Derivation of Base-line Geochemistry, Petrography, and Isotopic Data for the Host Rocks to the Lucky Strike Deposit and Comparison with Data from Other Alteration Zones, Buchans Mining Camp, Newfoundland

by

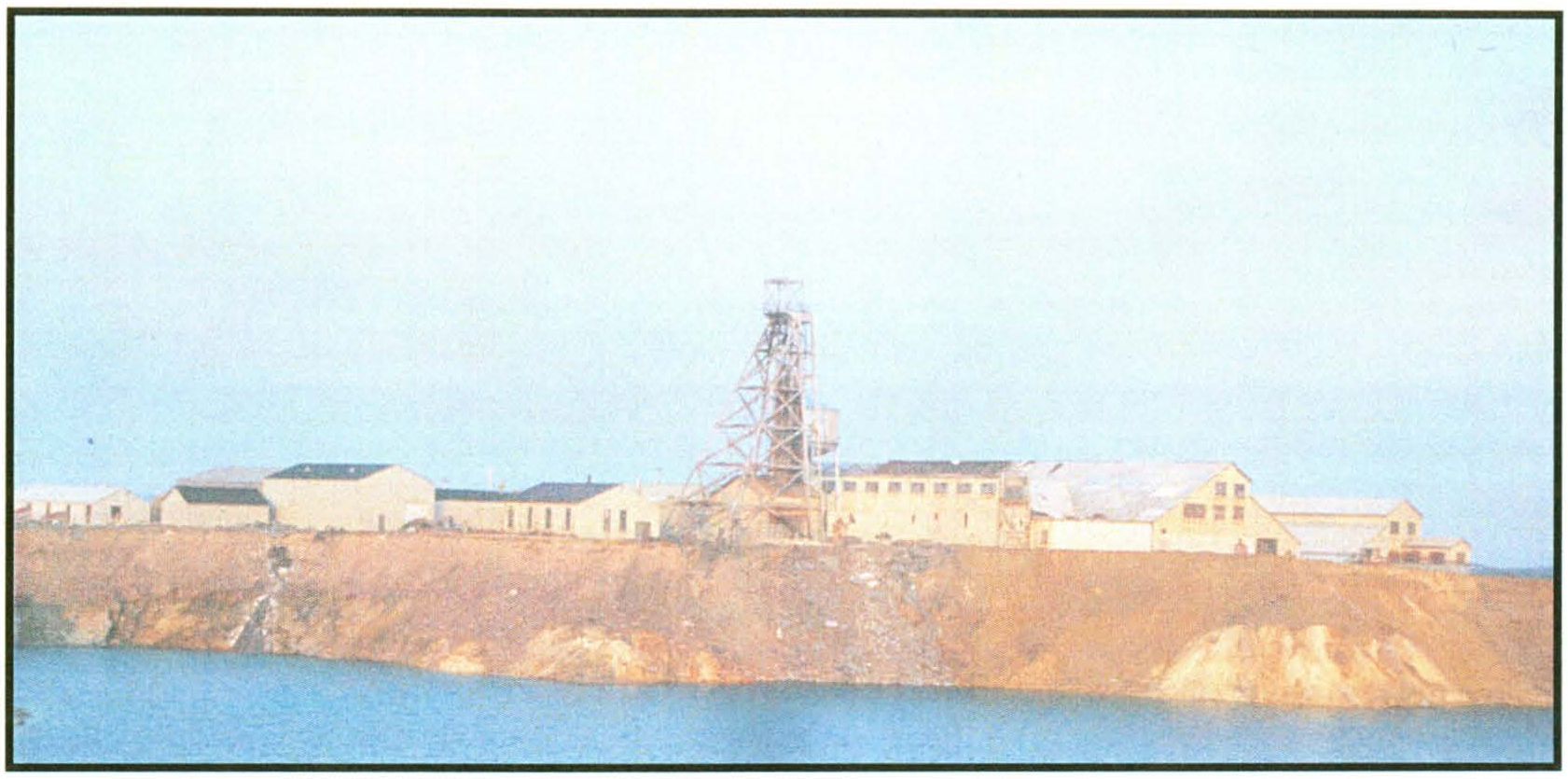
©Lawrence Stephen Winter, B.Sc. (Hons.)

A Thesis Submitted to the School of Graduate Studies
in Partial Fulfilment of the Requirements for the Degree of
Master of Science

Department of Earth Sciences
Memorial University of Newfoundland

February 2000

St. John's *Newfoundland*



Frontispiece
The Lucky Strike mill, headframe and glory hole and, as pointed out by John, plenty of blue sky.

Abstract

The Buchans ore bodies of central Newfoundland represent some of the highest grade VMS deposits ever mined. These Kuroko-type deposits are also known for the well developed and preserved nature of the mechanically transported deposits. The deposits are hosted in Cambro-Ordovician, dominantly calc-alkaline, bimodal volcanic and epiclastic sequences of the Notre Dame Subzone, Newfoundland Appalachians. Stratigraphic relationships in this zone are complicated by extensively developed, brittle-dominated Silurian thrust faulting.

Hydrothermal alteration of host rocks is a common feature of nearly all VMS deposits, and the recognition of these zones has been a key exploration tool. Alteration of host rocks has long been described to be spatially associated with the Buchans ore bodies, most notably with the larger in-situ deposits. This report represents a base-line study in which a complete documentation of the geochemical variance, in terms of both primary (igneous) and alteration effects, is presented from altered volcanic rocks in the vicinity of the Lucky Strike deposit (LSZ), the largest *in-situ* deposit in the Buchans camp. Packages of altered rocks also occur away from the immediate mining areas and constitute new targets for exploration. These zones, identified mostly by recent and previous drilling, represent untested targets and include the Powerhouse (PHZ), Woodmans Brook (WBZ) and Airport (APZ) alteration zones, as well as the Middle Branch alteration zone (MBZ), which represents a more distal alteration facies related to Buchans ore-formation. Data from each of these zones were compared to those from the LSZ in order to evaluate their relative propectivity.

Derived lithogeochemical data served two functions: (i) to define primary (igneous) trends and (ii) secondary alteration trends. Primary trends were established using immobile, or conservative, elements (*i.e.*, HFSE, REE, Th, TiO_2, Al_2O_3, P_2O_5). From these, altered volcanic rocks were interpreted in terms of composition (e.g., basalt - rhyodacite) and magmatic affinity (*e.g.*, calc-alkaline vs. tholeiitic). The information suggests that bimodality is a common feature of all zones, with most rocks plotting as either basalt/andesite or dacite (or rhyodacite); andesitic *senso stricto* compositions are rare. Magmatic affinities are more varied and complex, but indicate that all units are arc volcanic sequences. Rocks from the LSZ/MBZ represent a transitional to calc-alkalic sequence, however, a slight shift in key geochemical discriminants occurs between the foot-wall to the hanging-wall. Specifically, mafic and felsic lavas of the foot-wall are of transitional (or mildly calc-alkaline) affinity whereas the hanging-wall rocks are relatively more strongly calc-alkaline as indicated by enriched LREE/HREE and higher Zr/Y, Nb/Y and other ratios in the latter. The geochemical variations also serve as a means to separate the units (at least the felsic rocks) into hanging-wall and foot-wall sequences, therefore providing a valuable exploration tool. Volcanic rocks from the WBZ/PHZ (and probably the APZ) are more typical of tholeiitic to transitional suites, yielding flatter mantle-normalized REE patterns and lower Zr/Y ratios. Thus, the relationships between the

immediate mining area (represented by LSZ/MBZ) and the Buchans East (PHZ/WBZ) and the APZ are uncertain.

Host rocks for all zones consist of mafic to felsic volcanic rocks, though the proportion of pyroclastic and epiclastic rocks, is greatest at the LSZ. Phenocryst assemblages and textures are common in all zones, with minor exceptions, and are not useful for discrimination purposes. Felsic rocks from all zones are dominated by sericite-clay +/- silica alteration, whereas mafic rocks are dominated by chlorite - quartz - sericite alteration. Pyrite is ubiquitous in all moderately altered rocks and minor associated base metal sulphides occur locally. The exception is at Lucky Strike, where stockwork quartz-veining contains abundant base-metal mineralization and barite. Rocks completely comprised of chlorite (chloritite) also occur in the LSZ foot-wall. In addition, K-feldspar alteration occurs in felsic volcanic rocks at the MBZ associated with Zn-Pb-Ba and, notably, without chlorite. This zone represents a peripheral, but proximal, zone of alteration induced by lower temperature hydrothermal fluids, presumably with little influence from seawater.

Alteration geochemistry was interpreted from raw data as well as from mass balanced (recalculated) data derived from immobile element pairs. The data from the LSZ/MBZ indicate a range in the degree of alteration from only minor to severe modification of precursor compositions. Ba tends to show a strong positive correlation with K_2O, although most Ba occurs as barite. With respect to mass changes, Al_2O_3, TiO_2 and P_2O_5 were shown to be immobile. Nearly all rocks display mass loss of Na_2O, CaO, and Sr reflecting feldspar destruction. These trends are usually mirrored by K_2O-Rb and MgO addition, indicating sericitic and chloritic alteration, respectively. More substantial gains of K_2O often occur in rocks with K-feldspar alteration, whereas a few samples also displayed excessive MgO enrichment and represent chloritites. Fe_2O_3 indicates both chlorite and sulphide formation. SiO_2 addition is almost always the case for the altered mafic rocks as silica often infills amygdules and replaces the finer tuffaceous material. The felsic rocks display more variability in SiO_2. Silicic, sericitic and chloritic alteration trends were observed from the other zones, but not K-feldspar, chloritite, or barite.

Microprobe analysis of chlorites, sericites and carbonates indicate: (i) sericites from all zones are defined as muscovite and are not phengitic; (ii) at the LSZ, chlorites ranged from Fe-Mg chlorites (pycnochlorite) to Mg-rich chlorite (penninite), with the latter occurring in the stockwork zone and more proximal alteration facies; (iii) chlorites from the WBZ were typical of those from the more distal alteration facies of the LSZ, plotting as ripidolite to pycnochlorite; (iv) conversely, chlorite from the PHZ plot with Mg-Al-rich compositions (chlinochlore to penninite); and (v) carbonate species from each zone are also varied, with calcite occurring in each zone, in addition to dolomite and ankerite in the PHZ and WBZ, respectively.

Lead isotope ratios for galena separates from the different various zones, when combined with data from older studies, tend to cluster into four distinctive fields. Overall, the data plot on a broad mixing line and indicate evolution in a relatively low-μ

environment. Data from sulphide stringers in altered MBZ rocks, as well as from clastic sulphides (Sandfill prospect), plot in the Buchans ore field, as do the data for galena from altered rocks in the APZ. Samples from the Buchans East area are even more primitive than the Buchans ores, with lead from the PHZ plotting with the Connel Option prospect and data from the WBZ matching that of the Skidder prospect. A sample from a newly discovered debris flow-type sulphide occurrence (Middle Branch East) yields lead isotope ratios that are slightly more radiogenic than Buchans and plot with the Mary March alteration zone. Data within each cluster are interpreted to represent derivation from individual hydrothermal systems in which metals were derived from a common source.

Acknowledgments

The completion of any thesis is an arduous task that requires contributions from many sources. Derek Wilton presented me with the opportunity to study in the Buchans camp and also supervised this thesis. Derek exemplifies all of the qualifications of a great mentor, including patience, academic support and honest advice. His everlasting positive attitude and good humour have made this a most pleasurable learning experience. Thanks for the *big buller burgers*!

This study has been made possible by generous funding and employment opportunities from Buchans River Ltd., in particular: Brian Grant, John Tuach and Phil Saunders. You will get your forty metres of forty percent soon enough! Also, Ingrid Strelow drafted countless maps and sections and Debbie Doyle provided secretarial support from the office. Jim Harris directed much of this thesis in the early going and also shared many ideas on Buchans geology. The ever energetic Malcolm Oxford provided efficient field office management. Barry McCarthy and Rob Vaters are also thanked for assistance in the core shack and for their hospitality while at Buchans.

The receiving of the Buchans' Scholarship fund of ASARCO Incorporated of Memorial University is gratefully acknowledged.

The technical staff at the Department of Earth Sciences conducted very competent work, including Rock Soper (lapidary), Lakmali Hewa (ICP-MS) and Maggie Pyranian (microprobe). Special thanks are extended to Mike Tubrett and Pam King (XRF/ICP-MS) for their patience and efforts. Gerry Ford and Maureen Moore provided administrative support and quicky addressed all of my concerns. Time-efficient lead isotope analyses were provided by Clement Gariépy (UQAM).

Several individual are acknowledged for many thought-provoking discussions. In particular, Mark Wilson and George Jenner are greatly thanked for willingly sharing their knowledge of geology, geochemistry and mineral deposits. Fellow graduate students Steve Piercey, Rod Smith, Trevor McHattie, Jason Krauss, Richard Cox, and John Hinchey, as well as Brent Bromley, Sean Bailey and many others, have been eager to discuss academic, and not so academic, topics over the past few years. Brian Dalton and Roland Butler also provided me with some interesting field work opportunities and shared many ideas on Newfoundland geology. Thanks to all for the advice. Robbie Butler is thanked for playing half-decently on left wing.

I cannot express enough the gratitude towards my family for all of their support throughout my university career. My parents and sister have been a constant source of inspiration and have provided much emotional and financial support. Without their help I would not have reached this level. Last, but certainly not least, Angie has been my patient and ever supportive companion who has gone beyond the call of duty of see me complete this thesis. Her emotional support and understanding have been great sources of inspiration. Words cannot express my gratitude.

Table of Contents

Frontispiece ii

Abstract iii

Acknowledgments vi

Table of Contents vii

List of Tables xiii

List of Figures xix

List of Plates xviii

List of Abbreviations and Symbols xxii

Chapter One - Introduction

1.1 Introduction . . . . . Page 1
1.2 Location and Access . . . . . Page 2
1.3 Mining History . . . . . Page 2
1.3.1 Early Development . . . . . Page 2
1.3.2 Mining and New Discoveries . . . . . Page 4
1.3.3 New Explorers at Buchans . . . . . Page 5
1.4 Previous Technical Geological Studies . . . . . Page 6
1.5 Present Study . . . . . Page 12
1.6 Methods of Study . . . . . Page 13
1.7 VMS Deposits Overview . . . . . Page 14
1.7.1 Alteration Zones . . . . . Page 14

Chapter Two - Regional and Local Geological Setting

2.1 Introduction . . . . . Page 19
2.2 Regional Geological Setting of the Buchans Group . . . . . Page 19
2.2.1 The Dunnage Zone . . . . . Page 20
2.2.1.1 Tectono-Magmatic Development of Arc Sequences in the Notre Dame Subzone . . . . . Page 23

2.2.1.1.1 The Buchans - Robert's Arm Belt . . . . . Page 25
2.3 Geology of the Buchans Group . . . . . Page 26
2.3.1 Sandy Lake Formation . . . . . Page 28
2.3.2 Buchans River Formation . . . . . Page 29
2.3.3 Ski Hill Formation . . . . . Page 30
2.4.4 Lundberg Hill Formation . . . . . Page 32
2.4 Geology of the Skidder Basalt . . . . . Page 32
2.5 Structural Geology of the Buchans Area . . . . . Page 34
2.6 A Review of VMS-Style Mineralization in the Buchans-Roberts Arm Belt and Equivalent Groups . . . . . Page 35
2.6.1 Introduction . . . . . Page 35
2.6.2 The Buchans Polymetallic Volcanogenic Massive Sulphide Deposits . . . . . Page 37
2.6.3 Other Deposits/Significant Prospects . . . . . Page 40

Chapter Three - Alteration Zones

3.1 Introduction . . . . . Page 54
3.2 Lucky Strike Alteration Zone . . . . . Page 54
3.2.1 Location . . . . . Page 54
3.2.2 Dimensions . . . . . Page 55
3.2.3 Lithologies . . . . . Page 56
3.2.4 Alteration . . . . . Page 57
3.2.4.1 The Stockwork Zone . . . . . Page 57
3.2.4.2 Peripheral Alteration . . . . . Page 58
3.2.4.2.1 Proximal Alteration . . . . . Page 58
3.2.4.2.2 Distal Alteration . . . . . Page 62
3.2.4.3 Alteration Mineralogy . . . . . Page 63
3.3 Middle Branch Alteration Zone . . . . . Page 64
3.3.1 Location . . . . . Page 65
3.3.2 Dimensions. . . . . Page 65
3.3.3 Lithologies . . . . . Page 65
3.3.4 Alteration . . . . . Page 66
3.4 Woodman's Brook Alteration Zone . . . . . Page 68
3.4.1 Location . . . . . Page 68
3.4.2 Dimensions . . . . . Page 68
3.4.3 Lithologies . . . . . Page 69
3.4.5 Alteration . . . . . Page 71
3.5 Powerhouse Alteration . . . . . Page 74
3.5.1 Location . . . . . Page 74
3.5.2 Dimensions . . . . . Page 75
3.5.3 Lithologies . . . . . Page 75
3.5.4 Alteration . . . . . Page 76

3.6 Airport Alteration Zone . . . . . Page 78
3.6.1 Location . . . . . Page 78
3.6.2 Dimensions . . . . . Page 78
3.6.3 Lithologies . . . . . Page 79
3.6.4 Alteration . . . . . Page 80
3.7 Summary . . . . . Page 81

Chapter Four - Mineral Chemistry

4.1 Introduction . . . . . Page 120
4.2 Chlorite . . . . . Page 120
4.3 Sericite . . . . . Page 122
4.4 Carbonates . . . . . Page 123
4.5 Discussion and Applications to Exploration . . . . . Page 124
4.6 Summary . . . . . Page 127

Chapter Five - Lithogeochemistry and Lead Isotopes

5.1 Introduction . . . . . Page 137
5.2 Discrimination Diagrams . . . . . Page 139
5.2.1 Rock Types . . . . . Page 140
5.2.2 Normalized trace element data . . . . . Page 141
5.2.2.1 Primitive mantle normalized extended rare earth element plots . . . . . Page 141
5.2.2.2 Chondrite normalized rare earth element plots . . . . . Page 146
5.2.3 Mafic rocks as indicators of tectono-magmatic setting . . . . . Page 148
5.2.3 Bimodal suites - genetic relationships . . . . . Page 150
5.3 Lead Isotopes . . . . . Page 155
5.4 Discussion and Summary . . . . . Page 158

Chapter Six - Alteration Geochemistry

6.1 Introduction . . . . . Page 187
6.2 General Alteration Geochemistry . . . . . Page 188
6.2.1 Lucky Strike/Middle Branch Zones . . . . . Page 188
6.2.2 Powerhouse Alteration Zone . . . . . Page 193
6.2.3 Woodmans Brook Alteration Zone . . . . . Page 195
6.3 Mass Balance Calculations . . . . . Page 196
6.3.1 Mass Changes in the Lucky Strike Area/Middle Branch Area . . Page 199
6.3.1.1 Fractionation Trends . . . . . Page 199
6.3.1.2 Mass Changes . . . . . Page 203

6.3.1.2.1 $\triangle CaO$, $\triangle Na_2O$ and $\triangle K_2O$ . . . . . Page 203
6.3.1.2.2 $\triangle Fe_2O_3$ (total) - $\triangle MgO$ - $\triangle MnO$ . . . . . Page 204
6.3.1.2.3 $\triangle SiO_2$ . . . . . Page 205
6.3.1.1.4 $\triangle Al_2O_3$ - $\triangle TiO_2$ - $\triangle P_2O_5$ . . . . . Page 206
6.3.1.2.5 $\triangle Rb$ - $\triangle Ba$ - $\triangle Sr$ . . . . . Page 206
6.3.1.2.6 $\triangle$Totals . . . . . Page 207
6.3.1.3 Binary Mass Change Plots . . . . . Page 207
6.3.1.3.1 $\triangle SiO_2$ vs $\triangle K_2O$, $\triangle MgO$ . . . . . Page 207
6.3.1.3.2 $\triangle(MgO+K_2O)$ vs. $\triangle(Na_2O+CaO)$ . . . . . Page 208
6.3.1.3.3 $\triangle K_2O$ vs $\triangle Rb$ and $\triangle Ba$ . . . . . Page 208
6.3.2 Mass Changes at the Powerhouse Alteration Zone . . . . . Page 209
6.3.2.1 Fractionation Trends . . . . . Page 209
6.3.2.2 Mass Changes . . . . . Page 209
6.3.2.2.1 $\triangle CaO$, $\triangle Na_2O$ and $\triangle K_2O$ . . . . . Page 210
6.3.2.2.2 $\triangle Fe_2O_3$ (total) - $\triangle MgO$ - $\triangle MnO$ . . . . . Page 210
6.3.2.2.3 $\triangle SiO_2$ . . . . . Page 211
6.3.2.2.4 $\triangle Al_2O_3$ - $\triangle TiO_2$ - $\triangle P_2O_5$ . . . . . Page 211
6.3.2.2.5 $\triangle Rb$ - $\triangle Ba$ - $\triangle Sr$ . . . . . Page 211
6.3.2.2.6 $\triangle$Totals . . . . . Page 212
6.3.2.3 Binary Mass Change Plots . . . . . Page 212
6.3.2.3.1 $\triangle CaO$ vs $\triangle Na_2O$ . . . . . Page 212
6.3.2.3.2 $\triangle SiO_2$ vs. $\triangle K_2O$ . . . . . Page 212
6.3.2.3.3 $\triangle K_2O$ and $\triangle$ MgO vs. $\triangle$ CaO . . . . . Page 213
6.3.2.3.4 $\triangle$ Ba vs. $\triangle K_2O$ and $\triangle$Sr vs. $\triangle$ CaO . . . . Page 213
6.3.3 Mass Changes at the Woodmans Brook Alteration Zone . . . . . Page 214
6.3.3.1 Fractionation Trends . . . . . Page 214
6.3.3.2 Mass Changes . . . . . Page 214
6.3.3.2.1 $\triangle CaO$, $\triangle Na_2O$ and $\triangle K_2O$ . . . . . Page 215
6.3.3.2.2 $\triangle Fe_2O_{3(total)}$ - $\triangle MgO$ - $\triangle MnO$ . . . . . Page 215
6.3.3.2.3 $\triangle SiO_2$ . . . . . Page 216
6.3.3.2.4 $\triangle Al_2O_3$, $\triangle TiO_2$ and $\triangle P_2O_5$ . . . . . Page 216
6.3.3.2.5 $\triangle Rb$, $\triangle Ba$ and $\triangle Sr$ . . . . . Page 216
6.3.3.2.6 $\triangle$ Totals . . . . . Page 216
6.3.3.3 Binary Mass Change Plots . . . . . Page 217
6.3.3.3.1 Various $\triangle CaO$, $\triangle Na_2O$, $\triangle K_2O$ plots . . . . . Page 217
6.3.3.3.2 $\triangle SiO_2$ vs. $\triangle K_2O$, $\triangle$ MgO . . . . . Page 218
6.3.3.3.3 $\triangle MgO$ vs. $\triangle$K20, $\triangle Fe_2O_{3(total)}$ . . . . . Page 218
6.3.3.3.4 $\triangle Rb$, $\triangle Ba$ vs. $\triangle K_2O$ and $\triangle Sr$ vs. $\triangle CaO$ . . . . . Page 219
6.3.4 Summary of Mass Changes . . . . . Page 219
6.4 Downhole Geochemical Variation . . . . . Page 220
6.4.1 DDH 2871 . . . . . Page 220
6.4.2 DDH 202 . . . . . Page 221
6.5 Model for Hydrothermal Alteration Aureole at Buchans . . . . . Page 223

Chapter Seven - Summary and Applications to Exploration

7.1 Introduction . . . . . Page 263
7.2 Summary . . . . . Page 263
7.2.1 Primary Geochemistry . . . . . Page 263
7.2.2 Alteration Geochemistry, Mineral Analyses and Lead Isotopes . . Page 265
7.3 Applications to Exploration . . . . . Page 268
7.4 Unresolved Problems . . . . . Page 270

References . . . . . Page 271

Appendix A General Sample Preparation, XRF Technique and Analyses

A.1 General Sample Collection and Preparation A-1
A.2 X-Ray Fluorescence Technique A-1
A.3 Precision and Accuracy A-3

Appendix B ICP-AES Analyses

B.1 ICP-AES Analyses B-1

Appendix C ICP-MS Technique and Analyses

C.1 ICP-MS Analytical Technique C-1
C.2 Precision and Accuracy C-1

Appendix D Electron Microprobe Technique and Analyses

D.1 Electron Microprobe Technique D-1
D.2 Precision and Accuracy D-1

Appendix E Lead Isotope Analyses

E.1 Lead Isotope Analyses D-1

Appendix F Mass Balance Calculations

F.1 Methods and Calculations F-1

List of Tables

Table 2-1 Summary of formation lithologies of the Buchans Group. . . . . Page 28

Table A-1 Precision and accuracy for standard DNC-1. Data represent fourteen XRF analysis from December 1997 to June 1998. . . . . A-5

Table A-2 Pressed pellet XRF data from the Lucky Strike area.. . . . . A-6

Table A-3 Pressed pellet XRF data from the Middle Branch Zone. A-15

Table A-4 Pressed pellet XRF data from the Powerhouse Alteration Zone. A-18

Table A-5 Pressed pellet XRF data from the Woodmans Brook Zone A-24

Table A-6 Pressed pellet XRF data from the Airport Alteration Zone A-32

Table B-1 ICP-AES data from the Lucky Strike Zone B-3

Table C-1 ICP-MS data from various areas in the Buchans camp. C-4

Table D-1 Statistical parameters for 21 analyses of standard Kakanui hornblende D-2

Table D-2 Microprobe data for chlorite D-3

Table D-3 Microprobe data for sericite D-6

Table D-4 Microprobe data for carbonates D-9

Table E-1 Lead isotope ratios for six samples from the Buchans area. E-2

Table E-2 Description of host rock/mineralization style for lead isotope ratios. E-2

Table F-1 Various alteration indices and alteration indicator elements for the LSZ. F-4

Table F-2 Correlations for alteration indices and various elements for data from the LSZ. F-5

Table F-3 Various alteration indices and important alteration indicator elements for the PHZ F-6

Table F-4 Correlation Coefficients for Alteration indices and selected elements from the PHZ. F-7

Table F-5 Various alteration indices and important alteration indicator elements for the WBZ F-8

Table F-6 Correlation Coefficients for Alteration indices and selected elements from the WBZ. F-7

Table F-7 Calculated mass changes for volcanic rocks in the Lucky Strike and Middle Branch area. . . . . F-9 - F-13

Table F-8 Calculated mass changes for volcanic rocks in the PHZ . . . . . F-14 - F-16

Table F-9 Calculated mass changes for volcanic rocks in the WBZ. . . . . F-17 - F-20

List of Figures

1-1 Map of the island of Newfoundland showing location of Buchans. . . . . Page 17

1-2 Hydrothermal alteration models for various VMS deposits . . . . . Page 18

2-1 Tectonostratigraphic subdivisions of the island of Newfoundland . . . . . Page 47

2-2 Geological map of the Notre Dame Subzone showing major lithostratigraphic units and structures . . . . . Page 48

2-3 Local geological map for the immediate Buchans area . . . . . Page 49

2-4 Schematic stratigraphy of the Buchans Group . . . . . Page 50

2-5 Regional schematic geological section of the Buchans area illustrating relationships between thrusts and major units. . . . . Page 51

2-6 Camp scale schematic structural cross section. . . . . Page 52

2-7 Map of the Buchans-Robert's Arm Belt showing the location of VMS deposits and significant prospects. . . . . Page 53

3-1 Map of the Buchans area showing local geology, ore bodies, drill hole locations and the outline of alteration zones . . . . . Page 85

3-2 East-West cross section through the Lucky Strike area . . . . . Page 86

3-3 North-South cross section through the Lucky Strike area. . . . . Page 87

3-4 Schematic stratigraphy and alteration in the Lucky Strike area . . . . . Page 88

3-5 Block Model for the Middle Branch alteration zone area . . . . . Page 90

3-6 North-South cross section through the Woodmans Brook alteration zone showing a) lithological units . . . . . Page 91
and b) alteration . . . . . Page 92

3-7 Cross section through the Powerhouse alteration zone,
a) northwest - southeast . . . . . Page 94
b) north-south . . . . . Page 95
and c) east-west section. . . . . Page 96

3-8 Block Model for the Airport alteration zone (north) . . . . . Page 98

3-9 Northwest-Southeast cross section through Airport alteration zone (south) . . . . . Page 99

4-1 Chlorite compositional diagram based on the classification scheme of Hey (1954): a) Lucky Strike alteration zone . . . . . Page 128
b) Woodmans Brook alteration zone . . . . . Page 129
c) Powerhouse alteration zone. . . . . Page 130

4-2 Plot of Fe vs. Mg in number of cations for chlorite composition data. . . . Page 131

4-3 Chlorite compositional tetrahedron using Mg, Fe, Si, Al apexes. . . . . Page 132

4-4 Mica compositional ternary diagram. . . . . Page 133

4-5 Carbonate compositional ternary diagram . . . . . Page 134

4-6 Fe/Fe+Mg variations in coexisting sericites and chlorites from all zones. . Page 135

4-7 Distance from Lucky Strike ore vs. a) Fe/(Fe+Mg+Al) ratio in chlorite, b)Fe/(Fe+Mg) in sericite, c) Fe/(Fe+Mg) in chlorite, and d) modeled distance to ore vs. Fe/(Fe+Mg) for LSZ data and hypothetical distance to ore for PHZ and WBZ samples based on same equations. . . . . Page 136

5-1 Winchester and Floyd (1977) compositional plot for a) Lucky Strike alteration zone, b) Woodmans Brook alteration zone . . . . . Page 163
c) Powerhouse alteration zone, d) Airport alteration zone. . . . . Page 164

5-2 Representative primitive mantle-normalized extended rare earth element plot signatures for examples of recent volcanic rocks from various settings. . . . . Page 165

5-3 Primitive mantle normalized extended rare earth element plot for a) Ski Hill Formation, b) Buchans River Formation . . . . . Page 166
and c) Buchans East (PHZ and WBZ)) mafic and felsic volcanics . . . . . Page 167

5-4 Chondrite normalized rare earth element plots for various Buchans volcanic suites and comparison to the Hokuroko District, Japan.
a) Ski Hill Formation mafic volcanics, b) Buchans River Formation felsic volcanic rocks . . . . . Page 168
c) Buchans East felsic volcanic rocks , and d) Buchans East mafic volcanic rocks . . . . . Page 169

5-5 Ti vs. V plot (Shervais, 1982) discriminating arc and non-arc mafic volcanic rocks. a) Ski Hill Formation, b) Woodmans Brook, c) Powerhouse and d) Airport alteration zones. . . . . Page 170

5-6 Zr vs. Ti plot (Pearce and Cann,(1977) discriminating calc-alkaline basalts, island arc tholeiites and ocean floor basalts. a) Ski Hill and Buchans River formations, b) Woodmans Brook, c) Powerhouse, and d) Airport alteration zones. . . . . Page 171

5-7 Zr-Ti-Y plot (Pearce and Cann, (1977) discriminating mafic volcanic rocks as either within plate basalts, ocean floor basalts, low-K tholeiites, and calc-alkaline basalts. a) Ski Hill Formation, b) Woodmans Brook, c) Powerhouse and d) Airport alteration zones. . . . . Page 172

5-8 a) Zr - Th - Nb, b)Th - Hf - Nb, and c)Th - Hf - Ta ternary diagrams discriminating mafic rocks from various MORB, within plate and arc tectonic settings. . . . . Page 173

5-9 Zr vs. Y binary plots as monitors of fractionation and affinity.
a) Ski Hill and Buchans River formations b) Woodmans Brook alteration zone . . . . . Page 174
c) Powerhouse and d) Airport alteration zones . . . . . Page 175

5-10 Zr vs. Nb for data from all zones . . . . . Page 176

5-11 Y vs. Nb for data from all zones. . . . . Page 176

5-12 Various HREE vs. LREE plots for data from the Lucky Strike area (Ski Hill and Buchans River Formations) and Buchans East area (Powerhouse and Woodmans Brook alteration zones). . . . . Page 177

5-13 Various HREE vs. MREE plots for data from the Lucky Strike area (Ski Hill and Buchans River Formations) and Buchans East area (Powerhouse and Woodmans Brook alteration zones) . . . . . Page 178

5-14 Various LREE vs. MREE plots for data from the Lucky Strike area (Ski Hill and Buchans River Formations) and Buchans East area (Powerhouse and Woodmans Brook alteration zones). . . . . Page 179

5-15 Zr/TiO_2 (fractionation) vs. various LFSE/HFSE ratios for data from the Lucky Strike area (Ski Hill and Buchans River Formations) and Buchans East area (Powerhouse and Woodmans Brook Alteration. . . . . Page 180

5-16 Zr/TiO_2 (fractionation) vs. various LFSE/REE ratios for data from the Lucky Strike area (Ski Hill and Buchans River Formations) and Buchans East area (Powerhouse and Woodmans Brook Alteration . . . . . Page 181

5-17 Y vs.Nb for felsic volcanic rocks in the vicinity of the Lucky Strike deposit (Buchans River Formation), as well as Powerhouse and Woodmans Brook Alteration Zones. . . . . Page 182

5-18 $^{206}Pb/^{204}Pb$ vs. $^{207}Pb/^{204}Pb$ isotope plot illustrating published data from Cumming and Krstic (1987) for the Buchans ore bodies and various other VMS prospects in the Buchans Group. . . . . Page 183

5-19 Schematic model for volcanic stratigraphy in the Lucky Strike area . . . . Page 184

5-20 Regional tectonic model for the NDSZ. . . . . Page 185

5-21 Schematic model for potential setting of various volcanic suites from Buchans area . . . . . Page 186

6-1 $MgO - Al_2O_3 - (CaO-Na_2O-K_2O)$ ternary diagram for volcanic rocks from the Lucky Strike area (Ski Hill and Buchans River Formation). . . . . Page 226

6-2 Zr/TiO_2 vs SiO_2 for Ski Hill and Buchans River Formation mafic and felsic volcanic rocks (residual silica plot of Lavery, 1982). . . . . Page 227

6-3 Zr vs SiO_2 for Buchans River Formation dacites. . . . . Page 227

6-4 $(MgO + K_2O)$ vs. Na_2O for both the Ski Hill and Buchans River formations. . . . . Page 228

6-5 K_2O vs. Rb for a) Buchans River Formation dacites, b) Buchans River Formation rhyodacites and c) Ski Hill Formation mafic volcanic rocks. . Page 229

6-6 K_2O vs Ba for a) Buchans River Formation dacites, b) Buchans River Formation rhyodacites and c) Ski Hill Formation mafic volcanic rocks. . Page 230

6-7 $MgO - Al_2O_3 - (CaO-Na_2O-K_2O)$ ternary diagram for mafic and felsic volcanics rocks from the Powerhouse alteration zone. . . . . Page 231

6-8 K_2O vs. Ba, Rb for volcanic rocks from the Powerhouse alteration zone . . . . . Page 232

6-9 CaO vs. MnO, Sr for the Powerhouse alteration zone. . . . . Page 233

6-10 $MgO - Al_2O_3 - (CaO-Na_2O-K_2O)$ ternary diagram for mafic and felsic volcanic rocks from the Woodmans Brook alteration zone. . . . . Page 234

6-11 K_2O vs. Ba, Rb for volcanic rocks from the Woodmans Brook alteration zone. . . . . Page 235

6-12 Ba, CaO vs. Sr for volcanic rocks from the Woodmans Brook Alteration Zone. . . . . Page 236

6-13 Fractionation plots for the Ski Hill and Buchans River (dacites) formations: a) Zr vs. TiO_2, b) Zr vs. Al_2O_3 . . . . . Page 237
c) Zr vs. P_2O_5, d) TiO_2 vs. Al_2O_3 . . . . . Page 238

6-14 Zr vs TiO_2 plot for the Buchans River (rhyodacites) Formation . . . . . Page 239

6-15 Fractionation plots of Zr vs. TiO_2 for a) data from this study only and b) all existing data for the Ski Hill and Buchans River formations . . . . . Page 240
Fractionation plots of Zr vs. Al_2O_3 for c) data from this study only and d) all existing data for the Ski Hill and Buchans River formations . . . . . Page 241

6-16 Δ SiO_2 vs Δ K_2O, ΔMgO plots showing Ski Hill and Buchans River formations volcanic rocks . . . . . .Page 242

6-17 Δ ($MgO + K_2O$) vs. Δ (Na_2O +CaO) plot showing Ski Hill and Buchans River formations . . . . . Page 243

6-18 Δ MgO vs. Δ Na_2O and Δ K_2O vs. Δ Na_2O plots for data from the Ski Hill and Buchans River formations . . . . . Page 244

6-19 Δ K_2O vs Δ Rb, Δ Ba plots displaying data from the Ski Hill and Buchans River formations . . . . . .Page 245

6-20 Zr vs. TiO_2 and Zr vs. Al_2O_3 fractionation trends for the Powerhouse alteration zone . . . . . Page 246

6-21 Binary mass change plot of ΔCaO vs. ΔNa_2O for volcanic rocks of the Powerhouse alteration zone. . . . . Page 247

6-22 Δ SiO_2 vs. Δ K_2O plot for volcanic rocks of the Powerhouse alteration zone. . . . . Page 247

6-23 Binary mass change plot of Δ K_2O, Δ MgO vs. Δ CaO for Powerhouse alteration zone volcanic rocks . . . . . Page 248

6-24 Δ Ba vs. Δ K_2O and Δ Sr vs. Δ CaO plot for volcanic rocks of the Powerhouse alteration zone. . . . . Page 249

6-25 a) Zr vs Al_2O_3 and b) Zr vs TiO_2 fractionation trends for volcanic rocks from the Woodmans Brook alteration zone. . . . . Page 250

6-26 Binary mass change plots of a) ΔNa_2O vs. ΔK_2O, b) ΔCaO vs. ΔNa_2O and c) ΔCaO vs. ΔK_2O for volcanic rocks of the Woodmans Brook alteration zone . . . . . Page 251

6-27 Binary mass change plots of a) ΔSiO_2 vs. K_2O, b) ΔSiO_2 vs. MgO for volcanic rocks of the Woodmans Brook alteration zone. . . . . Page 252

6-28 Binary mass change plots of a) ΔMgO vs. K_2O, b) ΔMgO vs $Fe_2O_{3(total)}$ for volcanic rocks of the Woodmans Brook alteration zone. . . . . Page 253

6-29 Binary mass change plots of a) ΔBa vs ΔK_2O and b)ΔRb vs. ΔK_2O for volcanic rocks of the Woodmans Brook alteration zone. . . . . Page 254

6-30 Average calculated mass changes for a) Lucky Strike, b) Powerhouse, and c) Woodmans Brook alteration zones. . . . . Page 255

6-31 Geochemistry vs. depth in diamond drill hole 2871.
a) Zr/TiO_2 and Zr/Al_2O_3, b) Zr/Y and Nb/Y c) Cu, Pb, Zn, and Ba . . . Page 257
d) CaO, Na_2O and K_2O e) $Fe_2O_{3(total)}$ and MgO, f) SiO_2. . . . . Page 258

6-32 Geochemistry vs. depth in diamond drill hole 202.
a) Al_2O_3/TiO_2 and Y/TiO_2 . . . . . Page 259
b) Zr/Y c) $Fe_2O_{3(total)}$ and MgO, d) CaO, Na_2O and K_2O . . . . . Page 260
e) SiO_2 and f) Cu, Pb, Zn, and Ba . . . . . Page 261

6-33 Idealized hydrothermal alteration model for the Buchans VMS deposits showing alteration mineralogical assemblages and mass changes . . . . . Page 262

B-1 a) Duplicate and b) standards analysis by the ICP-AES method B-2

C-1 ICP-MS analysis of standard MRG-1 from this study and quoted values C-3

C-2 ICP-MS analysis of duplicate samples C-3

F-1 Element mass change histograms for SHF andesitic basalts F-21, F-22

F-2 Element mass change histograms for BRF dacites F-23, F-24

F-1 Element mass change histograms for PHZ dacites F-25

F-1 Element mass change histograms for WBZ dacites F-26, F-27

List of Plates

Plate 3-1 Chlorite - carbonate - epidote - hematite altered SLF mafic volcanic rocks. DDH 542, ~570'. . . . . Page 100

Plate 3-2 Quartz and sulphide-rich stockwork mineralization below the Lucky Strike orebody. DDH 542, 0-32'. . . . . Page 100

Plate 3-3 Mafic flow - hyaloclastite sequence of the SHF. DDH 2871, ~533'. . . . . Page 101

Plate 3-4 Various alteration textures in the SHF basaltic andesites. A) PPL and B)XPL illustrate silica-pyrite and sericite replacement of a feldspar phenocryst. Sample LS-39, FOV=1.3 mm. C)XPL and D)PPL illustrate chlorite, quartz and sericite replacement of phenocrysts. Sample LS-12, FOV=5 mm. . . . . Page 102

Plate 3-5 Photomicrograph of amygdules in SHF basaltic andesites typical of proximal alteration. A) PPL and B) XPL are from sample LS-39. Amygdules are zoned inwards from Mg-Fe chlorite (Mg end of pycnochlorite field) to quartz-pyrite. FOV=5 mm. C)PPL and D) XPL are from sample LS-35. This is the same unit but even closer to the ore horizon than previous. FOV=1.3 mm. . . . . Page 103

Plate 3-6 BRF dacitic flow/flow breccia. DDH 2889, ~516'. . . . . Page 101

Plate 3-7 Pyroclastic/volcaniclastic sequence within the BRF dacitic volcanic sequence. DDH, 2889, ~125'-145' . . . . . Page 104

Plate 3-8 Vitric and lithic tuff dominated by BRF dacitic volcanic fragments. DDH 2889, ~360. . . . . Page 104

Plate 3-9 Calcite-sulphide nodules in volcanic sandstone within the BRF. DDH 2889, 176'-212'. . . . . Page 105

Plate 3-10 Ore horizon breccia conglomerates. DDH 237, ~542'. . . . . Page 105

Plate 3-11 Chlorite-sericite(clay) altered crystal-vitric rhyodacitic tuff of the BRF in the LSZ. DDH 196, ~526' . . . . . .Page 106

Plate 3-12 Photomicrographs of devitrified and altered BRF rhyodacites. A flow is shown in A)PPL and B)XPL with quartz and plagioclase phenocrysts. Sample LS-25, FOV=7 mm. A more vitric flow is shown in C)PPL and D)XPL. This sample is also quartz and feldspar porphyritic and shows well developed classic perlitic fracturing. Sample LS-33, FOV=5 mm. . . . . Page 107

Plate 3-13 Strongly potassic (as well as silica and pyrite) altered pumiceous tuff of the BRF. DDH 237, ~443'. . . . . Page 106

Plate 3-14 Photomicrograph of zoned amygdules typical of weak, distal alteration in the SHF basaltic-andesite. Epidote and quartz (spheroidal) are the earliest phases and Fe-Mg chlorite is later. Sample LS-01 (Ski Hill Locality). a) PPL, Magnification is 10X, field of view is 1.3 mm. B) same view in XPL. . . . . Page 108

Plate 3-15 Distal alteration facies for the mafic volcanic foot-wall (SHF andesitic-basalt). MBZ, DDH 1916, 1826'. . . . . Page 109

Plate 3-16 Peripheral, proximal (potassic) alteration facies (at MBZ) in the felsic volcanics (BRF dacite). DDH 1162, ~ 1305'. . . . . Page 109

Plate 3-17 Photomicrographs of strong potassic alteration in BRF dacites in the MBZ. A) Relatively coarse masses of K-feldspar rimmed with sericite and epidote. MB-01, XPL, FOV=5mm. B) PPL and C) XPL are enlargements of the same area with FOV=1.3mm. . . . . Page 110

Plate 3-18 Quartz-feldspar porphyritic to aphyric dacite flows of the Woodmans Brook felsic volcanics. DDH BE-96-08, 278-287 m. . . . . Page 111

Plate 3-19 A) Quartz and feldspar porphyritic dacite from the WBZ. Sample is WB-19, XPL, FOV=5 mm. B) Well developed micropoikilitic texture in dacite from the WBZ. Sample WB-23, XPL, FOV=1.3 mm. . . . . Page 112

Plate 3-20 Spotty carbonate-sulphide texture peculiar to a portion of the WBZ felsic volcanics. DDH BJ-41, ~149' . . . . . .Page 111

Plate 3-21 Chlorite-sericite-quartz-pyrite altered basaltic andesite flows of the WBZ. DDH BE-96-10, ~120 m . . . . . .Page 113

Plate 3-22 Strongly foliated and sericite altered felsic volcanic sequence of the WBZ. DDH BE-95-01, ~60 m . . . . . Page 113

Plate 3-23 Chlorite - pyrite dominant alteration and brecciation in the WBZ mafic volcanic rocks. DDH BE-95-01, ~16.9 m. . . . . Page 114

Plate 3-24 A) Complete quartz-sericite-chlorite-pyrite-carbonate replacement of a mafic hyaloclastite? from the WBZ. Sample WB-10, XPL, FOV=5mm. B) Zoned amygdules in strongly altered mafic volcanics from the WBZ. WB-09, XPL, FOV=5mm. C) Foliated quartz -sericite-pyrite alteration in a felsic volcanic protolith; WB-02, FOV=1.3mm. . . . . Page 115

Plate 3-25 Sericite - quartz alteration and associated galena - sphalerite -pyrite mineralization in felsic volcanic rocks of the WBZ. DDH BE-95-03, ~ 108.3 m . . . . . Page 114

Plate 3-26 Hydrothermal breccia in felsic volcanic rocks from the WBZ. BE-96-10, ~113-114 m. . . . . Page 116

Plate 3-27 Photomicrograph of sample in plate 3-26. Fragments are altered to very fine grained sericite-clay and te matrix is quartz. Sample WB-15, PPL, FOV=5 mm. . . . . Page 116

Plate 3-28 Gossan exposed near powerhouse on Buchans River and representing the surface expression of the PHZ. . . . . Page 117

Plate 3-29 DDH BE-96-11 showing the mafic volcanics and the underlying felsic volcanic. . . . . Page 117

Plate 3-30 DDH BE-97-19, ~44m. Well developed in-situ breccia texture in a dacite flow from the PHZ. . . . . Page 118

Plate 3-31 Strongly altered feldspar porphyritic mafic volcanic unit from the PHZ. DDH BE-95-11, ~84 m. . . . . Page 118

Plate 3-32 Large carbonate-quartz-pyrite filled amygdule in altered PHZ mafic volcanics. DDH BE-95-11, ~92.5 m. . . . . Page 118

Plate 3-33 Photomicrographs of altered rocks from the PHZ. A) Quartz and feldspar porphyritic dacite. Sample BE-97-20, PPL, 5mm. B) Similar to above but with stronger resorption of quartz WB-9, XPL, FOV=8.45mm. C) Altered feldspar porphyritic mafic unit. Sample PH-3, XPL, FOV=8.45mm. . . . . Page 119

List of Abbreviations and Symbols

APZ	Airport Alteration Zone
APZ-N	Airport Alteration Zone - North
APZ-S	Airport Alteration Zone - South
BRAB	Buchans - Roberts Arm Belt
BRF	Buchans River Formation
CAB	Calc-Alkalic Basalts
E-MORB	Enriched Mid Ocean Ridge Basalts
ESZ	Exploits Subzone
HFSE	High Field Strength Elements
HREE	Heavy Rare Earth Elements
IAT	Island Arc Tholeiites
LOI	Loss On Ignition
LFSE	Low Field Strength Elements
LHF	Lundberg Hill Formation
LKT	Low-K Tholeiites
LREE	Light Rare Earth Elements
LSZ	Lucky Strike Alteration Zone
MBZ	Middle Branch Alteration Zone
MREE	Middle Rare Earth Elements
NDSZ	Notre Dame Subzone
N-MORB	Normal Mid Ocean Ridge Basalt
OFB	Ocean Floor Basalt
PHZ	Powerhouse Alteration Zone
REE	Rare Earth Elements
RIL	Red Indian Line
SHF	Ski Hill Formation
SLF	Sandy Lake Formation
VMS	Volcanogenic Massive Sulfide
WBZ	Woodmans Brook Alteration Zone
FOV	field of view
PPL	plane-polarized light
XPL	crossed-polarized light
Py	pyrite
Qtz	quartz
Ser	sericite
Chl	chlorite
Carb	carbonate
K-feld	K-feldspar
pum	pumice
vit	vitric
lith	lithic
bx	breccia
cgl	conglomerate
xtal	crystal
sst	sandstone (volcanic)

Chapter One - Introduction

1.1 Introduction

The Buchans ore bodies were originally discovered in 1905 by Matty Mitchell, a Micmac Indian employed by the Anglo Newfoundland Development (A.N.D.) Company to conduct prospecting around the Red Indian Lake area. A joint venture between the American Smelting and Refining Company (ASARCO) and A.N.D. in 1926 initiated what would eventually amount to 56 years of continuous mining from 1928 to 1984. Over this period, the prolific Buchans camp produced 16.2 million tonnes of ore at an average grade of 14.5% zinc, 7.6% lead, 1.3 % copper, 126 grams per tonne silver and 1.37 grams per tonne gold from 5 major volcanogenic massive sulphide deposits. After nearly a century of mining and exploration, the search for new ore continues in the Buchans area.

This study represents one of the few geological studies in Buchans carried out over this decade and is being conducted to advance exploration in the Buchans Group. It is based on lithogeochemistry supported by field work, core-logging and petrography. Mineral chemistry and lead isotope data provide important supplementary data. Although the Buchans camp has a long and historical record of mining, this study should be considered as reconnaissance in nature as opposed to advanced for two reasons. First, a major revision of the structure and stratigraphy of the Buchans area has recently been undertaken; this overhaul of Buchans geology occurred at the very end of mining and after the bulk of exploration. Secondly, a surprisingly small amount of lithogeochemical data exist for the Buchans camp, with most work having been compiled in the 1970's and early 1980's.

1.2 Location and Access

Buchans is located in central Newfoundland approximately 5 kilometres north of Red Indian Lake (refer to Figure 1-1). It is accessible via a two lane paved highway which branches off of the Trans Canada Highway at Badger. The 72 kilometre long highway parallels the Exploits River to Buchans Junction for about 40 kilometres while the remaining 30 kilometres trek the west side of Red Indian Lake. Vegetation dwindles from thick spruce forests to higher barrens and isolated stands of trees proceeding inland. The topography for this area is generally flat with gently rolling hills. Concentrates from the Buchans camp were hauled by railway line port of Botwood where they were transported by ship. All railway lines have since been decommissioned and stripped of their tracks.

1.3 Mining History

1.3.1 Early Development

Buchans has a very interesting and rich history which includes many pioneering methods of exploration and development in mining. An excellent record was compiled by Neary (1981) upon which the following summary relies heavily.

Matty Mitchell, a Micmac Indian from Halls Bay, Newfoundland, worked for the Anglo-Newfoundland Development (A.N.D.) Company during the seasons 1904, 1905, 1906. Along with his oldest son Lawrence and friend Jim Sheppard, Matty is credited with making the original discovery of the "Buchans River deposit" in 1905.

The first geological examination of the Buchans River prospect was carried out in

1905 by William F. Canning of the surveying firm Sullivan and Canning. The firm was hired by the A. N. D. Company. Through stripping, digging and trenching, Canning provided the first estimates of the extent of the orebody as well as assays of copper, lead, zinc, gold and silver.

In 1906 - 1907, William Scott, a civil engineer with the A.N.D. Company at Grand Falls, extended Canning's trenches and provided more assays. In the summer of 1906, Scott and Col. R. C. Fielding, an English geologist, produced the first geological map of the vicinity. A small number of miners were hired in 1907 who completed a total of 1700 linear feet of underground work, including an inclined shaft to a slope distance of 255 feet. Two deposits were delineated.

Terra Nova Properties were incorporated as a subsidiary of the A.N.D. Company in 1908. Metallurgical testing of the ores in the U.S. proved unsuccessful due to the fine-grained and intergrown nature of the ore.

In 1909, Fielding continued to oversee work on the property conducting mineralogical studies and metallurgical tests. A mining engineer, George Francis Laycock, was also introduced to the property. In 1910, Laycock sent a 1000 ton bulk sample of Buchans ore to Sweden for metallurgical testing. Some success was obtained from electrical smelting of the bulk sample but the transportation costs and smelting penalties hampered development.

Walter Harvey Weed, in 1911, conducted the first reserve calculation for the Buchans River Mine and estimated that it contained 93,900 tons of ore with a grade of 20.38% zinc, 8.14% lead, 2.36% copper, 6.7 ounces per ton silver and gold (worth $2.72

per ton). Weed's recommendations for further drilling and in order to test for new ore bodies were declined by the Terra Nova Properties limited.

1.3.2 Mining and New Discoveries

In 1926, the American Smelting and Refining Company (ASARCO), upon developing a successful metallurgical means (selective flotation) to mill the Buchans ore, signed a formal agreement with Terra Nova Properties Limited (A.N.D. Company) to develop the Buchans River Mine. Work began in the spring with prospecting and diamond drilling. Hans T. Lundberg, of the Swedish American Prospecting Corporation, was contracted to conduct a geophysical prospecting survey testing for electrical conductivity.

A couple of 'good anomalies' were detected. Initial trenching on the first in the west unearthed scattered lead-zinc mineralization, termed the "Black Fly". A 27 foot shaft was unsuccessful in reaching bedrock. Later trenching 300 feet west of this shaft revealed massive lead-zinc mineralization - the Lucky Strike orebody. Testing of the second anomaly also proved to be massive sulphide mineralization - the Oriental No.1 orebody.

In 1927, mine, mill and town construction began at the new and emerging town of Buchans. A subsidiary company was incorporated under the name the Buchans Mining Company Limited. In the following year, railway construction on a line from Millertown to Buchans began and hydro-electric power was generated. First ore concentrates were also produced. Proven ore reserves were in excess of 6 million tons in 1929. Then in

1930, the mill was expanded from 500 tons per day to 1250 tons per day.

In 1947, the 3.4 Mt high grade Rothermere orebody was discovered west of Lucky Strike. The MacLean orebody was discovered northwest on the same trend in 1950. MacLean also contained 3.4 Mt of high grade ore. The Oriental No. 2 orebody was discovered adjacent to the Oriental No. One orebody 1953. Oriental No.2 contained 0.9 Mt of good grade ore. After 57 years of continuous production, the Buchans mining operation closed in 1984 with reserves supposedly exhausted.

1.3.3 New Explorers at Buchans

In the period from 1985 to 1992, the Buchans camp proper was explored by BP Selco, who conducted a modest amount of surface exploration, including geological mapping, geochemical and geophysical studies, trenching and diamond drilling. B.P. Selco's mining division was later dissolved.

In 1993, the Buchans camp became available for ground claim staking for the first time in history. Several major, junior and private companies and individuals descended into the area. Much of the camp is currently controlled by Buchans River Ltd., through staking and a series of option agreements. Furthermore, at the time of writing, a joint-venture agreement between Buchans River and Billiton Exploration Canada Ltd. has been signed. Billiton now has an interest in much of the known Buchans Group, having conducted a *high resolution VLF-EM and Magnetics* geophysical survey over the region and are undertaking follow-up geochemical and geological studies and drilling.

1.4 Previous Technical Geological Studies

Considering the historical production at Buchans, and compared to many other mining camps, Buchans has seen relatively little in terms of technical geological studies. This section provides an account of all known published and unpublished geological information pertaining to the Buchans camp. Note that, in keeping with the overall aims of this report, an attempt is made to stress information from the literature that relates to issues such as regional geology and alteration, and less of the specific details on the ore bodies themselves. The section also provides some insight into the evolution of geological ideas and exploration criteria at Buchans.

Murray (1871) provided the first geological descriptions from the Red Indian Lake area and the only ones before the discovery of ore at Buchans. Murray correlated these rocks with those of the Bay of Exploits and considered them to be of Silurian age. He considered the granites to be of Laurentian (Archean) age.

A lengthy document was published by Snelgrove (1928) in which he defined the *Central Mineral Belt of Newfoundland* as a wedge-shaped belt extending and narrowing from Notre Dame Bay to the Rose Blanche - Cinq Cerf area on the south coast of the island. He also divided the rocks of the Red Indian Lake area into two series: (i) an older series of 'andesitic to trachytic' volcanic, volcaniclastic and epiclastic rocks, and (ii) a younger series of intruding 'granitic' rocks and basaltic dykes. In his petrographic examination of the lavas he commented that "As a rule, they are highly altered, the characteristic secondary minerals being chlorite, with lesser amounts of sericite, epidote and calcite". Snelgrove also noted the abundance of clastic rocks in the "Buchans

district", and a strong association of "quartz porphyry" with ore. He suggested that the granites were the source for the felsic volcanics and were, therefore, a key factor in the mineralization process. Snelgrove supported a Silurian age for the older series but considered the intrusive rocks to be of Devonian age.

Newhouse (1931) defined three groups of rocks in the vicinity of Buchans. He recognized a package of basaltic to rhyolitic lavas, flow breccia and tuffs, considered to Cambro-Ordovician age, which he labeled the Buchans series. Diabase, granite and rhyolite intruded this series. A later sequence of fossiliferous sedimentary rocks were considered to be Carboniferous. Interestingly, Newhouse noted the occurrence of several faults in the vicinity of the Lucky Strike and Buchans River orebodies, reporting that the most significant faults have a northeast-southwest strike. He also described alteration in the "wall rock" as being variable, "with highly chlorite altered andesite and andesite tuff, to the point where textures are obscured… with scattered pyrite crystals and local silicification". Newhouse also described light coloured, silicified tuffs, and strongly sericitized rhyolite porphyry and tuff close to the contact with the ore. He also pointed out that the strongly sericitized and chloritized zones, close or immediately adjacent to ore, are strongly sheared or broken.

A publication by the Buchans Staff (1954), mostly detailing the mining and milling operations, was the first documentation of the Rothermere orebodies. The staff also made brief reference to the alteration commenting that silicification was the most extensive, chloritization was common in the foot-wall to the Lucky Strike and Rothermere orebodies, and sericitization was most common immediately around the ore lenses.

Relly's (1960) doctoral thesis, largely based on extensive petrographic work, represents the first petrochemical study directed towards understanding alteration related to mineralization. Relly supported the epigenetic hydrothermal replacement model.

Swanson and Brown (1962), by summarizing all previous data, considered the relationship of host rocks/orebodies to local/regional structures. These authors ascribed a Lower to Middle Ordovician age to the Buchans Group and correlated it with the Roberts Arm Group to the north. The authors pointed to local similarities in stratigraphy in the vicinity of the orebodies, but considered three 'cycles' of volcanism, with all orebodies hosted in the two lowermost cycles. Sericitization was described as the most characteristic and widespread form of alteration. Quartz and pyrite alteration are also considered to be widespread, but most notably in the 'intermediate foot-wall', and chloritization is prevalent in the foot-wall. An epigenetic style of mineralization was favoured, with selective replacement of certain stratigraphic members in which the replacement zone occurred at structurally favourable locations.

Through published descriptions of the Buchans ores, Anger (1963) was able to make comparisons of Buchans to the Rammelsberg and Meggen deposits. As these were considered to be of syngenetic origin, and based on similarities, he considered Buchans to have formed by a similar syngenetic process.

The first published regional geological map (1:250,000) to include the Buchans area was that of Williams (1967). Williams ascribed a Silurian age to the rocks of the Buchans area owing to the presence of red sandstones on the southeast shore of Red Indian Lake and lithologic comparisons of the Buchans Group to the Springdale Group.

Anderson (1972) mapped the Buchans area at 1:50,000 scale, but produced only preliminary maps.

Entwistle and Barnes (1971) were the first to suggest that the Lucky Strike and Oriental sequences were actually fault repetitions of a single sequence. Walker and King (1975) supported the hypothesis.

Thurlow (1974) studied the relationships of lithogeochemistry to mineralization. A summary of this data and ideas on Buchans geology was published by Thurlow et al. (1975). These authors describe two major subgroups within the Buchans Group - the Upper and Lower subgroups. The Upper Buchans Subgroup encompassed most of the rocks to the east of Buchans. Within the lower subgroup, four cycles of calc-alkalic mafic to felsic volcanism were described, with ore occurring in the lower two cycles. They also suggested a volcanic-exhalative origin for the ore in a shallow water environment, most similar to the Kuroko deposits of Japan. Within 30 metres of either foot-wall or hanging wall, Zn, Pb, and Ba, and to a lesser extent Cu, Ag, Fe, Mg, Ca and Sr were described as the elements which "best indicate the presence of nearby mineralization" (*op cit*, p. 141). However, these authors also suggest that the dispersion patterns of most elements show erratic behavior and spatial inconsistencies.

A volume commissioned by ASARCO Inc. and the Price Co. Ltd. commemorating fifty years of geological development at Buchans (Swanson *et al.* 1981) represents the first significant collaboration of geological expertise on all aspects of Buchans geology. This volume contains contributions assessing regional, local and mine scale geology, geochronology, mineralogy, sedimentology, metamorphic petrology, stable

isotope geochemistry, metallogeny, glacial studies, geophysics, exploration methodology, and the history of the Buchans area. Concurrently, Thurlow (1981) completed a Ph.D. study on geology, ore deposits and geochemistry. His work is summarized in the volume. As part of his work, Thurlow also produced a 1:50,000 scale geology map for the Buchans area. Kean (1980) also published a map which included the Buchans area (12A/15).

Strong (1984) reported rare earth element (REE) analyses for 57 samples (from Thurlow's (1981) sample collection) including both mineralized and non-mineralized stratigraphic units at Buchans. He concluded that no systematic magmatic fractionation processes were indicated and, therefore, that such processes did not control ore formation at Buchans, as Campbell *et al.* (1982) had suggested for VMS deposits in the Archean Abitibi greenstone belt.

Dunning *et al.* (1986) reported U-Pb zircon ages of 473 $^{+3}/_{-2}$ and 473 $^{+}/_{-2}$ Ma for rhyolites of the Buchans and Roberts Arm Groups, respectively. These data supported the correlation of these groups and their description as early Ordovician sequences and quashed previous Rb-Sr whole-rock isochron ages of 447 Ma (Bell and Blenkinsop, 1981). These data were supported by the identification of late Arenig - early Llanvirn conodonts within the Buchans Group (Nowlan and Thurlow, 1987).

A second multi-disciplinary study of Buchans geology was published by the Geological Survey of Canada (Kirkham, 1987) in order to improve understanding of the Buchans deposits and advance exploration for VMS deposits in Newfoundland and elsewhere. Many excellent papers were included in this volume, including several

pertaining to structural and stratigraphic issues that have had a profound effect on geological concepts and exploration methodology at Buchans. Specifically, Calon and Green (1987), McClay (1987) and Thurlow and Swanson (1987) recognized that the Buchans Group was part of a fold and thrust belt in which older rocks were emplaced upon relatively younger sequences. Consequently, a complete reinterpretation of the stratigraphy was presented by Thurlow and Swanson (1987) where, simply, four formations were outlined with the ore bodies occurring at only one horizon.

Various geophysical methods have been tested at Buchans including tensor controlled source audio-magnetotellurics (CSAMT) (Boerner *et al.* 1993) and high resolution seismic reflection surveys (Thurlow *et al.* 1992; Spencer *et al.* 1993; and Wright *et al.* 1994). These surveys, notably the latter, have provided insight into the complex three dimensional distribution of major thrust faults in the Buchans camp.

Based on mafic volcanic rock trace and REE geochemical data, Swinden (1991) considered the Buchans Group to represent a mature arc sequence, displaying calc-alkalic, prominent arc geochemical signatures. Thurlow (1988) provides a concise summary of geology and ore bodies of Buchans.

Several unpublished B.Sc. theses on various geological topics at Buchans have been completed over the life of the operation (Woakes, 1954; Catherall, 1960; and Alcock, 1961) and several unpublished Asarco Inc. geological reports also exist (*e.g.*, MacLean, 1941; Larsen, 1973).

1.5 Present Study

The purpose of this study is to describe and document the hydrothermal alteration associated with the *in-situ* Lucky Strike massive sulphide deposit, particularly, with the aid of lithogeochemistry, mineral chemistry and petrology. In addition, the geochemical and petrological data will assist in determining protolith compositions for host rocks which are typically unidentifiable due to intense alteration. This represents the first substantial lithogeochemical study in the Buchans camp in nearly twenty years and is the first to employ modern analytical techniques with high precision detection limits for important trace elements. A major problem that this study aimed to surmount at Lucky Strike, and in Buchans in general, relates to the structural complexities in this area as panels of altered rocks may have misleading spatial relationships to associated massive sulphide mineralization.

The rationale for studying alteration at Lucky Strike is to produce a type-alteration model of the Kuroko-style VMS deposits at the Buchans camp which would allow for direct comparison with other prospective zones of alteration and mineralization throughout the region. It can be reasoned that, if through field, petrographic and geochemical studies, changes can be recognized from peripheral to proximal alteration facies in a known VMS-forming paleo-hydrothermal system (*i.e.*, Lucky Strike), then the same alteration template can be applied to untested alteration zones to focus exploratory drilling. Thus, four other hydrothermal alteration zones were documented and compared in this study.

Additionally, lead isotopic studies were undertaken to determine if the various

alteration zones could be subdivided. Lead isotope ratios from one single hydrothermal alteration system are normally homogenous and reflect metal sources.

1.6 Methods of Study

Most of the field work was conducted from mid-May to the end of August, 1997, and involved the re-logging of ASARCO drill core as well as drill core from the recent drilling programs by Buchans River Limited to the east of Buchans. Only a minor field mapping program was warranted due to the lack of outcrop exposure.

A total of 69 drill holes with a combined footage of approximately 22,000 metres were examined. Several hundred samples were collected and 131 of these were analyzed by pressed-powder pellet X-ray fluorescence (XRF) for trace elements and majors at the Department of Earth Sciences at Memorial University. Polished thin sections were also prepared at Memorial University for each sample analyzed. All of the Lucky Strike samples were also analyzed by Inductively Coupled Plasma - Atomic Emission Spectrometry (ICP-AES) at the Bondar Clegg lab in Vancouver, B.C, for high precision major elements. A sub set of samples were also analyzed by Na_2O sinter, Inductively Coupled Plasma - Mass Spectrometry (ICP-MS), Memorial University, for a complete rare earth element (REE) and trace element data set. Galena separates, from mineralized areas within each alteration zone, were collected and analyzed for lead isotopic compositions at GEOTOP Laboratories, Université du Québec à Montréal (UQAM), Québec.

1.7 VMS Deposits Overview

Volcanogenic massive sulphide (VMS) or volcanic-hosted massive sulphide (VHMS) deposits are typically modelled as syngenetic mound-shaped accumulations of polymetallic sulphide hosted in submarine volcanic or volcano-sedimentary successions. The deposits result from hydrothermal systems focussed and exhaled on the sea floor. VMS deposits occur throughout the geological record ranging from the Archean to active formation on the modern seafloor. Although all VMS deposits have the same fundamental characteristics, significant variation exists in the sizes, morphologies, metal contents, host rocks and alteration patterns from district to district and even within districts. The geological literature abounds with studies on VMS deposits and there have been numerous comprehensive reviews that summarize our understanding of this deposit type (Franklin *et al.* 1981; Lydon, 1988a, 1988b, 1996; Franklin, 1993; Ohmoto, 1996, and others)

Several classification schemes have been derived to subdivide VMS deposits including metallic compositions (*e.g.,* Franklin *et al.*, 1981; Poulsen and Hannington, 1995), host rock composition/geological setting (*e.g.,* Barrie and Hannington, 1999), and tectonic setting (Swinden, 1991; Franklin *et al.* 1999). For the purposes of this paper the classification scheme of Franklin *et al.* (1981) will be used since it adequately defines alteration styles for each deposit type.

1.7.1 Alteration Zones

Alteration zones associated with VMS deposits often form haloes that are orders

of magnitude greater in size than the orebodies which they surround. Undoubtably then, these zones are important clues to the presence of blind (or unknown) massive sulphide deposits and the correct identification of alteration assemblages is an essential prerequisite for successful exploration. There is, however, significant variance in the alteration mineralogy associated with different deposits that can be grouped broadly into two different types: alteration associated with (i) Cu-Zn or (ii) Zn-Pb-Cu deposits (Franklin *et al.,* 1981. Franklin, 1993).

Of the Cu-Zn type, two distinctive styles of alteration have been identified and attributed to water depth controls (*cf.* Franklin, 1993): (i) deep water or Noranda and Cyprus type and (ii) shallow water or Mattabi type. Noranda deposits have a distinctive pipe-like stockwork zones that have a characteristic chloritic core and a sericitic rim (Figure 1-2a). The alteration pipes generally taper downwards for up to hundreds of metres to a very narrow fault controlled zone. Mattabi type alteration zones (Figure 1-2b) typically have a pipe-like zone defined by silica-sericite alteration with lesser chlorite. Chlorite may be localized to the periphery of the pipes along with aluminosilicate, including pyrophyllite, andalusite and kyanite (Morton *et al.,* 1992).

Large zones of semi-conformable foot-wall alteration are also associated with the Cu-Zn type VMS deposits. These are often several kilometres in lateral extent and several hundred metres in thickness occurring a few hundred metres below the deposits (Franklin, 1993). Epidote-silica often characterize the alteration assemblage of this zone (*e.g.,* Noranda, Quebec; Gibson *et al.,* 1983), or carbonitization may be important (*e.g.,* Mattabi; Morton *et al.,* 1992). Franklin (1993) suggests that the semi-conformable alteration zones have undergone reaction with high temperature and low pH fluids under

low water/rock ratios, and therefore, are potential source regions for metals in the overlying ores.

Alteration around Zn-Pb-Cu VMS deposits is best exemplified by that of the Miocene Hokuroko district, Japan (Ohmoto and Skinner, 1983). Franklin (1993) summarizes the research of several workers on Kuroko VMS deposit types and reports four distinctive alteration zones (Figure 1-2b). Stockwork mineralization immediately below the ore is hosted in a quartz, sericite and lesser chlorite zone which represents the most intense alteration. A zone peripheral to the stockwork and immediately above the ore deposits consists of sericite, magnesian chlorite and montmorillonite. Both of these zones have incurred feldspar destructive alteration. Weaker sericite and mixed layer smectite alteration occurs peripheral to the previous zones. An outermost zone is defined mostly by the presence of zeolite (analcime) as well as montmorillonite. In older deposits that have undergone metamorphism and deformation, these alteration assemblages may not have preserved. The Carboniferous Tulsequah Chief deposit, British Columbia (Sebert and Barrett, 1996), has an associated sericite and quartz stringer zone surrounded by a biotite-cordierite rich zone interpreted to represent a metamorphosed chlorite, sericite, clay altered zone. When compared to the Cu-Zn type deposits, the Zn-Pb-Cu type generally lacks the chlorite-rich pipe-like zone. However, the Lucky Strike orebody at Buchans has an associated pervasively chlorite altered and quartz stockwork zone which represents the most intensively altered body of rock in the camp, although the zone does not resemble a pipe-like structure. Sericite generally occurs peripheral to this zone. Alteration at Lucky Strike is discussed in greater detail in Chapters 3, 4 and 6. In addition, there are other Zn-Pb-Cu deposits also display chlorite-rich zones (*e.g.,* Woodlawn deposit, New South Wales, Australia; Petersen and Lambert, 1979).

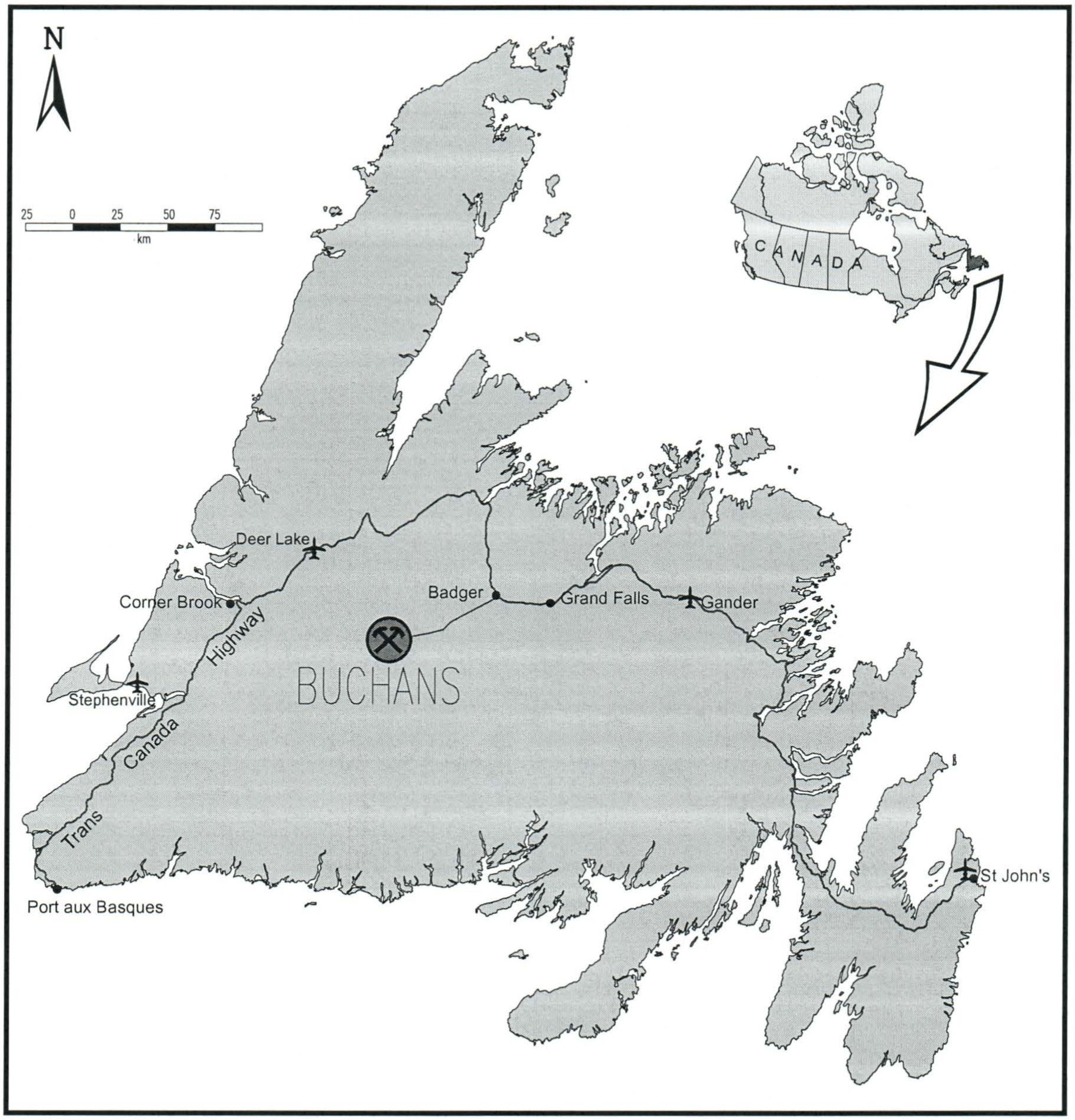


Figure 1-1 - Map of the island of Newfoundland showing the location of Buchans.

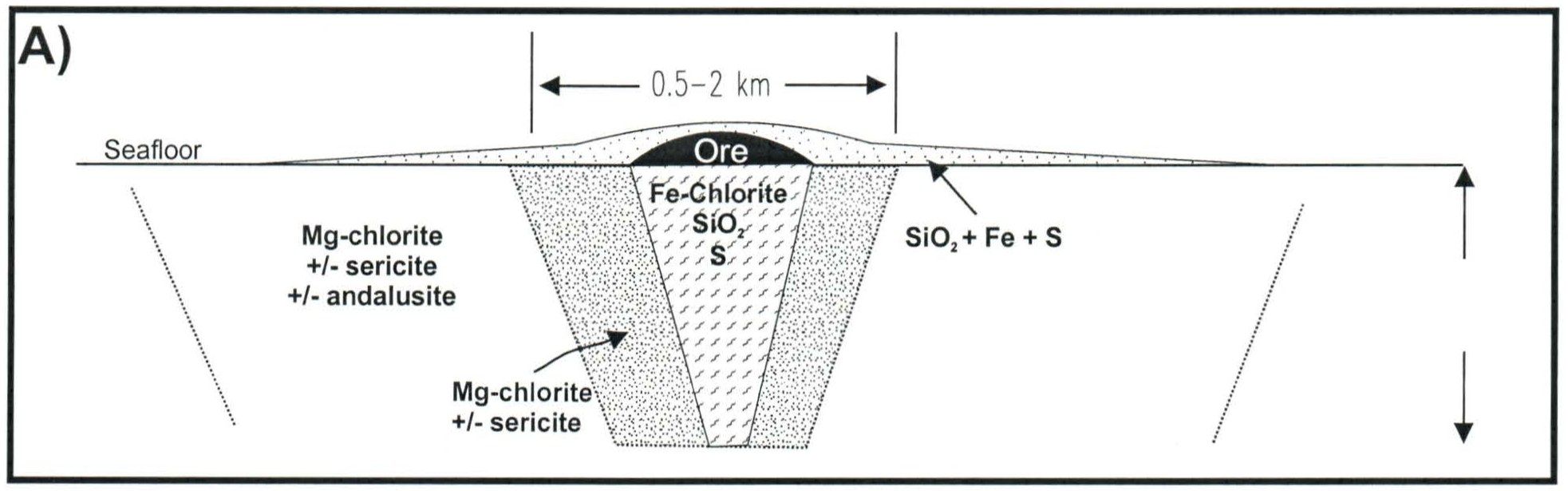


Figure 1-2 - Idealized hydrothermal alteration models for various styles of VMS deposits (after Franklin, 1993). Cu-Zn VMS deposits illustrated in A) Noranda/Cyprus-type (deep water) and B) Mattabi-type (shallow water). C) Zn-Pb-Cu or Kuroko-type.

Chapter Two - Regional and Local Geological Setting

2.1 Introduction

The Buchans Group comprises a portion of one of several volcanic belts in the Central Mobile Belt of Newfoundland. This chapter addresses the regional geology of Newfoundland with a focus on the tectonic development of these volcanic terranes. The geology of the Buchans camp is discussed with an emphasis on structural complications affecting stratigraphic interpretations. A brief geological overview of the Buchans camp is presented, including aspects of lithology, structural geology and alteration-mineralization. Other VMS-style mineral deposits and prospects hosted in other broadly coeval volcanic successions in the Central Mobile Belt, namely the Robert's Arm and Cutwell Groups, as well as the Skidder Basalt, are also reviewed.

2.2 Regional Geological Setting of the Buchans Group

The island of Newfoundland was initially described by Williams (1964) as a "two-sided symmetrical system" consisting of Precambrian continental platforms at the margins and an internal Paleozoic mobile belt. Further work led to the conclusion that the island represented the northeastern terminus of the Appalachian Orogen (Williams *et al.*, 1974), an ancient mountain belt extending a further 3000 kilometers south, into the southeast United States.

Based on stratigraphic and structural contrasts, Williams (1979) subdivided the Appalachian Orogen into five zones, including the Humber, Dunnage, Gander, Avalon,

and Meguma (the latter of which is not represented in Newfoundland). The Humber and Avalon Zones represent the early Paleozoic Laurentian and Gondwanan continental margins, respectively (Figure 2-1). These margins were separated by the early Paleozoic Iapetus Ocean of which vestiges are preserved in the Dunnage and Gander zones, collectively termed the Central Mobile Belt. The Gander Zone, comprised of monotonous turbiditic sequences, represents a marine shelf sequence developed along the peri-Gondwanan margin. The volcanic sequences of central Newfoundland, and hence, VMS deposits, are generally confined to the Dunnage Zone (*cf.* Swinden *et al*, 1988).

Hall *et al.* (1998) produced crustal seismic profiles through the Atlantic region from which the major structural boundaries have been imaged; the belt is considered allochthonous. They indicate that the central mobile belt has a thinner crust than its margins and that high velocity lower crust is found below the former Laurentian continental margin. These workers concluded that the orogen is probably more complex than a single process, doubly vergent collisional zone as proposed by Quinlan *et al.* (1993).

2.2.1 The Dunnage Zone

The Dunnage Zone consists of thick marine volcanic and epiclastic sequences and hypabyssal rocks of Cambrian to Silurian age representing vestiges of island arc/back arc tectono-magmatic systems which existed in the Iapetus ocean (Swinden, 1991; Swinden *et al.,* 1997, and references therein). The Dunnage Zone is bounded to the west by the Baie Verte - Brompton Line (Williams and St. Julien, 1978) and to the east by the Gander

River Ultramafic Belt (the "GRUB Line") (Blackwood, 1979).

In order to best describe the geology of the Dunnage Zone, the geological development should be viewed as a two-stage process: *pre-accretionary and post accretionary* (Swinden, 1991). Pre-accretion events refer to those which occurred in Iapetus during the Cambrian to Middle Ordovician, and include pre-accretionary volcanism and pre- and syn-sedimentation in island arc/back arc scenarios. Following the termination of subduction in the Mid to Late Ordovician, oceanic terranes were accreted to the Laurentian margin as Taconic allochthons (Kean and Strong, 1975; Swinden and Thorpe, 1984).

Pre-accretionary geology. The development of Iapetus was initiated in the Late Proterozoic (*ca.* 615 +/- 2 Ma; Kamo *et al.,* 1989) with rifting of the supercontinent. The rift-drift transition occurred in the Early Cambrian around 545 Ma (Williams and Hiscott, 1987). Oceanic crust generated during rifting is nowhere preserved (Dunning *et al.,* 1991). Therefore, all volcano-sedimentary successions in the Dunnage Zone are related to arc volcanism.

Following a review of geochemical, metallogenic, geochronological, paleontological and geophysical studies, Williams *et al.* (1988) suggested that the Dunnage Zone in Newfoundland is actually bipartite and two subzones were recognized: the Notre Dame Subzone (NDSZ), in the west and the Exploits Subzone (ESZ) in the east, separated by a structural boundary, the Red Indian Line (RIL) (named after the Red Indian Lake through which the boundary traces). The RIL is described as a rectilinear fault along most of its length, although mylonites occur in some places and intrusions

locally obscure its trace. The lithological packages associated with the Buchans mining camp are part of the NDSZ.

Based on fossils and other evidence, it was proposed that these two subzones formed in distinctly different paleogeographic settings (Colman-Sadd *et al.,* 1992, and references therein). The Notre Dame Subzone is considered to have formed close to the Laurentian margin whereas the Exploits Subzone formed closer to the Gondwanan margin. Williams *et al.* (1988) illustrated that the greatest contrast between the Notre Dame and Exploits Subzones is based on stratigraphy. Specifically, conformable Upper Ordovician and Silurian marine greywackes and conglomerates with underlying Caradocian black shales in the Exploits Subzone are not present in the Notre Dame Subzone. Otherwise, the Cambro-Ordovician arc/back-arc volcanic and epiclastic sequences of each zone record histories that are broadly contemporaneous. Hall *et al.* (1998, p. 1217) concluded that "the Taconic age of accretion of the Dunnage subzones to their respective continental margins is earlier than the ultimate closure of Iapetus that brought the subzones together in the Silurian along the RIL, which in turn occurred before final continental collision".

Post-accretionary geology. Shallow marine and non-marine Silurian sedimentary rocks, conformable in the ESZ but not the NDSZ, are related to the activation or reactivation of large strike-slip faults and the development of pull-apart basins (Szybinski *et al.,* 1990). Coeval epicontinental-type volcanism resulted in the deposition of subaeriel, mainly felsic volcanic rocks in caldera settings (Coyle and Strong, 1987).

The Siluro-Devonian Salinic Orogeny, related to the accretion of the ESZ,

(Dunning *et al.,* 1990) involved crustal thickening, regional greenschist to amphibolite grade metamorphism and crustal melting inducing widespread granitic plutonism (Dean, 1978; Strong, 1980; Colmann-Sadd, 1980; Kean *et al.,* 1981).

The Devonian-Carboniferous Acadian Orogeny (Williams and Hatcher, 1983), related to the accretion of the Avalon terrane, affected the entire Newfoundland Appalachians with transpressional tectonism. Although granitic plutonism was largely confined to the Gander Zone, non-marine sedimentation and much lesser volcanism occurred in several rift-related basins further west .

2.2.1.1 Tectono-Magmatic Development of Arc Sequences in the NDSZ

Drawing from an extensive geochemical, geochronological and isotopic database, and by analogies with modern environments, Swinden *et al.* (1997) provided the most current perspective on the tectonic development (pre-accretionary) of the Notre Dame Subzone; this section summarizes their work. In order to facilitate this model, the NDSZ was separated into five major components. These include the Western Ophiolite Belt, Western Notre Dame Bay, Eastern Ophiolite Belt, Eastern Notre Dame Bay, and the Buchans - Robert's Arm Belt (Figure 2-2).

Swinden and coworkers suggested that a subduction system existed in the Iapetus ocean at least in the Late Cambrian, prior to 506 Ma. These rocks are now preserved in the western and eastern Notre Dame Bay areas and are dominantly represented by tholeiitic arc and non-arc volcanic rocks, with the non-arc volcanic rocks generally occurring near the upper portion of the sequence. This led to the suggestion that this

back-arc system had evolved to a mature stage where there was little influence from a subducting slab. These rocks were accreted to the Laurentian margin very early in the Ordovician, as constrained by the intrusion of series of high-magnesium andesitic dykes (*ca.* 488 - 501 Ma; Szybinski, 1995)

The high-magnesium dykes also record an anomalously high thermal event at the time reflecting rifting and the initiation (or continuation) of a westward-dipping subduction zone under this composite margin. The ensuing development of an ensimatic arc - back-arc basin was recorded by Early Ordovician (490 - 475 Ma) tholeiitic rocks of the western and eastern ophiolite belts as well as tholeiitic rocks in the Buchans - Robert's Arm Belt. This system was outboard from the Laurentian margin as it does not show any petrogenetic influence from continental lithosphere (*i.e.*, it has tholeiitic geochemical signatures and positive ε_{Nd} values); the Skidder basalt is part of this group.

Temporally overlapping (484 - 469 Ma) calc-alkalic bimodal mafic - felsic volcanic rocks, however, have geochemical and isotopic signatures displaying significant influence from continental lithosphere. These volcanic sequences, occurring in the Western Arm, Cottrell's Cove, Cutwell, Buchans, and Robert's Arm Groups, record an arc event built upon the continental crust of the Laurentian margin. Ore-hosting volcanic rocks of the Buchans camp are considered to be part of this group. These volcanic units are generally spatially distinct from the aforementioned tholeiitic suites, nonetheless, there are local examples where these rocks display conformable relationships.

2.2.1.1.1 The Buchans - Robert's Arm Belt

The Buchans - Robert's Arm Belt, with a strike length of approximately 200 kilometers and a width of mostly less than 10 kilometers, encompasses the Buchans Group in the south, the Roberts Arm Group in the north, and the Cottrells Cove and Chanceport Groups further to the northeast (Kean *et al.,* 1981; Swinden *et al.,* 1997). The Cutwell Group in Notre Dame Bay has also been correlated with the belt (O'Brien and Szybinski, 1989). The belt is fault-bounded on both its margins. To the east it is bounded by the Red Indian Line. The western structural contacts include the Lobster Cove and Chanceport Faults in the northwest, the Mansfield Cove Fault south of Halls Bay, and the Hungry Mountain Thrust in the south near Buchans.

Lithological studies of the Buchans and Roberts Arm Groups (Swanson and Brown, 1962; Strong, 1977; Dean, 1978) were the initial grounds for correlation of these groups. U-Pb zircon ages of 473 $^{+3}$/-2 and 473 $^{+}$/-2 for calc-alkaline rhyolites in the Buchans and Roberts Arm Groups (Dunning *et al.,* 1987), respectively, provided evidence for their coeval formation. These ages are supported by fossil ages of latest Arenig-Early Llanvirn conodonts within a carbonate breccia in the Buchans Group (Nowlan and Thurlow, 1986). An older U-Pb zircon age of 484 $^{+}$/-2 was obtained from a calc-alkaline felsic tuff in the Cottrells Cove Group (Dec *et al.,* 1997) and suggests a minimum life span of ~10 Ma for the Buchans - Robert's Arm Belt. Accepting the Cutwell Group as an equivalent of the Buchans -Roberts Arm Belt, Late Arenig - Early Llanvirn conodonts and U-Pb zircon ages of ~469 Ma from the Cutwell Group may extend the lifespan of the arc to at least 15 Ma.

The Buchans - Roberts Arm Belt is dominated by bimodal mafic - felsic volcanic and lesser epiclastic rocks. As previously discussed, Swinden *et al.* (1997) have geochemically identified both tholeiitic and calc-alkaline volcanic rocks throughout the entire extent of the belt. These workers suggest that the tholeiitic rocks are most abundant towards the eastern side of the belt (close to the Red Indian Line) and are also distinct in containing a substantially greater component of epiclastic rocks than do the calc-alkaline sequences. Although there are no radiometric or fossil ages documented in the tholeiitic sequences, Swinden *et al.* (1997) considered them to be coeval with calc-alkaline rocks. The assumption is based on local stratigraphic relationships, such as the observations by Dec and Swinden (1994) of calc-alkaline lava clasts in a 484 Ma epiclastic flow stratigraphically overlying an E-MORB tholeiite.

2.3 Geology of the Buchans Group

In general, the Buchans Group represents a complex fault-bonded and internally thrust imbricated sequence of volcanic rocks (structural geology is discussed in detail section 2.5). The post-thrusting Siluro-Devonian Topsails granite cuts the Buchans Group/Hungry Mountain Complex to the north and Silurian flyschoid sediments unconformably overlie the Buchans Group. Subsequent Devonian-Carboniferous sedimentation with minor volcanism occurred in localized pull-apart basins.

The immediate Buchans area (Figure 2-3) represents the most extensively studied region of volcanic rocks in Newfoundland, though much of the detailed work has been focused in the mine areas. As a result, the Buchans Group geology peripheral

to the mined areas is comparatively poorly documented. Moreover, the geology of the Buchans Group has been largely re-written relatively recently, hinged largely on the identification of a complex structural history. The realization that the stratigraphy was repeated via thrust faulting has had a profound effect on stratigraphic models. The reconstructed stratigraphic column of the Buchans Group (Thurlow and Swanson, 1987) includes four formations: Lundberg Hill, Ski Hill, Buchans River and Sandy Lake Formations, yielding a collective thickness of less than 3 kilometers (Thurlow *et al.*, 1992). The schematic stratigraphy of the Buchans Group is shown in Figure 2-4.

Detailed lithological descriptions of the Buchans Group have been generated by Thurlow (1974, 1981, 1988), Thurlow and Swanson (1981, 1987), Thurlow *et al.*, 1995). Bimodal volcanic rocks of the Buchans Group display rapid lithologic variations and facies changes. Amygdaloidal, pillowed and brecciated mafic volcanic rocks are often plagioclase and, less commonly, augite porphyritic and range in composition from basalt to andesitic basalt. Felsic rocks are often quartz and plagioclase porphyritic with compositional ranges between dacite and rhyolite. A compositional gap commonly exists between mafic and felsic compositions, largely represented by the absence of andesitic rocks. Thurlow (1988, p. 111) described the clastic rocks as "commonly coarsely fragmental and characterized by a bewildering array of fragment types, sizes and transport, and by matrix compositions from pumiceous pyroclastics to volcanic wacke". Epiclastic rocks, including siltstone, wacke and volcanic conglomerate, often form discontinuous lenses within felsic pyroclastic sequences (Thurlow, 1988). Chemical sedimentary rocks are not common in the Buchans camp, unlike the adjacent

Skidder Group where Fe-chert (jasper) is associated with the Skidder massive sulphide prospect (Pickett, 1988) and further north of the Buchans area where cherts are associated with the Connell Option prospect (Thurlow, 1981). Graphitic and carbonaceous sediments are volumetrically less abundant than massive sulphide (Thurlow, 1988). A summary of the lithologies is provided below based on the work of Thurlow and Swanson (1987). In addition, each of the formations are described in more detail below.

Formation	**Maximum Thickness**	**Lithologies**
Sandy Lake Formation	2000 meters ?	Basaltic pillow lava, pillow breccia intertonguing with coarse grained, redeposited clastic rocks of felsic volcanic derivation (arkosic conglomerate, arkose, wacke, siltstone). Local abundant tuff, breccia, polylithic pyroclastic breccia and tuffaceous sedimentary rocks.
Buchans River Formation	400 meters ?	Felsic tuff, rhyolite, rhyolite breccia, pyritic siltstone, wacke, polylithic breccia-conglomerate, granite boulder conglomerate, high-grade in situ and transported sulphide bodies.
Ski Hill Formation	1000 meters ?	Basaltic to andesitic pyroclastic rocks, breccia, pillow lava, massive flows. Minor felsic tuff.
Lundberg Hill Formation	1000 meters ?	Felsic pyroclastic rocks, coarse pyroclastic breccia, rhyolite, tuffaceous wacke, siltstone, lesser basalt, minor chert and magnetic iron-formation.

Table 2-1: Summary of formation lithologies of the Buchans Group (after Thurlow and Swanson, 1987).

2.3.1 Sandy Lake Formation

The Sandy Lake Formation is the uppermost known formation of the Buchans Group. It lies conformably above the Buchans River Formation with an unknown top, and consequently, an unknown thickness. It is comprised dominantly of basaltic pillow

lava, pillow breccia and felsic epiclastic rocks (mostly arkose and arkosic conglomerate).

Thurlow and Swanson (1987) also suggest that the Sandy Lake Formation has a distinctively different origin than that of the Buchans River Formation and, additionally, that the mafic volcanic and felsic epiclastic rocks were probably deposited episodically from different sources and different directions. The Sandy Lake Formation mostly represents caldera infill material (*i.e.*, felsic epiclastic rocks) and has a very widespread distribution in the Buchans Group.

2.3.2 Buchans River Formation

The most economically important of all sequences within the Buchans Group, the Buchans River Formation hosts all major VMS deposits and has been mapped in great detail in the immediate mine area. Thurlow and Swanson (1987, p. 39) describe a 200 to 400 meter thick stratigraphic section as consisting of "quartz-poor pumiceous pyroclastic rocks, rhyolite and pyritic siltstone, overlain by quartz-rich rhyolite and crystal-vitric tuff and the transported ore breccias. A thick sequence of felsic tuff with local quartz and feldspar phyric rhyolite forms the upper part of the formation".

The composition of these rocks is generally dacitic to rhyodacitic, with magmatic affinities from transitional (or mildly calc-alkaline) to calc-alkaline, respectively. The geochemistry of these rocks is discussed in more detail in chapters 5 and 6.

2.3.3 Ski Hill Formation

The Ski Hill Formation is regarded as the foot-wall to the Buchans orebodies, hosting much of the epigenetic stockwork mineralization, especially in the Lucky Strike area. Thurlow and Swanson (1987) describe it as a thick pile (up to 1 km) of black to dark green breccia, pyroclastic rocks and pillow lava that conformably overlies pyroclastic and tuffaceous rocks of the Lundberg Hill Formation. The composition of the formation is generally basaltic-andesite. The texture of both flows and fragments is variably amygdular with plagioclase, and lesser augite, phenocrysts.

The Ski Hill Formation mafic volcanic rocks form several types of fragmental units including various autoclastic and hyaloclastic breccias (*cf.* McPhie *et al.,* 1993). Autoclastic breccias are best displayed at the type locality (Ski Hill). The fragments range in size from less than 1 cm, to more than 10 cm, but most are fist size and blocky, monolithic, variably porphyritic and amygdaloidal, and range in colour from dark green grey to green to faintly purplish. These clasts do not show quenched or chilled margins. Most clasts show a well developed trachytic texture, defined by feldspar microlites, and elongate amygdules suggestive of laminar flow and shear. The matrix to these clasts is a mixture of smaller clasts and infilling lava. These rocks form through mechanical brecciation, probably caused by temperature-controlled viscosity contrasts, *i.e.*, as a result of a relatively fast flowing lava that cooled and fractured at the outer margins of the flow due to an increase in viscosity.

Also common in the Ski Hill Formation mafic volcanic rocks are hyaloclastic breccias, notably in the panels of altered foot-wall below Lucky Strike. Locally, *in-situ*

hyaloclastite, evidenced from 'jig-saw fit' textures, is found adjacent to lava flow lobes. These lobes form 'fingers' or apophyses which are directly related to the hyaloclastite. Essentially, the flows are the source of the hyaloclastite, quenching and fragmenting at the margins, but continuing to inject into the pile of fragments. As with the Ski Hill autoclastic breccias, shear during laminar flow is also indicated in these rocks by elongate, flow foliated amygdules as well as banded perlitic fractures in the intact flows. The lobe flow hyaloclastite facies represents the surface areas of a flow, ideally outwards from the autoclastic breccias. Locally, both volcanic facies are observed together. Pillow textures are less common in these rocks, presumably owing to the lower viscosities, but do occur locally.

Elongate quartz-filled amygdules are characteristic of the Ski Hill Formation in addition to the calcite - chlorite - prehnite-pumpellyite filled amygdules typical throughout the Buchans Group (Thurlow and Swanson, 1987). Quartz-filling of amygdules and voids may be the result of a fairly extensive, low temperature silica precipitation process related to the formation of the Buchans orebodies. Hematite - chlorite - calcite - epidote alteration of mafic volcanic rocks, which appear to represent a diagenetic assemblage that is common in most mafic volcanic units in the belt, is not typical in the Ski Hill Formation, especially in the immediate vicinity of the ore bodies. Hematite is generally only abundant near the stratigraphic top of this unit (Thurlow and Swanson, 1987).

The respective recognition of, and relationships between, the Ski Hill and Buchans River formations in the vicinity of the Lucky Strike deposit is complicated by

intense alteration and faulting. These rocks comprise the former "Intermediate Foot-wall" (Thurlow and Swanson, 1981). Thurlow and Swanson (1987, p.39) acknowledge that this is a poorly understood stratigraphic package where "altered rocks of recognizable mafic composition are overlain by quartz-poor felsic lithologies. The former are assigned to the Ski Hill Formation and the latter to the Buchans River Formation".

2.4.4 Lundberg Hill Formation

The Lundberg Hill Formation represents the lowermost known unit within the Buchans Group and has a unknown base. A wide variety of felsic and mafic volcanic and epiclastic lithologies throughout the Buchans area are assigned to this formation, however, correlation of these units is difficult. Thurlow and Swanson (1987) described the rhyolitic pyroclastic rocks of this formation, at the base of the Oriental panel, as having 5-10 mm quartz phenocrysts (often termed 'prominent quartz') and smaller zoned plagioclase crystals. These rocks are described in other areas as interbedded with upward graded sequences of polylithic breccia through pumiceous pyroclastic rocks into tuffaceous wacke, siltstone and cherty mudstone. Locally, important rhyolite bodies with large or small quartz phenocrysts, bedded tuffaceous sedimentary rocks with multi-coloured mudstone-chert and basaltic pillow lava also occur (Thurlow and Swanson, 1987).

2.4 Geology of the Skidder Basalt

The Skidder Basalt unit occurs about 10 km south of Buchans and covers an area

of approximately 20 km^2. Pickett (1987, 1988a, 1988b) described the area as being comprised of basaltic pillow lava, pillow breccia, and massive flows with lesser diabase dykes, gabbro, mafic pyroclastics and chert. The Skidder Basalt has been locally intruded by trondhjemite pods and dykes. Presumably because of their textural similarites, Pickett (1988a) compared the Skidder Basalt to the Buchans Group (Sandy Lake Formation) basalt and suggested that the former differs in being spilitized, contains fewer and smaller amygdules, and is locally variolitic when compared to the Buchans Group rocks. The Skidder Basalt also represents an aeromagnetic susceptibility high when compared to the Buchans Group (G.S.C. map c40 097G, 1987).

The mafic volcanic rocks of the Skidder area were originally considered to be component of the former Foot-wall Basalt (now Sandy Lake Formation basalt considered to be the structural, but not stratigraphic, foot-wall) of the Buchans Group (Thurlow and Swanson, 1981). Pickett and Barbour (1984) suggested that these rocks represent a distinctly different suite of rocks from the Buchans Group and proposed the name Skidder Basalt. Geochemical data (Pickett, 1988) showed that these basalts have affinities between mid-ocean ridge basalt (MORB) and island arc tholeiites (IAT). Swinden *et al.* (1997) grouped the Skidder Basalt with the ophiolitic Annieopsquotch, Star Lake and King George IV Complexes in the south, and the Hall Hill Complex to the north near Halls Bay, collectively defining them as part of the eastern ophiolite belt. U-Pb ages of 478 $^{+3}/_{-2}$ and 481 $^{+4}/_{-2}$ Ma were obtained from the Annieopsquotch Complex (Dunning and Krough, 1985). Hence, Swinden *et al.* (1997) suggested that this belt of rocks was part of a 490 - 475 Ma back-arc basin outboard of the Laurentian

margin.

As suggested earlier in this chapter, this back arc basin was coeval with, or at least temporally overlapped, the Buchans - Roberts Arm Belt. As there is relatively little evidence for spatial relationships between the tholeiitic and calc-alkaline sequences in the belt, it is unclear how the Skidder Basalt relates to the Buchans Group.

2.5 Structural Geology of the Buchans Area

The Buchans Group, as part of a south-southeast directed imbricated thrust system, internally manifests itself as a series of duplex and antiformal stack geometries over a broad range of scales (Calon and Green, 1987; McClay, 1987; Thurlow and Swanson, 1987). Consequently, the Buchans Group is fault bounded along all margins (Thurlow *et al.,* 1992). The base of the group is in structural contact with the Victoria Lake and Harbour Round Groups along the Victoria River Delta Fault (Figure 2-5). The Hungry Mountain Complex, a deformed Cambro-Ordovician granitic suite, has been thrust above the Buchans group via the Hungry Mountain Thrust. The Skidder Basalt is also fault bounded at both its upper and lower contacts. It is in contact with the Buchans Group above and to the north and the northwest, possibly due to the continuation of the Tilleys Pond thrust fault (Thurlow and Swanson, 1987; Pickett, 1988). The Skidder Basalt has been thrust above the Harbour Round Formation via the Victoria River Delta Fault (Thurlow *et al.,* 1992). These workers concluded that the Powerline Fault is the floor thrust to a large duplex structure with the Airport Thrust in the roof. All of the known Buchans orebodies are found within this large duplex structure.

The orebodies were contained within two adjacent duplexes (Figure 2-6), namely the Sandy Lake and Lucky Strike Duplexes, separated by the Ski Hill - Buchans River Fault (Calon and Green, 1987). The Sandy Lake and Lucky Strike Duplexes are also often referred to as the Oriental and Lucky Strike panels, respectively. The orebodies themselves display antiformal stacking which structurally thickens the massive sulphide lenses (Calon and Green, 1987).

2.6 A Review of VMS-Style Mineralization in the Buchans-Roberts Arm Belt (BRAB) and Equivalent Groups

2.6.1 Introduction

A number of deposits, including seventeen past producers (mostly in the Buchans camp), and dozens of showings and developed prospects occur in the Buchans - Roberts Arm Belt, Cutwell Group and Skidder Basalt (although the relationship of Skidder Basalt to the other groups is uncertain). The locations of most these deposits and prospects are shown on Figure 2-7 (note that the Skidder Prospect plots just off of the map area south of Buchans). The characteristics of these deposits, however, such as metal ratios and morphology, are largely varied. Despite this, VMS deposits in these terranes have loosely been designated Kuroko-style, hosted in thick volcanic/epiclastic sequences with locally associated felsic volcanism. The Skidder prospect (in the Skidder Basalt), hosted in mafic volcanic rocks with ophiolitic affinities and interpreted as having formed in an oceanic or back-arc spreading center, is considered distinctive (Swinden, 1991). The Skidder prospect was compared with Cyprus-type VMS deposits (Galley and Koski, 1999).

However, an evaluation of the available information on VMS deposits in the

BRAB, such as morphology, host rock compositions, metal content, alteration, and so forth, suggests that there are two broad styles of mineralization in this region. Group One is characterized by:

- mafic volcanic hosted (felsic volcanic rocks may be more significant in foot-wall or hanging-wall).
- well-developed stockwork or stringer style mineralization +/- stratiform massive sulphides
- pyritic, Cu + Zn dominant +/- gold.
- dominantly chloritic alteration +/- silicification, lesser sericitization.
- and commonly, chemical sediments (*i.e.*, Fe-oxide-chert exhalative horizon)

This group includes the Gullbridge - Lake Bond deposits and prospects. The Skidder prospect and Skidder Alteration Zone prospect may also be inlcuded in this group. The Little Sandy prospect may belong to this group as well. This style of mineralization loosely resembles Cu-Zn-type VMS deposits (Franklin *et al.,* 1981; Franklin, 1993) and may be similar to VMS deposits in modern spreading centers.

Group Two differs from group one in the following manner:

- a more obvious association with felsic volcanism (rhyolite-dacite flows or domes and pyroclastic rocks)
- often both stratiform sulphides and an underlying stockwork zone are present
- more diverse metal content: Zn-Pb-Cu-Au-Ag, and very often Ba
- quartz-chlorite-sericite +/-K-feldspar +/-carbonate alteration
- lack of a laterally extensive exhalative component (*i.e.*, Fe-chert).

This group comprises the Buchans deposits, Pilleys Island deposits and

prospects, and the Oil Islands and Shamrock prospects. The Connell Option and Mary March prospects, may also be included in this group. The group more closely represents the Zn-Pb-Cu deposit (Franklin, 1993) and are more Kuroko-like.

A review of the geology of the Notre Dame subzone was provided in section 2.2.1.1. It was shown that there exists a variance in magmatic affinity/tectonic setting of the volcanic sequences within the BRAB (*i.e.* tholeiitic to calc-alkalic signatures corresponding to back-arc and island arc settings, respectively). The Group Two deposits are associated with the calc-alkalic sequences. Group One deposits (specifically the Lake Bond-Gullbridge area) are not well defined in terms of host rock petrochemistry and isotopic signatures. By analogy with the Skidder Basalt, it may be reasoned that the Group One deposits are hosted in tholeiitic, back-arc settings. Therefore, there may be a tectono-magmatic control on the style of these deposits within the belt. However, the factors controlling the characteristics of the different deposits are numerous and other factors, such as water depth, or a combination thereof may be more important.

2.6.2 The Buchans Polymetallic Volcanogenic Massive Sulphide Deposits

The Buchans orebodies consisted of five major and numerous smaller deposits that accounted for 16.2 million tons of ore that graded 14.51% Zn, 7.56% Pb, 1.33% Cu, 126 g/t Ag and 1.37 g/t Au (Kirkham, 1987). The total ore mined represented almost equal amounts of *in-situ* and mechanically transported, fragmental ore, which occurred up to two kilometers from their inferred source. Grades of the transported ores were only slightly less than *in-situ* deposits. A few smaller transported ore bodies with

lower, subeconomic grades occur at greater distances (*e.g.*, Clementine). The Lucky Strike Main (4.3 Mt at 18.36% Zn, 8.42% Pb and 1.67% Cu) and Oriental No.1 (2.5 Mt at 15.80% Zn, 8.47% Pb, 1.71% Cu) orebodies were the largest of the *in-situ* deposits (Hutchinson, 1981). All of the ore mined at Buchans would fit into a rectangular geographical area of roughly 1.5 by 4 km (refer to Figure 2-3).

The Buchans orebodies are all located at or near the base of the Buchans River Formation close to the contact with the underlying Ski Hill Formation (Thurlow and Swanson, 1981). All Buchans deposits are interpreted to have been contemporaneous, however, several pulses of hydrothermal activity and venting occurred, with the focus of discharge periodically shifting (Thurlow and Swanson, 1981; Jambor, 1987). This is indicated in the Lucky Strike area by isolated zones of stockwork mineralization, such as the Engine House orebody (Thurlow and Swanson, 1981) and the deposition of siltstone marking a period of quiescence between Engine House/North orebodies and the Lucky Strike/Two-level orebodies (Jambor, 1987).

The orebodies at Buchans occur in two paleotopographic depressions that extend northwest from the Lucky Strike orebodies and northeast from the Oriental deposits (Thurlow and Swanson, 1981). These depressions were later interpreted to be the expression of a submarine caldera, which underwent resurgence triggering debris-flows of lithic material and sulphide-barite ore (Kirkham and Thurlow, 1987). Transported orebodies, including MacLean, MacLean Extension, Rothermere, Two-level, and North orebody, were considered to have been derived from the *in-situ* Lucky Strike deposit. The transported Oriental No.Two and Old Buchans orebodies are interpreted to have been derived from the *in-situ* Oriental No.One deposit (Thurlow and Swanson, 1987).

Other, more distal prospects of mechanically transported sulphides, such as the Clementine prospect, 4 km northwest of Lucky Strike, are of less certain origin (probably derived from Lucky Strike). Therefore, the hydrothermal alteration zones at Lucky Strike and Oriental No.1 represent a greater amount of discharged sulphide than is represented in the overlying *in-situ* deposits.

The *in-situ* Lucky Strike Main deposit represents the largest and highest grade single massive sulphide body in the Buchans Camp. The orebody is described as a thick lense (up to 50 m) that is underlain by a thin bed of dacitic tuff (BRF) or the SHF andesite-basalt (Thurlow and Swanson, 1981). Compositional zoning within the deposit was noted by George (1937) who estimated that 90% of the ore was Pb-Zn rich (*black ore - Kuroko*) and the remainder formed an underlying zone of Cu-Zn rich ore (*yellow ore - oko*).

Ore Mineralogy. The mineralogy of the ores was fairly complex and generally fine-grained, consisting dominantly of sphalerite, galena, barite, chalcopyrite, and pyrite (less than 10 %), quartz and calcite, as well as very minor tetrahedrite, bornite, argentite, ruby silver, and native silver (Thurlow and Swanson, 1981).

Alteration. VMS-associated hydrothermal alteration mineralogy and geochemistry studies have not been a topic of major concern for researchers in the Buchans camp, with the exception of a few significant studies. Henley and Thornley (1981) provided detailed alteration mineralogical assemblages with some partial mineral analyses. Kowalik *et al.* (1981) described the mineralogy of the Lucky Strike stockwork zone and suggested paragenetic relationships.

Thurlow and Swanson (1981) described the stockwork zone at Lucky Strike as a

"stratigraphically controlled blanket" that has a width of 360 meters at bedrock and wedges out 600 meters down dip and attains a maximum thickness of 100 meters, although this zone has undergone structural modification. The alteration is dominated by patchy to pervasive, and vein/veinlet chloritization and silicification. Swinden and Thurlow (1981) described a sulphide assemblage dominated by fine to euhedral pyrite with much less chalcopyrite, sphalerite, galena, and barite. Outside of the stockwork zone the alteration is dominated by a clay mineral - pyrite assemblage (Thurlow and Swanson, 1981). Alteration is described in significantly more detail in section 3.2.4.

2.6.3 Other Deposits/Significant Prospects

The **Connel Option prospect** (Thurlow, 1981; Barrie, 1991), located 19 km east of Buchans and 1.6 km north of the Buchans Highway, was drill tested in the 1930's and 1940's by six diamond drill holes. A 60 cm interval at 30 m depth assayed 25.4% Zn, 11.9% Pb, 0.3% Cu, 156 g/t Ag and 3.43 g/t Au. The prospect is a thin blanket up to 60 cm thick and 200 m long of high grade massive sulphides consisting mostly of sphalerite, galena, chalcopyrite, and pyrite. Banded sulphide textures and colloform pyrite were noted by Thurlow (1981). The sulphides are non-baritic with pyrite and silica comprising the main gangue minerals. The prospect is hosted in a more than 100 m thick sequence of chert, siltstone, and fine-grained dacitic crystal-vitric tuff, with the immediate foot-wall and hanging-wall rocks being grey-green chert. There is no stockwork-style alteration zone known to be associated with the Connel Option, rather, minor disseminated and ~1 mm beds (?) of Zn-Pb-Cu-sulphide and pyrite mineralization occur in chert and tuff in the foot-wall, and one hole intersected a 30 cm

interval of strongly sericitized vitric dacite. At ~ 30 meters into the foot-wall, Thurlow described a contorted, 30 cm thick, Mn-rich bed within jasper. Thurlow also suggested that the host rocks and sulphide mineralization were deposited distal from a volcanic edifice. The host rocks were interpreted by Thurlow to be the former Foot-wall Arkose (now Sandy Lake Formation) of the Buchans Group, implying an undiscovered basemetal-rich, paleo-hydrothermal venting system. Barrie suggested that the host rocks were Buchans River Formation.

The **Little Sandy prospect** (Barrie, 1991) is located 13 km east of Buchans and 1.2 km north of the Buchans Highway. Defined by 18 drill holes, the prospect has a geological resource of 180,000 tons grading 1.91% Cu, 8.2 g/t Ag and 2.3 g/t Au. The mineralization is described as veinlet quartz-pyrite-chalcopyrite in chloritized, silicified mafic volcanics within a stratiform zone. Barrie suggested an epigenetic origin related to fault movement. My interpretation, however, is that the zone is typical of stringer style mineralization in foot-wall rocks associated with VMS deposits. Rhyolite and rhyolite breccia are spatially associated with the mafic rocks, but are not mineralized. The notable lack of zinc and lead suggests a unique metal assemblage for Buchans Group volcanic rocks. The host formation is uncertain.

The **Mary March prospect** (Barrie, 1991) is located 32 km east of Buchans, along the Buchans Highway, in the vicinity of the Mary March Provincial Park. The prospect is a quartz-sericite-altered zone, locally with vein and disseminated pyrite and barite, but generally low base metal content. However, several high grade sulphide and barite boulders have been discovered in the vicinity of the alteration zone. The host rocks are described as felsic to intermediate and mafic breccias and tuffs. Although the

prospect is within the Buchans Group, a host formation name has not been assigned to this prospect. At the time of writing, drilling by Phelps-Dodge is reported to have encountered significant base metal mineralization at this prospect (The Northern Miner, 1999).

The **Skidder Prospect** (Pickett and Barbour, 1984; Pickett, 1987, 1988a, 1988b), located 12 km southwest of Buchans, is an ophiolite-type pyritic massive sulphide deposit (two lenses) with a geological resource of 0.9 Mt grading 2.09% Zn, 2.05% Cu, 0.17% Pb, 8.8 g/t Ag and tr. Au. The prospect is hosted by basaltic pillow lava, pillow breccia and hyaloclastite of the Skidder Basalt. Abundant jasper is associated with the massive sulphides, included brecciated, quartz-veined, unlayered and lesser bedded jasper and jasper-rich siltstone. Pickett noted the occurrence of trondhjemite dykes in the vicinity of the Skidder deposit. Sulphide assemblages consist mostly of pyrite, with lesser chalcopyrite and low-Fe sphalerite, with very minor galena. Hematite and magnetite are also present. Other gangue minerals include quartz, chlorite and calcite. A chlorite +/- talc-rich stringer zone with disseminated pyrite (mostly) underlies the massive sulphides. More peripheral alteration, up to 150 m from the sulphide-bearing zones, include chlorite, quartz, and lesser phengitic sericite. Chlorites from the Skidder Prospect alteration zone are more Mg-rich than chlorites typical of the spilitized Skidder Basalt. Calcite and epidote, common in the spilitized basalt, are generally not present in the alteration zone.

The **Gullbridge Deposit** and **Southwest Shaft Prospect** (Swinden, 1988, and references therein) are located less than 70 km northeast of Buchans and generally in the central area of the BRAB. Production at the Gullbridge Mine, from 1967-1972, totaled

approximately 3 Mt of 1.1% Cu, although traces of Zn, Pb and Ag were reported. The main sulphides are pyrite, pyrrhotite and chalcopyrite. The Southwest Shaft Prospect, located 2.5 south of Gullbridge, is considered to lie along the same horizon as both are encompassed by a 4 km long alteration zone. Mineralization is described as disseminated, ribboned or lensoid in a silicate gangue with few features to indicate an exhalative processes. And, although the ore lenses are conformable on a broad scale with the surrounding stratigraphy, mineralization is locally discordant. These features are consistent with a zone of stringer-style mineralization. Alteration mineralogy includes a chlorite-cordierite-anthophyllite assemblage thought to represent contact-metamorphosed chloritized basalts (chlorite now is considered to be retrograde). South of the Southwest Shaft, quartz-sericite-pyrite altered rhyolite is observed. The 'Gullbridge iron formation', up to 20 m thick and traced 2.3 km from Gullbridge to the Southwest Shaft, is a hematitic-chert unit interbedded with fine-grained felsic tuff that may be considered as an exhalative component of the hydrothermal system.

The **Lake Bond deposit** (Swinden, 1988, and references therein), located approximately 55 km northeast of Buchans and 20 km south of Gullbridge, has reserves of 1.1 Mt at 2.12% Zn and 0.3% Cu. Lake Bond, considered a stratigraphic equivalent of Gullbridge deposit, is hosted in mafic volcanic rocks and also resembles a stockwork zone that lacks an exhalative component. An area of about 2 km^2 south of Lake Bond is characterized by irregular patched and veinlets of epidote. These rocks are also pervasively choritized and locally contain veinlets of black chlorite with minor pyrite and occasionally chalcopyrite. Epidotization is an uncommon alteration style for VMS deposits in the BRAB, and in general for VMS deposits. The proximity of the deposit

to a large post-mineralization granitic intrusion lends suspicion to other possibilities for the alteration style.

A cluster of massive sulphide deposits occur at **Pilley's Island** at the northern end of the BRAB, about 100 km northeast of Buchans. These include the Old Pilley's Island Mine and Bull Road Showings (Tuach, 1988, and references therein) and the more recently discovered Spencers Dock, Janes Cove and Rowsell's Cove deposits (Thurlow, 1996). The Old Pilley's Island Mine produced ~0.5 Mt of cupriferous pyritic ore from 1891-1908, with reserves estimated at 1.159 Mt at 1.23% Cu. This deposit consists dominantly of massive pyrite, with lesser chalcopyrite and minor sphalerite and barite in altered breccias in the upper parts of the deposit. Galena was observed in waste piles in massive pyritic samples at the adit entrance. The Bull Road showings are high grade Zn-Pb rich massive sulphide boulders, some more than 1 m in diameter, hosted within polymictic breccias. The Spencer's Dock deposit, comparable to the Old Pilley's Island Mine deposit, is a pyritic massive sulphide body with very low base and precious metal content. The Jane's Cove Deposit is also similar, but also consists of a breccia sulphide facies, with the potential to be a very large tonnage deposit. A siliceous, weakly hematitic horizon is also locally associated with the Janes Cove deposit. The Rowsell's Cove deposit is composed entirely of pyritic breccia and contains low grade Cu. Although Pilley's Island represents a bimodal volcanic environment, mineralization at Pilley's Island is closely associated with felsic volcanic rocks, specifically the extrusion of dacite domes, flows, hyaloclastic breccias and lithic breccias. Alteration includes sericitic, chloritic, silicic, pyritic, Fe-carbonate and K-feldspar alteration (Appleyard and Bowles, 1978; Santaguida *et al.,* 1992; Thurlow,

1996). Sericitization is the most widespread, mostly affecting felsic volcanic rocks. Chloritization affects mafic rocks below the Old Pilley's Island Mine and the Rowsell's Cove deposit. Santaguida *et al.* (1992) identified chlorites in the mineralized zone as being relatively Fe-rich. Thurlow also described a transition from base metal-bearing chlorite-pyrite alteration in a gabbro below the Rowsell's Cove deposit which gives way to epidote-pyrite alteration. K-feldspar alteration, affecting felsic volcanics, is interpreted to be a peripheral foot-wall alteration facies (Thurlow, 1996). Much of the pyritic massive sulphide mineralization appears to be subhalitive, or replacement style, within the hyaloclastic breccias and perlitically fractured lavas.

Significant thrust faulting occurs at Pilley's Island which, similar to Buchans, produces repetitions in stratigraphy and places older stratigraphic units above younger ones (Thurlow, 1996). Also, several of the deposits/prospects were shown to occur in different structural panels.

Several interesting prospects occur in the Cutwell Group in Notre Dame Bay. The **Oil Islands prospect** (Kean, 1973; McHale and McHale, 1984; Thurlow, 1995) is a pyritic and baritic Zn-Pb prospect located roughly 120 km northeast of Buchans on a small island east of Long Island in Hall's Bay. The mineralization includes disseminated, stringer, massive and clastic sulphides associated with sericite-quartz, and locally chlorite, alteration. Dalmatianite (presumed to be cordierite-anthophyllite) is described from hornfelsed rocks in the vicinity of the prospect (hornfelsing is presumed to be due to the Long Island Pluton). The main showings are located in felsic volcanic and pyroclastic rocks, although mineralization in mafic rocks does occur locally. The **Shamrock prospect** (Winter, 1999), located 3 km to the southeast on Long Island, is an

epigenetic-style zone of pyrite-sphalerite-galena-chalcopyrite mineralization within altered mafic volcanic and intrusive rocks that are variably hornfelsed. The mineralization is manifested as disseminated and stringer sulphides associated with epidote - K-feldspar - quartz - sericite +/- chlorite alteration within a zone at least 300 m in strike length. Consequently, the zone resembles stockwork-style mineralization. As with many other VMS prospects in the BRAB, structural complexities may have displaced associated massive sulphide lenses.

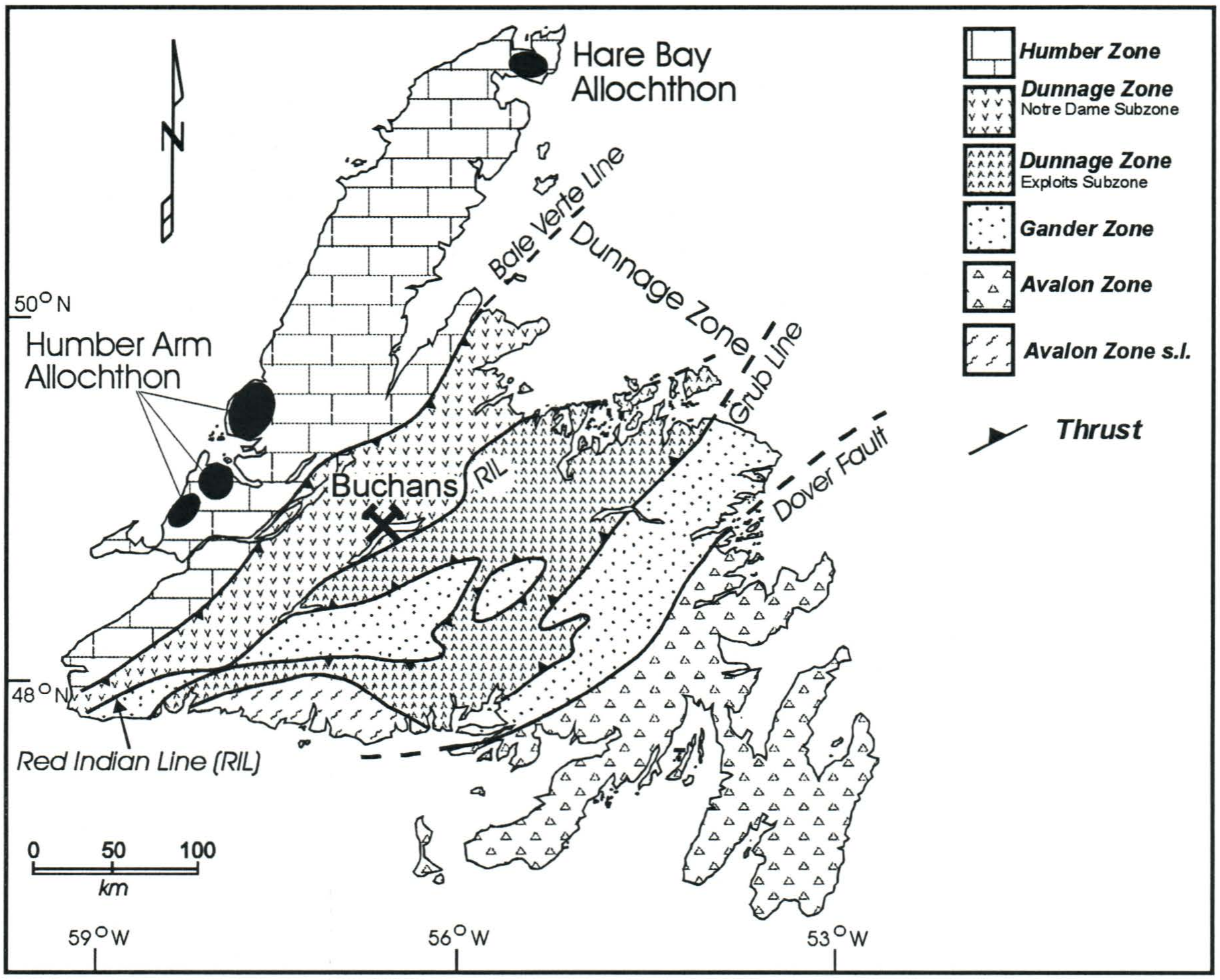


Figure 2-1 - Tectonostratigraphic subdivisions of Newfoundland (after Williams *et al.*, 1988).

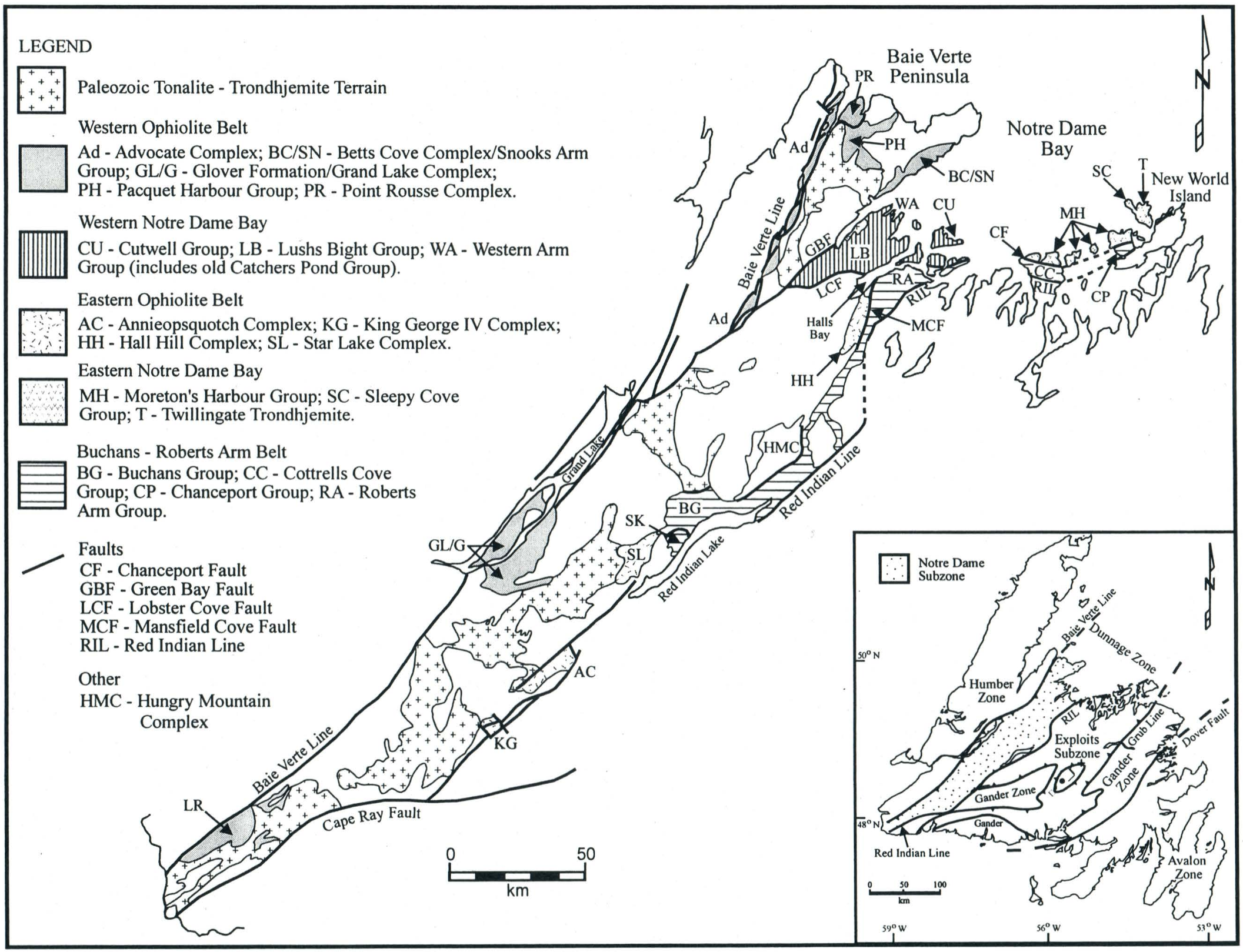


Figure 2-2 - Geological map of the NDSZ with separate lithostratigraphic units and major structures illustrated (from Swinden *et al.*, 1997).

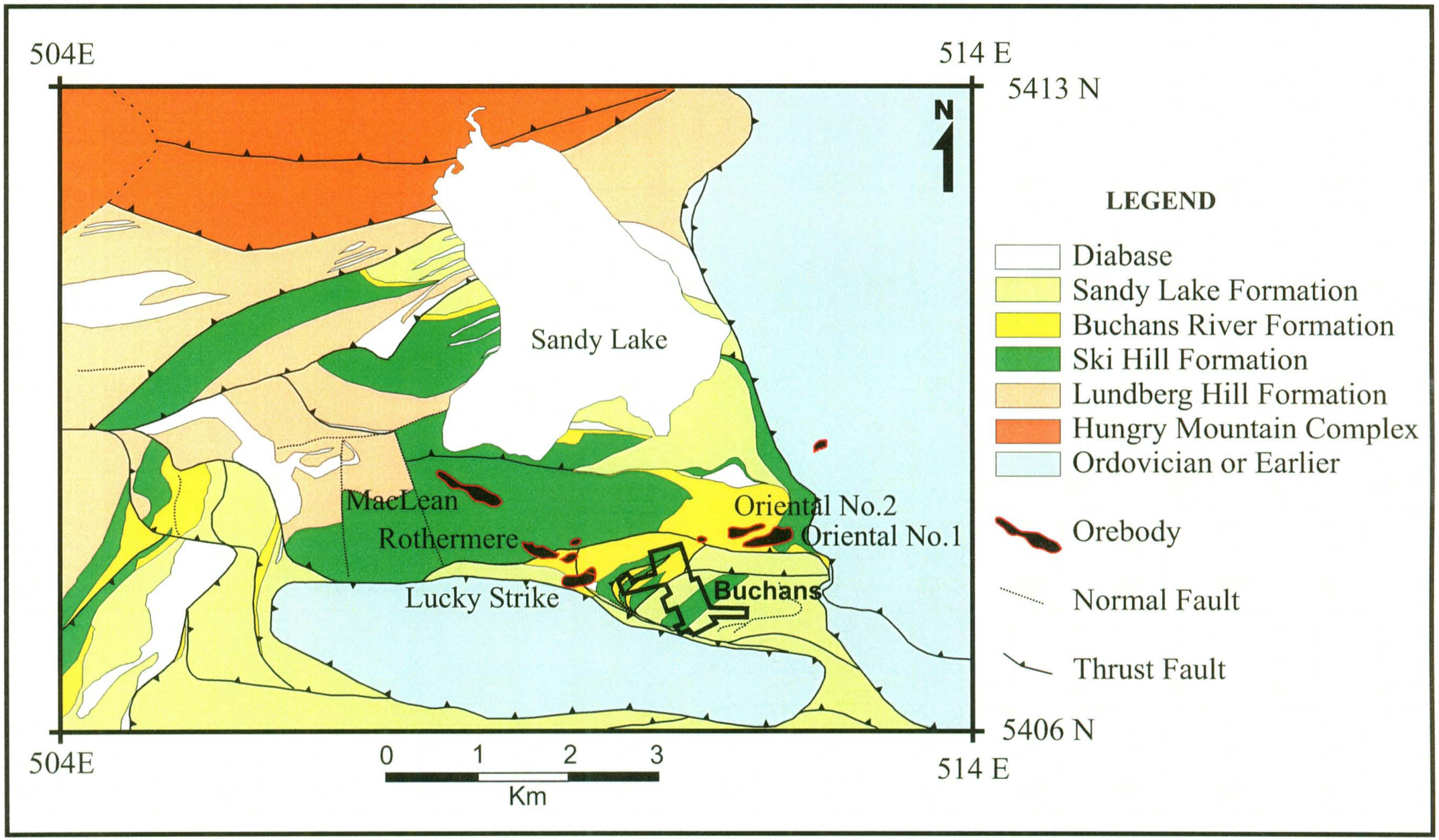


Figure 2-3 - Local geological map of the Buchans camp showing the main formations and orebodies (after Spencer et al., 1993)

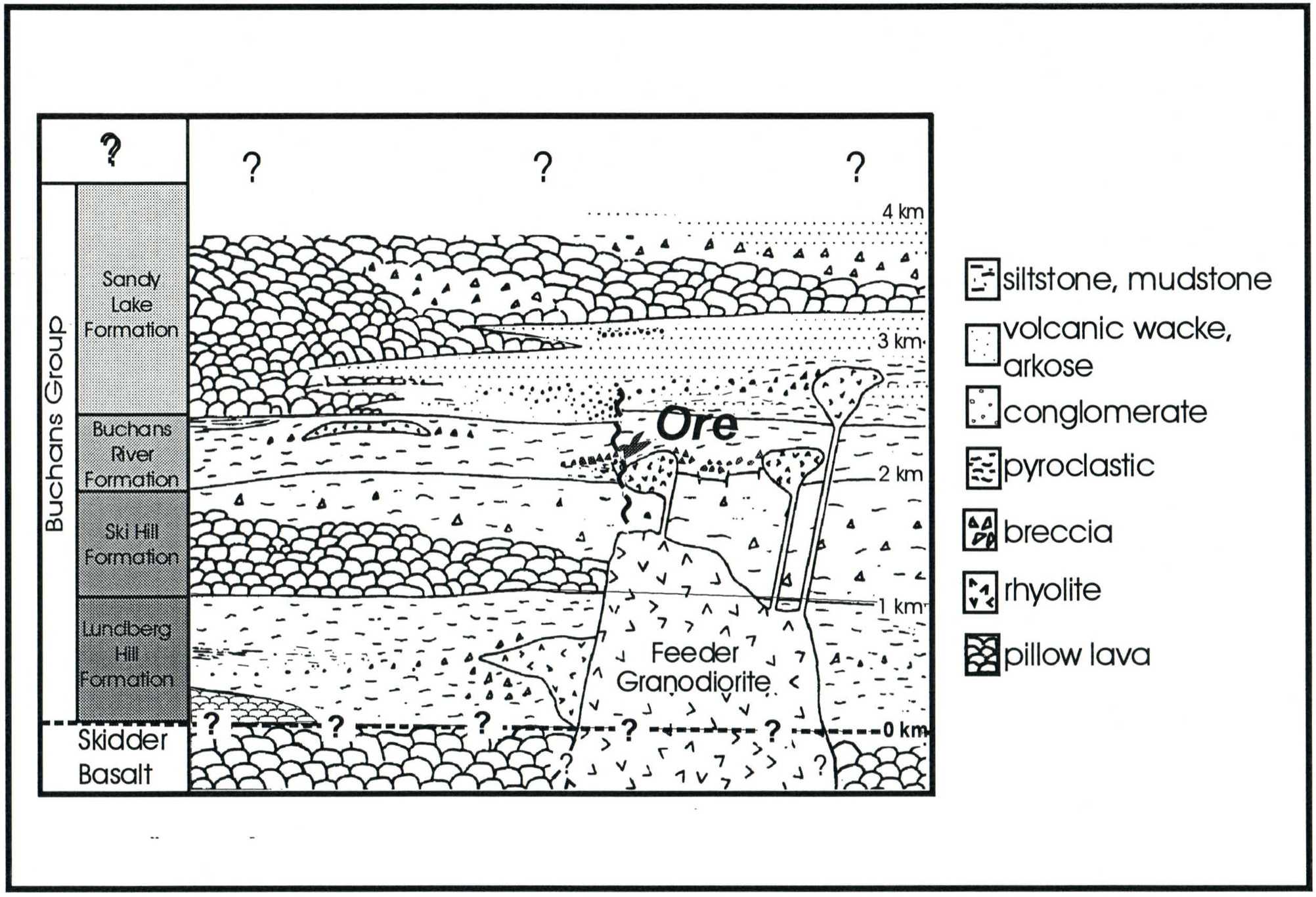


Figure 2-4 - Schematic stratigraphy of the Buchans Group (after Thurlow and Swanson, 1987).

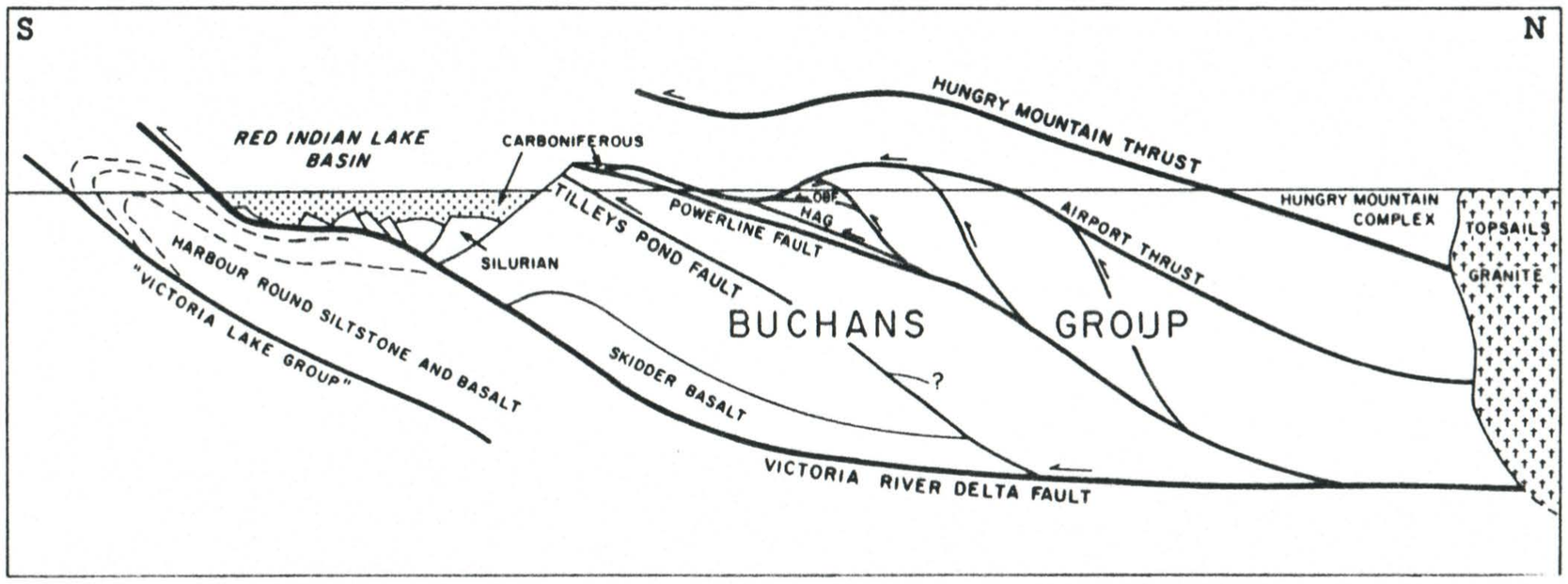


Figure 2-5 - Schematic geological cross section through the Buchans region from Thurlow et al. (1992).

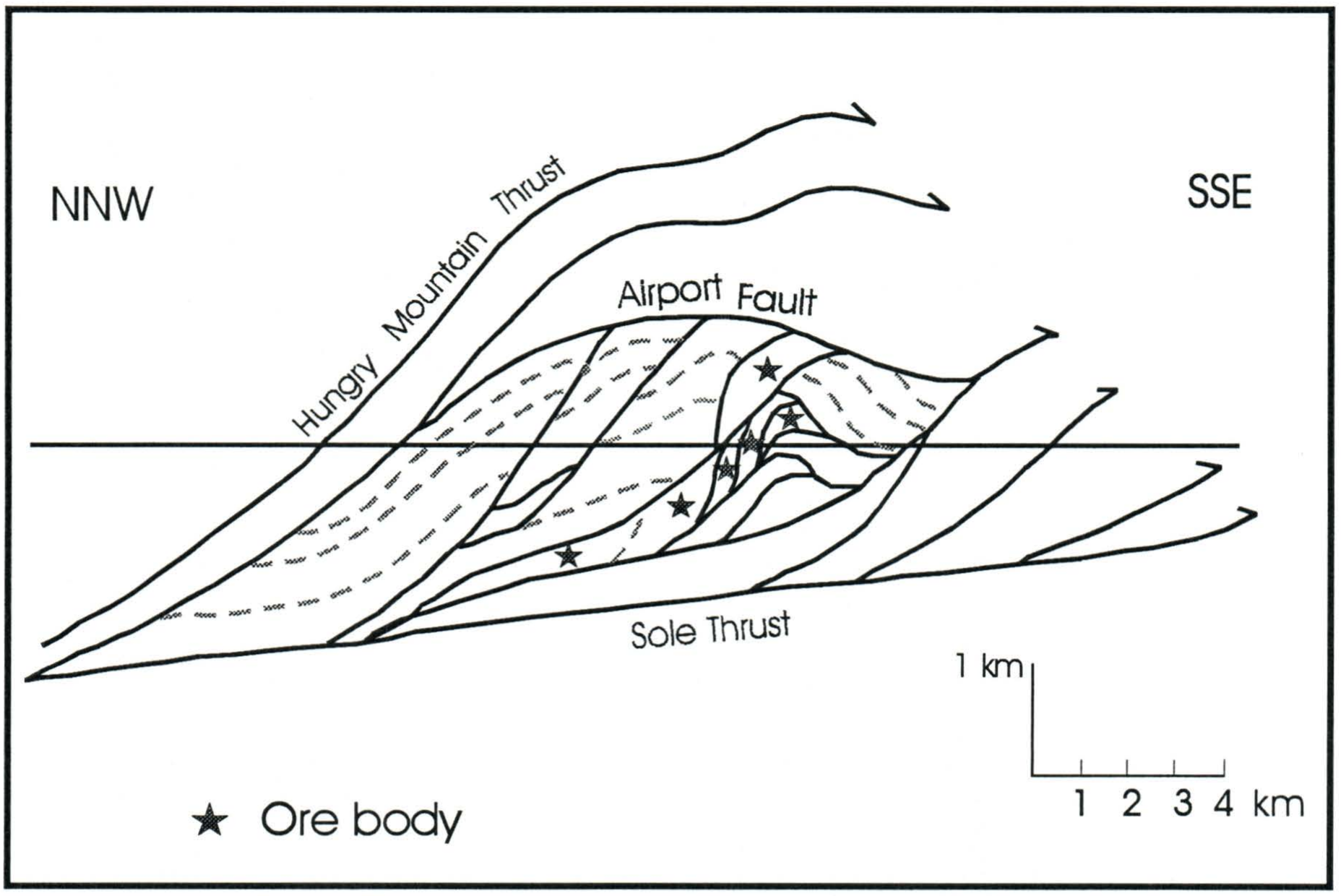


Figure 2-6 - Schematic cross section through the Buchans thrust stack (after Calon and Green, 1987).

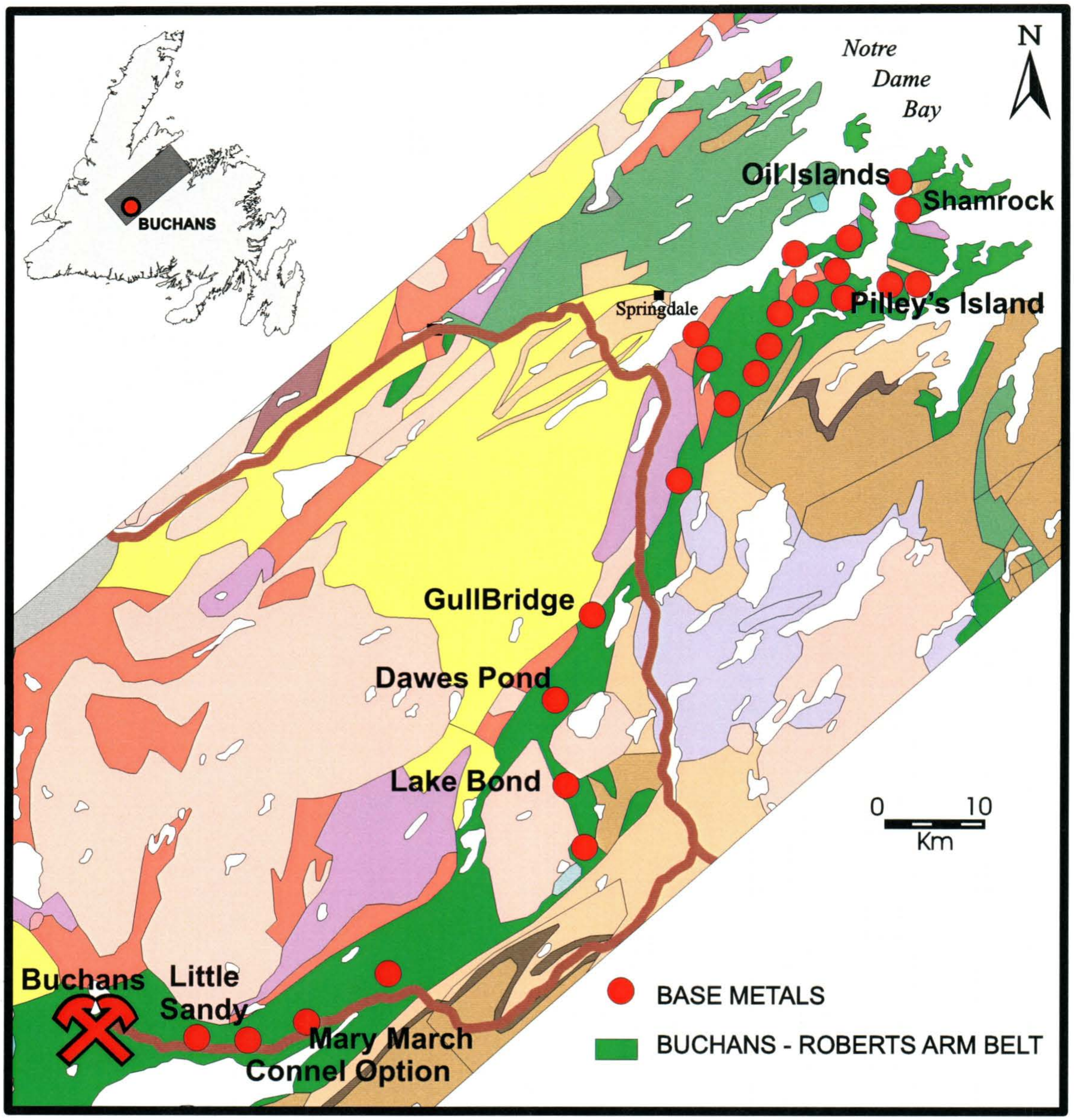


Figure 2-7 - The location of significant basemetal deposits and prospects in the Buchans - Roberts Arm Belt. 1:1,000,000 scale geology after Colman-Sadd et al. (1990).

Chapter Three - Alteration Zones

3.1 Introduction

Alteration in this thesis is defined as a change in the primary mineral assemblage through chemical (and physical) means, which are the direct result of the interaction of the rocks with hot fluids. The alteration is implied to be a function of volcanogenic processes and is considered broadly contemporaneous with the eruption of the host volcanic rocks. Zones are defined by particular secondary, or alteration, mineral assemblages and are described in both the surface and sub-surface as defined by outcrop and diamond drilling information as well as other means (*e.g.*, geophysics). In many instances, alteration zones are subdivided where internal zonation can be illustrated.

Five alteration zones were studied in the Buchans area. The Lucky Strike Zone and Middle Branch zones are the only zones studied which are known to be associated with massive sulphide mineralization. Three other zones, the Powerhouse, Woodmans Brook and Airport Alteration Zones, are 'grass-roots level' exploration targets and are being actively explored. These latter zones have much less outcrop exposure or drilling and represent new exploration targets in this part of the BRAB. The location and outline of these zones is shown on the map in Figure 3-1.

3.2 Lucky Strike Alteration Zone

3.2.1 Location

Albeit structurally modified, the Lucky Strike Alteration zone is spatially

associated with the Lucky Strike *in-situ* massive sulphide deposit. The most intense alteration occurs underneath and to the east of the Lucky Strike deposit.

3.2.2 Dimensions

The spatial relationships of altered host rocks to the Lucky Strike *in-situ* VMS deposit have been greatly modified by brittle structures mostly associated with thrust faulting. Consequently, the extent of the alteration zone and morphology with respect to ore is uncertain. Erosion has also removed much of the altered rocks, as well as an unknown and possibly substantial quantity of ore. The immediate stockwork system at surface forms a northeast-trending zone extending for approximately 500 m from the Lucky Strike deposit with a width of up to 100 m (Jambor, 1987). Thurlow and Swanson (1981, p.127) described it as an "irregular concordant wedge-shaped zone...360 m at bedrock and wedging out 600 m down dip with stratigraphic thicknesses varying up to 100 m". Figures 3-2 and 3-3 illustrate this zone in cross-sections through east-west and north-south lines, respectively. The zone is cut off at the base by the two-level fault and is also limited at the top by an unnamed fault and the erosional surface. Therefore, the stockwork zone is completely fault bounded and is not in contact with either the peripheral alteration zones or the massive sulphide deposits. The maximum dimensions of less intense, peripheral phyllosilicate alteration related to ore formation are not exactly known, but were probably in the 10's of km^2 in the pre-deformation surface area.

3.2.3 Lithologies

Of the four formations that define the Buchans Group, the lowermost unit, the LHF, is not present in the Lucky Strike area and is not considered in this section, In addition , the uppermost unit, the SLF, does not display any evidence of hydrothermal alteration. The mafic volcanic units of the SLF are readily distinguished by their diagenetic metamorphic assemblage of carbonate - chlorite - epidote - hematite (Plate 3-1). Only the BRF and SHF are discussed in terms of alteration.

As suggested earlier, the stockwork zone, although discordant, is best described as an individual and distinctive lithology. Primary volcanic textures are mostly obliterated in this zone, although lithogeochemical data suggest that the original compositions were either SHF mafic volcanics and/or BRF dacite.

Structural overprints in the immediate vicinity of the Lucky Strike massive sulphide deposits complicate stratigraphic interpretation. Based on lithological and lithogeochemical data, it appears that the stratigraphic sequence of SLF, BRF and SHF may be present in numerous panels due to thrust repetition, with the ore-bearing BRF possibly present several times within a section less than 400 m thick. Specifically, a less than 100 m thick lava flow/pyroclastic sequence, assigned to the BRF, is repeated in drill core. The BRF sequence from top to bottom consists of some or all of the following: quartz phyric rhyolite, crystal-vitric (+/-lithic) tuff, volcanic sandstone and/or breccia conglomerate (locally with high grade sulphide clasts), vitric-lithic tuffs (possible reworked) and, finally, aphyric dacite flows and related breccia. The BRF conformably overlies SHF mafic volcanic rocks which are dominated by flow-hyaloclastite sequences and auto-breccias.

3.2.4 Alteration

Alteration can be broken into two broad styles, namely, stockwork and peripheral. Peripheral alteration may be subdivided again into proximal and distal.

3.2.4.1 The Stockwork Zone

The stockwork zone, which has been documented by previous workers (Jambor, 1987; Thurlow and Swanson,1981; Kowalik *et al.*, 1981), represents a distinct 'body' of alteration within the Lucky Strike foot-wall whereby alteration was intense enough to effect complete obliteration of host lithologies. The alteration is dominated by milky white sulphide-bearing quartz stockwork veining, with lesser calcite and barite veins, in a pervasive and completely Mg-rich chlorite/sulphide/quartz replaced host rock (Plate 3-2). Multiple quartz vein generations cut earlier generations. Pink calcite veins form the latest stage, often with barite, cut all other alteration types and are considered to form in the waning stages of the hydrothermal system (Kowalik *et al.*, 1981). The contacts of the stockwork zone are generally knife-sharp against less intense alteration, however, many of these have been structurally modified.

Detailed discussions of the stockwork mineralogy are given by Kowalik *et al.* (1981) and much of the following paragraph summarizes their work. They described a relatively simple sulphide assemblage consisting almost exclusively of pyrite, chalcopyrite, sphalerite and galena, with quartz, barite and calcite as the only gangue minerals. Sulphides are associated with both quartz and chlorite in variable proportions, and pyrite is ubiquitous throughout the stockwork zone, locally

constituting as much as 30 %. Pyrite occurs as fine, disseminated, euhedral grains in the chloritized portions but forms considerably larger grains (up to several cm's) in quartz. Chalcopyrite content is proportionately higher in the stockwork than in the overlying massive sulphides and, therefore, the stockwork has higher Cu/(Zn+Pb) ratios. Anhedral blebs of chalcopyrite up to several cm's across are described as being strongly associated with stockwork structures that contain substantial quartz, and much less so with those that contain barite and calcite. Sphalerite is the most common base metal sulphide in the stockwork zone, occurring as subhedral to anhedral grains in veinlets with quartz, and more so with calcite and barite. Sphalerite often contains exsolved chalcopyrite. Euhedral galena is also common with sphalerite.

3.2.4.2 Peripheral Alteration

3.2.4.2.1 Proximal

Hydrothermal alteration has affected all units except for the upper part of the BRF and the SLF. In many cases, alteration textures are highly dependant on the nature of the primary lithologies. This section reviews the alteration in terms of lithological host. A schematic stratigraphic column is shown in Figure 3-4 illustrating the major alteration facies. At the base of the sections, the SHF has undergone strong silicification and chloritization. Quartz void-space filling is predominant where good primary permeability exists, notably replacing the matrix of hyaloclastic mafic breccias as well as infilling amygdules and perlitic cracks (Plate 3-3). Quartz is also the most abundant mineral precipitated in areas of secondary permeability (*e.g.,* veinlets).

Groundmass glass in the flows and flow fragments is strongly chloritized producing a very dark grey-green colour and black specks in the matrix of these flows represent completely chlorite-replaced mafic phenocrysts. Quartz also locally replaces phenocrysts. Examples of phenocryst replacement assemblages are shown in Plate 3-4. Other bright green specks are completely sericitized feldspar phenocrysts. The contrast between very dark green chloritic hyaloclastite fragments and the white to cream coloured silicic matrix greatly enhances the textures of these rocks. In fact, most of the hyaloclastic rocks have an apparent matrix supported texture due to the propagation of the silicification front into the fragments. Flow-banded textures are also enhanced by quartz along banded perlitic cracks. Pyrite, and locally base metals, are strongly associated with quartz which occurs in open spaces (*i.e.*, amygdules and veins). Variable and complex zonation occurs in amygdules from different samples. Commonly though, these amygdules are filled with a combination of quartz, chlorite and pyrite (Plate 3-5). Carbonate and base metal sulphides may also occur in amygdules but are much less abundant.

Silicification and pervasive sericitization continue into the overlying BRF dacitic lavas (Plate 3-6) where chloritization is limited more to fractures. Silicic alteration occurs as hard, light greyish patches that resemble chert, whereas the sericitic alteration effects a yellow-green colour. This texture does not appear to be related to fragmental texture common to parts of the unit, but may be controlled by phyllosilicate and quartzo-feldspathic devitrification textures. Minor sphalerite and galena are common as irregular stringers and disseminations throughout this unit.

The overlying vitric-lithic tuff displays weakly developed graded bedding and is intercalated with finer epiclastic rocks, including volcanic siltstone/sandstone (Plate 3-7). As such, the tuff has been partly reworked. Non-welded vitric fragments range from mm-sized to several cm's and are wispy-shaped fragments varying from light to dark green (Plate 3-8). The colour is the direct result of complete replacement by very fine-grained sericite and lesser chlorite. Lithic fragments are more blocky and light grey to cream coloured. These often contain mm sized sericite altered feldspar phenocrysts. The matrix of these fragments is quartzo-feldspathic and partly sericitized. A few fragment types display irregular, mm scale, light and dark bands indicative of flow banding. All fragments are apparently matrix supported and set in a quartz-rich groundmass. As with the underlying SHF mafic hyaloclastites, silicic alteration has replaced the finer-grained material as well as the margins of larger clasts producing a false matrix-supported texture. Silica-sericite alteration imparts a distinctive "bleached" appearance to this unit. The tuff is of the same composition as the underlying dacite flow and breccia.

These tuffs grade into, and are interbedded with, finer-grained epiclastic rocks, namely volcanic sandstone/siltstone and/or conglomerate-breccia deposits. The sandstones range from massive to laminated and locally contain minor, fine-grained disseminated pyrite and sphalerite-galena along diffuse fractures. In addition, abundant carbonate-sulphide 'spots', up to 1 cm or more in diameter, occur locally in the sandstones (Plate 3-9). Very fine, 'dusty' sericite also occurs in the matrix of these rocks. These features suggest some degree of hydrothermal alteration of these rocks.

More intense alteration has caused brecciation of these siltstones as indicated by an abundance of angular siltstone fragments with altered rims in the overlying ore horizon breccias (Thurlow and Swanson, 1981).

A breccia-conglomerate unit, the 'ore horizon breccia' (Walker and Barbour, 1981), represents the immediate host for the transported ore bodies at Lucky Strike (Plate 3-10). The breccia varies locally in composition, but generally consists of variably altered, breccia fragments of SHF mafic volcanics, BRF 'rhyolites', siltstone and, locally, rounded granodiorite pebbles, cobbles and boulders (Thurlow and Swanson, 1981). High grade sulphide clasts are common in the breccias, and locally the breccias are comprised dominantly of sulphide clasts constituting the transported ore bodies. Although many of the lithic fragments within this unit are highly altered, little post-deposition alteration appears to have occurred.

Crystal-vitric rhyodacite tuff (Plate 3-11), locally with lithic and pumice fragments, overlies the ore horizon breccias and can be considered as the immediate hanging wall to the ore horizon. The vitric component of the tuffs is altered to sericite and clay, with lesser chlorite, resulting in yellow to green colours in hand specimen. The groundmass to these vitric rocks often contains an abundance of very fine-grained, granular quartz which show a strong association with primary quartz phenocrysts, often enveloping several grains. Otherwise, the groundmass consists of very fine-grained phyllosilicates (Plate 3-12). This alteration may be better described as devitrification, equivalent to Thurlow and Swanson's (1981) regional diagenetic-metamorphic alteration. Therefore, it is not clear as to how much of an effect the

hydrothermal system had on the hanging wall stratigraphy. It appears, however, that most vitric and vitriclastic volcanic rocks in the ore horizon are strongly sericitized and clay altered but generally devoid of quartz veining, significant chlorite or sulphide mineralization. In addition, there does not seem to any spatial relationship between alteration intensity and distance to ore. Arguably then, this alteration is essentially a form of devitrification, although this too might have been enhanced by contemporaneous elevated heat and water circulation. More coherent rhyodacite (rhyolite) flows are often much less altered and retain a reddish or maroon red colour, except at the base where slight sericitization can occur. These units may be more impermeable or were erupted later when the hydrothermal system had been exhausted.

In addition, a peculiar alteration occurs holes 243, 244 and 237 just west of the Lucky Strike Main deposit in the structural foot-wall. K-feldspar - quartz +/-sericite alteration and pyrite - sphalerite - galena mineralization are well developed in pumiceous tuffs stratigraphically above an ore-clast bearing breccia-conglomerate and may represent a form of hanging-wall, or ore horizon, alteration at Lucky Strike (Plate 3-13). Otherwise, K-feldspar alteration is not common in the Lucky Strike area.

3.2.4.2.2 Distal Alteration

Distal alteration in the SHF is characterized as a weak, non-pervasive style of alteration mainly involving quartz, sericite, Fe-Mg chlorite, epidote-clinozoisite and carbonate. Pyrite is very minor to nil in this zone and base metal sulphides and barite

are generally absent. This alteration may be more diagenetic than hydrothermal, yet it is distinctly different from that of the SLF basalts.

Quartz tends to occupy open spaces, notably amygdules. Sericite is mostly confined to feldspar and chlorite typically replaces groundmass glass and augite phenocrysts, although it too can occur in amygdules. Epidote forms small clots in the matrix or in voids. Carbonate is also very common in voids, and to a lesser extent in feldspar. Amygdules are commonly filled by a combination of several phases. An example is illustrated in Plate 3-14.

3.2.4.3 Alteration Mineralogy

Alteration mineralogy is dominated by microcrystalline quartz, which is common throughout the stockwork zone, but most intense in the upper portions. Various styles quartz occur, including (i) silicification - pervasive replacement of groundmass and phenocrysts with quartz and (ii) as open-space (*e.g.* veinlets, amygdules) filling with coarser subhedral to euhedral quartz. With more distal, lower temperature alteration, amygdules are often encrusted by banded, chalcedonic(?) silica

Chloritization is a widespread alteration product, commonly occurring as a replacement of groundmass glass in all mafic volcanic rocks in the Buchans area, however, it is best developed in the mafic rocks of SHF in the Lucky Strike foot-wall. In addition to replacement of glass, chlorite also pseudomorphs mafic phenocrysts, and sometimes plagioclase, forms veinlets and margins to veins, and fills amygdules and

other voids. Chlorite chemistry is discussed in detail in the following chapter.

Barite typically occurs as veins or as needles in calcite veins. White calcite occurs mostly in veins. Vein calcite often forms central cores to quartz veins having utilized the same fracture systems. Kowalik *et al.* (1981) suggested a decrease in the amount of calcite in the upper portions of the stockwork zone in marked contrast to quartz.

Sericitization is a common product in nearly all volcanic rocks form the Buchans area, however, it is absent in the most intense stockwork altered zones. Sericite may have been present initially during the earlier stages of hydrothermal alteration but was subsequently replaced by chlorite as hydrothermal intensity peaked.

Thurlow and Swanson (1981) have suggested that the alteration has a roughly concentrical zonation, with an outer, peripheral zone of clay mineral alteration with pyrite and occasional base metal mineralization. Henley and Thornley (1981) have identified these clay minerals as illite, lesser montmorillonite and mixed-layer clays.

3.3 Middle Branch Alteration Zone

Alteration in the Middle Branch area has been attributed to the same hydrothermal activity which formed the Buchans orebodies (Thurlow and Swanson, 1981), with the closest *in-situ* deposit being the Oriental No.1 deposit.

3.3.1 Location

The MBZ is located a minimal distance of 1 km northeast of the *in situ* Oriental No.1 deposit (refer to map in Figure 3-1).

3.3.2 Dimensions

The zone has a minimum northeast strike length of 800 m by 100 m wide, and is essentially a part of the much larger zone that relates to known ore. Thicknesses of altered rocks range to over 100 m. The MBZ dimensions are really equivalent to the dimensions of the BRF in this area. The alteration is generally weaker at the top of the unit and does not extend into the conformably overlying SLF. Alteration is truncated at the base by a major structure, presumably the Ski Hill - Buchans River Fault system. Internal zones of more intense alteration have a very limited extent, often cut by a single drill hole. The zone is illustrated in a block-model in Figure 3-5.

3.3.3 Lithologies

Alteration and mineralization at the MBZ are hosted in the BRF, consisting of up to 260 m of rhyolite, rhyolite breccia and lesser tuffs. Well developed alteration occurs in the rhyolites and high grade Zn-Pb and barite clasts also occur in the breccias within this unit. Two holes, 1605 and 1916, also intersect SHF mafic volcanic rocks conformably below the BRF. Conformable above the BRF, and represented in all drill holes on the section, are 10-100 m of SLF, including arkose and mafic flows. This

package of rock is structurally bound within the Sandy Lake Duplex.

The Airport Thrust separates the Sandy Lake Duplex from the overlying Middle Branch Duplex. This structurally higher duplex consists of 120-320 meters of mafic to felsic flows, flow breccias, tuffs and agglomerates, historically considered to represent the LHF. Most of the drill holes at Middle Branch are deep enough to encounter a second major thrust zone under which the SLF reappears again. This panel is considered to represent either the Lake 3 or Lucky Strike Duplex.

3.3.4 Alteration

The MBZ is hosted primarily in felsic volcanic rocks of the BRF, although mafic volcanic rocks of the SHF are locally present. The latter contain only weak alteration characterized by quartz-filled amygdules with weak chloritization of groundmass and sericitization of feldspars, but essentially no sulphides (Plate 3-15).

Felsic rocks from this zone locally contain much more significant alteration and mineralization. The alteration may be described as a northeast-southwest trending zone highlighted by several isolated inner zones of stringer-style Zn-Pb-Ba mineralization (Plate 3-16). This stringer mineralization is associated with pervasive and intense K-feldspar - sericite(clay) - quartz +/- epidote alteration (Plate 3-17). Mineralization consists of irregular pyrite-sphalerite-galena-barite stringers with rare chalcopyrite. Also evident in these zones are late quartz - carbonate veins and later minor chlorite along fractures. In the south, hole 1662 intersected 120 m of stringer-

style mineralization, and in the north hole 1798 intersected 50 m of an equivalent style mineralization. This intense alteration causes a bleached appearance in the host rhyolites, characteristic of 'white rhyolites'. Thurlow and Swanson (1981) described these as intensely altered rocks, consisting of an assemblage almost entirely of secondary quartz and K-feldspar, with the only accessory minerals being minor leucoxene, barite and pyrite. Strong chlorite alteration and chalcopyrite mineralization are generally absent in this area. Therefore, although the alteration here can be considered fairly proximal to a venting system, none of these zones resemble the stockwork zone at Lucky Strike.

The stringer zones are isolated zones and appear to be in fault contact in several locations. For example, at the base in hole 1662, the alteration zone is truncated against underlying SLF arkose (?) via the Ski Hill - Buchans River Fault. Internally they are in sharp contact with much lesser altered rocks of the same lithology, presumably along minor faults.

All other holes presented on the section indicate some degree of incipient alteration in BRF units. This incipient alteration is characterized by various degrees of quartz - sericite - chlorite - hematite - epidote - carbonate with local pyritic sections and occasional Pb-Zn-Cu mineralization.

3.4 Woodman's Brook Alteration Zone

3.4.1 Location

The Woodmans Brook Alteration zone is located approximately 5 kilometers east of the Oriental No.1 deposit, the closest in situ massive sulphide deposit (refer to Figure 3-1).

3.4.2 Dimensions

The Woodmans Brook alteration zone has a poorly constrained north-south strike length measuring approximately 1.3 km (Figure 3-1). The width of the zone is somewhat uncertain due to the fact that the drill holes plot close to a north-south line and therefore do not permit a three-dimensional perspective of the sub-surface for this area. A gradient induced polarization (IP) survey (Spurvey and Scott, 1997), however, identified a significant anomaly in this area corresponding with pyrite mineralization. The IP survey suggests a width of up to 1000 m for the pyrite-bearing zone with maximum chargeability values of up to 35mV/V. In general, the WBZ is open in all lateral directions, and can be extended at depth in the north where it is at least 300 m thick. The zone is less than 150 m thick in the south, essentially limited at the base by the Airport Thrust. Presumably, this same structure defines the depth extent of the alteration in the north where drilling did not intersect the structure. Cross sections through this zone emphasizing lithologies and alteration are shown in Figure 3-6a.

3.4.3 Lithologies.

Describing the lithologies of this area in terms of the Buchans Group stratigraphy of Thurlow and Swanson (1987) is untenable. Therefore, only brief correlations will be attempted. Calon and Green (1987) considered the entire area northeast of the Airport Thrust as part of the LHF, although there are few exposures and limited drilling in this region. In addition, the LHF also contains a variety of rock types that are not as distinctive as lithologies in other formations.

A major division in stratigraphy may occur across a fairly significant structure, the Airport Thrust (Calon and Green, 1987). As a major brittle-ductile thrust fault zone, the Airport Thrust is characterized by shearing over a relatively wide interval (several m's) with minor gouge and is cut by abundant diabase dykes. The dykes are essentially unaltered relative to the host felsic volcanics. Below the thrust occurs a mixed sequence of felsic epiclastics with a lesser mafic component, mafic and felsic flows/breccias with minor fine grained clastic sedimentary rocks, interpreted to be the SLF. This unit shows rapid changes in lithology and contains relatively 'colourful' breccia fragments when compared to the units above the thrust. This unit contains locally strong chlorite in the matrix of some of the volcaniclastic rocks and occasional weakly anomalous Zn, but is not significantly altered and was not a focal point for this study. The unit is continuous at depth.

Unit 5a, represented in numerous drill holes immediately above the Airport Thrust, consists dominantly of quartz +/-feldspar porphyritic to aphyric dacite flows, mostly massive but with some breccias and local shearing (Plates 3-18, 3-19). Lesser

portions of this unit are tuffaceous. These rocks are tentatively termed the Woodman's Brook felsic volcanics. The colour of these rocks is mostly dependent upon alteration style and ranges from light grey (silicic) to cream coloured (sericitic) and pinkish (albitic). Quartz phenocrysts are variably colourless to white coloured (cloudy), mostly from 1-5 mm and up to a maximum of 7 mm and are subhedral-rounded. Quartz phenocrysts rarely account for more than 5 % of the rock. Pinkish, subhedral feldspar phenocrysts are finer, generally less than ~ 2 mm, and have low modal percentages, rarely greater than a few percent. A subunit, 5b, contains a distinctive texture - rounded blotches of black chlorite - pyrite - carbonate (Plate 3-20). These blotches may represent lithophysae produced during devitrification (*cf.* McPhie *et al.*, 1993).

Unit 4, conformable above unit 5, is a thin blanket (~ 1 meter) of cherty siltstone/shale, wacke and conglomerate which represents a relatively short period of quiescence. In hole BE-96-08, this unit is essentially absent but the contact between the felsic and mafic units contains minor hematitic-chert and chlorite-pyrite mineralization, including a ~20 cm band of massive pyrite.

Conformably above the sediments (unit 4), unit 3 records a period of dominantly mafic volcanism characterized by basaltic-andesitic flows and lesser breccia, tentatively termed the Woodman's Brook mafic volcanics (Plate 3-21). The unit attains a maximum thickness of less than 75 m in hole BE-96-10, however, true width may be considerably less. These rocks are variably amygdaloidal and feldspar porphyritic with weak to moderately developed foliation.

Unit 2, represented in six drill holes, represents a zone of strongly foliated felsic volcanic rocks, that are largely composed of fine-grained quartz, sericite and pyrite with very minor carbonate and chlorite (Plate 3-22). This unit shows very little variation owing to the well developed fabric which obliterates much of the protolithic textures. Contacts with the lower mafic rocks were not cored. Based on lithogeochemical data, this unit is considered a strongly foliated equivalent of the lower unit 5 felsic volcanics. The greater deformation in unit 2 was probably a result of proximity to the structurally overlying Hungry Mountain Thrust, the roof thrust to the imbricated Buchans Group (Calon and Greene, 1987; Thurlow *et al.*, 1992).

Unit 1 represents massive mafic volcanics that were intersected in only one drill

hole at the north end of the section. This unit is in fault contact with the underlying felsic volcanics and may be an equivalent of the unit 3 mafic volcanics.

3.4.5 Alteration

Some degree of alteration is evident in all rocks on the section above the Airport Thrust, however, stronger alteration and associated base-metal mineralization occur at two main areas, labeled A and B (Figure 3-6b). The host rock, alteration styles and metal ratios are distinct at each area.

Zone A is hosted in mafic volcanic rocks (Unit 3) and is best represented in drill hole BE-96-10. The mineralization consists of disseminated, stringer and vein pyrite with generally very minor sphalerite and chalcopyrite (Plate 3-23). No galena or

barite were observed within this zone. Associated alteration includes abundant quartz, which fills veins and stringers, as well as the matrix within brecciated zones. Chlorite is the most common replacement mineral for the groundmass glass but also replaces mafic(?) phenocrysts. Locally, it forms more intense patches and stringers and is often strongly associated with pyrite. Sericite is the most common replacement mineral for groundmass and porphyritic feldspar and is readily identifiable in hand specimen as a bright green phenocryst (after feldspar). It also occurs with quartz as a replacement of groundmass between fragments. In general, the sericitic - chloritic alteration lends a light grey-green to dark green colour to these mafic rocks. Carbonate forms a minor component, usually in the groundmass but also along fragment margins. Carbonate may represent a relatively early alteration phase. An example of typical alteration is shown in Plate 3-24a. Amygdules are mostly filled with quartz, lesser chlorite and pyrite, and rarely, contain minor sphalerite or chalcopyrite (Plate 3-24b). A weak to moderate fabric in these rocks is defined by phyllosilicate mineralogy, which commonly is displayed as flattened chloritized groundmass conforming around spherical quartz phenocrysts. Minor stringer mineralization and alteration occur below the mafic volcanic unit in the sedimentary unit, including fracture-controlled pyrite with minor sphalerite in quartz. The alteration does not persist with the same intensity in the lower porphyritic felsic rocks (unit 5) in hole BE-96-10.

Alteration/mineralization occur in the same unit in BE-96-08, although the mafic volcanic rocks thin towards the north. Jasper and pyrite in that hole appear to be related to the alteration.

The best base metal mineralization discovered at the WBZ occurs at Zone B, hosted in the felsic volcanic rocks of unit 5 about 450 m south of Zone A. Minor Zn-Pb mineralization occurs over a 50 meter interval in hole BE-95-03, including 0.5 m of 2.58% Pb and 1.92% Zn (Plate 3-25). Mineralization, consisting of 3-5% pyrite, with minor sphalerite and galena, also extends to drill hole BJ-46. Chalcopyrite is rare and barite is absent. The strongest mineralization appears to be associated with the more aphyric flows within the sequence. Alteration is considered to be roughly zoned, with an inner zone dominated by silicification with lesser sericitization, yielding a hard, grey rock cut by milky-white quartz veins. Carbonate may be present in this zone, but chlorite is generally absent. An outer zone is defined as having only 1-2% pyrite and trace Zn-Pb and less intense silicification. Sericite persists throughout this zone with variable carbonate. Chlorite is present in only minor amounts. An outer zone of weaker sericite-chlorite alteration includes the remainder of the WBZ felsic volcanics. Silicic alteration is not as significant in this outermost, incipient alteration facies. Carbonate is present in minor amounts throughout. This zone contains minor (~1% or less) pyrite and rare base metal sulphides.

The mineralogical assemblage of unit 2 can be considered to result from this alteration. The assemblage is dominated by very fine and strongly foliated quartz - sericite - pyrite (refer to Plate 3-24c) and is fairly homogenous throughout its known extent.

Boundaries for these alteration zones are arbitrary and are considered gradational. However, knife-sharp alteration fronts are present in drill core. For

example, the transition from relatively fresh feldspars to completely altered equivalents (replaced by sericite-pyrite) often occurs across mm scale boundaries within the same flow. The overall distribution of the alteration appears to be semi-conformable within unit 5. In addition, this zonation compares very well to the alteration model compiled for Miocene Kuroko deposits (Franklin, 1993). However, many of the hydrobreccia textures (Plates 3-26 and 3-27), which may be the result of over-pressurized fluids, appear to postdate the fabric in some of the felsic units and may not be synvolcanic. These textures are very similar to those which host the Pb-Zn mineralization (Plate 3-25). However, several lines of evidence exist to refute a syn or post-volcanic process These include: (i) The fault zones are cut by numerous diabase dykes that are very fresh compared to the very altered host rocks. Hence, the major later structures do not appear to have been fluid pathways. (ii) quartz-filled sulphide-bearing amygdules are undeformed within a foliated phyllosilicate-altered groundmass that conforms around them. The amygdules must have been filled at least prior to deformation. Therefore, it is uncertain if this mineralization is related to VMS-style processes.

3.5 Powerhouse Alteration

3.5.1 Location

The PHZ is located approximately 2.5 km east of the Lucky Strike in situ deposit and 700 m southeast of the Oriental in situ deposits. Figure 3-1 illustrates the location of this zone.

3.5.2 Dimensions.

The zone was intersected in several drill holes near the Buchans River and is also well exposed near the powerhouse on the Buchans River where it is represented as a gossanous zone (Plate 3-28) (the powerhouse referred to is a small, currently unused hydro-power generating station that was built by ASARCO). The zone trends northwest-southeast with a strike length of 1.2 km, likely in fault contact at the northwest but open at the southeast (refer to Figure 3-7 a,b,c). Based on current drilling, thicknesses range to more than 350 m, limited at the top by the erosional surface and at the base by a major fault - likely the Airport Thrust. Based on correlations of this zone with an IP geophysical anomaly, the zone has a width ranging from 150 m to 400 m and maximum chargeabilities of 14 mV/V (Spurvey and Scott, 1997). The zone thins to the southwest and is terminated where the Airport Thrust breaches surface. The zone is completely open both vertically and laterally to the northeast.

3.5.3 Lithologies

The zone is bounded at the base by a major structure, the Airport Thrust (?), below which arkosic and basaltic rocks of the SLF have been logged. Above the thrust, dacitic to rhyodacitic quartz and feldspar porphyritic volcanics and feldspar porphyritic and amygdaloidal mafics volcanics host the alteration (Plate 3-29). The felsic lithologies appear to be dominated by coherent lavas, with local breccias and well developed pseudobreccias. The colour of these felsic rocks varies from light grey

to yellowish and pinkish. Feldspar phenocrysts are mostly 1-3 mm and rarely comprise more than 5% of the rock. Pink to white plagioclase phenocrysts are mostly 1-2 mm.

Mafic volcanic rocks, despite being strongly altered, are easily recognizable due to the lack of quartz phenocrysts and abundance of relatively large feldspar phenocrysts, ranging from a few mm's to greater than 1 cm. These rocks have a fine-grained medium grey groundmass. Scattered, very discrete amygdules exist, ranging from mm sized and rounded to a few 1-3 cm sized and irregular shaped. The texture throughout the unit is fairly consistent, lacking obvious breccia or tuffaceous textures. Therefore, this unit is interpreted as a syn-volcanic mafic sill/dyke or a massive flow. This unit was intersected in only two drill holes, BE-96-11 and BE-96-19.

3.5.4 Alteration

Alteration is fairly homogenous in this zone and varies based on the composition of the host rocks. Alteration in the felsic rocks is dominated by sericite-clay, affecting feldspar phenocrysts and groundmass (Plate 3-33 a,b). Locally, minor chlorite occurs in the matrix of flow breccias. Fine-grained pyrite is associated with both sericite and chlorite in varying amounts, but rarely exceeds 5 % (modal). Minor carbonate also occurs as a replacement to feldspar phenocrysts. Pervasive silicification occurs in many samples, causing a greyish colour, but veining/veinlets of quartz are less common. Alteration in some of the pseudobreccias, localizing fractures, greatly enhanced the texture of these rocks (Plate 3-30).

Mafic rocks are equally altered but contain chlorite in addition to sericite, quartz and carbonate. Extremely fine disseminated pyrite is ubiquitous throughout the matrix of this rock causing a consistent grey colour to the matrix of this unit. Peculiar to this unit is the strong albitization of feldspar phenocrysts. Otherwise, sericite has a marked effect upon feldspars, completely replacing them with fine sericite yielding an emerald green colour (Plate 3-31, 3-33c). Chlorite is very hard to distinguish in hand specimen, but typically comprises 1-2% or more tiny dark spots often with pyrite, probably after mafic minerals. Pyrite appears to be much more common in this unit, comprising 5 - 10% on average, but up to 25 - 30%. Some networks or stringers of pyrite are slightly coarser than that of the groundmass and may have been remobilized. Amygdules are commonly filled with pyrite - quartz - carbonate (Plate 3-32). Late carbonate veinlets, presumably not related to the alteration assemblage, occur in both mafic and felsic units. It is unclear if the carbonate in the center of the amygdules is the same composition as the late veinlets. Traces of sphalerite and chalcopyrite are barely visible as fine grains in the matrix, but slightly coarser varieties occur locally in stringers, and occasionally in amygdules. Galena and barite were not observed. Assays from the mafic volcanic interval in hole BE-96-11 were particularly anomalous in Zn, Cu and Ag, with elevated levels of Pb and Au. One of the more interesting values was a 0.5 m intersection of 3.9 % Zn and 6.2 g/t Ag.

Overall, it was very difficult to outline distinctive alteration zones at the PHZ. The best mineralization from drill core appears to be focused in the mafic volcanics. The best alteration/mineralization within this zone, consisting of intense quartz - pyrite

with minor chalcopyrite and lesser sphalerite and galena, occurs on the banks of the Buchans River immediately south (downstream) of the Powerhouse. Mineralization is represented by a gossan over ten's of meters.

3.6 Airport Alteration Zone

3.6.1 Location

The Airport Alteration zone (APZ) will be described as two zones, the Airport North (APZ-N) and Airport South zones (APZ-S), due to the fact that such a large separation (750 m) exists between drill intervals. Therefore, these two zones cannot be correlated with any degree of confidence.

The Airport North (APZ-N) Zone is located approximately 2.25 km north of the Oriental No.1 deposit. A smaller zone, the Airport South (APZ-S) Zone, is located about 1.5 km north of the Oriental No.1 deposit and is defined by two short drill holes. EX-size core was used for both holes and all core has been split with core splitter leaving only small fragments to log.

3.6.2 Dimensions

The APZ-N, although poorly constrained, appears to be conformable with dimensions of the weakest, incipient alteration approximately 900 m in the east-west direction and 300 m in the north-south direction, although the strongest alteration occurs over only a few meters in each of holes 2837 and 2845 (refer to cross-section, Figure 3-8). The zone appears to be open in all directions except at the north where

drill holes 2838 and 2847 are barren of any significant mineralization/alteration.

The APZ-S, defined by holes 258 and 395, only 55 m apart in a northeast-southwest direction, is an intense zone of alteration (Figure 3-9). The zone is open in all directions and at depth. The upper limit of the zone is the erosional surface. There is little drilling and no outcrop exposed in the area.

3.6.3 Lithologies

Uncertainties also exist in this area with respect to the naming of units based on Buchans geology. The uppermost volcanic sequence at the AP zone consists dominantly of weakly foliated andesitic tuffs, originally considered Lundberg Hill. Conformably below are weakly foliated dacite tuffs, also likely to be LHF, though a significant zone of shearing has been logged at this contact. The APZ-N zone appears to be entirely hosted within these dacitic tuffs. In most instances these dacitic tuffs are underlain by a thick dacitic epiclastic and arkosic sequence of SLF. It is not clear of the relationship between this unit and the above dacitic tuffs (possibly a fault contact - the Airport Thrust?). There also appears to be a unit of rhyolite or rhyolite porphyry separating these sequences, which may be intrusive along the contact. This dacitic epiclastic/arkosic sequence thickens substantially to the north. Conformably(?) below this arkosic sequence is a basaltic sequence, also of SLF. Finally, SHF andesitic-basalts underlie these SLF basalts in holes 2842, 2845, 2837 and 2846 to the southeast. BRF felsic volcanic rocks may be present as a thin sequence above the SHF in holes 2845 and 2837.

Lithologies were indistinguishable at the APZ-S zone due to intense alteration and shearing and overall poor quality of core, however, the protoliths appear to be dacitic. This is verified geochemically in Chapter 5.

3.6.4 Alteration

APZ-N Zone - Alteration in the north zone is focused on a weakly mineralized zone in hole 2837; similar alteration is present in hole 2845. The mineralization is characterized by weak to moderate chloritization with quartz (+/- sericite +/- carbonate) alteration. Minor base metal sulphides are associated with quartz - pyrite stringers. Sphalerite and chalcopyrite are the most common base metal sulphide stringers. Galena is rare and barite is absent. Assays from hole 2845 yield values as high as 0.46% Zn over approximately 4.0 m. Values of 0.41% Zn over 1.8 m and 0.16% Cu over 1.5 metres from hole 2837 also indicate the presence of base metal sulphides within zones of dominantly quartz - chlorite alteration. This mineralized zone is enveloped by a zone of weaker incipient alteration. This style of alteration is characterized by variable, weak and localized sericite - quartz - chlorite - pyrite with only weakly anomalous of basemetal values.

APZ-S Zone - Alteration in the APZ-S zone is very intense and appears strongly 'bleached'. Close to surface, a shallow northwest dipping (?) 30 m (apparent thickness) zone of intense quartz - pyrite alteration was logged in core. This zone is anomalous in Au-Ag-Cu-Pb-Zn, yielding values as high as 0.3 g/t Au, 25 g/t Ag, 0.62% Zn, 0.18% Pb, and 0.11% Cu (from separate samples). Silicification and

pyritization decrease in intensity away from this zone accompanied by decreases in base metals and Au-Ag. At approximately 100 m depth in each hole, a zone containing minor fuchsite was observed and correlated. Strong shearing of the host rocks and significant diabase dyking occur in this zone, suggesting proximity to a major structure. The dykes are relatively fresh.

3.7 Summary of Alteration Zones

The LSZ is an altered package of rocks in the vicinity of the Lucky Strike massive sulphide deposit which represents a proximal hydrothermal facies. The stockwork zone, which can be regarded as an individual unit, is an extremely altered and mineralized zone. Alteration in this zone is typified by pervasive chloritization and quartz replacement and quartz veining. Quartz veining occurs as multiple generations displaying complex cross cutting relationships. Carbonate and barite are late vein-hosted constituents that probably were deposited in the waning stages of hydrothermal alteration. Pyrite is ubiquitous throughout, occurring commonly with both chlorite and quartz. Base metal sulphide mineralization, commonly yielding several percent combined Cu-Zn-Pb, occurs throughout the stockwork zone but is highly variable. Outside of the stockwork, the alteration is much less intense, consisting of various proportions of quartz (and chalcedony) - chlorite - sericite (and clays) , with locally K-feldspar. Chlorite tends to be ubiquitous throughout the mafic volcanics but is uncommon in the felsics. K-feldspar occurs only in felsic lithologies. In this outer zone protoliths are easily recognizable and base metal sulphides/barite are

typically in trace amounts. The extent of the peripheral alteration halo is uncertain. Hanging-wall alteration does not appear to be significant.

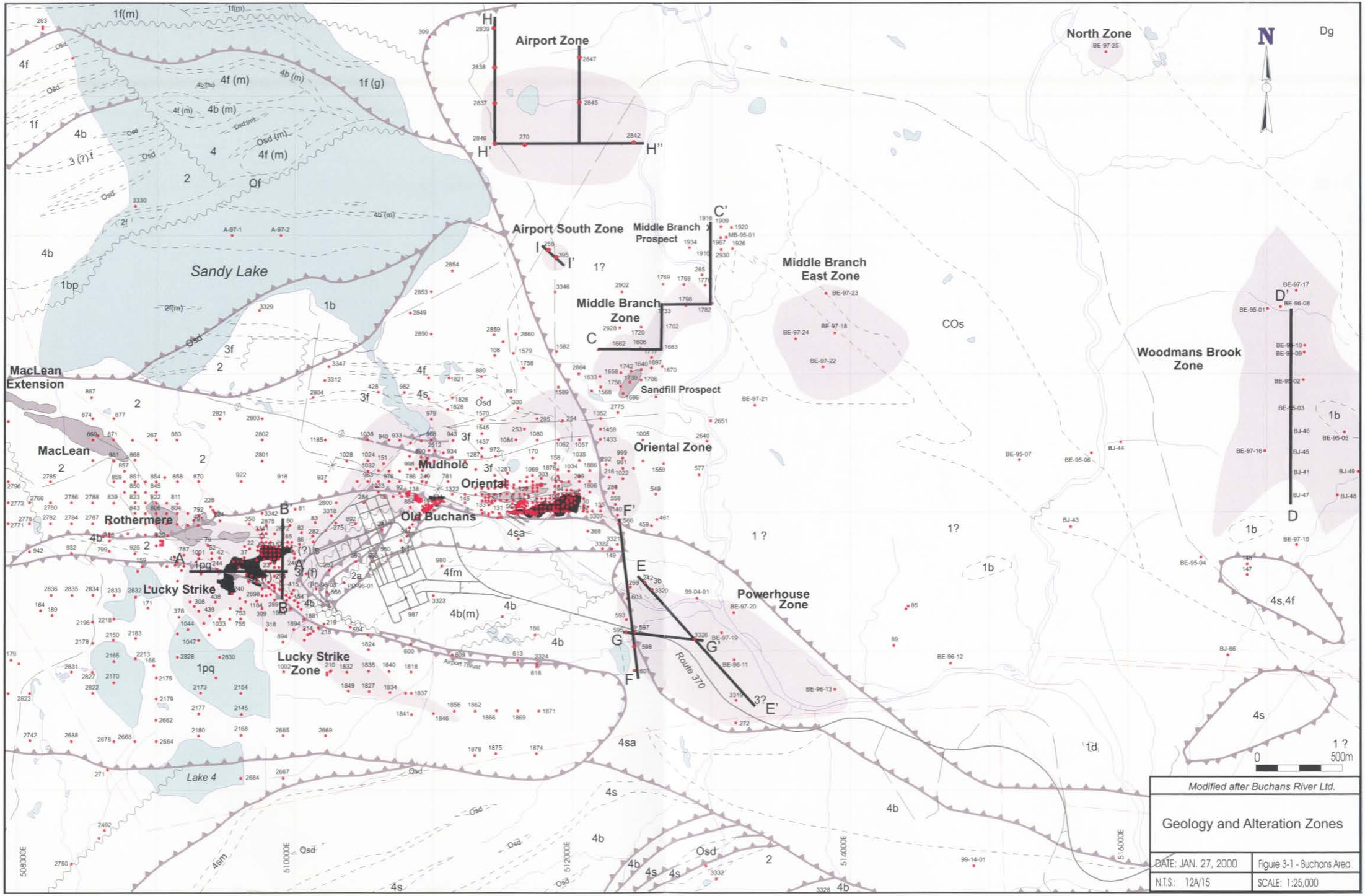
The MBZ, also regarded as alteration related to known massive sulphide mineralization, represents a more distal alteration facies. This alteration is characterized by strong sericite - quartz - K-feldspar alteration and sporadic Zn-Pb-Ba mineralization. Strong chlorite alteration or chalcopyrite mineralization are lacking from this zone and may reflect the lower temperatures expected at a distal venting facies.

The WBZ is an extensive zone of alteration which displays distinctly different styles of alteration which seem to be largely controlled by host lithology. Specifically, the zone contains a chlorite - sericite - quartz altered mafic sequence with abundant pyrite and very minor sphalerite - chalcopyrite. The felsics have been dominantly affected by sericite - quartz alteration, containing ubiquitous minor pyrite and occassional galena - sphalerite mineralization. Barite has not been observed in any of these rocks. Based on drilling, the volcanic package appears to be dominated by felsic units.

The PHZ contains strongly altered mafic and felsic rocks, dominated by sericitic-quartz alteration and minor conspicuous chlorite in the mafic rocks. Mineralization is dominated pyrite and also commonly has sphalerite - chalcopyrite. Galena is less common and barite appears to be absent. As with the WBZ, the host lithologies are dominated by felsic volcanics.

The APZ-N, in general, represents a weak, localized zone of altered and

mineralized dacitic volcanics, the style of which could be attributed to late fault-related processes. However, the alteration and mineralization at the APZ-S is much more intense and pervasive. Strong shearing and 'late' diabase dykes in the APZ-S suggest that these rocks are proximal to a major structure but does not suggest a structural control on mineralization. The alteration at the APZ-S zone can be likened to VMS-style typical of the peripheral facies in a felsic volcanic host.


Airport Zone
North Zone
Airport South Zone
Middle Branch Prospect
Middle Branch East Zone
Middle Branch Zone
Sandfill Prospect
Woodmans Brook Zone
MacLean Extension
MacLean
Mudhole
Oriental
Oriental Zone
Old Buchans
Rothermere
Lucky Strike
Lucky Strike Zone
Powerhouse Zone
Route 370
Sandy Lake
Lake 4
COs
Modified after Buchans River Ltd.
Geology and Alteration Zones
DATE: JAN. 27, 2000
Figure 3-1 - Buchans Area
N.T.S.: 12A/15
SCALE: 1:25,000
0
500m

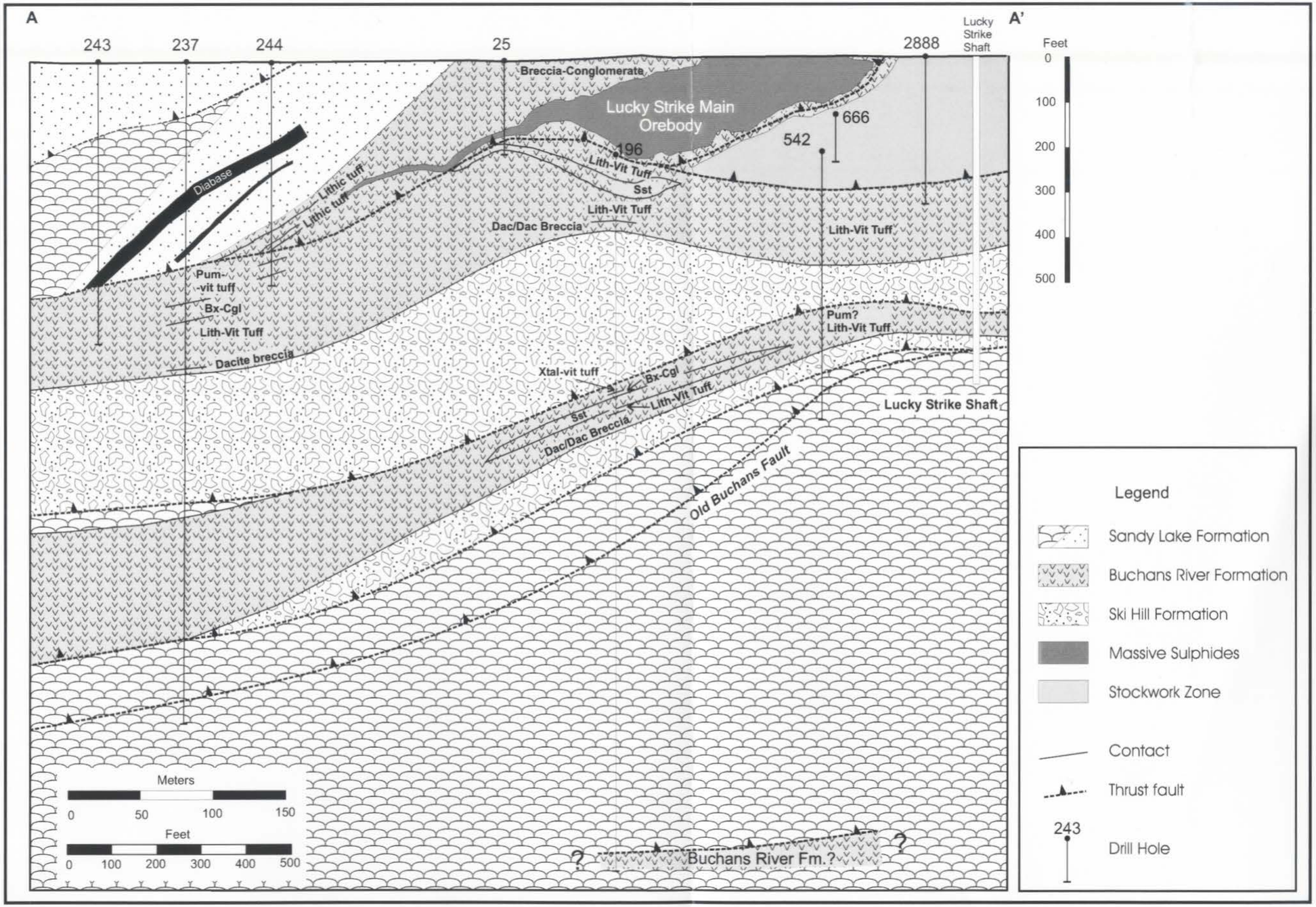


Figure 3-2 - East-west cross section through the Lucky Strike area (modified from Jambor, 1987).

LEGEND

Siluro-Devonian
Dg Topsail Granite

Ordovician-Silurian
Osd Diabase

Ordovician
Buchans Group
5 Feeder Granodiorite
4 Sandy Lake Formation
4s Volcanic sediment. Arkose and conglomerate, pyritic shale, chert
4b Basaltic Pillow lava, pillow breccia and pyroclastics.

3 Buchans River Formation
Felsic volcanic and volcaniclastic rocks, unseparated

2 Ski Hill Formation
Mafic volcanic and volcaniclastic rocks, unseparated.

1 Lundberg Hill Formation
1d Felsic volcanic, grey and greenish grey. Masisive to banded flows, breccia and agglomerate.
Quartz- feldspar crystal tuff. Locally altered and mineralized
1b Basaltic and andesitic pillow lavas, breccia and tuff
1i Intermediate fragmentals. Locally altered and mineralized.
1r Rhyolite flows and quartz crystal tuff
NOTE: Stratigraphic position uncertain; may be equivalent to Lundberg Hill Formation or Buchans River Formation area

ORDOVICIAN or EARLIER
COS Skidder Basalt. Pillow lava, breccia, jasper, chert (b)
COHM Hungry Mountain Complex. Foliated mafic to felsic plutonic rocks.

Geology after ASARCO Inc., Abitibi-Price Inc., and Nfld. Dept. Of Mines with revisions.

SYMBOLS

Contact

Thrust fault, normal fault

2809 Diamond Drillhole

Alteration Zone

Roads

Streams, Lakes

Ore body: In-situ, transported

A — A' Location of cross sections

Figure 3-1 - (on this and facing page) Geological map of the Buchans area showing alteration zones, ore bodies, major structures and drill hole locations.

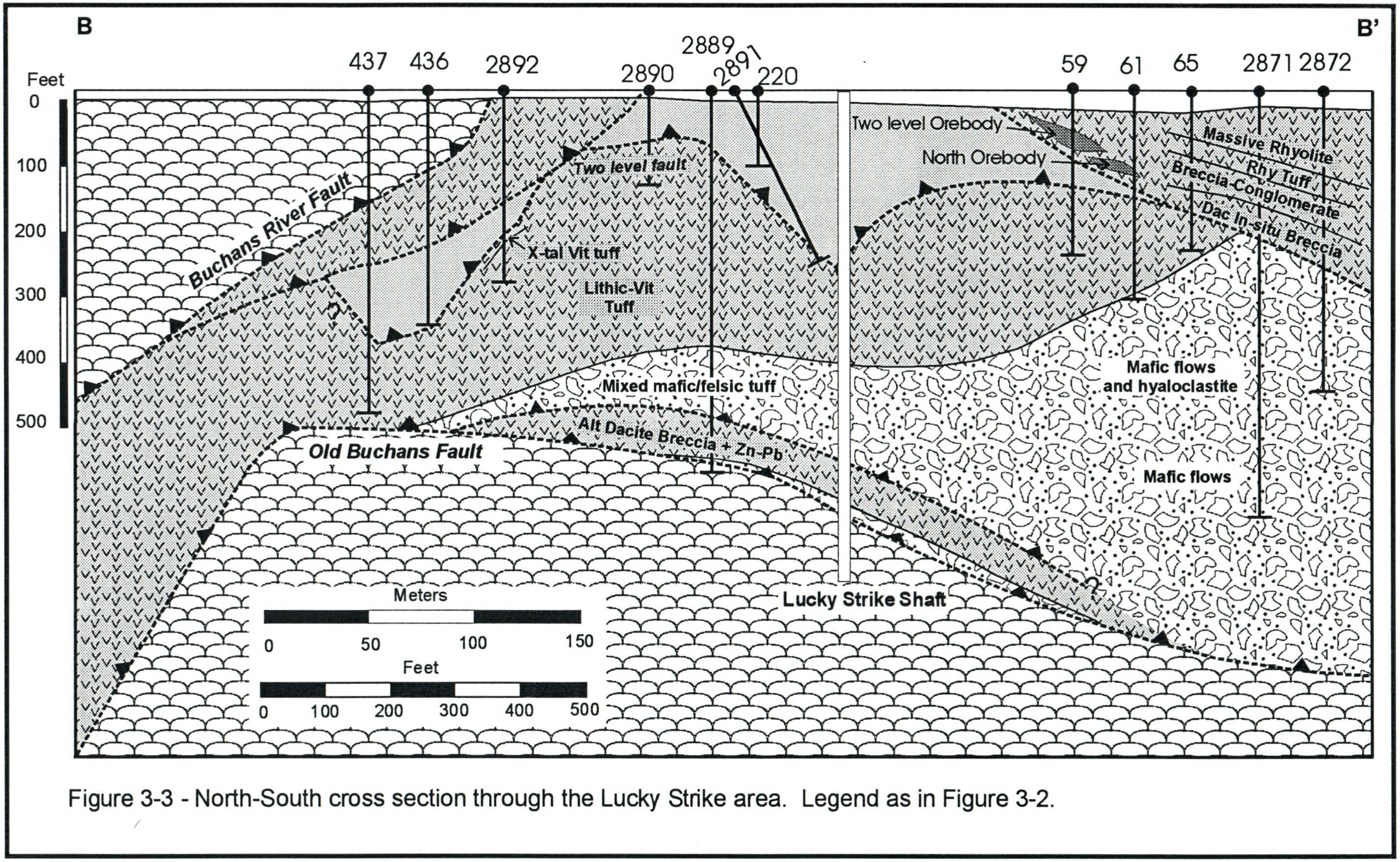


Figure 3-3 - North-South cross section through the Lucky Strike area. Legend as in Figure 3-2.

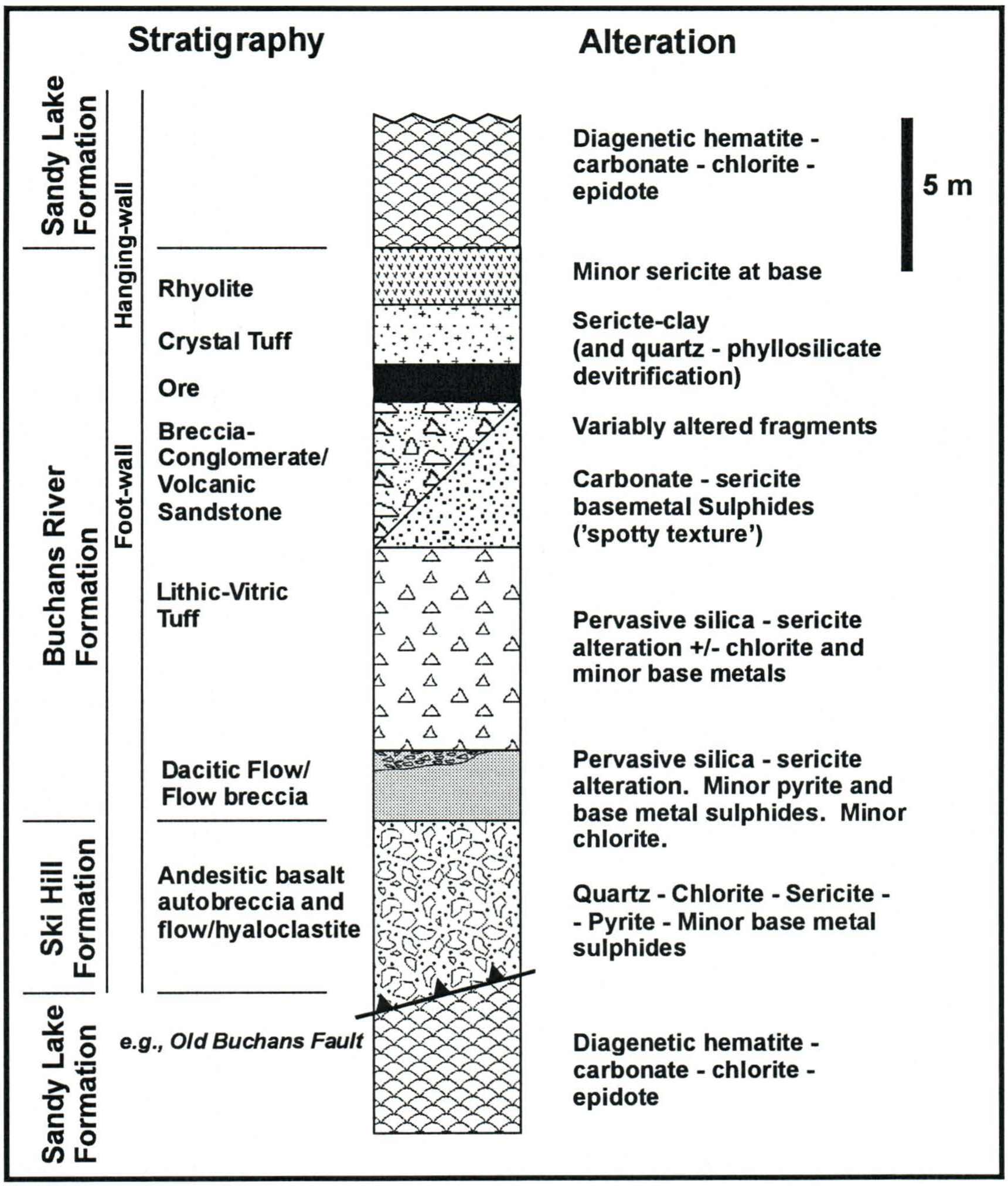


Figure 3-4 - Schematic stratigraphy and alteration in the Lucky Strike area. Note that the alteration assemblage is that in a peripheral (proximal) alteration zone. Note that fluid flow vectors may not be directly vertical, rather inclined upwards.

SYMBOLS

Fault: normal, thrust

1605 Diamond drill hole

Stratigraphy

Sandy Lake Formation
dominantly basaltic pillow lava, pillow breccia and pyroclastics: dominantly volcaniclastic and epiclastic sequences (arkose, arkosic conglomerate).

Buchans River Formation
dacitic to rhyolitic felsic volcanics\volcaniclastics; coarser debris flow breccia-conglomerates +/- ore clasts

Ski Hill Formation
andesitic basalt lava flows, hyaloclastite and breccia

Lundberg Hill (or Woodmans Brook Volcanics)
Unseperated mafic and felsic volcanics

Alteration

Strong potassic alteration and stockwork sphalerite - galena - barite. K-feldspar, sericite +/- silica +/-clay minerals +/- epidote.

Note that incipient alteration occurs throughout most of the BRF and SHF in this area consisting of variable silica - sericite - chlorite - epidote - carbonate - hematite.

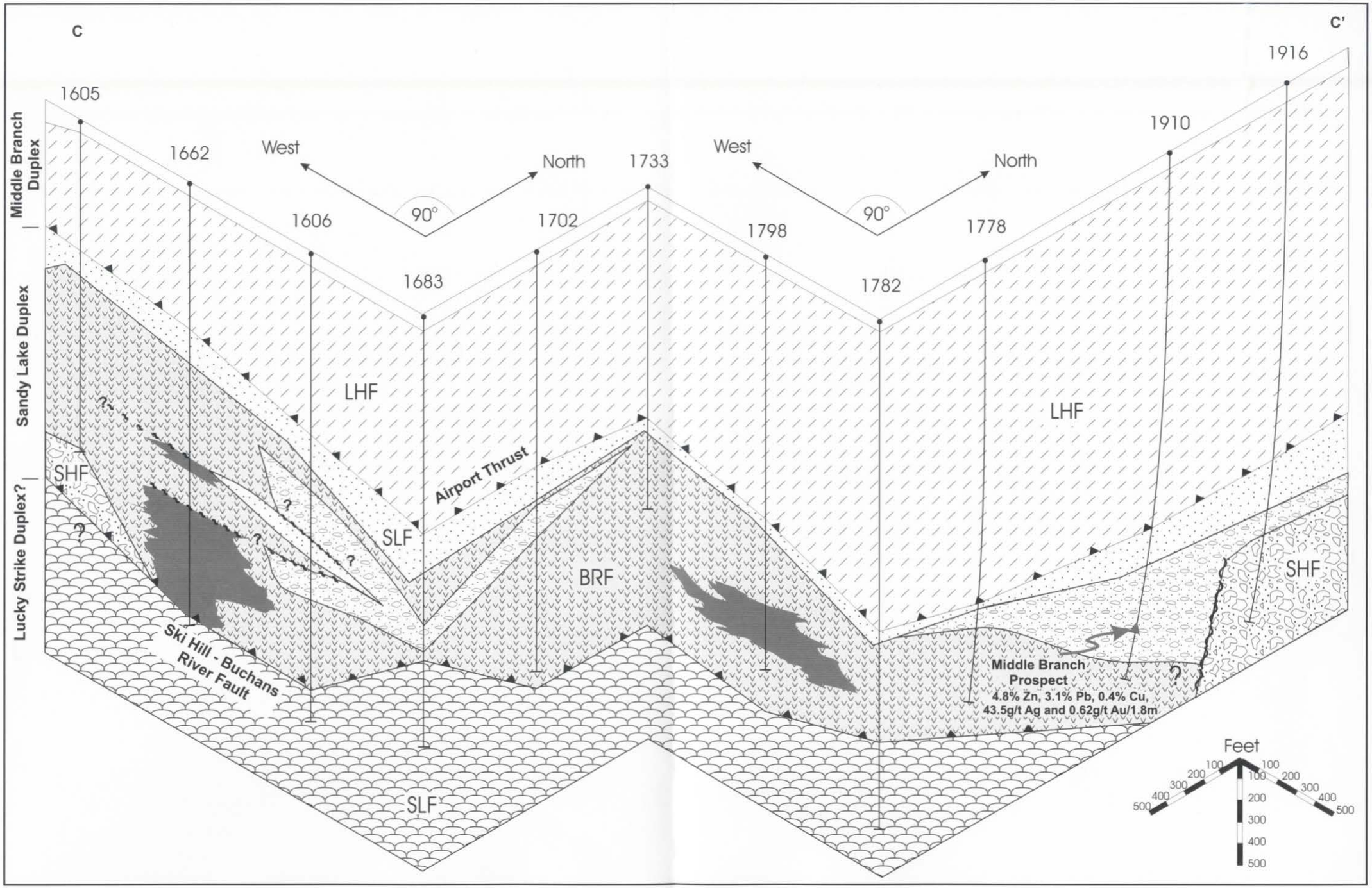


Figure 3-5 - The Middle Branch Alteration Zone. The strongest alteration is confined to the Buchans River Formation felsic volcanics.

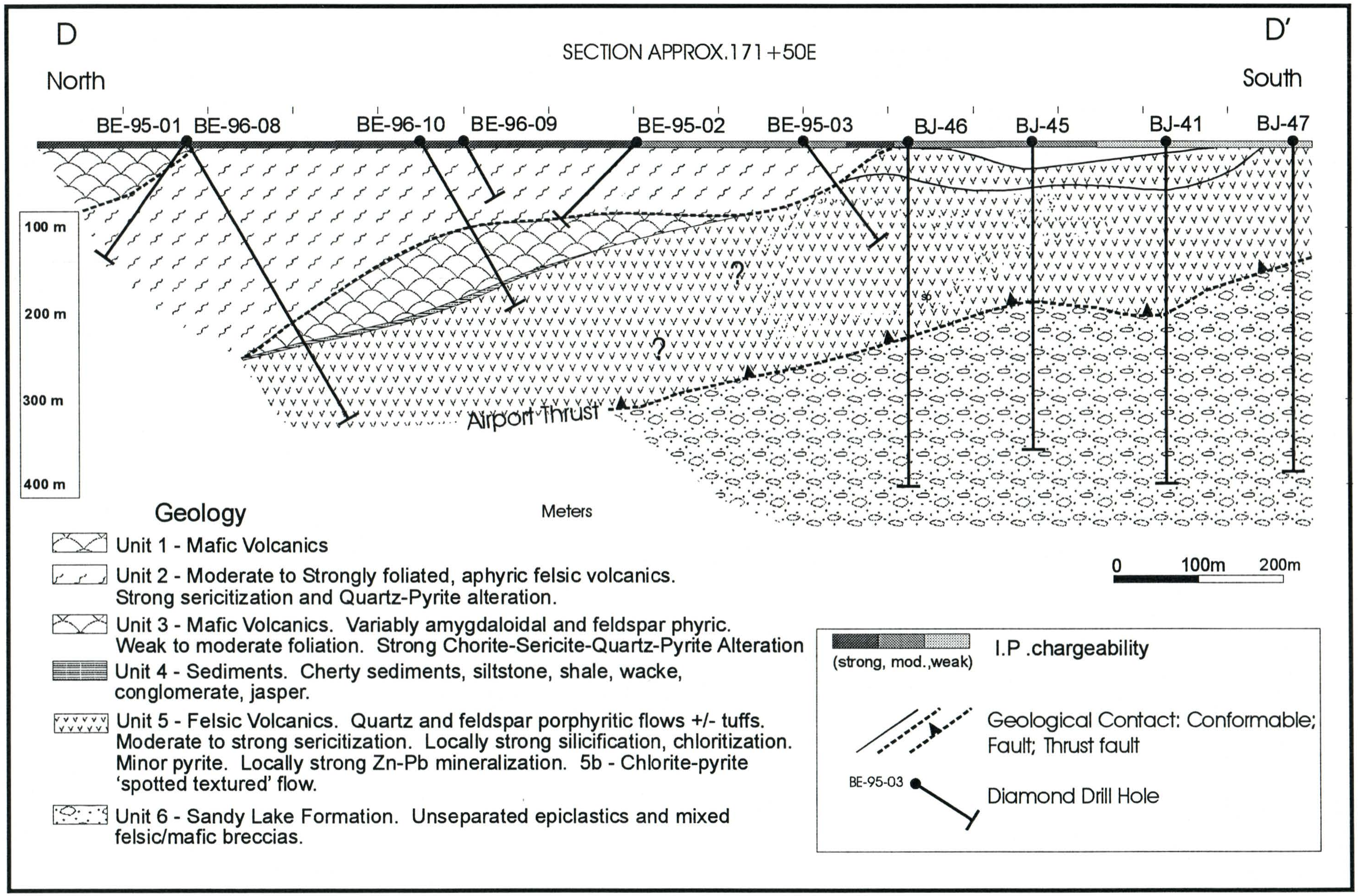


Figure 3-6a - Geological cross section through the Woodmans Brook Zone.

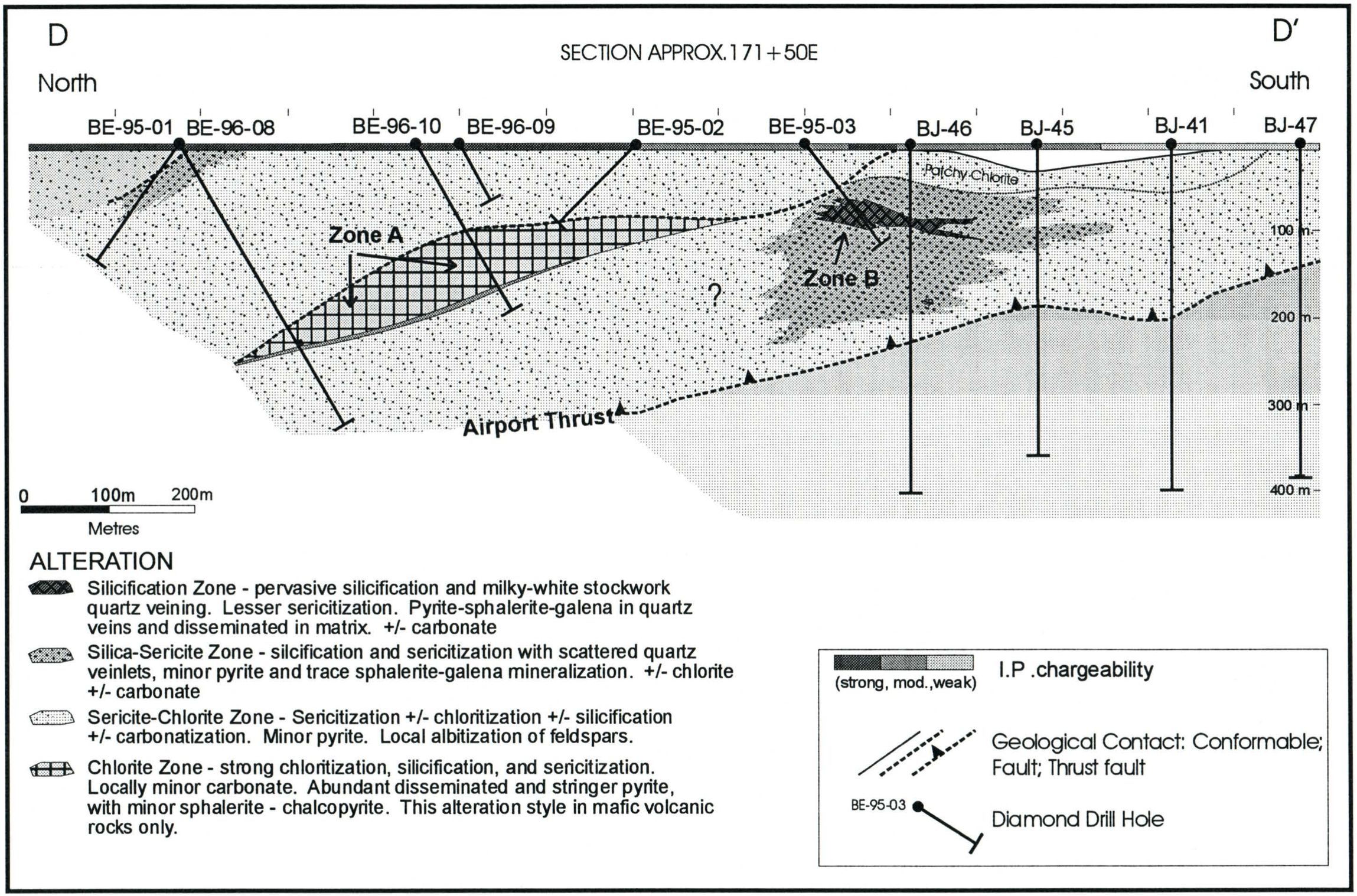


Figure 3-6b - Alteration zonation in the WBZ.

SYMBOLS

Fault: normal, thrust

1605 Diamond drill hole

Cu, Pb, Zn >1000 ppm/>0.5 m
Au > 100 ppb/>0.5 m
Ag > 6 ppm>0.5 m

Stratigraphy

Sandy Lake Formation
dominantly basaltic pillow lava, pillow breccia and pyroclastics: dominantly volcaniclastic and epiclastic sequences (arkose, arkosic conglomerate).

Lundberg Hill (or Powerhouse Volcanics)
Mafic volcanics; Felsic volocanics dominated by flows with much lesser breccia

Alteration

Pyrite - sericite(clays) - dolomite - quartz - chlorite alteration. Minor disseminated (and lesser stringer) chalcopyrite - sphalerite (rare galena) associated with pyrite. Albitization of feldspars may be metamorphic.

Sericite(clay) - quartz - pyrite +/- dolomite +/- chlorite. Anomalous basemetals.

Note that the alteration styles are largely protolithology dependent. Also note grey areas are essentially unaltered.

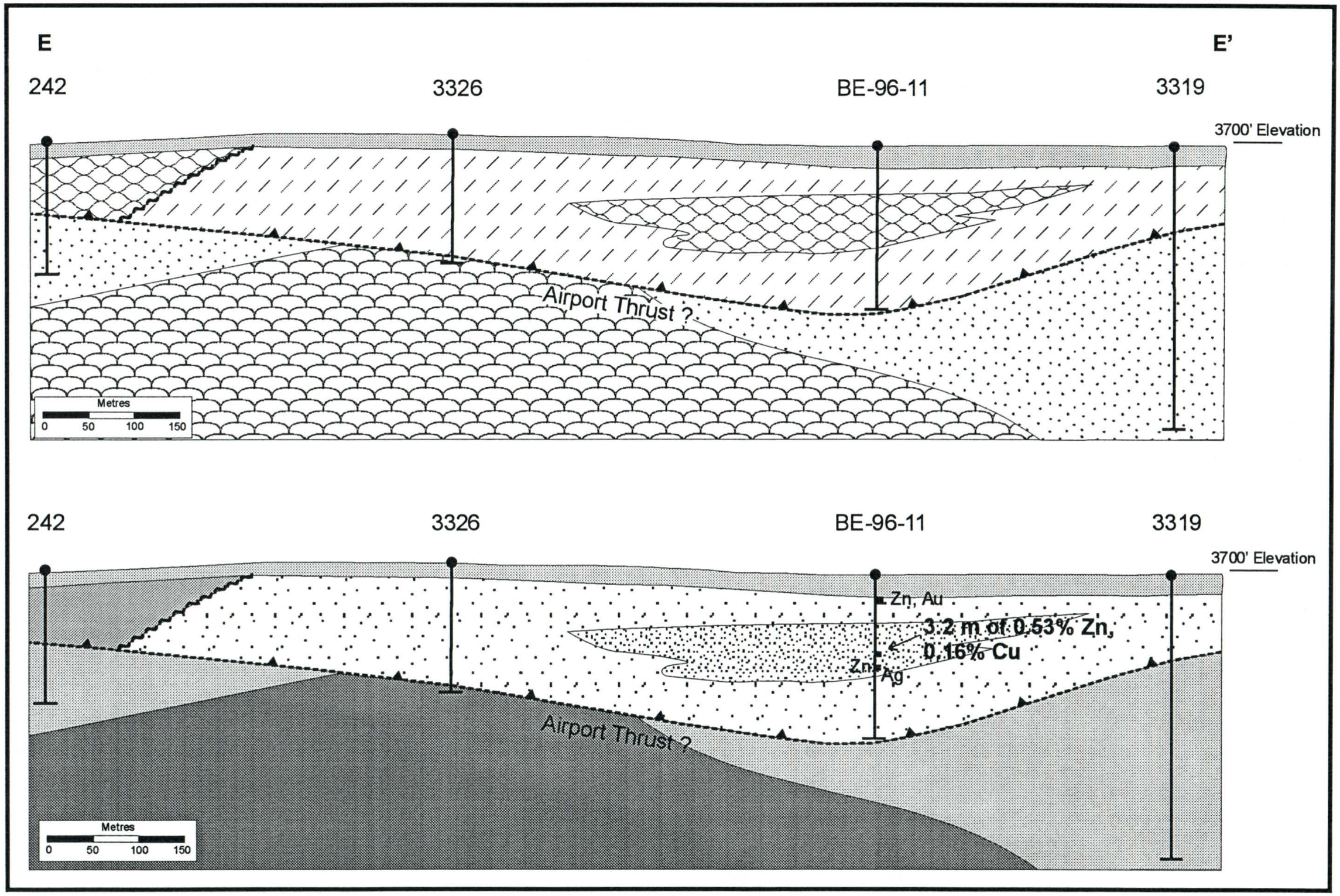


Figure 3-7a - Oblique northwest-southeast section through the Powerhouse Alteration Zone (~ 324°).

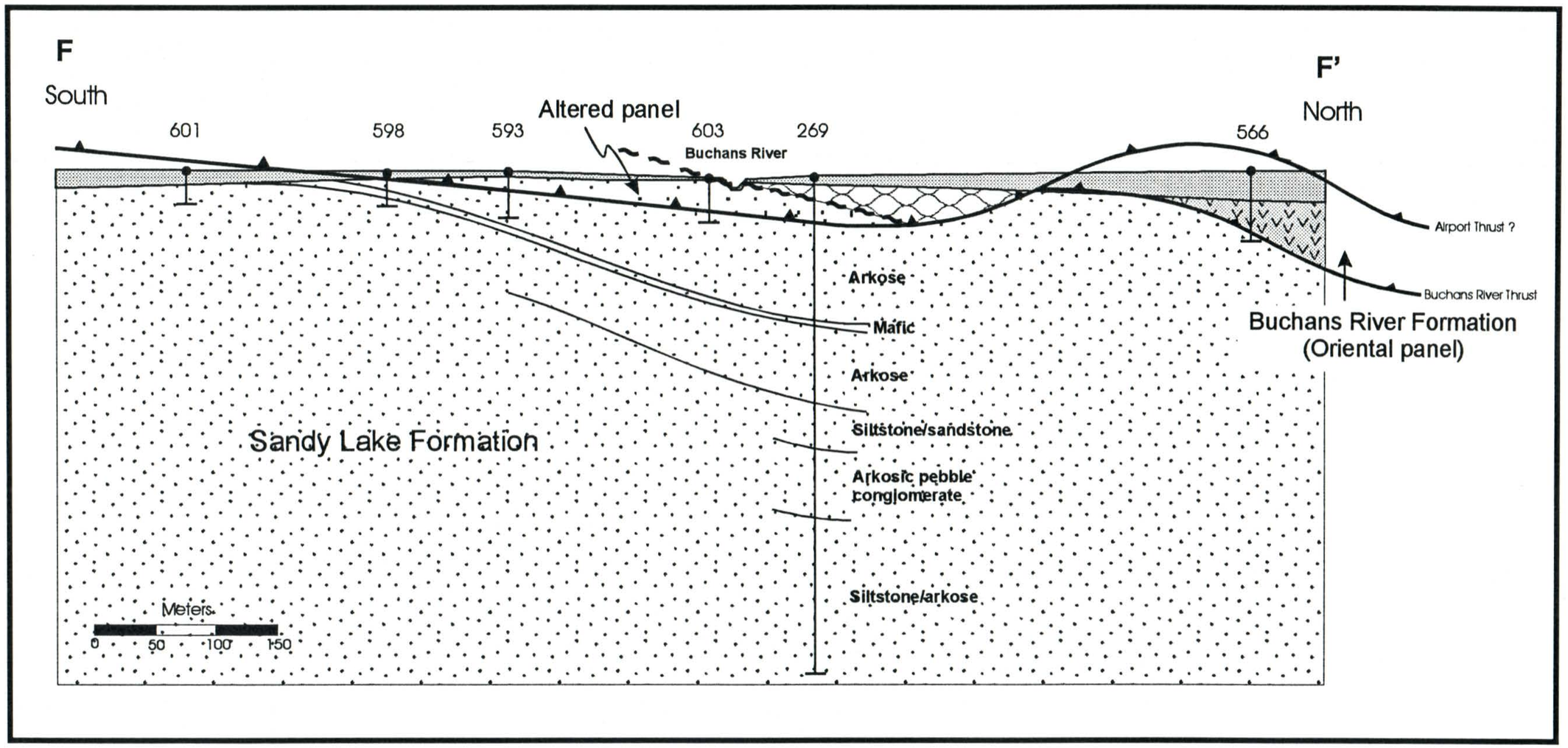


Figure 3-7b - Oblique north-south section through the Powerhouse Alteration Zone (~170°). Note that the alteration zone has thinned substantially here at western limits of the zone near the Airport Thrust.

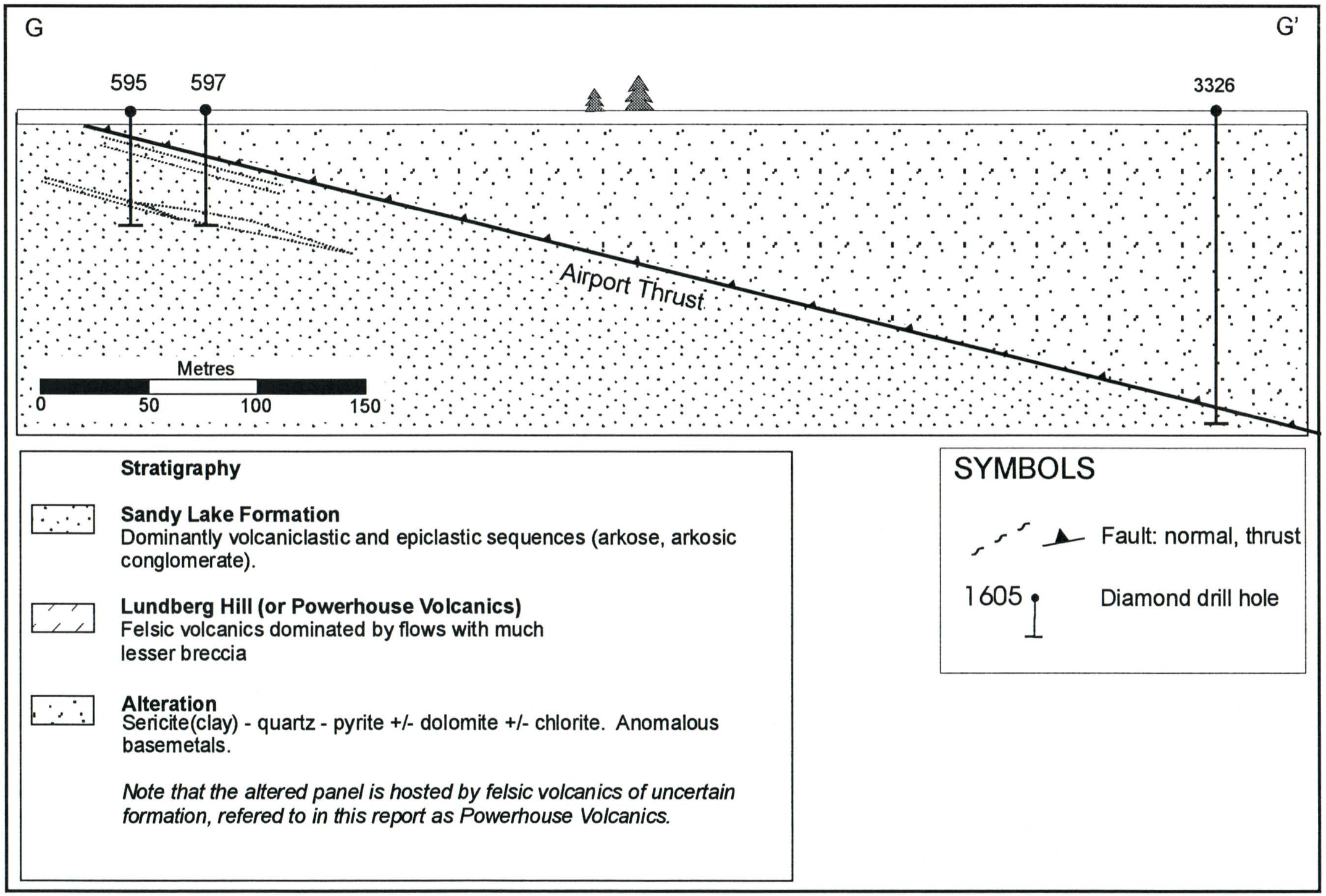


Figure 3-7c - Oblique east-west section through the Powerhouse Alteration Zone.

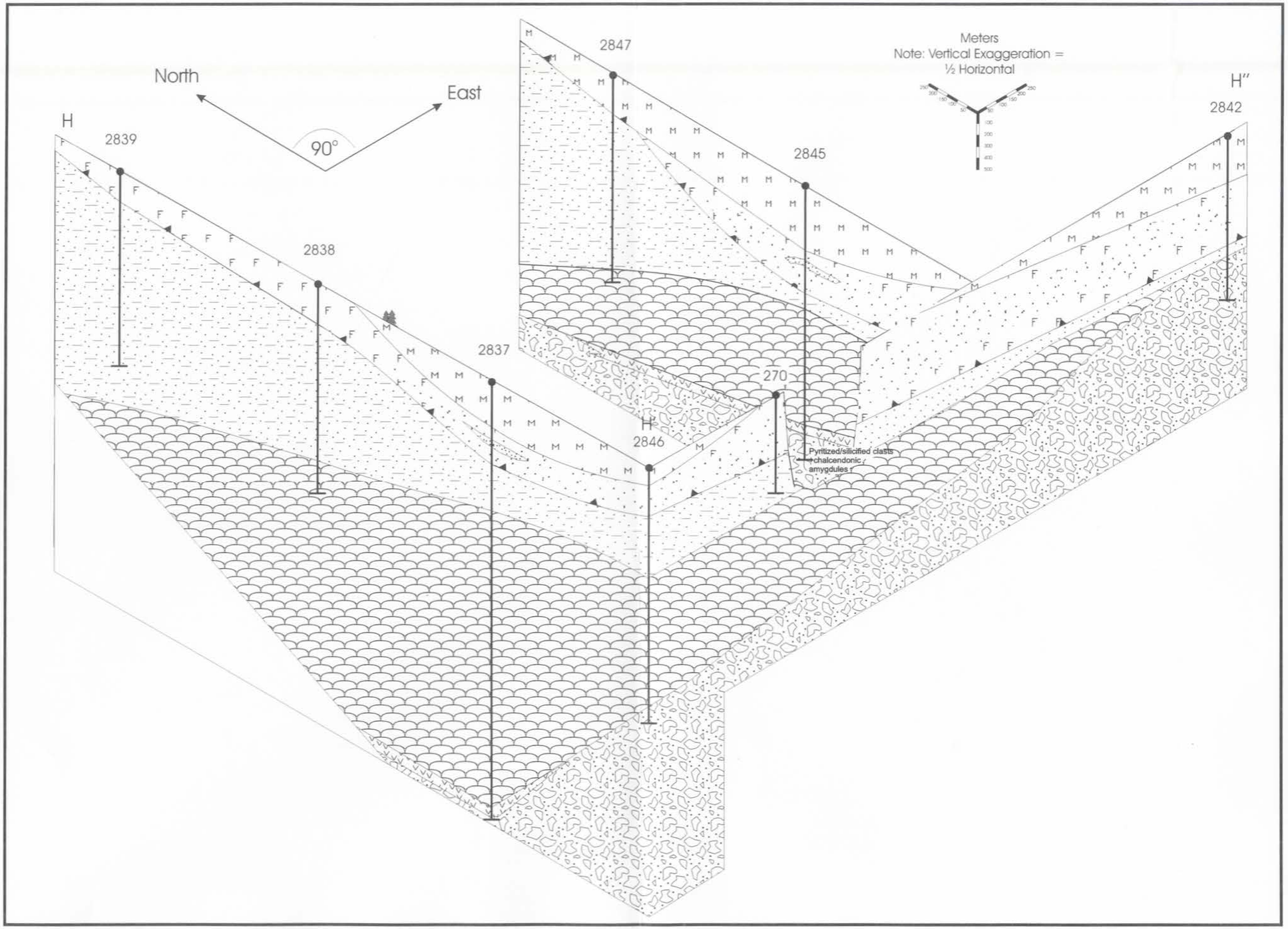


Figure 3-8a - Block model of the Airport Alteration Zone (north).

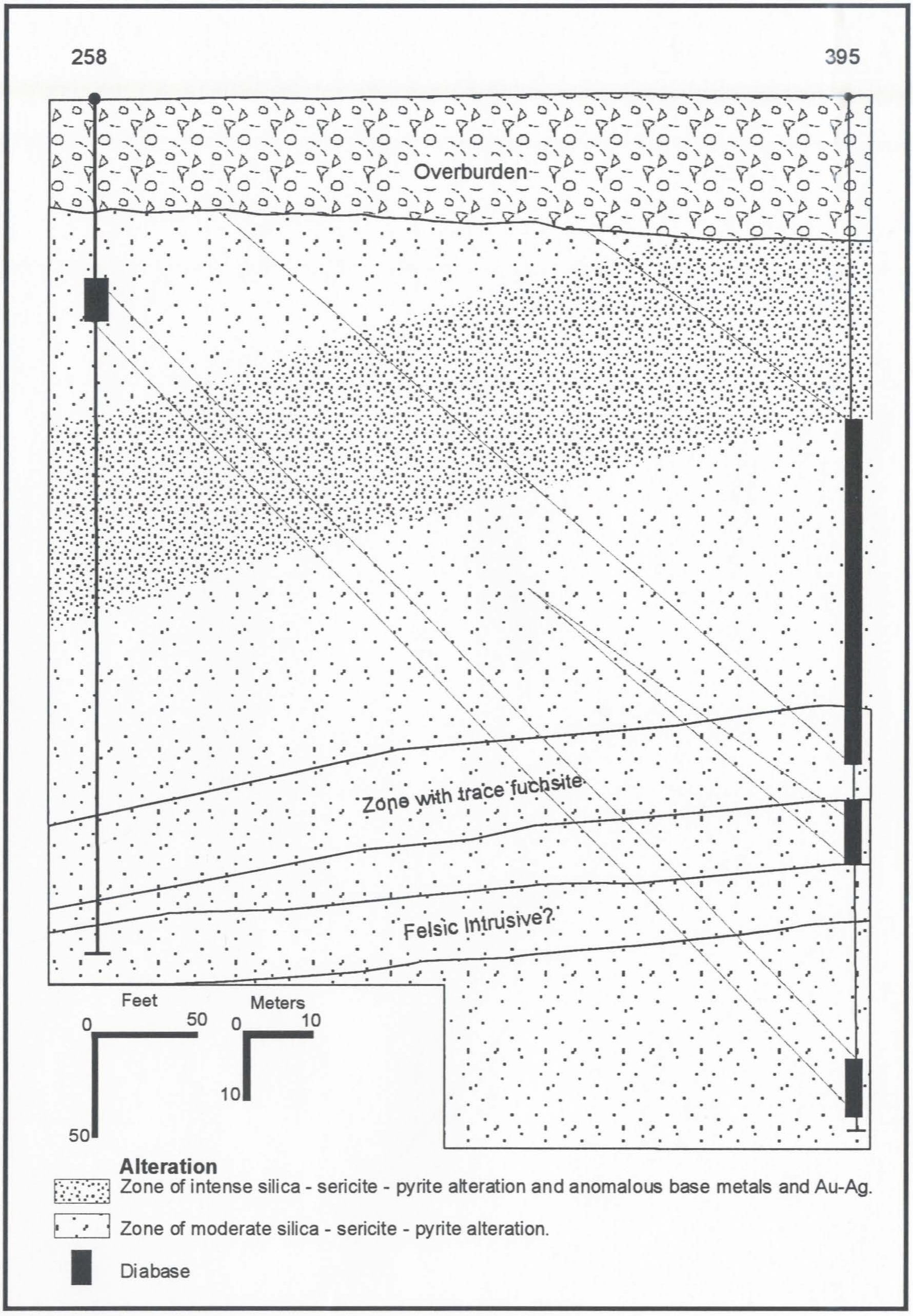


Figure 3-9 - Northwest-southeast cross-section through the Airport South Zone. Host rocks are dacitic volcanic rocks of uncertain association.

LEGEND

Fault: normal, thrust

1605 Diamond drill hole

Stratigraphy

Sandy Lake Formation
dominantly basaltic pillow lava, pillow breccia and pyroclastics: dominantly volcaniclastic and epiclastic sequences (arkose, arkosic conglomerate).

Buchans River Formation
dacitic to rhyolitic felsic volcanics\volcaniclastics

Ski Hill Formation
andesitic basalt lava flows, hyaloclastite and breccia

Lundberg Hill Formation?
Felsic Volcanics; Mafic Volcanics

Alteration

Localized chloritic alteration with lesser silica, carbonate and sericite alteration. Pyrite associated with quartz in stringers with minor sphalerite - chalcopyrite.

Incipient, variable alteration sericite - silica - chlorite - pyrite.

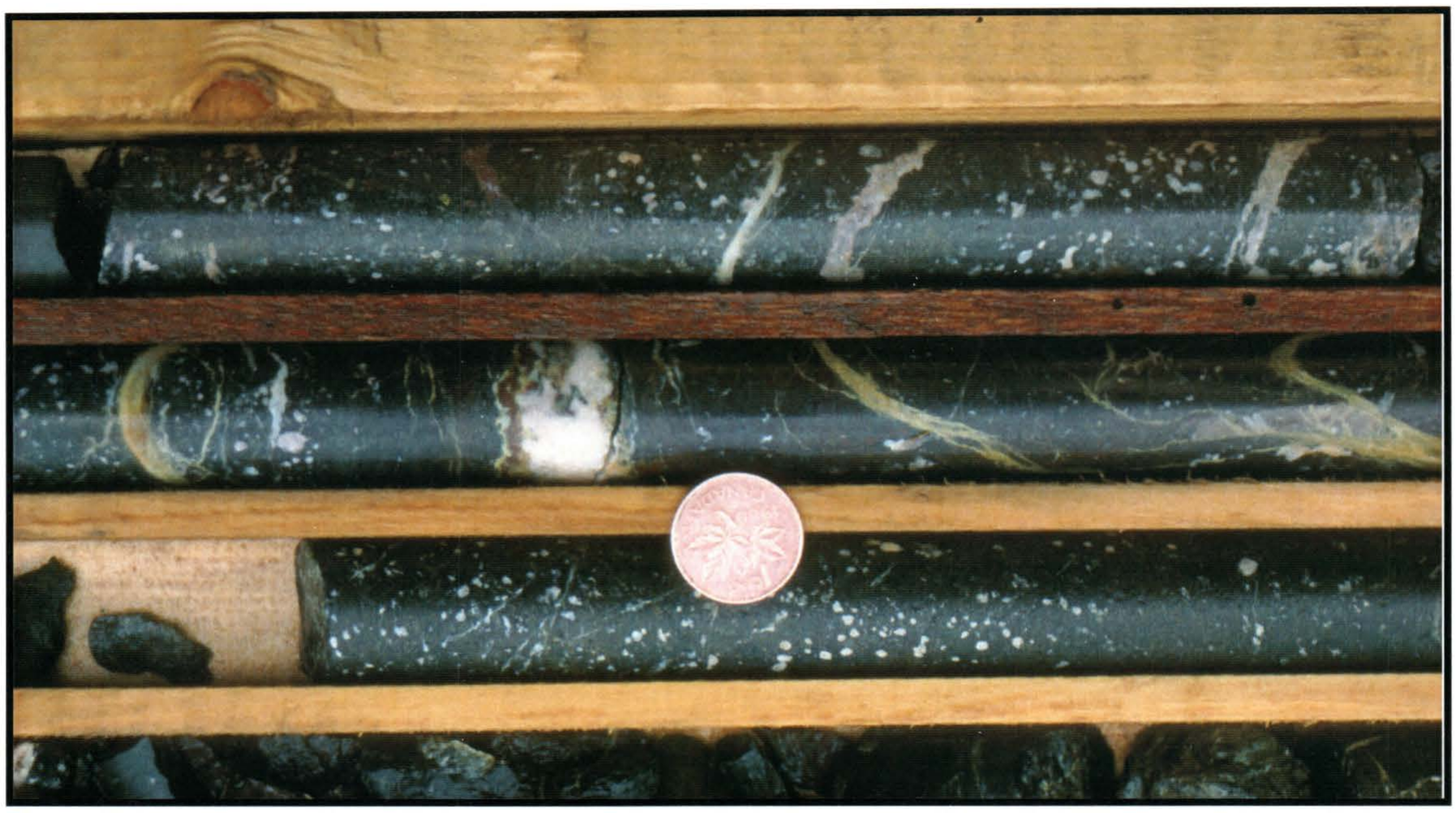


Plate 3-1 - Chlorite - Carbonate - Epidote - Hematite altered SLF mafic volcanics. This alteration assemblage is not related to the ore-forming hydrothermal fluids. DDH 542, ~570'.



Plate 3-2 - Quartz and sulphide-rich stockwork mineralization below the Lucky Strike orebody. DDH 542, 0-32'.

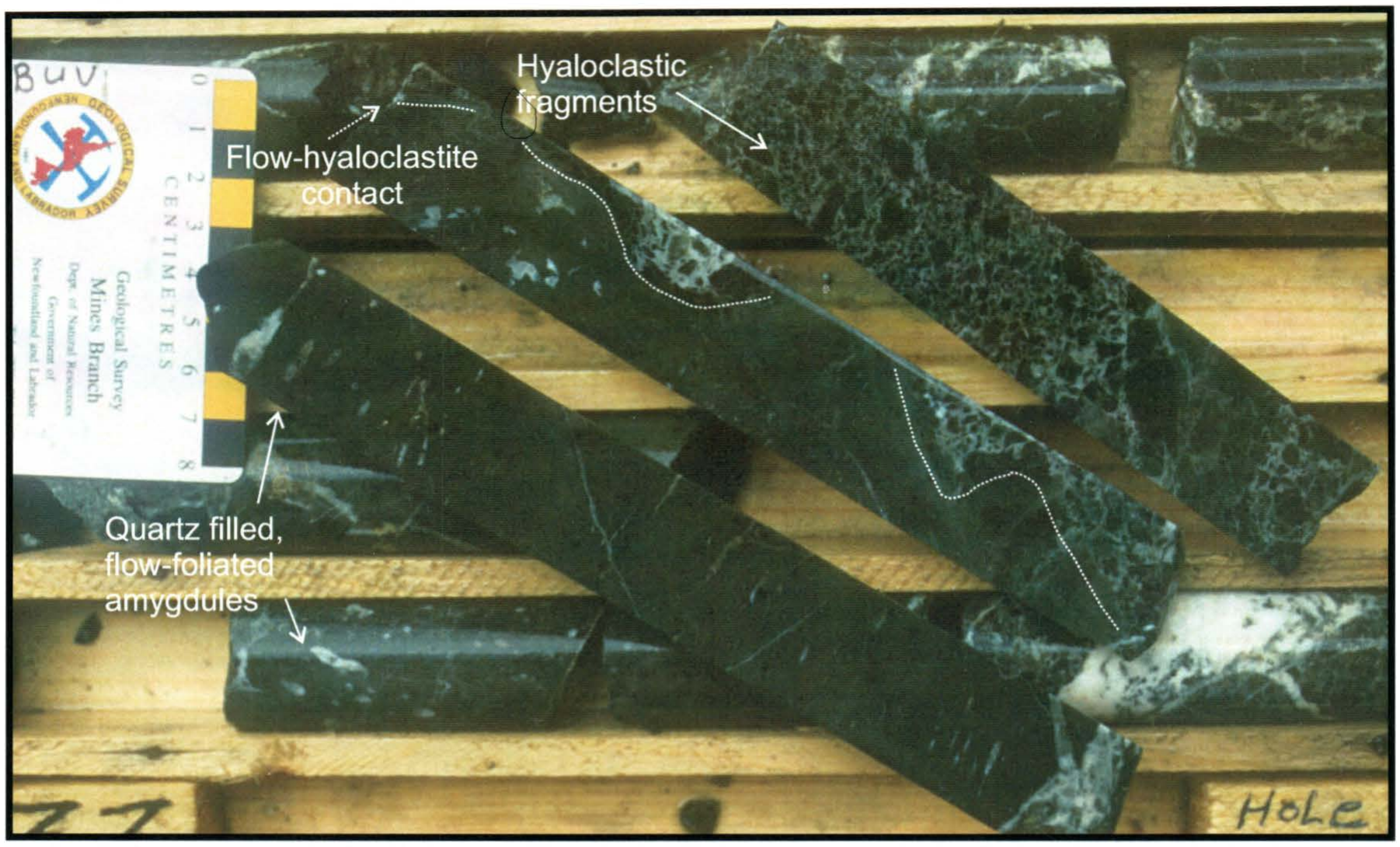


Plate 3-3 - Mafic flow - hyaloclastite sequence of the SHF. Note chloritic alteration of matrix and quartz infill of elongate amygdules and silicic replacement of matrix between hyaloclastite fragments. DDH 2871, ~533'.



Plate 3-6 - BRF aphyric dacitic flow/flow breccia. Note the strong alteration to sericite and silica. The sample also contains minor sphalerite and galena. DDH 2889, ~516'.

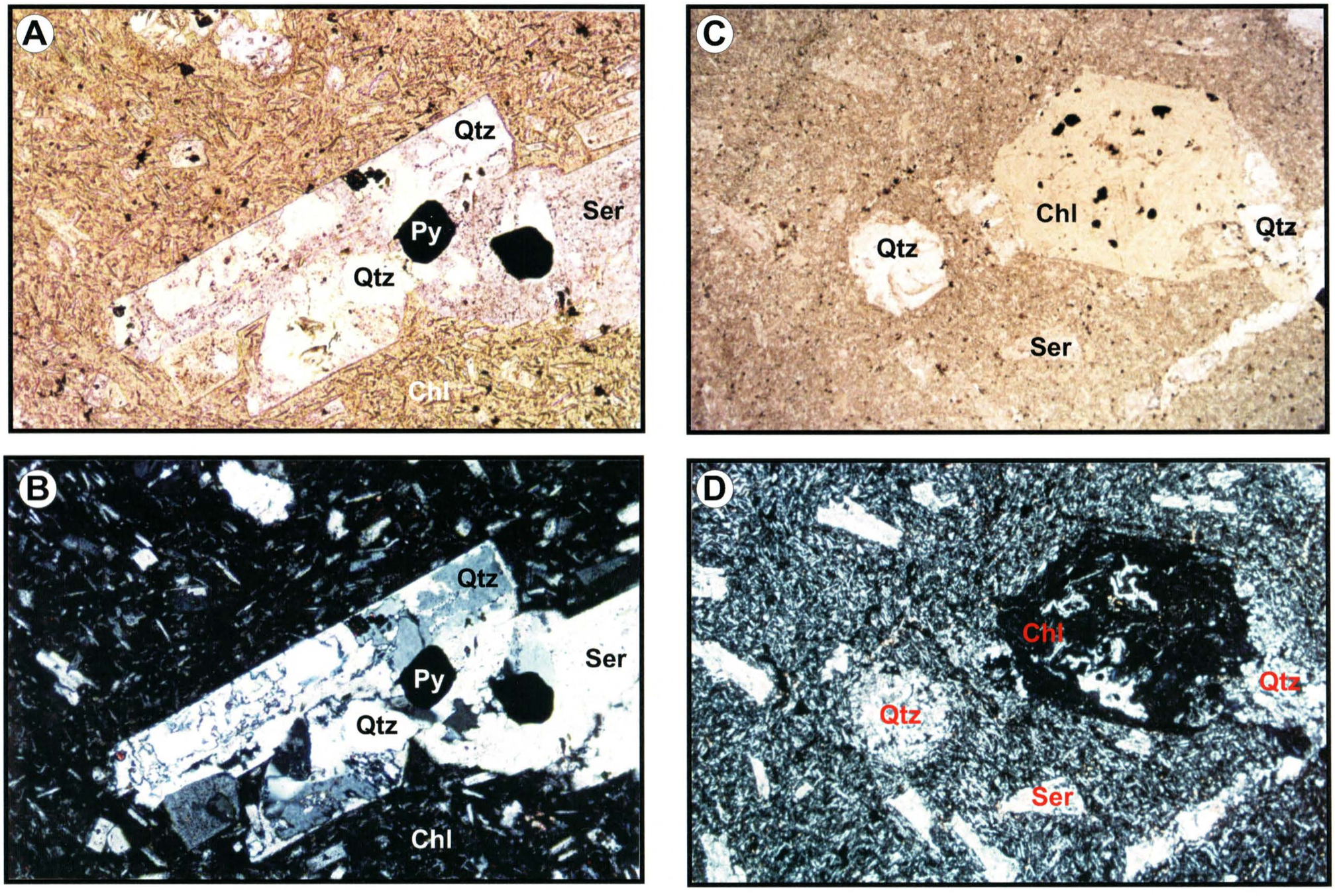


Plate 3-4 - Various alteration textures in the SHF basatic andesites. A) PPL and B)XPL illustrate silica-pyrite and sericite replacement of a feldspar phenocryst. Groundmass feldspars are altered to the same assemblage but glass has been chloritized. Sample LS-39, FOV=1.3 mm. C)XPL and D)PPL illustrate chlorite, quartz and sericite replacement of phenocrysts. The larger phenocrysts may be more mafic phases while the smaller ones were probably feldspar. Sample LS-12, FOV=5 mm.

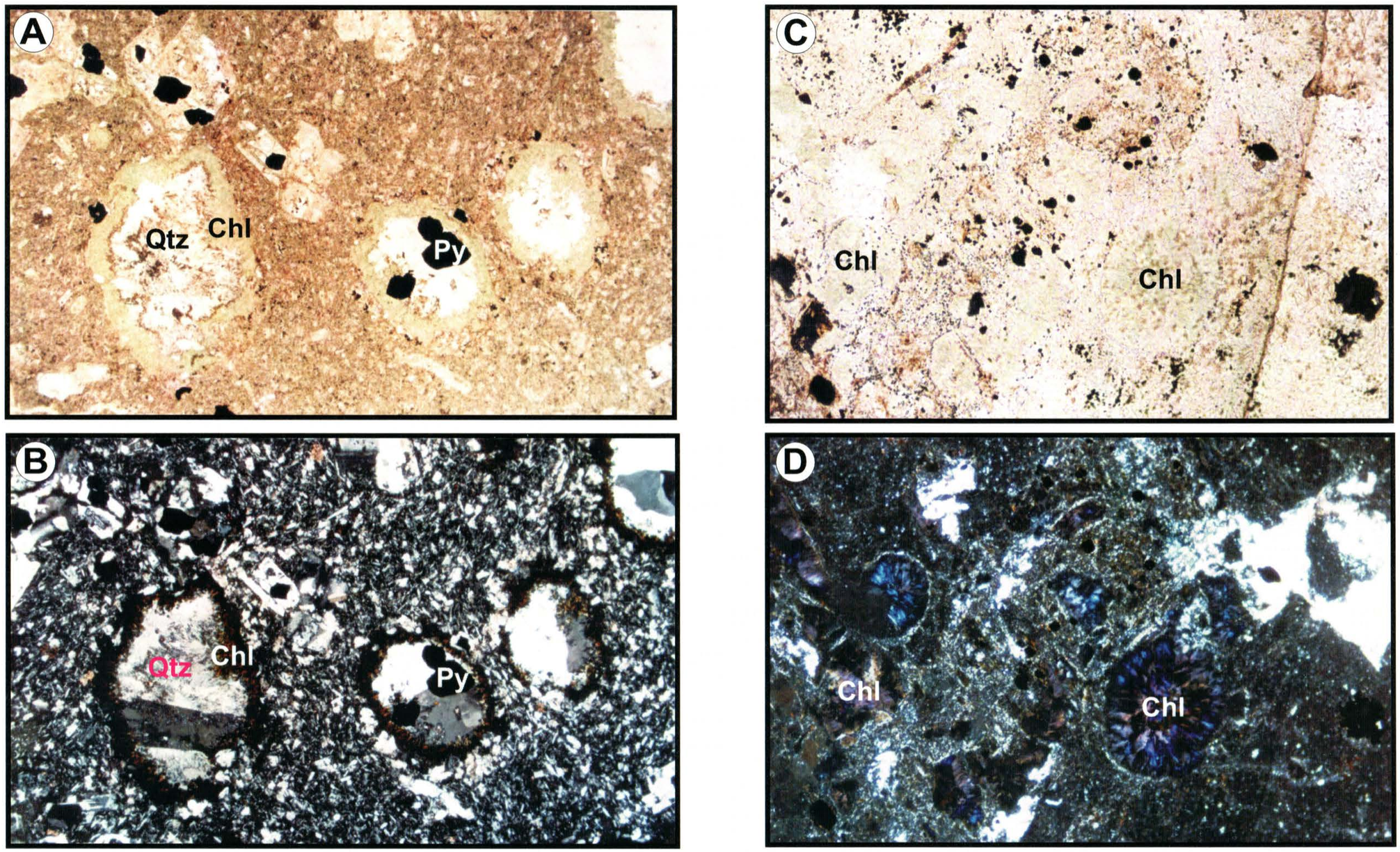


Plate 3-5 - Photomicrograph of amygdules in SHF basaltic andesites typical of proximal alteration. A) PPL and B) XPL are from sample LS-39. Amygdules are zoned inwards from Mg-Fe chlorite (*pycnochlorite*) to quartz-pyrite. FOV=5 mm. C)PPL and D)XPL from sample LS-35. This is the same unit but even closer to the ore horizon than LS-39. Amygdules are filled with Mg-rich chlorite (*chlinochlore-penninite*). Note the weaker pleochroism than previous and Berlin-blue and purple birefringence. FOV=1.3 mm.



Plate 3-7 - Pyroclastic/volcaniclastic sequence within the BRF dacitic volcanic sequence. DDH, 2889, ~125'-145'



Plate 3-8 - Vitric and lithic tuff dominated by BRF dacitic volcanic fragments. Vitric fragments are wispy and arcuate shaped and vary from light to darker green as a result of very fine sericite-chlorite replacement. Lithic fragments of the same composition are typically more blocky and vary in colour from light grey to pinkish. The matrix is a silicic mass probably produced by the quartz replacement of the finer material. DDH 2889, ~360.

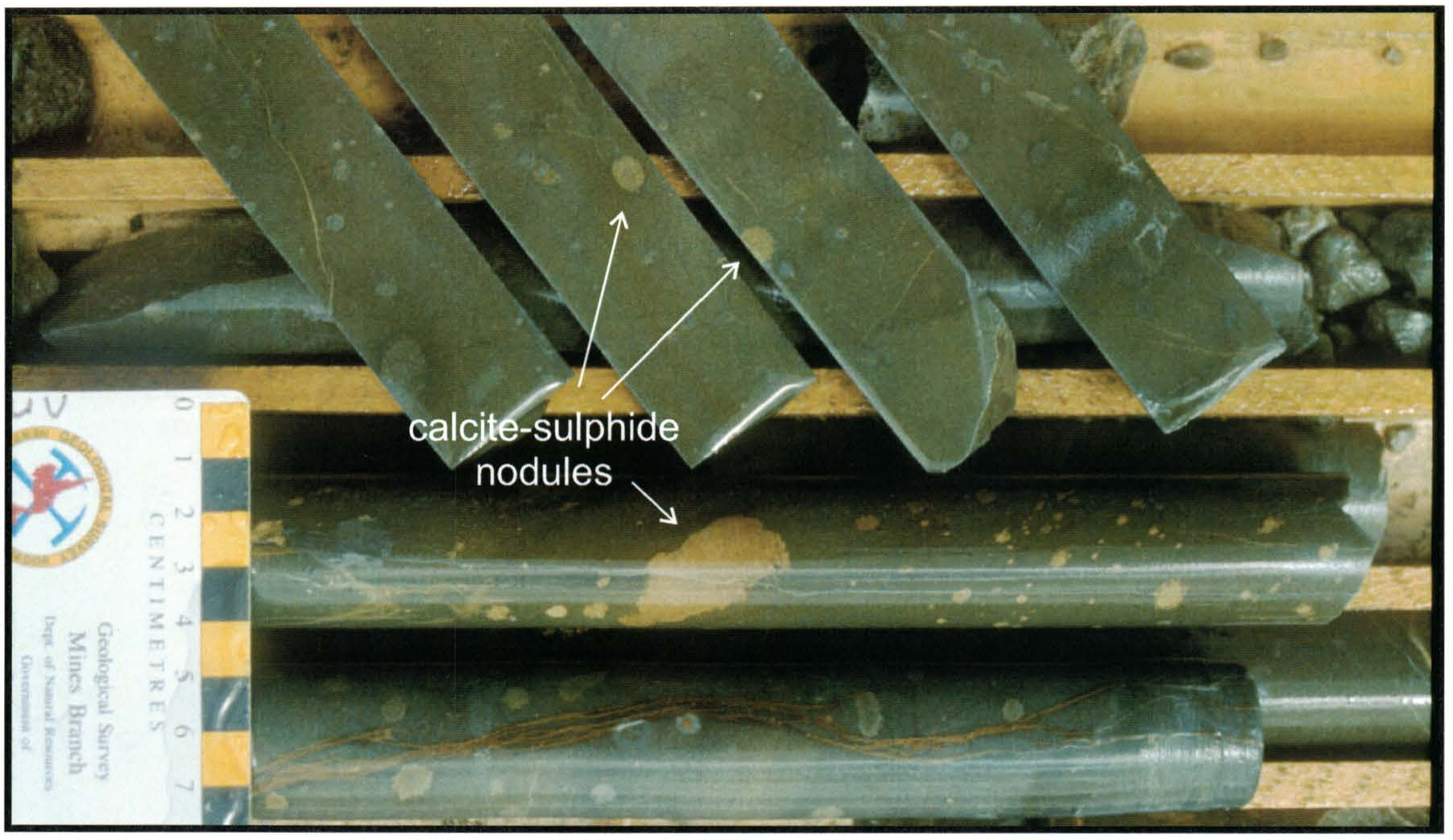


Plate 3-9 - Calcite-sulphide nodules in volcanic sandstone within the BRF. DDH 2889, ~176'-212'.

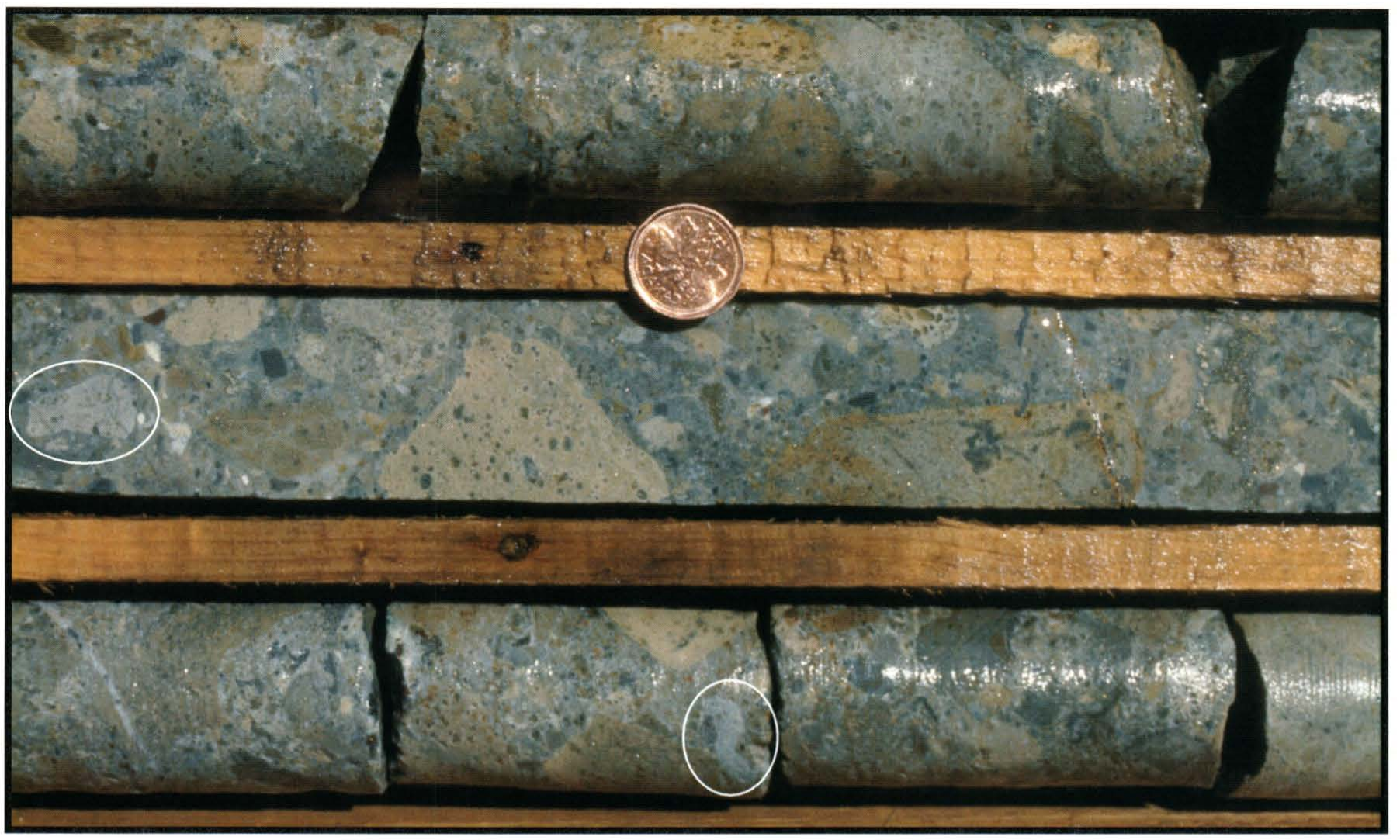


Plate 3-10 - Ore horizon breccia conglomerates containing altered clasts of both mafic and felsic lithologies as well as a few sulphide clasts (circled). Stringer sulphide mineralization also locally occurs in this unit suggesting contemporaneous hydrothermal activity and brecciation of co-existing ores. DDH 237, ~542'.



Plate 3-11 - Chlorite-sericite(clay) altered crystal-vitric rhyodacitic tuff of the BRF in the Lucky Strike Zone. DDH 196, ~526'.

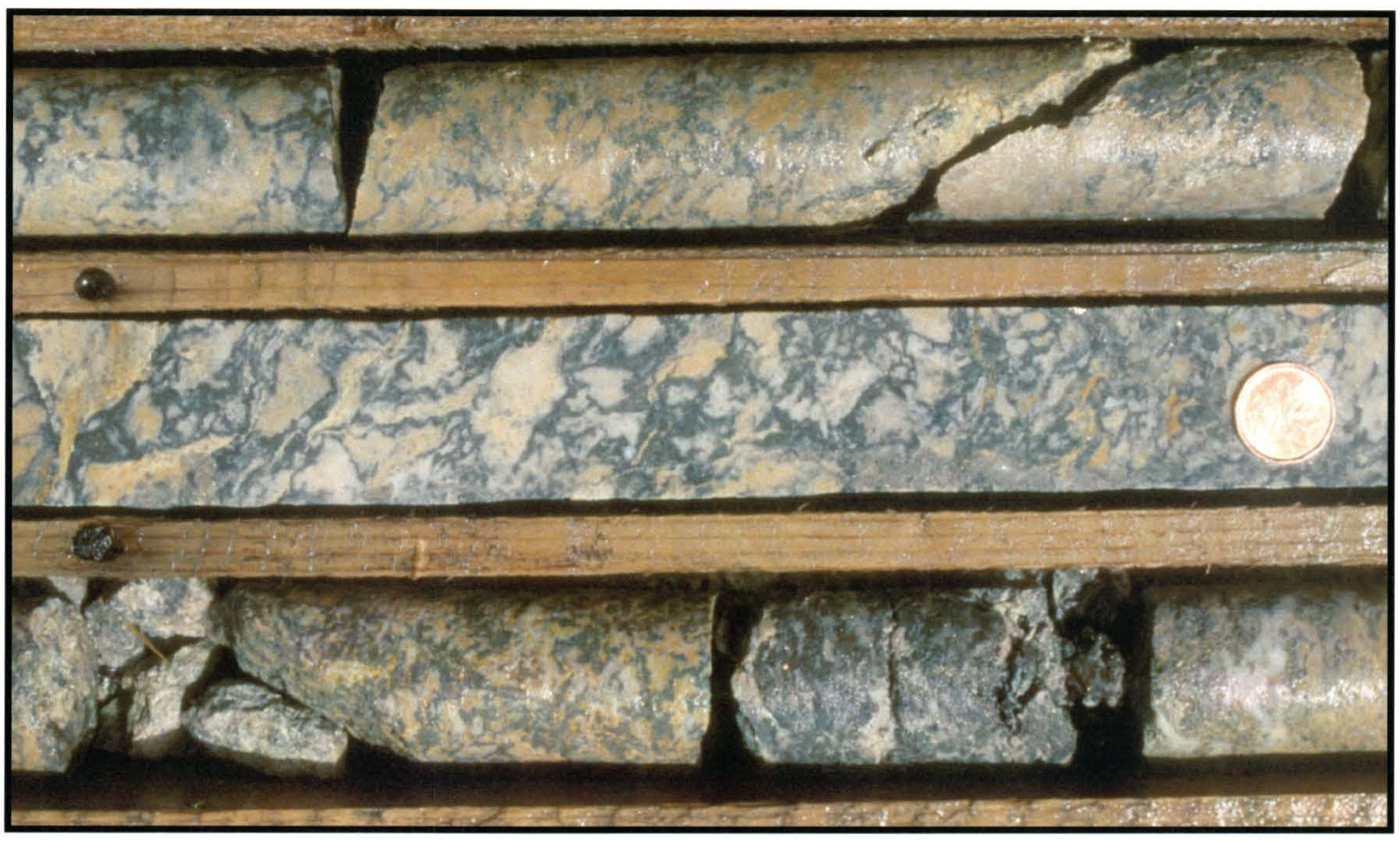


Plate 3-13 - Strongly potassic altered (K-feldspar, sericite, silica, pyrite) pumiceous tuff of the BRF. DDH 237, ~443'.

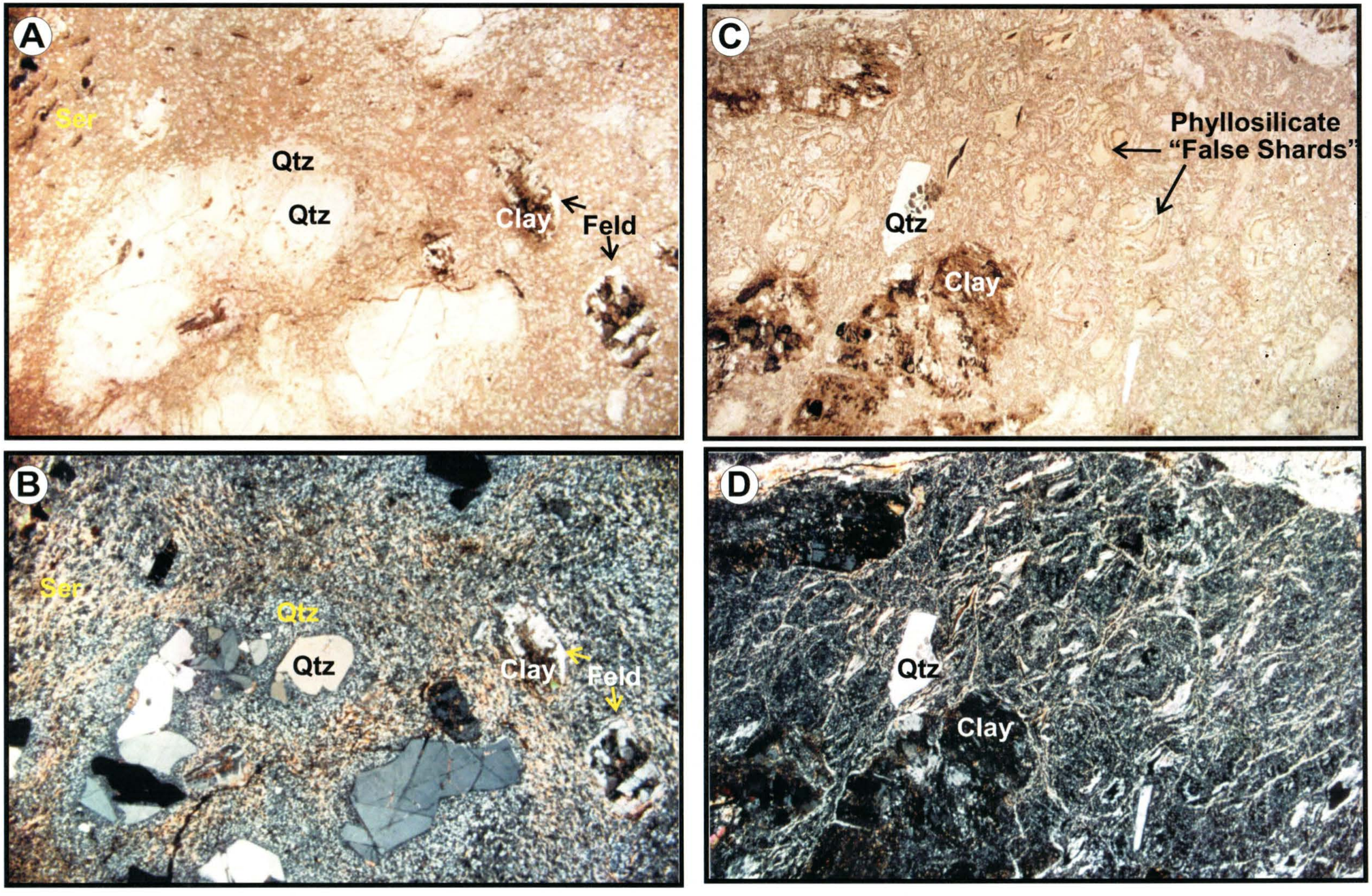


Plate 3-12 - Photomicrographs of devitrified and altered BRF rhyodacites. A flow is shown in A)PPL and B)XPL with quartz and plagioclase phenocrysts. The quartz phenocrysts are fractured and partly dismembered, showing slight resorption. The plagioclase phenocrysts are partly clay altered. Note the very fine-grained quartz in the groundmass that has nucleated on the larger quartz phenocrysts but not the plagioclase. Sample LS-25, FOV=7 mm. A more vitric flow is shown in C)PPL and D)XPL. This sample is also quartz and feldpsar porphyritic and shows well developed *classic perlitic fracturing*. The fracturing is emphasized by subsequent quartz-phyllosilicate devitrification producing a "false shard texture" (*cf.* Allen, 1988). Sample LS-33, FOV=5 mm.

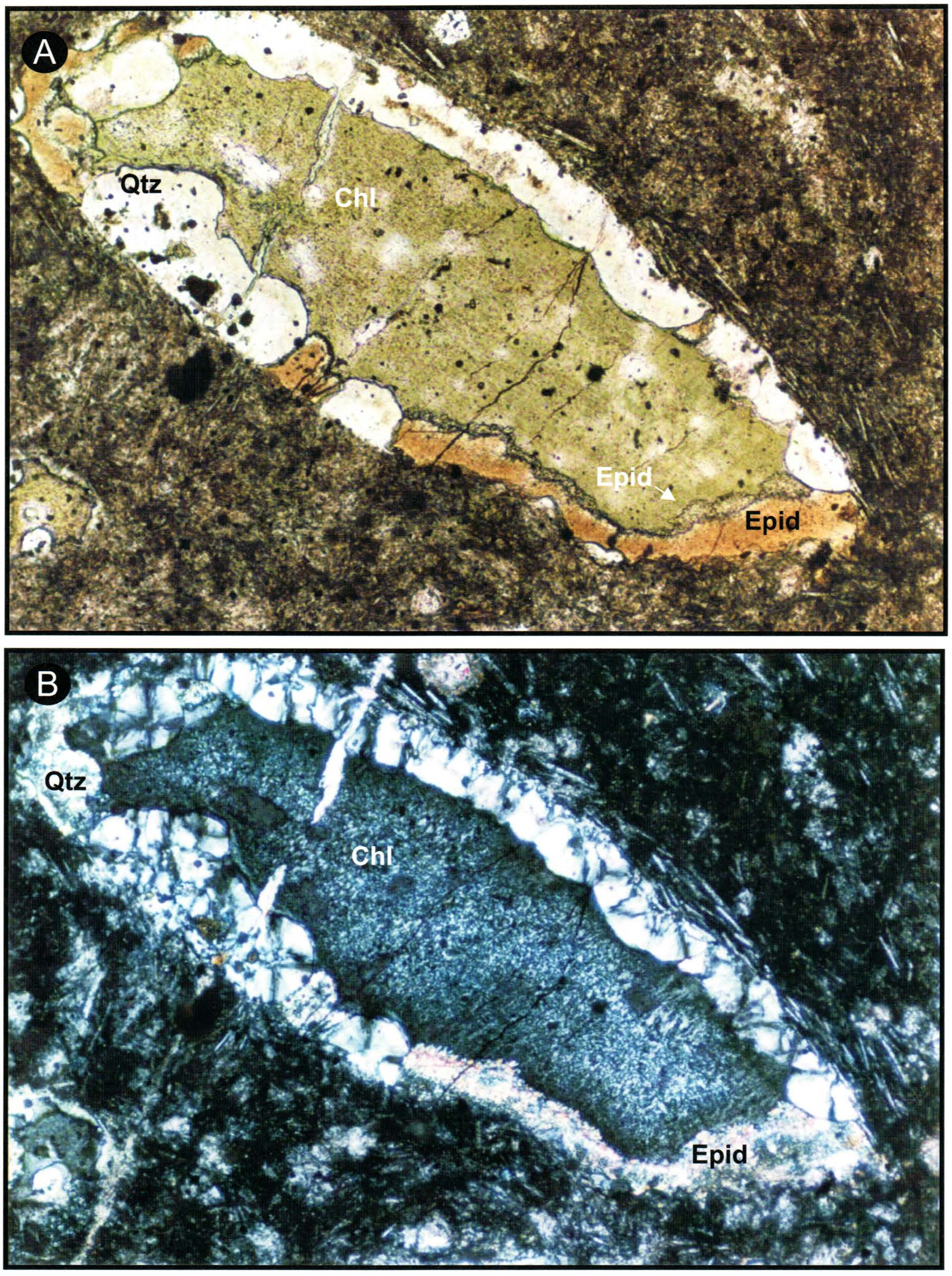


Plate 3-14 - Photomicrograph of zoned amygdules typical of weak, distal alteration in the SHF basaltic-andesite. Epidote and quartz (spheroidal) are the earliest phases and Fe-Mg chlorite is later. Sample LS-01 (Ski Hill Locality). a) PPL, Magnification is 10X, field of view is 1.3 mm. B) same view in XPL.

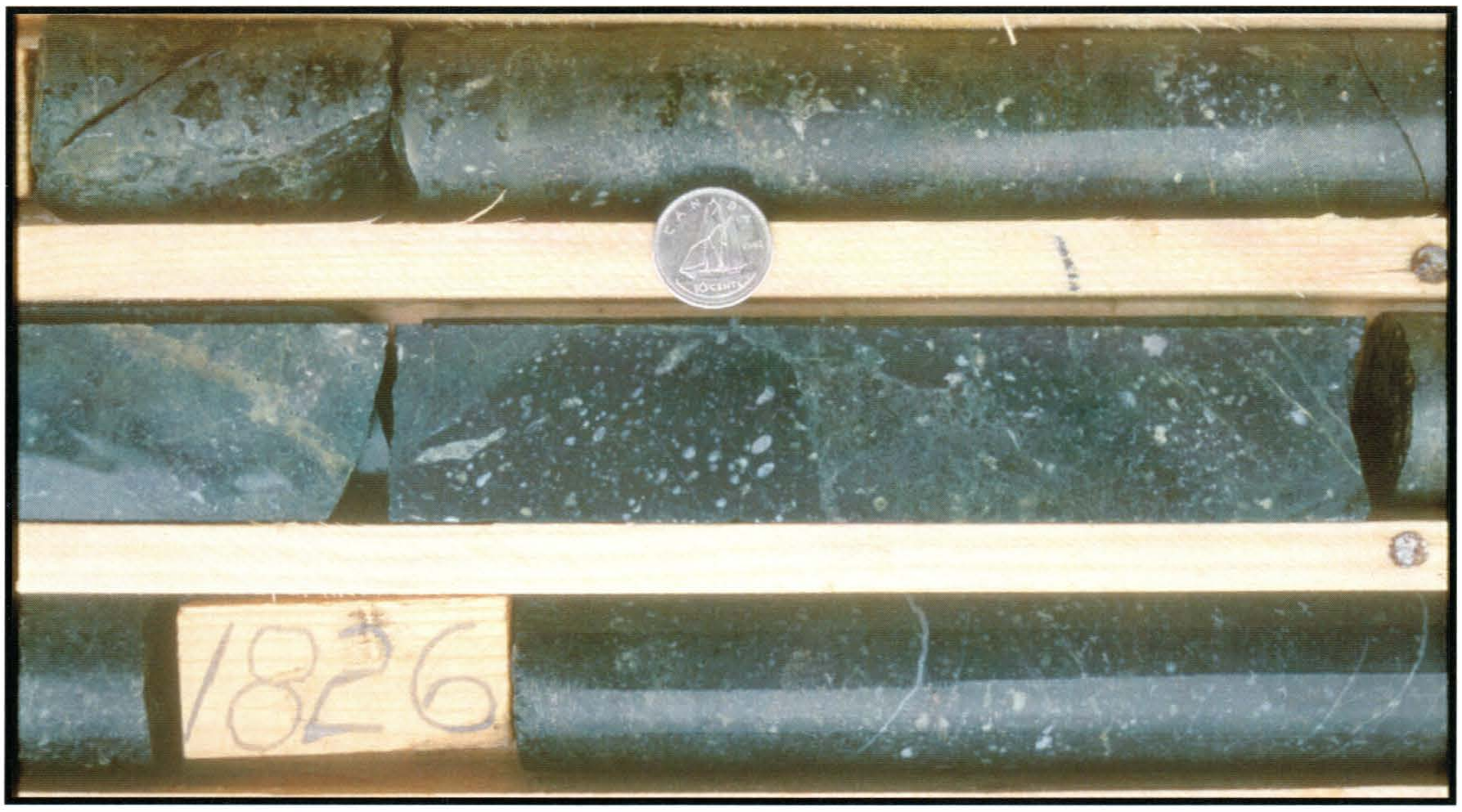
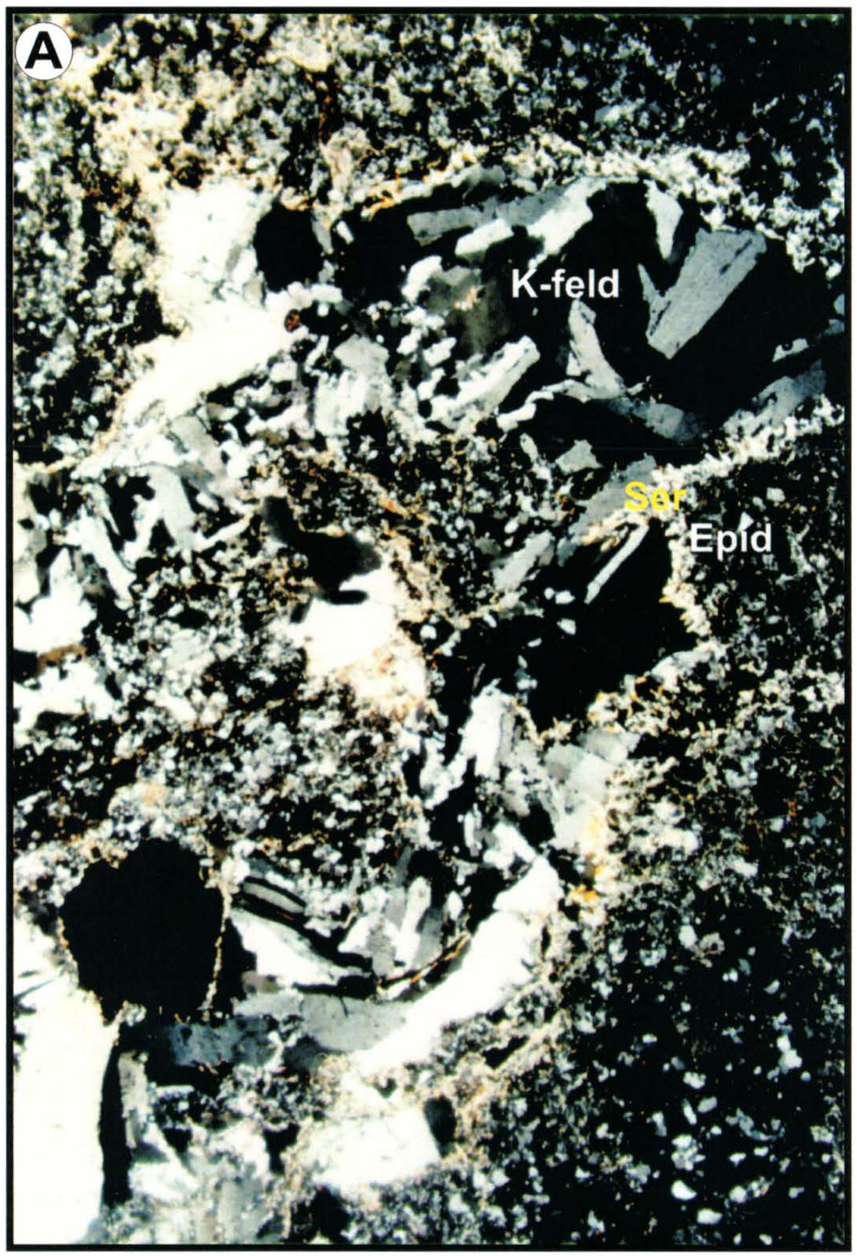
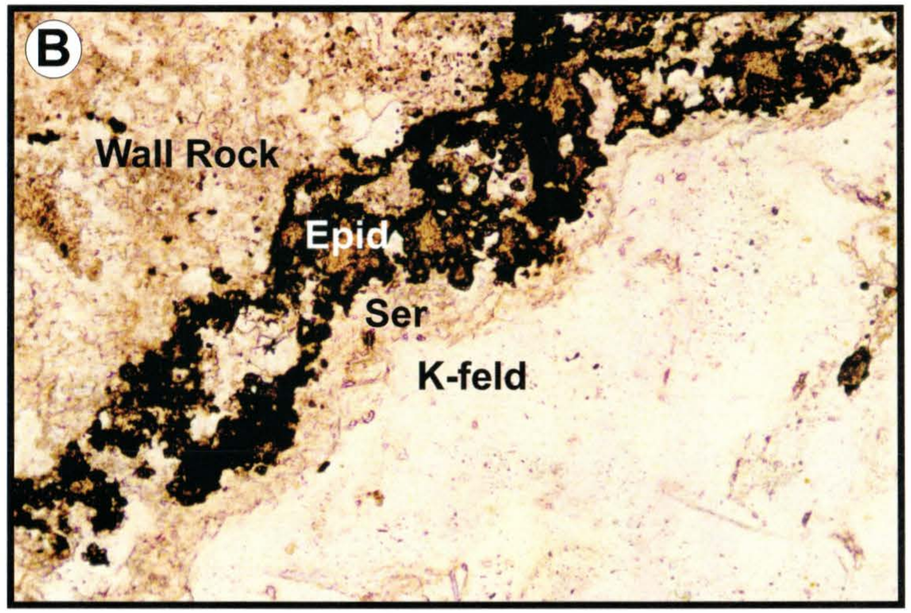


Plate 3-15 - Distal alteration facies for the mafic volcanic footwall (SHF andesitic-basalt). Minor Fe-chlorite and quartz are the predominant alteration minerals. MBZ, DDH 1916, 1826'.



Plate 3-16 - Potassic alteration facies at the Middle Branch Zone in the felsic volcanics (BRF dacite). Note the strong K-feldspar - sericitic (+/- silicic) alteration and Zn-Pb-Ba rich sulphide stringer. These rocks often contain 8-10 wt. % K2O and more than 1 wt. % Ba. DDH 1162, ~ 1305'.





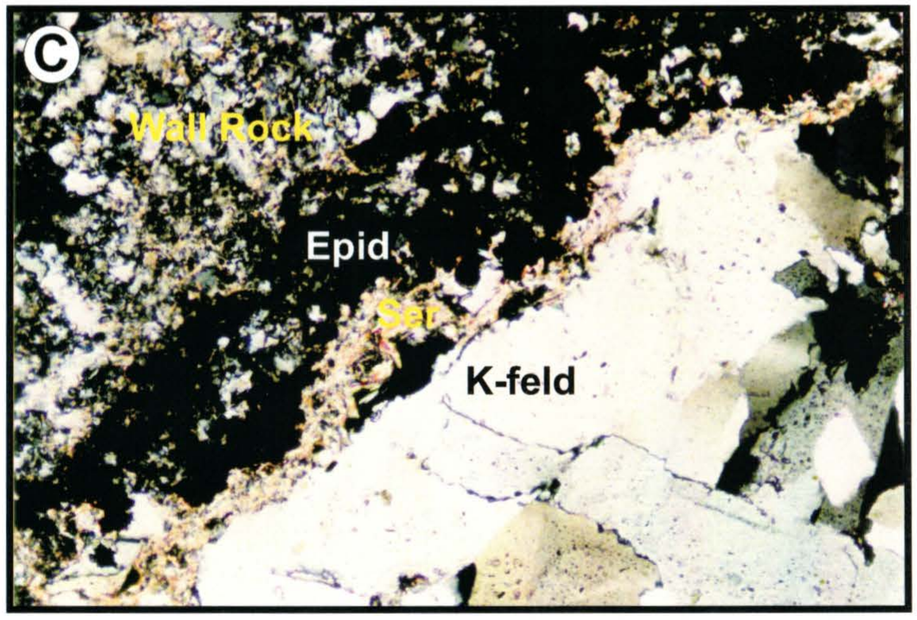


Plate 3-17 - Photomicrographs of strong potassic alteration in BRF dacites in the MBZ. A) Relatively coarse masses of K-feldspar rimmed by sericite and epidote. MB-01, XPL, FOV=5mm. B) PPL and C) XPL are enlargements of the same area as A with FOV=1.3mm. Wall rock contains an abundance of the same minerals, but much finer grained. Birefringence is slightly lower than normal due to thickness of thin section.



Plate 3-18 - Quartz-feldspar porphyritic to aphyric dacite flows of the Woodmans Brook felsic volcanics. DDH BE-96-08, 278-287 m.



Plate 3-20 - This texture is peculiar to a portion of the WBZ felsic volcanics. These chlorite-pyrite spots may represent lithophysae (devitrification texture), a feature common in some felsic volcanics. DDH BJ-41, ~149'.

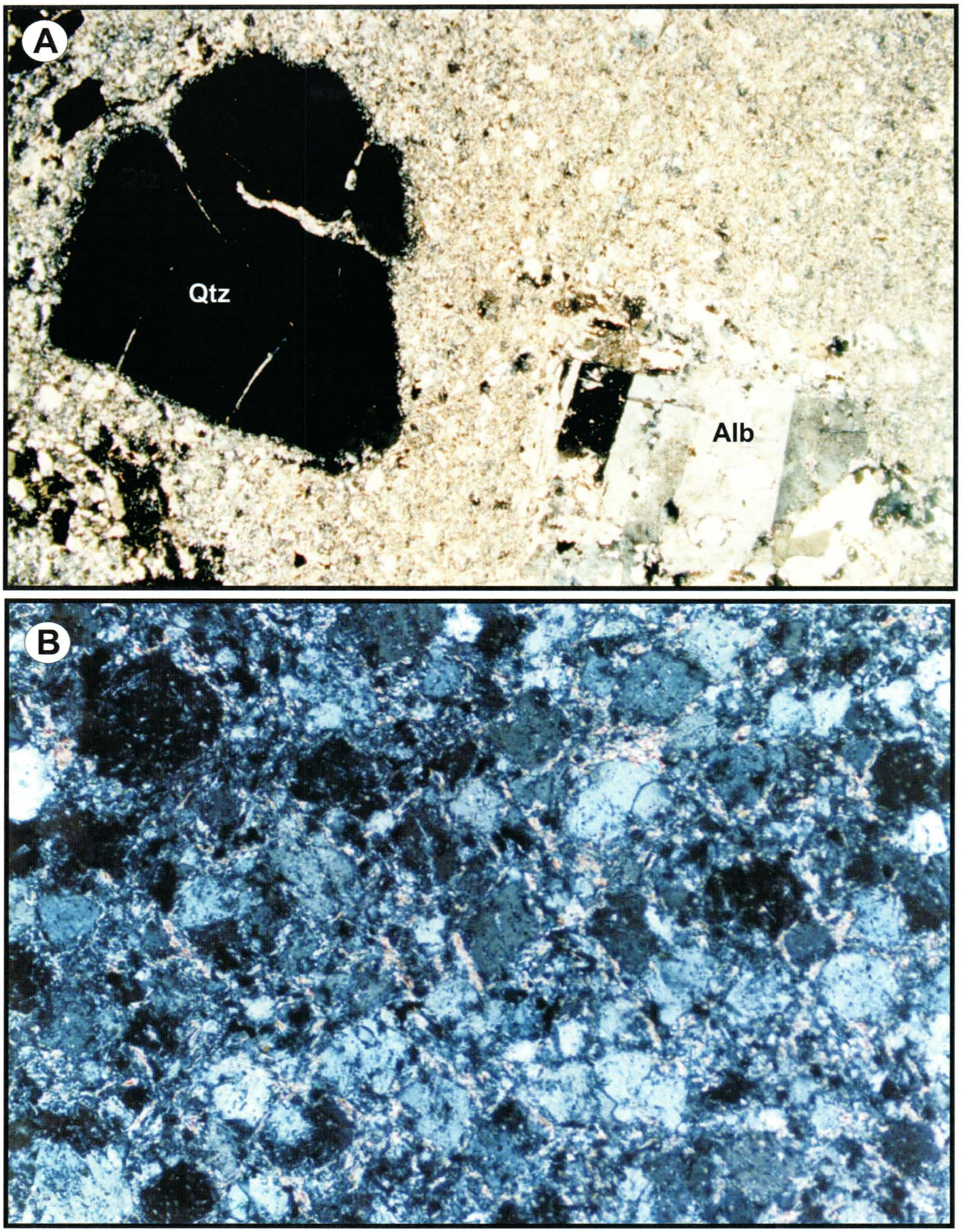


Plate 3-19 - A) Quartz and feldspar porphyritic dacite from the WBZ. The feldspar is albitized and quartz phenocrysts are embayed. Sample is WB-19, XPL, FOV=5 mm. B) Well developed *micropoikilitic* texture (*cf*. McPhie, 1993) in dacite from the WBZ. This texture commonly occurs glassy lavas and results from the devitrification. Note the very fine sericite (after feldspar) inclusions within the larger quartz grains. Sample WB-23, XPL, FOV=1.3 mm.

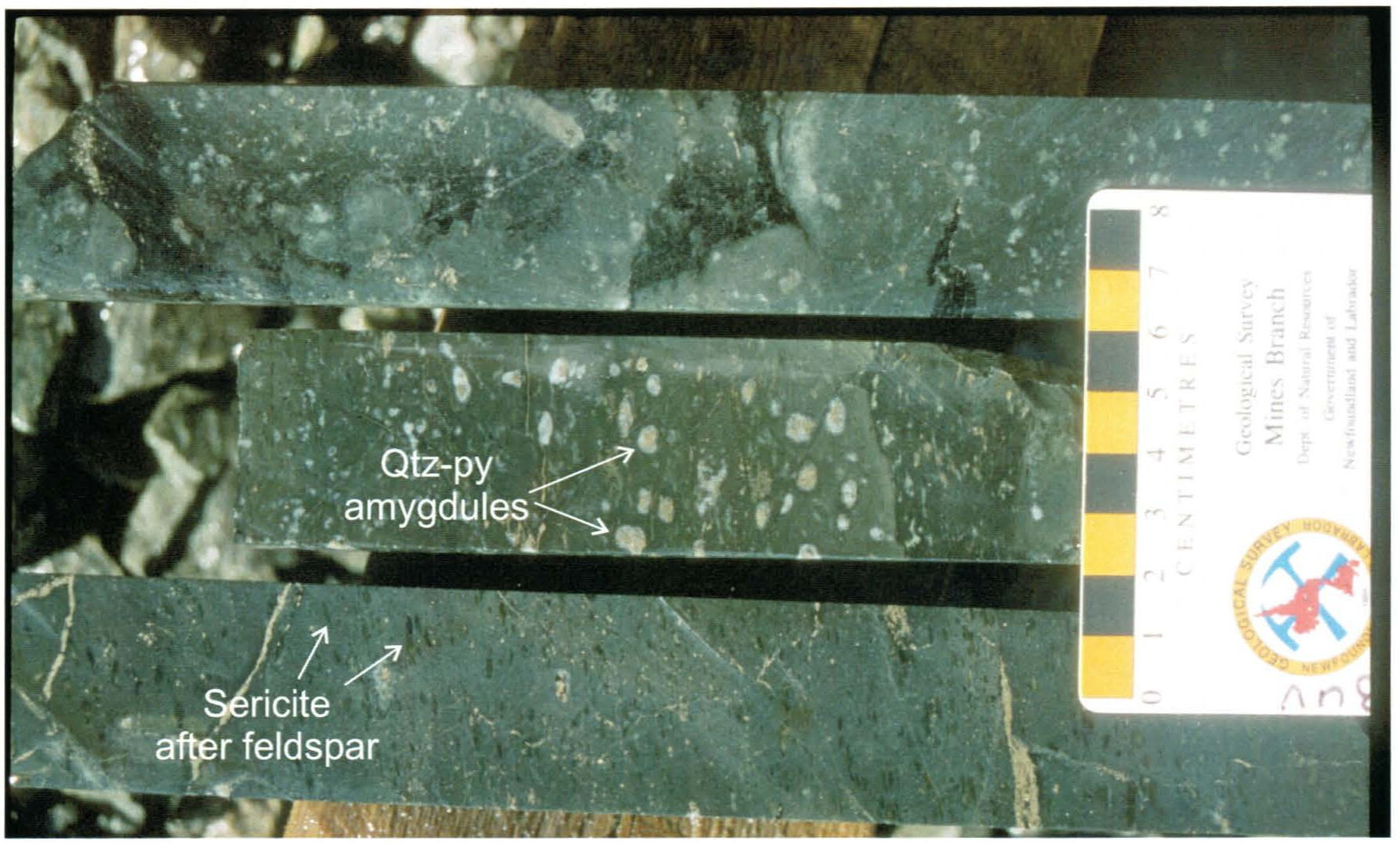


Plate 3-21 - Chlorite-sericite-quartz-pyrite altered basaltic andesite flows of the WBZ. These rocks are variably feldspar porphyritic and amygdular. DDH BE-96-10, ~120 m.



Plate 3-22 - Strongly foliated felsic volcanic sequence of the WBZ. These rocks are comprised almost wholly of sericite, quartz and pyrite. A few may contain minor albite and carbonate. DDH BE-95-01, ~60 m



Plate 3-23 - Chlorite - pyrite dominant alteration and brecciation in the WBZ mafic volcanic rocks. DDH BE-95-01, ~16.9 m.



Plate 3-25 - Sericite - quartz alteration and associated galena - sphalerite - pyrite mineralization in felsic volcanic rocks of the WBZ. DDH BE-95-03, ~ 108.3 m.

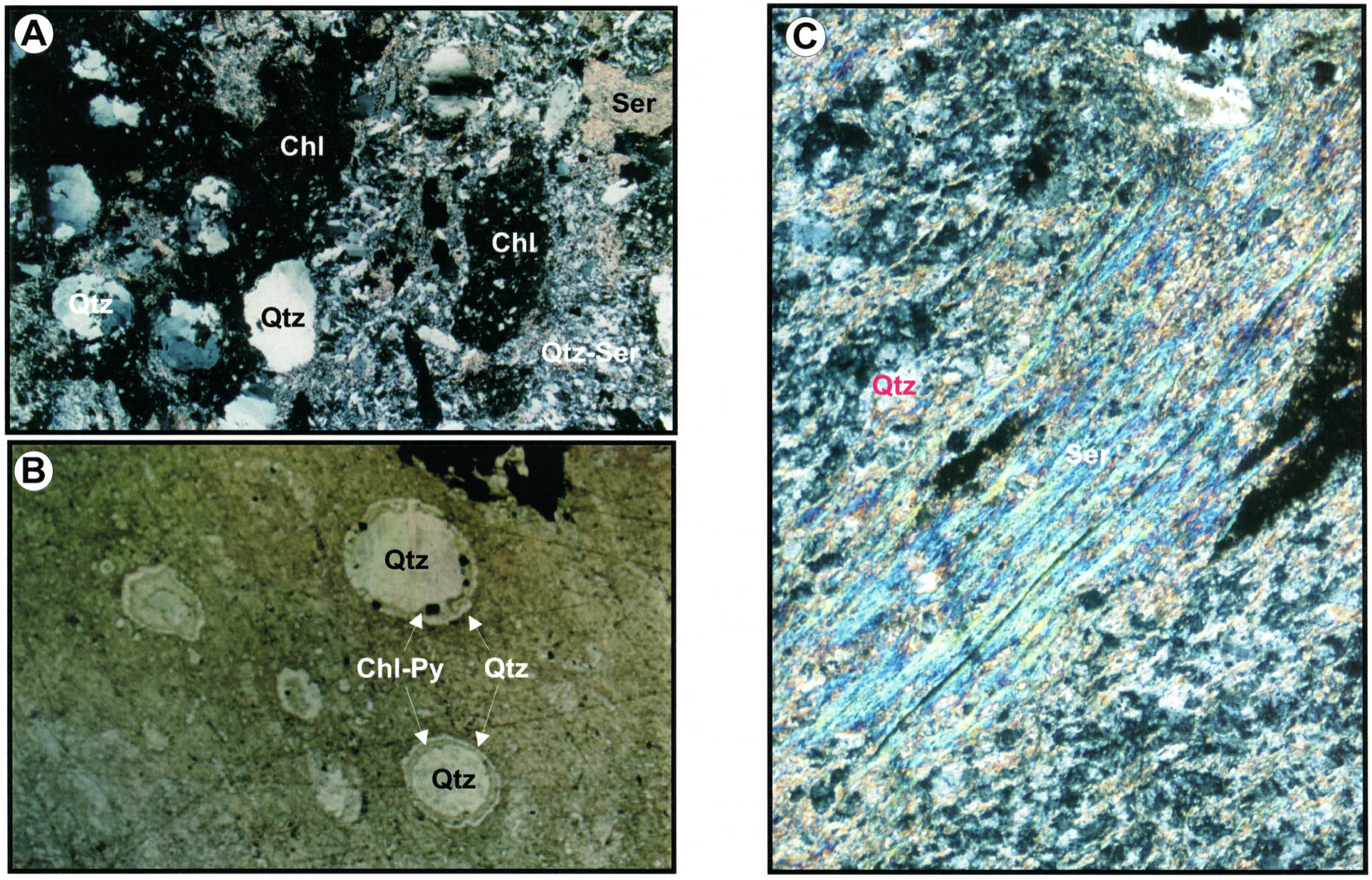


Plate 3-24 - A) Complete quartz-sericite-chlorite-pyrite-carbonate replacement of a mafic hyaloclastite? from the WBZ. Sample WB-10, XPL, FOV=5mm. B) Zoned amygdules in strongly altered mafic volcanics from the WBZ. Amygdules are zoned inwards from fine quartz to chlorite-pyrite to coarser quartz. Locally, these contain minor chalcopyrite. WB-09, XPL, FOV=5mm. C) Foliated quartz-sericite-pyrite alteration in a felsic volcanic protolith. WB-02, FOV=1.3mm.

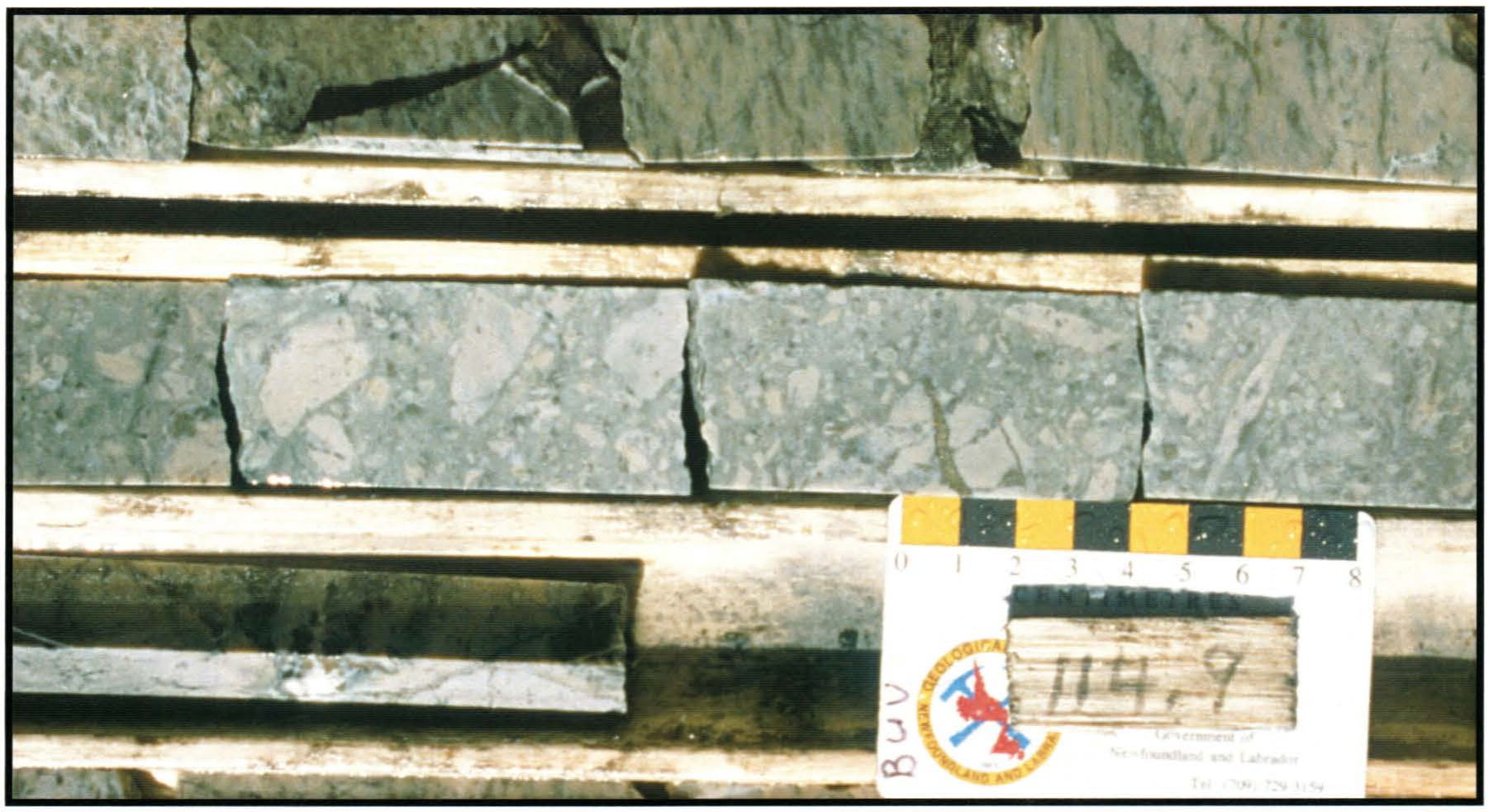


Plate 3-26 - Hydrothermal breccia in felsic volcanic rocks from the WBZ. The breccias appear to overprint the fabric in the rock and, as such, may be related to deformational process. BE-96-10, ~113-114 m.

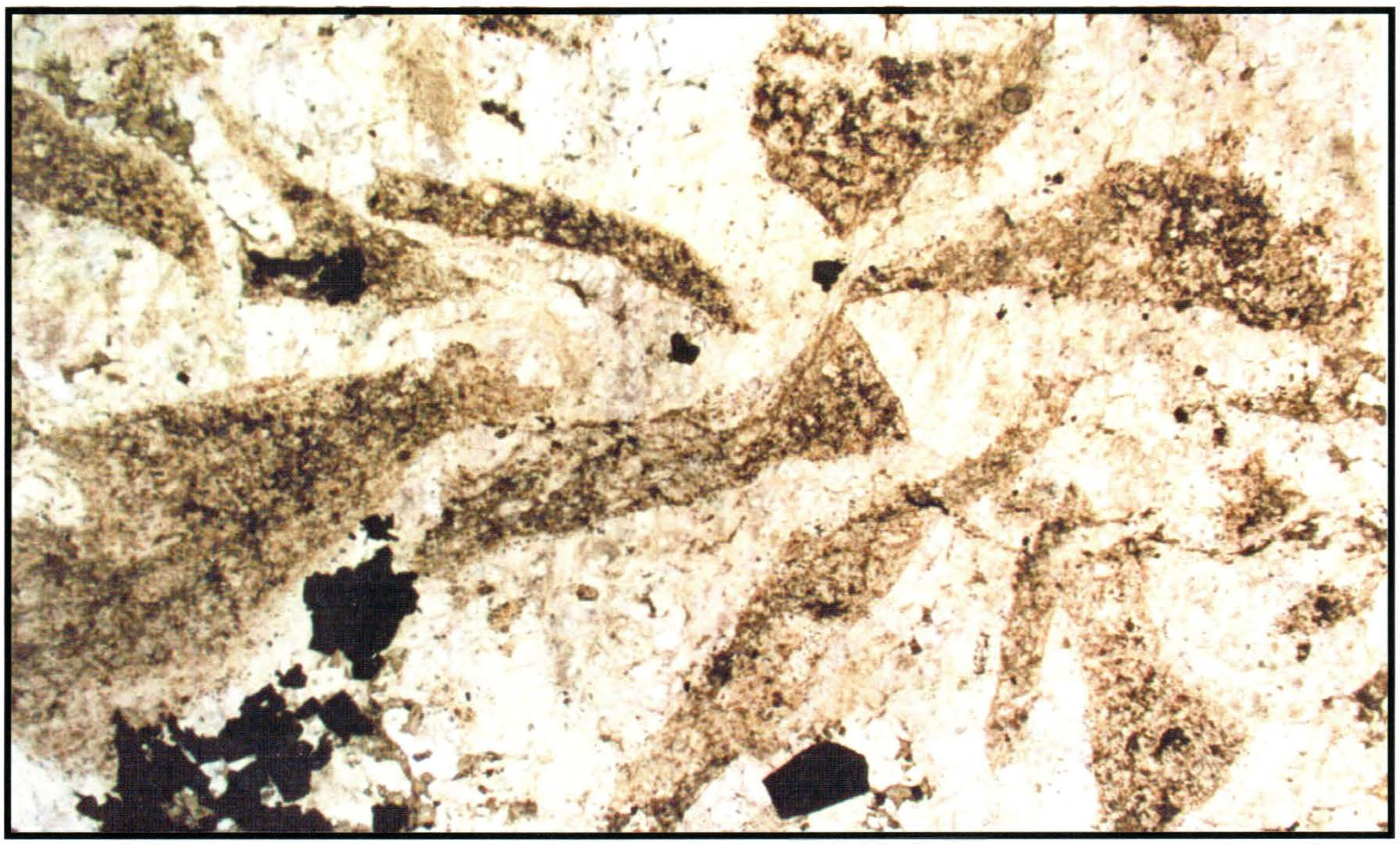


Plate 3-27 - Photomicrograph of sample in plate 3-26 Fragments are altered to very fine-grained sericite-clay and the matrix is quartz. Pyrite is associated mostly with the quartz. Sample WB-15, PPL, FOV=5 mm.



Plate 3-28 - Gossan exposed near powerhouse (abandoned hydro-station) on Buchans River which represents the surface expression of the PHZ.



Figure 3-29 - DDH BE-96-11 showing the mafic volcanics and underyling felsic volcanic rocks. Both units are strongly altered and mineralized. The mafics can be readily identified by the darker colour, coarse porphyritic texture and lack of quartz phenocrysts.



Plate 3-30 - DDH BE-97-19, ~44m. Well developed in-situ breccia texture in a dacite flow from the PHZ emphasized by sericite (+ minor carbonate) alteration.



Plate 3-31 - Strongly altered feldspar porphyritic mafic volcanic unit form the PHZ. Feldspars are altered to either sericite (bright green) or converted to pure albite (pink-orange). A few are altered to carbonate (whitish). The matrix is a mixture of very fine-grained pyrite - sericite - carbonate - chlorite. DDH BE-95-11, ~84 m.

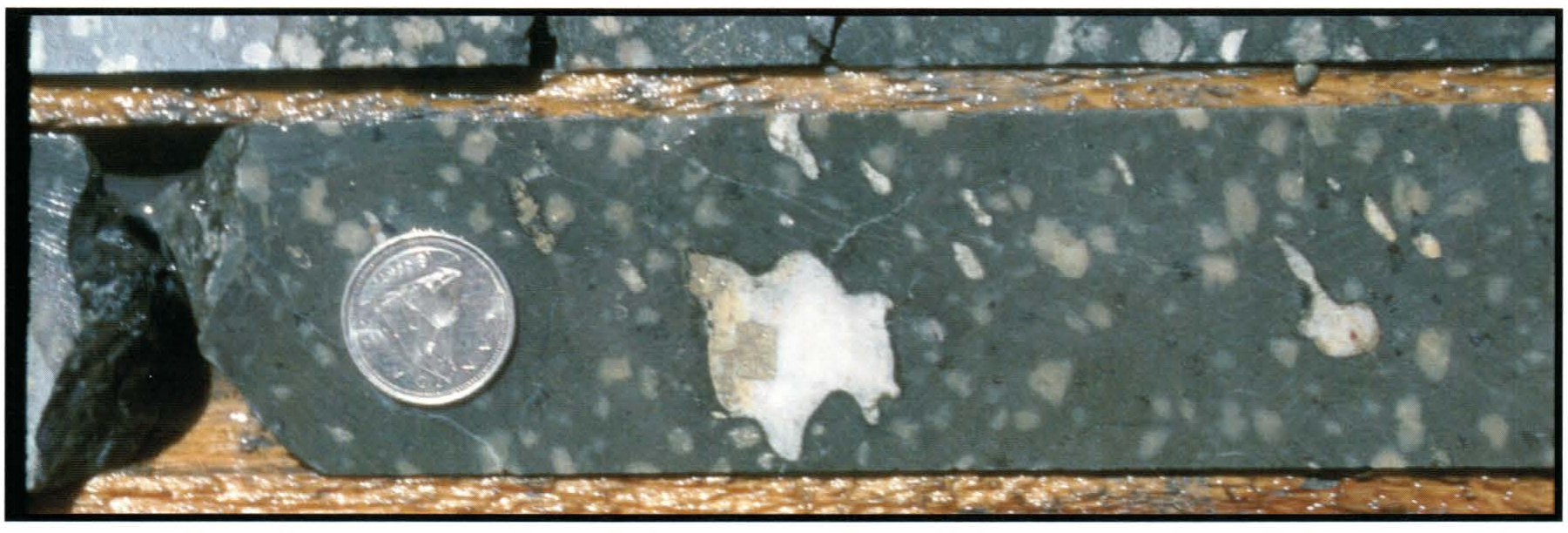


Plate 3-32 - Large carbonate-quartz-pyrite filled amygdule in altered PHZ mafic volcanics. A series of smaller amygdules define a weak flow? fabric. DDH BE-95 -11, ~92.5 m.

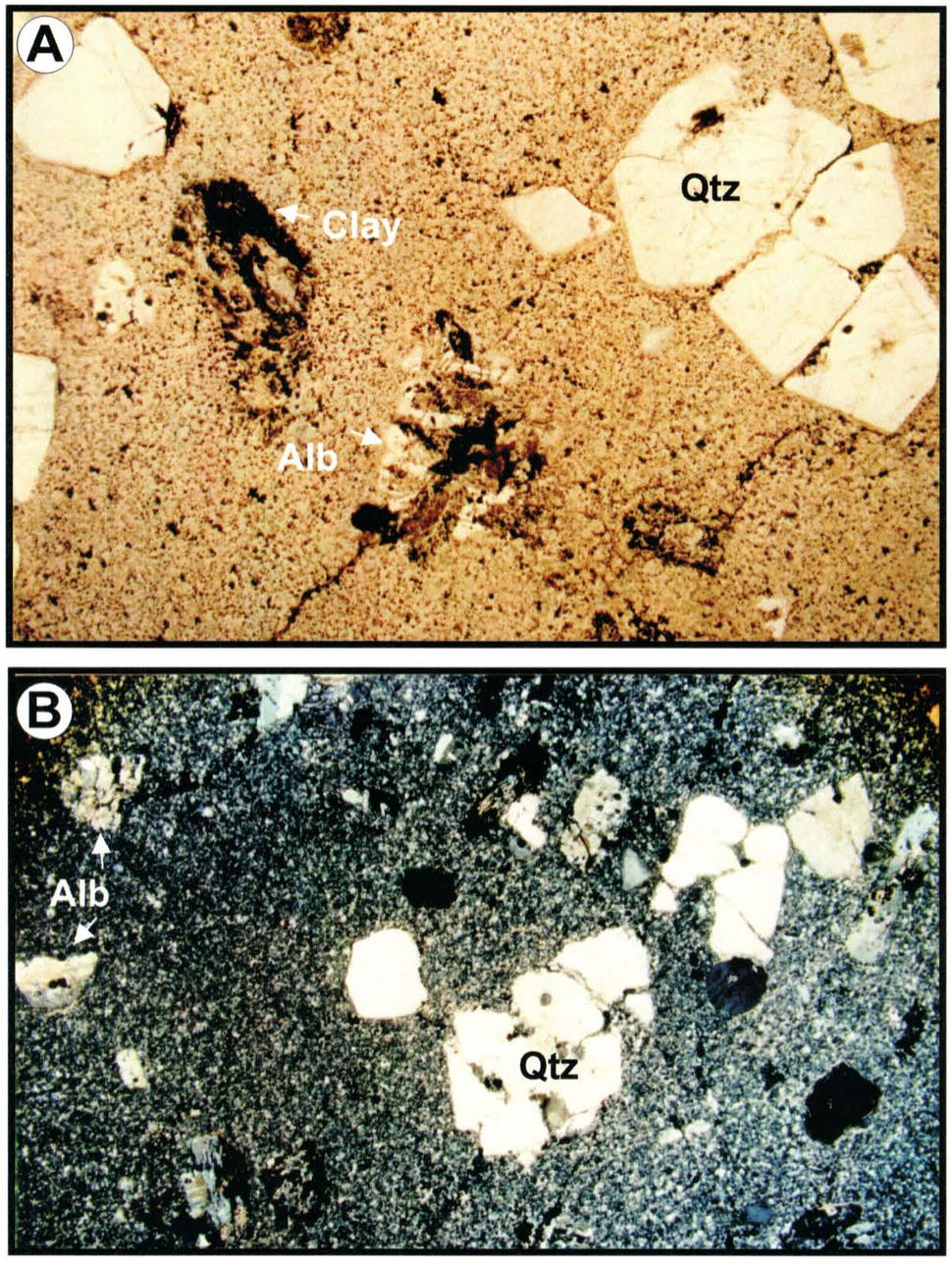


Plate 3-33 - Photomicrographs of altered rocks from the PHZ. A) Quartz and feldspar porphyritic dacite. Euhedral quartz phenocrysts are fractured and slightly resorbed. Feldspars are strongly altered to clay-sericite. Sample BE -97-20, PPL,FOV=5mm. B) Similar to above but with stronger resorption of quartz. Feldspars are altered to albite and sericite-clay-pyrite. WB-9, XPL, FOV=8.45mm. C) Altered feldspar prophyritic mafic unit. Phenocrysts and groundmass feldspar are completely albitized. Note the knife-sharp contact with the sericite-clay alteration front. Sample PH-3, XPL, FOV=8.45mm.

Chapter Four - Mineral Chemistry

4.1 Introduction

This chapter documents the chemistry of chlorite, sericite and carbonates from the LSZ, WBZ and PHZ. Each of these mineral species can have varying compositions depending upon the physicochemical conditions extant during formation, which can be estimated using the chemical data. Direct comparison of these zones can be used to rank their respective prospectivity for association with VMS-style mineralization. Additionally, variations within a zone could also be used to vector towards the hydrothermal focus.

The data were acquired using a Cameca SX50 electron microprobe analyser at the Department of Earth Sciences, Memorial University. An outline of the analytical techniques and the data are given in Appendix D. Thin sections used for petrographical studies were utilized for the microprobe analyses, and consequently, whole rock geochemical data also exists for each sample. Samples were selected in order to give a large spatial distribution, but also on the availability of the alteration minerals of interest.

4.2 Chlorite

A broad range of chlorite compositions are observed for the Lucky Strike Zone, with data overlapping from the Powerhouse and Woodmans Brook Zones (Table D-1). At Lucky Strike, Fe/(Fe +Mg) ratios range from 0.04 to 0.65 and atomic Si varies between 5.69 and 6.70. According to the classification scheme of Hey (1954), these

chlorites range from *pycnochlorite* (and *diabantite*) in the relatively higher Fe endmembers to *penninite* (and *chlinoclore*) in the Mg endmember (refer to Figure 4-1a) . This range in chlorite compositions is similar to that described by Henley and Thornley (1981). Chlorites from the Woodman's Brook Zone have Fe/(Fe +Mg) ratios from 0.30 to 0.57 and atomic Si from 5.44 to 5.81 and mostly range from *rapidolite* to *pycnochlorite* (Figure 4-1b). At much lower Fe/(Fe +Mg) ratios (0.14 to 0.31) and higher Si (5.74 to 6.36), the Powerhouse Zone chlorites would be classified mostly as *chlinochlore* and *penninite* (Figure 4-1c).

In most samples there is an inverse proportionality between Fe and Mg in the chlorites as is expected due to the continuous solid solution series between these two octahedral cations (Bailey, 1988). However, in some of the most Fe deficient samples, these sites are also commonly occupied by Al, in addition to Mg. This appears to be the case with a few of the Lucky Strike samples and most of the Powerhouse Zone chlorites (Figure 4-2).

Chlorite compositions are plotted in Figure 4-3 on a series of ternary diagrams. The four ternary plots represent a tetrahedron that is defined by the major components of chlorite: Mg, Fe, Si, and Al. Each point is projected normal to the face of each side of the tetrahedron which is then "unfolded" so that the data can be illustrated in two dimensions. The Lucky Strike data show the largest range in Fe/Mg ratios from intermediate to low values. The Woodman's Brook zone chlorite data overlap with the Fe-rich chlorites of the Lucky Strike area and have a more limited range. Chlorites from the Powerhouse Zone also have more limited ranges in Fe/Mg ratios, but are quite

different from those from Woodman's Brook and overlap with the most Mg-rich chlorites of the LSZ. These chlorites plot with low Fe/Mg ratios (Mg-rich), but show a wide range in Al/Mg. As suggested above, there is a greater range in octahedral Al in these samples due to substitution with Mg and a more limited range in octahedral Fe. Variations in tetrahedral Si and Al do not appear to be significant. The average compositions of chlorites from each of the three zones are as follows:

Lucky Strike: $Mg_{5.61}Al_{2.94}Fe_{2.72}Mn_{0.12}K_{0.13}Ca_{0.05}Na_{0.01}Ti_{0.03}[(Si_{6.17}Al_{1.83})O_{20}]OH_{16}$

Woodman's Brook: $Mg_{4.76}Fe_{4.01}Al_{2.98}Mn_{0.10}K_{0.07}Ca_{0.02}Na_{0.02}Ti_{0.01}[(Si_{5.63}Al_{2.37})O_{20}]OH_{16}$

Powerhouse: $Mg_{5.85}Al_{3.96}Fe_{1.40}Mn_{0.06}K_{0.05}Ca_{0.03}Na_{0.01}Ti_{0.01}[(Si_{6.12}Al_{1.88})O_{20}]OH_{16}$

4.3 Sericite

Microprobe analyses of micas (Table D-2) yielded very similar major element data from all three alteration zones and indicate that muscovite (sericite) is the only mica type present (Figure 4-4). The term sericite is a common term which is used to describe fine-grained white mica (Deer *et al.*, 1992); in this case it is muscovite, but the appellation can also be used for paragonite. Average Si/Al ratios are only slightly higher at Lucky Strike when compared to either the PHZ or the WBZ (1.35 versus 1.23 and 1.24, respectively). However, none of these sericites are considered phengitic which requires a Si/Al ratio of greater than 3 and also displays a substitution of Mg and Fe^{2+} for Al in octahedral sites accompanied by a Si increase (Deer *et al.*, 1992). Average formulae of sericites from each of the zones are as follows:

LSZ: $K_{1.67}Al_{2.43}[Si_6Al_2O_{20}](OH, F)_4$

WBZ: $K_{1.44}Al_{2.60}[Si_6Al_2O_{20}](OH, F)_4$

PHZ: $K_{1.47}Al_{2.55}[Si_6Al_2O_{20}](OH, F)_4$

However, adding the Na and Ca to the octahedral K and Fe, Mg, Mn and Ti to the octahedral Al, the the formulas are as follows:

LSZ: $(K,Na,Ca)_{1.75}(Al,Fe,Mg,Mn,Ti)_{2.88}[Si_6Al_2O_{20}](OH, F)_4$

WBZ: $(K,Na,Ca)_{1.59}(Al,Fe,Mg,Mn,Ti)_{2.98}[Si_6Al_2O_{20}](OH, F)_4$

PHZ: $(K,Na,Ca)_{1.66}(Al,Fe,Mg,Mn,Ti)_{2.96}[Si_6Al_2O_{20}](OH, F)_4$

The ideal formula for sericite requires 2 atoms of K and 4 atoms of Al in octahedral sites. Consequently, major element data account for only approximately $^3/_4$ of the octahedral cations in the sericites from all three zones. The remainder of the sites are probably occupied by trace elements. Trace elements that commonly substitute into sericite are Rb, Cs and Ba for K and Li, Cr and V for Al (Deer *et al.*, 1992).

Correlation coefficients for elemental data from the sericites are shown in Table E-2. Strong correlations between Mg and octahedral Al at the PHZ mimic relationships in chlorite from the same zone and reinforce the notion that the altering fluids were Fe depleted when compared to the WBZ and most of the LSZ.

4.4 Carbonates

Microprobe data from this study (Table D-3) and previous work (Henley and Thornley, 1981) suggest that calcite is the only carbonate species present in the Lucky Strike Zone. Several of the samples from the PHZ were also found to be calcite, however, many other carbonates contain equal amounts of Ca and Mg and, as such,

are dolomitic. Calcite also occurs at the at the WBZ, but additional samples were found to have approximately equal amounts of Ca and (Mg + Fe + Mn). These additional samples have Mg/Fe ratios of less than 4 typical of ankerite. Carbonate data are plotted on a ternary compositional plot in Figure 4-5.

4.5 Discussion and Applications to Exploration

Chlorites in alteration zones associated with VMS deposits commonly show systematic variations in Fe and Mg contents with respect to their proximity to the core of the hydrothermal alteration system (see references below). The most intensely altered altered rocks may be represented by either magnesian or ferroan chlorites, depending on the specific phyicochemical conditions and/or host rocks under which the deposit formed. Fe-rich chlorites occur in alteration pipes below many Cu-Zn VMS deposits in the Archean Abitibi (Doucet *et al.*, 1998 and references therein) and in other deposits such as the Prince Lyell, Tasmania (Hendry, 1981). However, many others display Mg-rich chlorites in their most altered zones, including the Kuroko deposits of Japan (Hattori and Sakai, 1979; Urabe *et al.*, 1983) and Buchans (Henley and Thornley, 1981). Therefore, the alteration style most preferred for a Buchans-type orebody would be that containing Mg-rich chlorite. In addition, data from VMS deposits indicate that Fe/(Fe+Mg) ratios have a strong spatial relationship to the focus of hydrothermal discharge, therefore suggesting their potential as powerful geochemical vectors to ore. The Fe/(Fe+Mg) ratios may increase towards the venting site (*e.g.*, Doucet *et al.*, 1998) or, alternatively, may show systematic decreases (*e.g.*,

Urabe *et al.*, 1983). Using data from this study, these relationships are illustrated graphically in Figure 4-7 with Fe/(Fe+Mg) ratios decreasing from approximately 0.65 at one kilometre from the deposit to 0.04 in the stockwork zone just metres from ore. A curve fitted to the data is probably a function of several factors ($[Fe^{2+}/Mg]$, pH, total dissolved S, T), but is mostly related to water/rock ratios which should increase exponentially towards the deposit. Water/rock ratios in the stockwork zone would have been many orders of magnitude greater than distal zones. Not surprisingly, Mg enrichment in the stockwork zone is also extreme, as evidenced from the formation of clinochlore and penninite. The curve flattens out at greater distances and approximates the Fe/(Fe+Mg) ratio of the precursor SHF andesitic basalt as only a relatively minor amount of seawater has affected these distal rocks.

Coexisting sericites and chlorites yield similar Fe/(Fe+Mg) ratios for all three zones, with the best correlation occurring in the WBZ (Figure 4-6). Fe/(Fe+Mg) in sericites have also been plotted against distance producing a curve similar to that of the chlorites (Figure 7b). The equations for each of these curves are as follows:

$$\text{Chlorite: Distance (m)} = 28.9 * \left[e^{[4.86 * Fe/(Fe+Mg)]} \right] \qquad R^2 = 0.646$$

$$\text{Sericite: Distance (m)} = 5.41 * \left[e^{[8.64 * Fe/(Fe+Mg)]} \right] \qquad R^2 = 0.703$$

Model distances were calculated for the chlorites and sericites from the Lucky Strike zone and then applied to the others using the above equations. Model distances for the LSZ had an average error of 47.2% for sericites and 26.5% for chlorites. Several sources of error contribute to these calculations. One source relates to the non-ideal,

non-symmetrical alteration zone associated with the deposit as well as the natural variations that exist, such as overprinting of alteration facies and shifting of fluid pathways. Probably most importantly, faulting has significantly hindered estimations of the distance of samples to the deposit. Therefore, although the model is tenable, it should be considered with much caution.

Assuming the PHZ and WBZ to represent VMS-style alteration, model distances to a potential deposit ranged from 173 - 472 metres for the WBZ and 57 - 129 metres for the PHZ, based on chlorite compositions. Comparable results were obtained from sericite compositions, but with larger ranges. Based on these results, the WBZ may represent an intermediate to distal alteration facies (mostly ~ 0.5 km) whereas the PHZ represents a much more proximal alteration facies (mostly less than 100 m). Data are reported in Table E-3.

Cathelineau and Nieva (1985) have demonstrated the potential use of chlorite as a geothermometer largely based Al_{IV} and octahedral vacancy. This method has been adapted to chlorites in alteration zones associated with VMS deposits such as Phelps Dodge, Matagami (Kranidiotis and MacLean, 1987) and the Horne, Noranda (MacLean and Hoy, 1991). Applying this procedure to the Lucky Strike area yields an improbable temperature gradient which has formation temperatures decreasing towards the deposit with decreasing $Al_{IV,}$ ranging from 161°C and 260°C. Possibly, some the relatively lower temperature, more Mg-rich chlorites are due to late- or post-mineralization, seawater dominated alteration.

4.6 Summary

Although the major element geochemistry of sericites is similar from all zones (all sericites are muscovite), the compositions of chlorite and carbonate are highly varied from each zone reflecting distinctive physicochemical conditions of formation.

Chlorite from the LSZ displays the greatest variation in Fe/(Fe+Mg), ranging from high Fe-chlorites to nearly pure endmember Mg-chlorite. The most Fe-rich chlorites are those in the SHF mafic volcanics most distal from the ore bodies whereas the most Fe-poor chlorites are those in the stockwork zone. The range in the ratios is attributed to a mixing of two sources of Fe and Mg, namely, the host rock and seawater. Chlorites more distal have experienced relatively lower water/rock ratios and reflect the Fe/(Fe+Mg) ratios of unaltered volcanic rocks. Chlorites more proximal have proportionately more Mg due to a greater influence of seawater, although this may not be related to ore-forming hydrothermal fluids. Modeling this relationship is possible but is complicated by the structural modification of the host lithologies.

Both the PHZ and the WBZ contain somewhat limited ranges in chlorite composition that are quite distinctive from each other but do overlap with chlorite compositions from the LSZ. The WBZ contains relatively Fe-rich, chlorites whereas the PHZ contains Fe-poor (Mg, Al-rich) chlorites. Based on the data from the LSZ, the PHZ would is considered to have more potential to host, or at least is more proximal to, a potential VMS deposit.

Carbonates from three zones were also analyzed. The data acquired here along with published data indicate that calcite is the only carbonate species at the LSZ. However, in addition to calcite, the PHZ contains abundant dolomite and the WBZ has ankerite. These results reinforce the dominance of Mg-metasomatism in the PHZ and Fe-metasomatism in the WBZ.

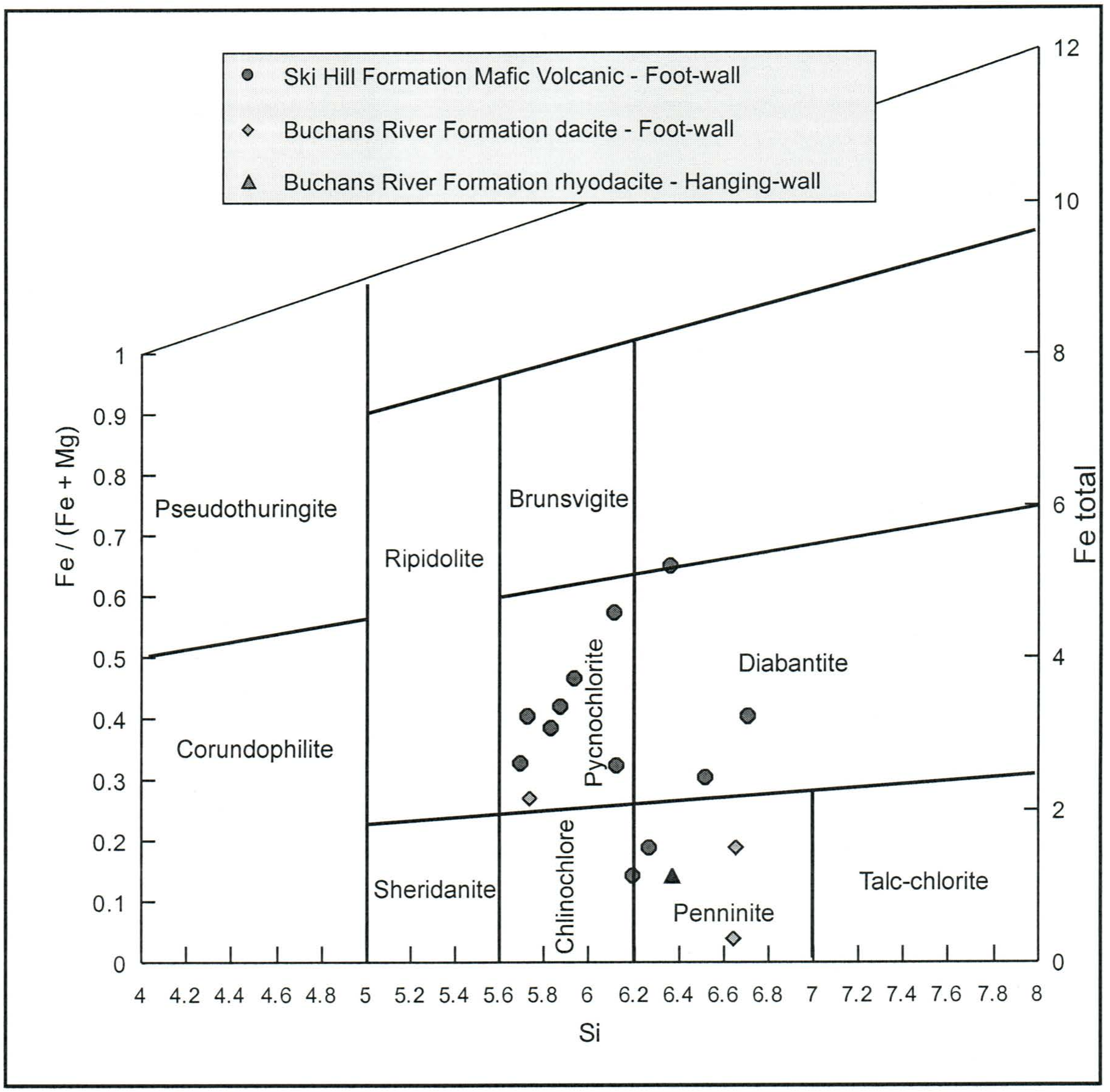


Figure 4-1a - Chlorite composition based on the classification scheme of Hey (1954). LSZ data.

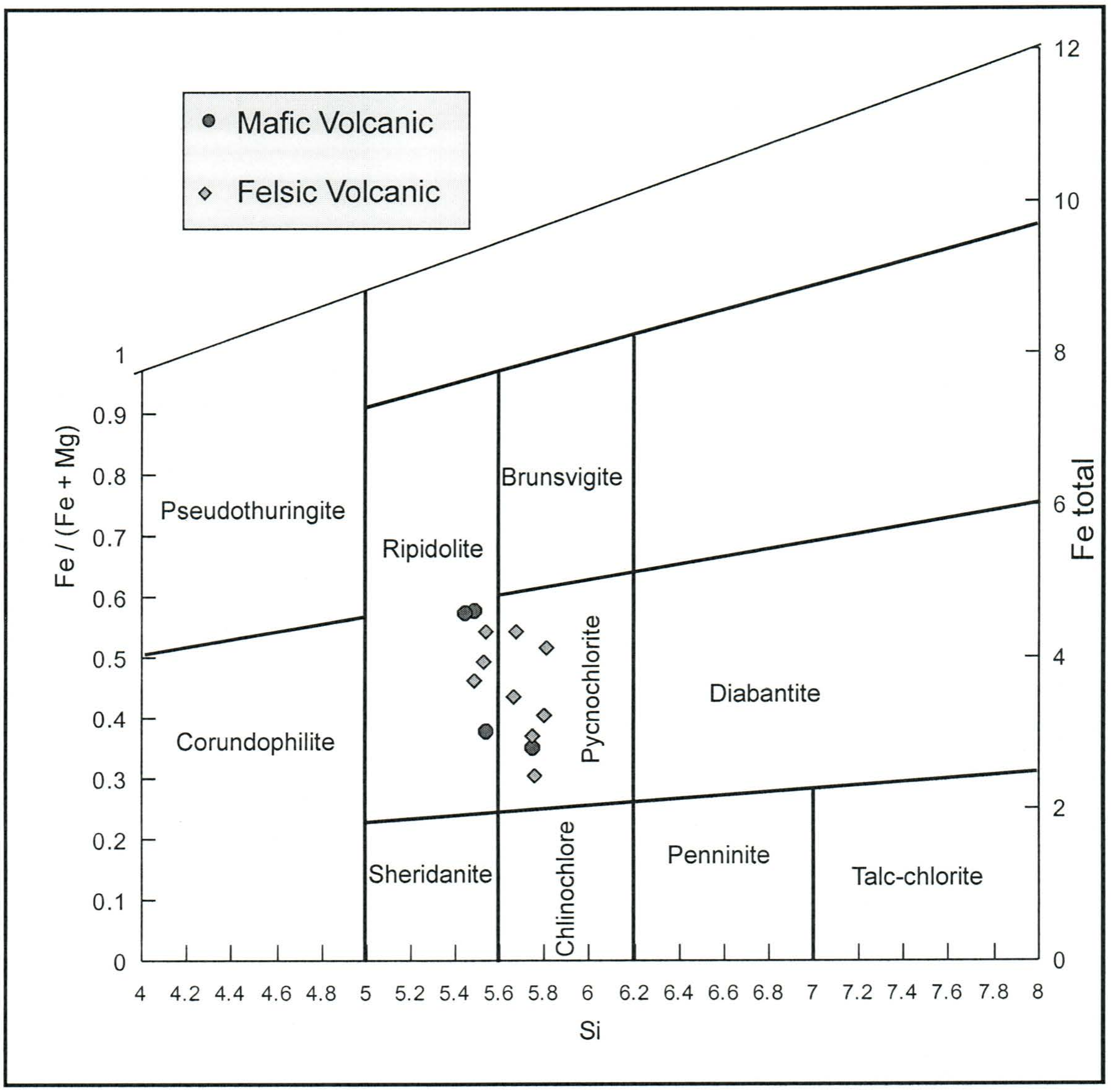


Figure 4-1b - Chlorite composition based on the classification scheme of Hey (1954). WBZ data.

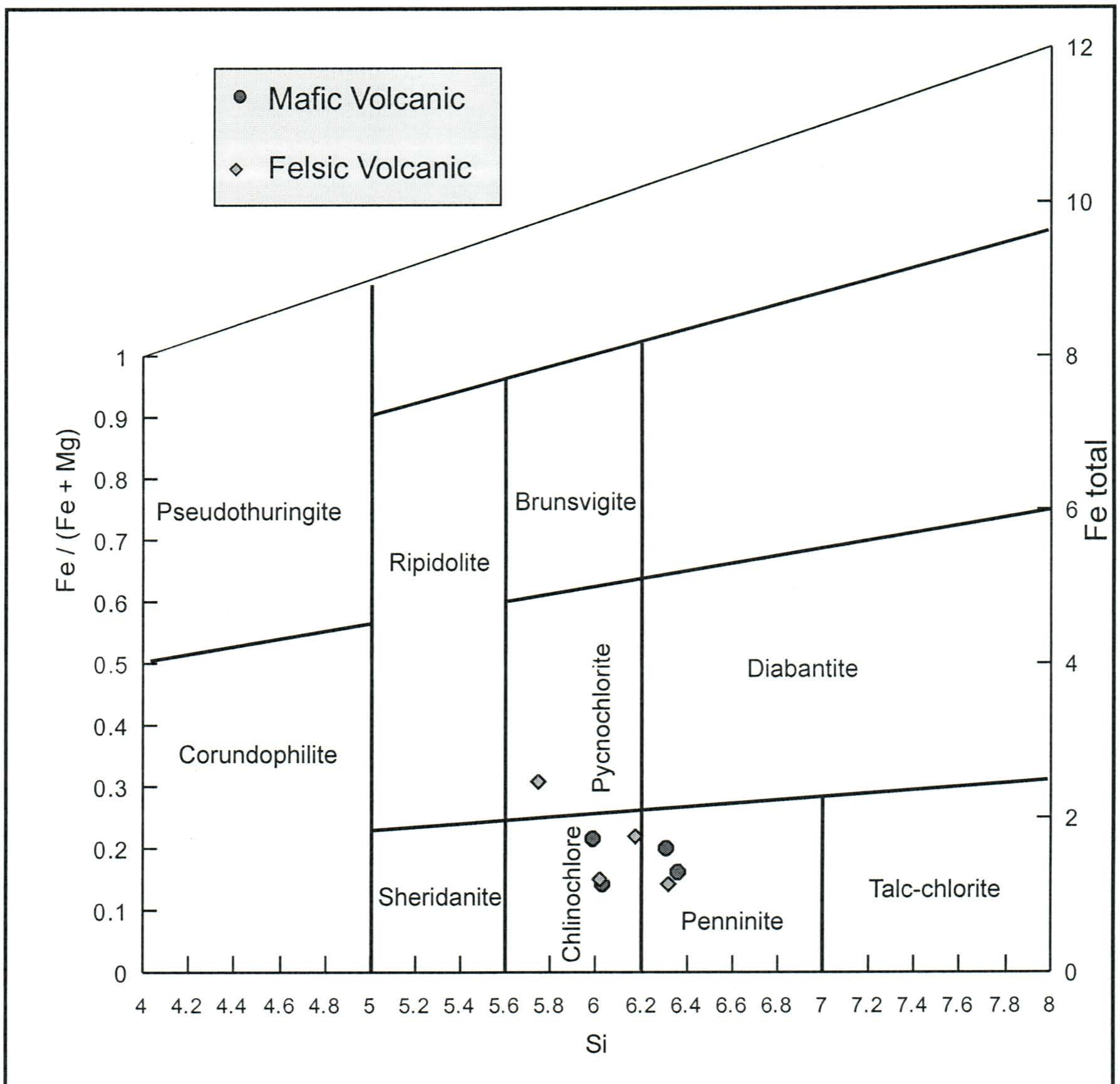


Figure 4-1c - Chlorite composition based on the classification scheme of Hey (1954). PHZ data.

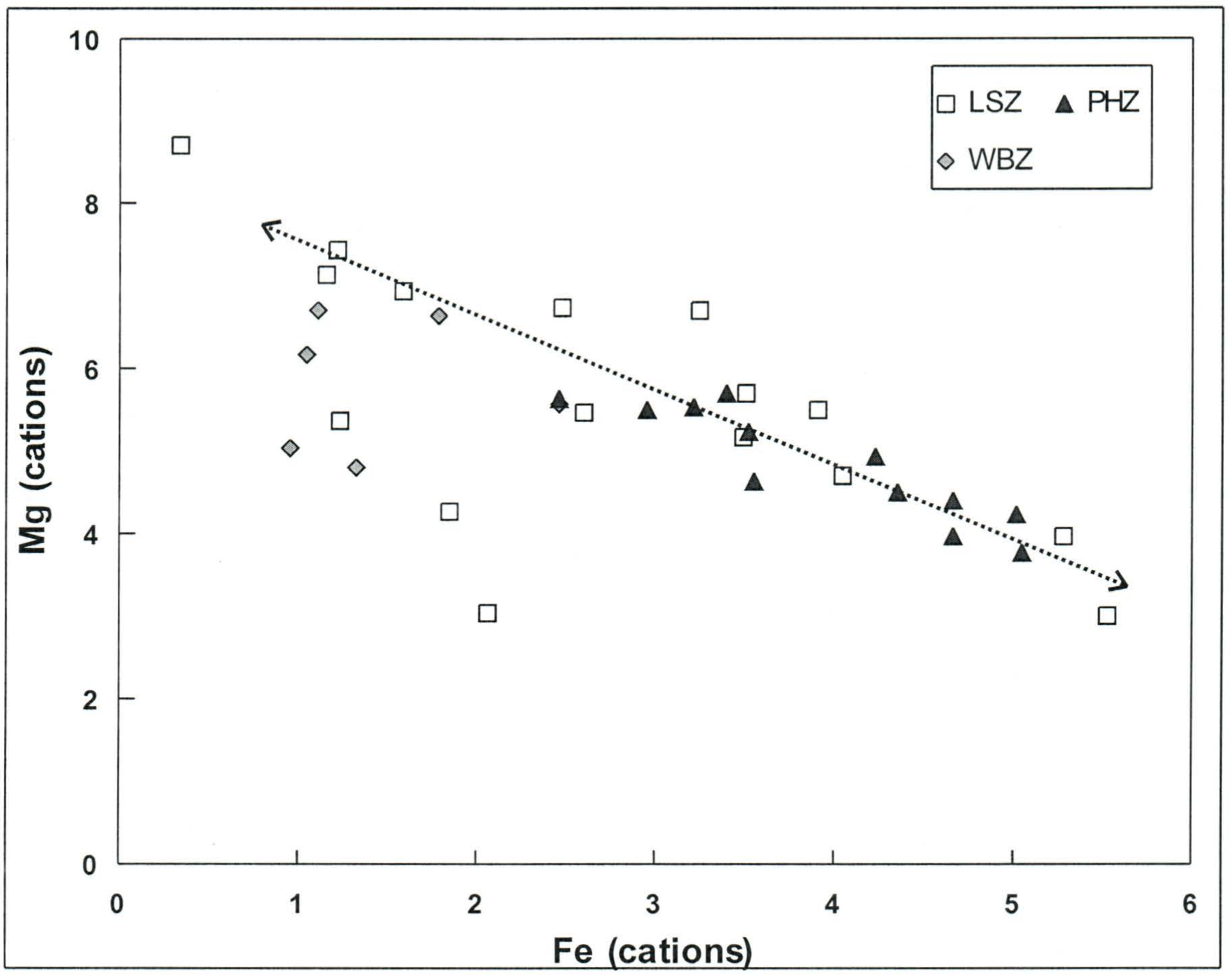


Figure 4-2 - Fe vs. Mg in number of cations in chlorites for each of the LSZ, WBZ, PHZ.

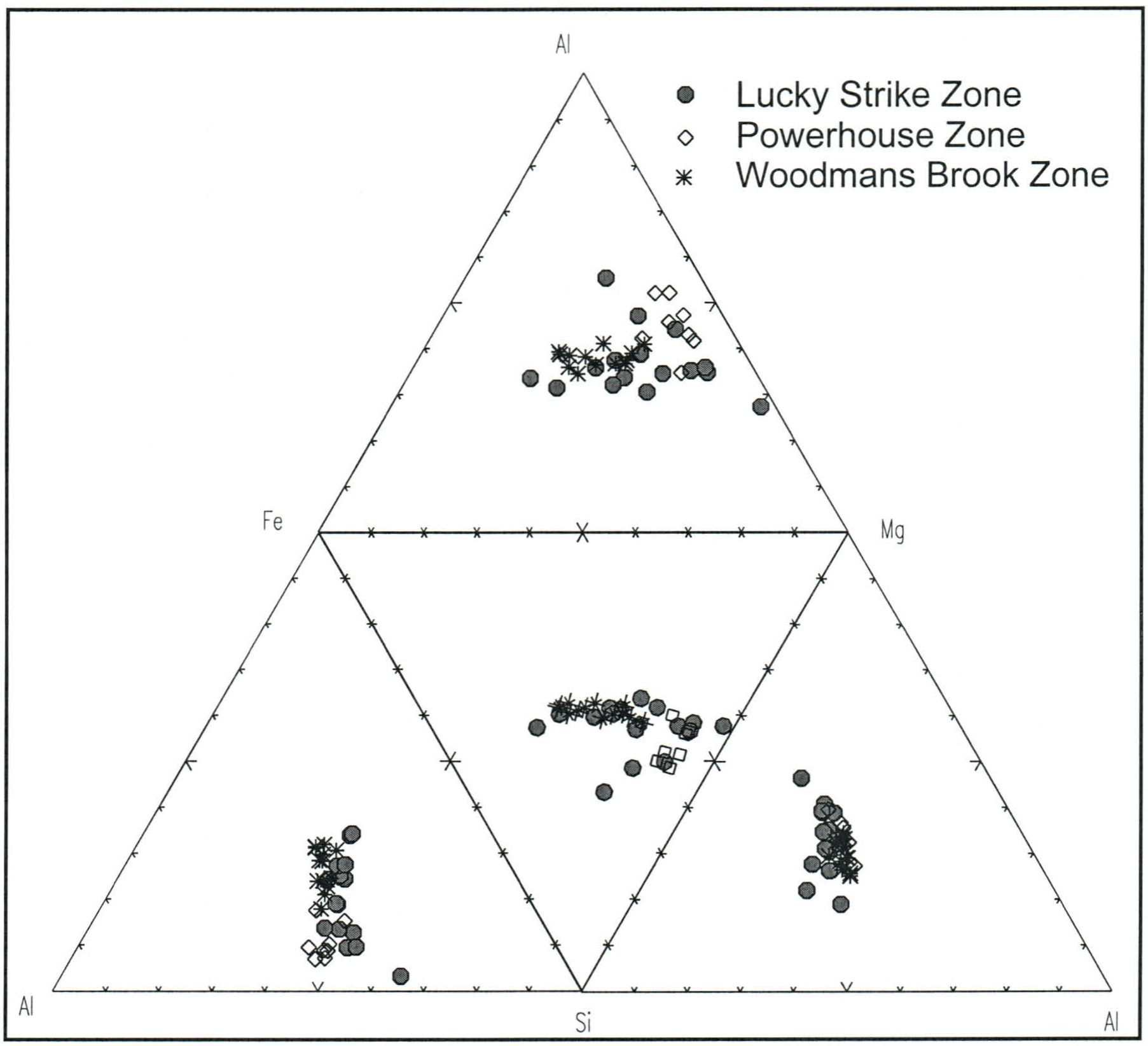


Figure 4-3 - Chlorite compositional tetrahedron showing data from the LSZ, WBZ and PHZ.

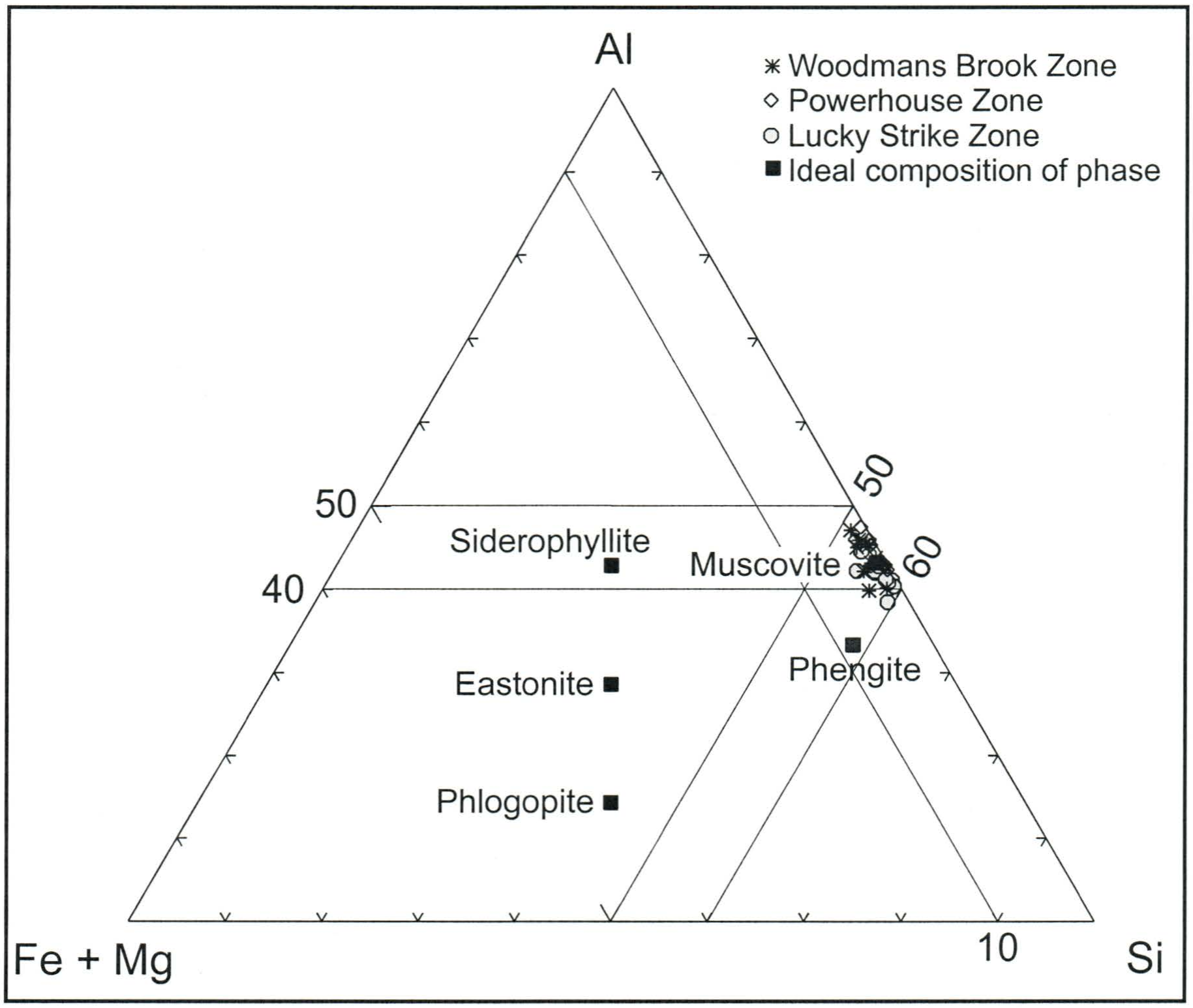


Figure 4-4 - Mica compositional ternary diagram (cationic) illustrating microprobe data from the LSZ, WBZ and PHZ. All samples plot as sericite (muscovite). Fields after Deer et al. (1992).

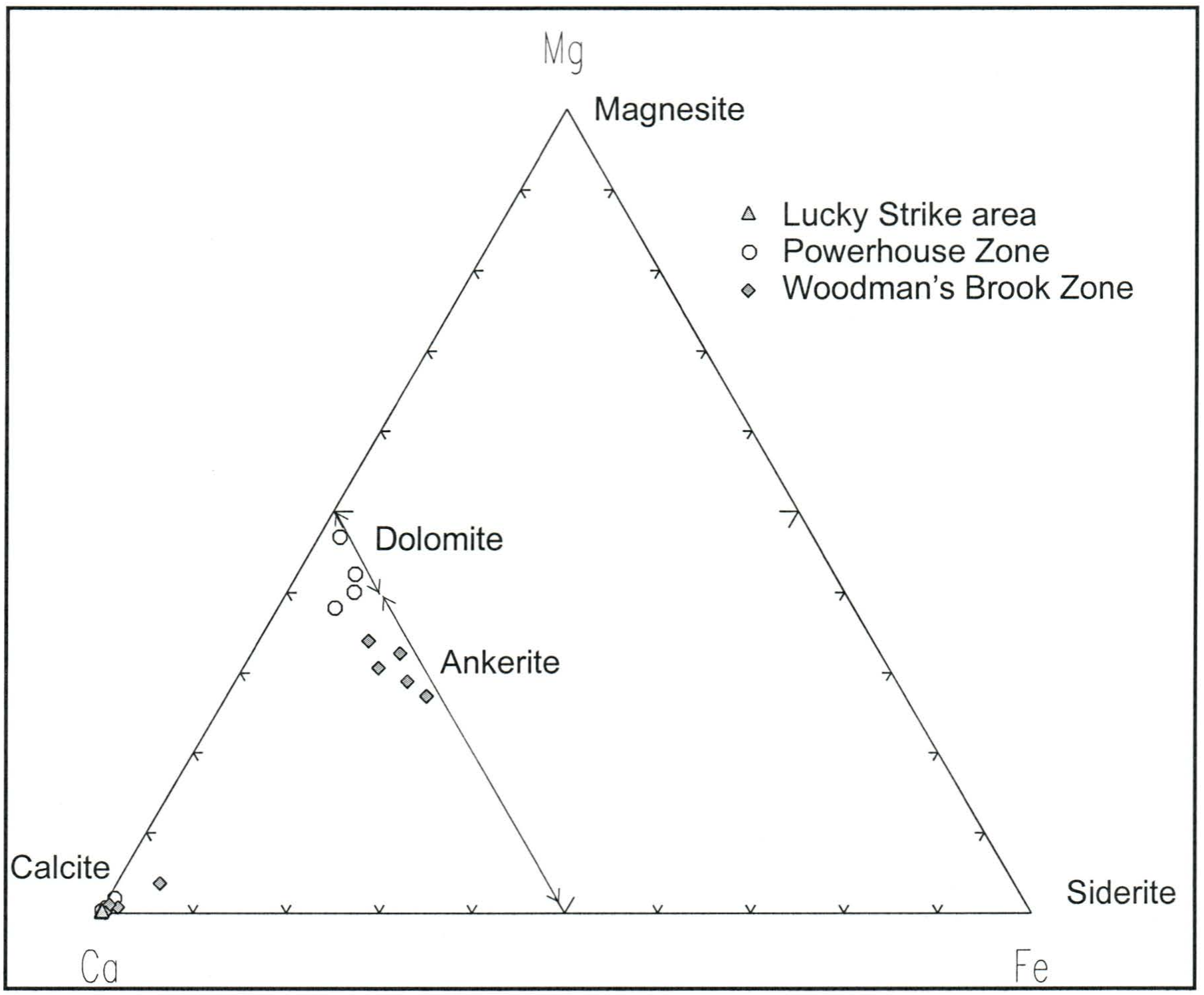


Figure 4-5 - Carbonate compositional ternary diagram based on idealized cationic formulas. Calcite contains almost pure Ca, whereas dolomite and ankerite contain about 50 per cent cationic Ca plus 50 per cent (Fe+Mg+Mn). Dolomite is recognized by Mg/Fe > 4 (*c f .* Deer *e t a l .* , 1992).

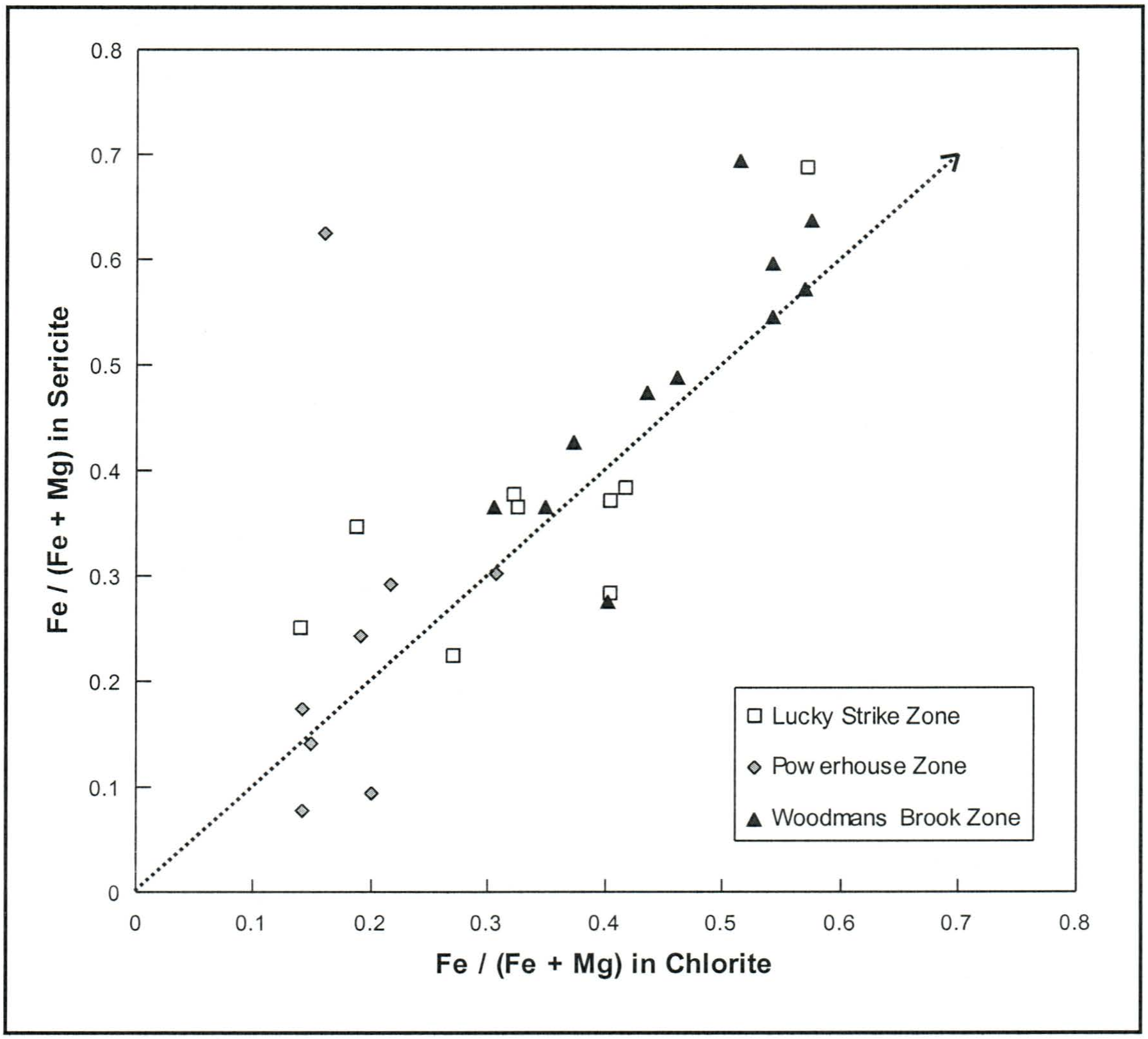


Figure 4-6 - Fe/(Fe+Mg) cationic ratios in co-existing sericites and chlorites from various zones. Note that nearly all data plot close to a line of unity.

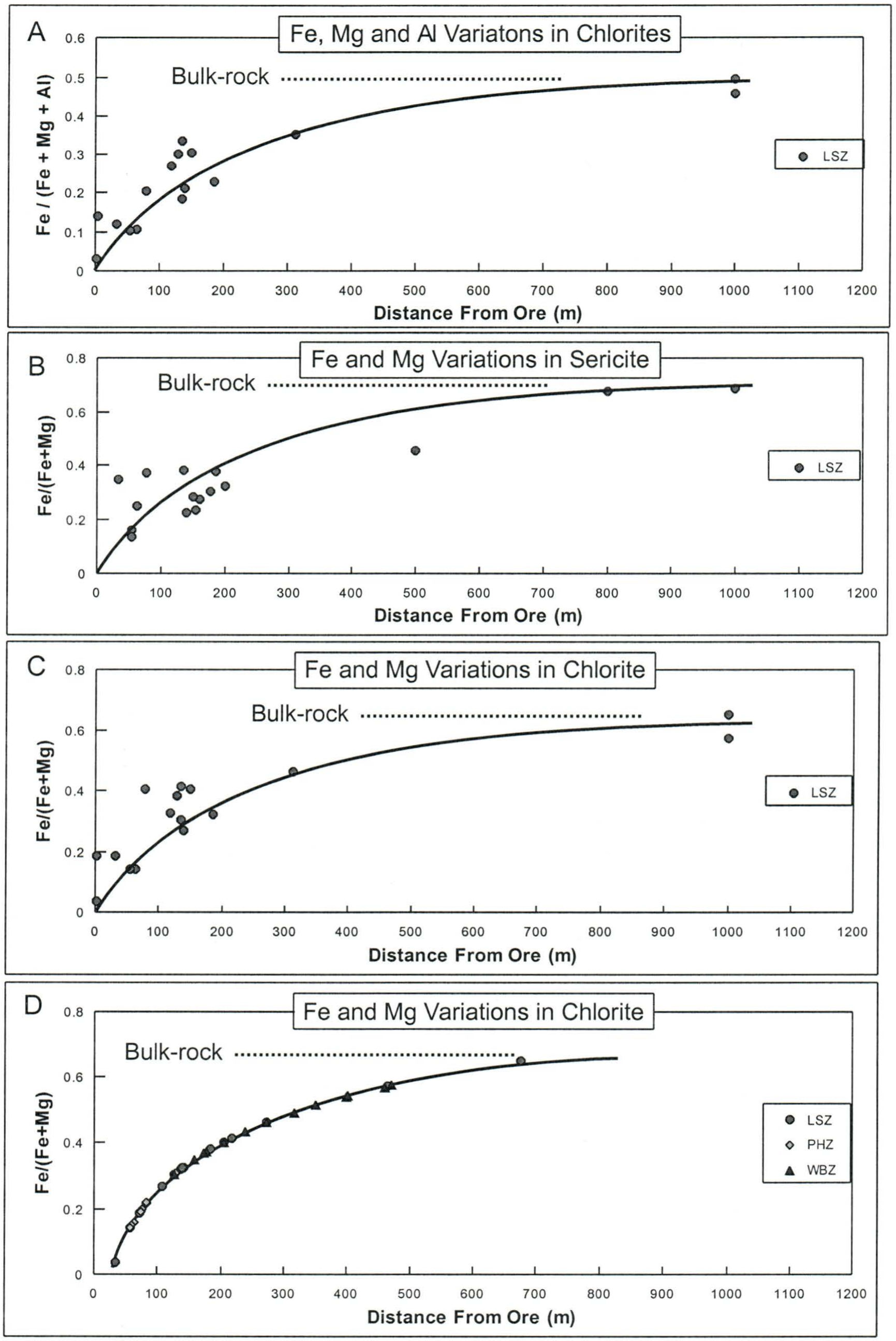


Figure 4-7 - Distance from Lucky Strike ore vs. a) Fe/(Fe+Mg+Al) ratio in chlorite, b) Fe/(Fe+Mg) in sericite, c) Fe/(Fe+Mg) in chlorite. D) modeled distance to ore vs. Fe/(Fe+Mg) for LSZ data and hypothetical distance to ore for PHZ and WBZ samples based on same equations. Bulk Rock refers to the least altered Ski Hill Formation andesitic-basalt.

Chapter Five - Lithogeochemistry and Lead Isotopes

5.1 Introduction

Trace element geochemical studies are an integral component to the understanding and interpretation of any given suite of volcanic rocks. In addition to their importance in classifying rock types and subdividing units within a stratigraphic sequence, trace element data serve as a key tool to test petrogenetic and tectonic models. The true power of trace elements lies in the inherent nature of some elements to remain immobile under hydrothermal and/or metamorphic alterations, an intrinsic feature not seen in the distributions of most major elements. Therefore, since most of the submarine volcanic rocks in the Buchans region have undergone some degree of chemical and physical transformation from their original state, examination of trace element systematics is vital to developing an understanding of the history of those rocks and consequently ore development processes.

Unraveling the geological history of the Buchans Group is not an easy task. Although metamorphism is generally low grade, prehnite - pumpellyite (Henley and Thornley, 1981) facies, hydrothermal alteration is often intensely developed and widespread and complexed by structural modification. Due to their inherent relationships to mineralization processes, the most hydrothermally altered and structurally complex areas that are also those areas of greatest interest to explorationists.

Much geological work has been completed at Buchans in the immediate mine area where underground workings and several thousand drill holes were studied in detail to

produce a very accurate mine-scale stratigraphy (Thurlow and Swanson, 1987). However, outside this immediate area, particularly in the east, the stratigraphic relationships are less certain. Limited field studies suggest that the presently defined stratigraphic sequence fails to incorporate much of the Buchans Group (outside of Buchans), rendering it unusable as a regional exploration tool. Trace element data should provide a broad scale comparison between underdeveloped areas within the Buchans area to areas that have been examined in more detail. Undoubtedly, the production of detailed stratigraphic successions for the entire Buchans Group is a major challenge which is beyond the scope of this project. However, as much as possible, lithogeochemical signatures will be assigned to the various lithologies and correlations will be suggested.

This chapter will use trace element geochemical data to achieve several purposes. First, each of four alteration zones in the Buchans area will be separated and treated as an individual suite of volcanic rocks. Lithologies will be categorized and classified based on rock composition (*i.e.*, mafic to felsic), alkalinity (*i.e.*, tholeiitic to alkalic) and tectonic setting (arc versus non-arc). The volcanic suites will also be compared to each other and to well documented modern tectonic settings. Note that ICP-MS data were not derived from either the MBZ or APZ. A summary of the data is provided at the end of the chapter along with comparisons to other ancient VMS-hosting volcanic belts, such as the Miocene Hokuroko district of Japan and the Archean Abitibi greenstone belt of Ontario and Quebec.

5-2 Discrimination Diagrams

The geological literature provides a myriad of trace element discrimination plots useful for the classification of magmatic suites. The selection and use of these plots depends largely on the nature and purpose of each particular geochemical study. The best approach is to use a combination of bivariate, ternary and normalized trace element plots combining different elements or groups of elements and to make use of published plots which have been designed using enormous data sets to define the fields. Finally, some understanding of the behavior of the trace elements is an essential prerequisite.

Immobile trace element data can be used to interpret the origin as well as provide classifications of igneous rocks. Trace elements considered to be immobile under typical water-rock reactions are the high field strength elements (HFSE): Ti, Zr, Hf, Nb, Ta, Y +/- P; the low field strength elements (LFSE): Th; and the rare earth elements (REE): La to Lu. The REE can be broken down into light REE (LREE): La, Ce, Nd, and Sm, middle REE (MREE): Gd, Tb, Dy, and Ho, and heavy REE (HREE): Er, Th, Yb and Lu. The MREE and HREE are considered to be the most immobile. Eu, a MREE, is generally mobile due to the result of feldspar breakdown during alteration. A complete discussion of geochemical nomenclature and analytical geochemistry with a focus on trace elements in igneous rocks is provided by Jenner (1996).

5.2.1 Rock Types

Winchester and Floyd (1977) have devised a trace element discrimination plot which distinguishes various volcanic rock types differentiates (*e.g.*, basalt-andesite-dacite) and magma series (*e.g.*, tholeiitic vs. calc-alkaline); it is based on a bivariate, log-log scale plot of Nb/Y vs. Zr/TiO_2. Altered and/or metamorphosed rocks can be plotted on this diagram from which differentiation products of various magma suites can be identified and classified. Since the Nb/Y ratio changes very little with differentiation (increases slightly in alkaline suite), then the ratio should represent *parental controls* and *alkalinity*. Nb/Y ratios greater than 0.67 reflect the higher Nb content typical of alkaline rocks. Zr/TiO_2, on the other hand, tends to increase significantly with *fractionation*, mostly as a function of magnetite crystallization which incorporates Ti. The Zr/TiO_2 ratio is used in the place of SiO_2.

Four zones from the Buchans area are compared in Figure 5-1. All four zones yielded samples with Nb/Y values of less than 0.67, indicative of subalkaline suites. In addition, each zone contains at least two distinctive compositional endmembers, typical of bimodal volcanism, with the compositional gap largely represented by the andesite field. The complex magmatic nature of the bimodal volcanism in the Lucky Strike area is illustrated on Figure 5-1a where the samples plot as andesitic-basalts and dacites/rhyodacites which would have been erupted in the same environment, and possibly contemporaneously. There are also two distinct clusters in the felsic field. The cluster further to the right has approximately 3 times higher Nb/Y as well as slightly higher Zr/TiO_2 ratios, consistent with rhyodacite. This more fractionated unit consists of

samples from the upper stratigraphic levels of the BRF. The other felsic cluster is more typical of dacite and generally represents the lower stratigraphic levels of the BRF.

The Woodman's Brook Zone samples also displays two distinctive endmembers (Figure 5-1b) with samples plotting within two very well delineated groups. The mafic endmember is subalkaline basalt, bordering andesitic-basalt. The more differentiated cluster plots in the uppermost andesite field, however, based on the petrographic evidence (refer to Chapter 3), a dacitic composition is considered more appropriate.

The PHZ mafic volcanic rocks are andesitic-basalts, bordering subalkaline basalts, similar to the WBZ mafic volcanics (Figure 5-1c). The felsic suite generally falls into the lower dacite/rhyodacite field but with several samples creating some scattering along the x-axis. This appears to be the result of Y mobility in a few samples.

Data from the APZ also display strong bimodality, approximately half of the samples plotting in the andesitic/basalt field and half plotting barely in the dacite field, bordering andesite (Figure 5-1d). Note also that there is significant spread in the Nb/Y ratios in both endmembers.

5.2.2 Normalized trace element data

5.2.2.1 Primitive mantle normalized extended rare earth element plots

In order to complete a detailed interpretation of the magmatic affinity and tectonic setting of a lithogeochemical data set representing volcanic rocks, the entire suite of trace elements must be examined. A first assessment of the data should include normalized extended trace element plots. These plots include LFSE, HFSE and the REE. Elements

are plotted according to their bulk distribution coefficients with the most incompatible elements on the left with decreasing incompatibility (*i.e.*, more compatible) to the right. There are several possible choices for normalizing factors available, but are usually either Mid-ocean ridge basalt (MORB), chondrite, or primitive mantle. MORB and chondrite are measured values from oceanic basalts and chondritic meteorites, respectively. Primitive mantle is a hypothetical reservoir that existed after core separation but prior to crust formation. Nonetheless, its composition is considered to be tightly constrained.

In this paper Jenner's (1996) element selection and order were normalized to Sun and McDonough's (1989) primitive mantle reservoir. This group of elements represents those considered unlikely to have been mobilized during hydrothermal alteration of the volcanic rocks and includes representatives of LFSE (Th), HFSE (Nb, Zr, Ti, Y) and REE (La-Lu).

Geochemical signatures of mafic volcanic rocks from all possible modern tectonic settings have been well documented. This database permits direct comparison of ancient settings with modern settings, assuming plate tectonic processes have not changed significantly over time. This appears to be the case at least during Proterozoic, though it may be more complicated in the Archean.

Modern settings fall into two dominant groups: (i) non-arc and (ii) arc settings (*cf.* Swinden *et al.*, 1997). Non-arc oceanic volcanic rocks plot as smooth patterns on extended trace element plots with variations in the slope representing the heterogeneity of the mantle sources from which these rocks were derived. The systematic behavior of elements with similar compatibility (or incompatibilty) suggests that only simple

fractionation processes have occurred. Based on current sampling, non-arc volcanic rocks are absent from the study area.

Arc volcanic rocks undergo the same fractionation processes that occur in non-arc volcanic rocks, but are more complex due to subduction-related effects (Pearce, 1983; Pearce and Peate, 1995). The general characteristics of these rocks include the enrichment of LFSE (represented by Th) to the most incompatible HFSE (Nb and Ta), and a depletion of Nb-Ta when compared to LREE (*i.e.*, La). This results in what is commonly termed 'the arc signature', a negative anomaly at Nb with respect to Th and La. Tholeiitic volcanic rocks from intra-oceanic island arc settings are recognized chiefly by this signature. When arcs are built upon continental lithosphere, the negative Nb anomaly and other LFSE/HFSE and REE/HFSE ratios become more fractionated, due to the enrichment of the LFSE and REE (especially LREE) from the crust and the retention of the HFSE in the source (Pearce and Peate, 1995). Tholeiitic and calc-alkaline arc volcanic rock types and their geochemical signatures are reviewed below, with typical primitive mantle-normalized extended trace element signatures shown in Figure 5-2.

Island arc tholeiites (IAT) are derived from a depleted mantle source that has undergone metasomatic modification due to the influence of a subducted slab. They generally produce flat patterns on mantle normalized trace element plots (range from slightly LREE-enriched to LREE-depleted) but always have a negative Nb anomaly (and possibly weak negative anomalies of other HFSE). They form in oceanic island arc settings or in advanced arc rifting (back-arc basins).

Calc-alkalic basalts (CAB), and commonly basaltic-andesites as well as andesites,

show the most pronounced enrichment of the highly incompatible trace elements seen in arc rocks. These rocks have the greatest LFSE and LREE enrichments and, therefore, the largest negative Nb anomalies on mantle normalized trace element plots. Strong negative anomalies at Ti as well as Zr or Y may also be apparent in these volcanics. The source of these volcanic rocks is similar to that of island arc tholeiites. However, as calc-alkalic basalts are mostly found in arc settings where continental crust is involved, it is assumed that crustal contamination plays a major role in genesis of these rocks.

Swinden *et al.* (1997) suggested that felsic volcanic rocks ranging from dacites to rhyolites are associated with calc-alkalic basalts throughout the Notre Dame subzone. These felsic rocks show strong enrichments of highly incompatible elements and produce pronounced negative Nb and Ti (and occasionally Eu) and positive Th anomalies on normalized trace element plots. Those workers considered several potential sources for these rocks including fractionation from mafic magmas or partial melting of sub-arc oceanic or continental crust.

Data from various mafic and felsic volcanics from several areas in the Buchans camp are plotted on extended rare earth element plots in Figure 5-3. All samples shown have distinctive negative Nb anomalies typical of arc volcanic rocks. However, there are numerous subtle variations amongst the data which require further explanation.

Ski Hill Formation mafic volcanics are shown in Figure 5-3a. Pronounced negative anomalies occur at Nb as well as Zr and Ti (except for LS-01 which has positive Zr and Ti), probably due to excess magnetite in this sample. Most samples also show minor troughs at Eu, although this may be due to plagioclase fractionation it is probably

alteration induced. Enriched LFSE/LREE ratios (*i.e.*, Th/La) produce overall negative slopes and suggest fractionation of the most incompatible elements. These signatures are typical of calc-alkaline basalts. Although there may be minor natural variations in the total REE contents, the large differences between total REE contents are caused mostly by mass changes due to hydrothermal alteration. That the signatures have not been noticeably modified, however, is evidence that the elements were indeed immobile.

Felsic volcanic rocks from the Buchans River Formation are plotted in Figure 5-3b. Again, prominent negative anomalies are present at Nb and Ti, however, no anomaly is present at Zr. Strong LFSE/HFSE (*i.e.*, Th/Zr) and LREE/HREE enrichments create the steep negative slope. LS-17 represents the BRF dacite (*i.e.,* stratigraphically lower or foot-wall) and the remaining samples (LS-02, 13, 46) represent rhyodacites (*i.e.*, stratigraphically higher or hanging-wall). The rhyodacites show steeper slopes consistent with the greater degree of fractionation. As is shown below in section 5.2.2.2, Y (and other HREE and MREE) have lower contents in the more fractionated suite indicative of the relative compatibility of these elements.

Felsic and mafic volcanic rocks from the Buchans East area are plotted on Figure 5-3c. Mafic and felsic endmembers have similar patterns on this diagram. Both endmembers show the prominent negative Nb anomaly typical of arc volcanic rocks but only felsic samples show the prominent negative Ti anomaly. A very weak negative anomaly occurs at Zr in the mafic samples, whereas a very weak positive Zr anomaly occurs in the felsic suite. Eu shows a weak to moderate negative spike in all samples which may be due to plagioclase fractionation and/or plagioclase destruction due to

alteration. The striking similarity in the overall patterns suggests common petrogenetic processes and source. It is assumed that the rocks were derived from a common source. TiO_2, as expected, would become incompatible beyond the mafic composition. Zr may have been very weakly compatible in the mafic magmas but appears to have behaved relatively incompatibly in the felsic suite, when compared to similar elements (*i.e.*, Nd and Sm). This suite is considered to be of island arc tholeiitic affinity.

5.2.2.2 Chondrite normalized rare earth element plots

On Figure 5-4, the REE have been normalized to Sun's (1980) chondrite values. The Ski Hill Formation plot on Figure 5-4a as negatively sloping patterns with enriched LREE relative to MREE and HREE. These rocks show only weak negative Eu anomalies, though ICP-MS analysis for Eu in some samples may have been complicated due to elevated barium contents (see Appendix B for ICP-MS analytical methods). These signatures are comparable to Kuroko pre- and post-ore mafic volcanics. Much of the offset in concentration is due to mass change effects which are discussed in the following chapter.

Felsic volcanic rocks from the Buchans River Formations are shown in Figure 5-4b. These samples show significant enrichment of LREE relative to HREE on the chondrite normalized plots, however, unlike the mafic samples, the felsic suites show distinctive concave upward patterns on the right side of the plot consistent with depletion of the MREE and HREE. This signature is commonly caused by partitioning of the MREE into hornblende, or possibly clinopyroxene (Rollinson, 1993). One sample, LS-

16 (not plotted), had such large mass gains that REE concentrations were close to or below detection limits for most elements. Negligible Eu anomalies are observed in these felsic rocks. The patterns are similar to Kuroko pre- and post-ore felsic volcanics, but with more fractionated LREE to HREE.

Mafic rocks from the Buchans East area have overall flat patterns on the chondrite-normalized plots (Figure 5-4c). They vary from slight LREE depleted at the Powerhouse Alteration Zone (PH-01) to slight LREE enriched at the Woodmans Brook Zone (WB-10) and have moderate negative Eu anomalies. These signatures lack the LREE fractionation observed in the more calc-alkaline Ski Hill Formation, and are also unlike the Kuroko felsic volcanic rocks.

Felsic volcanic rocks from both the PHZ and WBZ show the same chondrite-normalized REE patterns which can be described as fairly flat, weakly LREE enriched and with prominent negative Eu anomalies (Figure 5-4d). These rocks differ from the Buchans River Formation in terms of their lack of strong LREE enrichment. Also, the BRF has a distinctive concave upwards signature for the MREE-HREE whereas these felsic volcanic rocks are flat. These rocks also display less LREE enrichment than the Kuroko felsic volcanics. One anomalous sample from the Powerhouse Zone (PH-19) displays a rather unusual signature of strong HREE enrichment. This sample probably represents some mobility of the REE.

5.2.3 Mafic rocks as indicators of tectono-magmatic setting

The plots used in this section have been taken from the literature where extensive data sets were collected to determine the geochemical signatures of various tectonic settings. ICP-MS and XRF pressed powder pellet trace element data are both used here to reinforce the interpretation of the normalized plots.

V vs. Ti/1000 is used as an indicator of either arc or non-arc tectonic settings (Figure 5-5). Shervais (1982) uses a (Ti/V)/1000 ratio of 20 to divide the groups. The lower ratio, due to the depletion of Ti, is characteristic of arc volcanism. With only a few exceptions, all mafic rocks plotted occur within the arc field. The Buchans East area samples plot at lower Ti/V ratios than most of the Ski Hill Formation due to more depleted Ti in these rocks. The APZ rocks plot in both arc and non-arc fields.

Various igneous affinities are defined on Figure 5-6 for mafic rocks using a bivariate Zr vs. Ti plot (Pearce and Cann, 1973). Fields are outlined for ocean floor basalts (OFB), low-K tholeiites (LKT) and calc-alkalic basalts (CAB). Most samples from all groups overlap with each other in field A. The Ski Hill Formation and Airport Zone samples extend into fields B, C and D, C, respectively. These signatures are typical of calc-alkaline basalts (A,C) and ocean-floor basalts (B,D). The lack of elevated Zr in any of the Buchans East rocks suggests that they are more tholeiitic. Mass changes due to alteration may cause slight scattering on this plot.

Figure 5-7 is a ternary diagram from Pearce and Cann (1973) which utilizes Zr - Ti - Y to subdivide mafic volcanic rocks into various tectono-magmatic settings. In Figure 5-7a, most of the Ski Hill Formation mafic rocks plot into fields B and C typical

of calc-alkalic basalts. This is due to the depletion of Ti and Y relative to Zr in these suites. The Woodmans Brook zone data plot at the boundary of fields A and B and are consistent with a more low-K tholeiitic suite. The Powerhouse Alteration zone mafic rocks overlap with the B field, but again scattering of data normal to the Y apex (caused by mobility of this element) poses problems for interpretation. However, these rocks are also more akin to the low-K tholeiite type based on the relatively lower Zr contents. The Airport alteration zone data fall into fields A and B similar to the Ski Hill Formation and are more typical of calc-alkalic suites.

Wood (1980) developed a series of ternary diagrams for classifying mafic rocks utilizing various HFSE including: Zr, Th, Nb, Hf and Ta. Three of these plots are shown in Figures 5-8 a, b, and c and include fields for N-MORB, E-MORB, within plate basalts, and arc-related basalts. The arc-related field is characterized by proportionately lower contents of Nb and Ta. Within this field, the more calc-alkalic suites show higher proportions of Th relative to Zr or Hf. All of the data plotted here are categorized as arc-related volcanics and tend to show the high proportions of Th typical of calc-alkalic suites, or crustal contamination, with the greatest enrichment occurring in the SHF mafic volcanics. Several other key points are noted from these plots. First, there is remarkable consistency in the HFSE ratios for samples from the PHZ and WBZ. Also, the Ski Hill Formation mafic samples appear to be more calc-alkalic (*i.e.,* greater tendency towards Th endmember). Finally, Ta tends to show a greater range in data (Figure 5-8c) with Buchans East samples plotting close to the within plate basalt field. However, the trend of all data towards the Ta apex suggests a probable contaminant contributed to the element concentration.

5.2.3 Bimodal suites - genetic relationships

This section discusses the trace element geochemistry of both mafic and felsic volcanic rocks from several locations in the Buchans area. Trace element data will be used here to illustrate genetic relationships within bimodal volcanic suites, to compare the trace element signatures between volcanic suites, and to suggest petrogenetic processes responsible for their formation.

Incompatible and immobile HFSE data for a suite of volcanic rocks plotted on binary plots should produce linear enrichment trends from mafic to felsic endmembers. Related volcanic suites should maintain the constant HFSE ratios and therefore plot on the same line drawn from the origin. Caution is warranted, however, when assuming this in strongly calc-alkalic systems where HFSE can behave compatibly. Additionally, these ratios are also monitors of magmatic affinity. Since the HREE and Y are less incompatible than LREE and Zr, Nb, Hf, Ta, Th and U, ratios of LREE/HREE and Zr/Y, for example, are generally higher in calc-alkaline suites. These patterns are mimicked on trace element normalized plots.

Barrett and MacLean (1994a) have defined ranges of Zr/Y ratio ranges for tholeiitic to calc-alkalic affinities as follows:

Tholeiitic	2 - 4.5
Transitional	4.5 - 7
Calc-alkaline	7 - 25

The authors suggest that the transitional rocks have characteristics in common with flanking endmembers and border the field boundary on the standard AFM diagram,

falling somewhat into the calc-alkaline field.

On Figure 5-9a, data from the Lucky Strike area plot as two distinct trends. The strong linear upper trend, with a mean Zr/Y ratio of 4.2, falls within the tholeiitic field but near the transitional field. This trend, as defined, incorporates the mafic volcanic rocks of the Ski Hill Formation and the BRF dacites and implies a genetic link between these compositional endmembers (*i.e.*, these rocks appear to have had a common magmatic source). The other group, with an average Zr/Y ratio of approximately 9, suggests a distinctly stronger calc-alkalic affinity and corresponds to rhyodacitic volcanics from the Buchans River Formation. This separate trend may reflect different sources, or alternatively, a magmatic shift. Specifically, the group with higher Zr/Y can be produced from the other if Y becomes compatible. Indeed, the rhyodacites do have more lower concentrations of MREE and HREE than the dacites (concave patterns on REE plots, Figure 5-4b). These trends are supported by numerous other trace element ratios, such as Nb/Zr (Figure 5-10) and Nb/Y (Figure 5-11), both of which are distinctly higher for the Buchans River Formation. La/Yb, and other LREE/HREE ratios (Figure 5-12), also illustrate the more evolved nature of the Buchans River Formation. Finally, the dacites also have higher P_2O_5 contents, with twenty samples averaging 0.06 wt. % and only one below the detection limit of 0.03 wt.%. In contrast, most rhyodacites have P_2O_5 contents below the limits of detection.

In Figure 5-9b, bimodal volcanic rocks from the WBZ plot on a linear trend with a Zr/Y ratio of less than 4, consistent with a dominantly tholeiitic affinity. The fact that these mafic and felsic rocks show slight negative and slightly positive anomalies on

normalized extended trace element plots suggests that Zr behaved relatively more incompatibly in the felsic suites than the REE. Therefore, the fractionation line drawn on the plot may not be linear.

The PHZ bimodal suite plots on a similar trend to that of the WBZ suite with an average Zr/Y of about 4.5 (Figure 5-9c), suggesting an affinity close to the tholeiitic/transitional boundary based on the classification of Barrett and MacLean. Also evident on this plot is the large variation of Y with limited Zr ranges. This vertical scattering is exhibited by both the mafic and felsic clusters is quite unusual as it is not exhibited on the plots for other zones. No primary igneous process would generate this type of scattering of Y and, therefore, hydrothermal alteration is more likely responsible. That being said, the Powerhouse Alteration zone appears to contain a significant component of hydrothermal carbonate (calcite, dolomite) as an alteration product. Carbonate complexing is known to be a viable process for mobilizing the REE and Y (Taylor and Fryer, 1983). The unusual REE signature for sample PH-19 (Figure 5-4d), which also contains the lowest concentration of Y any felsic sample from this zone, was likely a function of alteration.

Figure 5-9d shows a scattering of data from the APZ on the Zr versus Y plot, with Zr/Y ratios ranging from approximately 2 to 17. The samples have affinities varying from tholeiitic to strongly calc-alkalic. Of note is the fact that some calc-alkalic felsic samples plot in the same Zr-Y space as those of the Buchans River Formation. These samples include those from the APZ-S and a few from the APZ-N. This obviously suggests some complexity for this zone.

Plotting all data on Zr vs. Nb and Y vs. Nb plots (Figures 5-10 and 5-11, respectively), the variation in HFSE for all groups can be illustrated. The Buchans East mafic volcanic rocks plot in the lower left hand corner having the lowest HFSE contents. Mafic rocks from the SHF also plot in the lower left hand corner, but with slightly higher contents than the Buchans East mafics. Felsic rocks from Buchans East have intermediate HFSE contents. The BRF has the greatest HFSE contents of all groups, however, the dacites and rhyodacites occupy distinctly different space on both plots. The Nb concentration is consistent for both dacites and rhyodacites, ranging from 3 to 8 ppm. However, Zr, and more notably Y, are both significantly lower in the rhyodacite as compared to the dacite.

In order to emphasize the variation amongst the REE data for the different alteration zone in the Buchans camp, numerous bivariate plots have been designed comparing chondrite-normalized LREE, MREE and HREE. Both mafic and felsic rocks are compared on these graphs. The grouping of the data in this section is as follows: (i) Ski Hill Formation mafics and BRF dacites, (ii) Buchans River Formation rhyodacites, and (iii) Buchans East (including mafic and felsic rocks from the Powerhouse and Woodman's Brook Zone).

In Figure 5-12, consistent results are obtained on plots of HREE versus LREE. The Buchans River Formation rhyodacite samples consistently display higher LREE/HREE ratios than the BRF dacites and SHF mafic lavas, which in turn have higher LREE/HREE ratios than the bimodal Buchans East samples. The lightest LREE (La) versus the HREE display this relationship best. These plots simply reinforce the data

from the normalized trace element plots which show distinctively higher degrees of LREE/HREE fractionation in the Buchans River Formation rhyodacites. The Buchans East samples, which produced flatter normalized trace element signatures, have the least fractionated LREE to HREE.

Chondrite-normalized HREE to MREE ratios were examined but do not display much variation. In fact, the samples overlap from all zones and cannot be separated into distinctive groups (Figure 5-13).

Comparing chondrite-normalized MREE vs. LREE (Figure 5-14), the highest LREE/MREE ratios are found in the BRF rhyodacites. SHF mafics and BRF dacites have intermediate LREE/MREE ratios, while the least amount of LREE to MREE fractionation has occurred in the Buchans East area.

In Figure 5-15, the variation in LFSE/HFSE ratios (Th/Nb, Th/Y and Th/Zr) is plotted against Zr/TiO_2 as a measure of fractionation. The BRF dacite has similar LFSE/HFSE ratios to the SHF, yet the BRF rhyodacites are typically much higher in these ratios, especially Th/Y owing to a decrease in Y contents. The Buchans East felsic volcanics show unremarkable changes in the ratios when compared to the mafic rocks from that zone. LFSE/REE ratios (*i.e.*, Th/La, Th/Yb, Th/Lu) display nearly identical trends (Figure 5-16). The greatest degree of fractionation in the ratios occurs of the LFSE/HREE (Th/Yb, Th/Lu).

The Y versus Nb tectonic discrimination diagram for felsic volcanic rocks (Pearce, *et al.*, 1984) has been used to classify the various suites in the Buchans area (Figure 5-17). The Buchans River Formation rhyodacites, with high Nb/Y ratios,

represent I-type arc magmatism. The BRF dacites and Buchans East felsic volcanics partially overlap and have lower Nb/Y typical of M-type arc magmatism. For comparison, the Kuroko felsic volcanics are shown to plot in the I-type field very similar to the BRF rhyodacites.

5.3 Lead Isotopes

Initial lead isotope studies in the Buchans camp (*i.e.,* Bell and Blenkinsop, 1981) suggested model ages that were too young considering the age of the host rocks and eliminated simple, single-stage models as an explanation for the evolution of the Pb isotope ratios in the rocks. These workers also suggested that the lead evolved in a primitive (low μ; $\mu=^{238}U/^{204}Pb$) environment and compared these values with those from Fletcher and Farquhar (1977) for the Grenville Province. The implication is that there is some relationship to the continental crust of Eastern North America. A more comprehensive study by Cumming and Krstic (1987) included all of the major ore bodies in the Buchans camp, including the Clementine prospect, as well as several other important VMS prospects in the region (*i.e.*, Connel Option, Mary March, Skidder, Tulks Hill/Tulks East and the Victoria Mine prospects). These workers illustrated that there is remarkable consistency in the lead isotope ratios of all data from the Buchans camp, with variations just larger than the limits of detection, and concluded that the distribution is due to a short period of Pb evolution in the volcanic environment soon after formation. Interestingly, the other prospects yielded distinctly different ratios. Cumming and Krstic (1987) presented the data as defining two lines which may be either multi-stage isochrons

or mixing lines. These workers supported the results of the previous study in that model ages were too young and that the metals were derived from a primitive source.

In a more regional scale study involving VMS deposits throughout the entire Central Mobile Belt of Newfoundland, Swinden and Thorpe (1984) identified Buchans as having one of the most primitive lead isotopic signatures. These workers showed that several other deposits hosted throughout the Roberts Arm and Cutwell Groups have similar lead isotopic signatures as Buchans. Additionally, the ophiolite-hosted York Harbour deposit, interpreted by Swinden and Thorpe (1984) as having a lead isotopic composition of Early Ordovician mantle, is strikingly similar to that of the Buchans.

For this study, six galena separates from the Buchans area were analyzed for their lead isotope ratios. These six samples are plotted in Figure 5-18 along with other data from the region from Cumming and Krstic (1987). Galena was collected from sulphide stringers in altered rocks from both the APZ, MBZ, PHZ and WBZ. Galena was also taken from sulphide-barite bearing breccia sequences from the Sandfill prospect and the newly discovered Middle Branch East prospect.

Samples from the Sandfill prospect, MBZ and APZ plot within the Buchans ore field of Cumming and Krstic (1987) on the $^{20b}Pb/^{204}Pb$ vs. $^{207}Pb/^{204}Pb$ plot (Figure 3-20) and are considered to have the same lead source as the Buchans ore deposits. It is not surprising that lead from the MBZ and Sandfill prospect match the Buchans ore leads as they are indeed part of the ore forming system. The APZ is apparently not part of that system, being immediately hosted in a different volcanic suite, but has matching lead isotopic ratios. It is reasonable that this lead may have been remobilized from the a

'Buchans source'. That the whole rock geochemistry from this zone indicated a mix of possible magmatic affinities, including calc-alkaline volcanics, suggests that this zone is not completely understood.

The Middle Branch East prospect, located ~2 km east of Oriental, is a newly discovered prospect of debris flow sulphide-barite mineralization that is associated with strongly potassic-altered mafic volcanic rocks. However, the prospect was discovered during the writing of this thesis and, as a result, is not discussed with respect to alteration. Galena from this fragmental unit indicates a slightly more radiogenic source than that for Buchans ore lead that is most like that of the Mary March Prospect (refer to section 2.6.3). This occurrence suggests that a potentially different and, as yet undiscovered, *in-situ* source of mineralization exists.

Galena recovered from sulphide stringers in pseudo-brecciated and weakly silicified and sericitized rhyodacites at the Powerhouse Zone have lead isotope signatures more primitive than Buchans, plotting on a mixing line intermediate between Buchans ore lead and the Skidder Prospect lead. The lead is strikingly similar to that of the Connel Option (refer to section 2.6.3).

At the Woodmans Brook Zone, galena was collected from a sulphide stringer with abundant galena and sphalerite. The host rocks are strongly silicified-sericitized dacites. Lead isotope ratios from this zone were the most primitive of all samples analyzed in this study and plotted amongst the Skidder prospect data (refer to section 2.6.3). These ratios are at or below the mantle growth curve of Doe and Zartman (1989).

The grouping of the data into distinctive clusters has interesting implications for

metallogeny in the Buchans region. Within a belt of volcanic rocks, VMS deposits from individual clusters have lead isotopic signatures that are very similar and group separately from other clusters (*e.g.*, Noranda and Matagami, Vervoort *et al.*, 1994). Consequently, it appears that the same is true for the Buchans region with at least four separate groupings being defined. Assuming a syn-volcanic origin, data that plot within the Buchans ore cluster should be considered as having a high probability of being associated with the Buchans ore-forming hydrothermal system. Data that plot with other clusters should be considered to have, as yet, unproven potential for economic VMS mineralization.

5.4 Discussion and Summary

The integrated results from the trace element and lead isotope data provide several interesting new ideas for the Buchans area geology. These new concepts have exciting and direct implications for VMS exploration at both regional and mine scales.

On a local scale, trace element data have successfully distinguished two previously undivided felsic volcanic sequences within the Buchans River Formation. These two suites comprise a transitional (or mildly calc-alkaline) dacitic unit and a more strongly calc-alkaline rhyodacitic unit. The transitional dacites have incompatible trace element ratios and REE profiles that mimic those of the SHF andesitic basalts. Therefore, it appears that these compositional endmembers are genetically related with the felsic volcanics representing a more fractionated product of the same source. The rhyodacitic volcanics have a lithogeochemical signature that is broadly similar to the

dacites but clearly distinctive. Their normalized trace element profiles are more inclined or steeper and key HFSE ratios differ (higher Zr/Y, Nb/Y, Nb/Zr). The rhyodacites may then represent a genetically unrelated suite. Alternatively, these felsic volcanic units may be related if the least incompatible elements (*i.e.*, MREE, Y, HREE) became compatible in the sub-volcanic source before eruption of the rhyodacites.

The stratigraphic relationship of these felsic units are complexed by structure, but generally the rhyodacitic composition volcanic rocks tend to be less abundant and stratigraphically higher. In addition, the main period of ore deposition may have occurred after the eruption of the dacites but prior to the eruption of the rhyodacites. The sequence of events is illustrated schematically in Figure 5-19. This has implications for exploration in the Buchans camp and the understanding of the genesis of VMS deposits in general. Other Phanerozoic examples of VMS deposits with distinctively stronger calc-alkalic felsic volcanics in the ore horizon/hanging-wall include Myra Falls (Barrett and Sherlock, 1996) and Kutcho Creek (Barrett *et al.*, 1996) representing mature arc and primitive arc settings, respectively. Some Archean VMS settings also commonly show these same characteristics. The Mobrun (Barrett *et al.*, 1992) and Delbridge (Barrett *et al.*, 1993) VMS deposits in the Noranda camp, Quebec, are located between two felsic lava series of tholeiitic and more calc-alkalic affinity, based on HFSE and REE ratios. Furthermore, Urabe (1987) reports a shift in the normative composition of the felsic magma from meta-aluminous in the foot-wall to alkaline in the hanging-wall with respect to the Kuroko deposits, although the trace element systematics are not discussed. As an aside, Urabe (1987) also proposes that an

aluminous felsic magma would have been favourable for the generation of a metal-rich magmatic fluid. He uses this and several other lines of evidence to support a magmatic hydrothermal theory for the the Kuroko deposits.

Regionally, based on immobile trace element and lead isotope data, two distinctive tectono-magmatic terranes are recognized. The subdivision occurs between the immediate Buchans mine area (based on data from the LSZ and MBZ) and the Buchans East area (hosting the Powerhouse and Woodmans Brook Zones). The two regions are separated by a significant fault, the Airport Thrust (Calon and Green, 1987) . The bimodal felsic and mafic rocks in the Buchans East area represent a distinctly different volcanic suite than those which host the Lucky Strike orebodies at Buchans. Volcanic rocks in the Buchans East area define a tholeiitic island arc volcanic sequence. Moreover, lead isotope data are also quite different in each of the two settings, with data from the Buchans East area representing more non-radiogenic lead sources. The more primitive lead source and tholeiitic trace element signatures suggest that this area represents an oceanic island arc that has not been influenced, at least to the same degree as the known ore-hosting rocks, by continental crust. Swinden *et al.* (1997) proposed several models for the tectonic development of the Notre Dame subzone, including subduction of oceanic crust under a highly irregular Laurentian continental margin (Figure 5-20). In this model, arc volcanism developed simultaneously through continental crust in promontories and through oceanic crust in reentrants. Rocks representing Early Ordovician intraoceanic island arc volcanism have not previously been documented in the Buchans-Robert's Arm Belt. The Buchans East area may

represent this type of setting.

Alternatively, the Buchans East rocks may represent more advanced rifting of the arc, which eventually evolves into a back-arc rift (Figure 5-21). This scenario has been suggested by Lentz (1998) to be a very important tectonic setting for the genesis of VMS deposits. In this scenario, continued extension the of the arc would tap sub-arc magmas that have faster ascent rates due to elevated heat flow and are not influenced by crustal contamination processes. Under this model the tholeiitic Buchans East rocks would be slightly younger. Unfortunately, the small amount of geochronolgical data that exist for the Buchans - Roberts Arm Belt have been limited to calc-alkaline sequences.

Furthermore, the WBZ and PHZ of Buchans East are hosted in slightly different volcanic suites, based on geochemistry, and have different lead isotopic signatures. Each appears to represent distinctive hydrothermal events or sources. Lead isotope ratios suggest possible correlations between prospects such as the Powerhouse zone and the Connel Option, approximately 15 km along strike to the east. The correlation of the WBZ lead isotopic ratios and those from the Skidder Group is less certain, however, both appear to represent components of primitive arc settings. These may be part of back-arc setting that existed adjacent to the calc-alkaline Buchans Group *senso stricto*.

Also interesting is that lead data from the debris flow-type East Branch prospect is unlike the Buchans ore which, consequently, are the only known *in-situ* sulphide sources or 'hydrothermal vent facies' in the Buchans area. This supports the possibility for as yet an undiscovered *in-situ* sulphide source in the Buchans East area. Deposits of

the Hokuroko district of Japan, for instance, are considered to have formed contemporaneously within one cluster, yet clusters themselves are not contemporaneous and have formed over periods of several million years (Tanimura *et al.*, 1983).

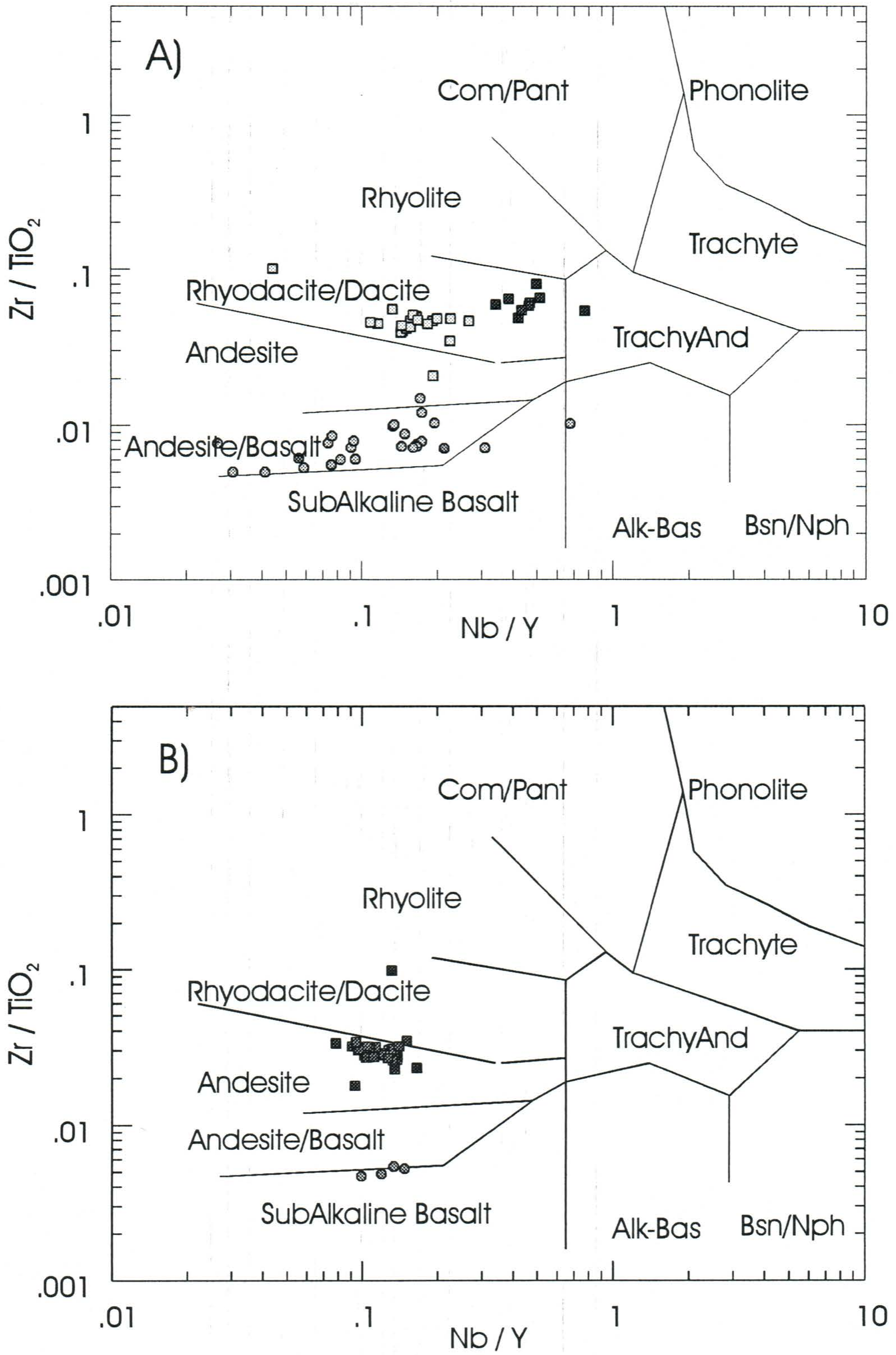


Figure 5-1 - Compositional plot based on immobile trace element ratios from Winchester and Floyd (1977) for (a) the Lucky Strike Zone, (b) the Woodmans Brook Zone, (c) the Powerhouse Zone and (d) the Airport Zone. Com/Pant = commendite/pantellite, Trachyand = trachyandesite, Alk-bas = alkali basalt, Bsn/Nph = basanite/nephelinite. Symbols for each group were defined primarily by this plot. Samples with Nb concentration below detection limit are not plotted.

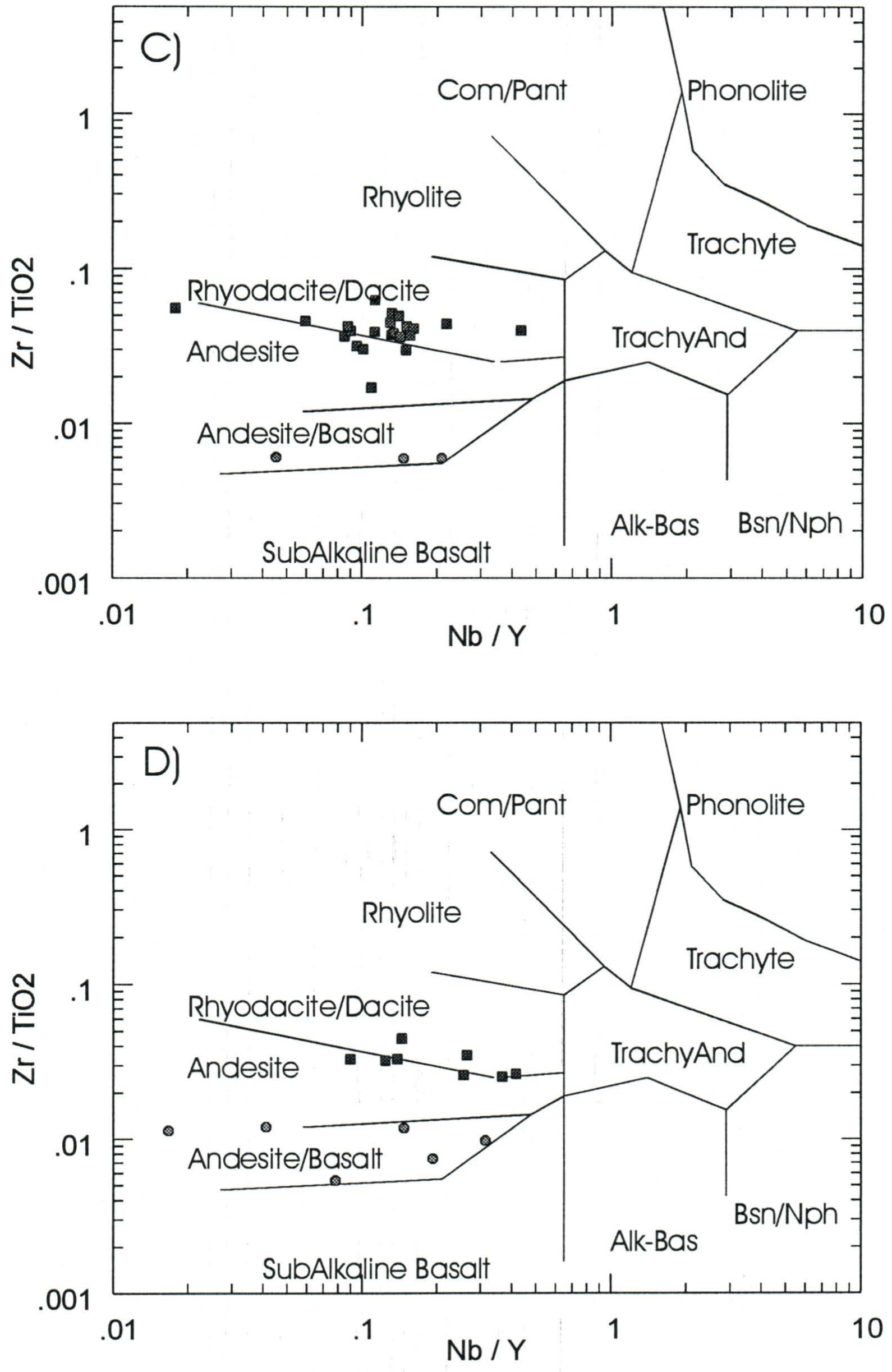


Figure 5-1 (continued)

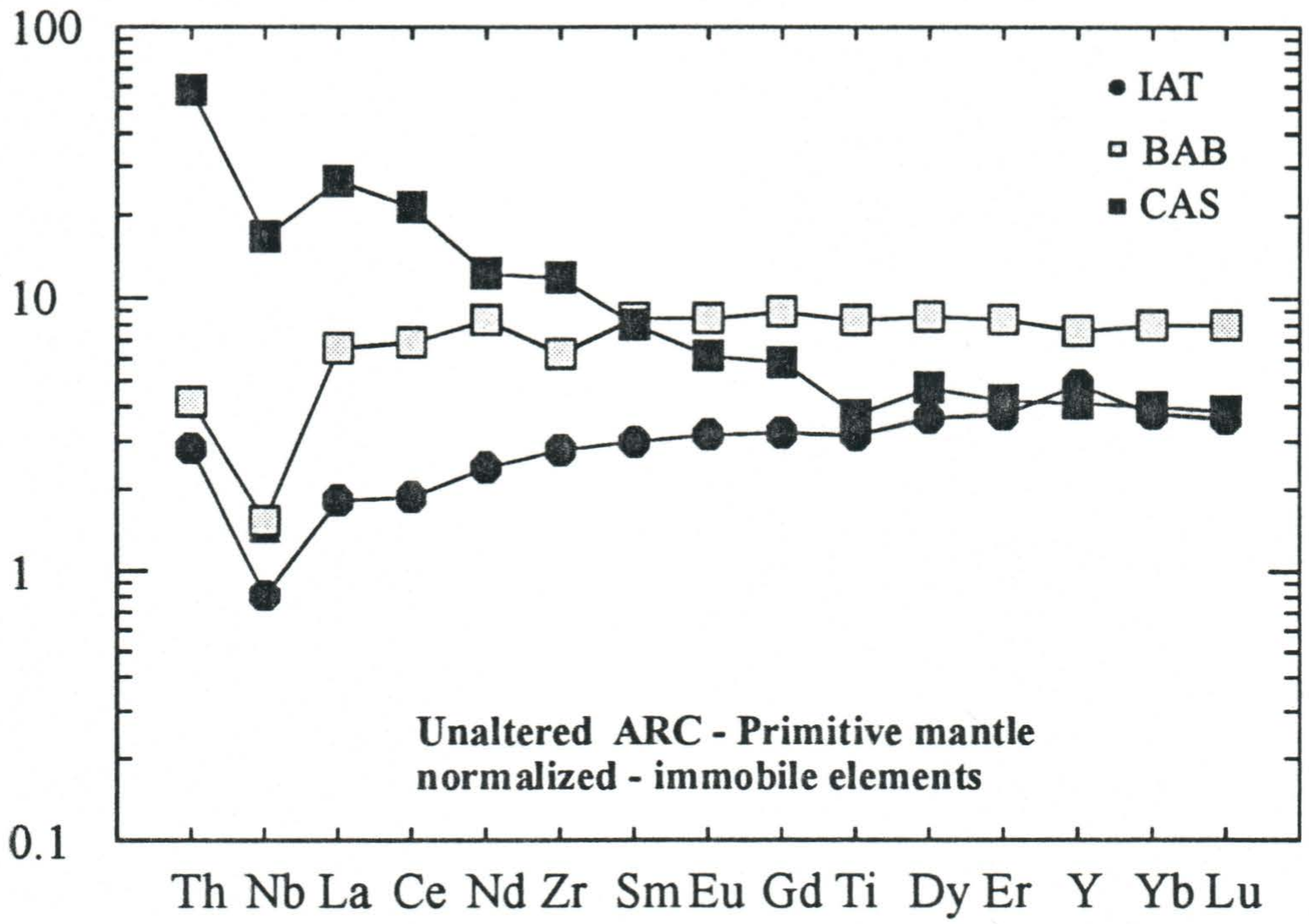


Figure 5-2 - Representative primitive mantle-normalized geochemical patterns of arc volcanic rocks (CAS = calc-alkalic basalt, IAT = island arc tholeiites, and BAB = back arc basin) from Jenner (1996). Normalization is to primitive mantle (Sun and McDonough, 1989).

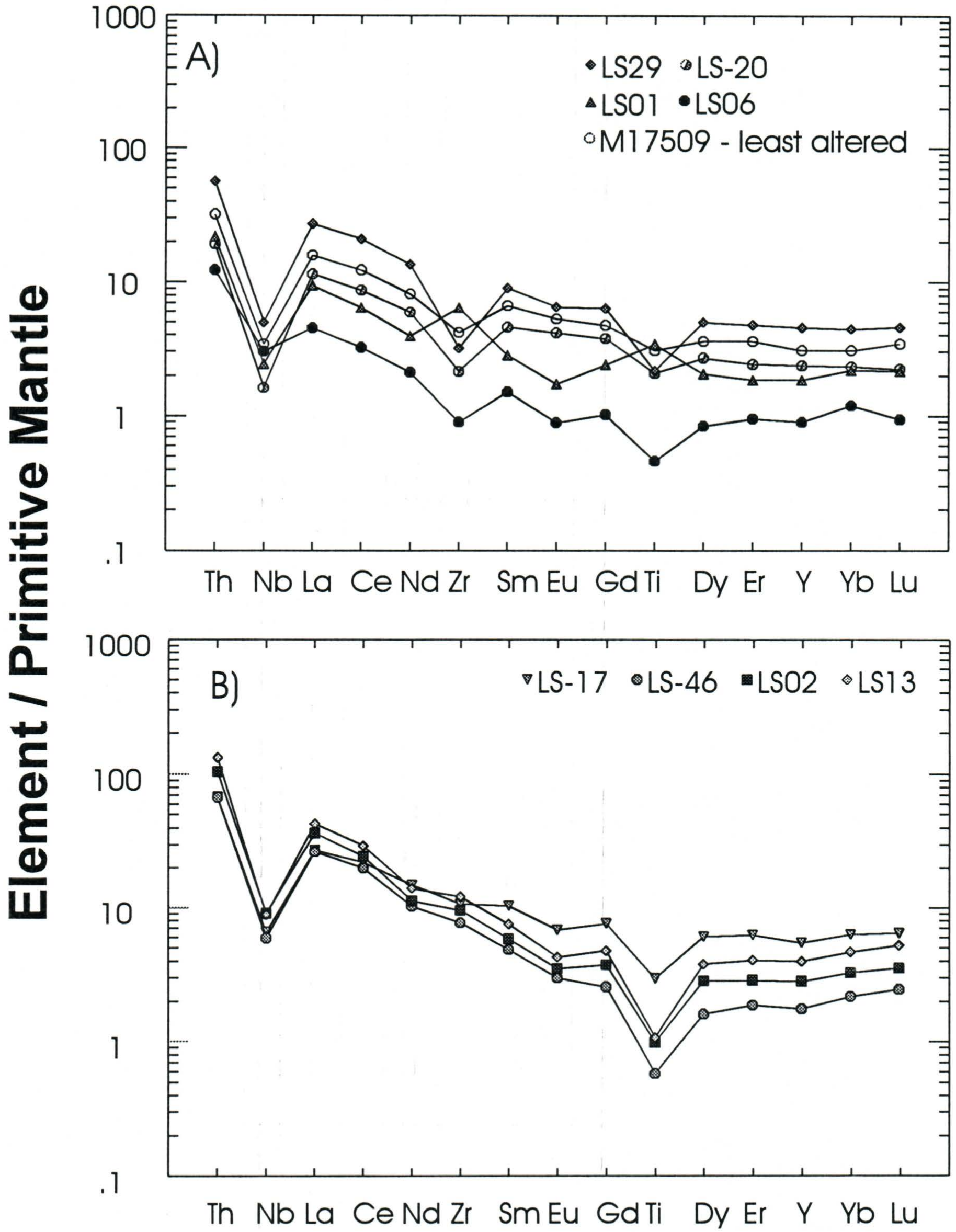


Figure 5-3 - Extended trace element plot for mafic and felsic rocks. Element selection and order are from Jenner (1996) and normalization is to the hypothetical primitive mantle of Sun and McDonough (1989); (a) Ski Hill Formation mafic volcanics, (b) Buchans River and Ski Hill Formation felsic volcanics, (c) Powerhouse/Woodmans Brook Alteration Zone mafic and felsic rocks.

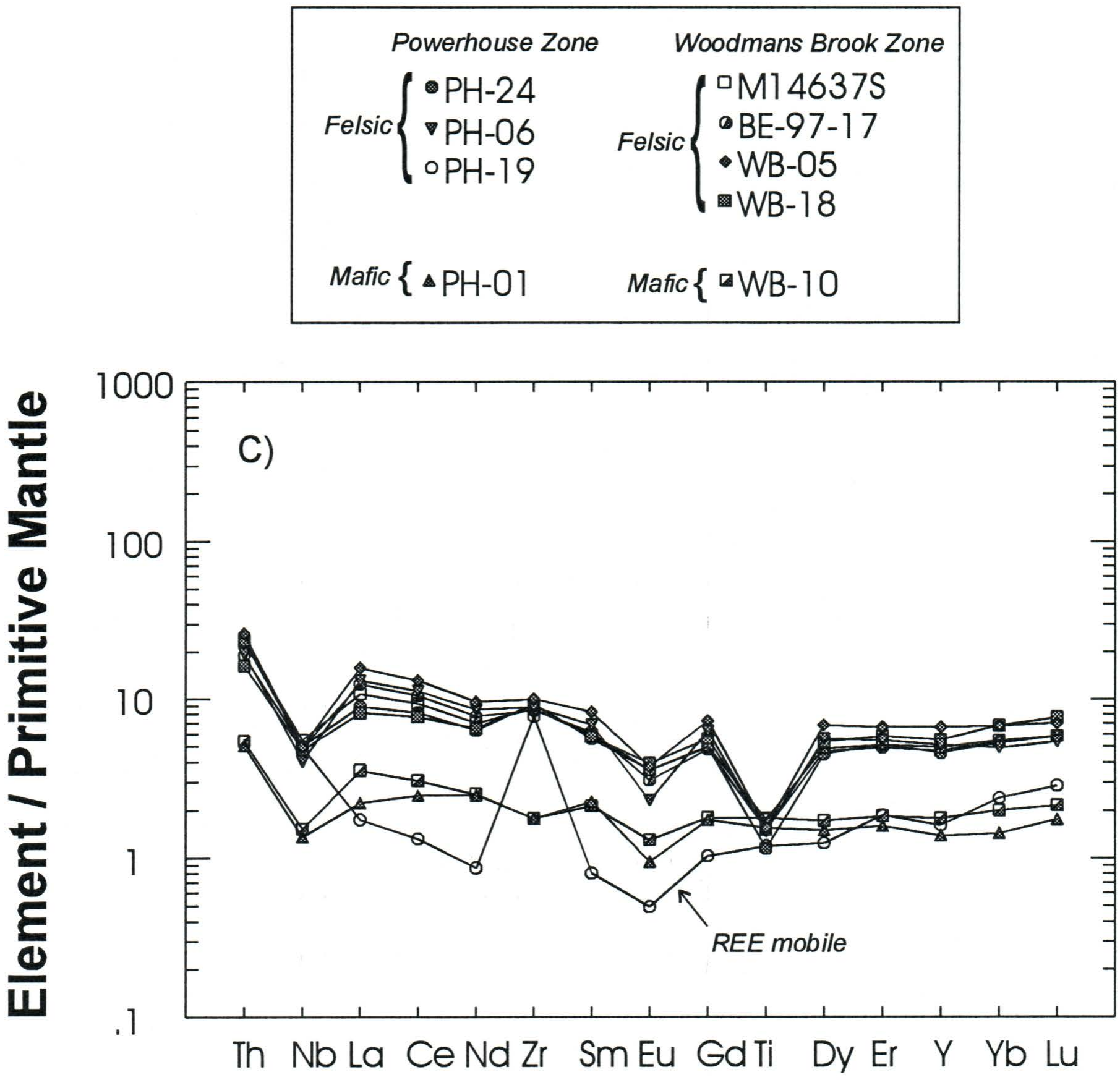


Figure 5-3 (continued)

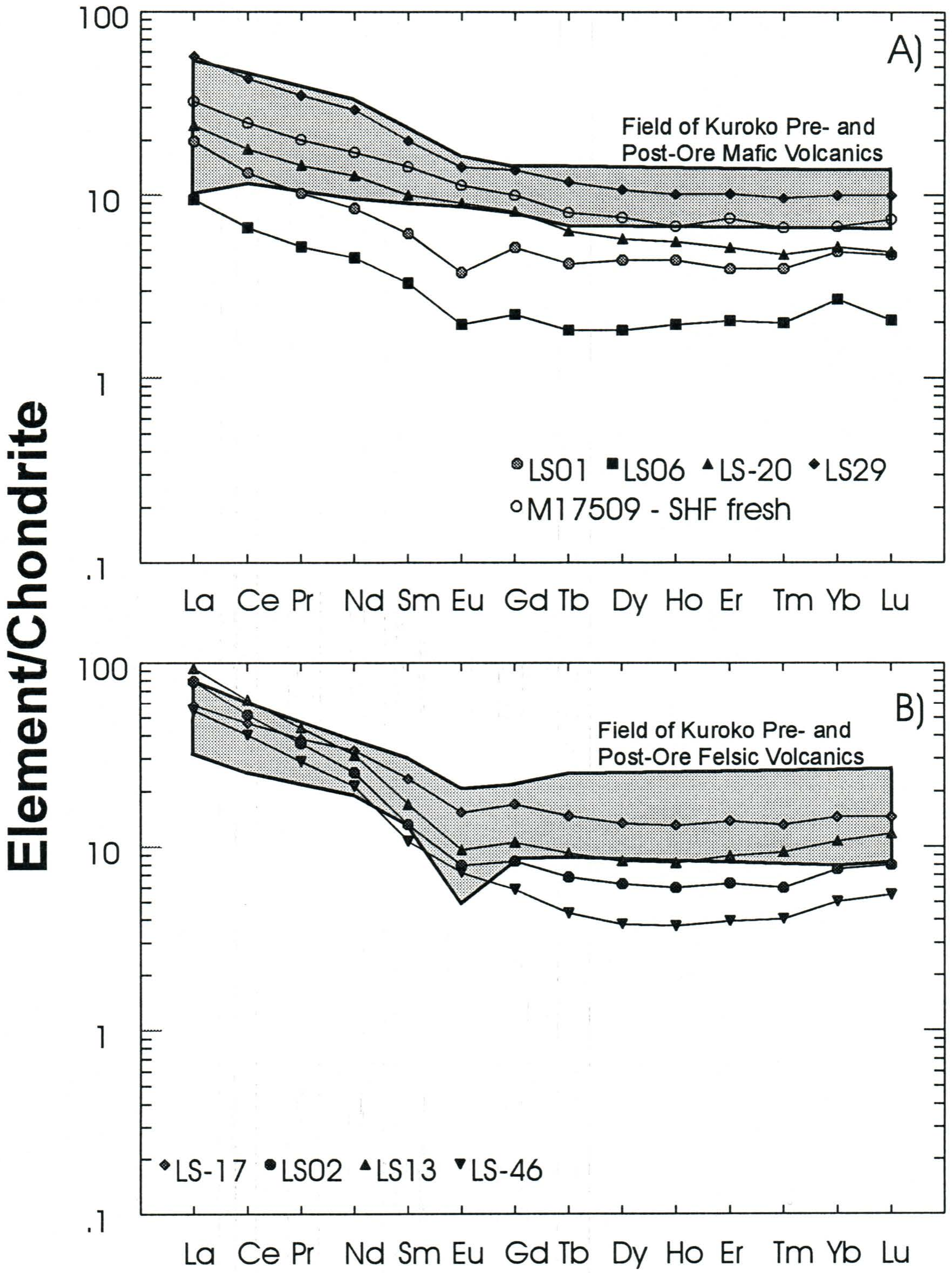


Figure 5-4 - Chondrite normalized REE profiles for mafic and felsic rocks from the Buchans area. Normalization factors from Sun (1980); (a) Ski Hill Formation mafic rocks, (b) Buchans River and Ski Hill Formation felsic volcanics, (c) Powerhouse/ Woodmans Brook zones mafic volcanics, (d) and Powerhouse/ WoodmansBrook zones felsic volcanics.

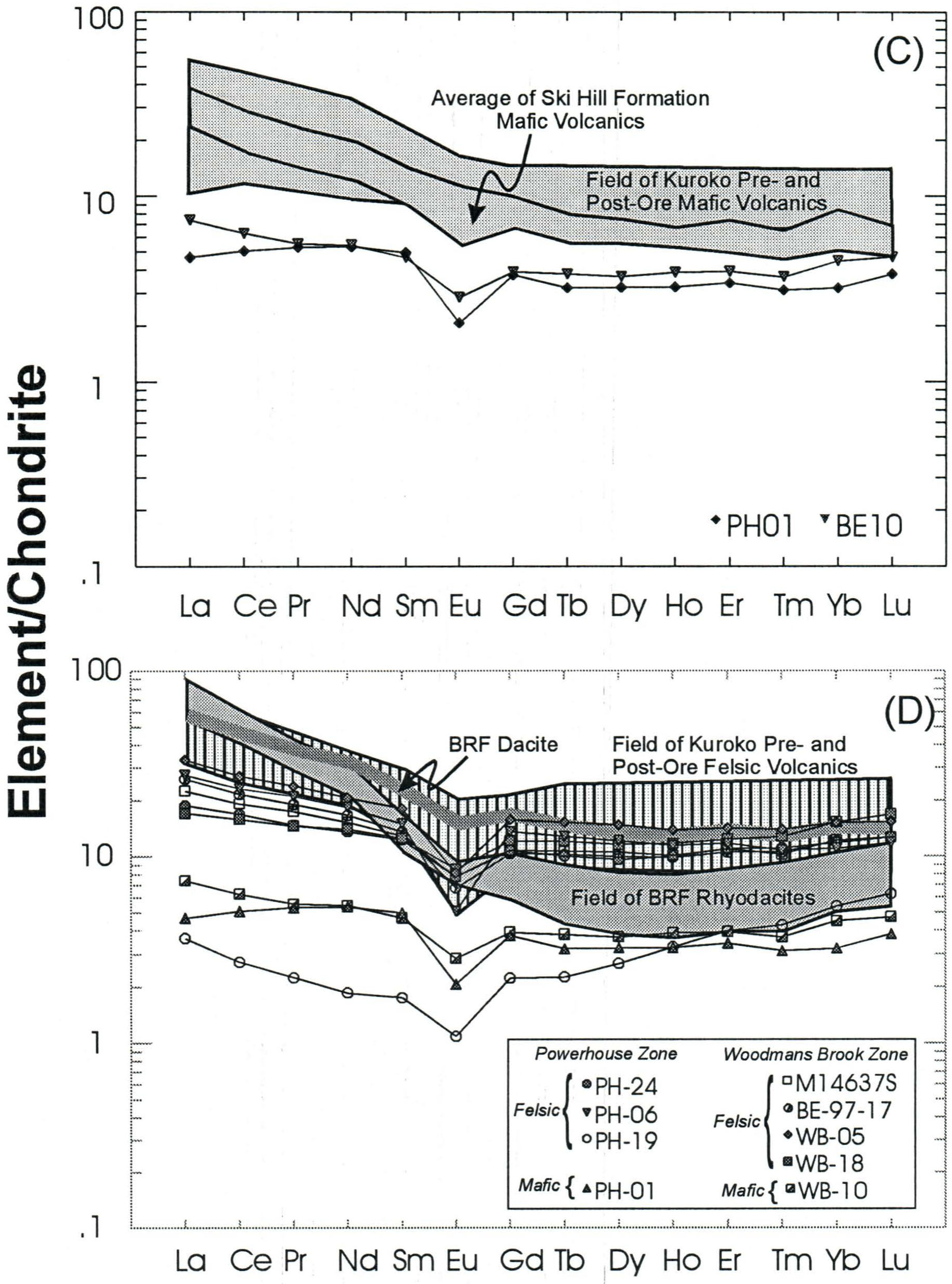


Figure 5-4 (continued)

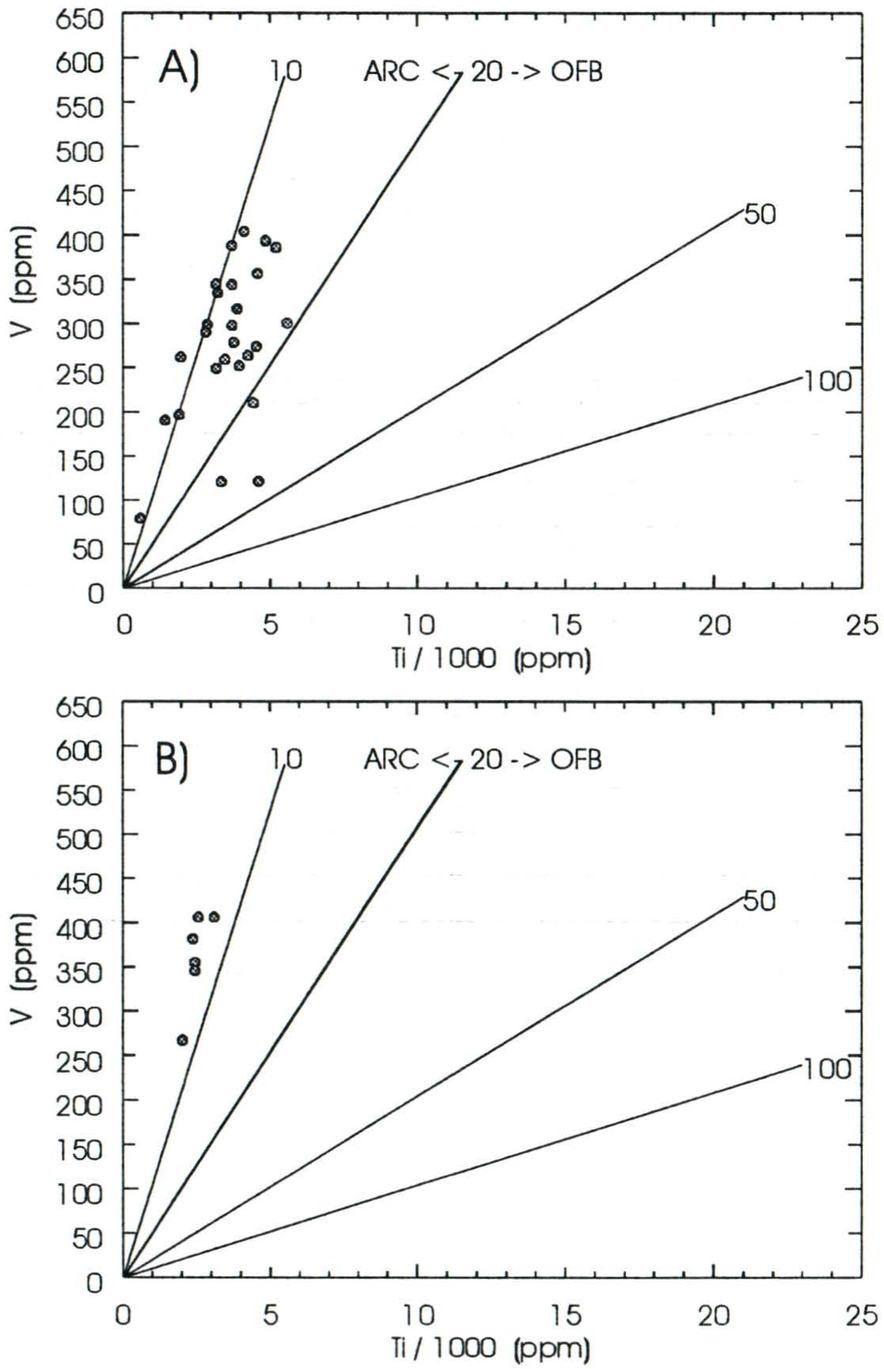
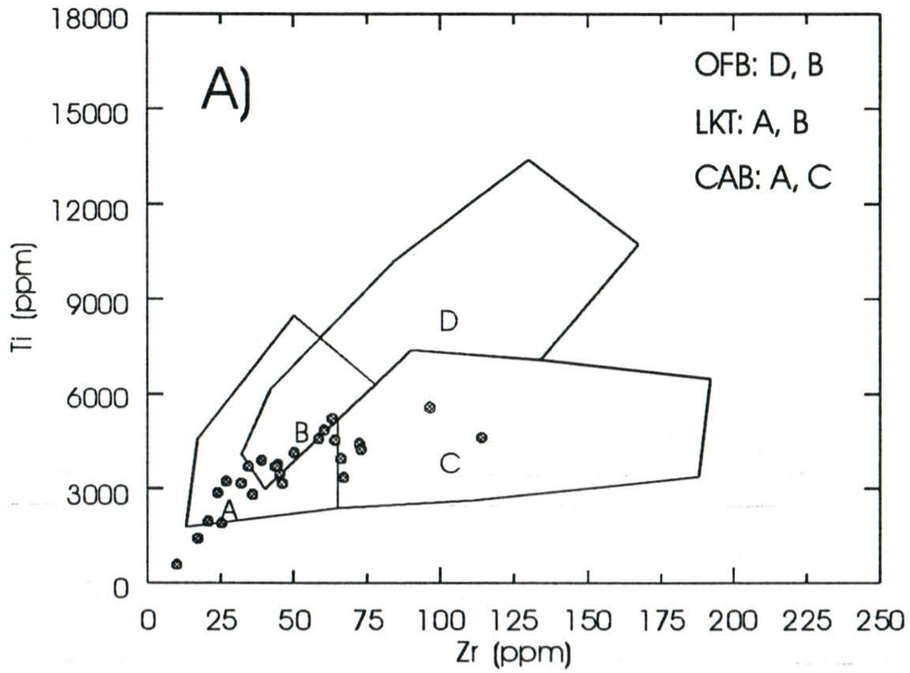
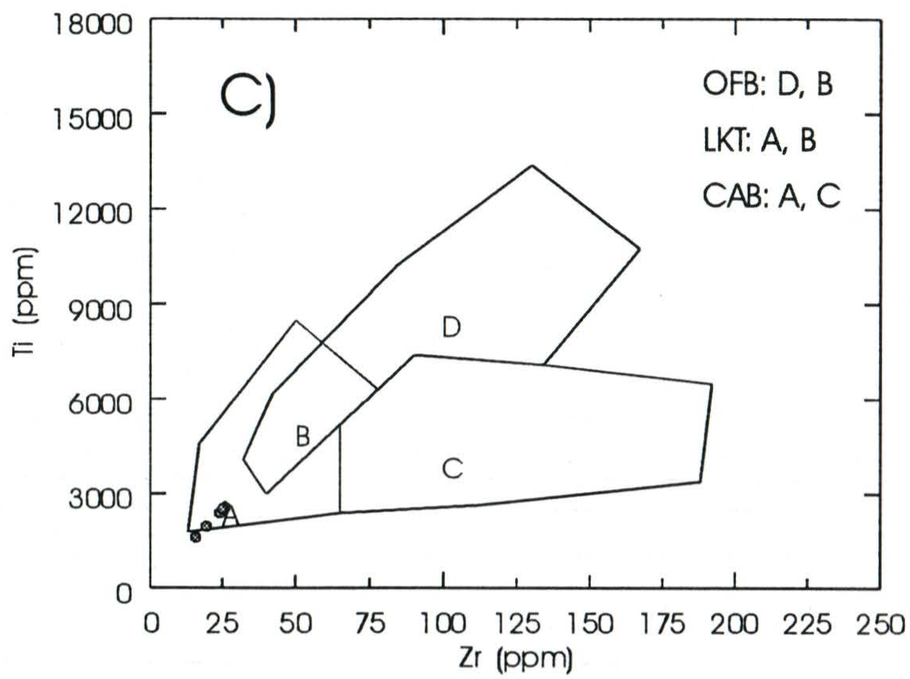
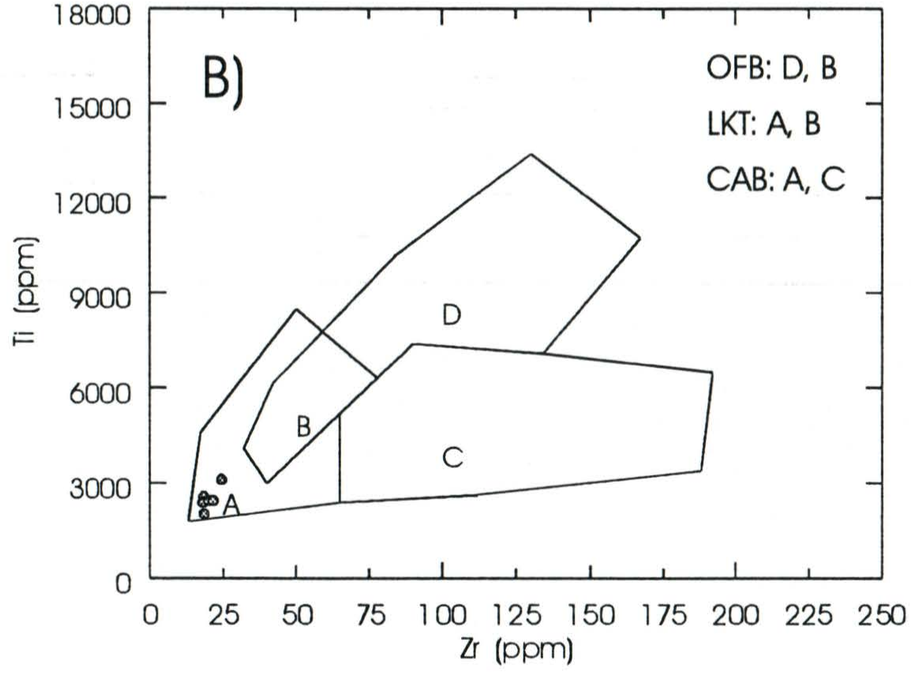


Figure 5-5 - Ti - V discrimination (Shervais, 1982) plot for mafic rocks which defines arc vs. non-arc affinities; (a) Ski Hill Formation, (b) Woodmans Brook Zone, (c) Powerhouse Zone, (d) Airport Zone.







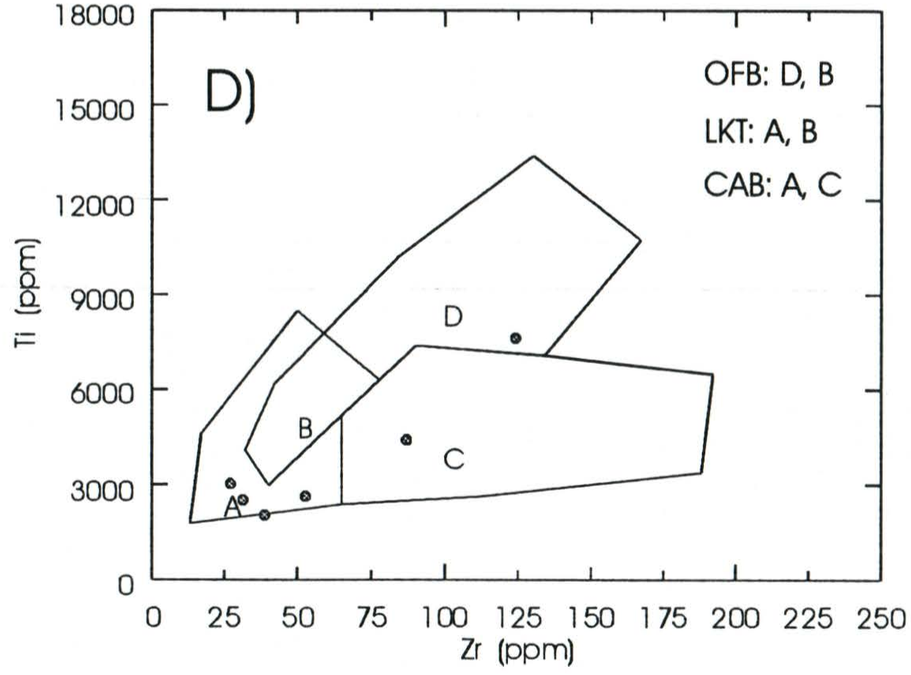


Figure 5-6 - Tectonomagmatic discrimination plot utilizing Zr and Ti in mafic rocks (Pearce and Cann, 1977). Rocks with high Ti and Zr contents are considered to be oceanic basalts. Lower Ti and Zr contents are typical of arc settings, with the calc-alkalic basalts at higher Zr/Ti ratios than the tholeiitic suites; (a) Ski Hill Formation, (b) Woodmans Brook zone, (c) Powerhouse zone, (d) and Airport Zone. OFB=ocean floor basalt, LKT=low K-tholeiite, and CAB=calc-alkaline basalt.

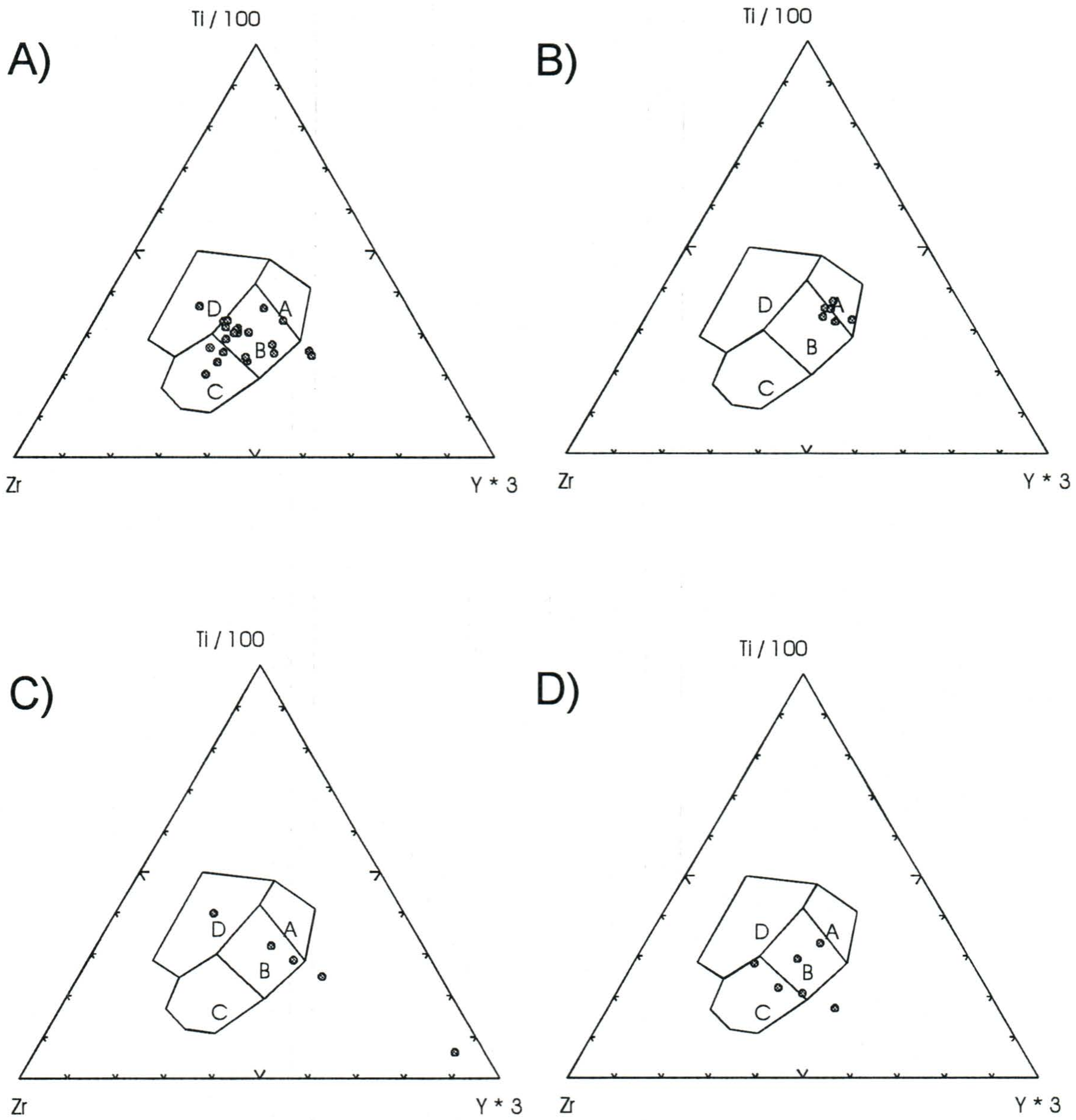
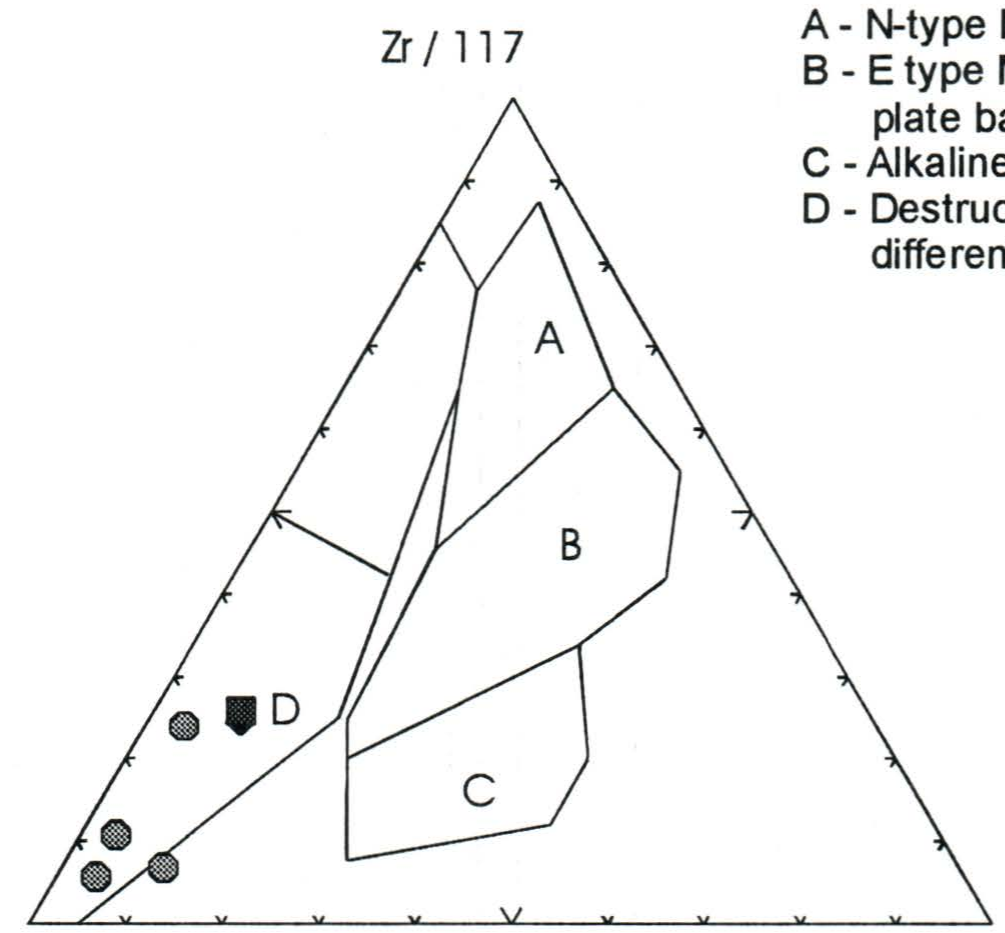
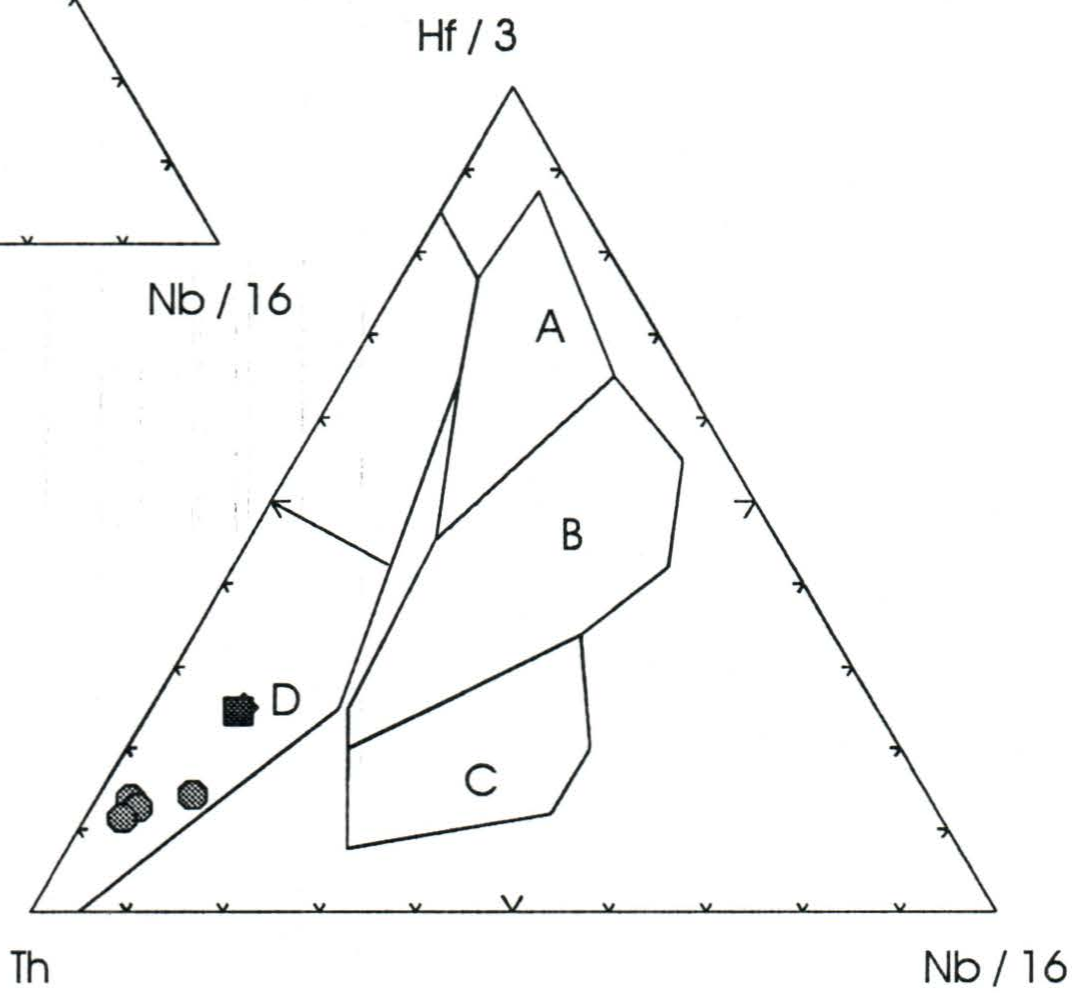
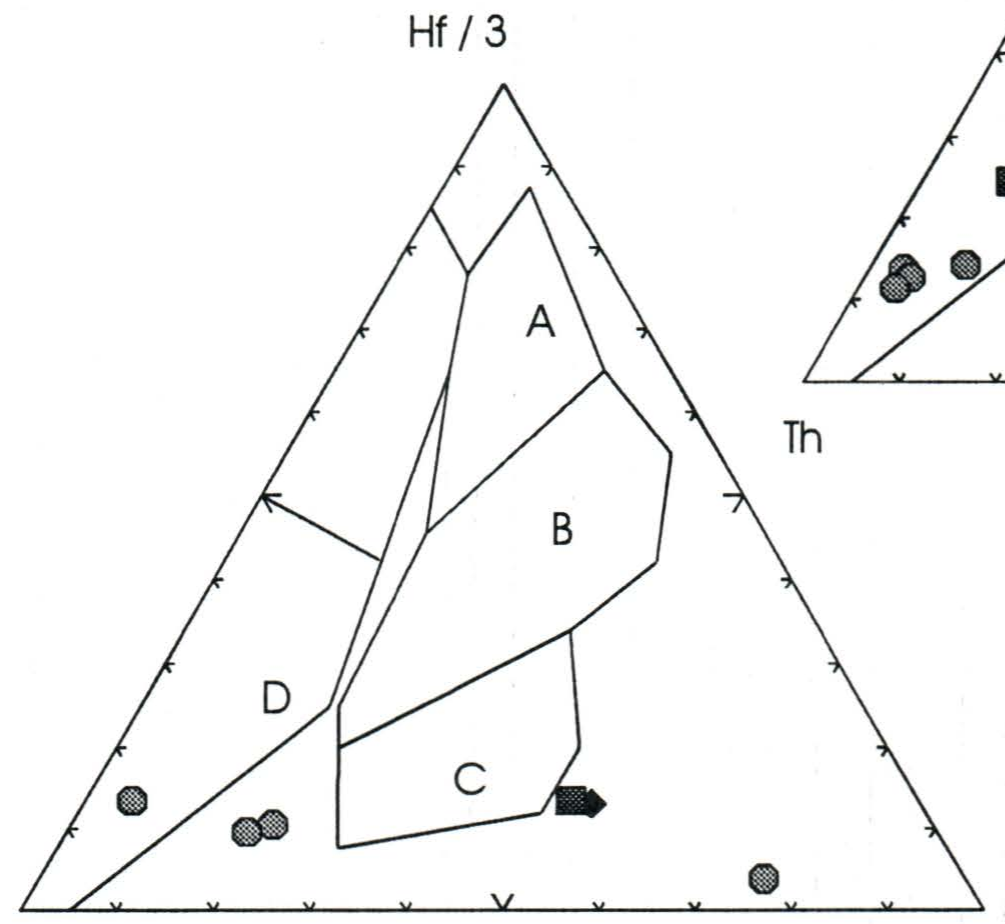


Figure 5-7 - Plots of tectonomagmatic setting based on Zr-Ti-Y systematics of mafic rocks (Pearce and Cann, 1977); (a)Ski Hill Formation, (b) Woodmans Brook zone mafics, (c) Powerhouse zone mafics, (d) and Airport zone. D = within plate basalts, B = ocean floor basalts, A + B = low-K tholeiites, and B + C = calc-alkalic basalts.



A - N-type MORB
B - E type MORB and tholeiitic within plate basalts and differentiates
C - Alkaline within plate basalts and differentiates
D - Destructive plate margin (arc-related) basalts and differentiates





Ski Hill Formation
Woodman's Brook Alteration Zone
Powerhouse Alteration Zone

Figure 5-8a (top left), 5-8b (middle right) and 5-8c (bottom left) - Ternary diagrams from Wood (1980) which utilize various HFSE to plot mafic rocks in terms of tectonomagmatic setting.

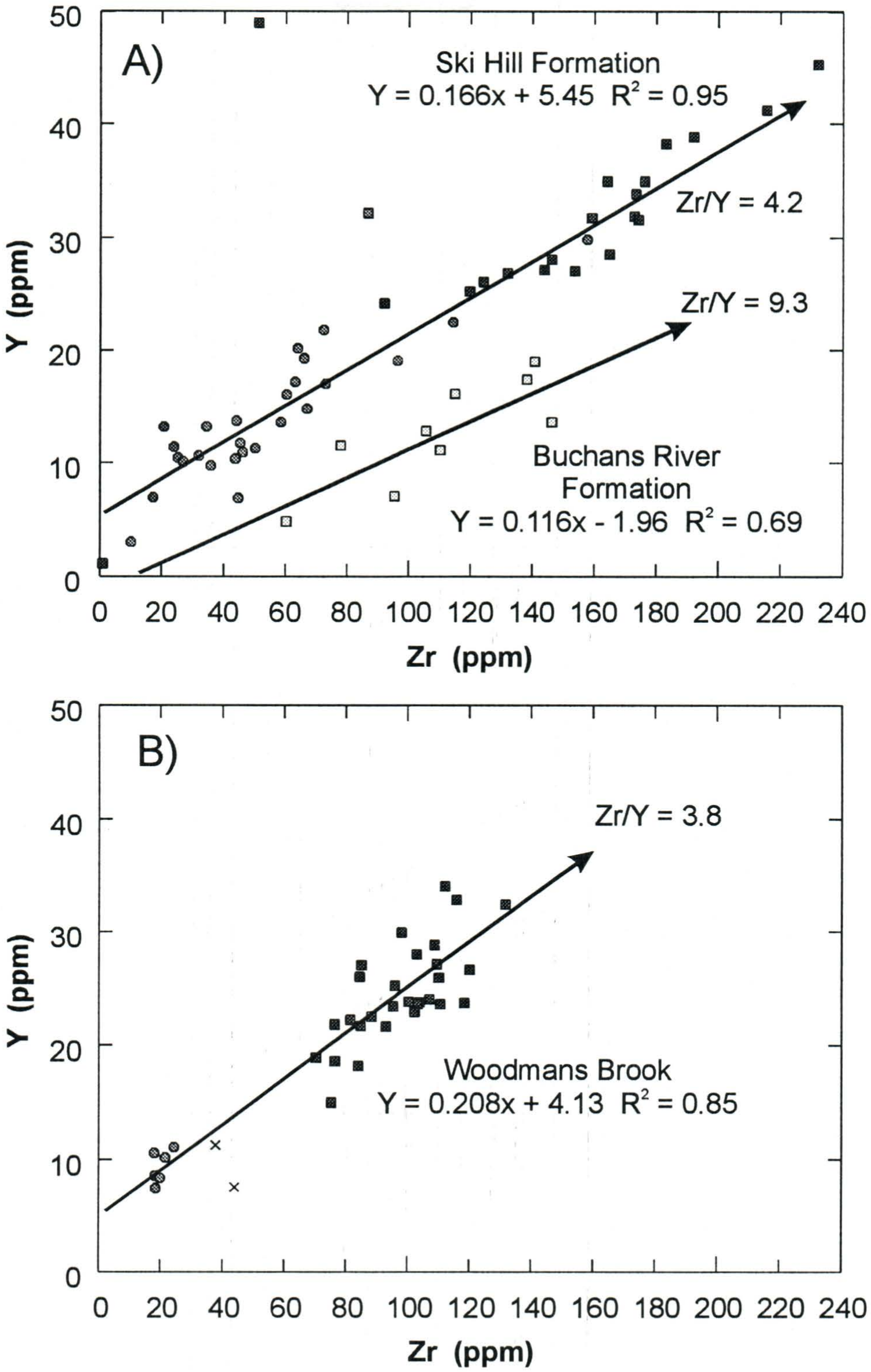


Figure 5-9 - HFSE plots (Zr versus Y) for different suites of volcanic rocks from the Buchans area. Zr/Y and other HFSE ratios are effective monitors of magmatic affintiy and petrogenetic relationships; (a) Lucky Strike area volcanics including mafic rocks from the Ski Hill Formations and felsic volcanics form the Ski Hill and Buchans River formations, (b) Woodmans Brook alteration zone bimodal suite, (c) Powerhouse alteration zone bimodal suite, and (d) various mafic and felsic rocks from the Airport alteration zone. Circles represent mafic rocks and squares are felsic samples.

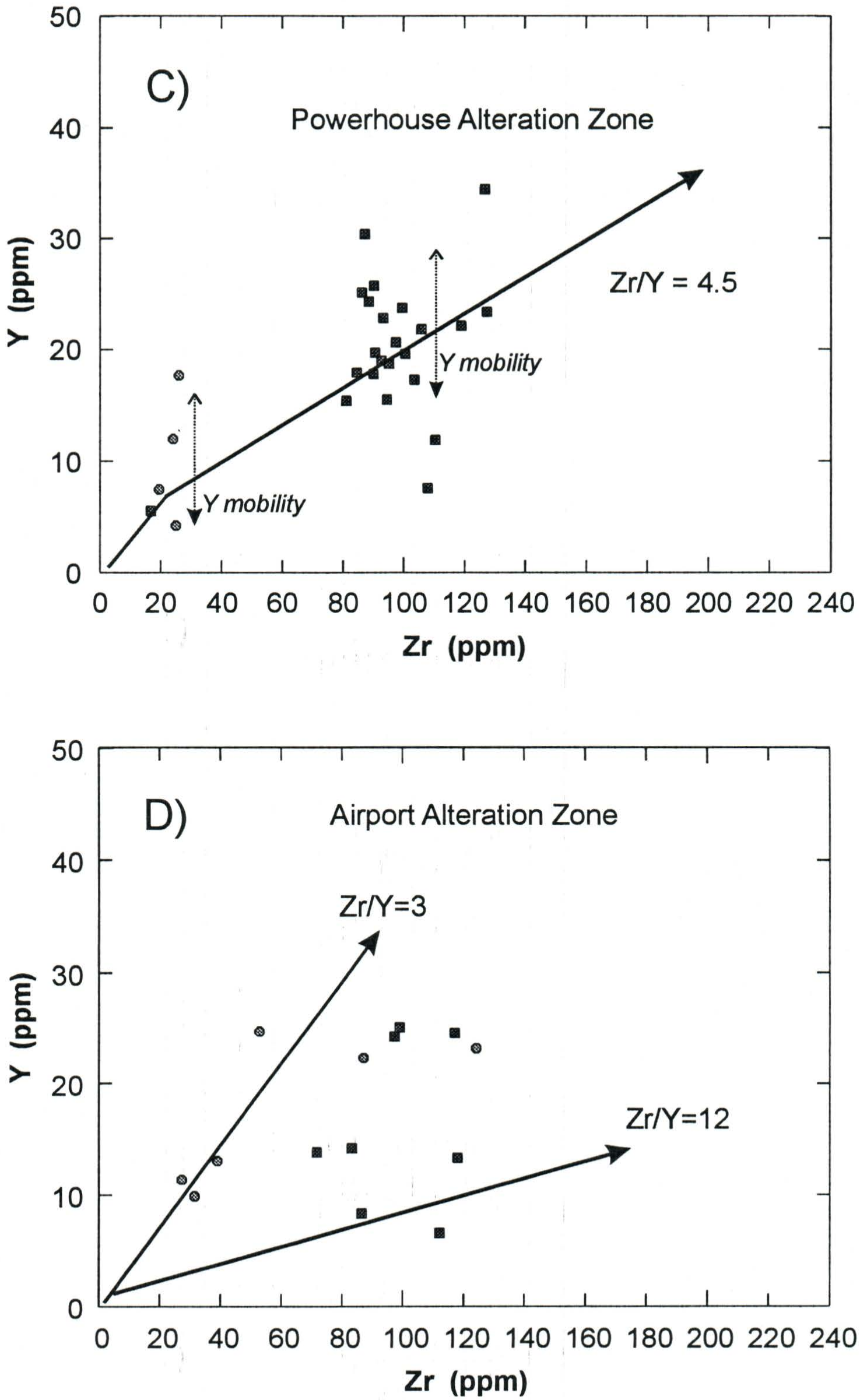
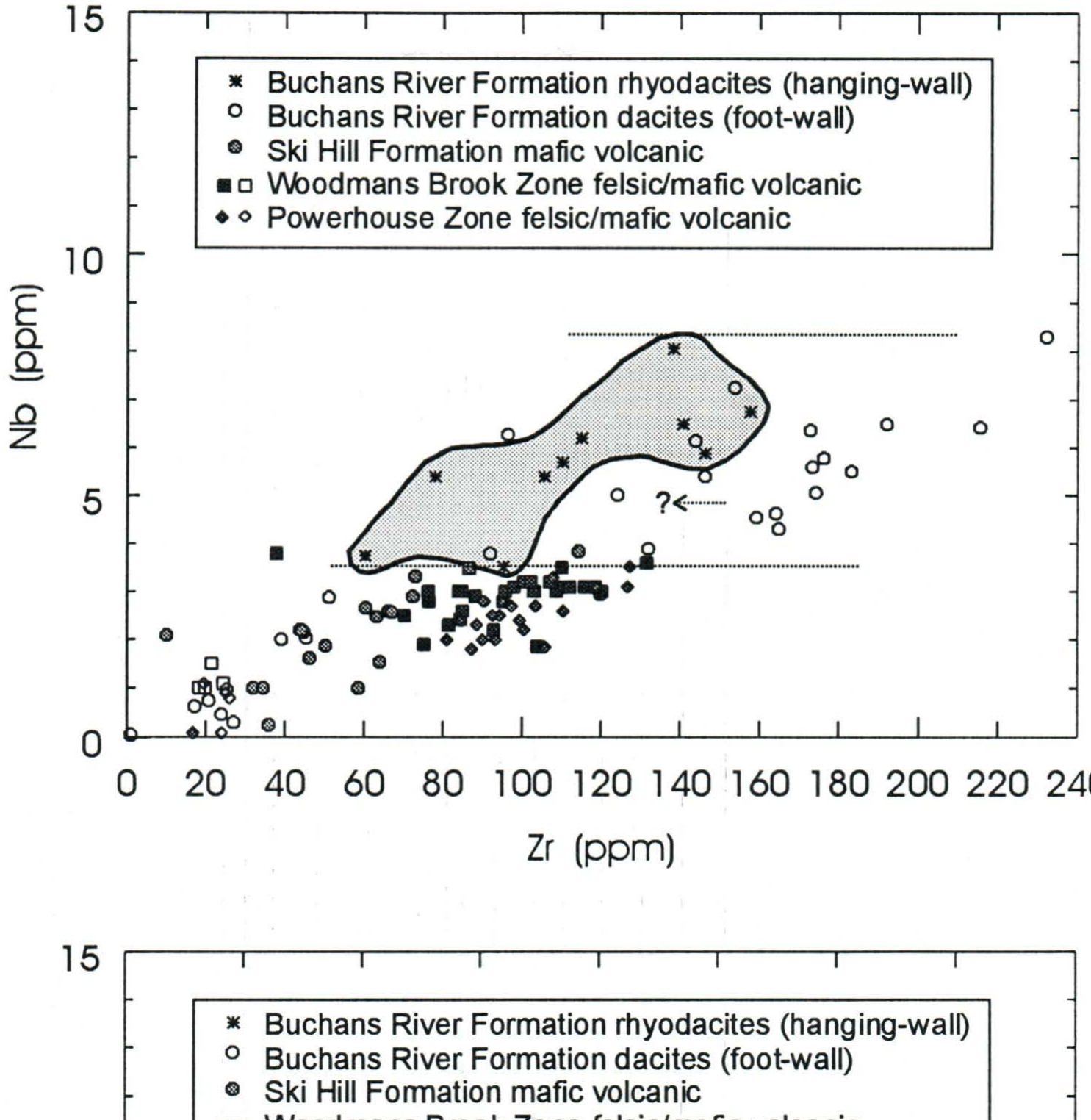


Figure 5-9 (continued)



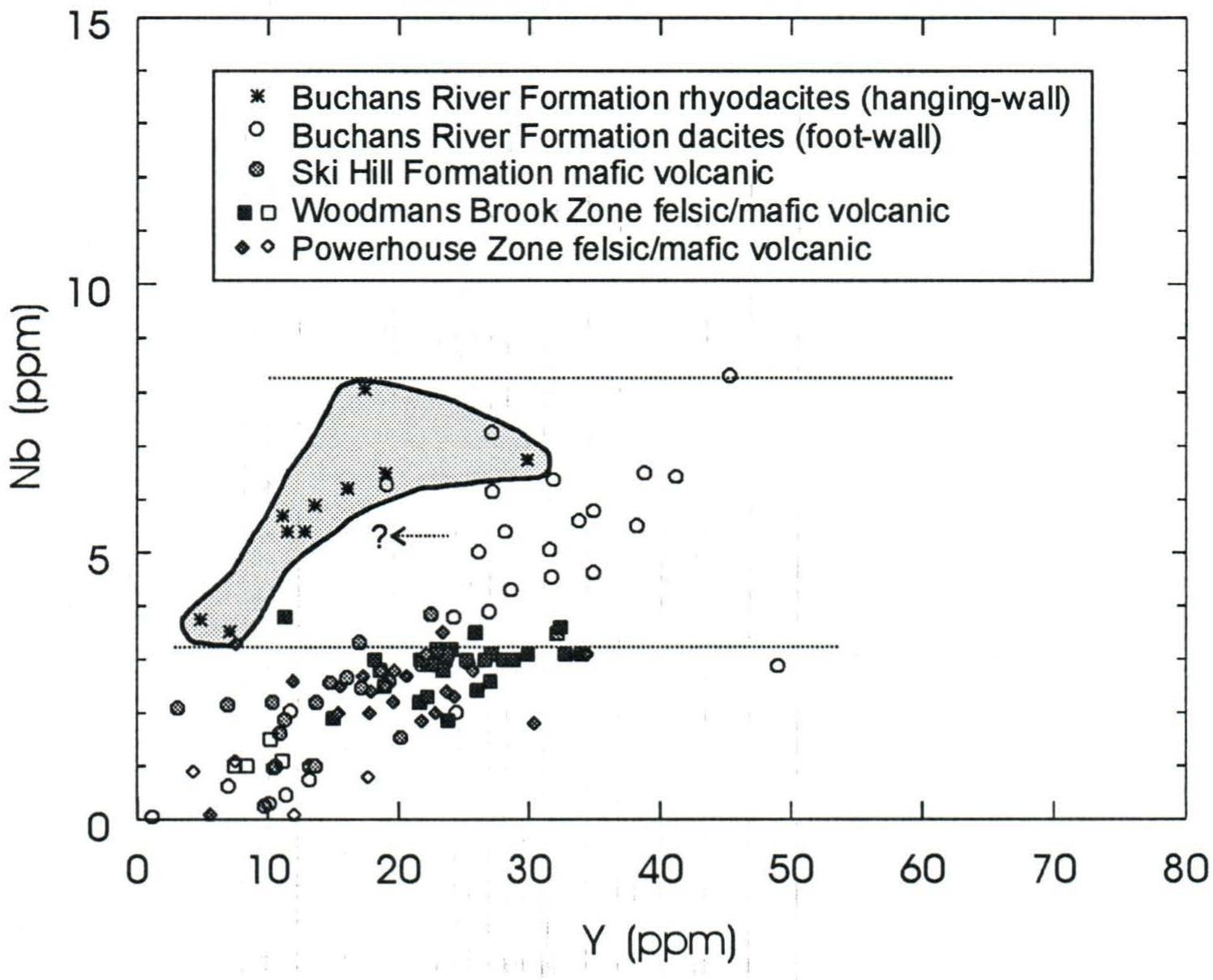


Figure 5-10 (above) - Zr versus Nb for entire data set. Buchans River Formation rhyodacites are outlined. Figure 5-11 (below) - Y versus Nb for entire data set. Buchans River Formation rhyodacites are outlined. In both plots, the hanging wall rhyodacites form a distinctive different suite, yielding relatively lower Zr and Y when compared to the Buchans River Formation foot-wall dacites. In fact, the rhyodacites are geochemically distinct from all other rock types in this data set.

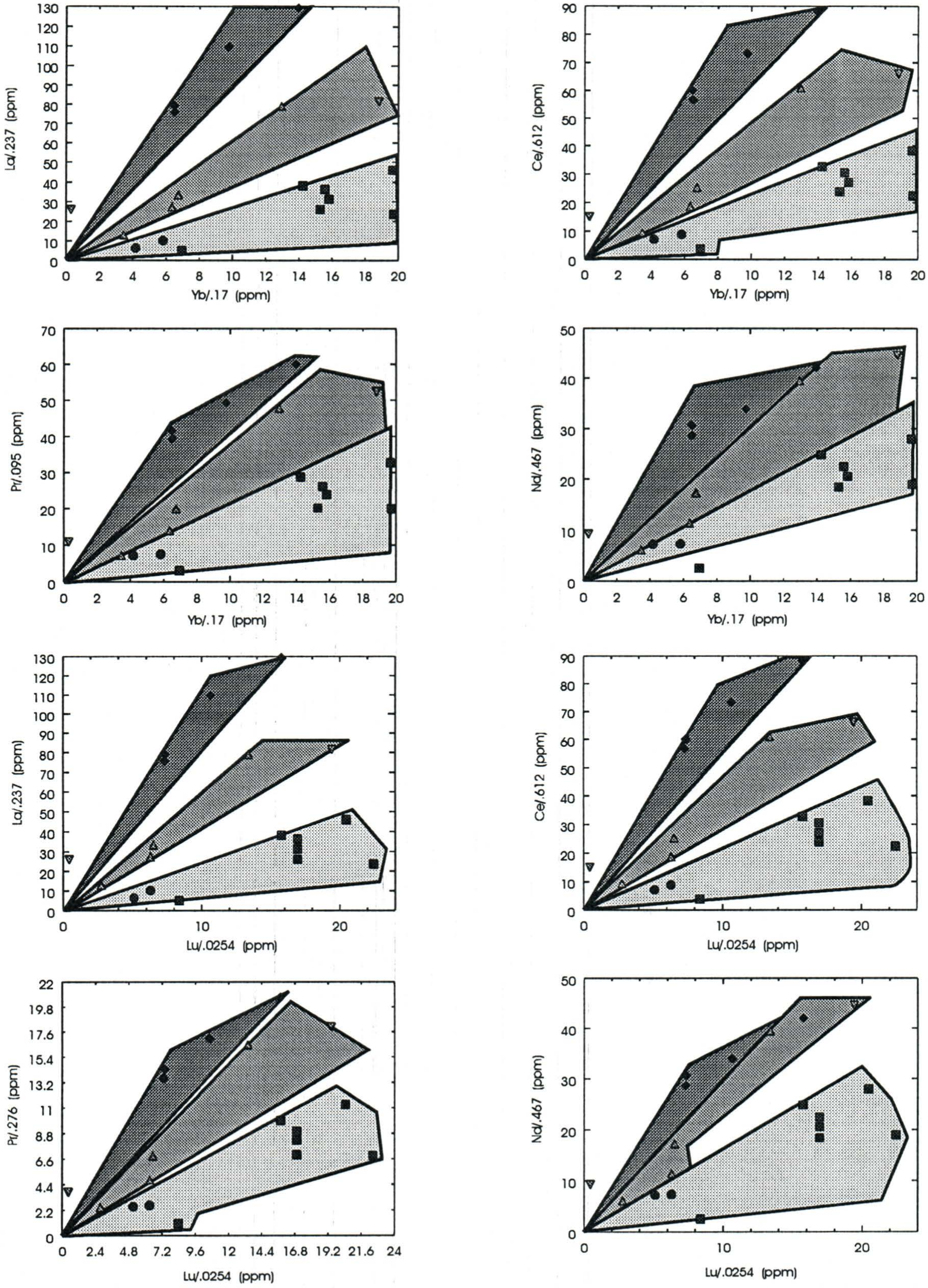
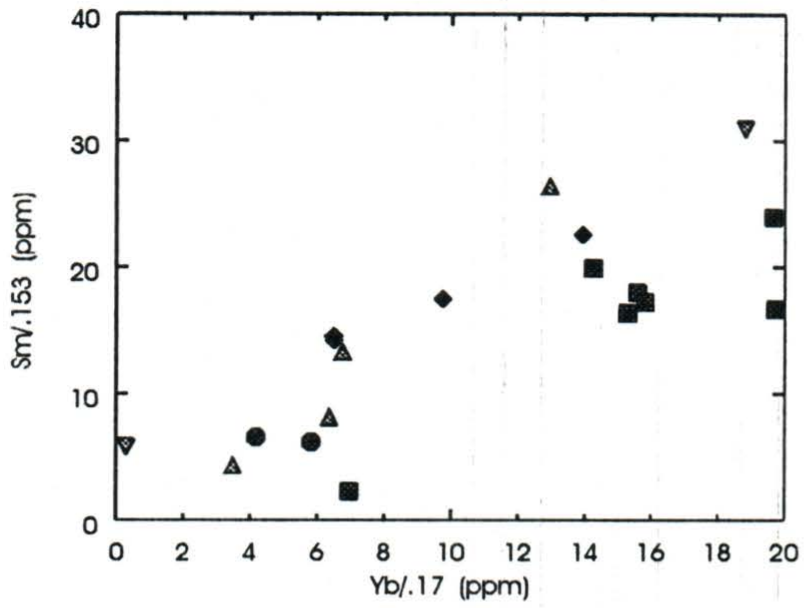
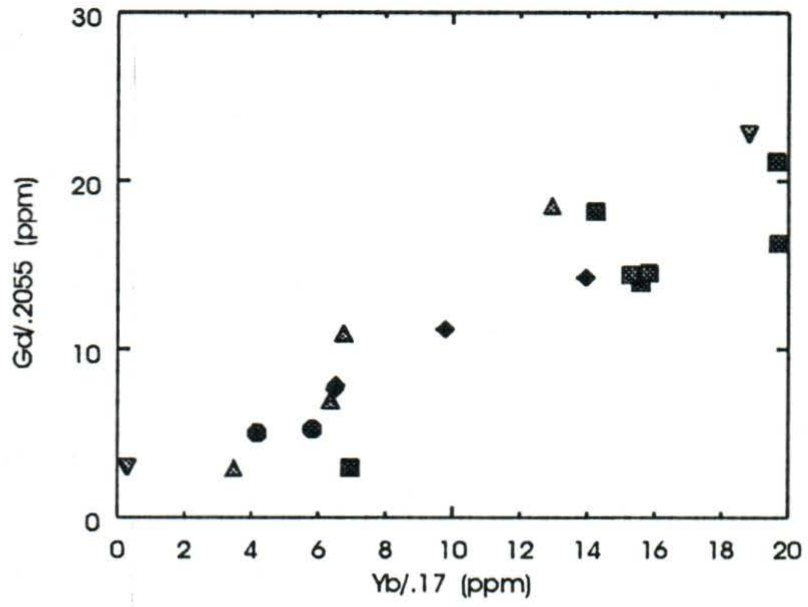
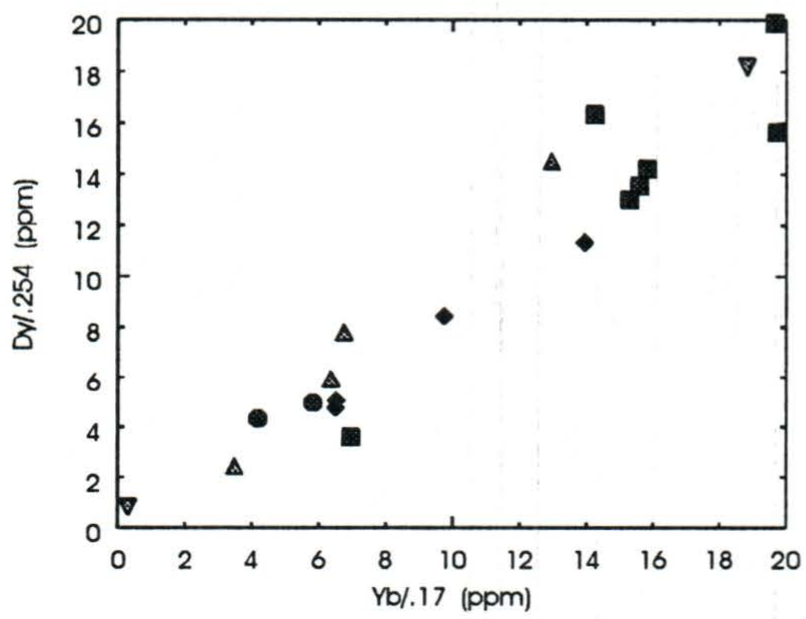
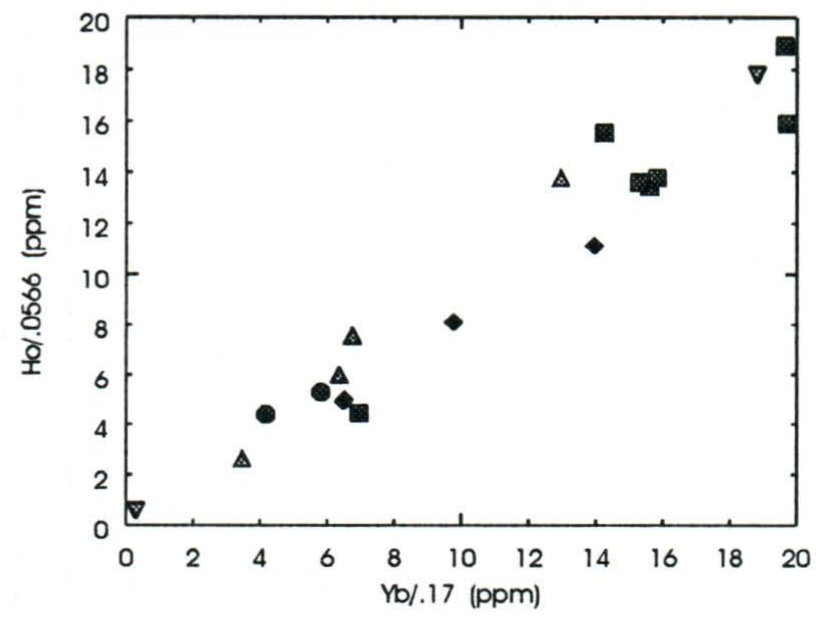


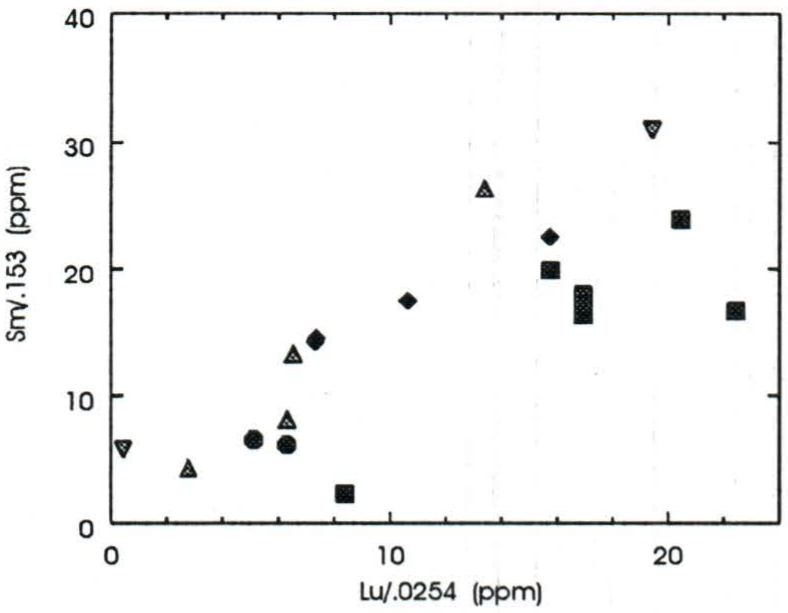
Figure 5-12 - Miscellaneous LREE vs. HREE plots, normalized to chondrite (Sun and McDonough, 1989).

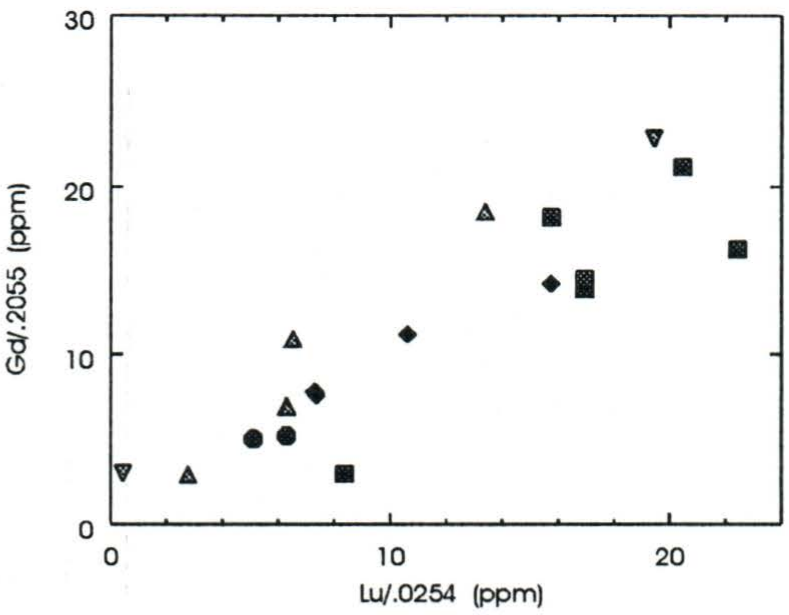


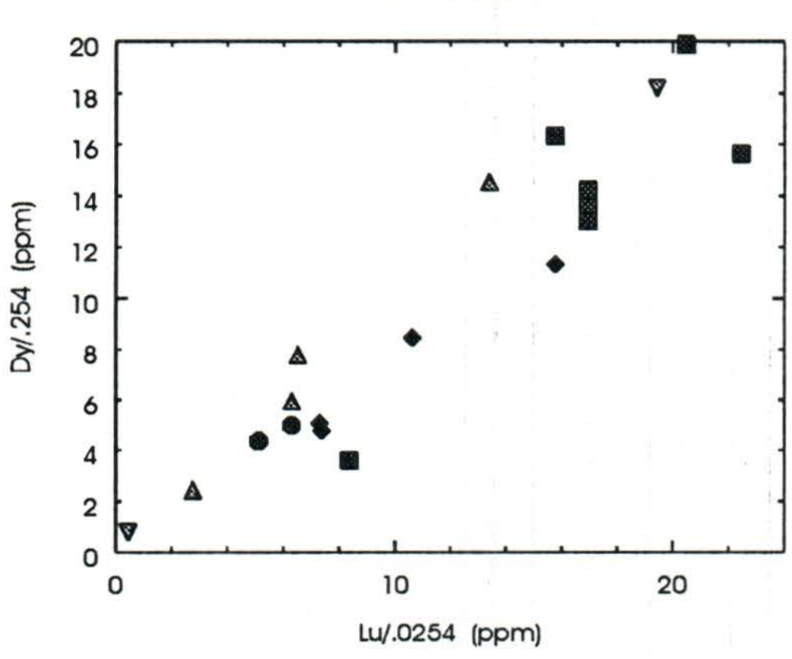


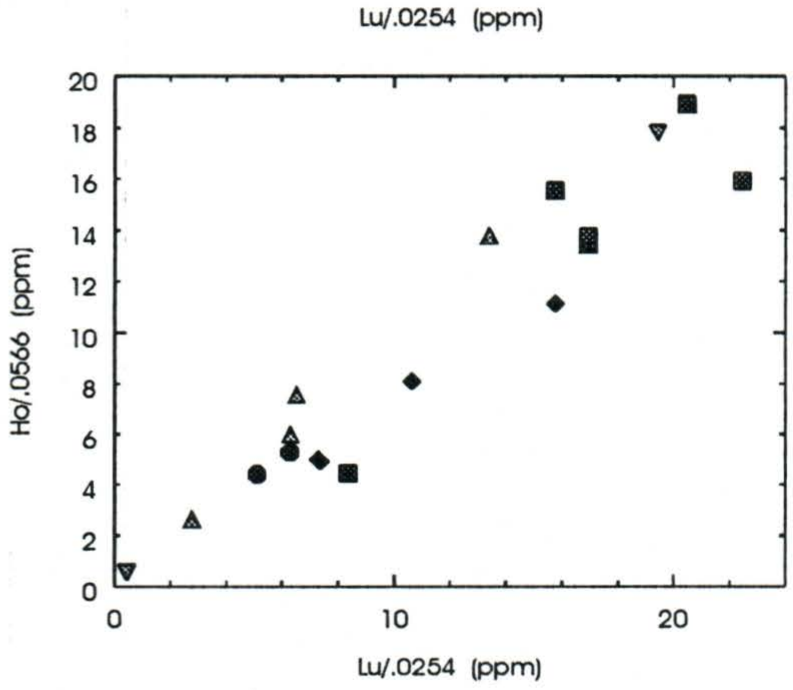












◆ ▽ Buchans River Formation rhyodacite/dacite
△ Ski Hill Formation mafic volcanics
■ ● Powerhouse and Woodmans Brook zones felsic/mafic volcanics

Figure 5-13 - Miscellaneous MREE vs. HREE plots.

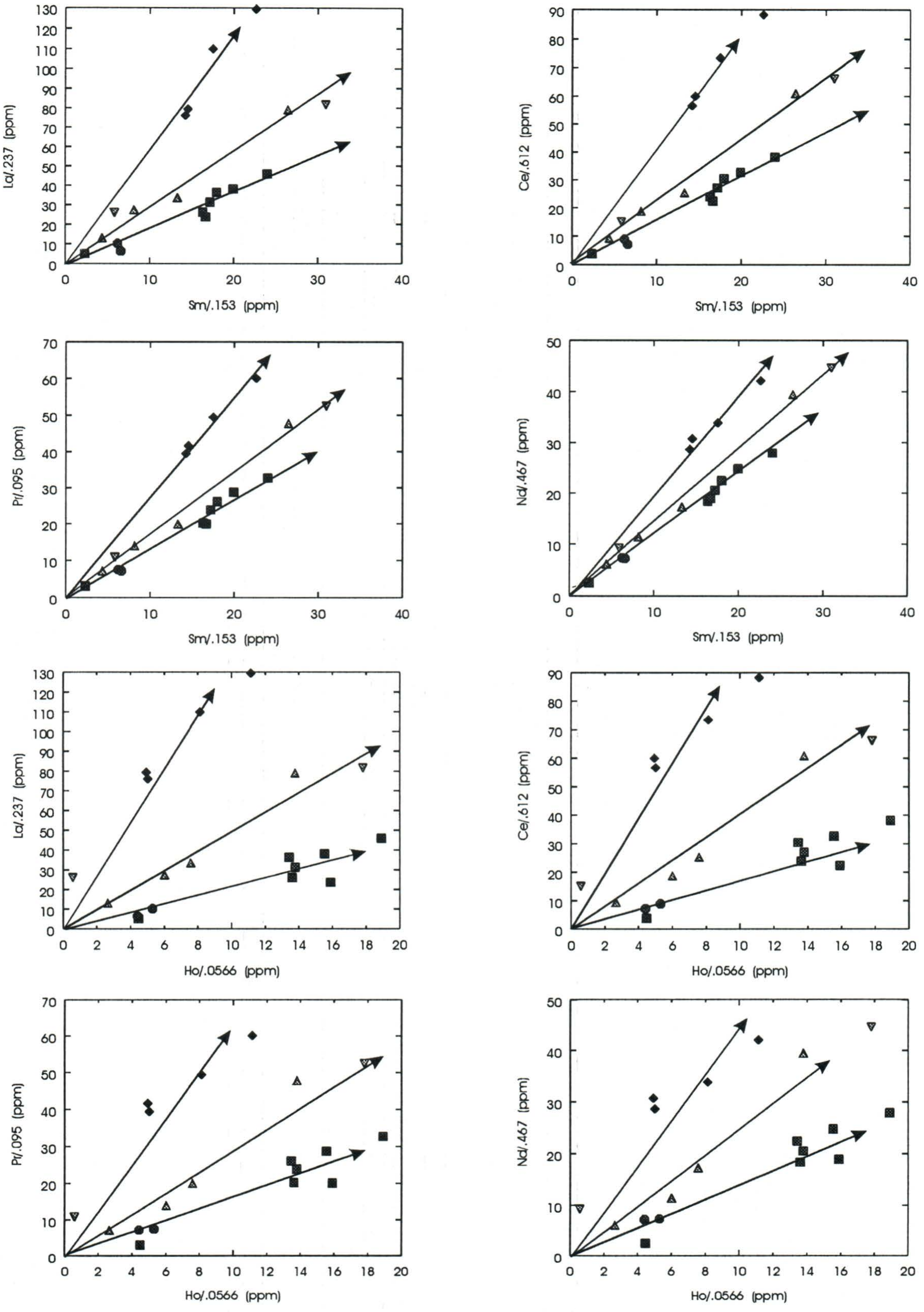


Figure 5-14 - Miscellaneous MREE vs. LREE plots.

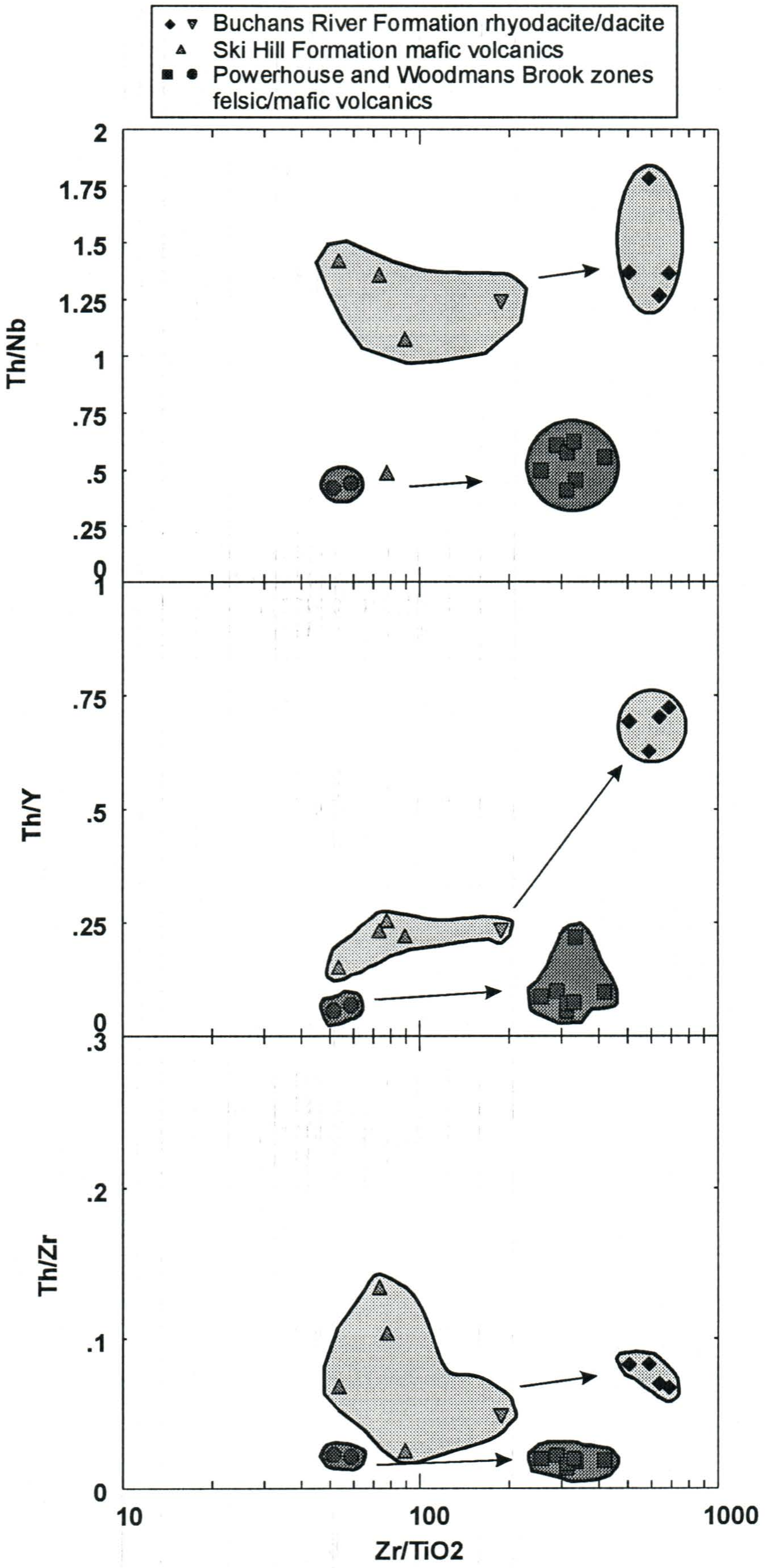


Figure 5-15 - Various LFSE/HFSE ratios plotted against Zr/TiO_2 for Buchans River Formation, Ski Hill Formation and the Buchans East area.

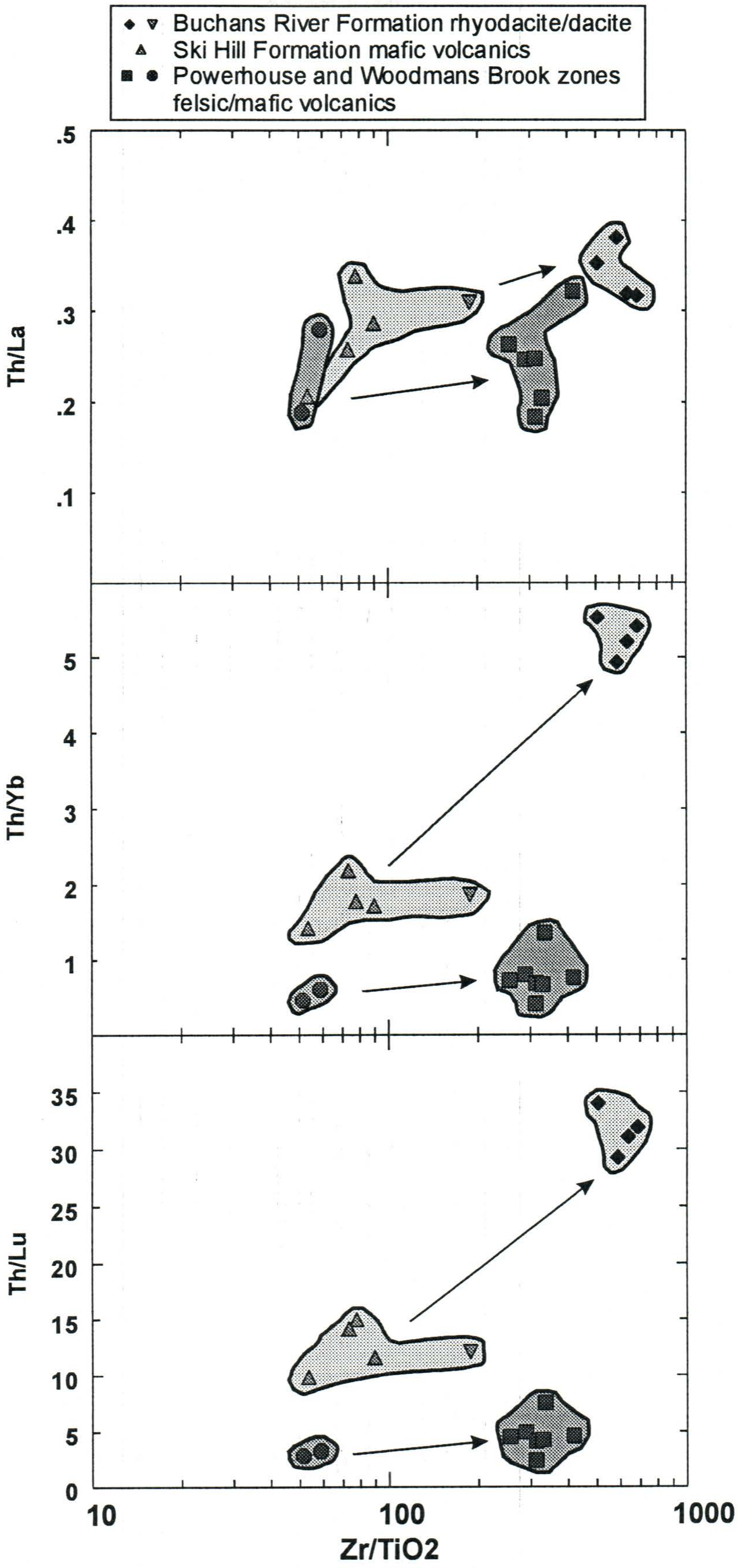


Figure 5-16 - Various LFSE/REE (*e.g.*, Th/Nb) ratios plotted against Zr/TiO2.

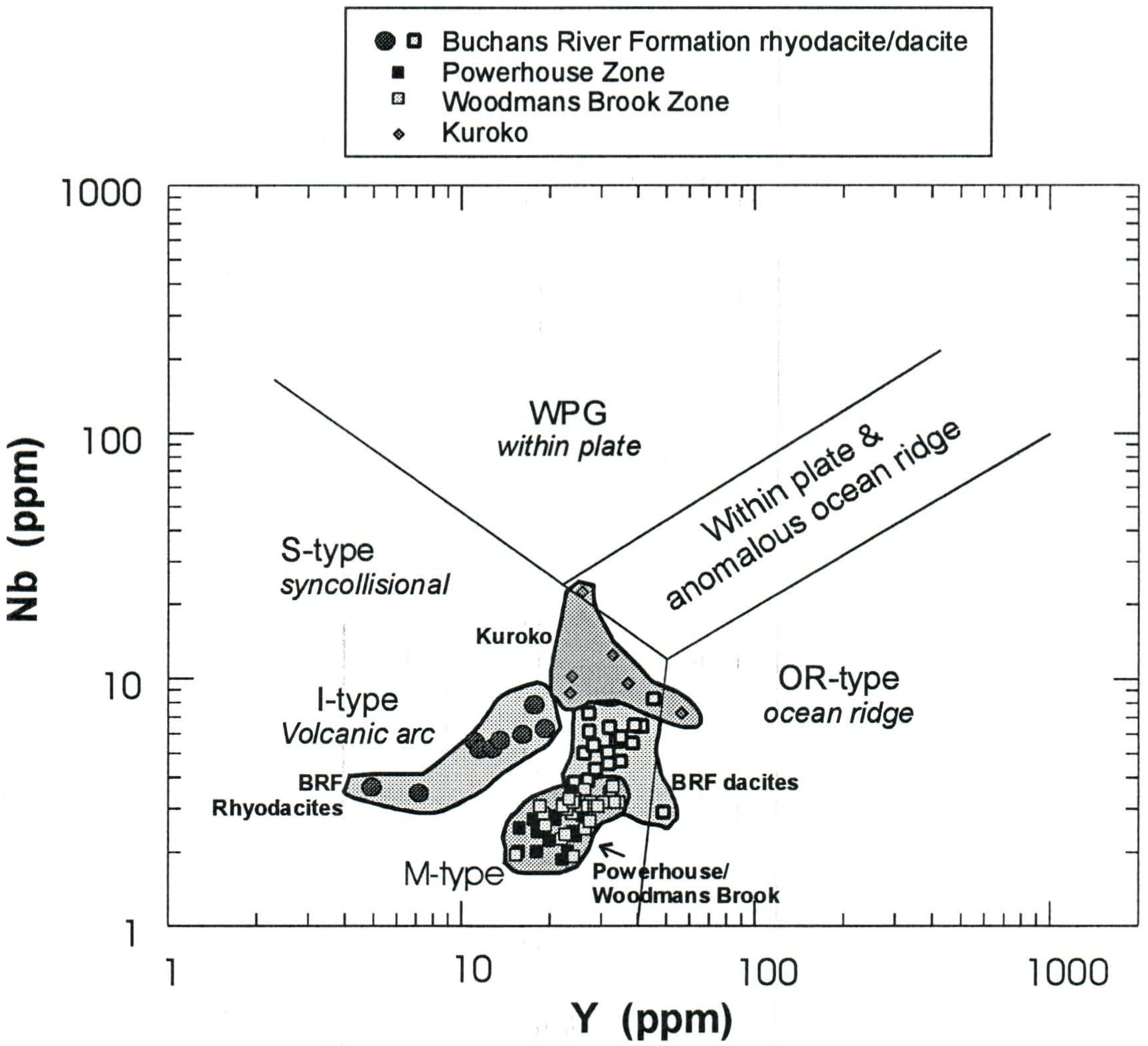


Figure 5-17 - Y versus Nb plot of Pearce *et al.* (1984). M-type volcanics are derived from a depleted mantle source and represent a primitive arc setting. I-type volcanic arcs represent more mature arc settings. Kuroko data from Dudas *et al.* (1983). For the Buchans East data, the WBZ samples are the light grey and PHZ samples are black.

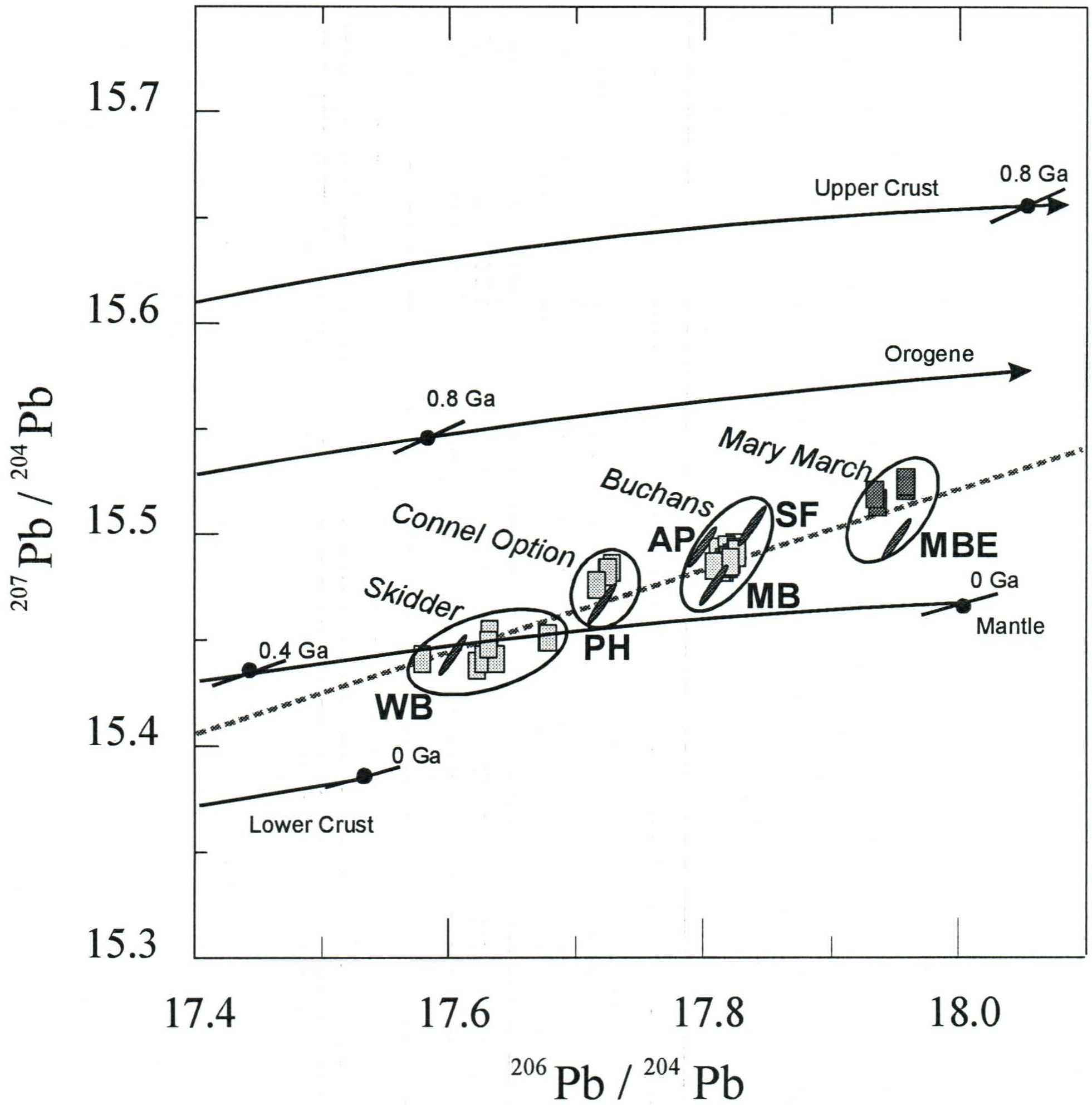
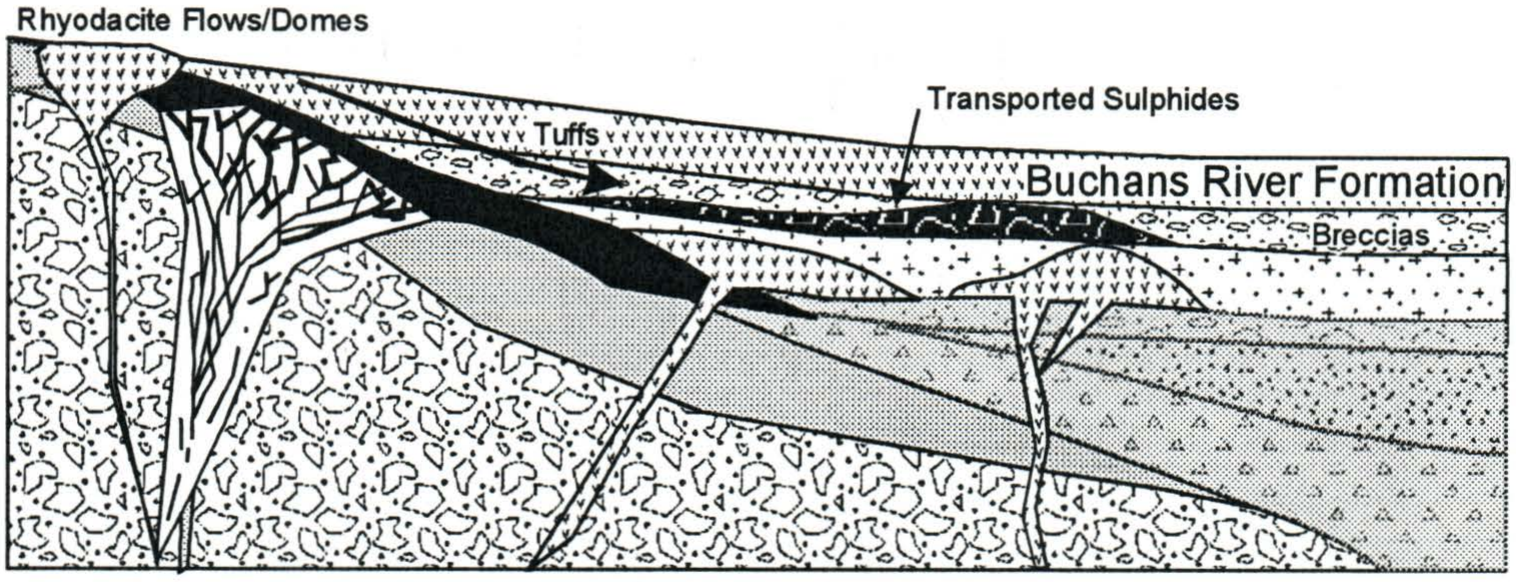
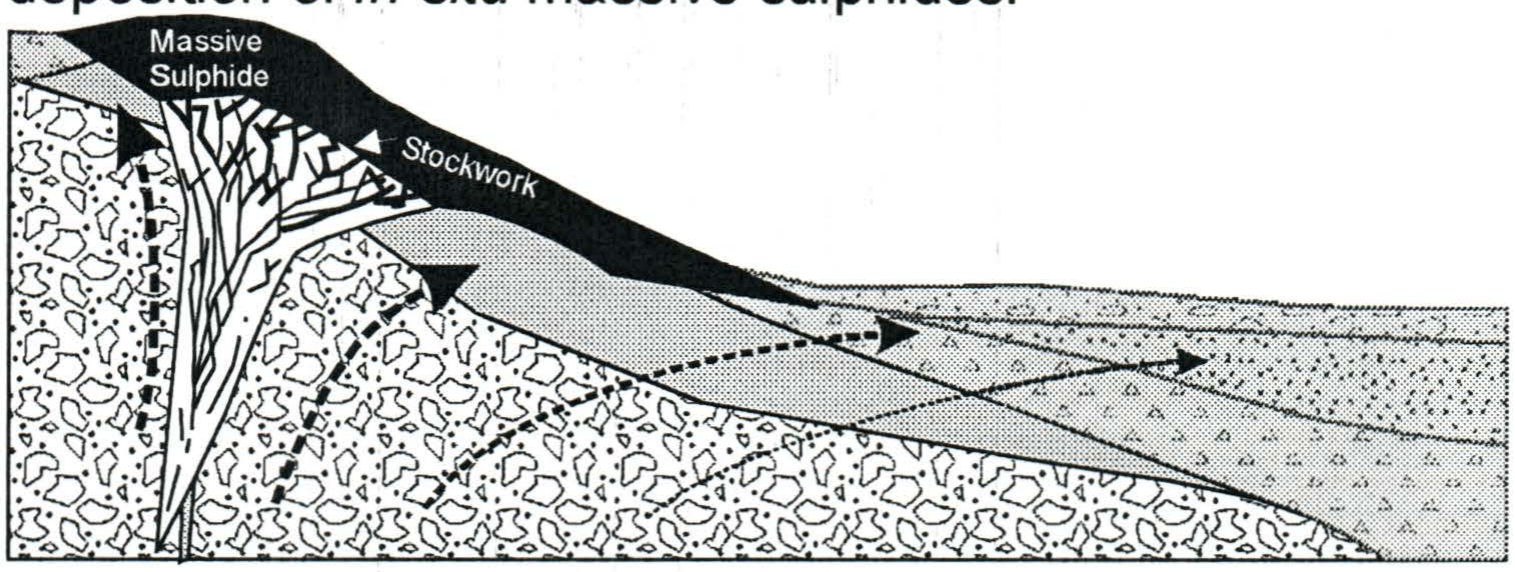


Figure 5-18 - Pb isotope data from this report (elipses) as well as previous studies (squares) in the Buchan region (Cumming and Krstic, 1987). Four clusters are outlined. Growth curves are from Doe and Zartman (1989). WB = Woodmans Brook Zone, PH = Power-house Zone, AP = Airport Zone, MB = Middle Branch Zone, SF = Sandfill Prospect, MBE = debris flow prospect at Middle Branch East. The Skidder, Connel Option, Buchans and Mary March groups are labelled.

Stage 3 - Eruption of Rhyodacitic volcanic rocks and end of major hydrothermal activity. Disruption and transport of *in-situ* orebodies along with extensive development of breccia - conglomerate deposits.



Stage 2 - Transitional from stage 1, development of the hydrothermal system, alteration of host rocks and deposition of *in-situ* massive sulphides.



Stage 1 - Eruption of dacitic volcanic rocks upon, or coeval with,Ski Hill Formation mafic volcanics.

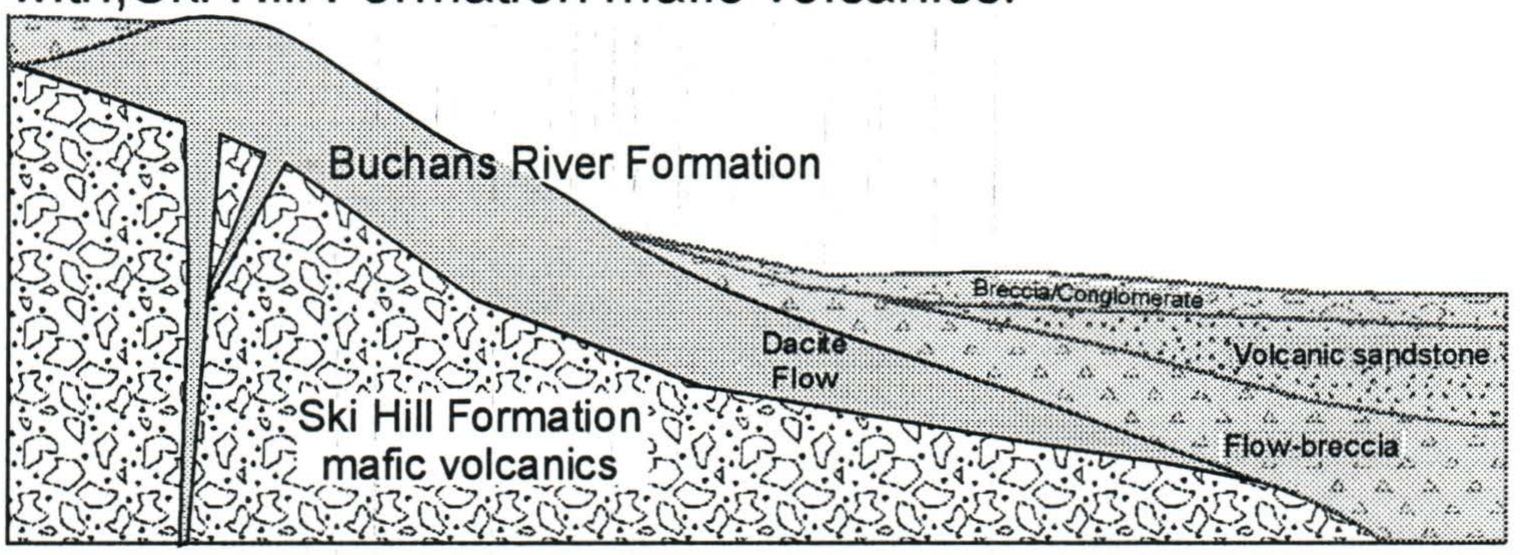


Figure 5-19 - A simplified and schematic interpretation of volcanism with respect to sulphide deposition and distribution. Note that the ore formation appears to occur after, or possible syn-, dacitic volcanism but prior to rhyodacitic volcanism. These felsic volcanic units form geochemically distinctive suites.

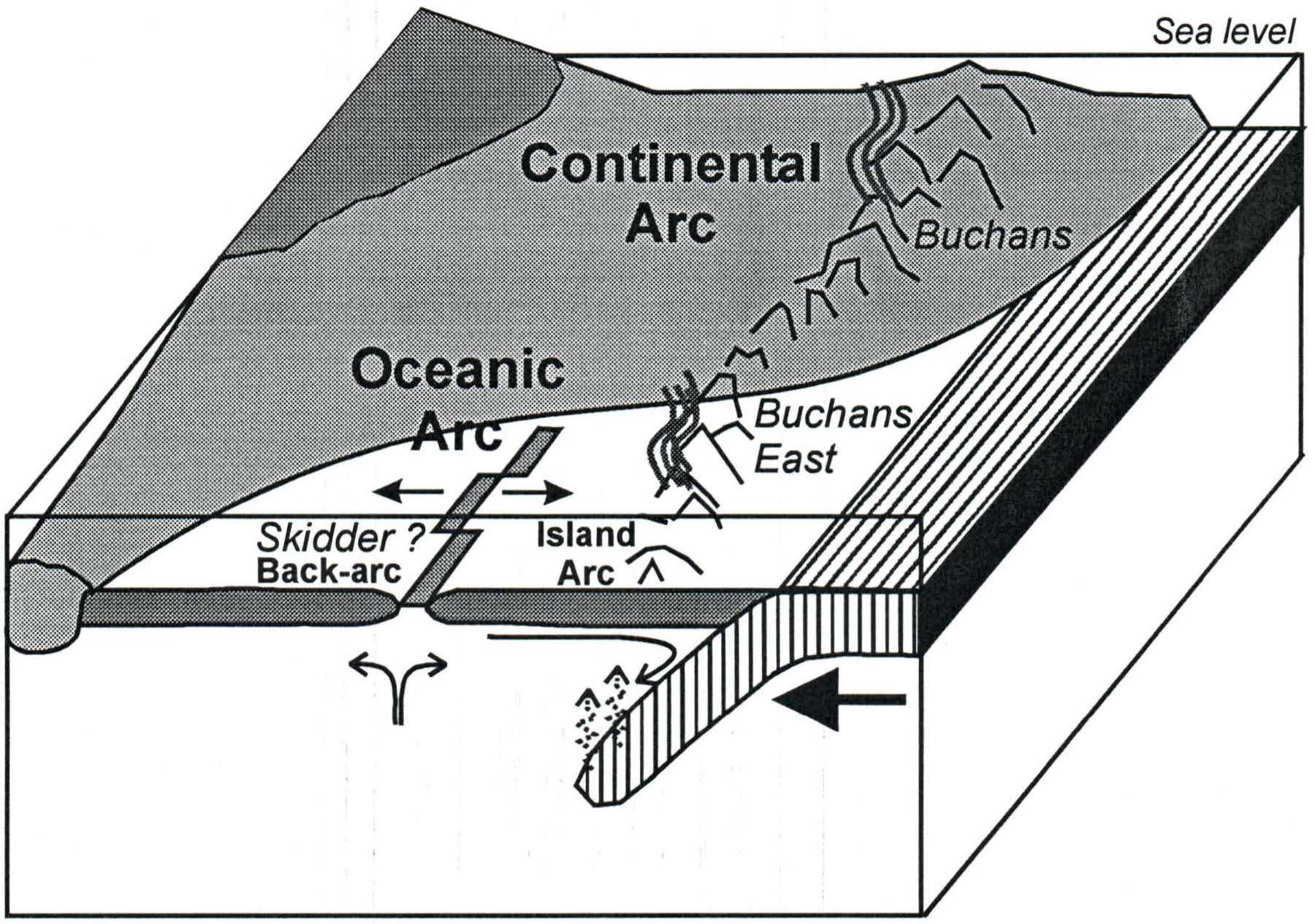


Figure 5-20 - Regional tectonic model for the Notre Dame subzone modified from Swinden et al. (1997). Proposed locations of various volcanic suites from the Buchans area are shown.

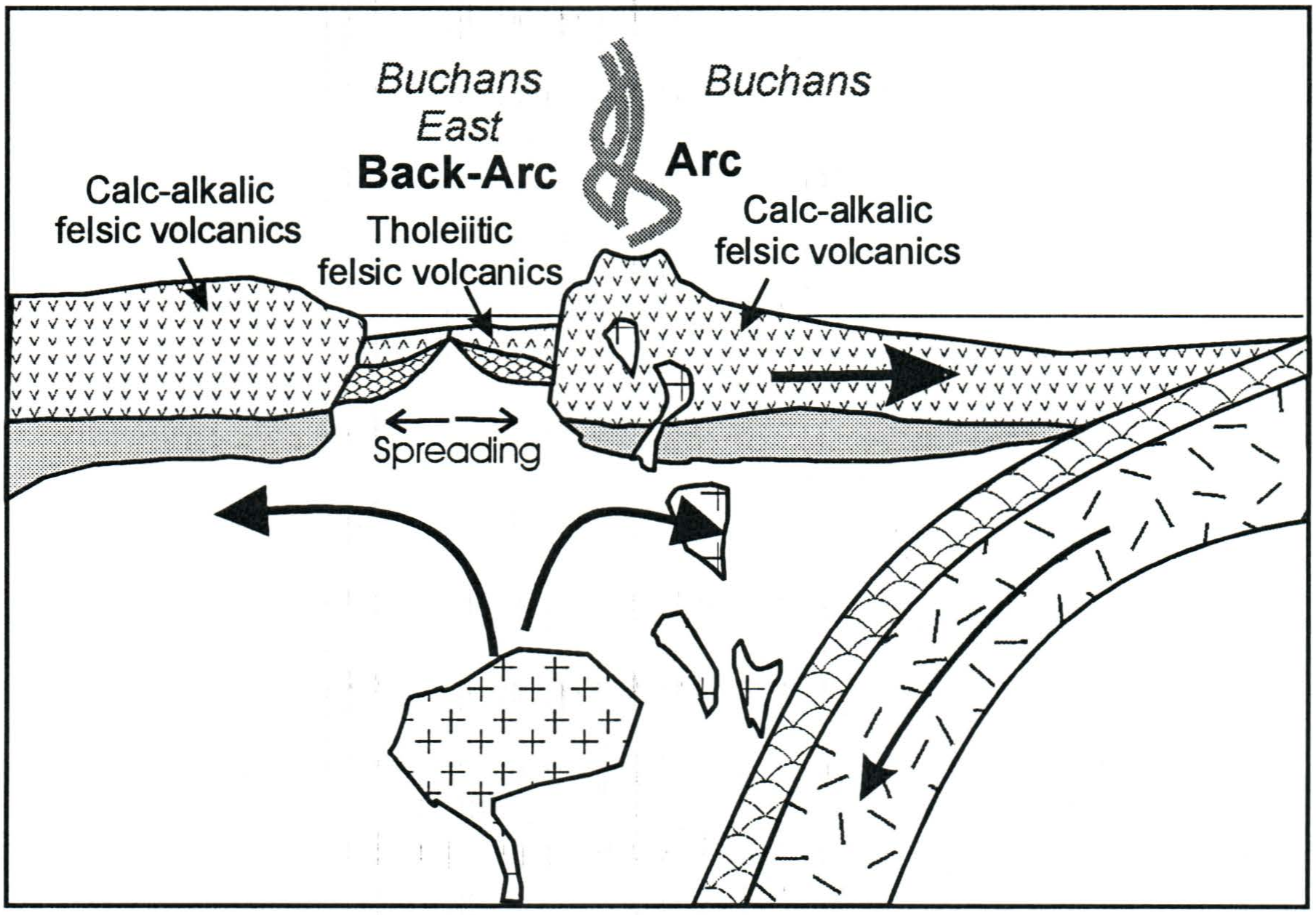


Figure 5-21: Schematic model for potential tectonic setting of various volcanic suites from the Buchans area (adopted from Lentz, 1997).

Chapter Six - Alteration Geochemistry

6.1 Introduction

Geochemical data from altered rocks can be used to identify, quantify and model hydrothermal alteration as the data are directly related to mineralogical processes. A major obstacle in geochemical data interpretation is the separation of hydrothermal alteration effects from primary (igneous) processes. With the added complexity introduced by the problem of closure, or constant sum, a recalculation of the data is required for proper interpretation.

This chapter is divided into three main segments. The first segment provides a qualitative analysis whereby the raw geochemical data are examined in order to detect the influence of various alteration mineral assemblages. The effects are recognized as changes in various ratios or the relative abundances of certain elements; the 'alteration trends' may be represented graphically. The second segment is a quantitative approach involving mass balance calculations which measure the true changes in the individual elemental components of each sample. This method provides a more accurate analysis of the effects of hydrothermal alteration and is most useful in modelling the hydrothermal system. The final segment displays downhole geochemical plots which are used to examine spatial relationships of rock geochemistry to ore.

6.2 General Alteration Geochemistry

6.2.1 Lucky Strike/Middle Branch Zones

As illustrated in Chapter 4, the hydrothermal alteration mineralogy assemblage associated with the Buchans orebodies is relatively simple, dominated by quartz, chlorite and sericite, with lesser clay minerals, carbonate and K-feldspar.

A ternary diagram defined by oxide wt. % MgO - Al_2O_3 - (CaO + Na_2O + K_2O) is shown in Figure 6-1. Data from the Lucky Strike/Middle Branch areas illustrate two main trends defining the main alteration pathways for each of the mafic and felsic rocks. The mafic rocks, from least altered to most altered, follow a path on the diagram from right to left and slightly concave downwards (shown by arrow). This trend mimics an alteration path from precursor to sericite-chlorite altered to strongly chloritized. The apparent initial relative increase in Al_2O_3 is due to the removal of CaO and Na_2O. Most of the mafic rocks plot on tie-lines from sericite to chlorite, with most samples plotting closer to the chlorite field. One sample plots directly on the MgO-Al_2O_3 axis and is considered to be chloritite. Also note that several samples do not plot within the alteration trend towards chlorite. These samples contain higher proportions of CaO indicative of carbonate alteration.

Felsic samples plot on a similar initial trend from least altered to proportionately higher Al_2O_3 contents. As with the mafic samples, this is due to feldspar breakdown and leaching of CaO and Na_2O. Most samples cluster around the sericite (+/-illite) composition, however, several other samples show greater proportions of Al_2O_3 than can

be attributed to sericite only and, therefore, these samples contain a proportion of Al-rich clays (*i.e.*, montmorillonite and mixed layered clays). These plots confirm the observations of Henley and Thornley (1981) that clay mineral alteration occurs chiefly in felsic rather than in mafic volcanic rocks at the Buchans camp.

Silica mobility has the greatest influence on the geochemistry of altered rocks at Buchans, as most altered rocks have undergone either silicification or silica-leaching. In Figure 6-2, Zr/Al_2O_3, as a measure of fractionation, is plotted against SiO_2 using the transitional SHF basaltic-andesites and BRF dacites suite. Least altered samples only are used to define the fractionation curve. The plot was designed to measure 'residual silica' (Lavery, 1985). In general, the plot suggests excess silica in many mafic rocks but deficient silica in most felsic samples. Although these values are affected by the closure problem and are not quantitative, they are broadly representative of the behavior of silica in these rocks.

In Figure 6-3, BRF dacites are shown as SiO_2 is plotted against Zr with a fractionation trend shown. In contrast to the last plot, where a ratio of immobile elements (*i.e.*, Zr/Al_2O_3) was used as a fractionation monitor, a single immobile component (*i.e.*, Zr) is used here. The advantage is that the offset of SiO_2 from the fractionation trend is proportional to a gain or loss. This plot represents part of the mass calculation process that is used to obtain quantitative information (see section 6.2). As in Figure 6-2, silica depletion is obvious in most of the dacites, although several samples show actual mass gains of SiO_2.

Due to its relative abundance and susceptibility to alteration, feldspar (mostly plagioclase) is a dominant mineral controlling the variation in alteration geochemistry around VMS deposits. Therefore, anomalously low values of Na and Ca are key indicators of hydrothermal alteration. Sericite (and chlorite) are generally the most common replacement products for plagioclase and, hence, K (and Mg) should show an inverse proportionality to Ca and Na. Sodium is generally more consistent as a feldspar destruction indicator since Ca is often re-precipitated as carbonate. A plot of (K_2O + MgO) vs. Na_2O is shown in Figure 6-4. In both mafic and felsic rocks types, Na_2O is consistently lower with higher (MgO and K_2O). Most altered samples have less than 1% Na_2O and many samples are nearly sodium free. Both mafic and felsic rock types can be shown to display very high MgO contents (> 25 wt.%) typical of rocks consisting almost entirely of chlorite (termed *chloritites*).

Rb shows a very good positive correlation with K_2O in both mafic and felsic suites (Figure 6-5). Rb commonly occurs with K_2O in alkali feldspar and during alteration as both are incorporated into sericite. In the BRF dacites, several samples have higher Rb/K_2O ratios suggesting the presence of hydrothermal K-feldspar in these rocks.

Unlike Rb, Ba does not show a strong correlation with K_2O for any suite of samples (Figure 6-6). Lower Ba values (~ 1000 ppm or less) correlate with K_2O and may define a sericite trend, yet most samples have much higher Ba irrespective of K_2O content indicating the presence of barite.

Numerous alteration indices have been formulated to evaluate raw data in order of the rank of hydrothermal alteration for each sample in a given suite (*e.g.*, Date et al, 1973; Ishikawa, 1976; Spitz and Darling, 1978; Saeki and Date, 1980; Lavery, 1985). Several of these were tested on the Lucky Strike data set.

The alteration scores (Appendix F, Table F-1) provide a rough estimation of the degree of alteration in each sample. Although the results are not quantitative, relative degrees of alteration can be outlined with the correct choice of indices. The 'Hashimoto index' (Ishikawa, 1976), uses the following ratio:

$$[(MgO+K_2O)/(MgO+K_2O+CaO+Na_2O)]*100.$$

The purpose of the index is to recognize sericite and chlorite as they are added to replace feldspar. The least altered mafic and felsic rocks have alteration scores of 28 and 25, respectively. Strongly altered rocks have scores typically greater than 90. A drawback of this index is that carbonate, especially calcite, reduces the scores. Locally, hydrothermal calcite is an important constituent of the alteration assemblage at Buchans.

A modified 'Spitz-Darling alteration index' (Spitz-Darling, 1978) is based on the ratio $Al_2O_3/(Al_2O_3 + Na_2O)*100$. This index is simple and effective relating the degree of soda-depletion due to feldspar destruction. Least altered samples have scores of less than 90 and the average is 93. Scores of 100 are not uncommon as sodium is often completely removed from these rocks.

The 'sericite index' (Saeki and Date, 1980) utilizes $K_2O/(Na_2O + K_2O)*100$ to express how much sericitic replacement of feldspar has occurred. From this data set, least

altered samples have scores of less than 50 and strongly sericitized rocks have scores of greater than 90. Rb/Sr, which can be used as a substitute for the sericite index, shows a similar trend with higher values for strongly sericitized rocks.

It is also common practice to use base metal and barium values to directly indicate the presence or absence of mineralization. Although these values are generally erratic, they show dramatic increases that are orders of magnitude higher in many altered samples when compared to least altered samples.

The indices are compared to other selected ratios and various individual elements (Pearson correlation coefficients are shown in Table F-2). Many of the best correlations occur amongst the aforementioned indices as they have common elements in the formulas. Surprisingly, there are only weak correlations amongst the various indices and base metals or barium. Rb shows a very strong positive correlation to K_2O and a much weaker positive correlation occurs between Sr and Ca (and Na). Consequently, the Rb/Sr ratio correlates very well with the Spitz & Darling, Sericite and Hashimoto Indices. The strongest correlation in the data set, other than K_2O -Rb, is Ba - Sr. It is suspected that Sr may substitute for Ba in barite. Chlorine, although with analytically uncertainties, has a strong and moderate positive correlation with CaO and Na_2O, respectively. As a result, Cl has a negative correlation with alteration indices suggesting that the depletion of chlorine may be an important indicator of hydrothermal alteration. Base metals and barium do not show strong correlation to any indice or other single element. Amongst them, Pb-Zn show the most significant correlation. Barium correlates only moderately (positive) with the

base metals and As shows a moderate positive correlation with Cu. The alteration indices show only weak positive correlation to the base metals and barium. Loss on Ignition (LOI) correlates positively MgO, MnO, and Fe_2O_3 but negatively with K_2O suggesting chloritized samples may have a higher volatile content than sericitized rocks.

6.2.2 Powerhouse Alteration Zone

A MgO - Al_2O_3 - (CaO + Na_2O + K_2O) ternary diagram is used to illustrate alteration pathways for rocks from the PHZ (Figure 6-7). Several important trends are evident. The alteration mineralogy at the PHZ is dominated by sericite(clay) alteration, as well as quartz, chlorite and Ca-Mg carbonates. The mafic rocks show significant displacement from the hypothetical precursor and plot close to a chlorite-albite tie line, with some tendency towards sericite. The felsic suite mostly clusters towards the Al_2O_3 apex, most likely due to strong calcic-soda depletion via sericite-clay mineral alteration. Most of the felsic samples plot between montmorillonite and sericite-illite. Some of these rocks may also be showing a weak influence of chlorite, which forms a minor constituent in a few rocks, typically as a replacement of glass. A single felsic and mafic sample form outliers from the main groups and plot roughly at the center of the diagram. These samples contain anomalously high proportions of CaO and MgO and low Al_2O_3 and are directed from the least altered sample towards dolomite.

Alteration indices for the PHZ are shown in Table F-3. Alteration scores show large ranges for the felsic rocks, but more limited and lower scores for the mafic rocks. The low alteration scores for the mafic rocks are due to the high Na_2O content.

Correlation coefficients are shown in Table F-4 for various alteration indices and elements. A cursory examination of the data suggests that the elements can be broken into two main inter-correlating groups: (i) Na_2O, MnO, CaO, FeO, Sr and Cl and (ii) SiO_2, K_2O, Rb, and Ba. Alteration indices correlate positively with group (ii). Cu, Pb and Zn show only weak correlation with alteration indices.

K_2O vs. Rb and Ba relationships are illustrated in Figure 6-8. Both trace elements show very strong positive linear correlations with K_2O, suggesting that both occur with K_2O in sericite. Only one sample shows significant deviation from the Ba-K_2O sericite trend, plotting at relatively high Ba. This sample may contain minor barite.

MnO correlates strongly with both CaO and MgO, and samples with elevated MnO (up to 0.89%) also have the highest CaO. The ratio of CaO/MnO varies mostly between 4 and 20 (Figure 6-9a). MnO is most likely substituting for MgO in dolomite. Sr, which typically has a strong affinity for Ca, shows only a modest statistical correlation. However, a plot of CaO vs. Sr (Figure 6-9b) shows a strong correlation of these elements, but on two distinct trends. The steeper Sr/CaO trend incorporates most of the mafic rocks and the least altered felsic samples, probably representing a feldspar control. The lower Sr/CaO, ratios represent dolomitic alteration.

6.2.3 Woodmans Brook Alteration Zone

The WBZ samples (Figure 6-10) are comparable to the previous zones and display two main trends on a MgO - Al_2O_3 - (CaO + Na_2O K_2O) ternary diagram. The mafic rocks are strongly displaced from a hypothetical precursor and plot in chlorite - illite/sericite - ankerite space, with chlorite providing the dominant influence. The felsic suite trends from least altered towards sericite with many samples overlapping sericite/illite compositions. Several felsic samples plot on a tie line from chlorite to sericite/illite, but are heavily weighted towards the latter. As with previous felsic suites, a number of samples also occur intermediate of sericite/illite and montmorillonite compositions.

Alteration indices applied to the WBZ data indicate an overall similarity in alteration scores when compared to previous zones (Table F-5). Correlation tests of the alteration indices and various elements (Table F-6) suggest that, as with the PHZ, Rb, Ba and Sr correlate well with the alteration indices. With respect to Ba and base metals, Pb-Ba and Pb-Zn show the best correlations. Arsenic, which correlated well with Cu at the LSZ and Cu and Pb at the PHZ, correlates well with Zn at the WBZ.

Sericite trends are illustrated on K_2O vs Rb, Ba plots (Figure 6-11). Rb shows a strong positive linear correlation with K_2O, however, there may be a change in the slope of the line on the plot at a point near approximately 2% K_2O. K_2O and Ba exhibit a more complex relationship. Specifically, there seems to be a strong correlation of Ba and K_2O below ~ 2% K_2O, but in samples with greater then 2% K_2O there appears to be a decoupling of these elements and several samples display much higher Ba. The cause of

the decoupling at ~2% K_2O is uncertain, however, it supports the observation from the Rb vs. K_2O plot wherein a change was also noted amongst those two elements at approximately the same K_2O content. It is speculated that the samples with less than 2% K_2O have not had significant K, Rb and Ba added and that the ratios reflect a primary control. All other samples above 2% K_2O may be the result of inhomogeneous, hydrothermal fluids. Some of these samples may contain minor barite.

CaO vs. Sr (Figure 6-12a) display a relationship comparable to that from the PHZ. Least altered sample plot on a steeply inclined trend (high Sr/CaO) with progressively more altered samples plotting closer to the origin. This trend is a function of feldspar breakdown. Conversely, a flatter trend (low Sr/CaO) represents hydrothermal carbonate. Sr and Ba (Figure 6-12b) are inversely proportional, and rocks containing greater than approximately 300 ppm Ba do not have more than 40 ppm Sr. This reflects the replacement of feldspar with sericite.

6.3 Mass Balance Calculations

Numerous methods have been developed over the past three decades to interpret lithogeochemical data from hydrothermally altered rocks (*e.g.*, Gresens, 1967; Pearce, 1968; Babcock, 1973; Grant, 1986; Stanley and Madeisky, (1994); Leitch and Lentz, 1994). These are generally referred to as the 'Gresens method' or a modified version thereof. Although these methods can test the relative mobility of elements and provide a qualitative analysis of elements gained or lost, they do not yield quantitative data because

the concept of closure (constant sum equal to 100%) is avoided and mass changes are not reported in weight percent. The 'MacLean method' (*e.g.*, MacLean and Kranidiotis, 1987; MacLean, 1990; MacLean and Barrett, 1993) is a more practical method of calculating mass changes that provides quantitative results, *i.e.*, true wt. % oxide additions or losses. This method is employed here to describe mass changes in hydrothermally altered rocks at Buchans.

The MacLean method is based on the premise that various elements (*i.e.*, TiO_2, Al_2O_3, P_2O_5, Zr, Y, Nb, etc) remain immobile, or conservative, under most water-rock reactions in VMS-forming environments (MacLean and Kranidiotis, 1987, MacLean, 1990, Elliot-Meadows and Appleyard, 1991, Richards *et al.*, 1989, and others). Therefore, the ratios of these elements will not be affected by the addition or removal of more mobile constituents. Initially, volcanic suites must be separated into individual suites according to magmatic affinity (as was described in Chapter 5). Fractionation trends for each suite are constructed using a subset of least altered samples. Using immobile elements, incompatible vs. compatible element binary plots (e.g., Zr vs. TiO_2, Y vs. Al_2O_3) produce fractionation trends on with negative slopes. Since these ratios remained unchanged, alteration lines ascending from the origin cut the fractionation trend. Samples displaying net mass loss or gain will plot on these lines and can be traced back to their respective precursor compositions on the fractionation trend. The displacement of a sample from the fractionation lines is representative of the *enrichment factor*, defined as the $X_{precursor}/X_{measured}$. An enrichment factor of greater than 1 indicates net mass gain and a

factor of less than 1 indicates net mass loss. With the subset of least altered samples, precursor compositions for all major and minor elements for each sample can be approximated by solving for the intersection of the alteration lines with the fractionation trends. Reconstituted compositions are then computed by multiplying analytically measured values by the enrichment factor. Mass changes are determined by subtracting precursor values from reconstituted values. If the data set represents a very minimal amount of fractionation, the single precursor method can be used whereby only one precursor composition exists for all samples (*i.e.*, fractionation trends are not required). With suites which display more complex fractionation, such as in bimodal suites, the multiple precursor method is used. The transitional SHF basaltic-andesites and BRF dacites appear to be genetically related (*i.e.*, single igneous suite) and therefore the multiple precursor method was utilized for these rocks. Conversely, since only smaller data sets have been established for the more calc-alkaline BRF rhyodacites, the single precursor method is used for this unit. Mass balance calculations used here are based on a Zr - Al_2O_3 fractionation trend, although Zr-TiO_2 based calculations yield very similar results. Mass changes were calculated for all major and minor oxides as well as Rb, Ba and Sr. The method, including equations used for fractionation trends, is described in more detail in section F.1. The results are presented in Table F-7.

6.3.1 Mass Changes in the Lucky Strike Zone/Middle Branch Zone

Fifty seven samples, including 21 'mafic' samples from the SHF and 20 BRF dacites, were evaluated using the multiple precursor method. Nine samples of BRF rhyodacitic composition were evaluated using a separate, single precursor system. Six samples of dacitic composition from existing data (*i.e.*, Thurlow *et al.*, 1981; Unpublished data from the Newfoundland Department of Mines and Energy) were also inserted into the data set as they were collected from drill hole 202, one of the holes studied in this report.

6.3.1.1 Fractionation Trends

The initial assignment of the data into igneous suites was based on immobile trace element data (section 5.2). Fractionation trends were constructed for each suite using least altered samples. The SHF mafic volcanic rocks and BRF dacites, which have been shown to be part of the same suite, were modeled together and were considered to plot on the same fractionation trend. Because of the altered nature of the host rocks, an extensive data set of relatively fresh rocks was not available. This was certainly the case for the dacites, which appear to almost always display intense alteration in the vicinity of the Lucky Strike deposits. However, the combination of the least altered samples from this data set, combined with the least altered samples taken from previous studies *(i.e.*, Thurlow *et al.*, 1981; Unpublished data from the Newfoundland Department of Mines and Energy), based on an examination of the raw geochemistry, permits a reasonable approximation of the protolithic compositions. A brief discussion about the use of this

older data is presented at the end of this section. The BRF rhyodacites are treated as a separate suite for the purposes of the mass balance calculations. Precursor compositions were readily estimated from 'fresh' rhyolite and all other data were applied using a single precursor method.

Fractionation trends for the SHF mafic volcanic and BRF dacite suite are shown in Figure 6-13. Altered samples retain their immobile element ratios (*e.g.*, Zr/TiO_2 and Zr/Al_2O_3 ratios, but due to the addition or removal of mobile constituents, they define the alteration lines or fans which pass through the origin and intersect the fractionation curve at high angles. The amount of offset from the precursor composition on the fractionation curve represents the degree of mass change. In Figure 6-13a, the data indicate an overall trend of decreasing TiO_2 (compatible) with increasing Zr (incompatible), with the resultant concave upwards curve flattening out at high Zr. The typical fractionation trend would also display a slight hump approximately the basalt to basaltic-andesite transition due to the fact that a Ti-bearing phase (*e.g.*, titanite) would start to crystallize and fractionate at this point. However, as most of the samples from this data set represent the more fractionated basaltic-andesite composition, there is insufficient data from which to define the curve at lower Zr values. The same data are plotted in Figure 6-13b, and define a similar trend with decreasing Al_2O_3 and increasing Zr with increasing fractionation. This trend differs, however, in that the removal of Al_2O_3 is constant, producing a line of constant slope. Fractionation trends are also shown for Zr - P_2O_5 (Figure 6-13c) and TiO_2 - Al_2O_3 (Figure 6-13d), either of which could be used as a basis for mass balance

calculations. It is clear from all plots that the mafic rocks have mostly undergone mass gain whereas the felsic rocks have display mostly mass losses, and that either suite displays a fairly narrow alteration fan indicating limited compositional ranges.. The mass balance calculation reported here was based on the Zr - Al_2O_3 fractionation trends.

The Buchans River Formation rhyodacites were treated as a separate suite and, as the single precursor method was used, fractionation trends were not needed to conduct mass balance calculations. The data are plotted on a Zr vs. TiO_2 plot in Figure 6-14 and define a fairly narrow alteration fan with most samples plotting at higher concentrations, but with the same ratios, of immobile elements indicating mass loss.

If all existing data from the Buchans camp are considered, including the data from this study and older data (an additional 180 samples from previous work), several interesting observations can be made. Note that much of the older data does not include important trace elements (*e.g., Y, Nb, REE*) used for discrimination purposes and, therefore, the designation as belonging to BRF or SHF is based on previous workers interpretations. As many of these samples are from the immediate mining areas of the Buchans camp, the assigned formations are probably fair. Based on data from this study, felsic rocks from the older data set are separated into dacites ($Zr/TiO_2 < 550$) and rhyodacites (and rhyolites) ($Zr/TiO_2 > 550$). As it is uncertain whether this more fractionated felsic unit is related, it is included here on a hypothetical basis only. Zr vs. TiO_2 is plotted with data from this study only in Figure 6-15 a and all available data in Figure 6-15 b. Zr vs. Al_2O_3 fractionation is also illustrated, first with data from this study

only (Figure 6-15c) and then with all existing data (Figure 6-15d). For simplicity, these rocks are temporarily treated as one suite. The same fractionation trends used previously are also plotted based on the suite of least altered samples, however, as to accommodate the rhyodacitic suite, the fractionation curve must be modified. Specifically, Zr must behave compatibly in these rocks beyond the dacitic composition in order to account for the lower Zr in the rhyodacitic suite.

There are several notable observations that can be made from these plots that reinforce the conclusions stated earlier in this study. Firstly, there is a general absence of relatively intermediate composition rocks (*i.e.*, andesites) on these plots and the mafic and felsic volcanic rocks are endmembers of the same suite. More importantly, there is significant scatter amongst the data, mostly attributed to alteration-induced mass changes. In particular, the greatest scattering (presumably along alteration lines) occurs amongst the SHF mafic rocks and BRF dacites, whereas the least amount of scatter occurs in the rhyodacitic suite. This suggests that greatest alteration occurs in the dacitic unit, inherent in the fact that it is more closely associated with mineralization whereas the lesser alteration occurs in the rhyodacitic unit. This supports the ideas presented in this study that the dacitic and rhyodacitic units represent the foot-wall and hanging-wall sequences, respectively. Furthermore, these units are easily distinguishable on these plots and are outlined. These same fields can also be discerned on the plots containing the larger data sets from previous work, giving order or form to an otherwise data 'cloud'. This is remarkable considering the even broader camp scale distribution of the samples and the

probable higher analytical uncertainty of much of the data. Therefore, these plots may be predictive in terms of distinguishing potential hanging-wall and foot-wall felsic lithologies. In addition, they can also be used to recalculate elemental concentrations in the older data to quantitatively determine the mass changes that occurred in these rocks.

6.3.1.2 Mass Changes

In this section, recalculated data as opposed to raw data are presented as a means to evaluate alteration. The data were derived from the method described above and are presented in terms of wt. % gain or loss. Graphical presentation of the recalculated data emphasizes the distribution of mass changes and depicts alteration mineralogy trends.

6.3.1.2.1 $\triangle CaO$, $\triangle Na_2O$ and $\triangle K_2O$

CaO and Na_2O are significantly depleted in most samples in the Lucky Strike and Middle Branch areas, owing largely to the destruction of plagioclase feldspar in these rocks. Na_2O is consistently depleted relative to the precursor, averaging losses of 3% in felsic rocks and 1% in mafic rocks. Few samples have non-negative values for mass change in Na_2O.

CaO also shows significant depletion from precursor, especially in mafic rocks. CaO is depleted at an average of 6.2% in mafic rocks and 0.3% in felsic samples. However, most of the mafic samples have losses in excess of 8% and many felsic rocks have lost more than 0.5%. These values correspond roughly to the precursor modal

anorthitic feldspar component in these rocks. Therefore, many of these samples have undergone near complete feldspar destruction. Only a few samples display CaO enrichment, however, the enrichment is often as high as 8 or 10 %. These values correlate with stockwork-related carbonate veining below the Lucky Strike deposit.

K_2O is dominantly enriched in both mafic and felsic rocks of the Lucky Strike Zone, as well as in the felsic units in the Middle Branch Zone. Losses in mafic rocks are calculated to have a maximum of 0.8% depletion but additions of up to 2.9% K_2O, corresponding to primary alkali feldspar breakdown and sericitic alteration of plagioclase, respectively. Felsic rocks display wider ranges of K_2O mass change, with losses of greater than 1% and gains as high as 4.8%. Gains in excess of 4% K_2O are attributed K-feldspar alteration and are most common in samples from the MBZ.

6.3.1.2.2 $\triangle Fe_2O_3$ (total) - $\triangle MgO$ - $\triangle MnO$

Fe_2O_3 shows moderate to strong enrichment in most mafic rocks, but generally shows less dramatic variations in felsic rocks. Other than a few samples hosting significant sulphide mineralization, Fe-enrichment in felsic samples rarely exceeds a few percent. In fact, many felsic rocks indicate Fe-loss.

MgO enrichment is more consistent than Fe_2O_3 enrichment and very few samples display MgO losses. As with Fe_2O_3, the largest gains of MgO generally occur in mafic rocks and commonly exceed 10% (averaging 8%). Felsic lithologies generally show only

slight gains in MgO, typically around 1-2 %, although a few intensely chloritized samples from the stockwork zone display 5-30 % MgO addition.

Modest MgO gains generally correspond to Fe_2O_3 additions, however, the greatest MgO enrichment does not show substantial Fe_2O_3 gain. This is due to the fact that the most strongly chloritized rocks are in the stockwork zone and have Mg-rich variety of chlorite (e.g., penninite). MnO mass changes show broad correlations to (Mg+Fe) changes, however, the strongest tendency appears to be towards MgO. MnO enrichment is typically less than 1%.

6.3.1.2.3 $\triangle SiO_2$

SiO_2, due to its relative mobility and abundance, has the greatest variation of any oxide and most often defines the bulk of the net mass change. Nearly all mafic samples have significant SiO_2 enrichments. This is attributed to in-filling of amygdules and other voids by quartz (and chalcedony), quartz stockwork veining, and pervasive replacement of groundmass. Felsic rocks, conversely, are typically SiO_2 depleted, presumable due to SiO_2 loss through feldspar breakdown and/or through leaching of quartz. Very large variations occur in stockwork zones where SiO_2 may be significantly enriched through pervasive silicification and quartz veining or significantly depleted due to intense chloritization. Stockwork zone alteration is independent of protolithic composition. SiO_2 losses are limited to protolithic SiO_2 content and may be up to about 40%, especially in strongly chloritized and/or sericitized felsic rocks.

6.3.1.1.4 $\triangle Al_2O_3$ - $\triangle TiO_2$ - $\triangle P_2O_5$

Deviations in Al_2O_3, TiO_2, and P_2O_5 ratios are insignificant and, therefore, these oxides are considered to be immobile. Although Al_2O_3 was assumed to be immobile, mass balance calculations based on Zr-TiO_2 fractionation also yielded no significant mass changes of Al_2O_3. This was supported by the consistency of the ratios of these elements from the raw data.

6.3.1.2.5 $\triangle$Rb - $\triangle$Ba - $\triangle$Sr

Ba shows minor losses in only a few samples, but substantial additions in most samples, often exceeding 10,000 ppm. Although Ba addition does not appear to be lithologically controlled, the largest gains are in the felsic samples. Ba gains also show modest correlations to K_2O additions. Rb mass gains appear to be even more strongly linked to K_2O. Both Rb and Ba were probably associated with primary K-feldspar and were probably re-incorporated into sericite. However, a surplus of Ba also caused the precipitation of barite.

$\triangle$Sr strongly correlates with $\triangle$CaO and the greatest depletions occur in mafic rocks. Sr losses are commonly around 400 ppm in the mafic rocks. Sr also shows strong Sr depletion in felsic rocks, released along with Ca during plagioclase breakdown. It is uncertain if Sr is associated with CaO in hydrothermal carbonate. Anomalously large Sr gains occur with strongly enriched Ba, suggesting that Sr may be incorporated into barite.

6.3.1.2.6 △Totals

The SHF mafic volcanics typically show large net gains, mostly due to the addition of SiO_2 (and MgO and Fe_2O_3), which are greater than the loss of CaO and Na_2O. Felsic lithologies usually display more variability and have average net mass losses, as well controlled by SiO_2 mobility.

6.3.1.3 Binary Mass Change Plots

6.3.1.3.1 △SiO_2 vs △K_2O, △MgO

The dominant styles of alteration at Lucky Strike, including silicification, chloritization and sericitization can be represented with SiO_2, MgO and K_2O mass changes, respectively. These relationships are shown on Figure 6-16. With a few exceptions, felsic rocks display potassium metasomatism, silica removal and very limited magnesium enrichment typical of sericite dominant alteration. Some felsic samples show negligible SiO_2 change but strong K_2O enrichment. These rocks are representative of K-feldspar alteration. The mafic rocks typically show quite different alteration styles from the felsic volcanic rocks, dominated by large SiO_2 and MgO gains but variable K_2O mass changes. These oxide changes illustrate the dominance of silica-chlorite alteration in the mafic rocks with local sericitization.

6.3.1.3.2 △($MgO+K_2O$) vs. △(Na_2O+CaO)

Mass changes of $CaO + Na_2O$ are broadly inversely proportional to $MgO + K_2O$ and represent the breakdown of feldspar to sericite and chlorite with nearly a one to one ratio of these groups (Figure 6-17). The trend continues to about -6 % and -12% ($CaO+ Na_2O$) for felsic and mafic samples, respectively, corresponding to the original concentration of these constituents in the precursors. The trend shifts toward horizontal as K_2O and MgO continue to be added to form additional phyllosilicates, limited only by the amount of conservative Al_2O_3. By separating these components, △MgO vs. △Na_2O and △K_2O vs. △MgO plots (Figure 6-18) reinforce the dominance of chloritization in the mafic suite and the general lack of strong chloritization in the felsic suite.

6.3.1.3.3 △K_2O vs △Rb and △Ba

Mass changes of K_2O vs. Ba and K_2O vs. Rb (Figure 6-19) illustrate several important alteration mineralogy features. For the mafic volcanic rocks, Rb tends to behave very similarly to K_2O in both gains and losses. The felsic volcanic rocks do not show the same degree of correlations. Ba and K_2O mass changes show good correlations for both losses and gains for many samples. Ba and Rb are assumed to occur in primary feldspar and are largely incorporated in sericite during alteration. In addition, a number of samples with very large Ba gains display no correlation to K_2O. These samples contain barite.

6.3.2 Mass Changes at the Powerhouse Alteration Zone

Mass changes at the PHZ were calculated for 28 samples, most of which were felsic. The mafic precursor compositions are estimated as no reasonably fresh samples of this unit occur in drill core.

6.3.2.1 Fractionation Trends

TiO_2-Zr and Al_2O_3-Zr fractionation trends are shown from the PHZ in Figure 6-20. Because of limited outcrop exposure and the fact that drilling targeted areas of strongest alteration, very few fresh rocks were available from this zone. The trends are based on the least altered felsic volcanic rocks and estimated for the mafic rocks. Based on either one of the plots shown, the mafic rocks display slight gains and losses whereas the felsic suite shows predominant net losses. The Al_2O_3-Zr fractionation trend was used to calculate mass balance calculations. The calculation procedure, equations and results are presented in Appendix F, section F.1.

6.3.2.2 Mass Changes

Recalculated mass changes are presented according to the method described above. Mass change data are presented in wt. % gains or losses for major oxides and ppm for trace elements.

6.3.2.2.1 $\triangle CaO$, $\triangle Na_2O$ and $\triangle K_2O$

Both CaO and Na_2O display consistent losses in the felsic volcanic rocks, with the exception of a few positive CaO values where significant carbonate alteration occurs

(Figure 6-21). Mass change of Na_2O averages -3.4 %. K_2O displays an antipathetic relationship to CaO and Na_2O, displaying gains in nearly all samples. The average K_2O gain is 1.7%.

The mafic rocks display pronounced CaO depletion (-7 to -8%) in these rocks (except one sample with large positive CaO). The CaO losses are typical of near complete removal of primary plagioclase and Na_2O would also be expected to mimic this trend. However, the mafic samples show a peculiar addition of Na_2O (averaging around +1.3%). Na_2O addition is attributed to the albitization of plagioclase. K_2O gains are comparable to those in the felsic suite and average about 1.7%. K_2O is very consistent for both mafic and felsic endmembers and no samples yield more than 2.9% addition.

6.3.2.2.2 $\triangle Fe_2O_3$ (total) - $\triangle$MgO - $\triangle$MnO

Fe_2O_3 (total) mass changes values are nearly all between about -2% and 4% in felsic rocks. MgO mobility is very similar, with nearly all values occurring between approximately -2% and 6%. One exception is sample BE-13-105 which has a MgO gain of 13%. MnO and CaO also yield 1.1% and 15% gains, respectively, likely due to dolomitic alteration.

Fe_2O_3 (total) displays slight losses to slight additions in the mafic rocks as well. MgO gains are also modest with the exception of one sample which yields a gain of 18%. This sample also has 0.7% MnO and 16% CaO addition and probably contains substantial dolomite

6.3.2.2.3 $\triangle SiO_2$

SiO_2 shows significant mobility in the felsic suite, dominated by SiO_2 loss with several samples in the -20% range. The average SiO_2 mass change is -4.6%. SiO_2 gains are more modest, though a few samples yield exceptionally large gains. Mafic rocks, surprisingly, display slight but consistent mass losses.

6.3.2.2.4 $\triangle Al_2O_3$ - $\triangle TiO_2$ - $\triangle P_2O_5$

There are no significant mass changes in either of Al_2O_3, TiO_2 or P_2O_5 in either mafic or felsic groups. Therefore, these oxides are considered immobile in the PHZ.

6.3.2.2.5 $\triangle$Rb - $\triangle$Ba - $\triangle$Sr

Both Rb and Ba prove to have been consistently added, although a few samples show slight losses of both Ba and Rb. About 80% of the both felsic and mafic rocks have less than 500 ppm Ba added, with no anomalously high values (the maximum addition is approximately 1300 ppm). Conversely, Sr has been largely removed, with the greatest Sr depletion occurring in the mafic suite.

6.3.2.2.6 $\triangle$Totals

Total mass gain or loss is dependent on the most mobile constituent, SiO_2. Therefore, most samples display net mass loss, averaging -5%.

6.3.2.1 Binary Mass Change Plots

6.3.2.3.1 △CaO vs △Na_2O

Both mafic and felsic rocks plot into distinctive clusters on the mass change plot of CaO vs. Na_2O (Figure 6-21). The felsic rocks plot in the lower left hand quadrant, displaying total removal of both CaO and Na_2O when compared to the precursors. This trend suggests near complete destruction of plagioclase due to alteration. A few samples display a drift into the positive △CaO field, probably as a result of carbonate alteration. The least altered felsic, not having been significantly altered, plots very close to the origin. Mafic samples plot in the upper left hand quadrant, displaying near complete CaO removal, but yielding Na_2O additions. It is unreasonable to assume that plagioclase might have been broken down and only leached CaO, and there are few minerals present in these rocks other than albite to explain significant Na_2O addition. Therefore, it can be reasoned that these mafic rocks were albitized, essentially replacing Ca with Na in primary feldspars. One mafic sample also shows strong CaO addition owing to carbonitization.

6.3.2.3.2 △ SiO_2 vs. △K_2O

K_2O enrichment may occur with either SiO_2 gain or loss (Figure 6-22). All mafic most felsic samples have undergone sericitization and silica loss. Other felsic samples show both sericite and silica alteration. There are no samples yielding silica gain or loss without K_2O mass change (*i.e.*, no silica leaching only).

6.3.2.3.3 △ K_2O and △ MgO vs. △ CaO

All samples which have undergone significant CaO depletion (most of the data) also show significant K_2O enrichment (Figure 6-23b), and some of these also display modest MgO gains (Figure 6-23a). Least altered samples show negligible mass changes and plot close to the origin on these plots. K_2O enrichment, limited to less than 3%, is typical of sericitization. MgO enrichment is generally less than 5% in both mafic and felsic samples. Since these do not correspond with CaO enrichment, the alteration is probably related to minor chloritization. A single mafic and a felsic sample display exceptionally high MgO and CaO additions, plotting in the upper right hand quadrant (Figure 6-23a). These samples have been intensely dolomitized.

6.3.2.3.4 △ Ba vs. △ K_2O and △Sr vs. △ CaO

Additions of both Ba and K_2O show strong positive correlation (Figure 6-24a). This trend represents a sericite alteration trend in which Ba substitutes for K in sericite. Very few samples plot off of this trend and some of these may contain very minor barite. Removal of both CaO and Sr also show positive correlation (Figure 6-24b). Removal of CaO and Sr occur during feldspar breakdown, however, Sr does not appear to be replenished to the same degree with CaO addition during carbonate alteration. This suggests that Sr may be a better indicator of feldspar destructive alteration in rocks with strong carbonate alteration.

6.3.3 Mass Changes at the Woodmans Brook Alteration Zone

Twenty nine felsic volcanic and 7 mafic volcanic samples from the WBZ were evaluated for mass changes. As with the mafic volcanics from the PHZ, the mafic rocks have a more limited extent and are strongly altered which makes precursor estimations difficult.

6.3.3.1 Fractionation Trends

Fractionation trends using Zr vs. Al_2O_3 and Zr vs. TiO_2 form trends that are broadly similar to the PHZ (Figure 6-25). The mafics, though only a few samples, plot on an alteration line with very consistent ratios. There is a little more scattering in the felsic endmembers due to greater Zr/Al_2O_3 ratios (*i.e.* broader alteration fan), suggesting more fractionation. The felsic suite also plot mostly above the fractionation trend indicating a predominance of mass loss.

6.3.3.2 Mass Changes

The following sections present recalculated data derived from the method described earlier. All data are presented as mass gain or loss in wt. % for major oxides and ppm for trace elements.

6.3.3.2.1 $\triangle CaO$, $\triangle Na_2O$ and $\triangle K_2O$

Na_2O and CaO are strongly depleted in felsic samples, averaging around -1.6% removal of each oxide. Many samples display essentially complete removal of both,

whereas very few samples show any gain in these oxides. Mass changes of CaO + Na_2O consistently combine for negative values. The frequency distribution of the mass changes for CaO and Na_2O are also different. Most samples show maximum CaO loss with fewer samples displaying lesser losses, however, the number of samples with Na_2O losses peaks at an intermediate value of depletion. This suggests that while many samples had almost complete removal of CaO, they have not been completely depleted in Na_2O.

A number of samples have also undergone K_2O loss but most samples have had K_2O added. The overall K_2O mass change is about 0.5% with maximum values of +2.7%. Almost all mafic samples have losses of CaO and Na_2O, approximately equal to precursor compositions, and K_2O additions that are comparable to the felsic suite.

6.3.3.2.2 $\triangle Fe_20_{3(total)}$ - $\triangle$MgO - $\triangle$MnO

Fe_2O_3 shows minor losses for most of the felsic samples, with only a few samples having modest gains, averaging -3%. MgO mass changes for felsic rocks are typically between -4% and +4%, with only a few samples with significantly greater enrichment. MnO does not display any significant variation in mass change.

Mafic rocks yield consistent modest mass gains of Fe_2O_3 and MgO, each averaging about 6%. Maximum gains of Fe_2O_3 and MgO are approximately 9% each. MnO mass changes are not anomalous and are up to a maximum of 0.3%.

6.3.3.2.3 △ SiO_2

Felsic samples have SiO_2 mass changes between -20% and +20%, with a maximum loss of -32%. Mafic rocks display less variability, typically showing only slight gains.

6.3.3.2.4 △Al_2O_3, △TiO_2 and △P_2O_5

No significant addition or depletion of Al_2O_3, TiO_2 or P_2O_5 appears to have occurred in either the mafic or felsic rocks from the WBZ.

6.3.3.2.5 △Rb, △Ba and △Sr

As with the previous zones, most samples display additions of Ba and Rb and losses of Sr. No samples yielded significant Ba additions (*i.e.*, no barite) akin to alteration typical of Buchans.

6.3.3.2.6 △ Totals

The removal of SiO_2, Na_2O and CaO outweighs the addition of K_2O in the felsic rocks and therefore the felsic rocks display average net mass loss. The mafic rocks have greater increases of SiO_2, Fe_2O_3, MgO and K_2O than losses of CaO and Na_2O. These rock show average net mass gains.

6.3.3.3 Binary Mass Change Plots

6.3.3.3.1 Various $\triangle CaO$, $\triangle Na_2O$, $\triangle K_2O$ plots

Inter-relationships between mass changes of CaO, Na_2O and K_20 are not as obvious in rocks from the WBZ (Figure 6-26). Both CaO and Na_2O display losses in most samples, however, the correlation of the two is less obvious than in previous zones. In fact, for the felsic rocks there appears to be two trends on a plot of $\triangle CaO$ vs. $\triangle Na_2O$ (Figure 6-26a). A few samples plot on a linear trend of proportional CaO and Na_2O mass loss. This trend is interpreted as representing the breakdown of primary feldspar. However, most samples plot on a trend of constant CaO loss (at -2 to 2.5%) but with a large range of $\triangle Na_2O$ values (-4 to +1%). The breakdown of feldspar cannot account for this trend (*i.e.* no alteration style for selective removal of CaO). This trend is interpreted to be the result of albitization of the un-sericitized feldspar component during lower greenschist metamorphism. The mafic rocks display similar trends, with near complete removal of CaO, but more variable Na_2O.

$\triangle Na_2O$ vs. $\triangle K_2O$ (Figure 6-26b) display a modest correlation of K_2O gain and Na_2O loss. The most altered samples cluster at approximately -3% Na_2O and +1.5% K_2O. A few samples with loss of both K_2O and Na_2O represent chlorite-pyrite replacement of primary feldspar. A plot of $\triangle CaO$ vs. $\triangle K_2O$ (Figure 6-26c) reinforces the fact that all samples range between strongly sericitized and strongly albitized.

6.3.3.3.2 $\triangle SiO_2$ vs. $\triangle K_2O$, $\triangle MgO$

A plot of $\triangle SiO_2$ vs. $\triangle K_2O$ (Figure 6-27a) displays three main styles of alteration. Most felsic samples have undergone either sericite or quartz-sericite alteration. A few samples, displaying losses of both K_2O and SiO_2, likely represent chloritized and/or albitized samples. Mafic samples generally show silica and sericite alteration. No samples display both SiO_2 gain and K_2O loss.

On a plot of $\triangle SiO_2$ vs. $\triangle MgO$ (Figure 6-27b), the felsic samples display a complete range of possibilities, with most having undergone slight MgO loss with variable SiO_2 mass changes. Those with the greatest MgO additions have undergone large SiO_2 loss, typical of strongly chloritized rocks. Mafic rocks have gains of both MgO and SiO_2 indicating chlorite and silica alteration.

6.3.3.3.3 $\triangle MgO$ vs. $\triangle K_20$, $\triangle Fe_20_{3(total)}$

A $\triangle MgO$ vs. $\triangle K_2O$ plot (Figure 6-28a) illustrates that the felsic samples have been dominantly sericitized, with smaller groups exhibiting sericite-chlorite and chlorite only alteration. All mafic rocks display both sericite and chlorite alteration. On a $\triangle MgO$ vs. $\triangle Fe_2O_3$ plot (Figure 6-28b), a majority of felsic samples display both Fe_2O_3 and MgO depletion. Those that have undergone chloritization have significant gains of both oxides. Nearly all mafic samples are chloritized and display both Fe_2O_3 and MgO addition. Several mafic samples with anomalously large Fe_2O_3 gains contain abundant sulphide mineralization (mostly pyrite).

6.3.3.3.4 △Rb, △Ba vs. △K_2O and △Sr vs. △CaO

Both Rb and Ba have mass gains that correlate well with addition of K_2O (Figure 6-29a,b). Furthermore, Rb and Ba both have losses that are highly correlated with K_2O losses. These trends are interpreted to represent the breakdown of K-feldspar, yielding loss of K, Ba, Rb, and subsequent incorporation of these constituents into sericite. Sericite trends appear to have slightly different slopes for the different compositional endmembers. A few samples with anomalously high Ba may contain minor barite.

Both mafic and felsic samples plot in negative space on a △Sr vs. △CaO plot (Figure 6-29c). These constituents are removed as plagioclase is broken down. Some CaO has been reintroduced into the system as carbonate, however, Sr does not appear to have been added in significant amounts with the hydrothermal carbonate.

6.3.4 Summary of Mass Changes

Calculated mass changes are broadly similar from all zones with a few exceptions (Figure 6-30). Al_2O_3, TiO_2 and P_2O_5 all display insignificant average mass changes and are considered to have been immobile in all zones. SiO_2 is greatly added and removed from mafic and felsic rocks, respectively, from the SHF and BRF. The WBZ rocks show a similar effect of SiO_2, although the average mass changes are not as great. The PHZ shows slight additions for both rock types. Fe_2O_3 has greatest additions in the SHF mafic volcanics, with lesser additions occurring in the WBZ mafic rocks and negative Fe_2O_3 mass changes occurring in mafics at the PHZ. Felsic rocks display little Fe_2O_3 mass change. Low average MnO mass changes are typical of all zones. MgO shows some degree of

mass addition in rocks from all zones, with the greatest additions occurring in mafic rocks. Likewise, CaO removal is common for mafic and felsic rocks in all zones. Na_2O mass loss is typical of all altered rocks from the SHF and BRF, but is less consistent in the PHZ and WBZ owing to low grade metamorphism. K_2O displays comparable mass gains in all rocks from all three zones.

6.4 Downhole Geochemical Variations

The vertical extent of alteration in the Lucky Strike area has been truncated by thrust faults which have cut the mineralized sequences and placed them upon younger, unaltered rocks. Drill hole 2871 was drilled through the Lucky Strike ore horizon and contains both hanging-wall and foot-wall lithologies. Drill hole 202 is one of the deepest and most continuously mineralized intervals cutting almost 370 meters of altered rock before intersecting a major fault (Old Buchans Fault). These holes have been used to illustrate the variation in alteration and host rock in the vicinity of the Lucky Strike deposits by plotting geochemistry vs. depth.

6.4.1 DDH 2871

Hole 2871 provides an intersection through the hanging-wall through the Lucky Strike ore horizon (North orebody) and into altered foot-wall rocks (Figure 6-31). The transition is marked by large variations in immobile element ratios (e.g., Zr, Y, TiO_2 and Al_2O_3) (Figure 6-31 a-b). The hanging-wall rocks are BRF calc-alkaline felsic rocks, specifically rhyodacitic lavas and tuffaceous volcanics. Immediately below the ore horizon

is BRF transitional dacite tuff, and below this are transitional SHF flow-hyaloclastite and autobreccia sequences.

In terms of alteration, there are several different trends indicated on these plots that can be illustrated with the use of recalculated (mass balanced) major oxide data. Na_2O is consistently and increasingly depleted upwards towards massive sulphides and, inversely, K_2O is increasingly enriched (Figure 6-31d). Both trends continue several meters into the hanging-wall where changes approach zero in the flows. CaO follows a similar trend with large losses in the deeper mafic samples and slight gains immediately below ore higher with little mass change in the hanging-wall. Total Fe_2O_3 and MgO show symmetrical trends, with large gains in the deeper mafic rocks of approximately 10 wt. % for each oxide (Figure 6-31e). These gains become weaker in the hanging-wall and eventually both Fe_2O_3 and MgO become depleted as alteration weakens. SiO_2 is spikey, showing large gains in the foot-wall but with depletion just below and above the ore horizon (Figure 6-31f). Base metal and Ba values (from raw data) tend to increase upwards towards the ore horizon but decrease sharply into the hanging-wall. Cu, Pb and Zn tend to mimic each other, yet Ba appears is independent of the base metals. Note the spike in Ba in the transitional dacite immediately below the ore horizon.

6.4.2 DDH 202

Hole 202 displays strong foot-wall alteration from the top of the hole to about 370 meters (~1250') where a major fault is intersected. Three different lithological units host the alteration, includin the calc-alkaline BRF rhyodacite unit, the transitional BRF

dacite and transitional SHF mafic volcanics. These units are easily separated with Zr, Y, TiO_2 and Al_2O_3 ratios (6-32a-b).

The relationship of calculated mass changes with depth is illustrated for CaO, Na_2O and K_2O in Figure 6-32d. CaO is significantly depleted in all rocks except in the uppermost chloritite zone where some CaO has been added as calcite (this may be related to post-ore faulting processes). Na_2O has also been largely removed from the felsic rocks in this section. The lower mafic rocks have been depleted almost consistently by -2 wt.% Na_2O, whereas as much as 4 wt.% Na_2O has been removed from the felsic rocks in the upper part of the section. Therefore, alteration has nearly removed nearly all of the Na_2O and CaO from foot-wall lithologies with similar effects in the hanging-wall. K_2O shows only marginal losses in the lower mafic rocks (< -1 wt.%) and overall gains in the upper felsic lithologies of greater than 2.5 wt.%.

Fe_2O_3 (total) and MgO (Figure 6-32c) have somewhat symmetrical patterns due to chlorite formation, but sulphide formation is also reflected through Fe_2O_3 addition. The largest gains of Fe and Mg occur in the foot-wall, with the highest Mg occurring just below the ore horizon in a zone of nearly pure chlorite (chlorite) affecting both mafic and felsic units. A value of $\triangle MgO \sim 0$ just below this corresponds to a large K_2O gain in a zone of strong sericite (and quartz) alteration. SiO_2 (Figure 6-32e) tends to be consistently and substantially enriched in the mid to lower mafic foot-wall, yet it is much more sporadic in the upper felsic rocks.

Base metal and Ba values (raw data) form somewhat spikey patterns on the downhole plot for drill hole 202 (Figure 6-32f), yet there is an overall enrichment trend towards the top of the hole. Most impressive are the very low values associated with the chloritite zone, indicating that this zone represented a pathway for a significant volume of hydrothermal fluids, yet very little sulphide precipitation occurred here.

6.5 Model for Hydrothermal Alteration at Buchans

It should first be stated that much of the work in this thesis focused on the what is considered here to be peripheral, proximal alteration. In addition, it is important to reiterate the post-ore structural disruption of the stratigraphy which is major factor in modeling hydrothermal alteration zones.

Two major factors control the style of alteration at Buchans: (1) the protolith and (2) the location relative to massive sulphide formation or relative to the maximum fluid flow and temperature. In the most proximal alteration facies (*i.e.*, stockwork zone), the alteration is independent of the host rock and alteration mineral assemblages and are fundamentally the same for both felsic and mafic rocks. The alteration has been divided into three main styles: distal, proximal and stockwork and is illustrated schematically on Figure 6-33. The following summarizes the alteration styles and associated geochemical mass changes that are typical of each zone.

The distal alteration in the felsic volcanics is dominated by a sericite-clay mineral assemblage. Most of these altered rocks yield anomalous base and precious metals and Ba.

Occasionally, narrow stringers of Zn-Pb-rich sulphides and barite occur. These stringers are unlike the more proximal style of quartz stockwork veins as they generally contain little or nil quartz, chlorite or chalcopyrite. Thus, they appear to represent a lower temperature style of mineralization. Large additions of K_2O and Ba are typical of these rocks. Ca and Na display modest depletion. Sr is also generally depleted and Rb is enriched.

Distal alteration in the mafic volcanic rocks is more complex and incorporates a mineral assemblage consisting of Fe-Mg-chlorite, quartz (and chalcedony), calcite, epidote-clinozoisite, and sericite. Pyrite is not common and base-metal sulphides and barite are rare. Minor gains in $_{SiO2}$ and K_2O occur in this zone. The alteration is not extremely different from diagenetic alteration in other mafic rocks in the region, but is distinguished by lower contents of epidote and carbonate, the general absence of hematite and the presence of quartz.

Felsic volcanics in proximal alteration zones are not extremely distinct from the distal zones. Ideally, they are affected by potassic alteration (sericite-clays +/-K-feldspar) and also silicic alteration. Pyrite and base metal sulphides are more abundant and a few quartz-stockwork veins occur. Mass changes are similar to that in the distal zone but may contain greater Na_2O and CaO depletion and $_{SiO2}$ enrichment.

Proximal alteration in mafic rocks is characterized by a dominant quartz - chlorite - sericite - pyrite assemblage. These rocks consistently display large SiO_2 gains as well as MgO and Fe_2O_3 addition. K_2O gains are less significant than in the felsic suite but larger

losses of CaO and Na_2O are typical. Ba and Rb are changes are variable unlike Sr which is consistently strongly depleted.

Stockwork zone alteration is independent of proto-lithologies and is dominated by complete chlorite - quartz alteration with abundant base metal sulphides and barite. Calcite, which may occur in small quantities in all zones, is locally abundant in the stockwork zone occurring as veins. Sericite - clay alteration is not present in this zone. In general, mass changes display the largest enrichment of MgO and SiO_2 of any zone. Fe additions are present where sulphides occur and CaO addition is significantly high when carbonate is present. Otherwise, CaO, Sr and Na_2O are completely removed.

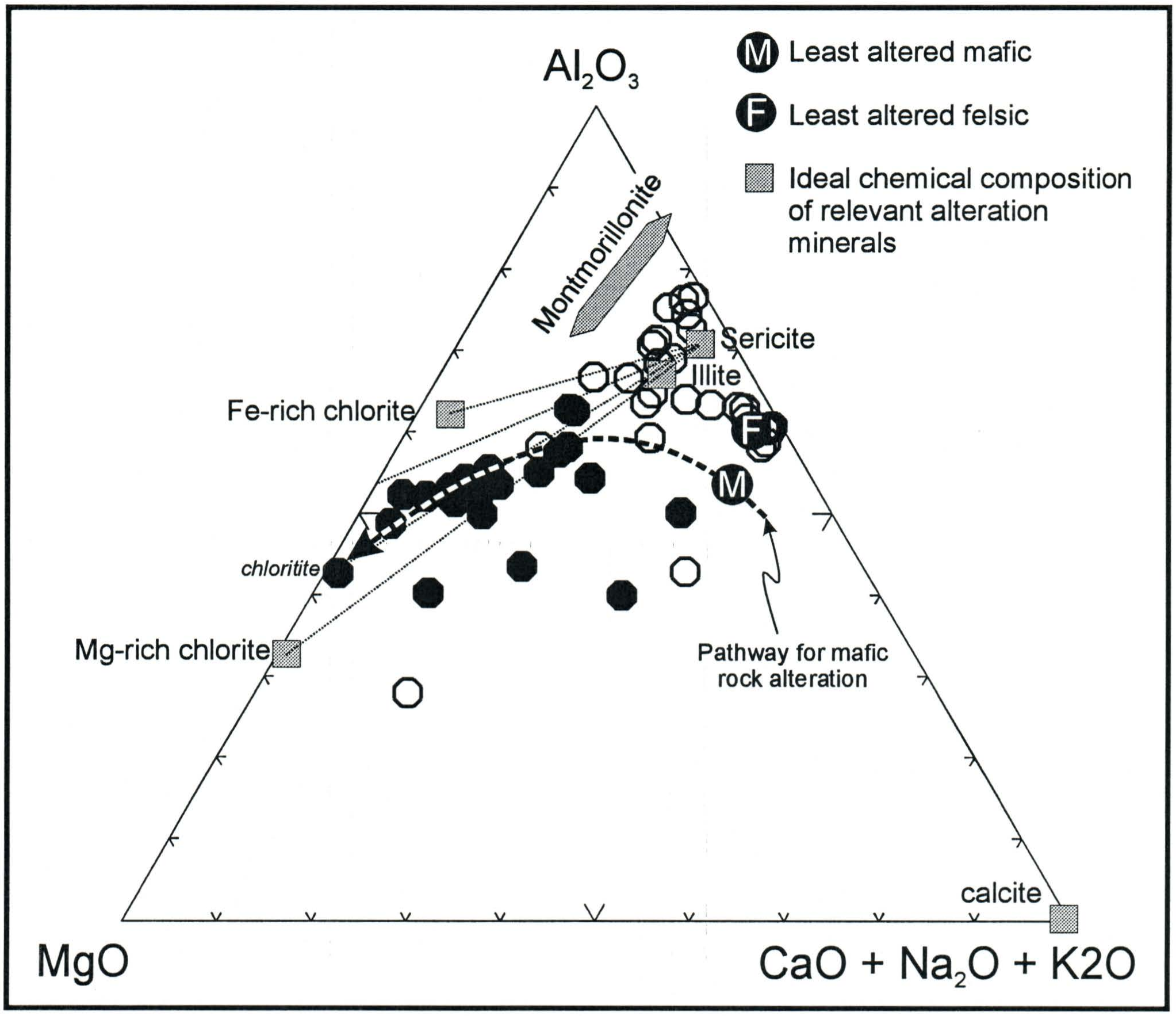


Figure 6-1 - Ternary diagram of MgO - Al_2O_3 - ($CaO+Na_2O+K_2O$) in oxide wt. %. SHF basaltic-andesites (solid circles) and BRF dacitic volcanics (open circles). Two main alteration trends are evident. The mafic rocks follow a trend towards a dominant chloritic alteration. Felsic rocks are generally more sericite-clay altered. Chlorite and sericite compositions are from microprobe analysis (this study). Montmorillonite and illite are derived from idealized formulas (Deer et al.,1992).

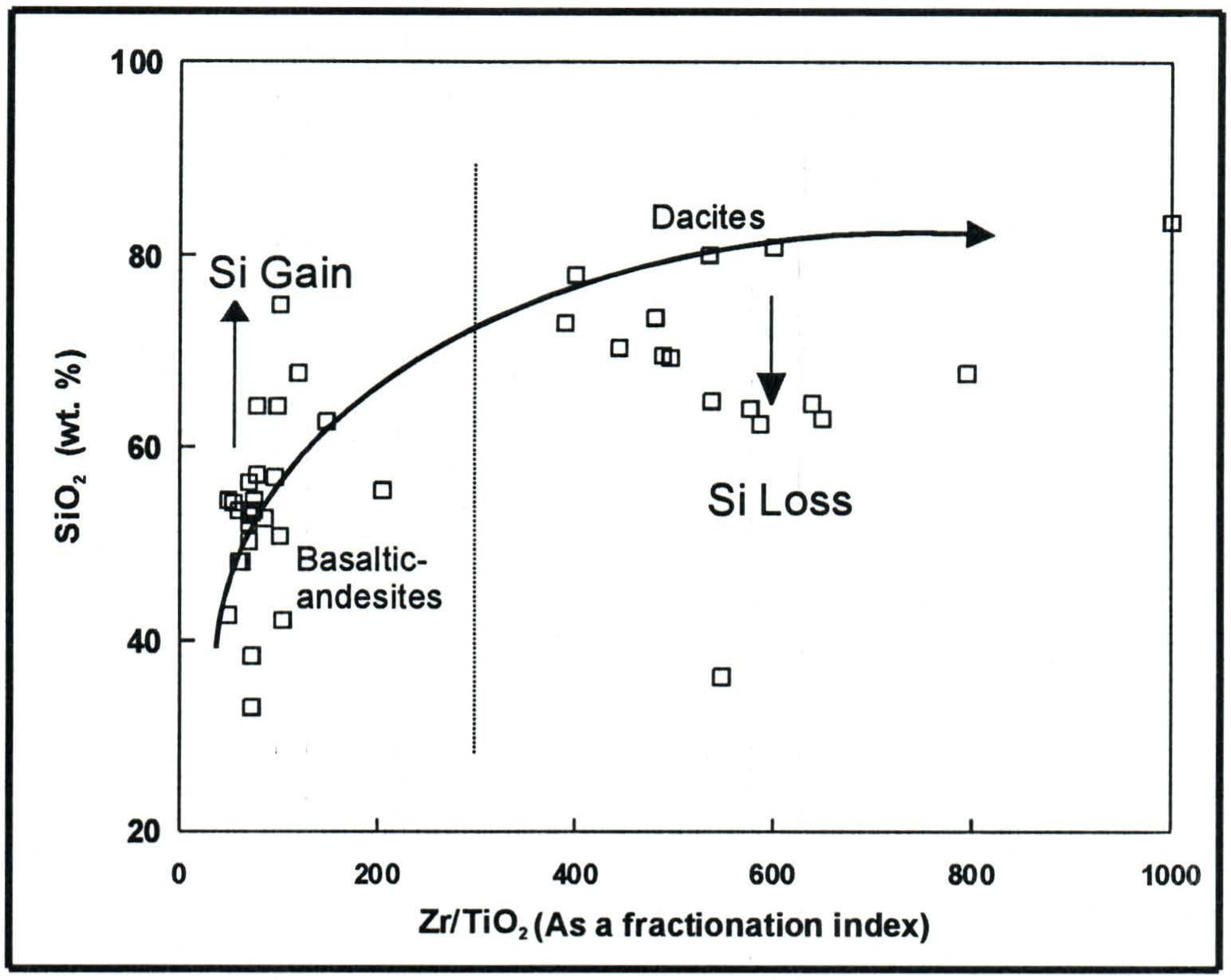


Figure 6-2 - 'Residual silica' plot of Lavery (1985). SHF andesitic-basalts show dominantly SiO_2 gains and BRF dacites appear to be SiO2 deficient. Data is raw whole-rock geochemistry. Results are not quantitative.

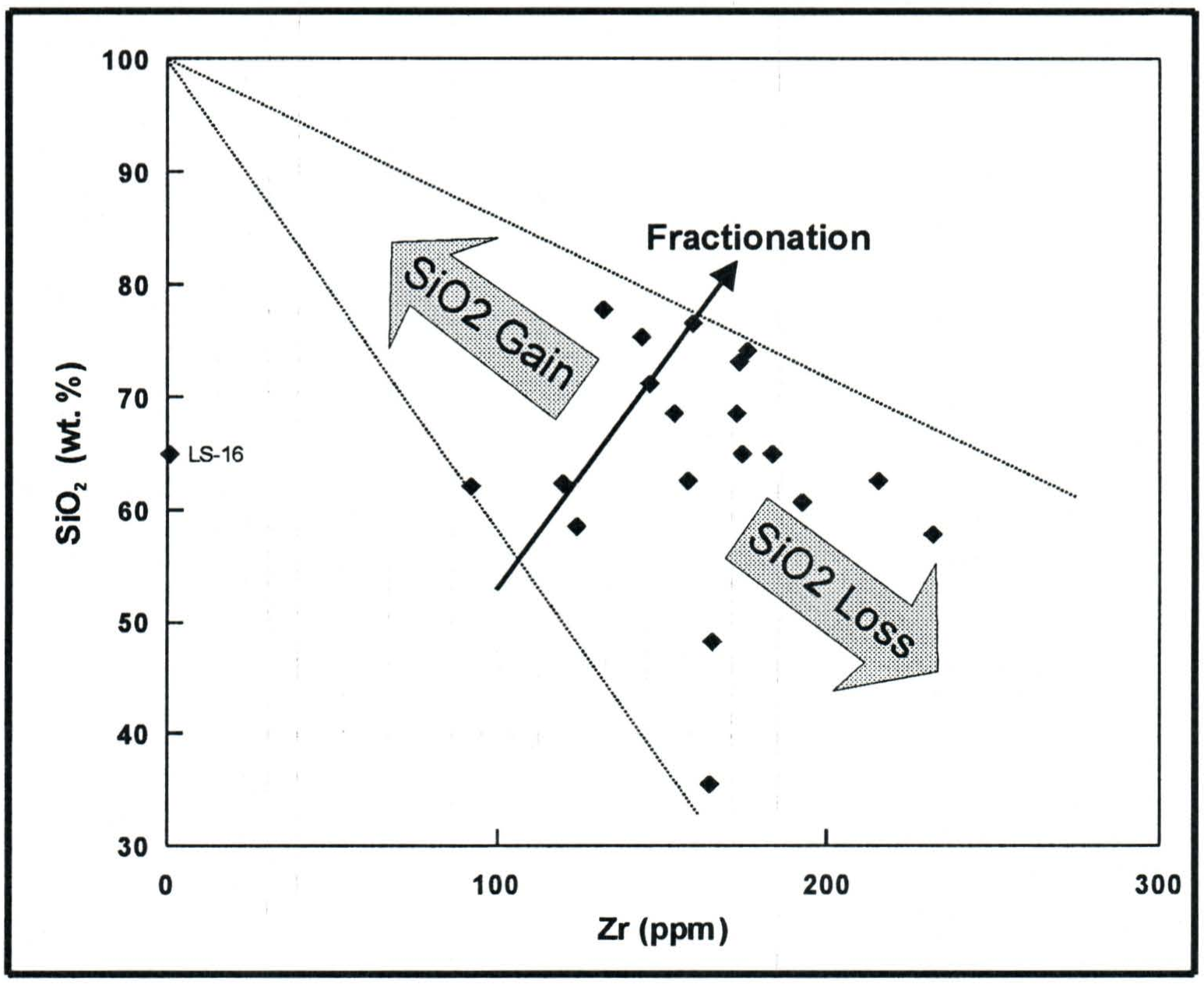


Figure 6-3 (below) - SiO_2 mobility in BRF dacites. Fractionation trend is based on least altered samples. Gains or losses of SiO_2 are proportional to displacement from fractionation trend. Data are raw whole-rock geochemistry. Results are quantitative.

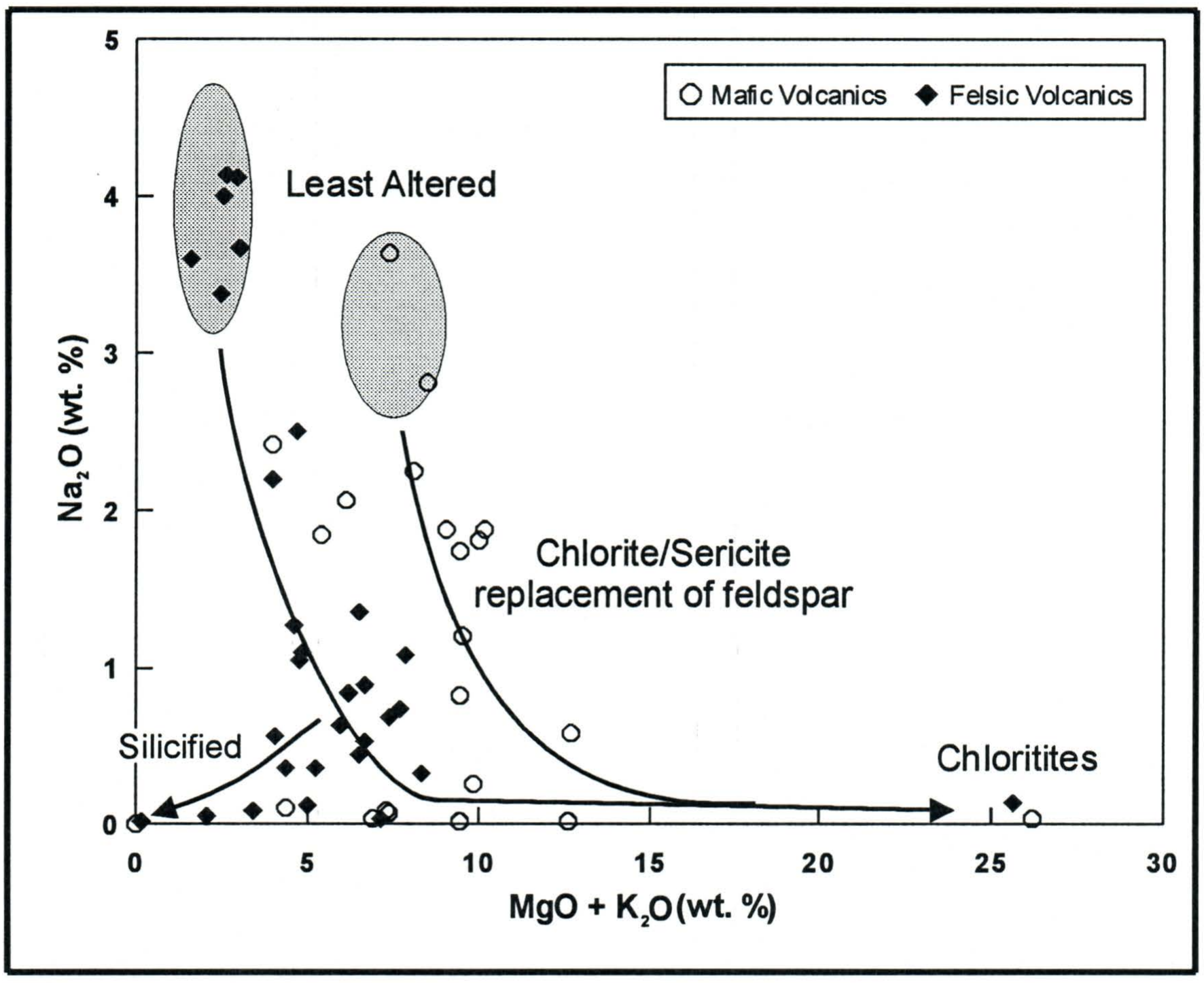


Figure 6-4 - Apparent removal of Na_2O during plagioclase breakdown and addition of ($MgO + K_2O$) through sericitization and chloritization. Note that both SHF mafic and BRF felsic rocks followed similar alteration pathways with the most extreme alteration represented by chlorite. Rocks that contain minimal amounts of Na_2O, MgO and K_2O are dominantly silicified. Data is raw whole-rock geochemistry.

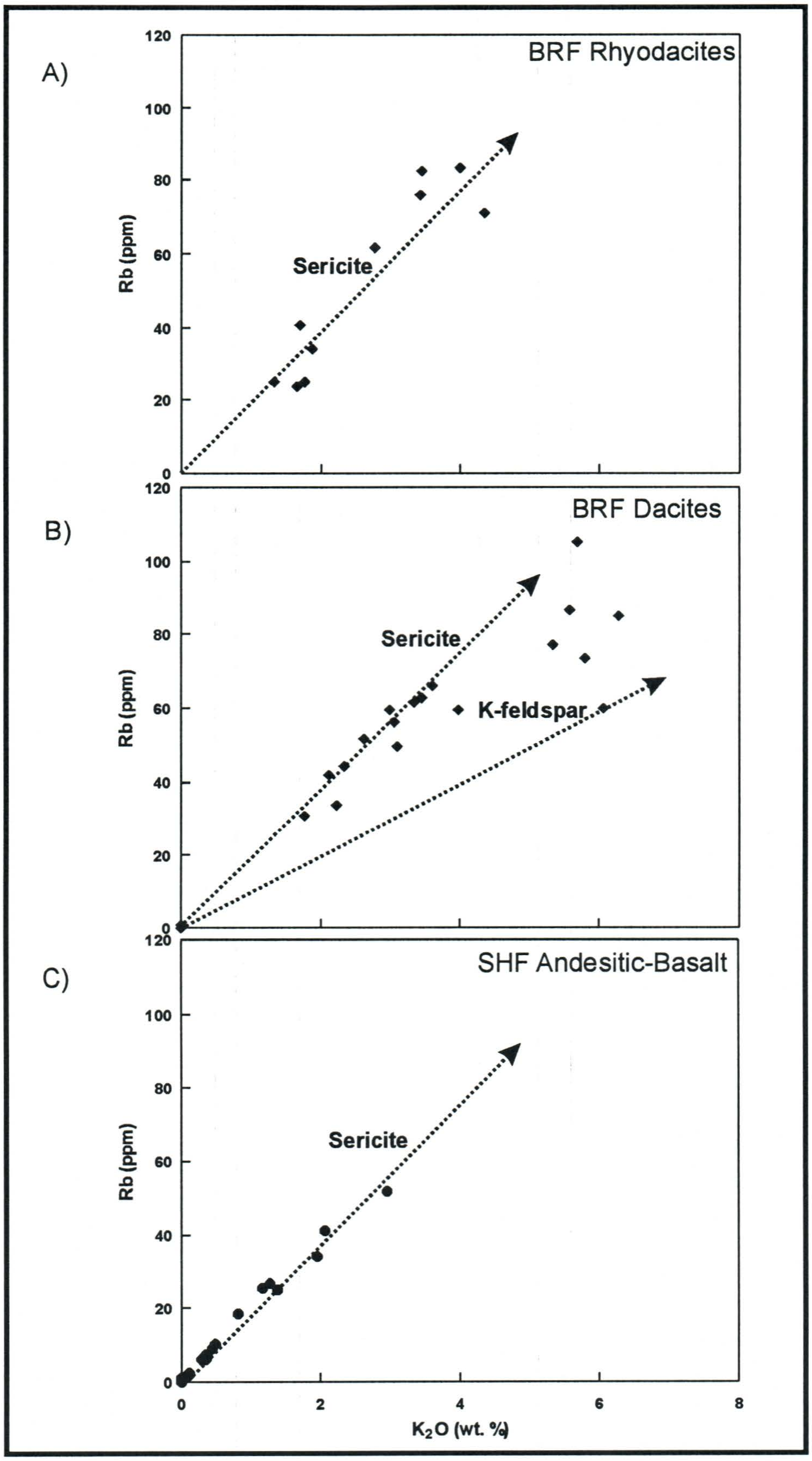


Figure 6-5 - K_2O vs. Rb plot for a) BRF rhyodacites, b) BRF dacites, c) SHF basaltic -andesites. K_2O and Rb show strong correlations in all three rock types. Rb/K_2O ratios for sericite (~ 20) are generally higher than those for K-feldspar. K-feldspar is apparent only in the BRF dacites.

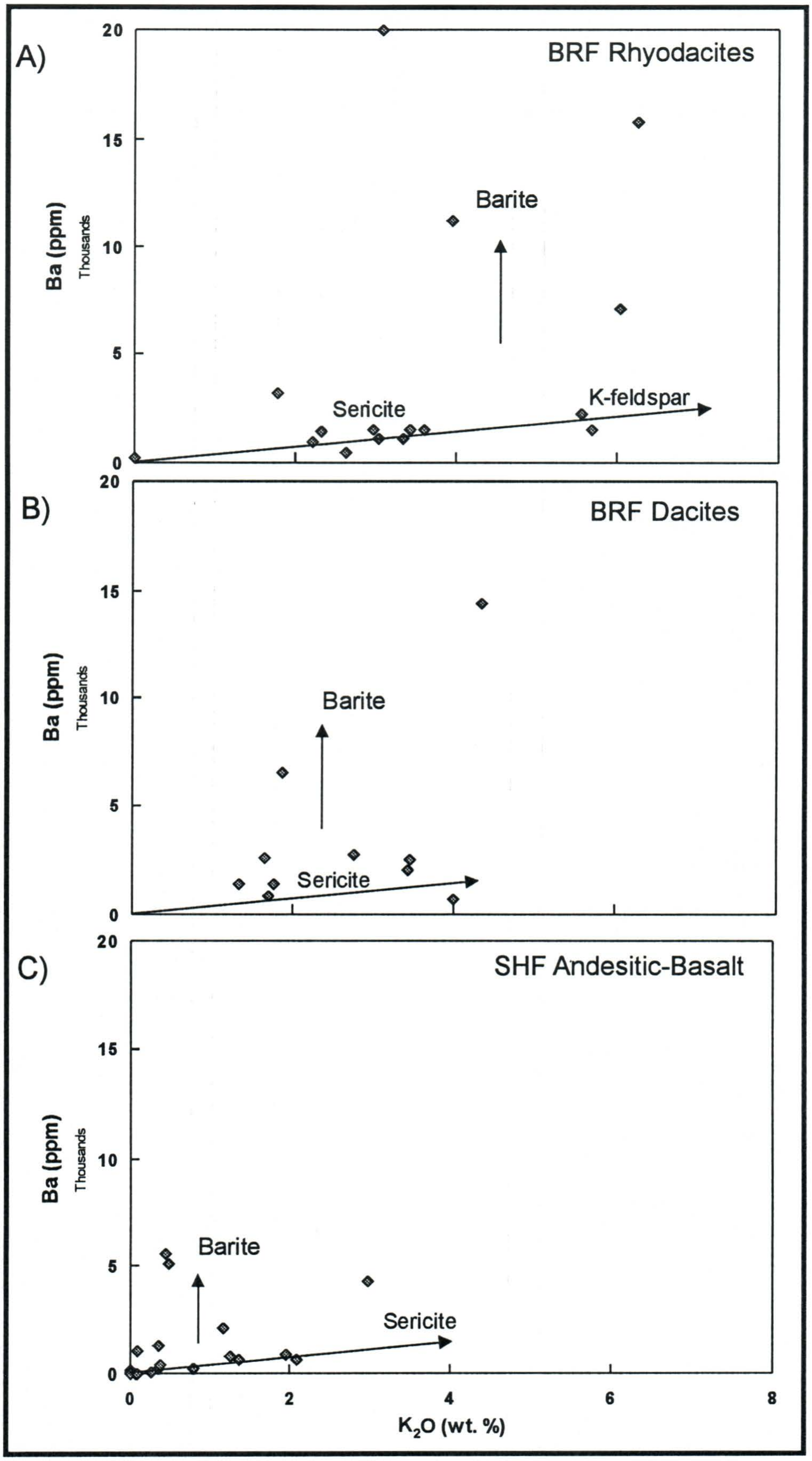


Figure 6-6 - K_2O vs. Ba plots for a) BRF rhyodacites, b) BRF dacites, c) SHF andesitic-basalts. Enough samples from each suite define trend of relatively low Ba/K_2Oratios. However, several samples from each suite show anomalously high Ba content due to the presence of barite.

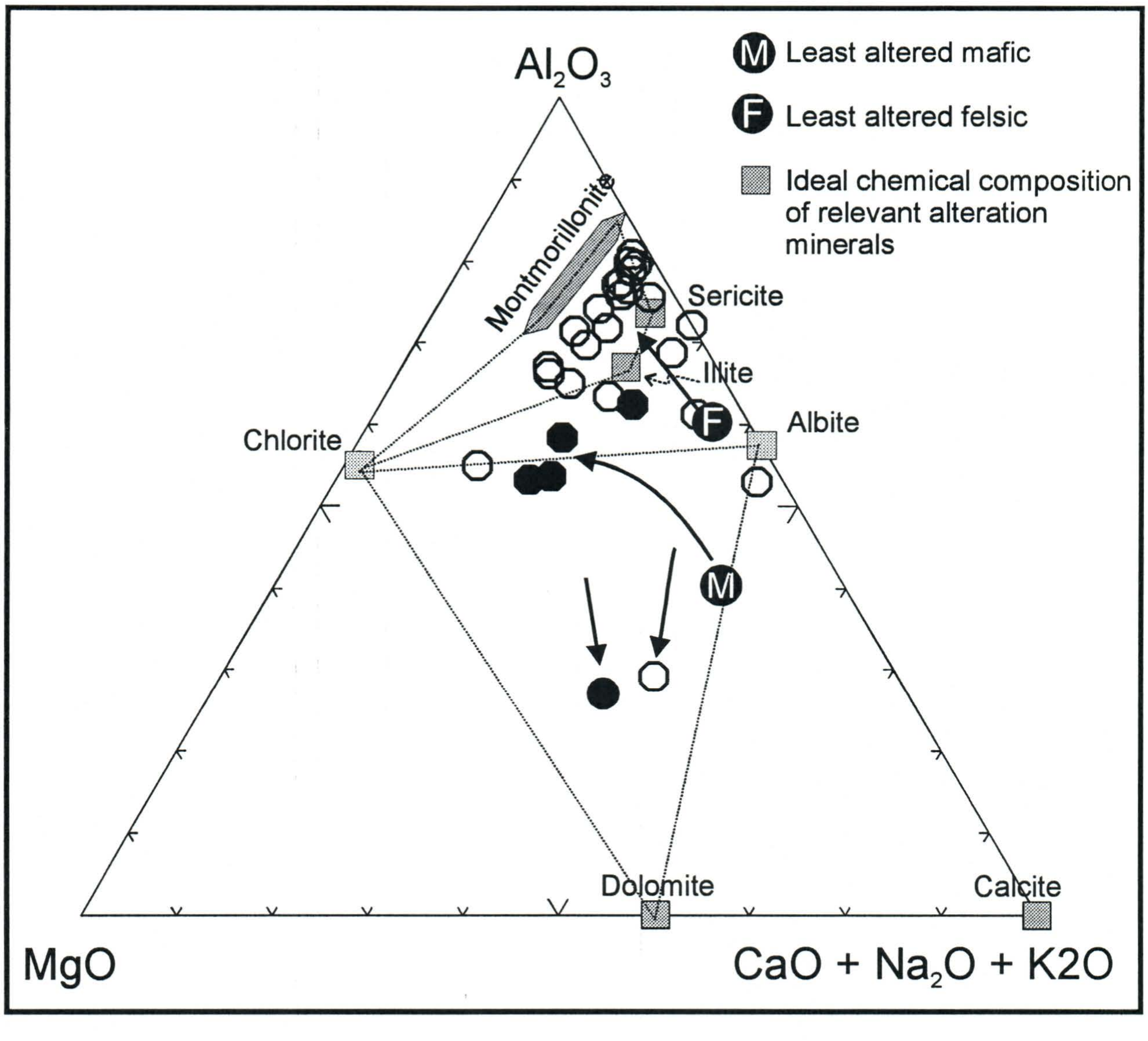


Figure 6-7. PHZ mafic volcanics (solid circles) and dacitic volcanics (open circles). Mafic rocks plot on a chlorite-albite tie line. Felsic rocks are dominated by sericite-clay alteration, although some samples are strongly dolomitized. Chlorite, sericite, albite and carbonate compositions are from microprobe analysis (this study). Montmorillonite and illite are derived from idealized formulas (Deer et al., 1992).

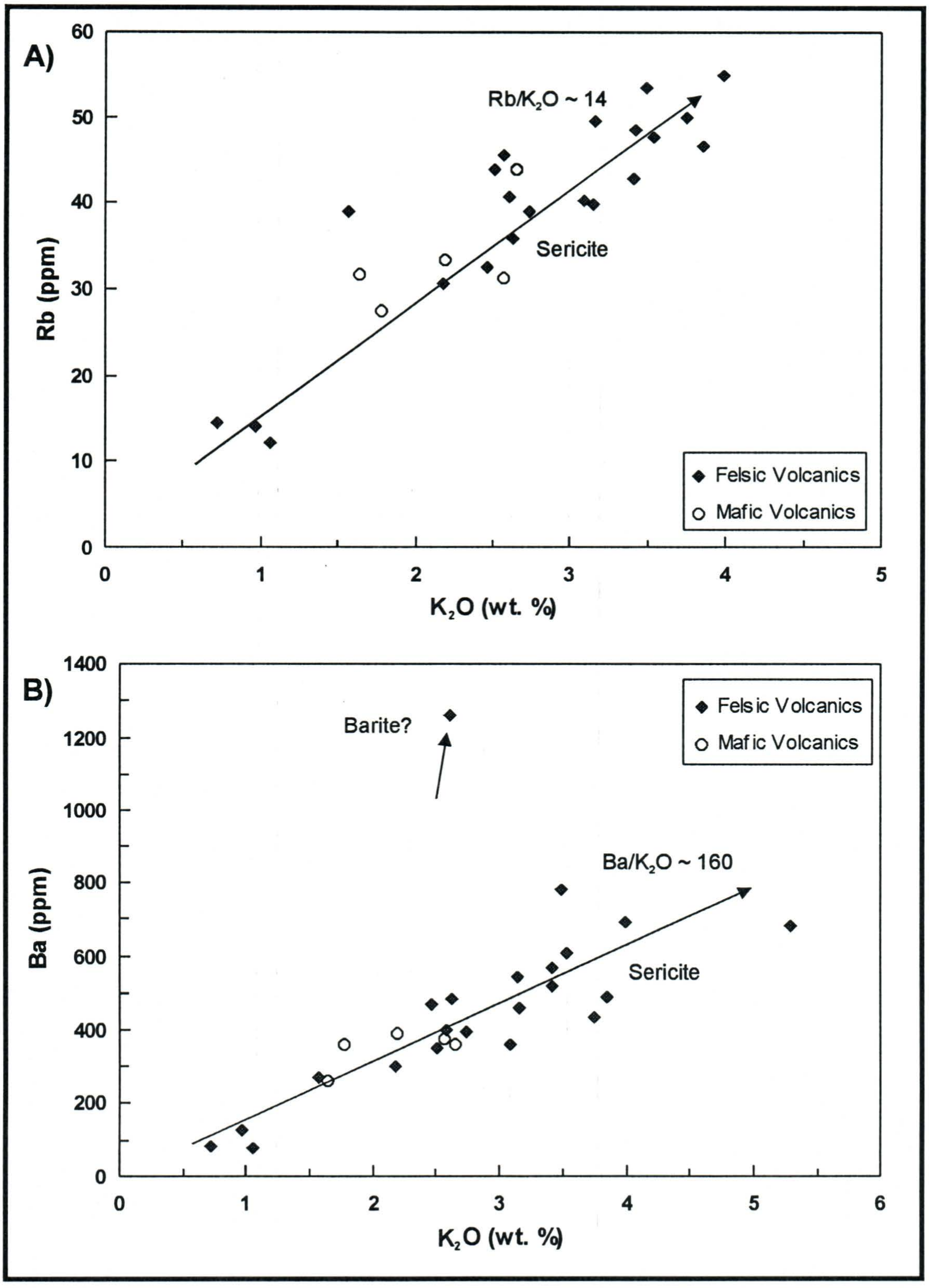


Figure 6-8 - WBZ sericite alteration trends. a) K_2O vs. Rb showing constant ratios typical of sericite. b) K_2O vs. Ba showing constant ratios for all but one sample; the outlier may contain barite.

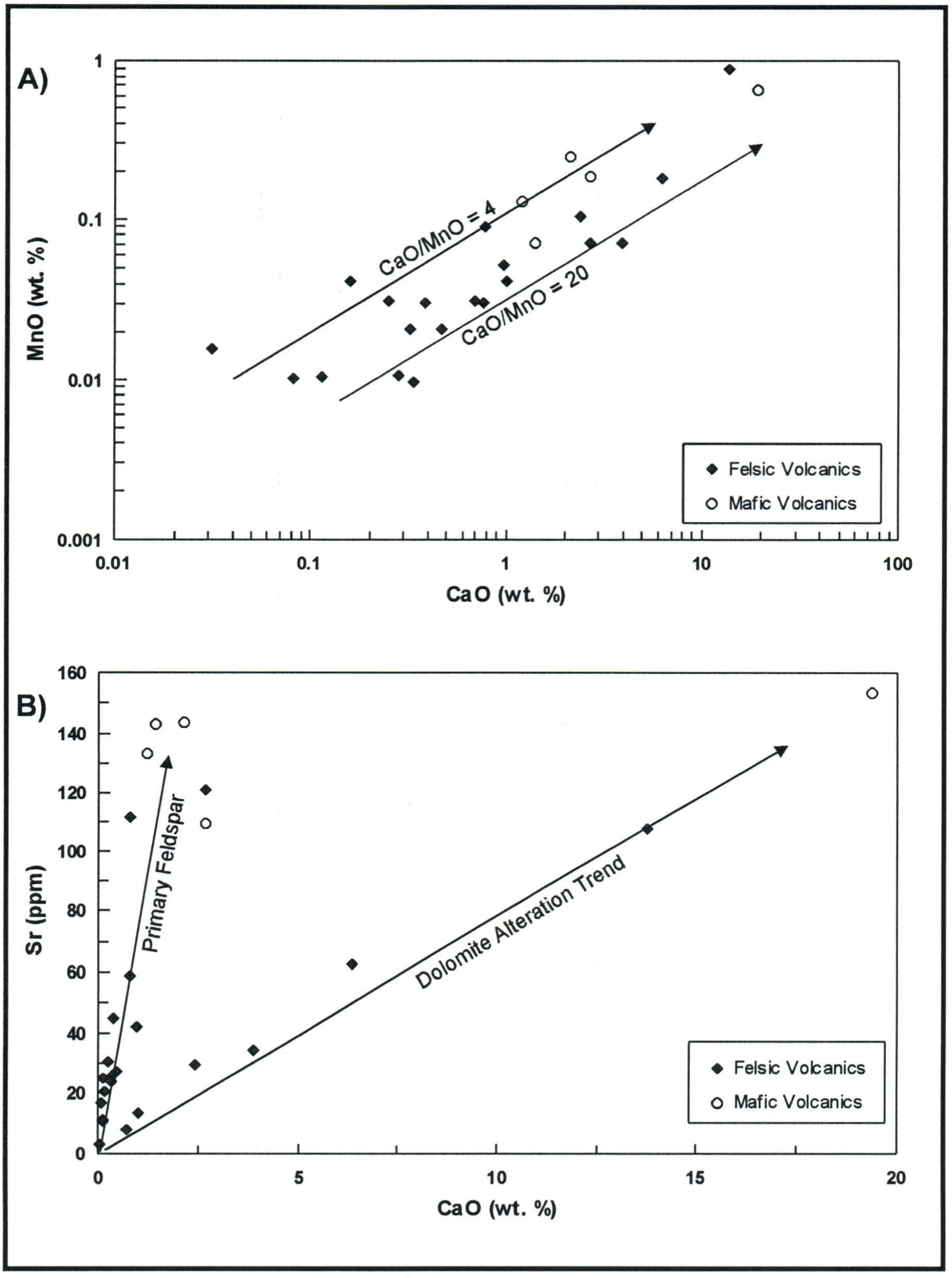


Figure 6-9 - a) CaO vs MnO for volcanic rocks of the PHZ. Ca/Mn ratios are fairly constant throughout the data set. Samples with greater than 10% CaO have greater than 0.5% MnO. B) Sr vs. CaO seperates the rocks into two main trends. The steeper trend corresponds to the feldspar component. The flatter trend with higher CaO represents carbonate alteration.

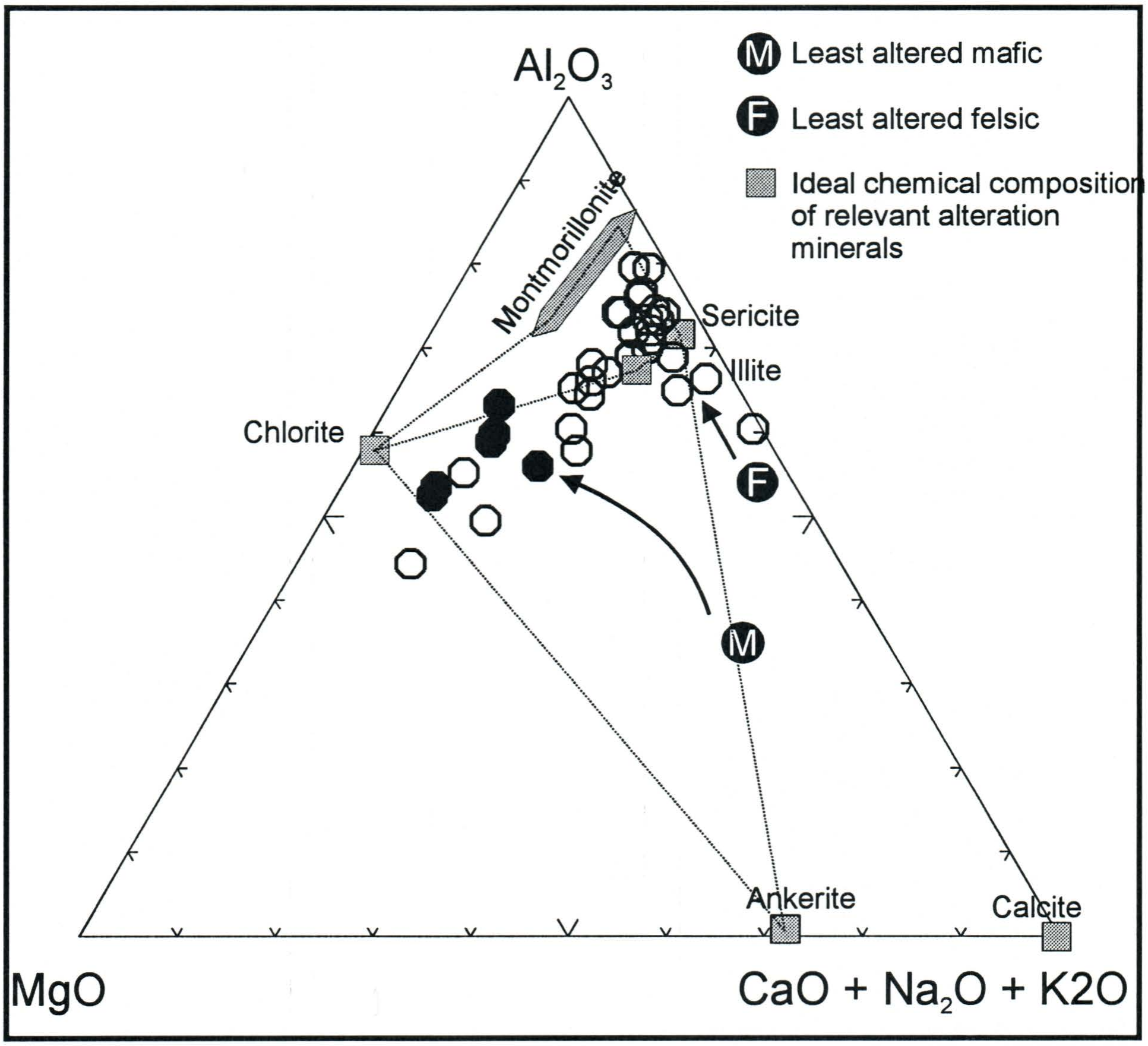


Figure 6-10. WBZ mafic volcanics (solid circles) and dacitic volcanics (open circles). Mafic rocks plot in a chlorite-sericite-ankerite field. Felsic rocks are dominated by sericite-clay alteration, although several samples trend towards higher proportions of MgO. Chlorite,sericite, and carbonate compositions are from microprobe analysis (this study). Montmorillonite and illite are derived from idealized formulas (Deer et al., 1992).

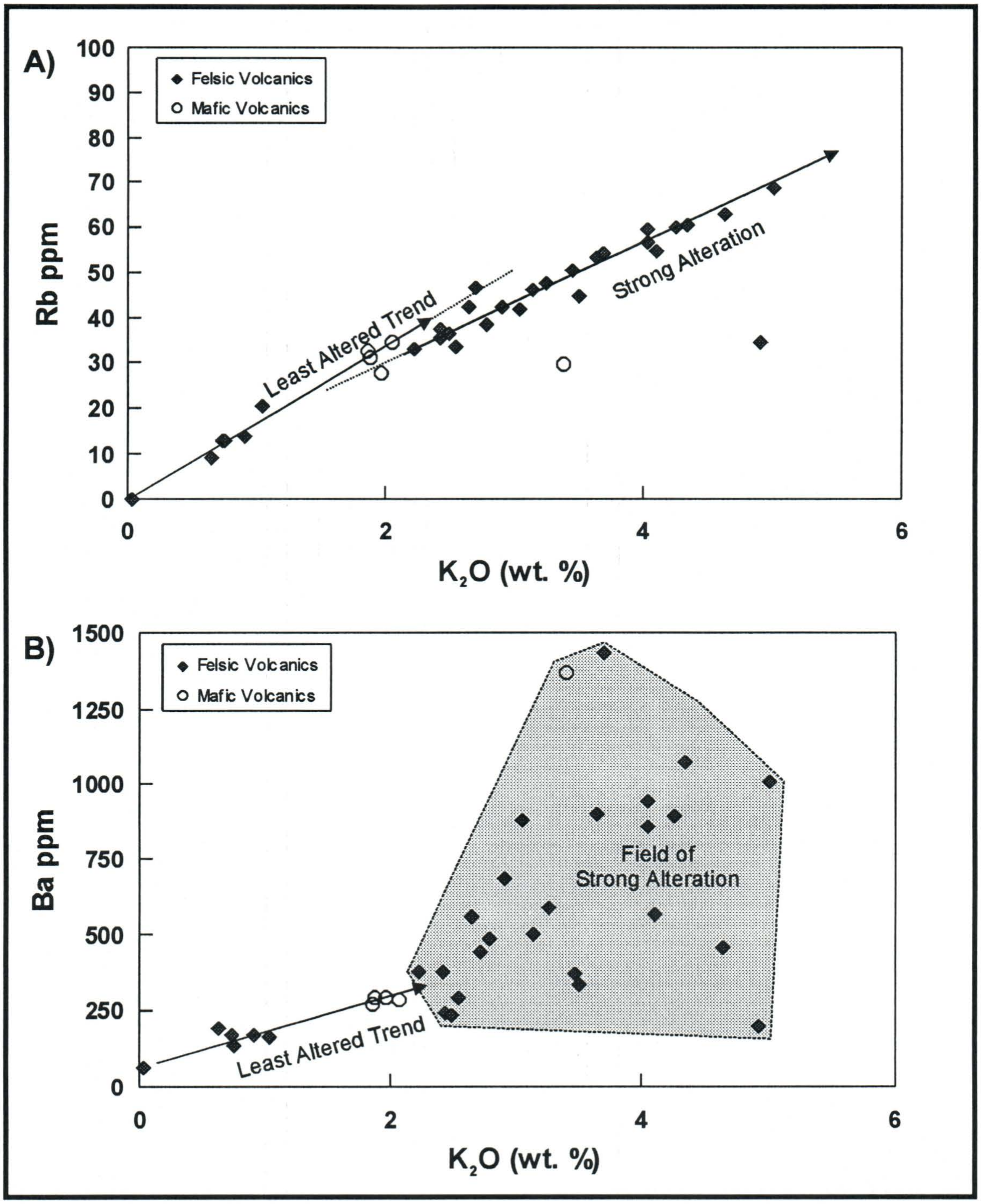


Figure 6-11 - Relationships between K_2O and Rb, Ba for WBZ data. Note that in figure (a) Rb and K_2O show a strong positive, somewhat curved, trend. This suggests that Rb occurs with K_2O in sericite. However, in figure(b), the Ba and K_2O show a correlation only up to approximately 2 wt. % K_2O and 300 ppm Ba. The field of grey represents samples where Ba probably occurs in another mineral than sericite (barite?).

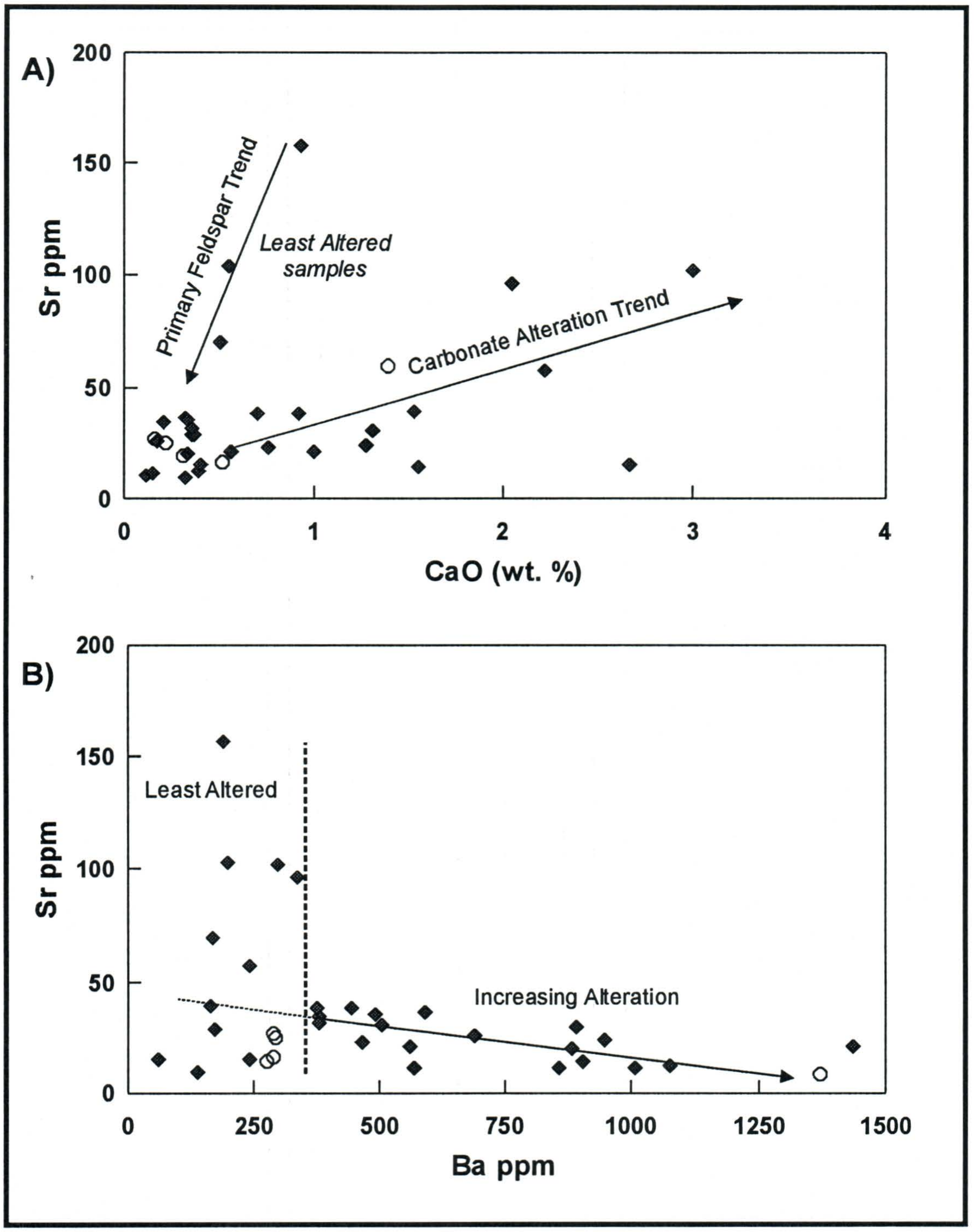


Figure 6-12 a) CaO vs. Sr for volcanic rocks from the WBZ. Note that the Sr/CaO ratio for carbonates is lower than that for feldspar. b) Ba vs Sr shows a trend of decreasing Sr with increasing Ba representing higher degrees of alteration. Least altered samples have relatively low Ba and high Sr.

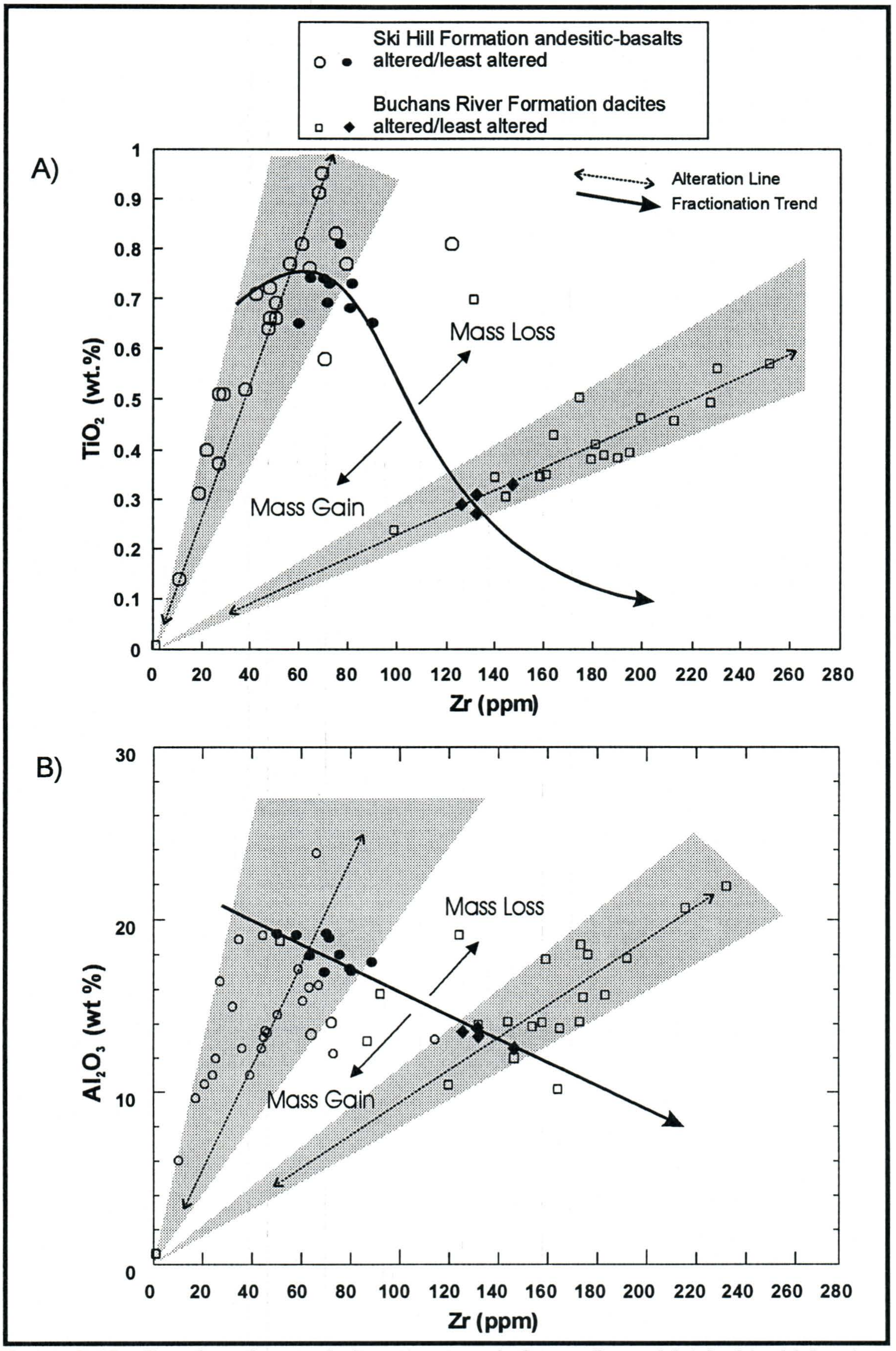


Figure 6-13 - Fractionation and alteration trends for mafic and felsic (dacitic) volcanic rocks of the SHF(open circles) and BRF (solid diamonds), respectively. Shaded areas represent 'alteration fans'. a) Zr vs. TiO_2 and b) Zr vs. Al_2O_3, c) P_2O_5 vs. Zr, and d) TiO_2 vs. Al_2O_3. Least altered samples are not shown in plots C) and D)

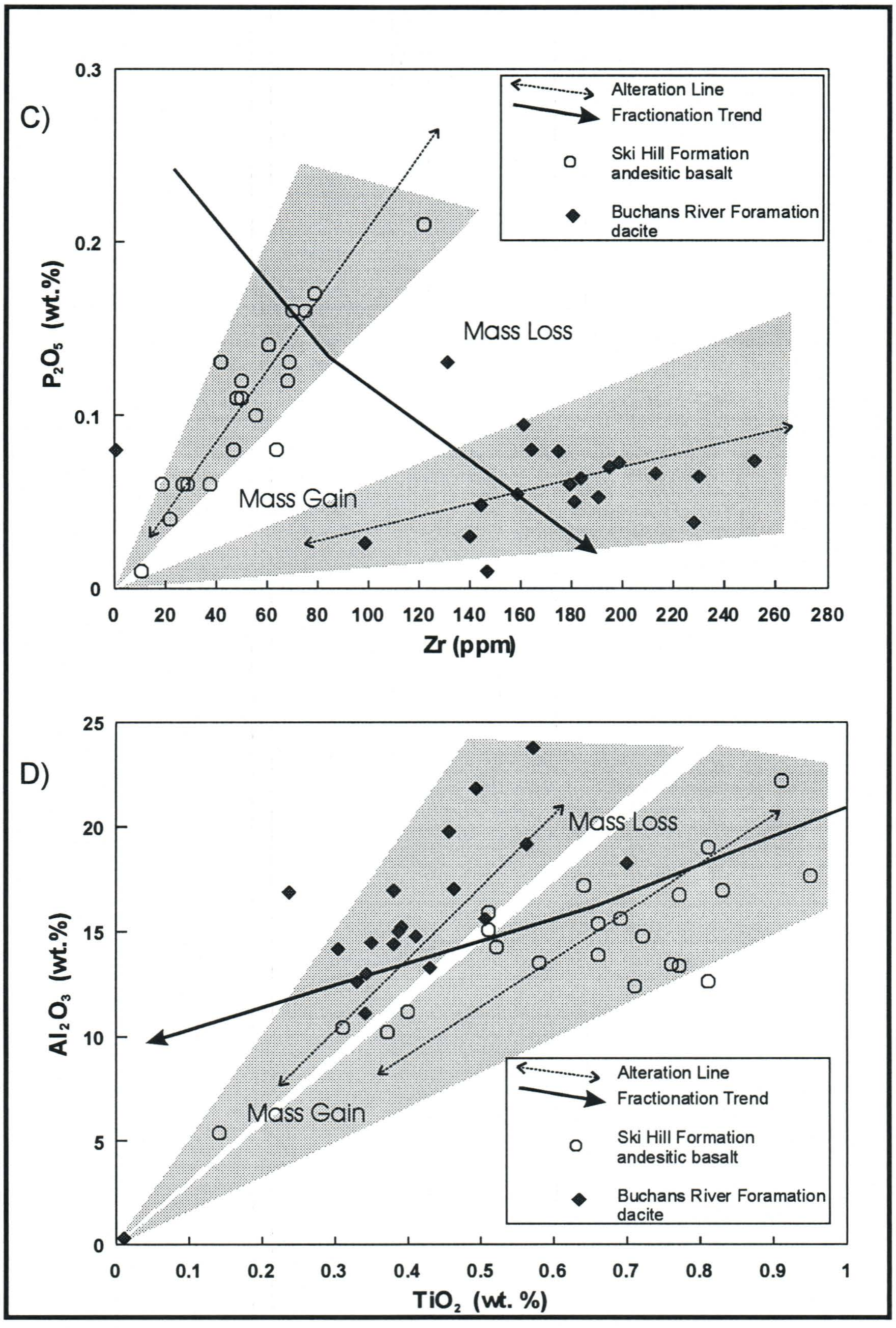


Figure 6-13 (continued)

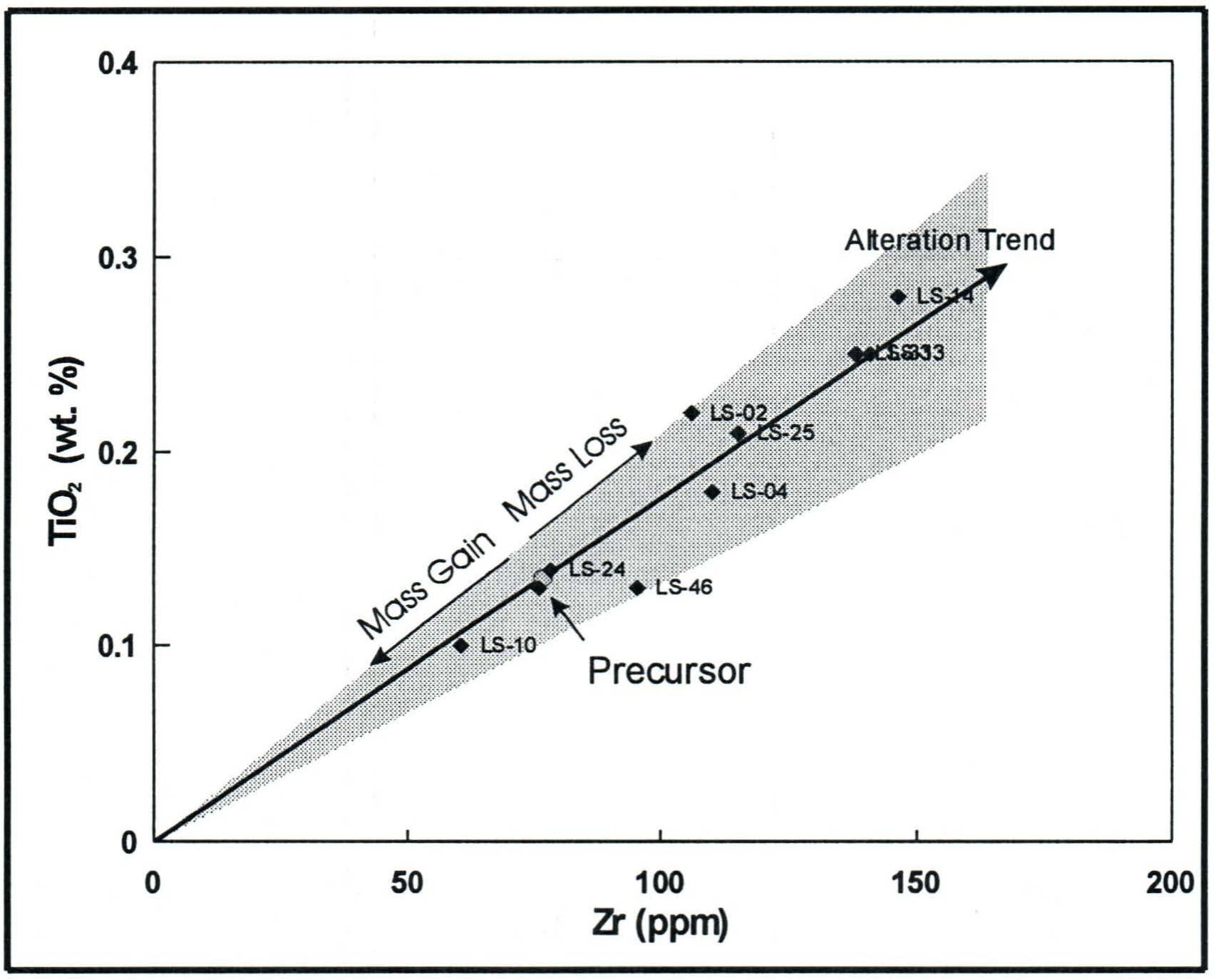


Figure 6-14 - Zr vs TiO_2 plot showing the alteration trend for felsic (rhyodacitic) volcanic rocks of the BRF. Shaded area represents 'alteration fans'.

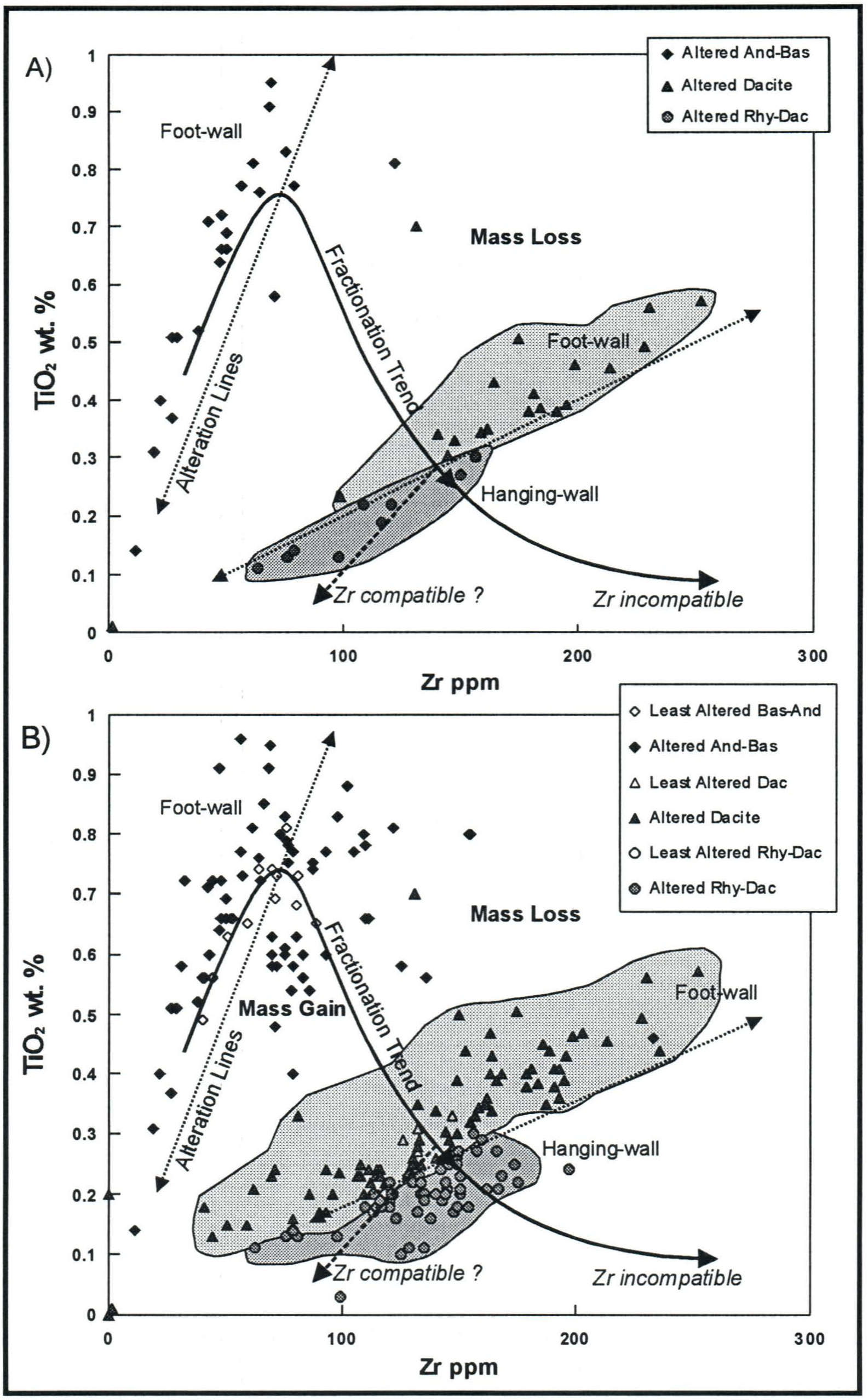


Figure 6-15 - Zr vs. TiO_2 for volcanic rocks from the Ski Hill and Buchans River formations. A) data from this study only are used to define fields (shaded grey areas) for each of the foot-wall dacites and hanging-wall rhyodacites (geochemical discriminants are discussed in Chapter 5). Fractionation trends, as defined by least altered samples, are also shown. B) Same plot as in A), but using all existing data from the Buchans camp (Thurlow, 1981; Unpublished data from the Newfoundland Department of Mines and Energy). Felsics were separated using Zr/TiO2 ratios. The plot illustrates that these fields may be predictive.

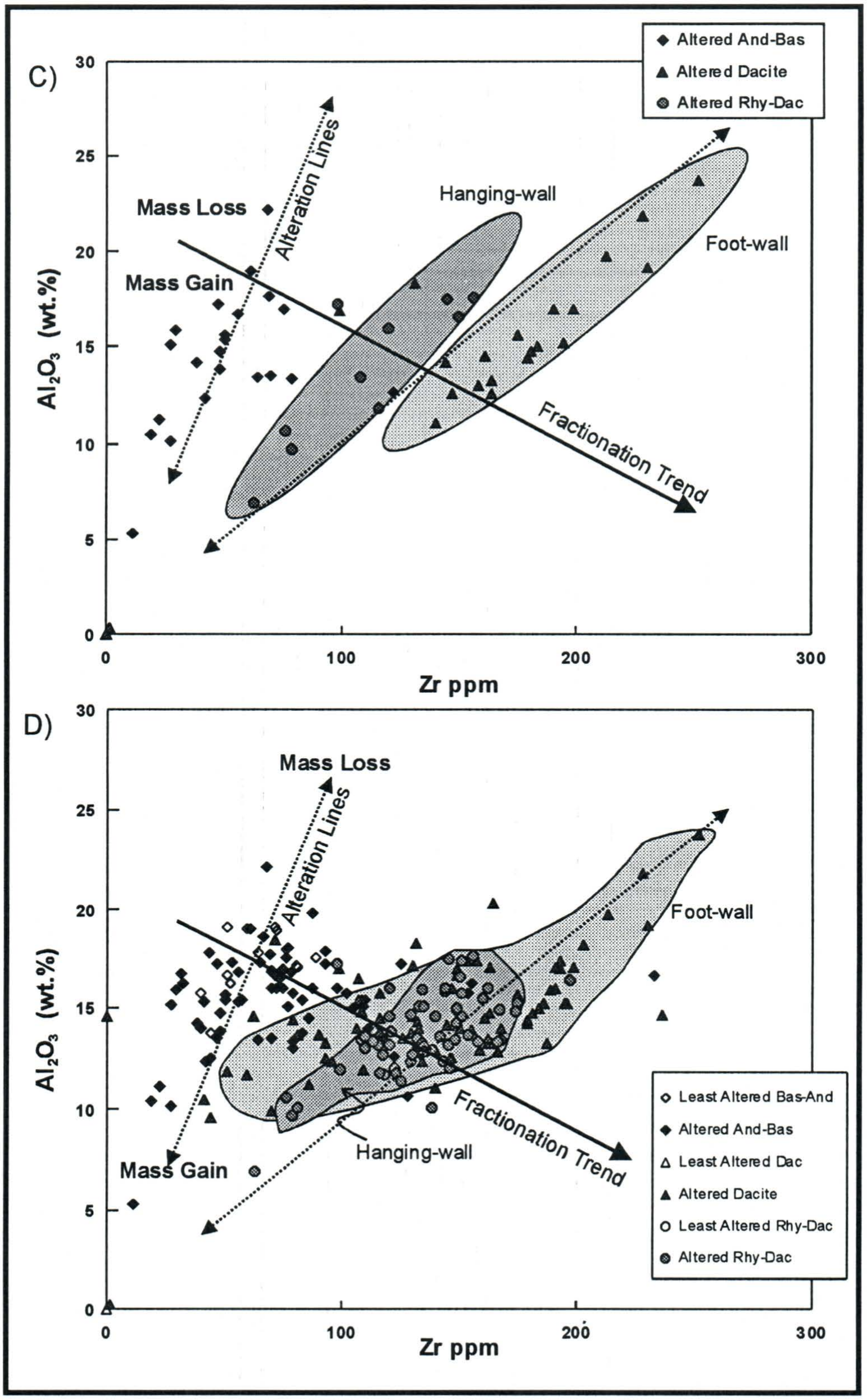


Figure 6-15 - Zr vs. Al_2O_3 for volcanic rocks from the Ski Hill and Buchans River formations. C) data from this study only are used to define fields (shaded grey areas) for each of the foot-wall dacites and hanging-wall rhyodacites. Fractionation trends, as defined by least altered samples, are also shown. D) Same plot as in C), but using all existing data from the Buchans camp (Thurlow, 1981; Unpublished data from the Newfoundland Department of Mines and Energy). Although not as diagnostic as in figures A) and B), these these fields may be predictive.

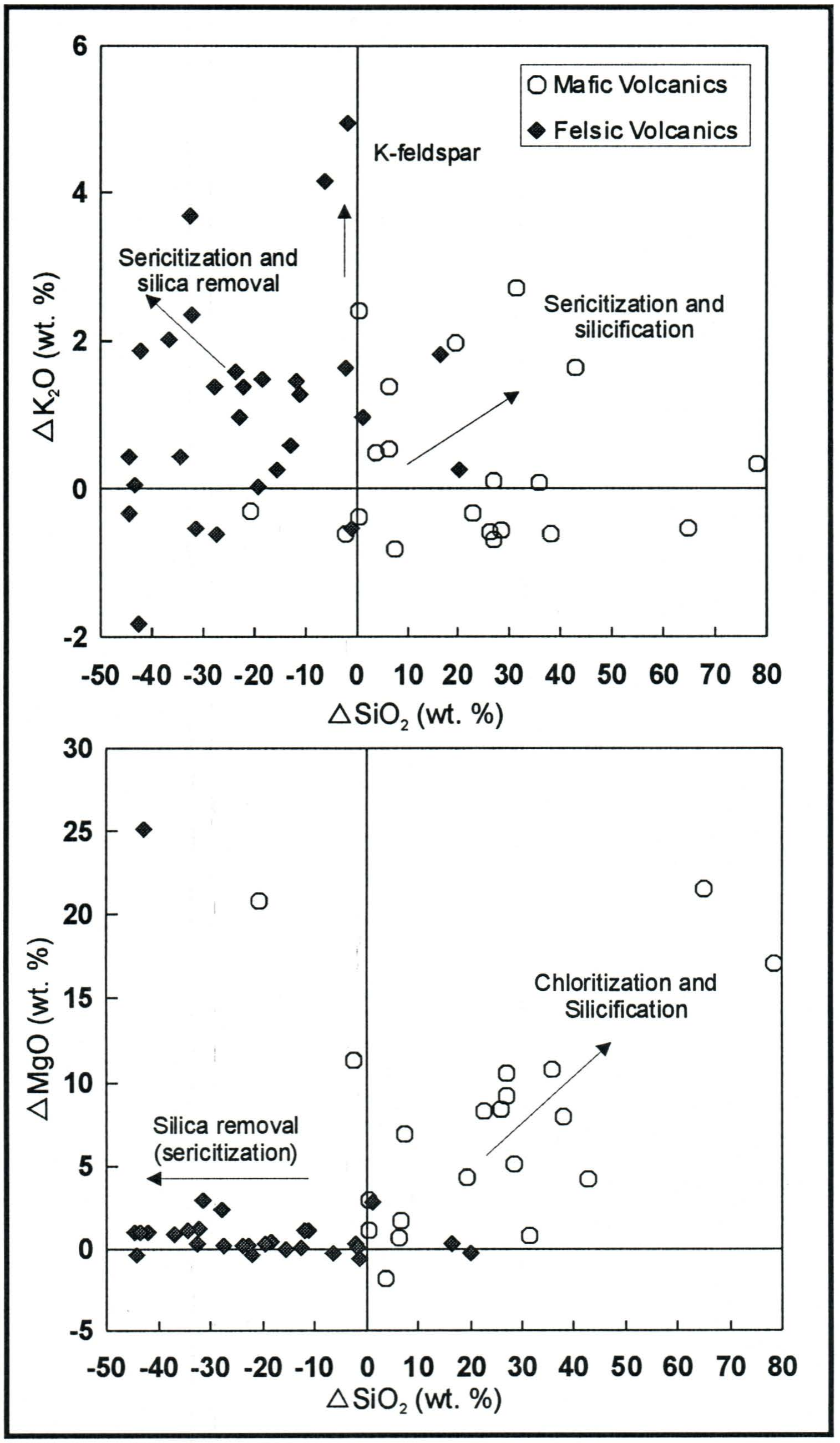


Figure 6-16 - Calculated mass change plots for mafic and felsic lithologies of the SHF and BRF. a) SiO_2 vs. K_2O and b) SiO_2 vs. MgO. Mass changes in wt.%.

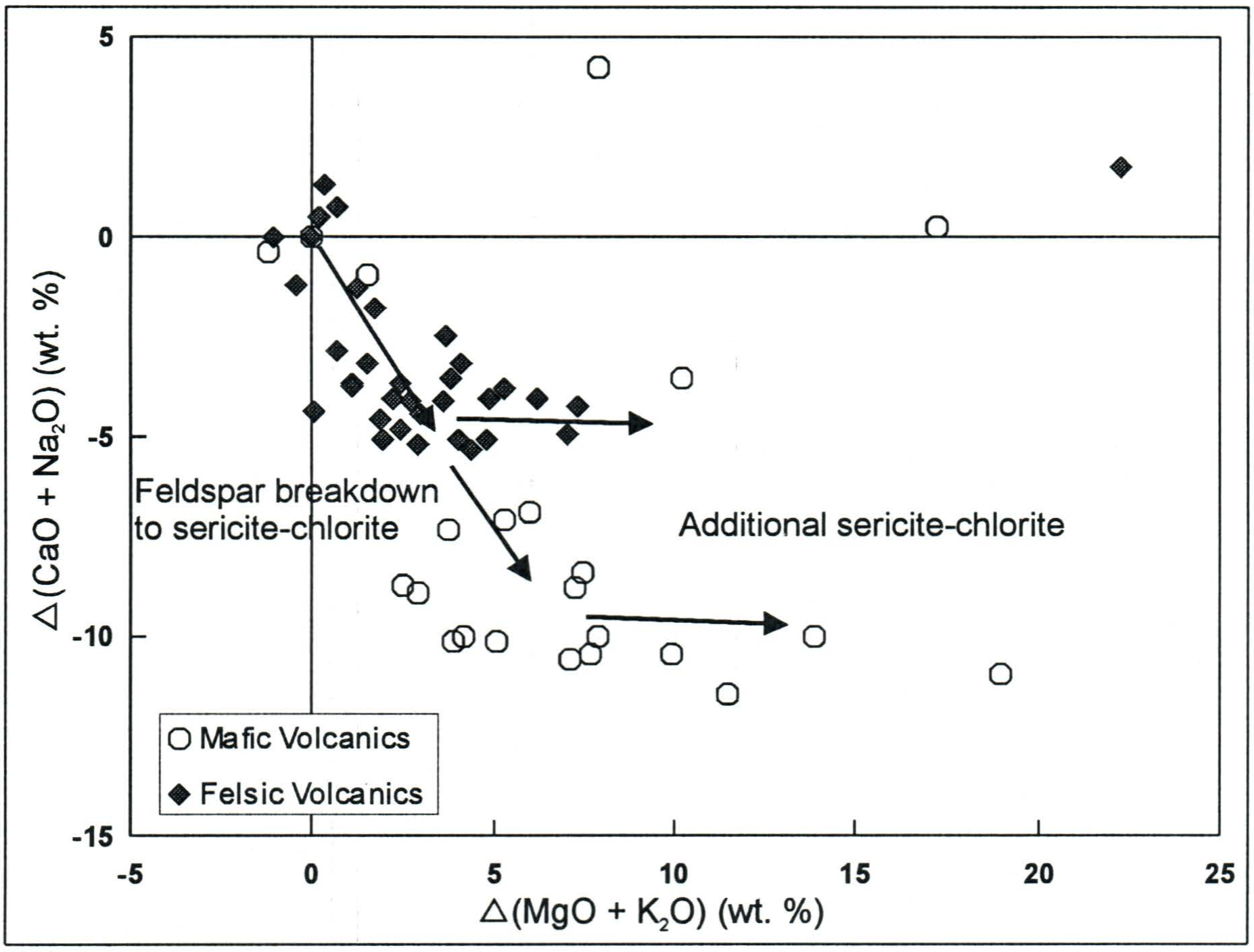


Figure 6-17 - Calculated mass changes in SHF mafic volcanics and BRF felsic volcanics. Mass changes in absolute wt.%.

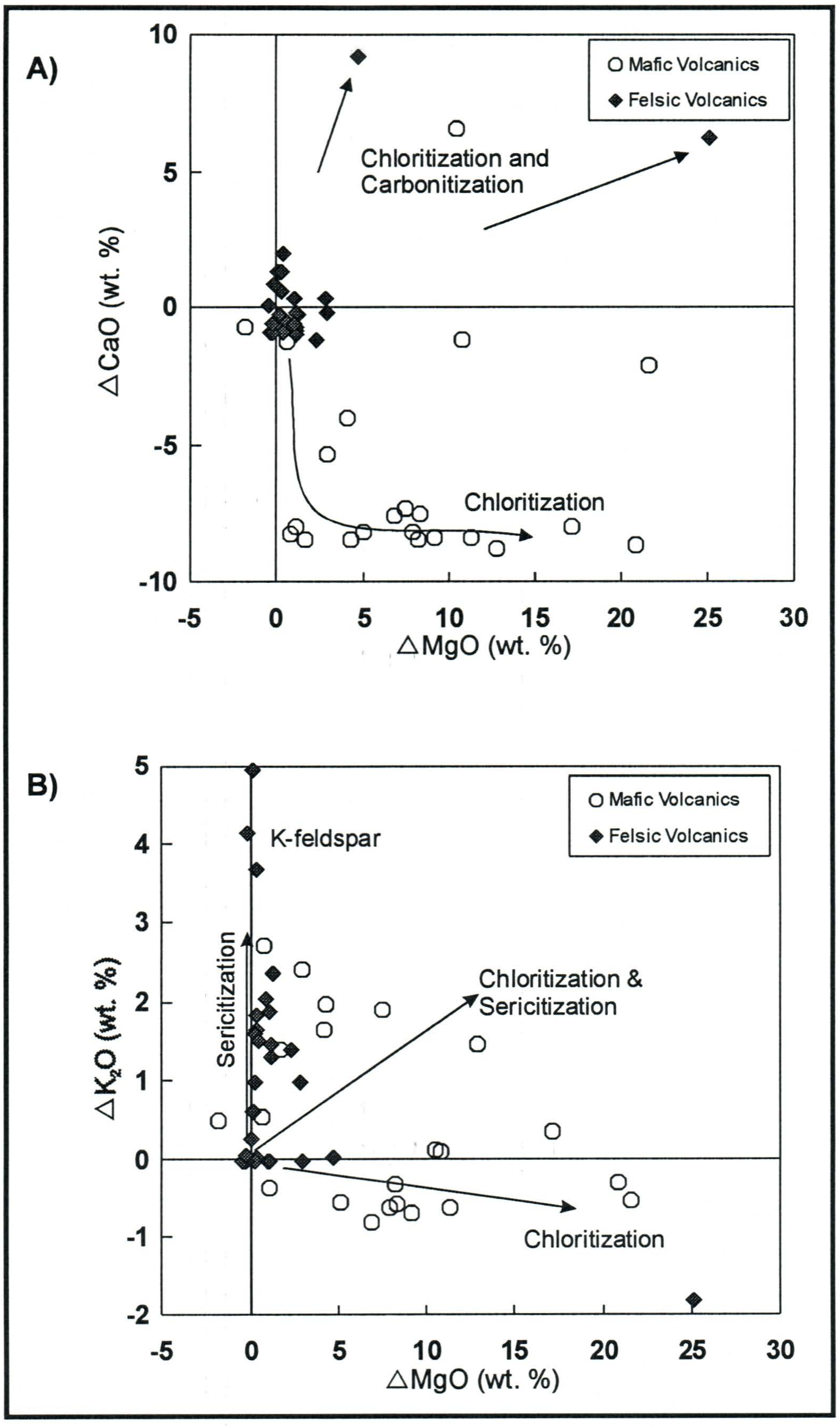


Figure 6-18 - Calculated mass changes for mafic and felsic rocks of the SHF and BRF, respectively. Mass changes are absolute wt. %. a) MgO vs. CaO and b) MgO vs K_2O.

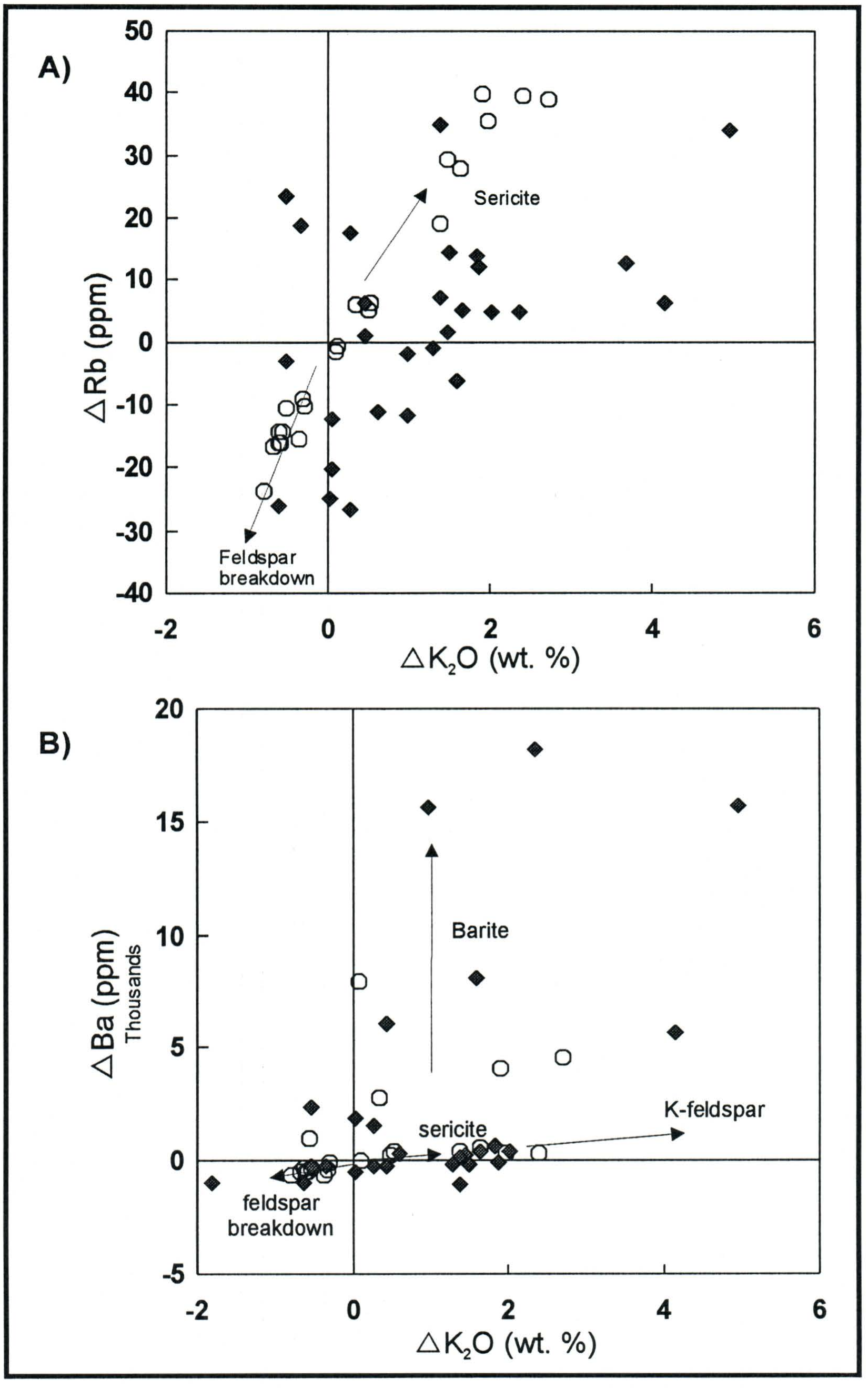


Figure 6-19 - Calculated mass changes for mafic rocks (SHF) and felsic rocks (BRF). Mass changes in absolute wt. %. a) K_2O vs. Rb and b) K_2O vs. Ba.

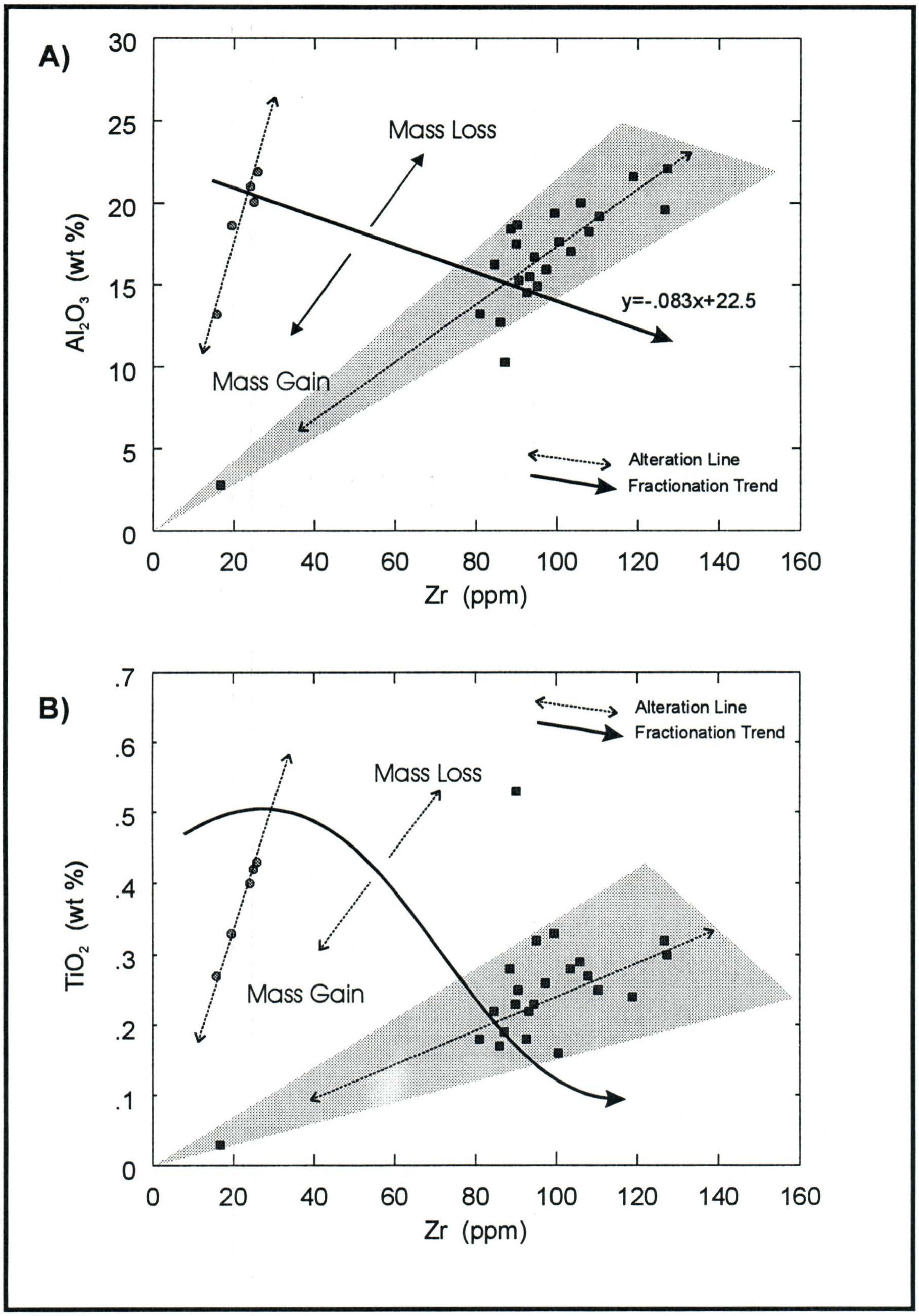


Figure 6-20 - Fractionation and alteration trends for mafic (solid circles) and felsic (solid diamonds) volcanic rocks of the PHZ, respectively. Shaded areas represent 'alteration fans'. a) Zr vs. Al_2O_3, b) Zr vs. TiO_2.

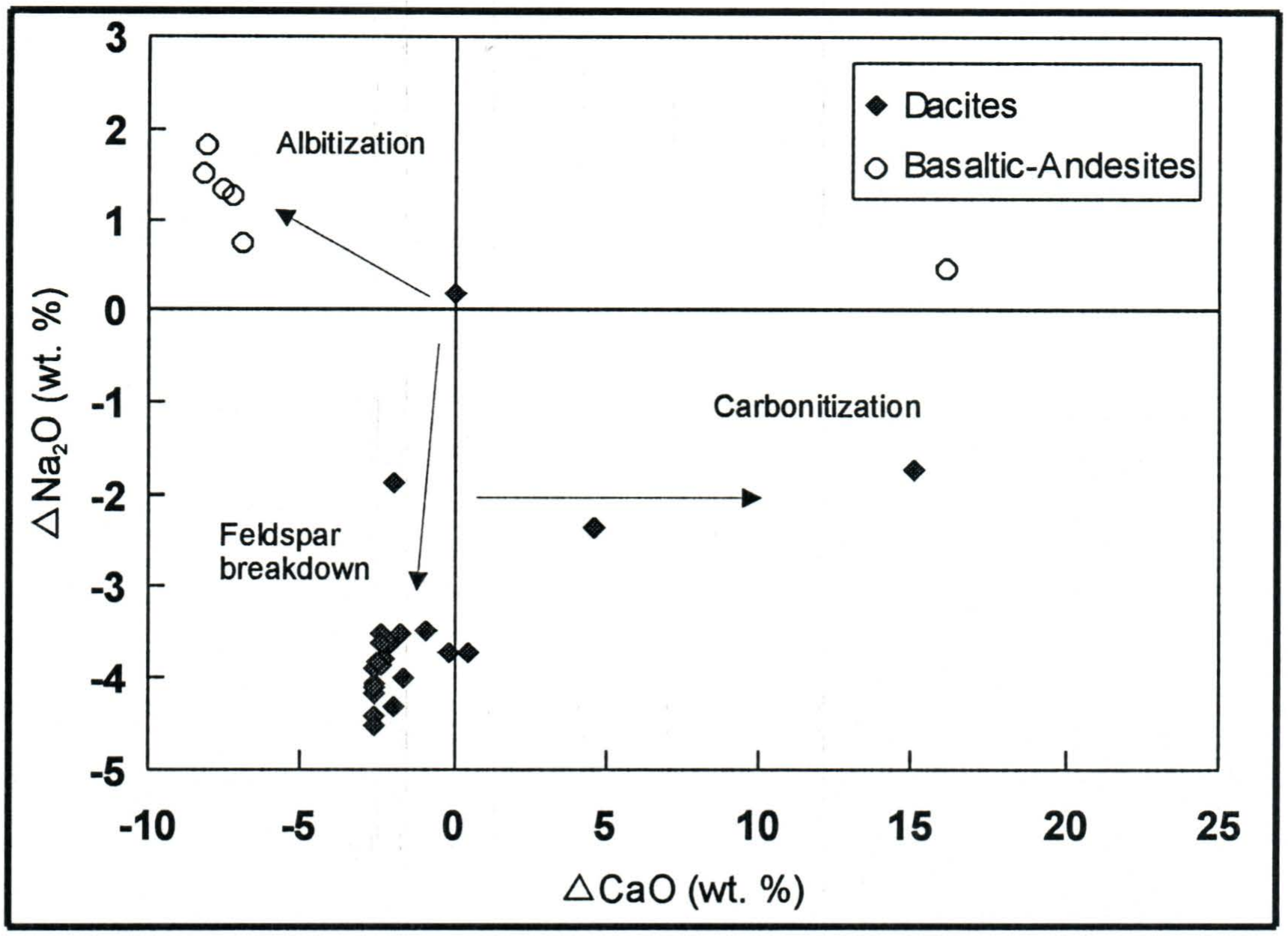


Figure 6-21 (above) - Calculated mass changes for CaO and Na_2O in mafic and felsic rocks from the PHZ. Mass changes in absolute wt. %. Note that mafic rocks display CaO loss but Na_2O gains.

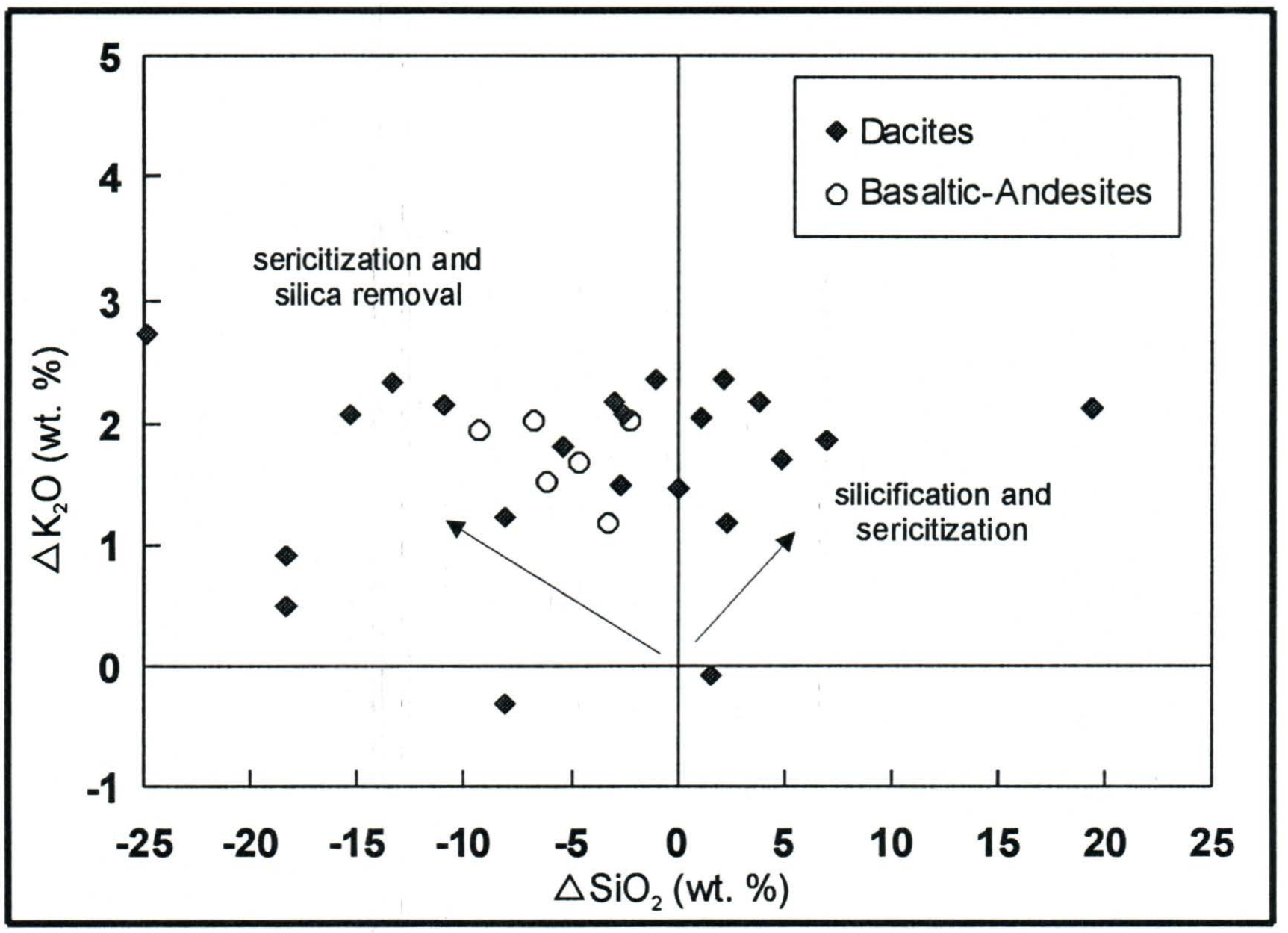


Figure 6-22 (below) - Calculated mass changes for SiO_2 and K_2O in mafic and felsic rocks from the PHZ. Values are in absolute wt. %. Nearly all rocks show K_2O gain, yet SiO_2 is more variable.

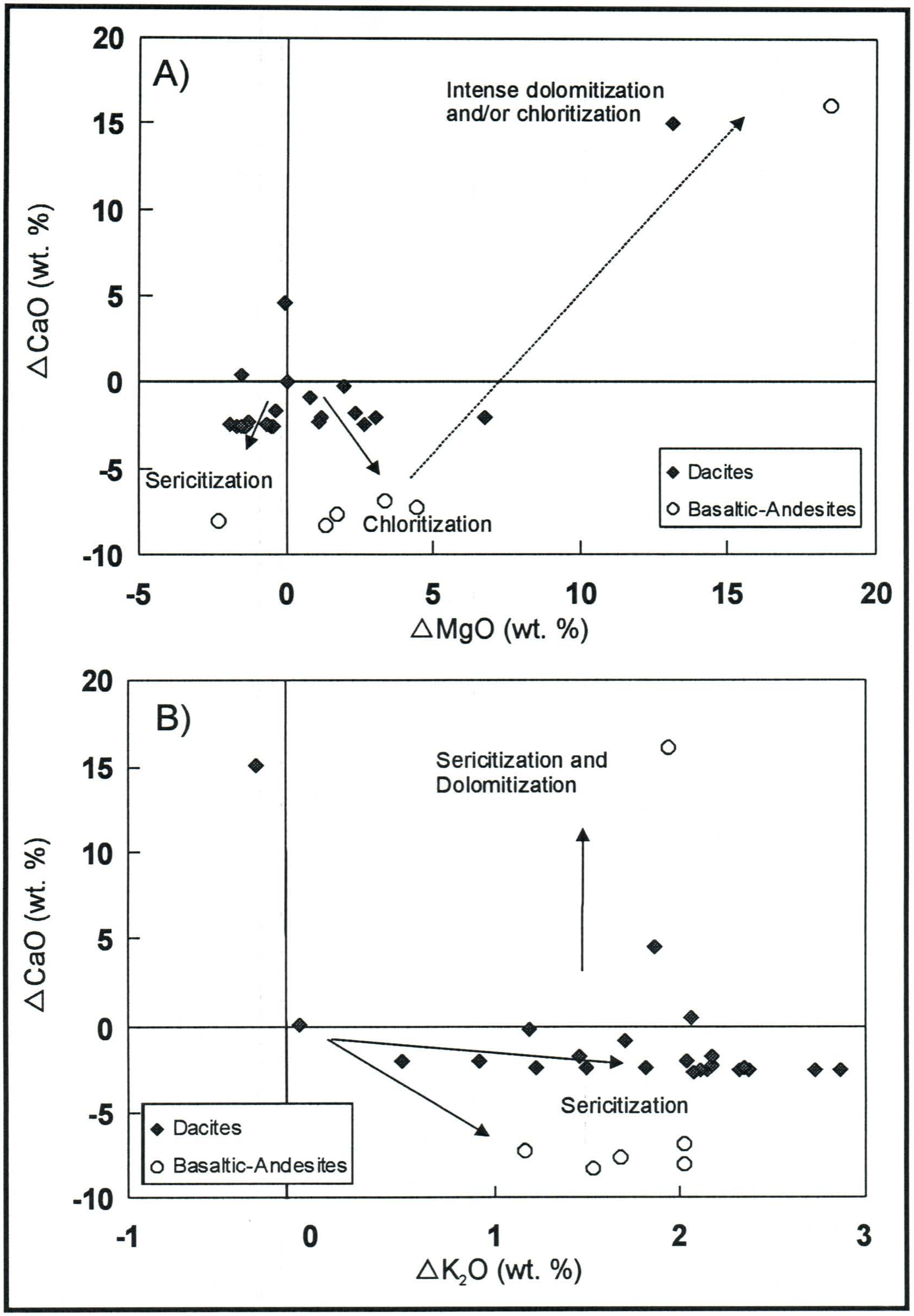


Figure 6-23 - Mass changes plots of mafic and felsic rocks from the PHZ. a) MgO vs.CaO and b) K_2O vs. CaO. All mass changes are absolute wt. %. The trends illustrate the dominance of sericitization, and less commonly, chlorite and dolomite alteration.

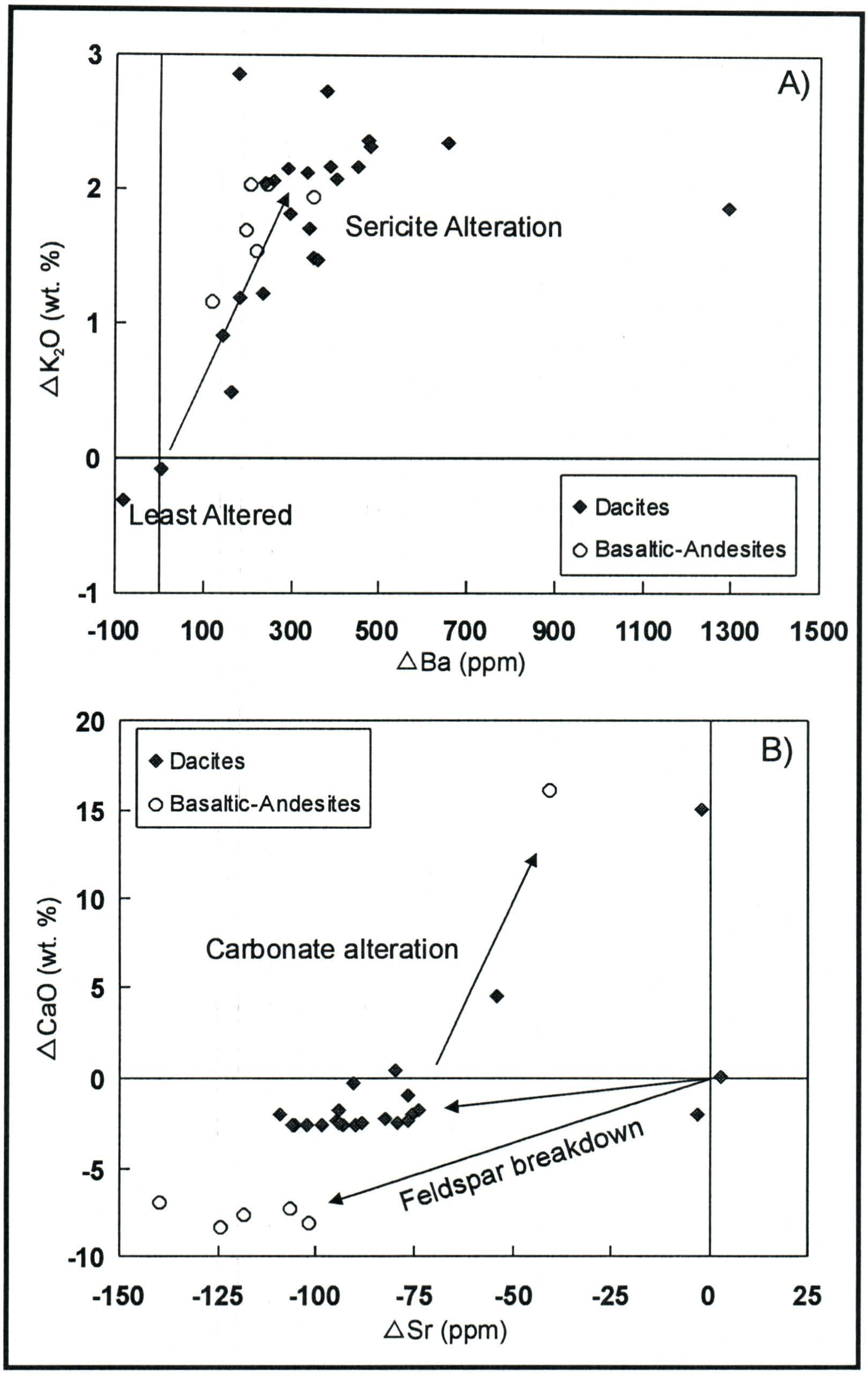


Figure 6-24 - Mass changes in altered mafic and felsic rocks from the PHZ. Mass changes are in absolute wt. % for oxides and ppm for trace elements. a) Ba vs K_2O illustrates a positive correlation. Ba is probably associated with sericite. b) Sr and CaO also show very good positive correlations, as both are strongly depleted. These constituents were removed during feldspar breakdown.

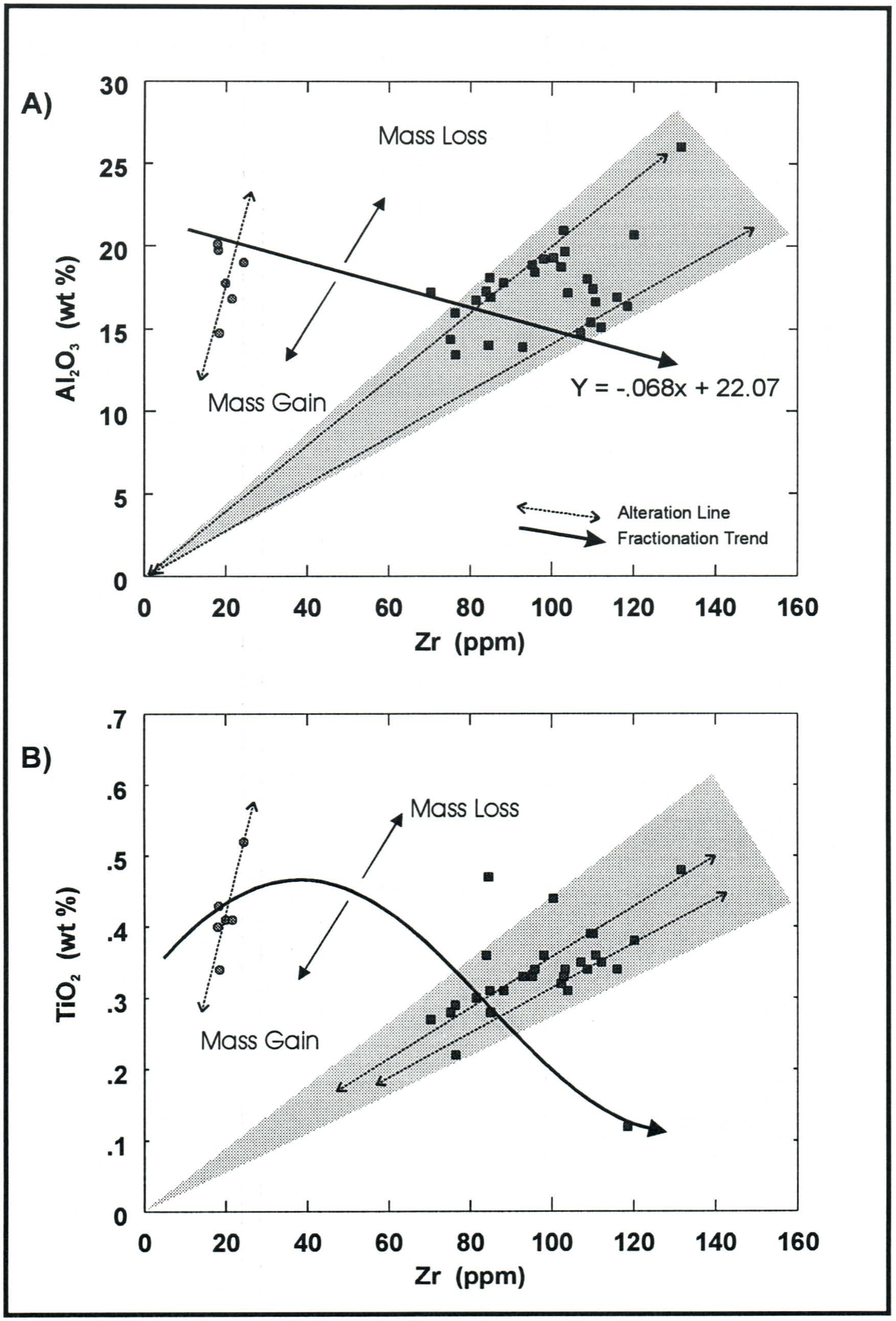


Figure 6-25 - Fractionation and alteration trends for mafic (solid circles) and felsic (solid diamonds) volcanic rocks of the WBZ, respectively. Shaded areas represent 'alteration fans'. a) Zr vs. Al_2O_3, b) Zr vs. TiO_2.

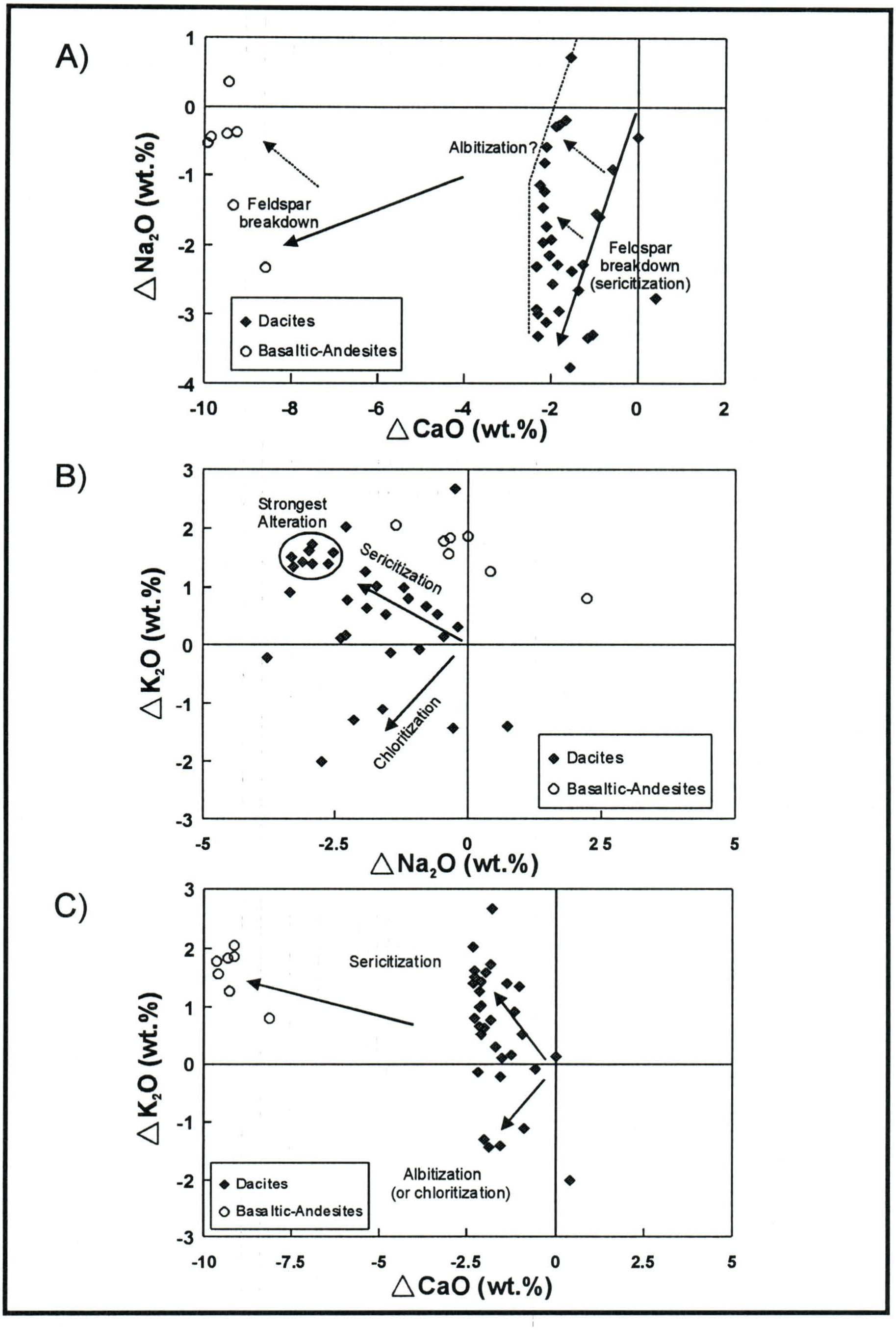


Figure 6-26 - Mass change plots for mafic and felsic volcanic rocks from the WBZ. Mass changes in absolute wt. %. a) Na_2O vs. K_2O, b) CaO vs. Na_2O, c) CaO vs. K_2O.

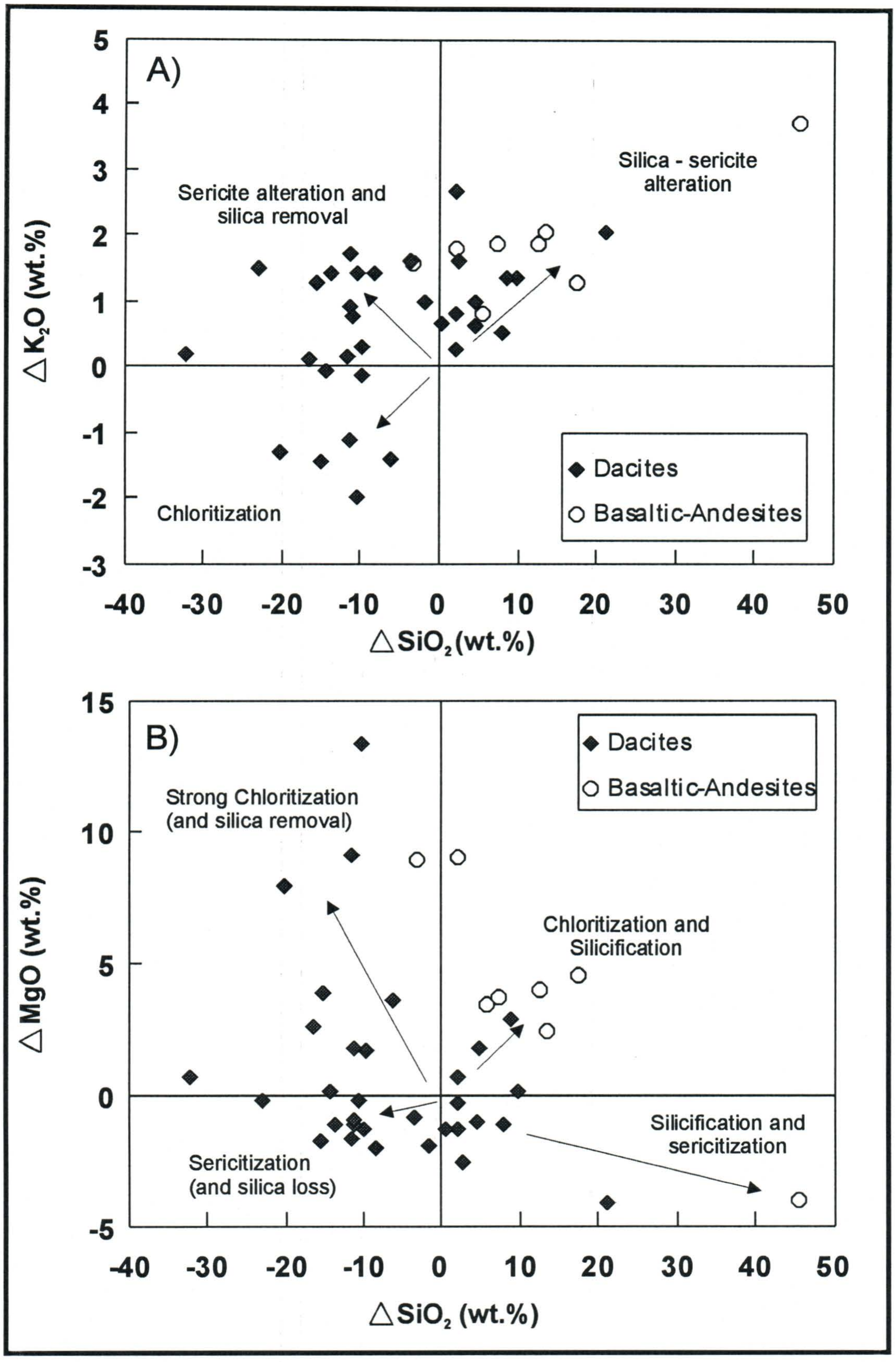


Figure 6-27 - Mass changes in mafic and felsic rocks from the WBZ. Mass changes are in absolute wt. %. a) SiO_2 vs K_2O and b) SiO_2 vs. MgO.

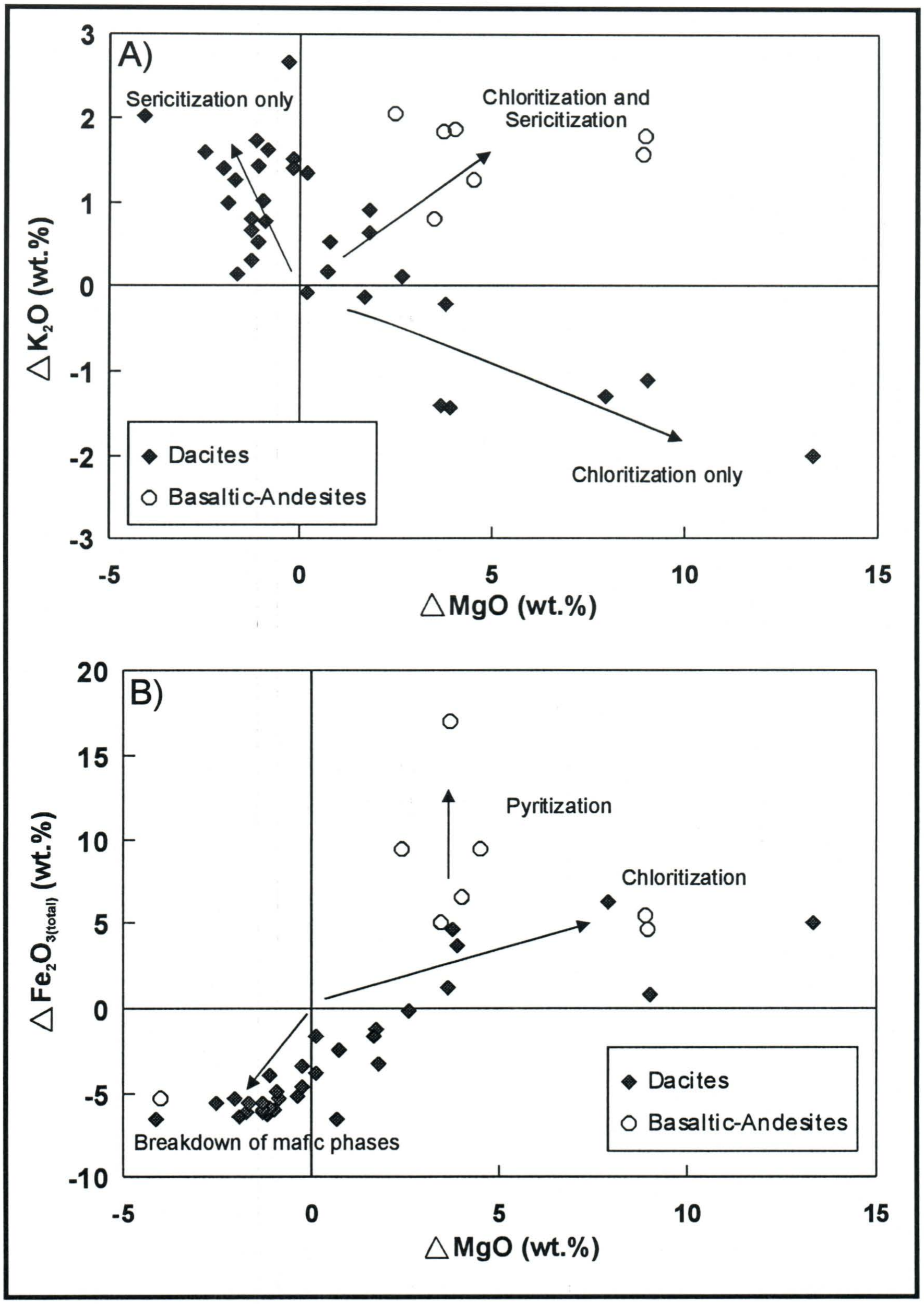


Figure 6-28 - Mass changes calculated for mafic and felsic volcanic rocks from the WBZ. Mass changes are in wt. %. a) MgO vs K_2O, b) MgO vs. $Fe_2O_{3(total)}$.

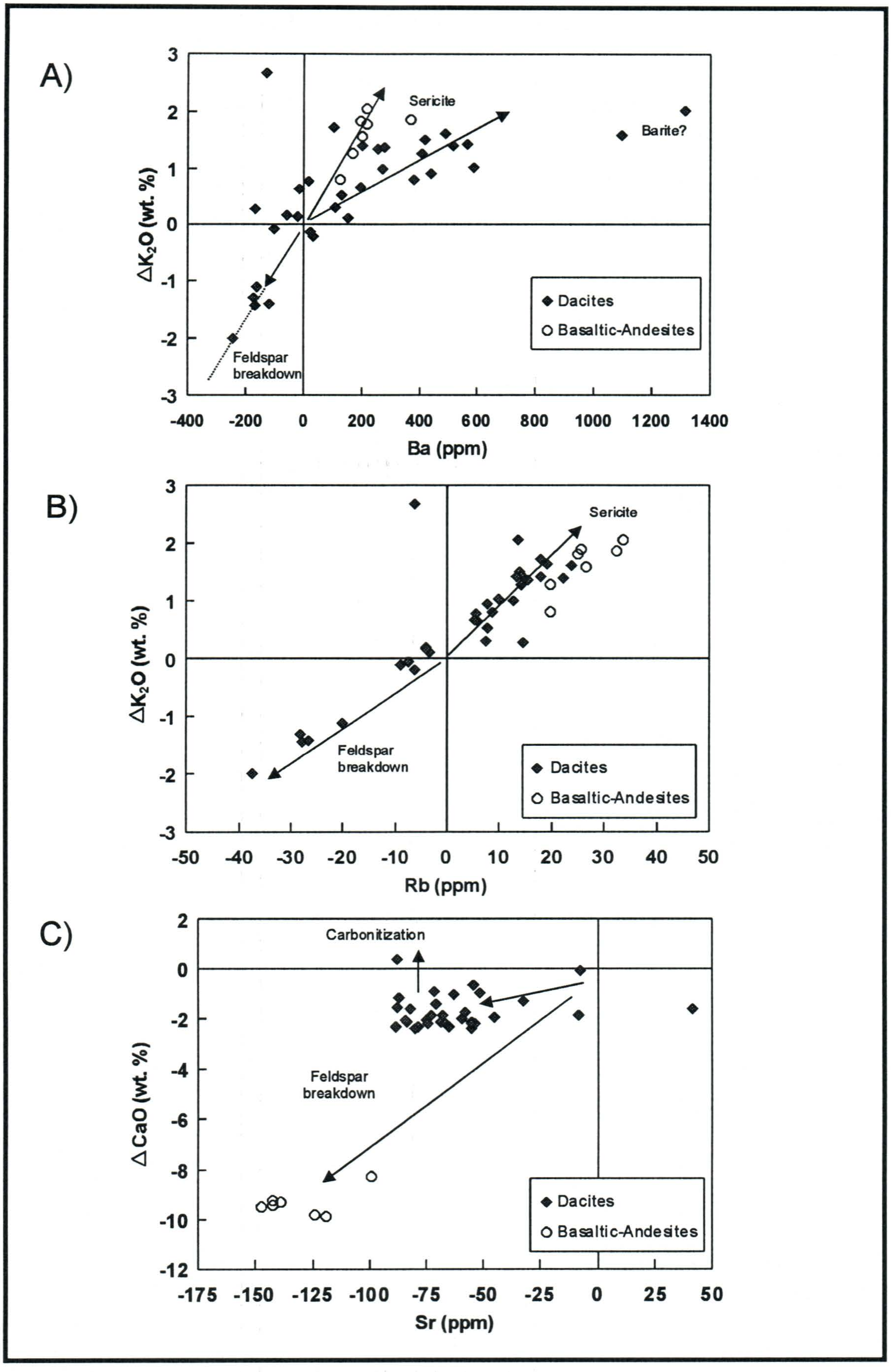


Figure 6-29 - Calculated mass changes in mafic and felsic rocks from the WBZ. Values are wt. % for oxides and ppm for trace elements. a) Ba vs. K_2O, b) Rb vs K_2O c) Sr vs. CaO.

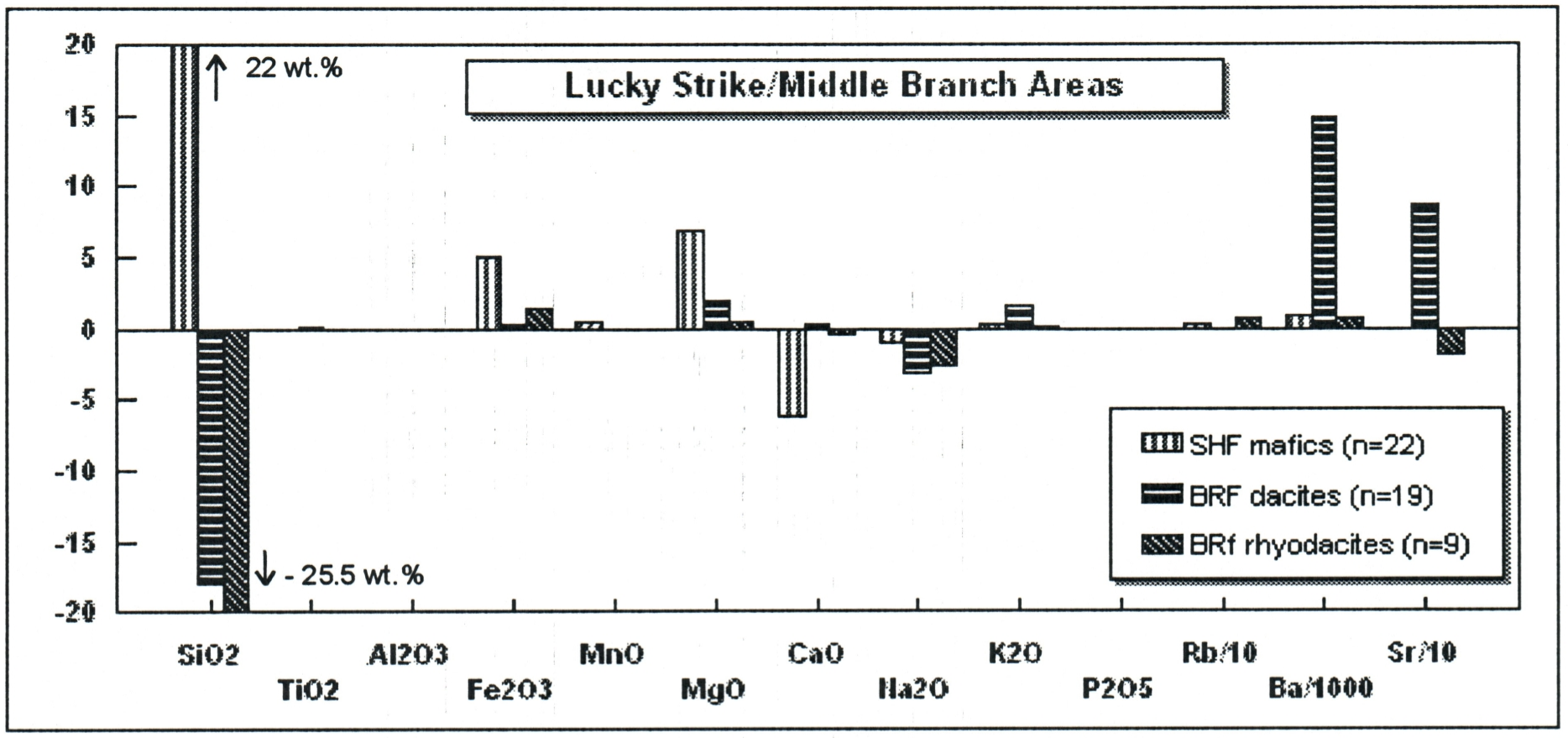
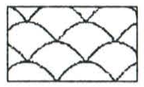
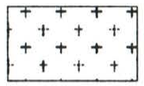


Figure 6-30 - Average calculated mass mass changes of major oxides and Rb, Ba and Sr for various lithologies from the Buchans area.

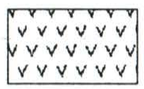
Legend



Sandy Lake Formation



BRF Rhyodacite (Rhyolite) Flow



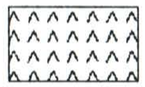
BRF Rhyodacite (Rhyolite) Tuff



BRF Ore Horizon Breccia/Comglomerate



Massive Ore



BRF Dacite tuff



SHF andesitic-basalt Flow/Breccia/Hyaloclastite



Fault (unknown type)



Thrust Fault

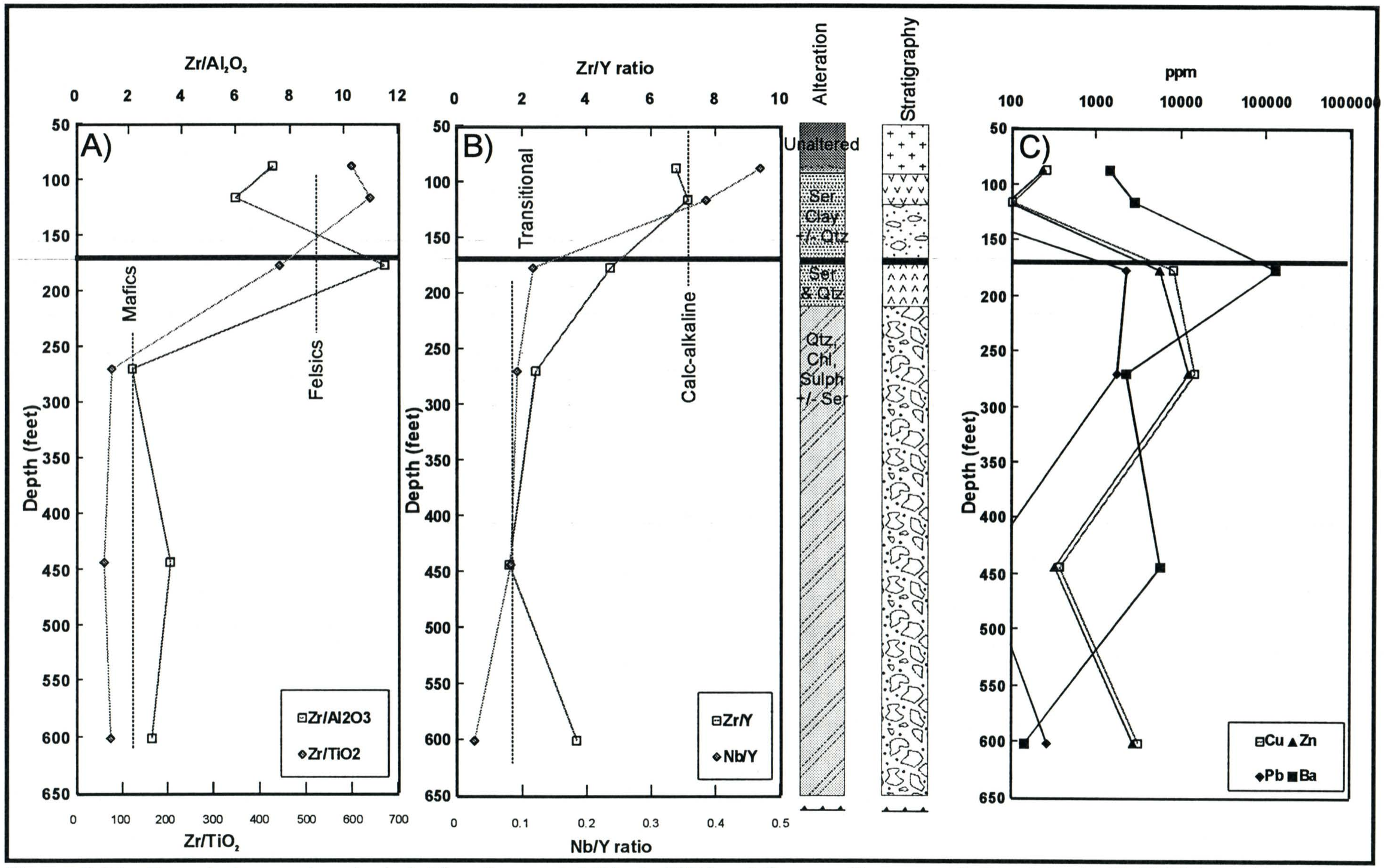


Figure 6-31 - Downhole geochemical plot for diamond drill hole 2871. a) Compositions are distinguished with Zr/TiO_2 and Zr/Al_2O_3 ratios. b) Magmatic affinity is discerned with Zr/Y and Nb/Y ratios. c) base metal values from raw geochemical data.

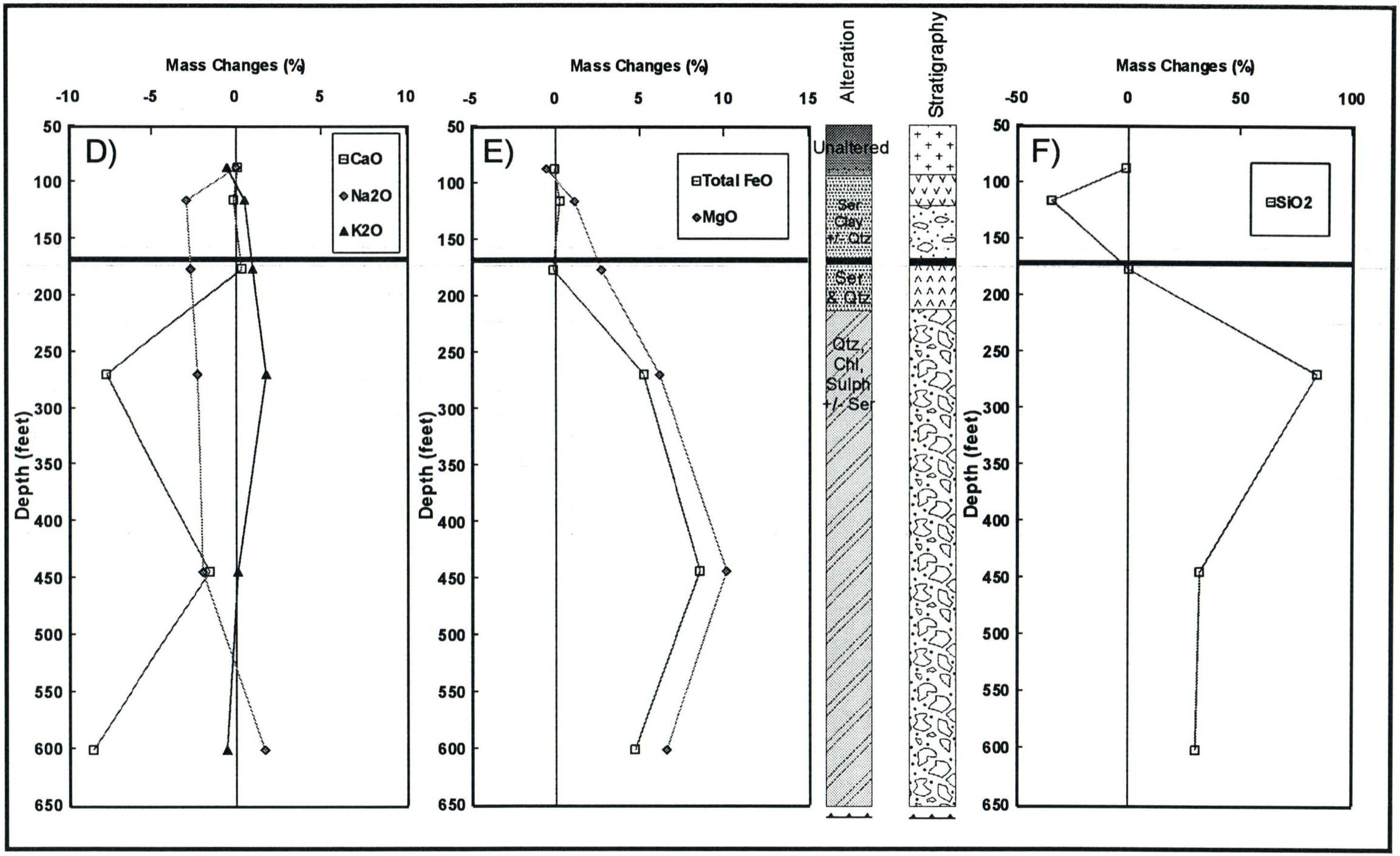


Figure 6-31 (continued) Calculated mass changes vs depth. d) CaO, Na_2O and K_2O, e) $Fe_2O_{3(total)}$ and MgO, f) SiO_2. Mass changes are wt. %.

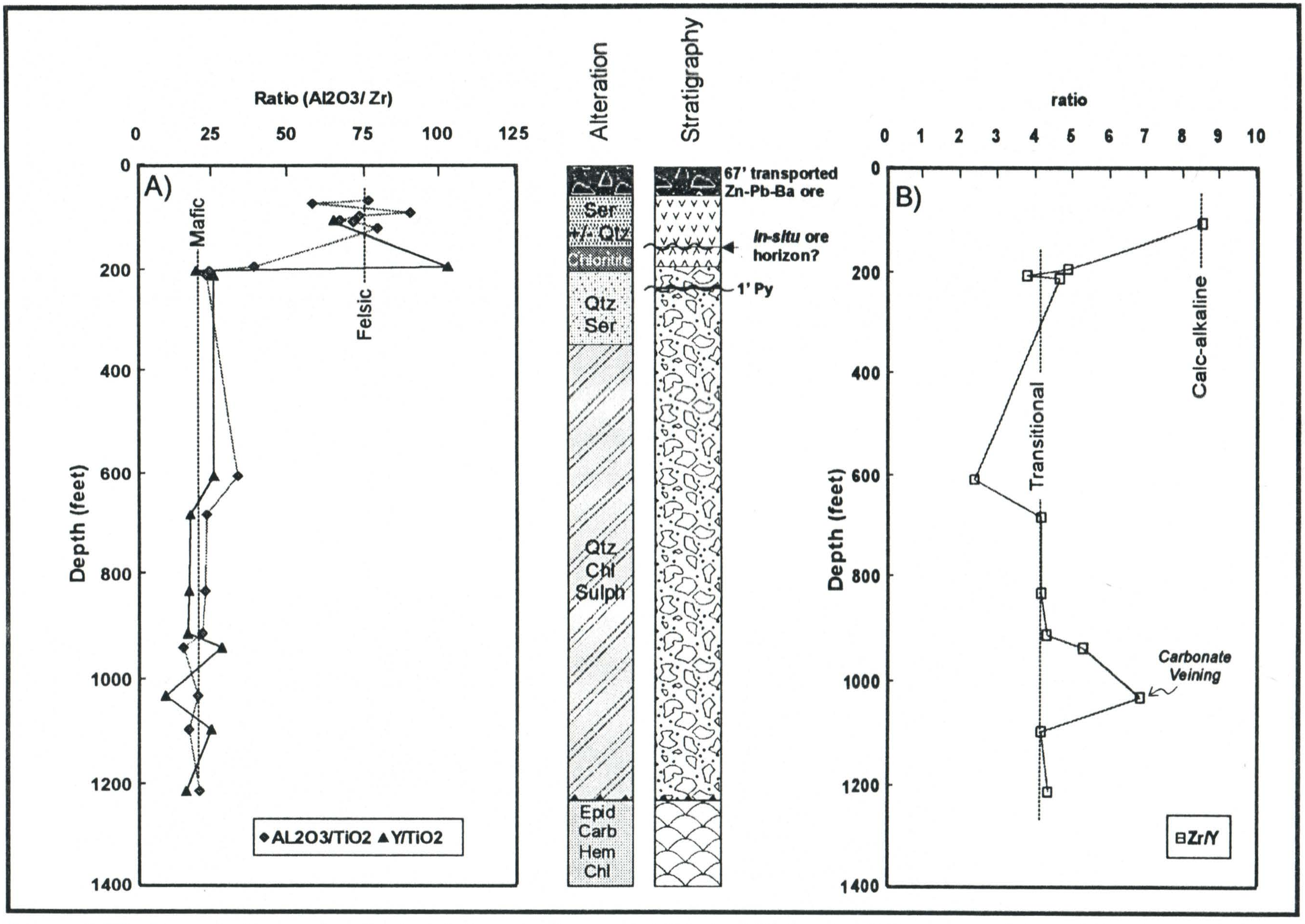


Figure 6-32 - Down hole geochemical variations in diamond drill hole 202, Lucky Strike area. a) immobile element ratios of Al_2O_3/TiO_2 and Y/TiO_2 indicating rock compositions. b) magmatic affinities indicated by Zr/Y.

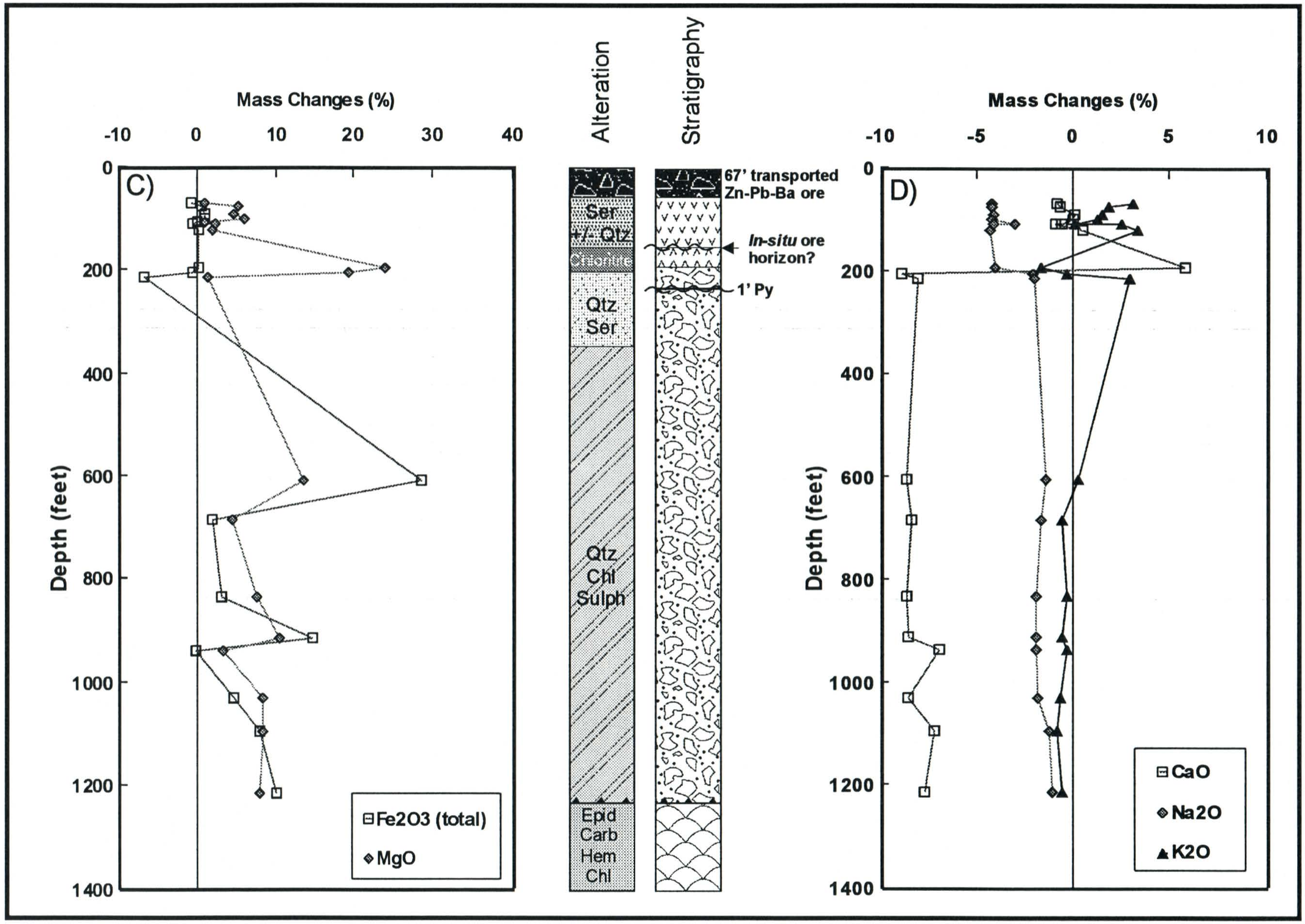


Figure 6-32 - (continued) Downhole geochemical variations in drill hole 202; c) $Fe_2O_{3(total)}$ and MgO, d) CaO, Na_2O and K_2O. Mass changes in wt. %.

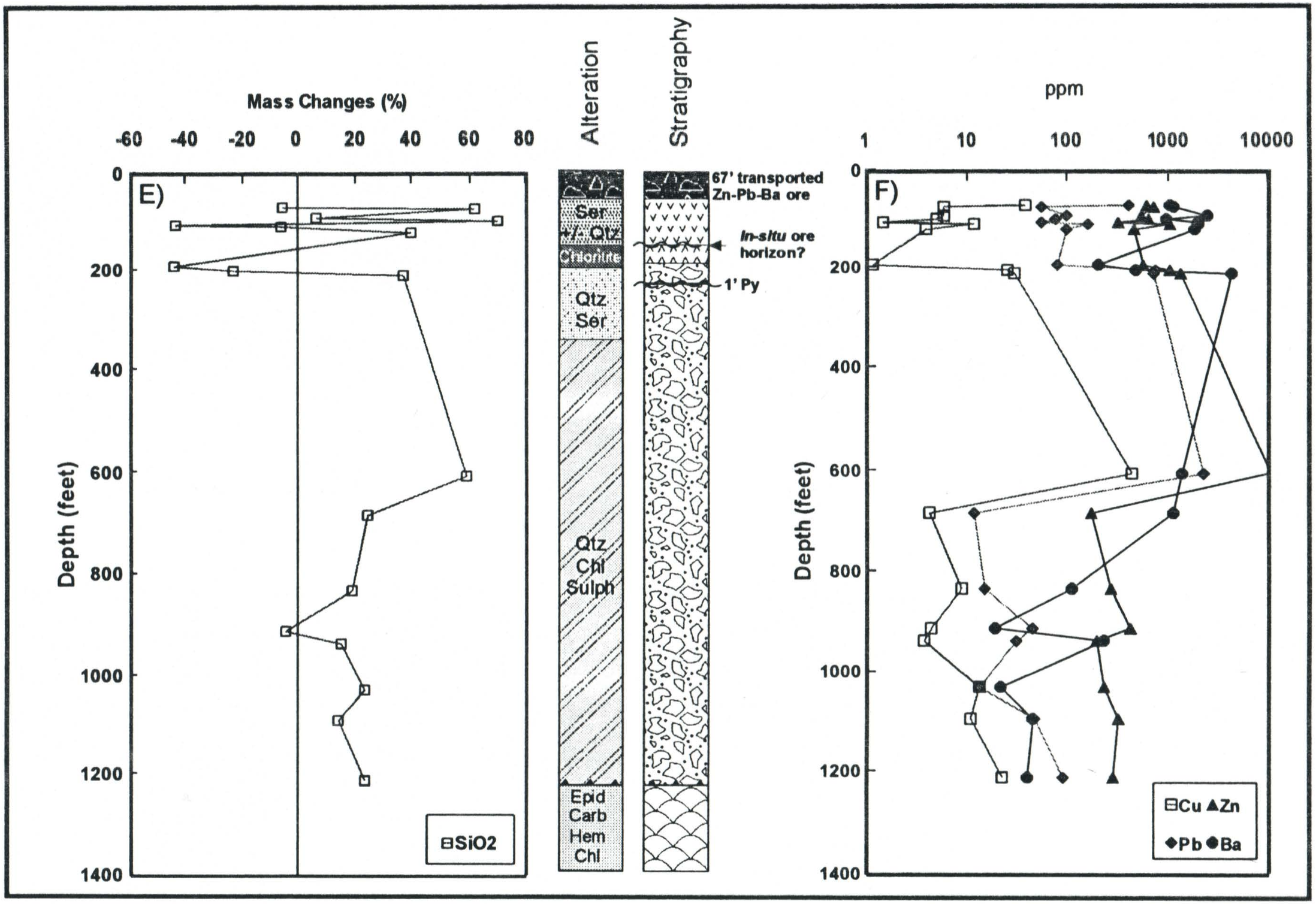


Figure 6-32 - (continued) Downhole geochemical variations in drill hole 202; e) SiO_2 mass changes in wt. %, f) base metal and Ba values in ppm (from raw data).

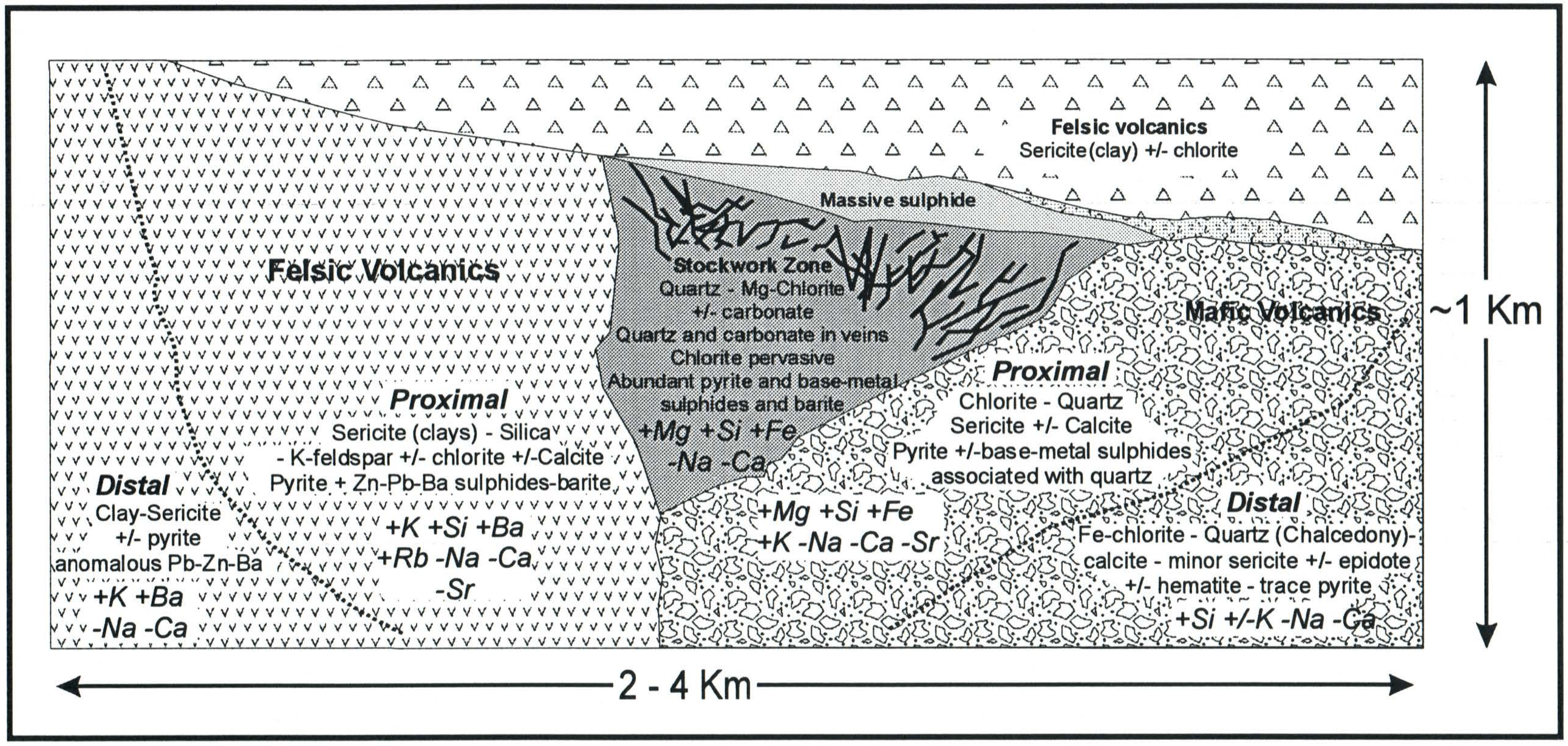


Figure 6-33 - Schematic hydrothermal alteration model for the Buchans Orebodies showing major alteration minerals and chemical mass changes.

Chapter Seven - Summary and Application to Exploration

7.1 Introduction

Whole rock and trace element geochemistry, petrography and microprobe analyses were applied to the hydrothermally altered host rocks in the immediate vicinity of the Lucky Strike orebody at Buchans (the LSZ). The same analytical methods were applied to other less explored areas (WBZ, PHZ, APZ) that have been considered to host potential significant alteration but no known massive sulphide mineralization. Lead isotopic studies were also applied to these 'new' zones. The purpose of this study was to compare alteration/mineralization/volcanic affinities in the new zones to that of the LSZ so that their prospectivity might be evaluated. The data indicate that the region is more complex in terms of tectonomagmatic history than previously thought. In addition, variations in alteration styles and isotopic ratios indicate that hydrothermal processes were also complex. Consequently, no single exclusive model can be used exclusively to explore for VMS deposits in this region.

7.2 Summary

7.2.1 Primary Geochemistry

Immobile trace and REE data indicate that at least two distinctive tectonomagmatic suites exist in the Buchans area: (i) a calc-alkaline island arc volcanic suite, defined for the immediate Buchans mining area and including at a minimum the SHF and BRF and (ii) an island arc tholeiitic suite, representing the rocks from the

Buchans East area. The LSZ and MBZ are within the calc-alkaline suite while the WBZ and PHZ are part of the tholeiitic suite. The APZ also appears to be of tholeiitic affinity yet several samples from the southern portion of this zone have calc-alkaline signatures.

Further information can be derived from the data within the calc-alkaline suite (Buchans Group *senso stricto*). The SHF andesitic-basalts and overlying BRF dacitic volcanics are very similar in their trace element-REE signatures and are considered to be genetically related. The higher stratigraphic levels of the BRF are characterized by rhyodacites. The rhyodacites are even more strongly calc-alkaline than the underlying units and may or may not represent a genetically different suite. The recognition of a large suite of genetically related, transitional (mildly calc-alkaline) to more strongly calc-alkaline volcanic rocks may be an important prerequisite for the formation of a Buchans type orebody. In addition, the main period of ore formation coincides with the transition from dacitic to rhyodacitic volcanics and a shift in trace element compatibility. If the least incompatible elements behaved compatibly in the subvolcanic source of the felsics after eruption of the dacites, but prior to eruption of the more evolved rhyodacite, then the shift in the trace element signature can easily be explained. As such, both felsics types would be considered genetically related. In either case, two very important implications are presented. Firstly, there may be important clues to the genesis of the Buchans ore deposits based on a comparison with the very similar Kuroko deposits where Urabe (1987) describes a shift from foot-wall to hanging-wall felsics of meta-aluminous to alkaline compositions, respectively. Urabe suggests that slightly aluminous felsic magmas would have been favourable for the generation of metal-rich magmatic fluids,

implying a magmatic-hydrothermal origin for those deposits. To be even more speculative, the observed signatures of the dacites and rhyodacites may indicate hornblende fractionation prior to eruption of the hanging-wall rhyodacites, assuming a common subvolcanic source. This would imply a build up of volatiles in the source coincident during the quiescence period, or ore-forming episode. A second implication, or rather an application, involves the exploration methodology for Buchans-type deposits. Obviously, lithogeochemical methods will readily distinguish these units as either hanging-wall or foot-wall and focus exploration to a specific "horizon".

7.2.1 Alteration Geochemistry, Mineral Analyses and Lead Isotopes

Alteration from all zones is broadly similar in that the assemblage is dominated by phyllosilicates (chlorite, sericite-clay) - quartz - pyrite with minor base metal sulphides also present locally. However, there are important but subtle differences that allow each of these zones to be characterized.

Host rocks to the Buchans orebodies (represented by the Lucky Strike Zone (LSZ)/Middle Branch Zone (MBZ)) consist of volcanic flows/breccias but also with a large tuffaceous component (pyroclastics and volcaniclastics). Felsic volcanics may comprise a slightly larger component and appear to have closer spatial and temporal associations to mineralization than the mafic volcanics. Alteration is characterized by a sericitic-clay - silicic style for felsic rocks and a silicic - chloritic +/- sericitic alteration in the mafics. K-feldspar also occurs locally in the felsics, and is best developed away from the zones of stockwork mineralization (such as occurs at Lucky Strike). The strongest K-

feldspar alteration observed occurs in the MBZ felsic volcanics. Hence, the alteration is largely controlled by the host lithology. Minor pyrite and anomalous base metals and Ba are ubiquitous in most altered rocks, although Cu sulphides are not well developed in zones of strong potassic (K-feldspar) alteration. This may reflect the lower temperatures of precipitation in this peripheral zone. The stockwork zone at Lucky Strike, however, is dominated by a quartz-chlorite-pyrite alteration and locally strong Cu-Zn-Pb mineralization and barite; sericite is absent. As protolithologies are often destroyed in this zone, immobile trace element geochemistry indicates that host rocks in the stockwork zone are both mafic and felsic in composition. Fe-Mg chlorites occur in intermediate to distal settings but Mg-rich chlorites occur in the stockwork zone presumably representing the highest seawater/rock ratios. Calcite is the only carbonate species occurring. Both calcite and Mg-rich chlorite may be due to a late, lower temperature flux of seawater as the hydrothermal system collapsed. Mass changes can easily be used to identify the style and quantify the degree of alteration.

The Woodmans Brook Zone (WBZ) has alteration assemblages that are also largely controlled by the protolithology, which appears to be dominated by felsic lithologies. Host rocks are dominated by coherent volcanics (*i.e.*, flows, sills) with a much smaller component of fragmental rocks and tuffs. Felsic rocks are dominated by silicic-sericitic(clay) alteration and only minor chloritization while mafic rocks are largely chlorite-sericite and silica altered. Fe-rich black chlorites typical of this zone and carbonate species include calcite and ankerite. Pyrite is ubiquitous in both rock types. Base metal mineralization may be controlled by the host rock as well since mafic rocks

generally contain anomalous Zn and Cu but rarely Pb. Mafic rocks may also contain more pyrite. Significant mineralization in felsic rocks consists of Pb-Zn rich mineralization with scarce Cu. Ba contents were typically less than 1000 ppm and appear to be controlled by potassic phases. Albitization of feldspars, more likely as a result of lower greenschist metamorphism is most obvious in the felsic suite. The style of alteration and mineralization in the mafic volcanics appears to be contemporaneous with volcanism, however, mineralization in breccia zones in felsic volcanics may represent later processes. Lead isotopic data suggest a very primitive source that is most comparable to the Skidder prospect.

The Powerhouse Zone (PHZ) is hosted dominantly in felsic volcanics, though some of the best mineralization and alteration occur in a mafic volcanic unit. This bimodal sequence contains few breccias and essentially no volcaniclastics similar to the WBZ, perhaps indicating a proximal volcanic facies. The alteration is dominated by sericite, silica and carbonate alteration, with only minor chloritic alteration for both mafic and felsic units. Chlorites contain much less Fe than those of the WBZ and are Mg-Al rich, more comparable to the Mg-rich chlorites at the LSZ. Carbonate alteration is more significant in this zone and is dominated by calcite-dolomite. Albitization of feldspar in the mafic suite is quite significant. Very fine disseminated and lesser stringer-style pyrite occur throughout both units but is more significant in the mafic rocks. Much of the base metal mineralization is Zn-Cu dominated, yet significant Pb mineralization is also locally abundant. Barite appears to be absent and contents of Ba are similar to the those at the WBZ. The strong Mg-metasomatism implies seawater as the source of the fluids for the

alteration. Lead isotope values are more primitive than Buchans, but more radiogenic than the WBZ, and overlap with the Connel Option lead isotope field.

The Airport Zone (APZ) is hosted mainly in felsic volcanics that range in volcanic affinity from tholeiitic to calc-alkaline, with the latter occurring towards the south. The APZ-N (north) contains locally strong chloritic-silicic alteration, with weakly anomalous Zn, that appears not to have a significant extent relative to the other alteration zones. The APZ-S (south) contains much more intense alteration and anomalous base metal concentrations, characterized by sericite-silica and trace fuchsite. Lead isotopic ratios from mineralization in the north part of the zone group closely to Buchans ore lead.

7.3 Applications to Exploration

Exploration in the immediate Buchans area for additional Buchans ore bodies should focus in the strongly calc-alkaline suites and specifically target the geochemical transition from the dacitic to rhyodacitic volcanism as an approach to pinpointing the ore horizon. Ba remains perhaps the best indicator of widespread alteration within this suite. Silicification, Mg-chloritization and increasing base metal mineralization are key indicators of proximal alteration. Zones of strong potassic alteration with anomalous Zn-Pb-Ba may indicate peripheral, but proximal, hydrothermal alteration facies.

Although the APZ has only localized alteration in the north, there is significant alteration at the south, and a significant geographical gap between these two areas. As such, the area requires further grass-roots level work before it can be deemed non-prospective for VMS mineralization. Obviously, the within this overall zone, the area

north of the APZ-S should be targeted.

Although this study did not include a systematic and detailed study on the entire region east of Buchans, the results suggest that it is unlikely that the ore-hosting SHF-BRF sequence is present towards the Buchans East area above the Airport Thrust. Firstly, these rocks are lithogeochemically distinct and represent a different volcanic affinity. In addition, they are lithologically dissimilar containing noticeably fewer pyroclastic and volcaniclastic sequences and mixed breccias. These rocks appear to be more deformed and metamorphosed, although this is probably a function of proximity to the Hungry Mountain Thrust. Finally, the alteration, although broadly similar, does not appear have the same degree of Ba enrichment. Although this may be spatially related to distance from the focus of hydrothermal activity, even the most mineralized intervals contain little Ba.

It is difficult to speculate on the style of mineral deposits which may occur in the Buchans East suite. Considering the data, the WBZ appears have potential for a Skidder-type (Cu-Zn) VMS deposit. As the host rocks for the WBZ and PHZ are broadly similar, a similar style of mineralization might be considered for the PHZ, although this zone is isotopically similar to the high grade (Zn-Pb-Cu) Connel Option prospect. Based on this correlation, and the degree of alteration at the PHZ, this zone appears to have the greatest potential for massive sulphide mineralization. As the lithogeochemical and isotopic signature of this zone is distinctive from that of the Buchans ore bodies, there is considerable potential that a new discovery would represent a new 'cluster' of VMS deposits.

7.4 Unresolved Problems

- With respect to the Buchans orebodies, is there an inherent magmatic control on the source of ore fluids/metals from the SHF-BRF suite? Does the shift in the trace and REE geochemistry from the dacitic to the rhyodacitic volcanism relate to any such process or is it simply coincidental?
- How significant is the spatial or temporal difference between volcanism in the Buchans camp (calc-alkaline) and the Buchans East area (tholeiitic), or is the variation simply a result of different magma sources occurring in the same setting? How does each relate to the Skidder Group?
- What is the distribution of the calc-alkaline and tholeiitic suites in the region?

References

Aeromagnetic vertical gradient map, Buchans, Newfoundland, 12A/15. Geological Survey of Canada, Geophysical Series, Map C40 097G. *In* Buchans Geology, Newfoundland. *Edited by* R.V. Kirkham. Geological Survey of Canada, Paper 86-24 (in pocket).

Alcock, J.B. 1961. Oriental No. 2 Orebody. Unpublished B.Sc. Thesis. Royal School of Mines, London, 56 p.

Allen, R.L. 1988. False pyroclastic textures in altered silicic lavas, with implications for volcanic-associated mineralization. Economic Geology, **83**: 1424 - 1446.

Anderson, F.D. 1972. Unpublished Geological Survey of Canada maps (Buchans 12A/15, Badger 12A/16).

Anger, C., 1963. The Lead-Zinc-Copper deposits of Buchans, middle Newfoundland. Neues Jahrbuch fuer Geologie und Palaeontologie. Monatshefte: **6**: 126-136.

Appleyard, E.C. and Bowles, E.G. 1978. The geology of the west mine, Pilley's Island, Newfoundland. Geological Survey of Canada, Paper 78-1A, pp. 199-203.

Babcock, R.S. 1973. Computational models of metasomatic processes: Lithos, **6**: 279-290.

Bailey, S.W. 1988. Chlorites: structures and crystal chemistry. *In* Hydrous Phyllosilicates. *Edited by* S.W. Bailey. Reviews in Mineralogy, Mineralogical Society of America,**19**: 347 - 398.

Barrett, T.J., Cattalani, S., Hoy, L., Riopel, J., and Lafleur, P.-J. 1992. Massive sulphide deposits of the Noranda area, Quebec. IV. The Mobrun mine. Canadian Journal of Earth Sciences, **29**: 1349 - 1374.

Barrett, T.J., Cattalani, S. and MacLean, W.H. 1993. Volcanic lithogeochemistry and alteration at the Delbridge massive sulphide deposit, Noranda, Quebec. Journal of Exploration Geochemistry, **48**: 135 - 173

Barrett, T.J. and MacLean, W.H. 1994a. Chemostratigraphy and hydrothermal alteration in exploration for VHMS deposits in greenstones and younger volcanic rocks. *In* Alteration and alteration processes associated with ore-forming systems. *Edited by* D.R. Lentz. Geological Association of Canada, Short Course Notes, **11**: 433 - 467.

Barrett, T.J. and MacLean, W.H. 1994b. Mass changes in hydrothermal alteration zones associated with VHMS deposits in the Noranda area: Exploration and Mining Geology, **3**: 131-160.

Barrett, T.J. and Sherlock, R.L. 1996. Volcanic stratigraphy, lithogeochemistry and seafloor setting of the H-W massive sulphide deposit, Myra Falls, Vancouver Island, British Columbia. Exploration and Mining Geology, **5**: 421 - 458.

Barrett, T.J., Thompson, J.F.H. and Sherlock, R.L. 1996. Stratigraphy, lithogeochemical and tectonic setting of the Kutcho Creek massive sulfide deposit, northern British Columbia. Exploration and Mining Geology, **5**: 309 - 338.

Barrie, C.T. 1991. New insights into the geology, geochemistry and mineral potential of the Buchans and Skidder Groups, central Newfoundland. Unpublished report prepared for B.P Resources Canada Ltd.

Barrie, C.T. and Hannington, M.D. 1999. Classification of volcanic-associated massive sulphide deposits based on hostr-rock composition. *In* Volcanic-associated massive sulphide deposits: processes and examples in modern and ancient settings. *Edited by* C.T. Barrie and M.D. Hannington. Reviews in Economic Geology, Volume 8, pp. 1 - 11.

Bell, K. and Blenkinsop, J. 1981. A Geochronological study of the Buchans area, Newfoundland. *In* The Buchans Orebodies: Fifty Years of Mining and Exploration. *Edited by* E.A.. Swanson, D.F. Strong and J.G. Thurlow. Geological Association of Canada. Special paper No.22, 91 p.

Bell, K. and Murton, J. B. 1995. A new indicator of glacial dispersion: lead isotopes. Quaternary Science Reviews, **14**: 275 - 287.

Blackwood, R.F. 1979. Geology of the Gander River area (2E/2), Newfoundland. *In* Report of Activities for 1978. *Edited by* R.V. Gibbons. Newfoundland Department of Mines and Energy, Mineral Development Division, Report 80-1, pp. 3 - 61.

Boerner, D.E., Wright, J.A., Thurlow, J.G., and Reed, L.E. Tenser CSAMT studies at the Buchans Mine in central Newfoundland. Geophysics, **58**: 12 - 19.

Buchans Staff. 1955. Buchans Operation, Newfoundland. Canadian Institute of Mining and Metallurgy Bulletin, **48**: 349 - 353.

Calon, T.J. and Green, F.K. 1987. Preliminary results of a detailed structural analysis of the Buchans mine area. *In* Buchans Geology, Newfoundland. *Edited by* R.V. Kirkham. Geological Survey of Canada, Paper 86-24, pp. 273 - 288.

Campbell, I.H., Coad, P., Franklin, J.M., Gorton, M.P., Scott, S.D., Sowa, J. and Thurston, P.C. 1982. Rare earth elements in volcanic rocks associated with Cu-Zn massive sulphide mineralization: a preliminary report. Canadian Journal of Earth Sciences, **19**: 619 - 623.

Cathelineau, M. and Nieva, D. 1985. A chlorite solid solution geothermometer: the Los Azufres (Mexico) geothermal system. Contributions to Mineralogy and Petrology, **91**: 235 - 244.

Catherall, D.J. 1960. Engine House Orebody. Unpublished B.Sc. thesis. Royal School of Mines, London, 92 p.

Cathles, L.M., Guber, A.L, Lenagh, T.C. and DuDäs, F.O. 1983. Kuroko-type massive sulphide deposits of Japan: Products of an Aborted Island-Arc Rift. *In* The kuroko and related volcanogenic massive sulphide deposits. *Edited by* H. Ohmoto and B.J. Skinner. Economic Geology, Monograph 5, pp. 96 - 114.

Colman-Sadd, S.P. 1980. Geology of South Central Newfoundland and the evolution of the eastern margin of Iapetus; American Journal of Science, **280**: 991-1017.

Colman-Sadd, S.P. and Swinden, H.S. 1984. A tectonic window in central Newfoundland? Geological Evidence that the Appalachian Dunnage Zone may be allochthonous. Canadian Journal of Earth Sciences, **21**: 1349 - 1367.

Colmann-Sadd, S.P., Stone, P., Swinden, H.S., and Barnes, R.P. 1992. Parallel geological development in the Dunnage Zone of Newfoundland and the Lower Paleozoic terranes of southern Scotland: An assessment. Royal Society of Edinburgh Transactions, Earth Sciences, **83**: 571 - 594.

Colman-Sadd, S.P., Hayes, J.P., aand Knight, I. 1990. Geology of the Island of Newfoundland. Map 90-01. Geological Survey Branch, Newfoundland Department of Mines and Energy, St. John's, Newfoundland.

Coyle, M. and Strong, D.F. 1987. Geology of the Springdale Group: A newly recognized Silurian epicontinental-type caldera in Newfoundland. Canadian Journal of Earth Sciences **24**: 1135 - 48.

Cumming, G.L. and Krstic, D. 1987. Detailed lead isotopes study of Buchans and related ores; *In* Buchans geology, Newfoundland. *Edited by* R.V. Kirkham. Geological Survey of Canada, Paper 86-24, pp. 227-233.

Date, J., Watanabe, Y. and Saeki, Y. 1983. Zonal alteration around the Fukazawa kuroko deposits, Akita prefecture, northern Japan. *In* The Kuroko and Related Volcanogenic Massive Sulfide deposits, Economic Geology Monograph 5. *Edited by* H. Ohmoto and B.J. Skinner. pp. 365-386.

Dean, P.L. 1978. The volcanic stratigraphy and metallogeny of Notre Dame Bay. Memorial University of Newfoundland, St. John's, Geological Report 7, 204 p.

Dec, T., Swinden, H.S. and Dunning, R.G. 1997. Lithostratigraphy and geochemistry of the Cottrells Cove Group, Buchans - Roberts Arm volcanic belt: new constraints for the paleotectionic setting of the Notre Dame Subzone, Newfoundland Appalachians. Canadian Journal of Earth Science, **34**: 86 - 103.

Deer, W.A., Howie, R.A. and Zussman, J. 1992. An Introduction to the Rock-Forming Minerals, Second Edition. Longman Scientific and Technical, Hong Kong, 696 p.

Dec, T. and Swinden, H.S. 1994. Lithostratigraphic model, geochemistry and sedimentology, Cottrells Cove Group, Buchans - Roberts Arm volcanic belt, Notre Dame Bay. Current Research, Newfoundland Department of Mines and Energy, Geological Survey Branch, Paper 94-1, p. 77 - 100.

Doe, B.R. and Zartman, R.E. 1979. Plumbotectonics. *In* Geochemistry of Hydrothermal Ore Deposits. *Edited by* H. Barnes. Wiley, New York, pp. 22 - 70.

Doucet, P., Mueller, W. and Chartrand, F. 1998. Alteration and ore mineral characteristics of the Archean Coniagas massive sulphide deposit, Abitibi belt, Quebec. Canadian Journal of Earth Science, **35**: 620 - 636.

Dudäs, F.O., Campbell, I.H. and Gorton, M.P. 1983. Geochemistry of ingeous rocks in the Hokuroko district, northern Japan. *In* The Kuroko and related volcanogenic massive sulphide deposits. *Edited by* H. Ohmoto and B.J. Skinner. Economic Geology Monograph 5, pp. 115 - 133.

Dunning, G.R., Kean, B.F., Thurlow, J.G., and Swinden, H.S. 1987. Geochronology of the Buchans, Robert's Arm, and Victoria Lake groups and Mansield Cove Complex, Newfoundland. Canadian Journal of Earth Sciences, **24**: 1175 - 1184.

Dunning, G.R. and Krogh, T.E. 1985. Geochronology of ophiolites of the Newfoundland Appalachians. Canadian Journal of Earth Science, **22**: 1659 - 1670.

Dunning, G.R. and Krogh, T.E. 1991. Stratigraphic correlation of the Appalachian Ordovician using advanced U-Pb zircon geochronology techniques. *In* Advances in Ordovician Geology. *Edited by* C.R. Barnes and S.H. Williams. Geological Survey of Canada Paper 90-9, p. 85 - 92.

Dunning, G.R., O'Brien, S.J., Colman-Sadd, S.P., Blackwood, R.F., Dickson, W.L., O'Neill, P.P. and Krogh, T.E. 1990. Silurian Orogeny in the Newfoundland Appalachians Journal of geology, **98**: 895-913.

Dunning, G.R., Swinden, H.S., Kean, B.F., Evans, D.T.W., and Jenner, G.A. 1991. A Cambrian Island arc in Iapetus: Geochronology and Geochemistry of the Lake Ambrose volcanic belt, Newfoundland. Appalachians Geological Magazine, **128**: 1-17.

Elliot-Meadows, S.R. and Appleyard, E.C. 1991. The alteration geochemistry and petrology of the Lar copper-zinc deposit, Lynn Lake area, Manitoba, Canada: Economic Geology, **86**: 486-505.

Entwistle, L.P. and Barnes, M.P. 1971. Report on exploration possibilities at the Buchans Unit, Newfoundland. ASARCO unpublished company report.

Fletcher, I.R. and Farquhar, R.M. 1977. Lead isotopes in the Grenville and adjacent paleozoic formations: Canadian Journal of Earth Sciences, **14**: 56-66.

Franklin, J.M. 1993. Volcanic-associated massive sulphide deposits. *In* Mineral Deposit Modelling. *Edited by* R.V. Kirkham, W.D. Sinclair, R.I. Thorpe and J.M. Duke. Geological Association of Canada, Special Paper 40, pp. 315 - 334.

Franklin, J.M., Hannington, M.D., Jonasson, I.R., and C.T. Barrie. Volcanogenic massive sulphide deposits. *In* Exploration Tools for Volcanogenic Massive Sulphide Deposits. *Edited by* J. Franklin and H Gibson. MDD-GAC and MDRU-UBC short course notes, January 24-25, Vancouver.

Franklin, J. M., Lydon, J. W. and Sangster, D.F. 1981. Volcanic-associated massive sulphide deposits. Economic Geology, 75th Anniversary Volume, pp. 485 - 627.

Galley, A.G. and Koski, R.A. 1999. Setting and characteristics of ophiolite-hosted volcanogenic massive sulphide deposits. Reviews in Economic Geology, Volume 8, pp. 221 - 246.

George, P.W. 1937. Geology of the lead-zinc-copper deposits at Buchans, Newfoundland. American Institute of Mining and Metallurgical Engineering, technical publication no. 816, Class I, Mining Geology, pp. 488-511.

Gibson, H.L., Watkinson, D.H. and Comba, C.D.A. 1983. Silicification: Hydrothermal alteration in an Archean geothermal system within the Amulet rhyolite formation, Noranda, Quebec. Economic Geology, **78**: 954 - 971.

Govindajaru, K. 1989. 1989 compilation of working values and sample description for 272 geostandards. Geostandards Newsletter, 13: 1 - 114.

Grant, J.A. 1986. The isocon diagram: a simple solution of Gresens' equation for metasomatic alteration. Economic Geology, **81**: 1976-1982.

Gresens, R.L. 1967. Composition-volume relationships of metasomatism. Chemical Geology, **2**: 47-55.

Hall, J., Marille, F., and Dehler, S. 1998. Geophysical studies of the structure of the appalachian orogen in the Atlantic borderlands of Canada. Canadian Journal of Earth Sciences, **35**: 1205-1221.

Harland, W.B. and Gayer, R.A. 1972. The Arctic Caledonides and earlier oceans. Geological Magazine, **109**: 289 - 314.

Hattori, K. and Sakai, H. 1979. D/H ratios, origins, and evolution of the ore forming fluids for the Neogene veins and Kuroko deposits of Japan. Economic Geology, **74**: 535-555.

Hendry, D.A.F. 1981. Chlorites, phengites and siderites from the Prince Lyell ore deposit, Tasmania, and the origin of the deposit. Economic Geology, **84**: 1978 - 1995.

Henley, R.W. and Thornley, P. 1981. Low grade metamorphism and the geothermal environment of massive sulphide formation, Buchans, Newfoundland. *In* The Buchans Orebodies: Fifty Years of Mining and Exploration. *Edited by* E.A.. Swanson, D.F. Strong and J.G. Thurlow (eds.) Geological Association of Canada. Special Paper 22, pp. 205-228.

Hey, M.H. 1954. A new review of the chlorites. Mineralogical Magazine, **30**: 277-292.

Huthinson, R.W. 1981. A synthesis and overview of Buchans Geology. *In* The Buchans Orebodies: Fifty Years of Mining and Geology. *Edited by* E.A. Swanson, D.F. Strong and J.G. Thurlow. Geological Association of Canada, Special Paper 22, pp. 325-347.

Ishikawa, Y., Sawaguchi, T., Iwaya, S., and Horiuchi, M. 1976. Delineation of prospecting targets for kuroko deposits based on modes of volcanism of underlying dacite and alteration haloes. Mining Geology, **26**: 105-117.

Jambor, J.L. 1987. Geology and origin of orebodies in the Lucky Strike area. *In* Buchans geology, Newfoundland. *Edited by* R.V. Kirkham. Geological Survey of Canada, Paper 86-24, pp. 75 - 106.

Jenner, G.A., Longerich, H.P., Jackson, S.E. and Fryer, B.J. 1990. ICP-MS - A powerful tool for high precision trace element analysis in earth sciences: Evidence from analysis of selected USGS reference samples. Chemical Geology, **83**: 133 - 148.

Jenner, G.A. 1996. Trace element geochemistry of igneous rocks: geochemical nomenclature and analytical geochemistry. *In* Trace element geochemistry of volcanic rocks: Applications for massive sulphide exploration. *Edited by* D.A. Wyman. Geological Association of Canada, Short Course Notes, Volume 12, pp. 51 - 57.

Jensen, L.S. 1976. A new plot for classifying subalkalic volcanic rocks. Ontario Division of Mines, MP 66, 22 pp.

Kamo, S.L., Gower, C.F., Krogh, T.E. 1989. Birthdate for the Iapetus Ocean? A precise U-Pb zircon and beddeleyite age for the Long Range dikes, southeast Labrador. Geology, **17**: 602 - 605.

Kean B.F. 1973. Stratigraphy, petroogy and geochemistry of volcanic rocks of Long Island, Newfoundland. Unpublished M.Sc. Thesis, Memorial University of Newfoundland, 155 p.

Kean, B.F. 1980. Buchans map sheet (12A/15), Newfoundland. Newfoundland Department of Mines and Energy Map 79-125.

Kean, B.F., Dean, P.L. and Strong, D.F. 1981. Regional Geology of the Central Volcanic Belt of Newfoundland. *In* The Buchans Orebodies: Fifty Years of Mining and Geology. *Edited by* E.A. Swanson, D.F. Strong and J.G. Thurlow. Geological Association of Canada, Special Paper 22, pp. 65 - 78.

Kean, B.F. and Strong, D.F. 1975. Geochemical evolution of an Ordovician island arc of the central Newfoundland Appalachians. American Journal of Science, **275**: 97-118.

Kirkham, R.V. 1987. Introduction. *In* Buchans Geology, Newfoundland. *Edited by* R.V. Kirkham. Geological Survey of Canada, Paper 86-24, pp. 1-6.

Kirkham, R.V. and Thurlow, J.G. 1987. Evaluation of a resurgent caldera and aspects of ore deposition and deformation at Buchans. *In* Buchans Geology, Newfoundland. *Edited by* R.V. Kirkham. Geological Survey of Canada, Paper 86-24, pp. 177 - 194.

Kowalik, J., Rye, R., and Sawkins, F.J. 1981. Stable isotope study of the Buchans polymetallic sulphide deposits. *In* The Buchans Orebodies: Fifty Years of Mining and Geology. *Edited by* E.A. Swanson, D.F. Strong and J.G. Thurlow. Geological Association of Canada, Special Paper 22, pp. 229-254.

Kranidiotis, P. and MacLean, W.H. 1987. Systematics of chlorite alteration at the Phelps Dodge massive sulphide deposit, Matagami, Quebec. Economic Geology, **82**: 1898 - 1911.

Larsen, K.B. 1973. The formation and penecontemporancous deformation of tuffaceous sediments in Buchans, Newfoundland. Unpublished ASARCO report.

Lavery N.G. 1985. Quantifying chemical changes in hydrothermally altered volcanic sequences; silica enrichment as a guide to the Crandon massive sulfide deposit, Wisconsin, U.S.A. Journal of Geochemical Exploration, **24**: 1 - 27.

Leitch, C.H.B and Lentz, D.R. 1994. The Gresens approach to mass balance constraints of alteration systems: methods, pitfalls, examples. *In* Alteration and alteration processes associated with ore-forming systems. *Edited by* D.R. Lentz. Geological Association of Canada, Short Course Notes, Volume 11, pp. 161-192.

Le Maitre, R.W. 1989. A classification of igneous rocks and a glossary of terms. Blackwell, Oxford. 193 p.

Lentz, D.R. 1998. Petrogenetic evolution of felsic volcanic sequences associated with phanerozoic volcanic-hosted massive sulphide systems: the role of extensional geodynamics. Ore Geology Reviews, **12**: 289-327.

Longerich, H.P., Jenner, G.A., Fryer, B.J., and Jackson, S.E. 1990. Inductively coupled plasma-mass spectrometric analysis of geological samples: A critical evaluationbased on case studies. *In* Microanalytical Methods in Mineralogy and Geochemistry. *Guest Edited by* P.J. Potts, C. Dupuy, and J.F.W. Bowles. Chemical Geology, **83**: 105 - 118.

Longerich, H.P., Jenner, G.A., Fryer, B.J., and Jackson, S.E., 1990. Inductively coupled plasma-mass spectrometric analysis of geological samples: A critical evaluation based on case studies. Chemical Geology, **83**:105-118.

Lydon, J.W. 1988a. Volcanogenic massive sulphide deposits, Part 1: A descriptive model. *In* Ore Deposit Models. *Edited by* R.G. Roberts and P.A. Sheahan. Geoscience Canada, Reprint Series 3, pp. 145 - 154.

Lydon, J.W. 1988b. Volcanogenic massive sulphide deposits, Part 2: Genetic models. *In* Ore Deposit Models. *Edited by* R.G. Roberts and P.A. Sheahan. Geoscience Canada, Reprint Series 3, pp. 155 - 181.

Lydon, J.W. 1996. Characteristics of volcanogenic massive sulphide deposits: Interpretations in terms of hydrothermal convection systems and magmatic hydrothermal systems. Boletin Geologico y Minero, 107: 215 - 264.

MacLean, H.J. 1941. Memorandum on prospecting in the Little Sandy Brook area. Unpublished ASARCO report.

MacLean, H.J. 1943. Memorandum on prospecting in the Woodmans Brook-No. 2 siding area. Unpublished ASARCO report.

MacLean, W.H. 1990. Mass change calculations in altered rock series: Mineralium Deposita, **25**: 44-49.

MacLean, W.H. and Barrett, T.J. 1993. Lithogeochemical techniques using immobile elements: Journal of Geochemical Exploration, **48**: 109-133.

MacLean, W.H. and Hoy, L.D. 1991. Geochemistry of hydrothermally altered rocks of the Horne Mine, Noranda, Quebec. Economic Geology, **86**: 506 - 528.

MacLean, W.H. and Kranidiotis, P. 1987. Immobile Elements as monitors of mass transfer in hydrothermal alteration: Phelps Dodge massive sulphide deposit, Matagami, Quebec; Economic Geology, **82**: 951-962

Marillier, F., Keen, C.E., Stockmal, G.S., Quinlan, G.S., Williams, H., Colman-Sadd, S.P. and O'Brien, S.J. 1989. Crustal structure and surface zonation of the Canadian Appalachians: Implications of deep seismic reflection data. Canadian Journal of Earth Sciences, **26**: 305 - 321.

McClay, K.R. 1987. Aspects of the structural geology of the Buchans area. *In* Buchans geology, Newfoundland. *Edited by* R.V. Kirkham. Geological Survey of Canada, Paper 86-24, pp. 47 - 58.

McHale, K.B. and McHale, D.E. 1984. Oil Island, an Ordovician volcanogenic sulphide prospect (abstract). Geological Association of Canada, Newfoundland Section, Annual Spring Meeting, Program with Abstracts, p.5.

McPhie, J., Doyle, M. and Allen, R. 1993. Volcanic Textures: A guide to the interpretation of textures in volcanic rocks. Centre for Ore Deposit and Exploration Studies, University of Tasmania, Hobart, Tasmania. 198 p.

Moritz, R. and Malo, M. 1996. Lead isotope signatures on Devonian Acadian structurally controlled mineral occurrences in the Gaspe peninsula, Quebec Appalachians: constrains on source rocks. Economic Geology: **91**: 1145 - 1150.

Morton, R.L., Hudak, G.J., Walker, J.S. and Franklin, J.M. 1992. Physical volcanology and hydrothermal alteration of the Sturgeon Lake caldera complex. MDRU short course SC-9, April 7-10. *Presented by* J. Franklin, H. Gibson, R. Morton and A. Galley. pp. 74 - 94.

Murray, A. 1881. Survey of Exploits and River and Red Indian Lake. Geological Survey of Newfoundland, Report for 1871. *In* Geological Survey of Newfoundland. *Edited by* A. Murray and J.P. Howley. Edward Stanford, London, pp. 250-278.

Neary, G.N. Mining history of the Buchans Area. *In* The Buchans Orebodies: Fifty Years of Mining and Geology. *Edited by* E.A. Swanson, D.F. Strong and J.G. Thurlow. Geological Association of Canada, Special Paper 22, pp. 1-64.

Newhouse, W.H. 1931. Geology and ore deposits of Buchans, Newfoundland. Economic Geology, **26**: 399 - 414.

Nowlan, G.S. and Thurlow, J.G. 1987. The significance of Middle Ordovician conodonts from the Buchans Group. *In* Buchans geology, Newfoundland. *Edited by* R.V. Kirkham. Geological Survey of Canada, Paper 86-24, pp. 59 - 62.

O'Brien, F.H.C. and Szybinski, Z.A. 1989. Conodont faunas from the Catchers pond and Cutwell groups, central Newfoundland. *In* Current Research, 121-5. Newfoundland Department of Mines, Geological Survey of Newfoundland report 89-1.

Ohmoto, H. 1996. Formation of volcanogenic massive sulphide deposits: The Kuroko perspective. Ore Geology Reviews, **10**:135 - 177.

Ohmoto, H. and Skinner, B.J. 1983. Introduction. *In* The kuroko and related volcanogenic massive sulphide deposits. *Edited by* H. Ohmoto and B.J. Skinner. Economic Geology, Monograph 5, pp. 1-8.

Pearce, T.H. 1968. A contribution to the theory of variation diagrams. Contributions to Mineralogy and Petrography, **19**: 142-157.

Pearce, J.A. 1983. Role of the sub-continental lithosphere in magma genesis at active continental margins. *In* Continental Basalts and Mantle Zenoliths. *Edited by* C.J. Hawkesworth and M.J. Norry, pp. 231-249.

Pearce, J.A. and Cann, J.R. 1973. Tectonic setting of basic volcanic rocks determined using trace element analyses. Earth and Planetary Science Letters, **19**: 290 - 300.

Pearce, J.A., Nigel, B.W.H. and Tindle, A.G. 1984. Trace element discrimination diagrams for the tectonic interpretation of granitic rocks. Journal of Petrology, **25**: 956 - 983.

Pearce, J.A. and.Cann, J.R. 1973. Tectonic setting of basic volcanic rocks determined using trace element analyses. Earth and Planetary Science Letters, **19**: 290 - 300

Pearce, J.A. and Peate, D.W. 1995. Tectonic implications of the composition of volcanic arc magmas. Annual Reviews in Earth Planetary Science, **23**: 251-285.

Petersen, M.D. and Lambert, I.B. 1979. Mineralogical and chemical zonation around the Woodlawn Cu-Pb-Zn ore deposit, southeastern New South Wales. Journal of the Geological Society of Australia, **26**: 169 - 186.

Pickett, J.W. 1987. Geology and geochemistry of the Skidder Basalt. *Edited by* R.V. Kirkham. Geological Survey of Canada, Paper 86-24, pp. 195 - 218.

Pickett, J.W. 1988a. A geological and geochemical study of the Skidder Basalt and Skidder trondhjemites: and the geology, ore petrology and geochemistry of the Skidder prospect and its accompanying alteration zone: Buchans area, central Newfoundland. Unpublished M. Sc. Thesis, Memorial University of Newfoundland, St. John's, Newfoundland, 465 p.

Pickett, J.W. 1988b. The Skidder prospect, Buchans area, Newfoundland. *In* The volcanogenic massive sulphide deposits of central Newfoundland. *Edited by* H.S. Swinden and B.F. Kean. Geological Association of Canada, Mineral Deposits Division, pp. 123 - 125.

Pickett, J. W. and Barbour, D.M. 1984. Geology of the Skidder prospect, Buchans, Newfoundland. In Current Research, Part A, Geological Survey of Canada, Paper 84-1A, pp. 581 - 586.

Poulsen, K.H. and Hannington, M.D. 1996. Volcanic-associated massive sulphide gold. *In* Geology of Canadian Mineral Deposit types. *Edited by* O.R. Eckstrand, W.D. Sinclair and R.I. Thorpe. Geological Survey of Canada, No.8, pp. 183 - 196.

Quinlan, G.G, Beamont, C., and Hall, J. 1993. Tectonic model for crustal seismic reflectivity patterns in compressional orogens. Geology, **21**: 663-666.

Relly, B.H. 1960. The geology of the Buchans Mine, Newfoundland. Unpublished Ph.D. Thesis, McGill University, 281 p.

Richards, H. G., Cann, J.R., and Jensenius, J. 1989. Mineralogical zonation and metasomatism of the alteration pipes of Cyprus sulphide deposits: Economic Geology. **84**: 91-115.

Rollinson, H. 1993. Using Geochemical Data: Evaluation, Presentation, Interpretation. Longman Scientific and Technical, NewYork.

Saeki, Y. and Date, J. 1980. Computer application to the alteration data of the footwall dacite lava at the Ezuri kuroko deposits, Akita Prefecture, Mining Geology: **30**: 241 - 250.

Santaguida, F., Hannington, M., and Jowett, C. 1992. A alteration and sulphur isotope study of the Pilley's Island massive sulphides, central Newfoundland. *In* Current Research, Part D: Geological Survey of Canada, paper 92-1D, pp. 265-274.

Serbert, C. and Barrett, T.J. 1996. Stratigraphy, alteration and mineralization at the Tulsequah Chief massive sulphide deposit, northern British Columbia. Exploration and Mining Geology, 5: 281 - 308. Survey Department, Cyprus, pp. 193 - 204.

Shervais, J. W. 1982. Ti - V plots and the petrogenesis of modern and ophiolitic lavas. Earth and Planetary Science Letters, **59**: 101 - 118.

Snelgrove, A.K. 1928. The geology of the Central Mineral Belt of Newfoundland. Canadian Mining and Metallurgical Bulletin, **21**: 1057 - 1127.

Spencer, C., Thurlow, G., Wright, J., White, D., Carroll, P., Milkereit, B. and Reed, L. 1993. A vibroseis reflection seismic survey at the Buchans Mine in central Newfoundland. Geophysics, **58**: 154 - 166.

Spitz, G. and Darling, R. 1978 Major and minor element lithogeochemical anomalies surrounding the Louvem copper deposit, Val d'Or, Quebec. Canadian Journal of Earth Sciences, **15**: 161 - 1169.

Spurvey, P.E. and Scott, W.J. 1997. Time-domain EM and gradient induced polarization survey on the Buchans east grid mineral licences 4547M, 4744M, 4293M, 4294M, and 4805M. Buchans Area, Newfoundland. NTS Map 12A/5. Unpublished report.

Stanley, C.R. and Madeisky, H.E. 1994. Lithogeochemical exploration for hydrothermal ore deposits using Pearce element ratio analysis. *In* Alteration and alteration processes associated with ore-forming systems: Geological Association of Canada, Short Course Notes. *Edited by* D.R. Lentz. Volume 11, pp. 161-192.

Strong, D.F. 1977. Volcanic Regimes of the Newfoundland Appalachians. *In* Volcanic Regimes in Canada. *Edited by* W.R.A. Baragar, L.C. Coleman and J.M. Hall. Geological Association of Canada, Special Paper Number 16, pp. 61 - 90.

Strong, D.F. 1980. Granitoid rocks and associated mineral deposits of eastern Canada and western Europe. *In* The continental crust and its mineral deposits. *Edited by* D.W. Strangway. Geological Association of Canada, special paper 20, pp. 741-769.

Strong, D.F. 1984. Rare earth elements in volcanic rocks of the Buchans area, Newfoundland. Canadian Journal of Earth Sciences, **21**: 775 - 780.

Sun, S.S. 1980. Lead isotope study of young volcanic rocks from mid-ocean ridges, ocean islands, and island arcs.; Philosophical Transactions of the Royal Society of London, A297, pp. 409-445.

Sun, S.S. and McDonough, W.F. 1989. Chemical and isotopic systematics of oceanic basalts: Implications for mantle composition processes. *In* Magmatism in the Ocean Basins. *Edited by* A.D. Saunders and M.J. Norry. Geological Society Special Publication No. 42, pp. 313 - 345.

Swanson, E.A. and Brown, R.L. 1962. Geology of the Buchans Orebodies. Canadian Institute of Mining and Metallurgy Bulletin, **55**: 618 - 626.

Swanson, E.A., Strong, D.F., and Thurlow, J.G. 1981. *In* The Buchans Orebodies: Fifty Years of Mining and Geology. *Edited by* E.A. Swanson, D.F. Strong and J.G. Thurlow. Geological Association of Canada, Special Paper 22, 350 p.

Swinden, H.S. 1988. Geology and mineral deposits of the southern part of the Robert's Arm Group, including the Gullbridge and Lake Bond areas. *In* The Volcanogenic Sulphide Districts of Central Newfoundland. *Edited by* H.S. Swinden and B.F. Kean. Geological Association of Canada, Mineral Deposits Division, pp. 96 - 109.

Swinden, H.S. 1991. Paleotectonic settings of volcanogenic massive sulphide deposits in the Dunnage Zone, Newfoundland Appalachians. CIM Bulletin, **84**: 59 - 69.

Swinden, H.S., Jenner, G.A. and Szybinski, Z.A. 1997. Magmatic and tectonic evolution of the Cambrian-Ordovician Laurentian margin of Iapetus: Geochemical and isotopic constraints from the Notre Dame subzone, Newfoundland. *In* The nature of magmatism in the Appalachian Orogen. *Edited by* A.K. Sinha, J.B. Whalen and J.P. Hogan. Geological Society of America, Memoir 191, pp. 337 - 365.

Swinden, H.S., Kean, B.F. and Dunning, G.R. 1988. Geological and paleotectonic settings of volcanogenic sulphide mineralization in central Newfoundland. *In* The Volcanogenic Sulphide Districts of Central Newfoundland. *Edited by* H.S. Swinden and B.F. Kean. Geological Association of Canada, Mineral Deposits Division, pp. 5 - 26.

Swinden, H.S. and Thorpe, R.I. 1984. Variations in style of volcanism and massive sulphide deposition in early to middle Ordovician aisland-arc sequences of the Newfoundland central mobile belt. Economic Geology, **79**: 1596 - 1619.

Szybinski, Z.A. 1995. Paleotectonic and structural setting of the western Notre Dame Bay Area, Newfoundland Appalachians. Unpublished Ph.D Thesis. Memorial University of Newfoundland, St. John's, Newfoundland.

Szybinski, Z.A., Swinden, H.S., O'Brien, F.H.C., Jenner, G.A., and Dunning, G.R. 1990. Correlation of ordovician volcanic terranes in the Newfoundland Appalachians: Lithological, geochemical and age constraints (abstract). Geological Association of Canada, Program with Abstracts 15, A40.

Tanimura, S., Date, J., and Takahashi, T. 1983. Stratigraphy and structure of the Hokuroku district, Part II. *In* The Kuroko and related volcanogenic massive sulphide deposits. *Edited by* H. Ohmoto and B.J. Skinner. Economic Geology Monograph 5, pp. 24-38.

Taylor, R.P. and Fryer, B.J. 1983. Rare earth element lithogeochemistry of granitoid mineral deposits. Canadian Mining and Metallurgical Bulletin, **76**: 74-84.

The Northern Miner, Volume 85, no. 24, Aug 9-15, 1999, p.1. Buchans area heats up, by James Whyte.

Thurlow, J.G. 1974. Lithogeochemical studies in the vicinity of the Buchans massive sulphide deposits, central Newfoundland. Unpublished M. Sc. Thesis, Memorial University of Newfoundland, St. John's, Newfoundland.

Thurlow, J.G. 1981. Geology, ore deposits and applied rock geochemistry of the Buchans Group, Newfoundland. Unpublished Ph. D. Thesis, Memorial University of Newfoundland, St. John's, Newfoundland.

Thurlow, J.G. 1988. Geology of the Buchans orebodies - a 1988 summary. *In* The volcanogenic massive sulphide deposits of central Newfoundland. *Edited by* H.S. Swinden and B.F. Kean. Geological Association of Canada, Mineral Deposits Division, pp. 177 - 194.

Thurlow, J.G. 1995. Report on diamond drilling during 1994 and 1995 on Oil Islands, Licence 4233, NTS 2E/12, Notre Dame Bay, Central Newfoundland. Unpublished report prepared for Phelps Dodge Corporation of Canada Limited.

Thurlow, J.G. 1996. Geology of a newly discovered cluster of blind massive-sulphide deposits, Pilley's Island, central Newfoundland. *In* Current research, Newfoundland and Labrador Department of Natural Resources, Geological Survey Branch, Report 96-1, pp. 181-189.

Thurlow, J.G., Swanson, E.A. 1981. Geology and Ore deposits of the Buchans area, Central Newfoundland. *In* The Buchans Orebodies: Fifty Years of Mining and Geology. *Edited by* E.A. Swanson, D.F. Strong and J.G. Thurlow. Geological Association of Canada, Special Paper 22, pp. 113 - 142.

Thurlow, J.G., Swanson, E.A. 1987. Stratigraphy and structure of the Buchans Group. *In* Buchans geology, Newfoundland. *Edited by* R.V. Kirkham. Geological Survey of Canada, Paper 86-24, pp. 35 - 46.

Thurlow, J.G., Spencer, C.P., Boerner, D.E., Reed, L.E., Wright, J.A. 1992. Geological interpretation of a high resolution reflection seismic survey at the Buchans mine, Newfoundland. Canadian Journal of Earth Sciences, **29**: 2022 - 2037.

Thurlow, J.G., Swanson, E.A. and Strong, D.F. 1975. Geology and lithogeochemistry of the Buchans polymetallic sulfide deposits, Newfoundland. Economic Geology, **70**: 130 - 144.

Tuach, J. 1988. Geology and volcanogenic sulphide mineralization in the Robert's Arm Group on Pilley's Island, Central Newfoundland. *In* The Volcanogenic Sulphide Districts of Central Newfoundland. *Edited by* H.S. Swinden and B.F. Kean. Geological Association of Canada, Mineral Deposits Division, pp. 117 - 122.

Urabe, T. 1987. Kuroko deposit modelling based on magmatic hydrothermal theory. Mining Geology: 37: 159 - 176.

Urabe, T. and Marumo, K. 1991. A new model for kuroko-type deposits of Japan. Episodes, **14**: 246 - 251.

Urabe, T., Scott, S.D, and Hattori, K. 1983. A comparison of footwall-Rock alteration and geothermal systems beneath some Japanese and Canadian volcanogenic massive sulfide deposits. *In* The kuroko and related volcanogenic massive sulphide deposits. *Edited by* H. Ohmoto and B.J. Skinner. Economic Geology, Monograph 5. pp. 345-364.

Vervoort, J.D., White, W.M., and Thorpe, R.I. 1994. Nd and Pb isotope ratios of the Abitibi greenstone belt: new evidence for early differentiation of the earth. Earth and Planetary Science Letters, **128**: 215 - 229.

Walker, P.N. and Barbour, D.M. 1981. Geology of the Buchans ore horizon breccias. *In* The Buchans Orebodies: Fifty Years of Mining and Geology. *Edited by* E.A. Swanson, D.F. Strong and J.G. Thurlow. Geological Association of Canada, Special Paper 22, pp. 161 - 186.

Walker, P.N. and King, J. 1975. Preliminary Report, Buchans Project. Unpublished Asarco report, 4 p.

Williams, H. 1964. The Appalachians in Newfoundland - A two sided symmetrical system. American Journal of Science, **262**: 1137 - 1158.

Williams, H. 1967. Silurian Rocks of Newfoundland. Geological Association of Canada, Special Paper 4, pp. 93 - 137.

Williams, H. 1979. Appalachian Orogen in Canada. Canadian Journal of Earth Sciences, **16**: 792 - 807.

Williams, H. and Hatcher, R.D. Jr. 1983. Appalachian suspect terranes. *In* Contributions to the Tectonic and Geophyiscs of Mountain Chains. *Edited by* R.D. Hatcher Jr., H. Williams, and I. Zietz. Geological Society of America, Memoir 158, pp. 33 - 53.

Williams, H. and Hiscott, R. N. 1987. Definition of the Iapetus rift-drift transition in western Newfoundland. Geology, **15**: 1044 - 1047.

Williams, H. and St. Julien, P. 1978. The Baie Verte - Brompton Line in Newfoundland and regional correlations in the Canadian Appalachians. Current Research: Geological Survey of Canada Paper 78-1A, p. 225 - 229.

Williams, H, Colman-Sadd, S.P., Swinden, H.S. 1988. Tectonic - stratigraphic subdivisions of central Newfoundland. *In* Current Research, Part B. Geological Survey of Canada, Paper 88-1B, pp. 91 - 98.

Williams, H, Kennedy, M.J. and Neale, E.R.W. 1974. The northeastward termination of the Appalachian Orogen. *In* The ocean basins and margins, Volume 2: The north Atlantic. *Edited by* A.E.M. Nairn and Francis G. Stehli. Plenum Press, New York, pp. 79 - 119.

Winchester, J.A. and Floyd, P.A. 1977. Geochemical discrimination diagrams on different magma series and their differentiation products using immobile elements. Chemical Geology, **20**: 325 - 343.

Winter, L.S. 1999. Report on mapping and lithogeochemistry at the Shamrock Property, Licence 6217m, NTS 2E/12 Notre Dame Bay, Newfoundland. Unpublished Report prepared for Altius Minerals Corporation

Woakes, M. 1954. A microscopic study of the ore sulphides from the Buchans mine, Buchans, Newfoundland. Unpublished B.Sc. Thesis. Royal School of Mines, London, 59 p.

Wood, D.A. 1980. The application of a Th - Hf - Ta diagram to problems of tectonomagmatic classification and to establishing the nature of crustal contamination of basaltic lavas of the British Tertiary volcanic province. Earth and Planetary Science Letters, **50**: 11 - 30.

Wright, C., Wright, J.A. and Hall, J. 1994. Seismic reflection techniques for base metal exploration in eastern Canada: examples from Buchans, Newfoundland. Journal of Applied Geophysics, **32**: 105 - 116.

Appendix A

APPENDIX A

A.1 General Sample Collection and Preparation

Samples were collected from the drill core stored at the government core shed building at Buchans. A few samples were also collected from outcrop in the Buchans area. Samples from core were cut with a rock saw at the core shed so that half of the sample could be placed back in the core racks. Outcrop samples were trimmed of all weathered surfaces to ensure a fresh sample. Samples were selected for study with one portion for thin section, one for a representative hand specimen and the largest portion for analysis.

Samples were crushed in a steel jaw crusher to reduce to the samples to ~ 1 cm size chips and then placed in a tungsten-carbide bowl-puck mill and ground for ~1 minute to reduce the sample to a very fine powder (-200 mesh/74 μ). All processing occurred at the Department of Earth Sciences, Memorial University. The powder preparation was the initial step for whole rock analysis (*e.g.*, ICP-MS, ICP-AES, XRF).

Thin sections were produced at the Department of Earth Sciences, Memorial University. Each sample selected for geochemical analysis was also used to produce a polished thin section. Polished thin sections were used for general petrographic examination as well as for microprobe analysis.

A.2 X-Ray Fluorescence Technique

All X-Ray Fluorescence (XRF) analyses were carried out at the Department of Earth Sciences, Memorial University of Newfoundland, using pressed powder pellets on a

Fisons/ARL (Mississauga, Ontario, Canada) model 8420+ sequential wavelength-dispersive x-ray spectrometer. Analyses are reported for 30 elements, including quantitative (P, S, Cl, K, Ca, Sc, Ti, V, Cr, Mn, Fe, Ni, Cu, Zn, Ga, As, Rb, Sr, Y, Zr, Nb, Ba, Ce, Pb, Th and U) and semi-quantitative (Na, Mg, Al, Si). The analytical technique, including sample preparation, limits of detection, precision and accuracy are discussed in detail by Longerich (1995) and the following briefly summarizes these topics.

Pressed powder pellets are prepared by mixing 5.00 g of rock powder with 0.70 g of BRP-5933 Bakelite phenolic resin (Bakelite Thermosets, Brampton, Ontario, Canada) in a 100 ml glass jar. Two 1.25 cm diameter stainless steel ball bearings were added and a plastic lid attached. The jar is placed on a roller mixer for 10 minutes or longer to ensure complete mixing. The powder is placed in a Herzog (Germany) pellet press (29 mm diameter mould) and pressed for 5 s at a pressure of 20 tonnes. Finally, the pellets are baked for 15 minutes at a temperature of 200°C. Care was taken to ensure all utensils were thoroughly cleaned prior to use.

Twenty samples were analysed per run, along with four quality control samples (AGV-1, DNC-1, JG-2, and BCR-1) and four repeats of six reference materials (DTS-1, BHVO-1, SY-2, SY-3, SiO_2 and PACS-1). Data are collected by an automated computer system attached to the XRF. An in-house written program is used to transfer the raw data from the XRF to a spreadsheet format where the data are reduced using commercial spreadsheet software on a personal computer.

Detection limits vary as the data acquisition protocol is based the geological

abundances of the elements. For example, detection limits for major oxides are generally 100's of ppm whereas trace elements such as Zr, Y and Nb are around 1 ppm or less. The limits of detection for all elements analysed are provided by Longerich (1995).

A.3 Precision and Accuracy

Fourteen analyses of a standard (DNC-1, diabase) are considered from the period of December 1997 to June 1998 (refer to Table A-1). The XRF runs that were selected represent the runs that contained the data included in this thesis. Precision is typically considered good (RSD of 3-7%) to excellent (RSD < 3%) for all major oxide data. All trace element data also yield good to excellent accuracy and precision, with the exceptions of Zn, Pb, Ba, Ga, Rb, Sc, and Nb. Many of these elements, notably Nb, have very low concentrations in this standard which cause the unusually high RSD values (*e.g.*,., the average concentration of Nb in the standard DNC-1 is 1.6 ppm which is below the limit of quantification, 2.3 ppm). Longerich (1995) lists a long term Nb RSD value of 0.16% and typically all RSD values of the lower concentration elements are lower in that study as compared with this report.

Accuracy is considered good (RD from 3-7%) to excellent (RD < 3%) for all elements analysed, with minor exceptions occurring at P_2O_5, S and Zn (Table A-1) More importantly, Nb has a RD ~ -15% indicating poor accuracy. However, as stated above the low concentration of this element in the standard contributes significantly to the erroneous statistical value.

Finally, although the light major elements (Na, Mg, Al, Si) are considered semi-quantitative (Longerich, 1995), they do yield good to excellent accuracy and precision. Therefore, caution has been exercised in the use of data and the interpretations derived are considered valid.

Table A-1 - Precision and accuracy for XRF analysis of standard DNC-1. Data represent fourteen analyses from December 1997 to June 1998.

Element[1]	Minimum	Maximum	Std. Deviation	Mean (n=14)	Quoted MUN Values[1,2]	RSD (%)[3]	RD (%)[4]
Na_2O	1.92	2.06	0.04	2.02	1.94	1.76	4.02
MgO	9.75	10.25	0.11	10.01	9.9	1.11	1.07
Al_2O_3	18.18	19.09	0.20	18.61	17.67	1.07	5.31
SiO_2	42.56	44.49	0.46	43.58	43.56	1.05	0.04
P_2O_5	0.09	0.10	0.00	0.10	0.09	4.83	7.93
K_2O	0.25	0.27	0.00	0.26	0.26	1.82	0.27
CaO	10.83	11.26	0.11	11.02	11.02	1.00	-0.02
TiO_2	0.44	0.46	0.01	0.45	0.45	1.82	0.64
MnO	0.14	0.15	0.01	0.15	0.15	3.53	-2.87
$Fe_2O_{3(total)}$	9.90	10.24	0.09	10.05	10.12	0.93	-0.73
S	1093	1168	24.5	1134	1032	2.16	9.90
Zn	45	58	4	50	60	7.80	-17.28
Ga	13	17	1	15	14	10.10	4.44
Rb	2.0	4.5	0.6	3.5	3.4	17.05	3.76
S	141.8	145.6	1.1	143.5	142.2	0.74	0.93
Y	14.9	16.8	0.6	16.1	15.9	3.72	1.03
Zr	34.0	36.0	0.6	35.2	36.0	1.77	-2.25
Nb	0.0	3.6	0.6	1.6	1.9[5]	40.03	-14.93
Cu	79	88	2	84	87	2.79	-3.22
Ni	233	248	4	239	252	1.64	-4.97
Cr	295	307	4	301	307	1.35	-1.86
V	131	150	6	144	148	3.85	-2.61
Sc	25	43	5	32	31	16.60	2.77
Ba	90	135	14	113	115	11.97	-1.49
Pb	1	11	3	7	7	36.67	-6.44

[1] Major element oxides reported as wt. % and traces reported as ppm. [2] Data represent extended duration means of Longerich (1995). [3] RSD is relative standard deviation (standard deviation/mean). [4] RD is the relative difference to the standard value [(mean-quoted value)/quoted value]. [5] Nb values in this standard are below the limit of quantification (Nb=2.3ppm). RSD for Nb from Longerich (1995) is 0.16%.

Table A-2 - Pressed pellet XRF data from the Lucky Strike area. Rock type based on immobile element ratios (*cf.* Winchester and Floyd, 1977). SLF Basalt = Sandy lake Formation basalt, And-Bas = Ski Hill Formation Andesitic-Basalt, Dacite = Buchans River Formation dacite, Rhyodacite = Buchans River Formation rhyodacite.

Sample	LS-09	LS-01	LS-03	LS-06	LS-07
Drill Hole	542	*Outcrop*	196	542	542
From	564	*at Ski Hill*	146	8	262
To	566	-	148	10	265
Rock Type	SLF Basalt	And-Bas	And-Bas	And-Bas	And-Bas
SiO2	37.51	51.92	51.89	69.35	47.93
TiO2	0.93	0.74	0.62	0.10	0.76
Al2O3	13.09	14.12	19.11	6.06	17.17
Fe2O3	12.29	9.36	9.95	8.63	11.44
MnO	0.22	0.18	0.66	0.11	0.41
MgO	10.13	3.76	12.29	7.83	7.81
CaO	11.54	8.22	0.43	0.12	0.48
Na2O	2.07	1.74	0.74	0.06	1.67
K2O	1.14	1.16	2.43	0.47	2.17
P2O5	0.22	0.12	0.10	0.02	0.11
LOI	7.78	2.81	6.48	7.79	5.16
Total	96.92	94.13	104.70	100.54	95.11
Cr	440	<LD	165	113	51
Ni	112	<LD	21	<LD	6
Sc	36	27	40	9	36
V	301	210	344	79	357
Cu	60	41	<LD	3087	9
Pb	4	14	26	4041	15
Zn	47	49	356	5341	241
S	142	211	8628	59064	5079
As	21	<LD	38	53	38
Rb	28.3	26.7	41.0	9.0	34.0
Ba	610	800	635	5514	893
Sr	320.1	363.7	18.0	83.6	55.3
Ga	16	15	19	28	18
Nb	6.3	2.9	2.2	2.1	1.0
Zr	96.4	72.4	44.2	10.1	58.6
Y	19.1	21.8	13.7	3.1	13.6
Th	<LD	5	5	<LD	3
U	<LD	<LD	4	<LD	<LD
Ce	<LD	59	<LD	<LD	<LD
Cl	116	129	66	85	7

Table A-2 - (continued) Pressed pellet XRF data from the Lucky Strike area.

Sample	LS-12	LS-20	LS-22	LS-23	LS-27
Drill Hole	237	2889	2889	2891	2871
From	864	385	537	258	270
To	866	388	540	260	272.5
Rock Type	And-Bas?	And-Bas	And-Bas?	And-Bas	And-Bas
SiO2	48.95	36.24	48.47	48.45	59.08
TiO_2	0.53	0.48	0.87	0.62	0.32
Al2O3	15.02	11.00	16.11	18.88	11.98
Fe2O3	11.34	12.05	11.82	9.43	6.73
MnO	0.78	1.44	0.15	0.17	0.40
MgO	11.14	11.00	6.95	8.23	10.83
CaO	1.03	11.27	3.13	0.28	1.11
Na2O	2.25	1.10	0.68	0.14	0.29
K2O	0.67	0.43	2.84	3.19	1.38
P2O5	0.10	0.05	0.12	0.08	0.05
LOI	0.00	12.50	6.84	0.00	5.52
Total	91.81	97.56	97.98	89.47	97.69

Cr	509	719	10	843	90
Ni	94	128	<LD	139	12
Sc	52	49	34	67	20
V	345	299	386	388	197
Cu	70	50	75	12	463
Pb	64	18	39	26	1649
Zn	290	273	163	196	11328
S	2631	454	1884	5647	16503
As	31	<LD	61	114	24
Rb	11.4	6.2	54.2	51.9	25.4
Ba	400	258	821	1354	2064
Sr	103.9	74.8	83.0	12.8	19.5
Ga	15	10	19	17	24
Nb	1.0	<LD	2.5	1.0	1.0
Zr	32.0	24.0	63.2	34.5	25.3
Y	10.6	11.4	17.2	13.2	10.4
Th	<LD	<LD	4	<LD	<LD
U	<LD	<LD	<LD	<LD	4
Ce	<LD	46	<LD	<LD	<LD
Cl	48	299	39	44	73

Table A-2 - (continued) Pressed pellet XRF data from the Lucky Strike area.

Sample	LS-28	LS-29	LS-32	LS-35	LS-36
Drill Hole	2871	2871	2892	202	202
From	444.5	601.5	264	205	214
To	447	604	265	207	216
Rock Type	And-Bas	And-Bas	And-Bas	And-Bas	And-Bas
SiO2	43.71	49.56	50.05	29.84	66.56
TiO_2	0.65	0.47	0.54	0.81	0.56
Al2O3	11.01	12.58	16.47	15.34	16.26
Fe2O3	12.24	11.39	9.23	10.71	2.38
MnO	0.77	0.76	0.70	0.63	0.11
MgO	13.69	13.58	9.40	31.93	8.44
CaO	7.92	0.73	3.72	0.30	0.56
Na2O	0.17	1.98	0.09	0.20	0.18
K2O	0.58	0.03	1.70	0.46	3.30
P2O5	0.10	0.06	0.05	0.10	0.11
LOI	8.16	5.41	7.63	0.00	0.00
Total	99.00	96.55	99.58	90.32	98.46
Cr	39	99	755	83	9
Ni	<LD	17	137	19	<LD
Sc	32	43	42	47	26
V	317	290	335	394	121
Cu	9	58	63	23	30
Pb	42	243	78	697	724
Zn	294	2545	748	939	1337
S	14180	9204	3861	4350	8372
As	16	<LD	52	215	137
Rb	10.3	1.0	25.3	7.2	51.7
Ba	5092	129	642	446	4251
Sr	57.0	22.4	39.1	16.6	61.0
Ga	11	17	15	23	14
Nb	2.0	<LD	<LD	2.7	2.6
Zr	39.0	35.8	26.9	60.5	67.0
Y	24.4	9.8	10.1	16.1	14.8
Th	5	<LD	<LD	<LD	<LD
U	<LD	<LD	5	<LD	<LD
Ce	<LD	<LD	55	97	73
Cl	75	89	88	54	88

Table A-2 - (continued) Pressed pellet XRF data from the Lucky Strike area.

Sample	LS-37	LS-38	LS-39	LS-40	LS-41
Drill Hole	**202**	**202**	**202**	**202**	**202**
From	**557**	**608**	**686**	**835**	**914**
To	**560**	**611**	**688**	**837**	**916**
Rock Type	**And-Bas**	**And-Bas**	**And-Bas**	**And-Bas**	**And-Bas**
SiO2	44.81	50.15	54.10	47.73	34.38
TiO_2	0.33	0.24	0.58	0.53	0.69
Al2O3	10.47	9.67	13.63	13.50	14.54
Fe2O3	12.13	12.69	9.51	10.99	18.79
MnO	0.73	0.33	0.49	0.59	0.86
MgO	19.39	14.75	12.64	15.11	19.60
CaO	5.15	0.57	0.62	0.38	0.47
Na2O	0.12	0.30	2.86	1.42	0.48
K2O	0.03	0.37	0.10	0.28	0.09
P2O5	0.04	0.04	0.10	0.08	0.08
LOI	0.00	0.00	0.00	0.00	0.00
Total	93.20	89.11	94.63	90.61	89.98

Cr	537	18	101	84	39
Ni	122	<LD	24	21	8
Sc	45	10	34	21	37
V	262	191	259	249	404
Cu	310	396	4	8	4
Pb	658	2030	11	14	41
Zn	953	9881	163	249	387
S	7187	51937	7909	5022	20924
As	<LD	49	<LD	<LD	34
Rb	<LD	7.3	2.3	6.2	1.7
Ba	68	1267	1069	99	<LD
Sr	14.1	20.9	62.6	23.1	12.6
Ga	18	34	11	14	21
Nb	0.8	<LD	2.0	1.6	1.9
Zr	20.7	17.2	45.3	46.1	50.2
Y	13.2	7.0	11.7	10.9	11.3
Th	<LD	4	<LD	<LD	4
U	<LD	<LD	<LD	<LD	<LD
Ce	<LD	<LD	<LD	<LD	<LD
Cl	81	53	134	107	38

Table A-2 - (continued) Pressed pellet XRF data from the Lucky Strike area.

Sample	LS-42	LS-43	LS-44	LS-45	M17509
Drill Hole	202	202	202	202	Outcrop at
From	939	1031	1095.5	1214	Ski Hill
To	941	1032	1098	1216	
Rock Type	And-Bas	And-Bas	And-Bas	And-Bas	And/Bas
SiO2	60.35	48.49	46.22	46.01	53.8
TiO_2	0.77	0.63	0.71	0.62	0.67
Al2O3	13.11	13.23	12.27	12.57	15.87
Fe2O3	8.66	11.96	13.45	13.68	9
MnO	0.38	0.63	0.62	0.57	0.16
MgO	9.48	16.17	15.40	15.24	2.75
CaO	0.84	0.41	1.27	1.28	8.57
Na2O	1.81	1.42	0.98	1.41	2.26
K2O	0.87	0.05	0.08	0.08	0.87
P2O5	0.17	0.09	0.13	0.08	0.07
LOI	0.00	0.00	0.00	0.00	n/a
Total	96.44	93.08	91.13	91.54	94.31
Cr	<LD	32	9	32	12
Ni	<LD	<LD	<LD	<LD	bdl
Sc	23	30	24	27	21
V	121	278	264	298	311
Cu	4	12	10	21	89
Pb	30	12	43	84	12
Zn	190	218	292	265	20
S	13442	7515	21081	20396	446
As	<LD	<LD	29	26	bdl
Rb	18.7	1.3	2.0	1.9	20.2
Ba	221	<LD	41	37	483
Sr	31.3	18.9	22.0	27.2	295.2
Ga	15	15	16	18	15
Nb	3.8	2.2	3.3	2.2	bdl
Zr	114.3	44.7	73.0	43.8	42.4
Y	22.5	6.9	17.0	10.3	15.3
Th	8	4	5	4	bdl
U	<LD	<LD	<LD	<LD	bdl
Ce	<LD	<LD	<LD	<LD	23
Cl	82	103	84	73	102

Table A-2 - (continued) Pressed pellet XRF data from the Lucky Strike area.

Sample	LS-08	LS-11	LS-16	LS-17	LS-18
Drill Hole	542	237	2889	2889	2889
From	376	703	17	167	214
To	378	705	18	170	216
Rock Type	Dacite	Dacite	Dacite?	Dacite	Dacite
SiO2	70.11	62.69	65.28	49.82	67.64
TiO_2	0.41	0.66	0.00	0.60	0.35
Al2O3	17.73	23.80	0.63	19.14	18.57
Fe2O3	1.58	2.80	11.70	8.74	2.91
MnO	0.02	0.05	0.00	0.44	0.22
MgO	1.38	1.79	0.10	6.62	3.02
CaO	0.26	0.05	0.38	0.68	0.43
Na2O	0.56	0.35	0.01	0.53	0.81
K2O	4.02	5.24	0.04	3.33	3.68
P2O5	0.06	0.13	0.04	0.12	0.07
LOI	3.11	0.00	10.07	5.95	0.00
Total	99.23	97.56	88.25	95.97	97.70
Cr	<LD	27	94	33	<LD
Ni	<LD	<LD	<LD	<LD	<LD
Sc	10	45	<LD	27	15
V	16	252	<LD	219	34
Cu	36	151	18082	14	18
Pb	1493	36	1620	46	25
Zn	3031	27	3661	406	541
S	9677	9632	111516	9385	3543
As	32	66	186	41	<LD
Rb	63.0	80.2	<LD	56.2	61.5
Ba	1524	1683	35509	1117	1096
Sr	23.8	24.9	497.6	19.0	23.3
Ga	23	17	<LD	20	16
Nb	4.5	2.6	<LD	5.0	5.6
Zr	159.2	66.1	<LD	124.1	173.4
Y	31.7	19.3	1.2	26.1	33.8
Th	<LD	<LD	<LD	7	8
U	<LD	<LD	<LD	<LD	4
Ce	42	<LD	<LD	64	74
Cl	100	50	49	57	91

Table A-2 - (continued) Pressed pellet XRF data from the Lucky Strike area.

Sample	LS-19	LS-26	LS-34	LS-46	LS-05
Drill Hole	**2889**	**2871**	**202**	**2865**	**196**
From	**279**	**177.5**	**194.5**	**3209.5**	**579.5**
To	**281**	**180.5**	**195.5**	**3211**	**583.5**
Rock Type	**Dacite**	**Dacite**	**Dacite**	**Dacite**	**Dacite**
SiO2	63.98	50.49	31.60	62.83	73.21
TiO_2	0.36	0.27	0.30	0.12	0.33
Al2O3	17.99	10.42	10.18	21.95	13.97
Fe2O3	2.21	1.56	2.97	1.69	1.80
MnO	0.15	0.04	0.49	0.03	0.03
MgO	2.84	4.29	33.13	0.98	0.90
CaO	0.30	1.68	8.51	0.55	0.16
Na2O	0.38	0.84	0.30	0.43	0.22
K2O	3.93	2.31	0.01	4.21	3.36
P2O5	0.06	0.04	0.04	0.07	0.04
LOI	3.18	3.48	0.00	0.00	2.87
Total	95.38	75.42	87.53	92.86	96.88
Cr	16	55	<LD	<LD	20
Ni	<LD	<LD	<LD	<LD	<LD
Sc	6	<LD	14	<LD	14
V	19	<LD	<LD	7	38
Cu	48	259	<LD	<LD	482
Pb	1029	1646	72	<LD	2910
Zn	3648	3895	493	7	5239
S	4780	25227	566	270	11673
As	15	63	<LD	17	33
Rb	66.2	42.0	1.0	83.5	59.6
Ba	1486	95063	180	654	1491
Sr	15.3	943.1	59.5	52.4	15.2
Ga	21	<LD	13	16	29
Nb	5.8	2.9	4.6	3.5	3.9
Zr	176.1	119.7	164.1	95.4	131.9
Y	34.9	25.3	34.9	7.1	26.9
Th	8	<LD	6	6	<LD
U	4	<LD	<LD	<LD	<LD
Ce	92	<LD	65	<LD	119
Cl	95	109	170	107	90

Table A-2 - (continued) Pressed pellet XRF data from the Lucky Strike area.

Sample	LS-04	LS-10	LS-13	LS-14	LS-24
Drill Hole	196	237	237	243	2871
From	525	441	1025	561	88
To	527	443	1027	563	89
Rock Type	Rhyodac	Rhyodac	Rhyodac	Rhyodac	Rhyodac
SiO2	58.64	76.00	55.27	60.65	76.76
TiO_2	0.17	0.11	0.24	0.27	0.13
Al2O3	15.19	11.06	18.59	24.50	10.62
Fe2O3	5.25	4.35	2.87	1.38	0.93
MnO	0.28	0.01	0.07	0.01	0.03
MgO	9.29	1.04	4.76	1.44	0.46
CaO	1.81	0.18	3.14	0.28	1.59
Na2O	0.07	0.06	0.57	0.24	3.06
K2O	2.54	2.33	3.06	5.10	1.40
P2O5	0.02	0.01	0.02	0.01	0.03
LOI	4.41	4.58	6.05	4.23	1.19
Total	97.67	99.73	94.64	98.11	96.20
Cr	<LD	<LD	<LD	<LD	<LD
Ni	<LD	<LD	<LD	<LD	<LD
Sc	<LD	<LD	7	6	<LD
V	59	32	17	24	9
Cu	<LD	15	<LD	74	<LD
Pb	19	159	24	3110	17
Zn	223	26	76	4308	222
S	1591	32208	222	9377	129
As	<LD	251	<LD	49	<LD
Rb	34.0	24.0	61.6	71.2	25.2
Ba	6513	2584	2760	14378	1368
Sr	50.9	23.1	76.9	199.9	143.5
Ga	19	6	13	23	9
Nb	5.7	3.8	6.5	5.9	5.4
Zr	110.2	60.4	140.8	146.3	78.0
Y	11.1	4.9	19.0	13.6	11.5
Th	10	18	11	7	7
U	6	<LD	<LD	5	5
Ce	<LD	<LD	80	108	43
Cl	56	85	60	41	138

Table A-2 - (continued) Pressed pellet XRF data from the Lucky Strike area.

Sample	LS-25	LS-33	LS-02	*M16969H*
Drill Hole	**2871**	**202**	**25**	**2871**
From	**116.5**	**108**	**57**	**58.75**
To	**117.5**	**111**	**61**	**60**
Rock Type	**Rhyodac**	**Rhyodac**	**Rhyodac**	**Rhyodac**
SiO2	59.60	63.64	69.79	**77.64**
TiO_2	0.18	0.24	0.22	0.13
Al2O3	19.23	22.13	14.26	10.63
Fe2O3	2.10	1.80	2.32	0.8
MnO	0.05	0.05	0.08	0.03
MgO	5.22	5.71	2.54	0.69
CaO	1.42	1.00	1.08	0.97
Na2O	0.54	0.98	2.76	3.39
K2O	4.04	3.89	2.04	1.77
P2O5	0.02	0.03	0.03	0.03
LOI	0.00	0.00	1.85	n/a
Total	92.41	99.47	96.97	96.44

Cr	<LD	<LD	15	77
Ni	<LD	<LD	<LD	-
Sc	7	9	<LD	6
V	13	8	17	6
Cu	<LD	<LD	4	-
Pb	9	55	27	4
Zn	84	320	34	15
S	71	104	152	564
As	<LD	<LD	<LD	23
Rb	82.6	76.0	40.7	24.9
Ba	2541	2017	878	1421
Sr	171.6	114.0	197.6	96.4
Ga	11	12	9	6
Nb	6.2	8.1	5.4	5.0
Zr	115.0	138.3	105.7	75.8
Y	16.1	17.4	12.8	13.8
Th	13	15	10	7
U	4	<LD	<LD	4
Ce	<LD	68	53	30
Cl	82	89	107	133

Table A-3 - Pressed pellet XRF data from the Middle Branch Zone. Rock type based on immobile element ratios (*cf.* Winchester and Floyd, 1977). Dacite = Buchans River Formation dacite, And/Bas = Ski Hill Formation andesitic-basalt, SLF Basalt = Sandy Lake Formation basalt, LHF dacite = Lundberg Hill Formation dacite.

Sample	**MB-10**	**MB-01**	**MB-02**	**MB-03**	**MB-04**
DDH	**1916**	**1662**	**1662**	**1683**	**1798**
From	**1819.5**	**1052.0**	**1500.5**	**1267.0**	**1463.5**
To	**1822.5**	**1054.0**	**1502.5**	**1269.0**	**1465.0**
Rock Type	**And/Bas**	**Dacite**	**Dacite**	**Dacite**	**Dacite**
SiO2	50.05	48.27	62.66	71.15	75.44
TiO_2	0.76	0.40	0.47	0.32	0.30
Al2O3	13.41	13.74	20.66	11.98	14.13
Fe2O3T	10.93	0.63	0.86	0.84	0.47
MnO	0.17	0.00	0.02	0.00	0.01
MgO	4.26	0.72	2.31	0.39	0.45
CaO	6.16	0.72	0.91	0.74	2.29
Na2O	1.84	1.35	1.09	0.53	0.45
K2O	1.12	5.79	5.57	6.27	6.05
P2O5	0.08	0.05	0.04	0.05	0.05
LOI	2.41	3.31	3.13	1.60	2.18
Total	89.11	92.02	95.28	96.42	101.38
Cr	<LD	23	<LD	16	<LD
Ni	<LD	<LD	<LD	<LD	<LD
Sc	25	<LD	18	10	<LD
V	274	<LD	<LD	8	<LD
Cu	71	97	<LD	69	19
Pb	16	1514	38	592	205
Zn	53	3703	37	2182	483
S	291	29018	1417	7876	3173
As	15	131	42	88	31
Rb	24.0	73.8	86.9	85.1	59.9
Ba	869	110053	2234	15758	7108
Sr	375.6	1854.1	69.5	160.0	100.8
Ga	19	<LD	12	7	<LD
Nb	1.5	4.3	6.4	5.4	6.1
Zr	64.0	164.8	215.5	146.3	143.9
Y	20.2	28.6	41.2	28.1	27.2
Th	6	<LD	11	<LD	5
U	<LD	6	<LD	<LD	<LD
Ce	<LD	<LD	131	<LD	88
Cl	121	45	76	103	136

Table A-3 - (continued) Pressed pellet XRF data from the Middle Branch Zone.

Sample	MB-05	MB-07	MB-08	MB-09	MB-11
DDH	**1662**	**1778**	**1910**	**1910**	**1798**
From	**1244.0**	**1537.0**	**1791.0**	**2006.0**	**1348.0**
To	**1246.0**	**1539.0**	**1792.7**	**2008.0**	**1350.0**
Rock Type	**Dacite**	**Dacite**	**Dacite**	**Dacite**	**Dacite**
SiO2	68.62	68.63	64.91	57.75	65.13
TiO_2	0.36	0.33	0.35	0.53	0.43
Al2O3	14.13	13.85	15.54	21.89	15.67
Fe2O3T	1.62	2.82	1.41	2.77	1.51
MnO	0.03	0.03	0.02	0.05	0.01
MgO	0.34	0.62	0.86	2.69	0.72
CaO	2.68	2.66	2.99	0.42	2.10
Na2O	4.01	4.12	2.19	0.33	2.51
K2O	2.22	2.34	3.10	5.69	3.97
P2O5	0.06	0.09	0.05	0.07	0.07
LOI	1.83	1.66	3.96	3.64	2.77
Total	94.28	95.81	96.57	92.54	95.64
Cr	<LD	20	<LD	<LD	<LD
Ni	<LD	<LD	<LD	<LD	<LD
Sc	<LD	13	15	15	11
V	<LD	40	<LD	13	19
Cu	<LD	<LD	27	<LD	30
Pb	3	10	518	8	691
Zn	32	8	580	37	688
S	133	185	10690	409	7950
As	16	<LD	218	<LD	214
Rb	33.6	44.5	49.7	105.4	59.5
Ba	927	1444	19999	1505	11165
Sr	139.7	272.6	338.6	23.8	238.7
Ga	13	14	<LD	19	16
Nb	6.4	7.3	5.1	8.3	5.5
Zr	172.9	153.7	174.2	232.1	183.1
Y	31.9	27.1	31.6	45.3	38.2
Th	8	9	<LD	11	6
U	<LD	<LD	<LD	<LD	4
Ce	88	96	<LD	92	131

Table A-3 - (continued) Pressed pellet XRF data from the Middle Branch Zone.

Sample	MB-14	MB-15	MB-13	MB-12	MB-06
DDH	**1768**	**1768**	**1768**	**1768**	**1778**
From	**1572.5**	**1627.0**	**1144.0**	**873.0**	**975.0**
To	**1575.5**	**1630.0**	**1146.0**	**876.0**	**978.0**
Rock Type	**Dacite**	**Dacite**	**SLF Basalt**	**LHF dacite**	**LHF dacite**
SiO2	62.75	60.80	45.19	62.13	60.17
TiO_2	0.46	0.41	0.99	0.22	0.19
Al2O3	14.10	17.79	18.78	15.74	13.01
Fe2O3T	2.64	1.34	5.35	7.64	10.41
MnO	0.05	0.02	0.10	0.08	0.13
MgO	0.84	2.36	2.00	2.10	1.72
CaO	3.42	1.29	10.17	1.49	2.33
Na2O	4.14	0.73	2.52	1.05	1.68
K2O	1.78	5.33	3.06	2.63	1.62
P2O5	0.07	0.06	0.20	0.03	0.03
LOI	2.33	3.85	8.24	4.58	5.39
Total	91.73	96.06	89.69	99.06	99.21
Cr	<LD	<LD	<LD	<LD	<LD
Ni	<LD	<LD	<LD	<LD	<LD
Sc	13	<LD	43	10	14
V	24	<LD	433	37	34
Cu	<LD	56	19	3493	1400
Pb	29	401	15	73	192
Zn	29	818	74	102	209
S	4239	10973	4274	21607	30603
As	<LD	175	37	21	<LD
Rb	31.0	77.3	56.5	51.8	44.7
Ba	3166	26208	909	448	146
Sr	284.8	346.8	147.7	43.5	51.0
Ga	12	<LD	17	12	13
Nb	6.8	6.5	2.9	3.8	3.5
Zr	157.7	192.1	51.2	92.0	86.7
Y	29.9	38.8	49.0	24.2	32.2
Th	7	5	<LD	<LD	5
U	<LD	<LD	<LD	<LD	<LD
Ce	<LD	<LD	42	<LD	<LD
Cl	117	108	95	60	57

Table A-4 - Pressed pellet XRF data from the Powerhouse Alteration Zone. And/Bas = Powerhouse Zone andesitic-basaltic volcanics and dacite = Powerhouse Zone dacites (*i.e.*, Buchans Group formational names not used). Rock type based on immobile element ratios (*cf.* Winchester and Floyd, 1977).

Sample	PH-01	PH-02	PH-03	PH-08	BE-11A-85*
Drill Hole	BE-96-11	BE-96-11	BE-96-11	BE-96-11	BE-96-11
From	58.5	71.2	84.0	97.9	85.9
To	59.4	72.0	85.1	98.7	86.4
Rock Type	And/Bas	And/Bas	And/Bas	And/Bas	And/Bas
SiO2	43.12	44.50	47.25	46.34	26.51
TiO_2	0.33	0.40	0.43	0.42	0.27
Al2O3	18.61	20.99	21.87	20.05	13.18
FeO	9.94	7.46	7.03	7.76	7.50
MnO	0.06	0.17	0.12	0.23	0.54
MgO	3.30	9.39	7.66	9.98	15.43
CaO	1.16	2.45	1.12	1.98	16.11
Na2O	4.17	3.65	4.62	4.04	2.12
K2O	2.13	2.43	2.02	1.52	1.48
P2O5	0.02	0.02	0.03	0.02	0.02
LOI	8.97	7.72	6.92	6.61	n/a
Total	102.04	96.90	97.48	92.02	96.81
Cr	31	34	29	33	69
Ni	<LD	<LD	<LD	<LD	<LD
Sc	46	42	35	40	29
V	224	334	318	289	173
Cu	620	70	130	2364	5862
Pb	198	281	22	41	253
Zn	306	502	96	162	37015
S	67848	32922	30329	28368	45257
As	80	44	<LD	47	19
Rb	25.9	40.1	30.8	29.3	22.9
Ba	313	328	361	243	300
Sr	118	100	123	133	128
Ga	15	25	22	18	31
Nb	1.1	0.1	0.8	0.9	<LD
Zr	19.5	24.1	25.9	25.0	15.8
Y	7.5	12.0	17.7	4.3	74.6
Th	5	<LD	<LD	<LD	4
U	<LD	<LD	<LD	<LD	<LD
Ce	<LD	<LD	<LD	<LD	<LD
Cl	71	61	642	116	111

Table A-4 - (continued) Pressed pellet XRF data from the Powerhouse Alteration Zone.

Sample	PH-04	PH-05	PH-06	PH-07	PH-09
Drill Hole	BE-96-11	BE-96-11	BE-96-11	BE-96-11	3326
From	121.7	141.1	151.7	168.5	312
To	122.4	141.6	152.4	168.9	314
Rock Type	Dacite	Dacite	Dacite	Dacite	Dacite
SiO2	71.53	75.25	65.15	76.45	69.83
TiO_2	0.25	0.23	0.33	0.18	0.26
Al2O3	19.16	16.68	19.37	13.23	15.91
FeO	1.53	1.29	3.88	2.48	2.95
MnO	0.00	0.00	0.04	0.01	0.03
MgO	0.51	0.62	2.28	0.92	4.19
CaO	0.12	0.10	0.15	0.11	0.24
Na2O	0.44	0.22	0.33	0.16	0.78
K2O	3.75	3.46	3.80	2.63	2.54
P2O5	0.03	0.03	0.03	0.03	0.05
LOI	3.18	2.89	4.69	3.52	4.04
Total	98.69	99.35	97.28	100.58	98.23
Cr	<LD	<LD	<LD	<LD	<LD
Ni	<LD	<LD	<LD	<LD	<LD
Sc	12	14	25	10	16
V	26	39	84	23	22
Cu	22	<LD	38	6	<LD
Pb	14	11	36	14	16
Zn	785	<LD	188	55	14
S	9795	7895	17513	14923	12254
As	29	17	39	65	<LD
Rb	45.3	46.6	52.4	37.6	34.8
Ba	474	596	659	380	471
Sr	25	11	20	11	30
Ga	10	14	15	12	17
Nb	2.6	2.5	2.4	2.0	2.7
Zr	110.4	94.5	99.5	81.0	97.4
Y	11.9	15.5	23.7	15.4	20.6
Th	<LD	<LD	<LD	3	<LD
U	<LD	<LD	<LD	<LD	<LD
Ce	<LD	<LD	<LD	<LD	<LD
Cl	80	103	73	64	43

Table A-4 - (continued) Pressed pellet XRF data from the Powerhouse Alteration Zone.

Sample	PH-10	PH-11	PH-12	PH-13	PH-14
Drill Hole	**3326**	**3326**	**3326**	**3326**	**3326**
From	**193.5**	**73.8**	**379**	**133.2**	**405**
To	**195.5**	**75.3**	**380.5**	**134.7**	**406.8**
Rock Type	**Dacite**	**Dacite**	**Dacite**	**Dacite**	**Dacite**
SiO2	69.73	71.51	69.89	71.00	71.86
TiO_2	0.23	0.28	0.18	0.32	0.22
Al2O3	17.47	17.02	14.54	14.89	16.22
FeO	2.91	2.61	2.97	1.82	2.38
MnO	0.02	0.02	0.10	0.07	0.04
MgO	1.29	0.98	3.00	1.22	2.05
CaO	0.45	0.31	2.31	2.61	0.98
Na2O	0.42	0.75	0.90	4.63	0.21
K2O	3.27	3.05	2.09	0.95	3.05
P2O5	0.04	0.04	0.02	0.06	0.03
LOI	4.15	3.63	5.05	3.07	3.80
Total	101.75	98.70	101.02	96.46	100.49
Cr	<LD	<LD	<LD	<LD	<LD
Ni	<LD	<LD	<LD	<LD	<LD
Sc	11	11	12	19	15
V	17	20	13	18	12
Cu	42	10	673	<LD	<LD
Pb	439	349	47	17	26
Zn	1529	1579	94	<LD	29
S	15540	12179	15376	9328	11516
As	21	19	141	<LD	<LD
Rb	41.0	47.9	29.5	13.7	38.7
Ba	498	445	288	126	528
Sr	26	25	28	118	13
Ga	18	16	12	10	12
Nb	2.0	2.7	2.5	2.8	2.4
Zr	90.0	103.5	92.6	95.2	84.6
Y	17.8	17.3	19.0	18.7	17.9
Th	<LD	4	<LD	<LD	<LD
U	<LD	<LD	<LD	<LD	<LD
Ce	<LD	<LD	<LD	<LD	<LD
Cl	87	73	108	124	45

Table A-4 - (continued) Pressed pellet XRF data from the Powerhouse Alteration Zone.

Sample	PH-15	PH-16	PH-17	PH-18	PH-19
Drill Hole	3326	3319	3319	3319	3319
From	235.5	237	163.5	112	282.5
To	237	239.5	165.5	113.75	285
Rock Type	Dacite	Dacite	Dacite	Dacite	Dacite
SiO2	68.53	68.95	55.30	71.02	72.47
TiO_2	0.25	0.32	0.53	0.22	0.27
Al2O3	15.26	19.57	18.62	15.48	18.25
FeO	3.72	0.80	9.04	3.08	1.16
MnO	0.05	0.03	0.09	0.03	0.03
MgO	3.84	5.30	10.54	2.74	3.23
CaO	0.93	0.77	0.78	0.67	0.38
Na2O	0.97	1.42	2.38	0.23	1.12
K2O	2.37	2.50	1.55	2.98	2.56
P2O5	0.04	0.03	0.03	0.04	0.02
LOI	5.15	3.51	4.81	3.85	2.55
Total	103.21	95.56	90.77	99.02	95.23

Cr	<LD	<LD	<LD	<LD	<LD
Ni	<LD	<LD	<LD	<LD	<LD
Sc	15	22	41	8	12
V	19	52	248	20	47
Cu	327	12	40	137	30
Pb	16	8	26	10	21
Zn	29	30	176	1670	29
S	15940	409	3179	12826	1117
As	31	<LD	<LD	38	<LD
Rb	31.3	43.8	38.6	38.8	45.3
Ba	450	348	267	347	398
Sr	40	59	110	8	45
Ga	16	10	20	13	4
Nb	2.8	3.1	2.8	2.0	3.3
Zr	90.6	126.7	90.2	93.3	107.9
Y	19.7	34.4	25.7	22.8	7.6
Th	3	<LD	<LD	<LD	<LD
U	<LD	<LD	<LD	<LD	<LD
Ce	<LD	<LD	<LD	<LD	<LD
Cl	73	110	148	85	98

Table A-4 - (continued) Pressed pellet XRF data from the Powerhouse Alteration Zone.

Sample	PH-20	PH-21	PH-22	PH-23	PH-24
Drill Hole	o/c along	BE-97-19	BE-97-19	BE-97-19	BE-97-20
From	Buchans	44	169.4	184	74.5
To	River	44.5	169.7	184.3	74.8
Rocky Type	Dacite	Dacite	Dacite	Dacite	Dacite
SiO2	47.98	66.17	74.90	72.87	67.90
TiO_2	0.03	0.29	0.16	0.28	0.30
Al2O3	2.79	20.01	17.64	18.39	22.06
FeO	12.76	0.00	0.00	0.00	0.00
MnO	0.01	0.07	0.00	0.01	0.00
MgO	0.00	1.10	0.59	1.13	0.51
CaO	0.02	3.75	0.07	0.34	0.19
Na2O	0.00	0.58	0.36	0.40	0.45
K2O	0.68	3.67	3.41	3.48	4.06
P2O5	0.01	0.04	0.02	0.04	0.05
LOI	20.25	n/a	n/a	n/a	n/a
Total	123.80	100.24	99.63	109.65	100.47

Cr	<LD	<LD	<LD	<LD	<LD
Ni	<LD	<LD	<LD	<LD	<LD
Sc	<LD	11	9	10	13
V	10	53	15	22	22
Cu	51733	<LD	<LD	79	<LD
Pb	3482	10	24	80	<LD
Zn	142	<LD	<LD	55	<LD
S	120096	8047	5896	23441	2393
As	116	26	11	47	41
Rb	7.8	48.2	46.3	53.7	56.0
Ba	51	427	531	767	355
Sr	2	33	16	25	19
Ga	16	13	10	15	16
Nb	<LD	1.9	2.2	2.3	3.5
Zr	16.7	105.9	100.5	88.6	127.3
Y	5.6	21.8	19.6	24.3	23.4
Th	15	3	<LD	<LD	<LD
U	<LD	8	<LD	<LD	<LD
Ce	<LD	48	11	13	25
Cl	33	90	99	102	52

Table A-4 - (continued) Pressed pellet XRF data from the Powerhouse Alteration Zone.

Sample	BE-11-115*	BE-13-62.4*	BE-13-105*
Drill Hole	**BE-96-11**	**BE-96-13**	**BE-96-13**
From	**115.8**	**62.4**	**105.8**
To	**117.6**	**63.1**	**106.4**
Rocky Type	**Dacite**	**Dacite**	**Dacite**
SiO2	60.36	67.03	49.64
TiO_2	0.24	0.17	0.19
Al2O3	21.58	12.71	10.27
FeO	3.96	2.80	6.12
MnO	0.01	0.17	0.82
MgO	0.77	0.67	8.95
CaO	0.26	5.96	12.67
Na2O	0.66	2.06	2.61
K2O	4.90	2.45	0.67
P2O5	0.01	0.03	0.03
LOI	n/a	n/a	n/a
Total	110.72	104.61	95.40

Cr	135	180	125
Ni	<LD	<LD	<LD
Sc	16	8	20
V	20	20	21
Cu	326	142	675
Pb	36	9110	5237
Zn	6550	19055	24862
S	26934	9527	16550
As	38	<LD	<LD
Rb	56.4	38.2	13.4
Ba	633	1185	77
Sr	23	59	99
Ga	18	71	52
Nb	3.1	<LD	1.8
Zr	118.9	86.1	87.2
Y	22.1	25.1	30.4
Th	<LD	<LD	<LD
U	<LD	<LD	<LD
Ce	<LD	<LD	<LD
Cl	69	144	159

* indicates sampling by Buchans River Limited; analysis by XRF at MUN.

Table A-5 - Pressed pellet XRF data from the Woodmans Brook Zone. Rock type based on immobile element ratios (*cf.* Winchester and Floyd, 1977). Buchans Group formational names are not used.

Sample	WB-6	WB-9	WB-10	WB-12	BE-10-14*
Drill Hole	**BE-96-08**	**BE-96-10**	**BE-96-10**	**BE-96-10**	**BE-95-10**
From	**249**	**124.3**	**154.7**	**190.7**	**140**
To	**249.5**	**124.8**	**155.5**	**191.1**	**143**
Rock Type	**Basalt**	**Basalt**	**Basalt**	**Basalt**	**Basalt**
SiO2	44.11	47.50	52.57	50.16	52.01
TiO_2	0.43	0.40	0.41	0.52	0.41
Al2O3	19.74	20.10	17.76	19.00	16.81
FeO	14.33	13.23	15.82	13.40	14.78
MnO	0.21	0.20	0.22	0.43	0.32
MgO	14.12	13.78	7.13	8.50	8.09
CaO	0.21	0.16	0.50	1.37	0.30
Na2O	1.67	1.53	0.68	3.92	1.99
K2O	1.81	1.95	2.00	1.10	1.30
P2O5	0.03	0.02	0.02	0.04	0.04
LOI	7.38	5.74	5.67	4.88	n/a
Total	93.30	94.38	95.58	90.27	99.05

Cr	<LD	<LD	10	16	104
Ni	<LD	<LD	<LD	<LD	<LD
Sc	58	68	46	47	45
V	406	382	355	406	346
Cu	5	<LD	<LD	<LD	<LD
Pb	16	10	20	<LD	10
Zn	98	123	85	124	5102
S	12733	3891	10730	5374	12525
As	50	<LD	17	11	<LD
Rb	30.0	27.5	33.5	24.4	21.0
Ba	282	287	281	238	241
Sr	23.6	26.5	15.7	58.7	18.5
Ga	19	19	19	20	19
Nb	<LD	<LD	<LD	<LD	1.5
Zr	18.2	18.0	19.9	24.4	21.5
Y	8.6	10.6	8.4	11.1	10.2
Th	<LD	<LD	<LD	<LD	<LD
U	<LD	<LD	<LD	<LD	<LD
Ce	<LD	<LD	<LD	<LD	<LD
Cl	73	108	159	76	132

Table A-5 - (continued) Pressed pellet XRF data from the Woodmans Brook Zone

Sample	BE-10-18*	BE-3-111*	WB-1	WB-2	WB-3
Drill Hole	BE-95-10	BE-95-03	BE-95-01	BE-95-01	BE-95-01
From	186.1	111.7	19.4	53.2	129.7
To	186.6	112.7	20.2	53.6	130.1
Rock Type	Basalt	Tuff	Dacite	Dacite	Dacite
SiO2	40.11	70.29	60.35	69.48	68.74
TiO_2	0.34	0.26	0.39	0.34	0.36
Al2O3	14.77	15.79	15.40	19.66	16.64
FeO	18.56	3.24	10.44	1.71	5.33
MnO	0.21	0.01	0.15	0.05	0.07
MgO	6.80	0.70	4.95	1.40	3.09
CaO	0.25	0.18	0.49	0.75	0.20
Na2O	1.28	0.00	3.92	0.43	2.65
K2O	1.56	3.18	0.71	4.56	2.21
P2O5	0.03	0.04	0.05	0.05	0.05
LOI	n/a	n/a	3.38	3.47	2.27
Total	107.60	95.11	95.87	101.60	97.58

Cr	62	274	<LD	<LD	<LD
Ni	<LD	<LD	<LD	<LD	<LD
Sc	38	14	33	27	26
V	267	38	42	28	31
Cu	<LD	<LD	<LD	<LD	<LD
Pb	132	604	6	6	<LD
Zn	2440	2379	<LD	<LD	<LD
S	62433	21548	12179	5950	2132
As	57	<LD	<LD	24	14
Rb	27.3	28.0	12.5	62.0	32.8
Ba	230	1285	163	456	377
Sr	12.1	7.4	67.8	22.6	33.8
Ga	22	147	20	15	13
Nb	1.0	12.5	3.1	3.0	3.1
Zr	18.4	43.9	109.5	103.3	110.7
Y	7.5	7.6	27.1	23.6	23.6
Th	<LD	<LD	3	4	4
U	<LD	<LD	4	<LD	<LD
Ce	<LD	116	<LD	<LD	<LD
Cl	66	98	82	81	78

Table A-5 - (continued) Pressed pellet XRF data from the Woodmans Brook Zone

Sample	WB-4	WB-5	WB-7	WB-8	WB-11
Drill Hole	BE-96-08	BE-96-08	BE-96-08	BE-96-10	BE-96-10
From	18.6	109.4	281.8	114.5	78.3
To	19.1	110	282.2	115.1	78.8
Rock Type	Dacite	Dacite	Dacite	Dacite	Dacite
SiO2	68.80	55.34	70.91	68.02	65.53
TiO_2	0.33	0.35	0.31	0.22	0.34
Al2O3	18.85	15.11	18.08	13.46	18.42
FeO	2.94	12.93	1.89	4.87	3.51
MnO	0.01	0.22	0.01	0.03	0.05
MgO	0.50	9.02	1.02	1.76	2.45
CaO	0.11	0.34	0.32	1.21	1.22
Na2O	0.34	1.99	2.07	0.13	0.73
K2O	3.93	0.87	3.18	2.91	3.89
P2O5	0.05	0.05	0.06	0.03	0.05
LOI	4.23	5.34	2.82	6.20	4.38
Total	106.97	97.17	101.43	107.44	99.18
Cr	<LD	<LD	<LD	<LD	<LD
Ni	<LD	<LD	<LD	<LD	<LD
Sc	23	26	18	16	22
V	26	39	39	22	37
Cu	<LD	42	6	14	<LD
Pb	16	17	5	30	9
Zn	<LD	199	<LD	<LD	<LD
S	15988	14528	8369	29271	14657
As	135	74	25	62	15
Rb	52.3	13.4	46.4	42.8	57.5
Ba	546	164	577	466	910
Sr	10.3	27.8	35.5	27.9	23.2
Ga	13	18	16	11	17
Nb	2.8	3.1	3.0	2.8	3.0
Zr	95.3	112.1	84.8	76.4	95.8
Y	23.4	34.0	21.7	18.6	25.2
Th	3	3	<LD	3	3
U	<LD	<LD	<LD	<LD	<LD
Ce	<LD	<LD	<LD	<LD	<LD
Cl	74	94	76	74	47

Table A-5 - (continued) Pressed pellet XRF data from the Woodmans Brook Zone

Sample	WB-13	WB-14	WB-15	WB-16	WB-17
Drill Hole	BE-96-10	BE-96-10	BE-96-09	BE-95-02	BE-95-02
From	193.7	208.5	62	9.9	119.5
To	194.2	208.8	62.5	10.5	120.1
Rock Type	Volcanic sandstone	Dacite	Dacite	Dacite	Dacite
SiO2	82.37	68.48	69.62	61.14	57.03
TiO_2	0.18	0.36	0.31	0.38	0.33
Al2O3	5.61	19.21	17.79	20.67	13.91
FeO	4.19	2.53	2.85	4.83	10.89
MnO	0.05	0.07	0.03	0.02	0.19
MgO	1.83	1.36	1.88	2.10	13.75
CaO	0.31	0.91	0.15	0.14	2.66
Na2O	0.00	3.70	0.22	0.23	0.96
K2O	0.72	2.69	3.91	4.73	0.04
P2O5	0.17	0.07	0.05	0.06	0.04
LOI	2.57	2.24	3.78	5.22	5.87
Total	105.87	96.94	102.00	101.50	92.64
Cr	35	<LD	<LD	<LD	<LD
Ni	63	<LD	<LD	<LD	<LD
Sc	11	18	16	21	24
V	430	46	31	30	36
Cu	<LD	4	9	14	4
Pb	128	<LD	11	11	11
Zn	2645	16	9	49	132
S	14805	2194	12199	22264	708
As	1012	<LD	28	34	<LD
Rb	12.3	46.4	54.9	65.0	<LD
Ba	132	442	830	951	60
Sr	8.5	38.2	10.8	10.8	15.1
Ga	9	17	14	14	13
Nb	3.8	3.1	2.9	3.0	2.2
Zr	37.8	98.0	88.2	120.2	92.9
Y	11.3	29.9	22.5	26.6	21.6
Th	4	<LD	3	3	3
U	7	<LD	<LD	<LD	<LD
Ce	84	<LD	<LD	<LD	<LD
Cl	186	67	78	71	120

Table A-5 - (continued) Pressed pellet XRF data from the Woodmans Brook Zone

Sample	WB-18	WB-19	WB-20	WB-21	WB-22
Drill Hole	BE-95-03	BE-95-03	BJ-46	BJ-46	BJ-46
From	157.8	133.1	226	352	501
To	158.2	133.5	228	355	503
Rock Type	Dacite	Dacite	Dacite	Dacite	Dacite
SiO2	65.87	72.85	73.28	71.10	64.57
TiO_2	0.33	0.29	0.30	0.36	0.39
Al2O3	20.93	15.96	16.72	17.26	17.41
FeO	2.30	2.15	1.98	2.15	3.19
MnO	0.01	0.03	0.05	0.03	0.06
MgO	1.12	1.59	1.72	1.48	1.71
CaO	0.35	0.35	0.33	0.33	2.11
Na2O	1.59	2.52	1.48	2.52	3.24
K2O	4.12	2.38	3.01	2.73	2.31
P2O5	0.06	0.07	0.06	0.07	0.05
LOI	3.77	2.31	2.34	2.50	4.85
Total	100.13	100.87	96.45	98.27	97.52
Cr	<LD	<LD	<LD	<LD	<LD
Ni	<LD	<LD	<LD	<LD	<LD
Sc	25	13	15	<LD	25
V	50	30	39	32	63
Cu	<LD	17	4	<LD	<LD
Pb	10	15	6	6	8
Zn	<LD	90	87	5	<LD
S	12832	6831	3641	7584	19507
As	<LD	21	17	<LD	16
Rb	57.9	36.7	41.2	37.5	33.8
Ba	863	372	873	480	228
Sr	28.0	30.7	19.5	34.5	54.8
Ga	16	15	15	12	16
Nb	3.0	3.0	2.3	3.0	3.5
Zr	102.9	76.3	81.4	83.9	110.1
Y	28.0	21.8	22.2	18.2	25.9
Th	<LD	<LD	<LD	<LD	<LD
U	<LD	<LD	<LD	<LD	<LD
Ce	<LD	<LD	<LD	<LD	<LD
Cl	71	85	98	72	84

Table A-5 - (continued) Pressed pellet XRF data from the Woodmans Brook Zone

Sample	WB-23	WB-24	WB-25	WB-26	WB-27
Drill Hole	BJ-46	BJ-46	BJ-45	BJ-45	BJ-41
From	646	1298.5	109	149	266.5
To	647.5	1300.5	111	151	268.5
Rock Type	Dacite	Dacite	Dacite	Dacite	Dacite
SiO2	68.87	62.47	72.57	63.25	56.96
TiO_2	0.34	0.35	0.28	0.34	0.48
Al2O3	18.01	14.78	16.91	16.91	26.04
FeO	2.35	6.85	1.80	6.95	2.19
MnO	0.02	0.19	0.02	0.24	0.07
MgO	0.77	10.06	1.30	4.10	5.18
CaO	0.67	1.52	0.17	0.97	2.00
Na2O	1.53	2.46	2.22	1.69	1.58
K2O	3.32	1.03	2.86	2.57	3.44
P2O5	0.04	0.05	0.05	0.05	0.05
LOI	4.04	3.83	2.41	3.90	5.62
Total	93.99	93.64	98.32	93.41	93.61
Cr	12	<LD	<LD	<LD	13
Ni	<LD	<LD	<LD	<LD	<LD
Sc	22	29	<LD	25	26
V	48	44	26	54	48
Cu	38	<LD	24	77	<LD
Pb	32	<LD	6	50	6
Zn	449	125	<LD	433	16
S	15663	612	6772	10977	7616
As	28	<LD	16	18	<LD
Rb	48.5	20.7	41.6	41.1	43.9
Ba	361	164	675	543	329
Sr	36.5	38.8	25.0	20.6	94.4
Ga	16	15	14	16	24
Nb	3.0	3.2	2.6	3.1	3.6
Zr	108.7	107.1	85.0	115.9	131.6
Y	28.8	24.0	27.0	32.8	32.4
Th	<LD	<LD	<LD	<LD	<LD
U	<LD	<LD	<LD	<LD	<LD
Ce	<LD	<LD	<LD	<LD	<LD
Cl	62	72	87	54	71

Table A-5 - (continued) Pressed pellet XRF data from the Woodmans Brook Zone

Sample	WB-23	WB-24	WB-25	WB-26	WB-27
Drill Hole	BJ-46	BJ-46	BJ-45	BJ-45	BJ-41
From	646	1298.5	109	149	266.5
To	647.5	1300.5	111	151	268.5
Rock Type	Dacite	Dacite	Dacite	Dacite	Dacite
SiO2	68.87	62.47	72.57	63.25	56.96
TiO_2	0.34	0.35	0.28	0.34	0.48
Al2O3	18.01	14.78	16.91	16.91	26.04
FeO	2.35	6.85	1.80	6.95	2.19
MnO	0.02	0.19	0.02	0.24	0.07
MgO	0.77	10.06	1.30	4.10	5.18
CaO	0.67	1.52	0.17	0.97	2.00
Na2O	1.53	2.46	2.22	1.69	1.58
K2O	3.32	1.03	2.86	2.57	3.44
P2O5	0.04	0.05	0.05	0.05	0.05
LOI	4.04	3.83	2.41	3.90	5.62
Total	93.99	93.64	98.32	93.41	93.61
Cr	12	<LD	<LD	<LD	13
Ni	<LD	<LD	<LD	<LD	<LD
Sc	22	29	<LD	25	26
V	48	44	26	54	48
Cu	38	<LD	24	77	<LD
Pb	32	<LD	6	50	6
Zn	449	125	<LD	433	16
S	15663	612	6772	10977	7616
As	28	<LD	16	18	<LD
Rb	48.5	20.7	41.6	41.1	43.9
Ba	361	164	675	543	329
Sr	36.5	38.8	25.0	20.6	94.4
Ga	16	15	14	16	24
Nb	3.0	3.2	2.6	3.1	3.6
Zr	108.7	107.1	85.0	115.9	131.6
Y	28.8	24.0	27.0	32.8	32.4
Th	<LD	<LD	<LD	<LD	<LD
U	<LD	<LD	<LD	<LD	<LD
Ce	<LD	<LD	<LD	<LD	<LD
Cl	62	72	87	54	71

Table A-5 - (continued) Pressed pellet XRF data from the Woodmans Brook Zone

Sample	BE-3-106*	BE-8-267*	M14637S
Drill Hole	BE-95-03	BE-95-08	BE-96-08
From	106.5	267.8	357.15
To	108.2	269.6	357.55
Rock Type	Dacite	Dacite	Dacite
SiO2	67.90	65.37	68.44
TiO_2	0.27	0.28	0.38
Al2O3	17.20	14.39	17.18
FeO	3.35	5.80	3.73
MnO	0.02	0.06	0.03
MgO	0.93	3.71	1.76
CaO	0.53	0.38	0.91
Na2O	0.31	1.25	2.55
K2O	3.47	2.33	2.77
P2O5	0.04	0.04	0.06
LOI	n/a	n/a	n/a
Total	99.61	111.69	101.91
Cr	219	149	8
Ni	<LD	<LD	<LD
Sc	20	14	25
V	48	52	34
Cu	<LD	<LD	<LD
Pb	585	34	<LD
Zn	1855	191	<LD
S	21718	24226	15886
As	51	16	<LD
Rb	51.0	34.0	40.7
Ba	1351	224	432
Sr	19.8	14.4	76.1
Ga	18	15	15
Nb	2.5	1.9	3.6
Zr	70.3	75.2	97.1
Y	18.9	15.0	23.5
Th	<LD	<LD	<LD
U	<LD	<LD	<LD
Ce	<LD	<LD	<LD
Cl	103	81	307

* indicates sampling by Buchans River Limited; analysis by XRF at MUN.

Table A-6 - Pressed pellet XRF data from the Airport Alteration Zone. Rock type based on immobile element ratios (*cf.* Winchester and Floyd, 1977). Buchans Group formational names not assigned.

Sample	AP-05	AP-06	AP-07	AP-08	AP-13
Drill Hole	2845	2845	2845	2845	2837
From	719	890	912	2357	695.4
To	722	892	914	2362	697
Rock Type	And/Bas	And/Bas	And/Bas	And/Bas	And/Bas
SiO2	53.55	48.73	60.03	52.44	44.04
TiO_2	0.34	0.42	0.44	0.74	0.51
Al2O3	14.28	13.85	17.32	14.36	12.31
Fe2O3	13.69	16.53	5.40	9.32	13.97
MnO	0.23	0.27	0.11	0.16	0.58
MgO	5.62	6.73	2.68	5.32	12.17
CaO	0.78	0.25	0.36	3.84	5.69
Na2O	1.26	0.35	2.94	1.96	0.76
K2O	1.35	1.61	2.36	1.40	0.73
P2O5	0.04	0.03	0.06	0.12	0.05
LOI	5.15	8.24	3.41	3.83	7.60
Total	95.41	98.27	95.30	90.30	92.48

Cr	9	<LD	17	<LD	473
Ni	<LD	<LD	<LD	<LD	77
Sc	31	40	31	39	63
V	220	281	168	149	295
Cu	194	91	6	17	311
Pb	81	28	13	23	52
Zn	351	347	69	68	188
S	16413	37436	13899	1921	5707
As	20	33	47	<LD	11
Rb	20.7	23.8	34.7	37.0	26.1
Ba	160	128	261	638	225
Sr	26.6	9.4	74.2	348.1	46.4
Ga	13	13	12	15	13
Nb	<LD	1.9	1.0	3.3	0.9
Zr	39.0	31.5	52.9	87.0	27.3
Y	13.0	9.9	24.7	22.3	11.4
Th	4	<LD	<LD	6	<LD
U	<LD	4	<LD	4	<LD
Ce	<LD	<LD	<LD	<LD	<LD
Cl	111	122	70	94	66

Table A-6 - (continued) Pressed pellet XRF data from the Airport Alteration Zone.

Sample	AP-15	AP-14	AP-01	AP-03	AP-09
Drill Hole	**2837**	**2837**	**270**	**2846**	**395**
From	**3176**	**2148.5**	**371**	**406**	**335**
To	**3178**	**2150**	**375**	**407**	**338**
Rock Type	**And/Bas**	**And/Bas**	**Dacite**	**Dacite**	**Dacite**
SiO2	46.61	45.24	61.29	55.75	60.03
TiO_2	0.70	1.27	0.46	0.33	0.42
Al2O3	14.80	13.23	17.83	18.74	20.53
Fe2O3	12.38	11.17	1.22	4.00	1.00
MnO	0.17	0.17	0.06	0.14	0.03
MgO	7.02	7.65	5.06	1.71	4.68
CaO	7.69	8.77	5.22	6.67	0.32
Na2O	2.29	2.08	2.93	1.87	1.36
K2O	0.51	0.27	1.81	3.24	4.05
P2O5	0.07	0.21	0.26	0.15	0.07
LOI	3.18	5.74	5.31	6.50	3.19
Total	92.72	90.49	96.27	92.94	92.69

Cr	81	39	12	<LD	303
Ni	38	41	<LD	<LD	11
Sc	39	20	30	6	24
V	260	217	110	75	146
Cu	61	28	<LD	<LD	<LD
Pb	19	<LD	5	15	<LD
Zn	50	53	30	27	15
S	1019	1004	100	337	69
As	<LD	11	<LD	<LD	<LD
Rb	9.2	6.3	40.3	60.0	72.7
Ba	385	268	206	1607	702
Sr	337.6	338.4	111.8	236.4	87.9
Ga	16	16	14	15	7
Nb	3.0	7.3	4.9	2.1	2.7
Zr	49.8	124.2	118.0	86.5	112.2
Y	13.8	23.2	13.3	8.3	6.6
Th	7	<LD	4	7	<LD
U	<LD	<LD	<LD	4	<LD
Ce	<LD	<LD	<LD	79	<LD
Cl	235	200	62	67	99

Table A-6 - (continued) Pressed pellet XRF data from the Airport Alteration Zone.

Sample	AP-11	AP-02	AP-04	AP-10	AP-12
Drill Hole	**258**	**2846**	**2842**	**395**	**2837**
From	**322**	**259.5**	**573**	**141**	**510**
To	**326**	**261.5**	**575.5**	**145**	**511.5**
Rock Type	**Dacite**	**Dacite**	**Dacite**	**Dacite**	**Dacite**
SiO2	61.01	70.56	68.46	72.81	71.39
TiO_2	0.36	0.30	0.21	0.25	0.22
Al2O3	20.43	14.75	12.93	16.20	15.90
Fe2O3	1.69	2.29	8.93	1.65	1.86
MnO	0.01	0.03	0.09	0.00	0.01
MgO	2.10	1.58	1.89	0.40	1.86
CaO	0.56	1.96	0.43	0.13	0.79
Na2O	0.63	4.33	0.22	0.85	2.70
K2O	4.07	1.06	2.35	3.06	1.76
P2O5	0.04	0.05	0.04	0.02	0.04
LOI	3.51	2.69	6.24	3.40	2.57
Total	92.42	100.78	106.41	101.69	99.16
Cr	9	<LD	<LD	<LD	<LD
Ni	<LD	<LD	<LD	<LD	<LD
Sc	28	11	10	17	17
V	61	42	24	38	14
Cu	35	<LD	255	392	<LD
Pb	8	5	763	47	<LD
Zn	<LD	<LD	2233	15304	<LD
S	5514	15241	41558	16157	10333
As	<LD	<LD	68	84	<LD
Rb	51.1	18.9	30.9	42.4	23.3
Ba	685	165	346	2386	217
Sr	60.7	101.7	11.7	30.6	61.1
Ga	12	13	15	22	13
Nb	3.0	2.2	3.7	2.0	3.6
Zr	117.1	97.4	71.7	83.3	99.0
Y	24.6	24.3	13.8	14.2	25.1
Th	3	<LD	<LD	<LD	<LD
U	<LD	<LD	<LD	<LD	<LD
Ce	<LD	<LD	<LD	<LD	<LD
Cl	84	119	95	98	62

Appendix B

APPENDIX B

B.1 ICP-AES Analyses

Forty-seven samples from the LSZ were analyzed via the lithium borate fusion ICP-AES method by Intertek Testing Services - Bondar Clegg, Val-d'Or, Quebec. Sample powders were prepared at Memorial University using the method described in Appendix A1.

All oxides have lower detection limits quoted as 0.01 wt.%, except P2O5 (0.03 wt.%), and K2O and Loss on Ignition (0.05 wt.%). Trace elements Ba and Cr are quoted at 10 ppm and Sr at 5 ppm for lower limits of detection. The samples analysed included blind duplicates for samples LS-01, 10 and 41 and standards BCR-2 and SY-3. The duplicate analyses were reproduced within reasonable error. Standards also yielded results that are consistent with accepted values.

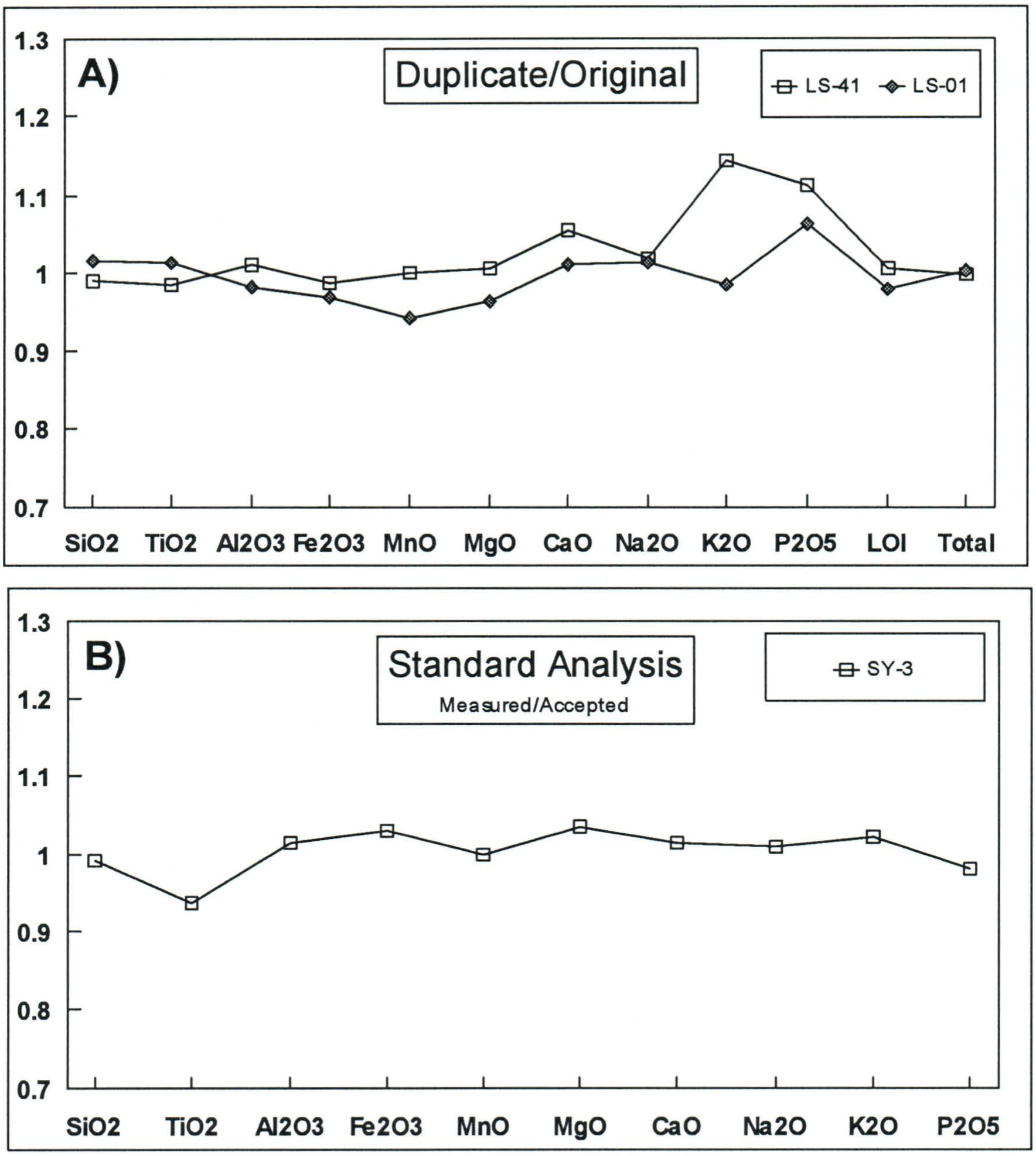


Figure B-1 - a) Duplicate and b) standards analysis from the ICP-AES method in this study. The larger peaks in plot A for K_2O and P_2O_5 result from the very low values (<0.1 wt. %) of these oxides in the samples.

Table B-1 - ICP-AES data for rocks from the Lucky Strike Zone. All intervals in feet.

Sample	LS-01	LS-01 Dup*	LS-02	LS-03	LS-04
Drill Hole	*Outcrop*	*Outcrop*	*25*	196	196
From	*at Ski Hill*	*at Ski Hill*	*57*	146	525
To			*61*	148	527
SiO2	56.37	57.21	75.12	56.01	70.83
TiO2	0.81	0.82	0.22	0.60	0.18
Al2O3	16.48	16.16	3.21	16.28	11.23
Fe2O3	8.93	8.65	2.02	10.05	4.14
MnO	0.17	0.16	0.08	0.58	0.23
MgO	2.71	2.61	1.30	7.39	5.28
CaO	7.86	7.94	1.04	0.37	1.19
Na2O	2.42	2.45	3.68	0.83	0.04
K2O	1.26	1.24	1.71	2.07	1.88
P2O5	0.16	0.17	< .03	0.08	< .03
LOI	2.74	2.68	2.02	6.53	4.60
Total	100.03	100.21	100.49	100.87	100.16
Ba	774	731	736	617	5591
Cr	<10	<10	<10	118	<10
Sr	362	365	203	18	58

Sample	LS-05	LS-06	LS-07	LS-08	LS-11
Drill Hole	196	*542*	542	542	237
From	579.5	*8*	262	376	703
To	583.5	*10*	265	378	705
SiO2	77.83	69.21	54.88	76.45	69.72
TiO2	0.32	0.13	0.77	0.42	0.65
Al2O3	10.48	4.92	18.11	12.91	16.64
Fe2O3	2.32	13.10	10.30	2.51	3.77
MnO	0.03	0.13	0.37	0.02	0.05
MgO	0.44	3.96	6.17	0.62	0.91
CaO	0.10	0.04	0.39	0.21	0.38
Na2O	0.08	0.10	2.25	0.57	0.27
K2O	2.99	0.44	1.94	3.45	4.54
P2O5	0.03	< .03	0.13	0.08	0.13
LOI	3.14	8.10	5.36	3.39	4.51
Total	97.89	100.27	100.74	100.67	100.70
Ba	1292	2256	649	1369	1519
Cr	<10	119	33	<10	13
Sr	14	32	56	24	24

Table B-1 - (continued) ICP-AES data for rocks from the Lucky Strike Zone.

Sample	LS-10	LS-10 Dup	LS-12	LS-13	LS-14
Drill Hole	237	237	237	*237*	243
From	441	441	864	*1025*	561
To	443	443	866	*1027*	563
SiO2	80.07	79.14	55.32	66.69	69.42
TiO2	0.10	0.10	0.55	0.25	0.28
Al2O3	6.21	6.58	16.55	15.51	16.41
Fe2O3	6.61	6.82	9.77	2.38	2.01
MnO	< .01	< .01	0.70	0.06	0.02
MgO	0.38	0.38	7.84	3.17	0.65
CaO	0.10	0.08	0.89	2.44	0.19
Na2O	0.04	0.05	2.84	0.63	0.12
K2O	1.66	1.65	0.64	2.77	4.36
P2O5	< .03	< .03	0.13	< .03	< .03
LOI	4.83	4.91	5.53	6.25	4.60
Total	100.22	99.95	100.84	100.38	
Ba	2263	2376	344	2291	>10000
Cr	<10	<10	447	<10	<10
Sr	24	25	108	81	215

Sample	LS-15	LS-16	LS-17	LS-18	LS-19
Drill Hole	244	*2889*	*2889*	2889	2889
From	460	*17*	*167*	214	279
To	462	*18*	*170*	216	281
SiO2	71.97	65.06	58.49	73.09	74.06
TiO2	0.42	< .01	0.66	0.37	0.40
Al2O3	8.92	0.27	17.25	13.98	14.37
Fe2O3	7.95	18.73	8.79	2.88	2.45
MnO	0.11	0.01	0.39	0.20	0.14
MgO	3.30	0.12	4.36	1.50	1.60
CaO	0.21	0.21	0.53	0.34	0.25
Na2O	0.06	0.02	0.68	1.10	0.36
K2O	1.69	< .05	3.06	3.35	3.61
P2O5	0.12	0.07	0.12	0.06	0.05
LOI	5.70	9.82	6.15	3.27	3.28
Total	100.62		100.57	100.25	100.70
Ba	1882	>10000	902	970	1290
Cr	<10	<10	16	<10	<10
Sr	27	470	20	23	17

Table B-1 - (continued) ICP-AES data for rocks from the Lucky Strike Zone.

Sample	LS-20	LS-21	LS-23	LS-24	LS-25
Drill Hole	*2889*	2889	2891	2871	2871
From	*385*	505	258	88	116.5
To	*388*	506.5	260	89	117.5
SiO2	43.62	72.80	60.18	81.61	70.12
TiO2	0.45	0.45	0.57	0.14	0.21
Al2O3	13.36	13.60	17.11	9.55	15.24
Fe2O3	9.55	1.70	8.48	0.79	1.68
MnO	1.21	0.09	0.15	0.03	0.04
MgO	9.10	0.66	5.31	0.22	2.73
CaO	8.89	2.63	0.20	1.09	1.28
Na2O	1.74	0.12	0.08	3.60	0.84
K2O	0.36	3.89	2.78	1.34	3.46
P2O5	0.05	0.07	0.08	< .03	< .03
LOI	11.17	3.78	5.58	1.15	4.91
Total	99.58	100.70	100.69	99.64	100.72
Ba	186	8965	1026	1310	1921
Cr	530	<10	702	<10	<10
Sr	78	96	13	148	178

Sample	LS-26	LS-27	LS-28	LS-29	LS-32
Drill Hole	2871	2871	2871	*2871*	2892
From	177.5	270	444.5	*601.5*	264
To	180.5	272.5	447	*604*	265
SiO2	62.42	68.13	52.94	58.26	58.27
TiO2	0.27	0.35	0.65	0.49	0.47
Al2O3	10.26	9.51	11.39	13.53	14.71
Fe2O3	1.46	7.54	11.49	10.32	7.74
MnO	0.05	0.37	0.62	0.64	0.63
MgO	2.53	5.77	9.41	8.47	6.04
CaO	1.16	0.72	4.62	0.47	3.14
Na2O	1.27	0.03	0.26	2.82	0.07
K2O	2.11	1.16	0.48	< .05	1.37
P2O5	< .03	0.06	0.12	0.06	0.06
LOI	3.87	5.35	7.97	5.72	7.62
Total		99.18	100.33	100.80	100.22
Ba	>10000	1841	3776	98	495
Cr	<10	65	15	53	540
Sr	996	21	61	23	41

Table B-1 - (continued) ICP-AES data for rocks from the Lucky Strike Zone.

Sample	LS-33	LS-34	LS-35	LS-36	LS-37
Drill Hole	**202**	**202**	**202**	**202**	**202**
From	**108**	**194.5**	**205**	**214**	**557**
To	**111**	**195.5**	**207**	**216**	**560**
SiO2	68.30	35.40	31.24	71.59	54.01
TiO2	0.25	0.33	0.81	0.56	0.38
Al2O3	16.58	12.80	19.72	12.97	10.74
Fe2O3	1.56	2.11	9.78	2.50	11.01
MnO	0.05	0.40	0.52	0.10	0.60
MgO	3.20	25.58	25.80	4.34	12.67
CaO	0.75	7.29	0.26	0.40	3.23
Na2O	0.89	0.14	0.04	0.08	0.02
K2O	3.44	< .05	0.38	2.96	< .05
P2O5	< .03	0.06	0.11	0.15	0.04
LOI	5.26	16.32	12.04	4.38	7.84
Total	100.47	100.44	100.75	100.45	100.61
Ba	1840	111	381	4256	64
Cr	<10	<10	62	<10	433
Sr	115	63	20	70	15

Sample	LS-38	LS-39	LS-40	LS-41	LS-41 Dup
Drill Hole	**202**	**202**	**202**	**202**	**202**
From	**608**	**686**	**835**	**914**	**914**
To	**611**	**688**	**837**	**916**	**916**
SiO2	51.52	58.60	56.17	39.28	38.90
TiO2	0.28	0.60	0.64	0.69	0.68
Al2O3	9.39	14.04	14.58	14.94	15.09
Fe2O3	18.08	9.01	10.23	19.99	19.75
MnO	0.32	0.42	0.53	0.69	0.69
MgO	9.10	7.26	9.88	12.65	12.70
CaO	0.40	0.49	0.34	0.37	0.39
Na2O	0.02	3.65	1.88	0.58	0.59
K2O	0.35	0.10	0.28	0.07	0.08
P2O5	0.05	0.11	0.10	0.09	0.10
LOI	10.57	4.85	5.79	10.81	10.88
Total	100.22	99.23	100.44	100.16	99.87
Ba	1273	891	93	24	18
Cr	<10	71	50	26	28
Sr	23	64	24	13	14

APPENDIX C

C.1 ICP-MS Analytical Technique

ICP-MS methods were used for quantitative determinations of the REE, Y and Th, and data were also derived for Zr, Nb, Ba, Hf and Ta. The latter elements are generally collected quantitatively (particularly Nb and Ta) by the digestion procedure but on occasion may not be (particularly Zr, Hf, Ba). These are treated as semi-quantitative and Zr, Nb and Ba concentrations from the XRF technique were used instead. It should be noted that grinding of samples in tungsten carbide-lined equipment has lead to Ta contamination. Nb, which can also be contaminated by tungsten carbide, is consistent in the data and thus, not contaminated in the data set.

The analytical procedure was as follows: (1) sintering of a 0.2 g sample aliquot with sodium peroxide, (2) dissolution of the sinter cake, separation and dissolution of REE hydroxide-bearing precipitate, (3) analysis by ICP-MS using internal standardisation to correct for matrix and drift effects. The advantage of the sintering technique is that it practically ensures complete digestion of resistant REE-bearing accessory phases (*e.g.*, zircon, fluorite) which may not dissolve during an acid digestion. Full details of the procedure are given in Longerich *et al.* (1990).

C.2 Precision and Accuracy

A pure quartz reagent blank (BLANK) and two certified geological reference standards (gabbro MRG-1 (CCRMP) and basalt BR-688 (NIST SRM 688) were prepared

and analysed with the samples. For comparison, recommended values for DNC-1, MRG-1 and W-2 are given by Govindaraju (1989). A plot of analyzed vs. quoted values are shown for MRG-1 in Figure C-1. Reagent blank concentrations are generally insignificant and have not been subtracted from sample concentrations. Samples PH-06 and LS-46 were prepared and analysed in duplicate (Figure C-2). Sample detection limits in ppm (3 standard deviations of the background) are quoted for each analytical run. Detection limits and reagent blanks are generally about 10% of chondrite values.

Several inter-element interferences are present in ICP-MS analysis. The instrument is optimised such that for most rock types the interferences are at a sufficiently low level to be adequately corrected. Problems can occur, however, for certain samples. The most significant is a Ba molecular ion interference on Eu. Although a correction is applied, at very high Ba/Eu ratios (Ba(ppm)/Eu(ppm) > 1000, chondrite-normalised Ba/Eu > 25), the interference becomes larger than the Eu signal and any error in the correction starts to be significant. Similarly, in samples with very steep LREE enriched REE patterns, the LREE interferences on the MREE become severe, particularly for Gd. Data are acquired on two Gd isotopes (^{157}Gd and ^{160}Gd). In samples with low Ba/Gd and flat or LREE depleted REE patterns, the interferences on ^{157}Gd are smaller. However, in highly Ba and/or LREE enriched samples, the interferences on ^{160}Gd are smaller and this isotope provides more reliable data.

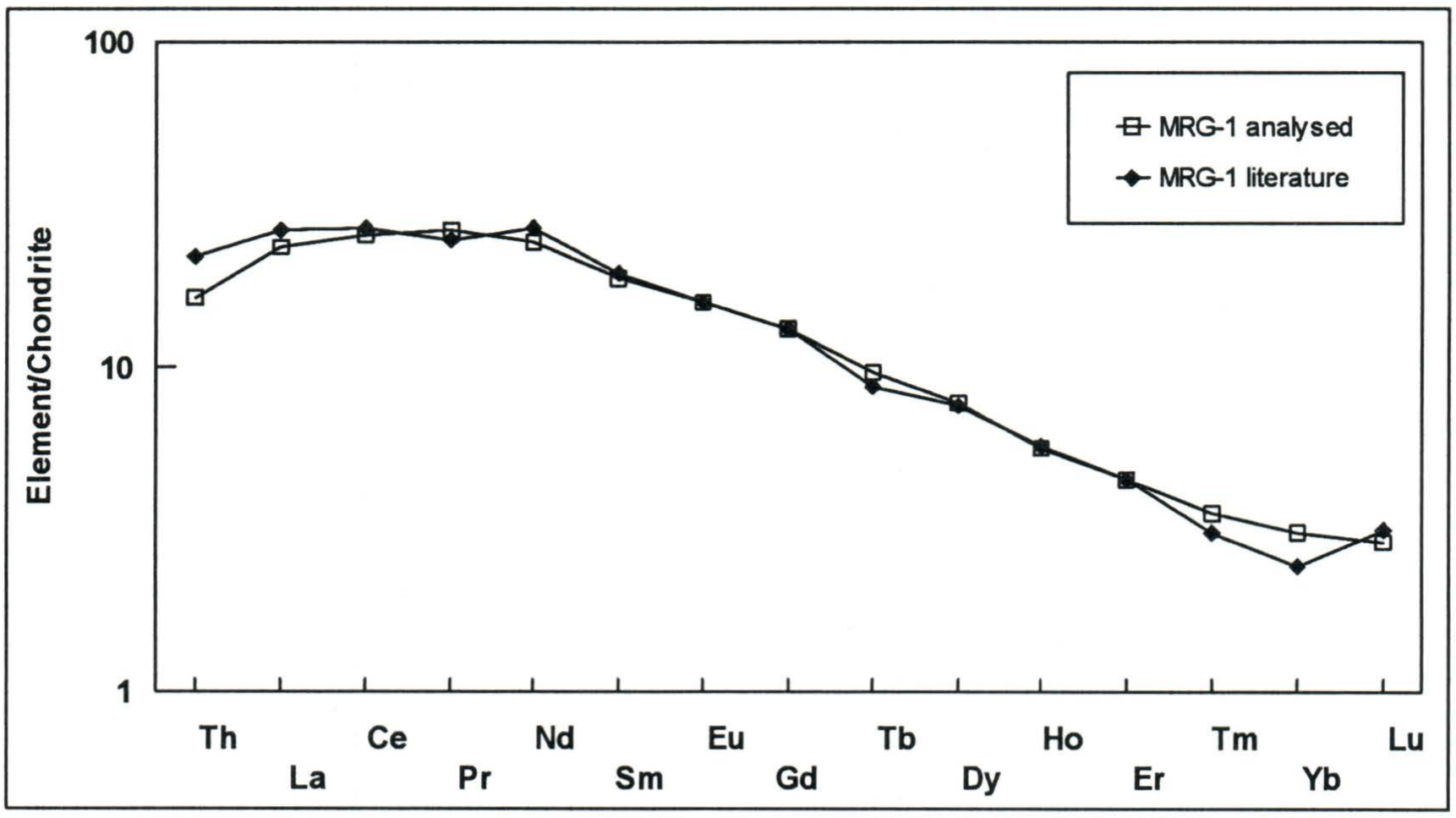


Figure C-1 - Analyses of standard MRG-1 from our run and that from quoted values in Govindaraju (1989) normalized to chondrite values of Sun and McDonough (1989).

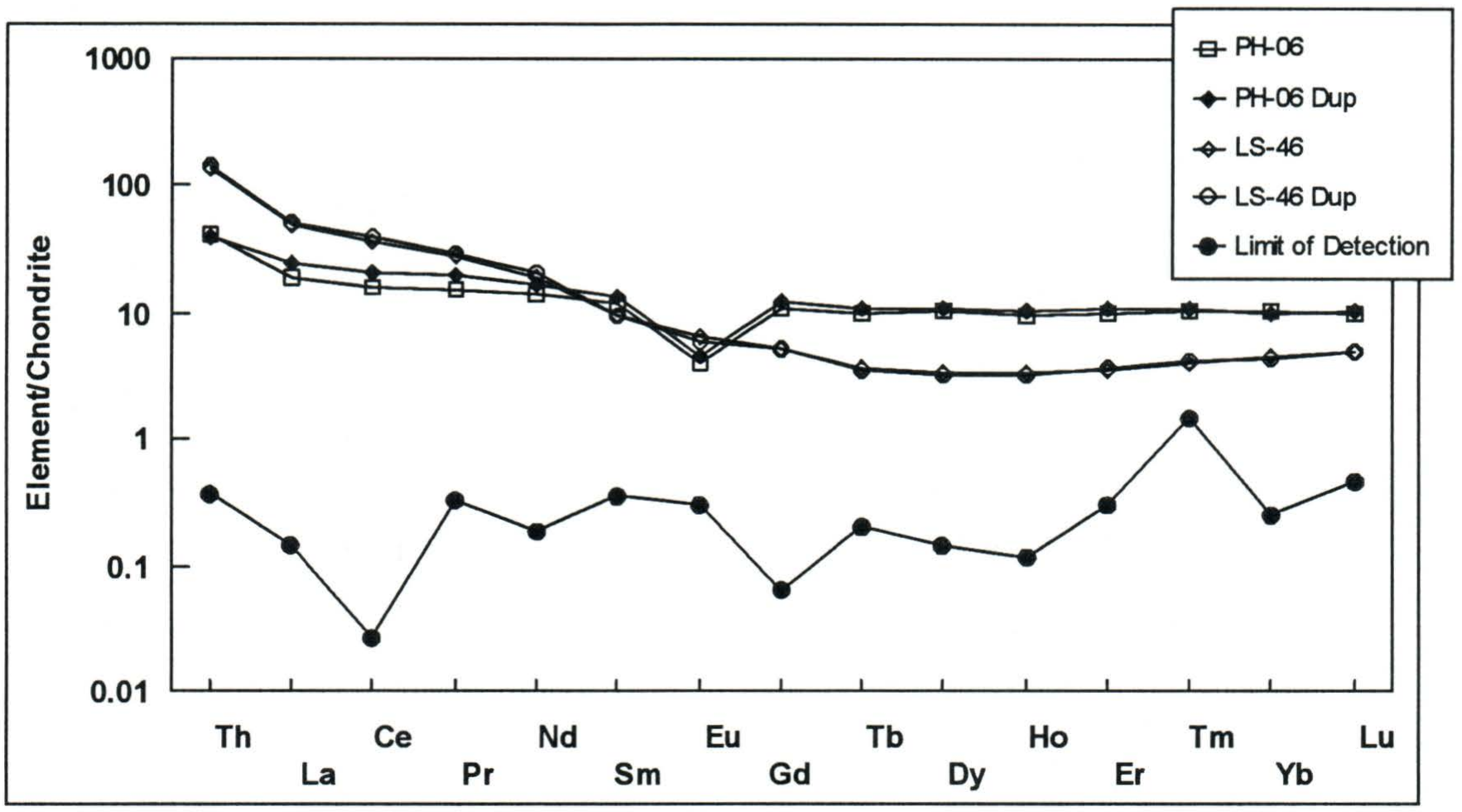


Figure C-2 - Duplicate analyses for samples PH-06 and LS-46, as well as detection limits, normalized to Chondrite values (Sun and McDonough, 1989).

Table C-1 - Na_2O sinter ICP-MS data from various areas in the Buchans camp.

Sample	WB-18	M14637S	WB-10	M14564U	WB-5
Drill Hole	BE-95-03	BE-96-08	BE-96-10	BE-97-17	BE-96-08
From	157.8	357.15	154.7	-	109.4
To	158.2	357.55	154.7	-	110
Th	1.39	1.95	0.46	2.12	2.23
La	5.61	7.41	2.44	8.60	10.90
Ce	13.70	16.60	5.45	18.69	23.41
Pr	1.90	2.27	0.72	2.48	3.11
Nd	8.86	9.60	3.44	10.50	13.05
Sm	2.55	2.63	0.95	2.75	3.67
Eu	0.66	0.60	0.22	0.52	0.63
Gd	3.35	2.98	1.08	2.86	4.35
Tb	0.60	0.53	0.19	0.51	0.76
Dy	3.97	3.61	1.27	3.44	5.05
Ho	0.90	0.78	0.30	0.76	1.07
Er	2.79	2.46	0.89	2.36	3.19
Tm	0.45	0.36	0.13	0.37	0.49
Yb	3.35	2.69	0.99	2.65	3.34
Lu	0.57	0.43	0.16	0.43	0.52

Sample	LS-01	LS-02	LS-06	LS-13	LS-16
Drill Hole	Outcrop	25	542	237	2889
From	at Ski Hill	57	8	1025	17
To	-	61	10	1027	18
Th	1.86	9.19	1.05	11.70	0.03
La	6.49	26.04	3.10	30.68	6.16
Ce	11.49	45.00	5.73	54.05	9.23
Pr	1.33	4.70	0.68	5.71	1.04
Nd	5.32	15.84	2.86	19.65	4.32
Sm	1.25	2.68	0.67	3.46	0.89
Eu	0.29	0.61	0.15	0.74	0.11
Gd	1.43	2.30	0.61	2.93	0.62
Tb	0.21	0.34	0.09	0.46	0.05
Dy	1.51	2.15	0.62	2.88	0.21
Ho	0.34	0.46	0.15	0.63	0.03
Er	0.89	1.42	0.46	2.01	0.07
Tm	0.14	0.21	0.07	0.33	0.01
Yb	1.08	1.66	0.59	2.37	0.05
Lu	0.16	0.27	0.07	0.40	0.01

Table C-1 - (continued) Na_2O sinter ICP-MS data from various areas in the Buchans camp.

Sample	LS-17	LS-20	LS-29	LS-46	LS-46 Dup	PH-24
Drill Hole	**2889**	**2889**	**2871**	**2865**	**2865**	**BE-97-20**
From	**167**	**385**	**601.5**	**3209.5**	**3209.5**	**74.5**
To	**170**	**388**	**604**	**3211**	**3211**	**74.8**
Th	5.97	1.64	4.82	5.77	5.97	1.99
La	19.32	7.93	18.74	18.03	18.83	6.18
Ce	40.48	15.52	37.30	34.69	36.75	14.60
Pr	4.98	1.90	4.54	3.75	3.96	1.92
Nd	20.84	8.08	18.42	13.39	14.36	8.60
Sm	4.74	2.03	4.04	2.18	2.22	2.50
Eu	1.19	0.70	1.10	0.56	0.52	0.60
Gd	4.69	2.24	3.81	1.61	1.57	2.96
Tb	0.73	0.32	0.59	0.22	0.21	0.50
Dy	4.62	1.98	3.69	1.30	1.22	3.31
Ho	1.01	0.43	0.78	0.28	0.28	0.77
Er	3.10	1.16	2.30	0.89	0.92	2.48
Tm	0.46	0.17	0.34	0.14	0.15	0.39
Yb	3.20	1.15	2.20	1.11	1.10	2.60
Lu	0.49	0.17	0.34	0.19	0.19	0.43

Sample	M17509	M16969H	PH-01	PH-06	PH-19
Drill Hole	**Outcrop**	**2871**	**BE-96-11**	**BE-96-11**	**3319**
From	**at Ski Hill**	**58.75**	**58.5**	**151.7**	**282.5**
To		**60**	**59.4**	**152.4**	**285.0**
Th	2.72	9.03	0.43	1.66	1.61
La	10.94	26.35	1.54	9.03	1.21
Ce	21.95	43.97	4.40	20.01	2.36
Pr	2.68	4.34	0.69	2.73	0.29
Nd	11.09	14.52	3.38	11.59	1.18
Sm	2.97	2.47	1.01	3.05	0.36
Eu	0.89	0.57	0.16	0.39	0.08
Gd	2.83	2.09	1.04	3.74	0.62
Tb	0.41	0.31	0.16	0.64	0.11
Dy	2.65	2.00	1.11	4.15	0.92
Ho	0.53	0.46	0.25	0.88	0.25
Er	1.72	1.60	0.77	2.63	0.90
Tm	0.24	0.25	0.11	0.38	0.15
Yb	1.52	1.83	0.71	2.42	1.18
Lu	0.26	0.31	0.13	0.40	0.21

Appendix D

APPENDIX D

D.1 Electron Microprobe Technique

Mineral analyses were carried out on a Cameca SX50 electron microprobe analyser at the Department of Earth Sciences, Memorial University. The beam current was set at 20 nA with a 15 kV accelerating potential. Analyses for Al, Si, K, Ca, Ti and Mn were done in energy-dispersive (ED) mode whereas wave-dispersive (WD) mode was used for analyses of Na, Mg and Fe. Count times were 100 s. Analyses were primarily for chlorite (Table D-2) and sericite (Table D-3), although some data on carbonate species were also collected (Table D-4).

D.2 Precision and Accuracy

Several silicate standards (hornblende and pyroxenes) were used for calibration and were analysed several times with each successive run. The Kakanui Hornblende was analysed twenty-one times. RSD values indicate that most of the data are either good (3-7% RSD) or excellent (<3% RSD) (Table D-1). The most notable exceptions include Na_2O and MnO. The MnO variation can be attributed to the low concentrations, however, Na_2O is more problematic and shows minor drift. Accuracy, as indicated by RD values, is also mostly good or excellent, with the exception of MnO and K_2O. Average K_2O values were slightly higher in the measured values for the standards than in the accepted values.

OXIDE (wt. %)	Quoted Values	Mean	Minimum	Maximum	Standard Deviation	RSD[1](%)	RD[2] (%)
Na_2O	2.6	2.59	1.55	2.87	0.38	14.67	-0.24
MgO	12.8	12.07	9.83	12.56	0.77	6.35	-5.70
Al_2O_3	14.9	14.09	13.76	14.41	0.18	1.27	-5.42
SiO_2	40.37	40.60	40.16	41.00	0.25	0.61	0.56
K_2O	2.05	2.33	2.01	2.55	0.19	7.94	13.70
CaO	10.3	10.23	9.98	10.52	0.14	1.36	-0.66
TiO_2	4.72	4.75	4.63	4.88	0.07	1.40	0.56
MnO	0.09	0.08	0.01	0.20	0.06	71.61	-12.49
$FeO_{(Total)}$	10.95	11.21	10.81	11.52	0.21	1.84	2.40
Total	98.78	97.91	95.71	99.28	0.91	0.93	-0.88

Table D-1 - Statistical parameters for 21 analyses of standard Kakanui Hornblende. [1]RSD (Relative Standard Deviation) = standard deviation/ mean. [2] RD (Relative Difference) = (mean - quoted value)/quoted value.

Table D-2 - Chlorite compositions from the Lucky Strike area

Sample	SH-1a	LS-01	LS-43	LS-38	LS-15	LS-28	LS-28	LS-29	Ls-20	LS-23	LS-35	LS-26	LS-03	LS-33	LS-06	LS-34
Points	3	9	4	3	9	2	6	9	8	5	2	6	1	6	8	3
SiO2 (wt. %)	27.45	28.76	27.48	28.63	28.32	33.24	27.54	27.64	28.59	33.93	30.72	32.37	26.68	34.67	31.06	34.75
TiO2	0.00	0.05	0.03	0.04	0.05	0.35	0.05	0.04	0.04	0.07	0.04	0.03	0.00	0.10	0.03	0.76
Al2O3	16.16	16.49	19.14	20.29	20.35	23.53	17.68	18.80	18.61	27.15	19.40	19.95	20.47	23.10	19.39	15.07
FeO	28.37	29.91	22.38	14.55	14.67	11.31	21.91	19.93	19.44	12.45	7.17	7.04	19.51	7.68	9.34	2.10
MnO	0.53	0.49	1.14	0.82	0.65	0.71	1.04	1.08	0.48	0.27	0.54	0.45	1.58	0.28	0.64	0.32
MgO	11.94	9.10	14.61	17.18	22.29	14.59	17.27	18.12	22.57	10.34	24.72	24.29	16.17	18.75	23.02	30.46
CaO	0.34	0.40	0.07	0.21	0.19	0.59	0.09	0.06	0.13	0.19	0.07	0.15	0.08	0.36	0.06	0.43
Na2O	0.01	0.03	0.01	0.02	0.01	0.09	0.06	0.03	0.02	0.09	0.00	0.00	0.12	0.08	0.02	0.01
K2O	0.02	0.52	0.01	0.05	0.02	3.34	0.03	0.03	0.10	2.08	0.11	0.04	0.11	1.81	0.02	0.01
Total	84.79	85.67	84.80	81.74	86.47	87.71	85.61	85.67	89.90	86.52	82.70	84.29	84.66	86.78	83.51	83.94
Number of Ions based on 28 O																
Si	6.11	6.36	5.93	6.12	5.74	6.52	5.87	5.83	5.69	6.7	6.19	6.37	5.72	6.65	6.27	6.65
Al (iv)	1.89	1.64	2.07	1.88	2.26	1.48	2.13	2.17	2.31	1.3	1.81	1.63	2.28	1.35	1.73	1.35
Al (vi)	2.34	2.66	2.8	3.23	2.6	3.95	2.31	2.5	2.06	5.03	2.8	3	2.9	3.88	2.88	2.04
Na	0	0.01	0	0	0	0.02	0.01	0.01	0	0.02	0	0	0.03	0.01	0	0
Mg	3.96	3	4.7	5.47	6.73	4.26	5.49	5.7	6.7	3.04	7.43	7.13	5.17	5.36	6.92	8.68
K	0.01	0.15	0	0.01	0	0.83	0.01	0.01	0.03	0.53	0.03	0.01	0.03	0.44	0	0
Ca	0.08	0.09	0.01	0.05	0.04	0.12	0.02	0.01	0.03	0.04	0.02	0.03	0.02	0.07	0.01	0.09
Ti	0	0.02	0.01	0.01	0.01	0.1	0.02	0.01	0.01	0.02	0.01	0.01	0	0.03	0.01	0.22
Mn	0.1	0.09	0.21	0.15	0.11	0.12	0.19	0.19	0.08	0.05	0.09	0.08	0.29	0.05	0.11	0.05
Fe	5.28	5.53	4.04	2.6	2.48	1.85	3.91	3.51	3.24	2.06	1.21	1.16	3.5	1.23	1.58	0.34
Fe/ (Fe+Mg)	0.57	0.65	0.46	0.32	0.27	0.3	0.42	0.38	0.33	0.4	0.14	0.14	0.4	0.19	0.19	0.04

Table D-2 (continued) - Chlorite compositions from the Powerhouse Zone

Sample	PH-08	PH-02	PH-03	PH-12	PH-7	PH-18
Points	8	3	2	7	1	5
SiO2 (wt. %)	30.11	31.11	33.25	31.65	31.66	28.22
TiO2	0.05	0.00	0.03	0.01	0.02	0.04
Al2O3	20.99	24.37	28.86	25.50	29.02	24.35
FeO	10.55	6.82	5.97	6.51	8.18	14.47
MnO	0.49	0.30	0.09	0.58	0.31	0.19
MgO	21.99	23.18	17.65	21.29	16.57	18.31
CaO	0.15	0.11	0.15	0.14	0.16	0.05
Na2O	0.05	0.04	0.05	0.02	0.04	0.05
K2O	0.25	0.16	0.09	0.01	0.05	0.36
Total	84.59	86.07	86.03	85.69	85.95	85.96
Number of loNumber of Ions based on 28 O						
Si	6.06	6.03	6.36	6.14	6.17	5.74
Al (iv)	1.94	1.97	1.64	1.86	1.83	2.26
Al (vi)	3.05	3.6	4.87	3.98	4.84	3.58
Na	0.01	0.01	0.01	0.00	0.01	0.01
Mg	6.61	6.7	5.03	6.16	4.81	5.55
K	0.06	0.04	0.02	0.00	0.01	0.09
Ca	0.03	0.02	0.03	0.03	0.03	0.01
Ti	0.01	0	0.01	0.00	0.01	0.01
Mn	0.09	0.05	0.01	0.10	0.05	0.03
Fe	1.78	1.11	0.96	1.05	1.33	2.46
Fe/ (Fe+Mg)	0.22	0.14	0.16	0.15	0.22	0.31

Table D-2 (continued) - Chlorite compositions from the Woodman's Brook Zone

Sample	WB-10	WB-9	WB-6	WB-15	WB-3	WB-1	WB-17	WB-25	WB-14	WB-26	WB-30	WB-31
Points	14	5	6	3	2	4	5	2	3	2	4	3
SiO2 (wt. %)	25.16	26.44	27.83	26.21	26.61	25.57	27.64	27.83	27.12	25.92	25.34	27.14
TiO2	0.05	0.06	0.04	0.06	0.06	0.06	0.03	0.02	0.04	0.05	0.01	0.00
Al2O3	22.02	21.38	22.19	21.61	21.40	20.79	21.40	20.70	18.90	21.75	20.09	23.19
FeO	27.82	19.42	17.12	13.39	26.13	23.56	18.56	20.28	26.03	24.47	27.42	20.43
MnO	0.44	0.42	0.31	0.72	0.47	0.98	0.31	0.44	1.12	0.83	0.46	0.56
MgO	11.69	18.28	17.89	17.20	12.45	15.44	17.91	16.88	13.80	14.16	13.01	14.91
CaO	0.04	0.15	0.07	0.15	0.06	0.08	0.10	0.06	0.19	0.08	0.07	0.08
Na2O	0.08	0.09	0.24	0.23	0.10	0.05	0.22	0.08	0.06	0.06	0.04	0.09
K2O	0.10	0.00	0.53	0.50	0.60	0.08	0.01	0.43	0.03	0.01	0.06	0.74
Total	87.32	86.22	86.13	79.99	87.85	86.51	86.18	86.67	87.21	87.23	86.46	87.13
Number of INumber of Ions based on 28 O												
Si	5.46	5.54	5.74	5.75	5.67	5.48	5.74	5.8	5.81	5.53	5.54	5.66
Al (iv)	2.54	2.46	2.26	2.25	2.33	2.52	2.26	2.2	2.19	2.47	2.46	2.34
Al (vi)	3.09	2.82	3.14	3.35	3.04	2.74	2.98	2.89	2.58	2.99	2.72	3.36
Na	0.02	0.02	0.05	0.05	0.02	0.01	0.04	0.02	0.01	0.01	0.01	0.02
Mg	3.78	5.71	5.51	5.63	3.96	4.94	5.54	5.24	4.41	4.5	4.24	4.64
K	0.03	0	0.14	0.14	0.16	0.02	0	0.11	0.01	0	0.02	0.2
Ca	0.01	0.03	0.01	0.04	0.01	0.02	0.02	0.01	0.04	0.02	0.02	0.02
Ti	0.02	0.02	0.01	0.02	0.02	0.02	0.01	0.01	0.01	0.02	0	0
Mn	0.08	0.07	0.05	0.13	0.08	0.18	0.05	0.08	0.2	0.15	0.09	0.1
Fe	5.05	3.4	2.96	2.46	4.66	4.23	3.22	3.53	4.66	4.36	5.01	3.56
Fe/ (Fe+Mg)	0.57	0.37	0.35	0.3	0.54	0.46	0.37	0.4	0.51	0.49	0.54	0.43

Table D-3 - Sericite compositions from the Lucky Strike Area

Sample Points	LS-10 n=7	Sh-1a n=2	LS-08 n=7	LS-15 n=7	LS-26 n=2	LS-46 n=4	LS-46 n=4	LS-38 n=4	LS-35 n=2	LS-04 n=6	LS-23 n=2	LS-33 n=4	LS-28 n=3	LS-13 n=4	LS-05 n=3	LS-3 n=4
SiO2 (wt. %)	48.96	45.82	48.88	50.62	52.68	50.55	47.42	49.22	47.73	49.76	49.62	47.46	46.73	51.19	51.36	49.02
TiO2	0.4	0.07	0.25	0.26	0.17	0.23	0.18	0.3	0.24	0.3	0.19	0.17	0.27	0.21	0.13	0.18
Al2O3	32.1	30.24	31.14	30.54	31.4	29.36	33.47	31.15	28.4	31.11	32.68	30.51	29.74	28.25	31.03	31.59
FeO	1.06	3.56	0.91	1.06	0.55	0.68	2.04	1.86	1	1.05	1.21	2.04	1.71	2.31	1.13	1.03
MgO	1.25	0.9	1.65	2.05	1.66	2.5	0.54	1.72	1.69	1.56	1.15	2.15	1.55	1.55	1.45	1.47
MnO	0.02	0.12	0.01	0.07	0.02	0.02	-0.01	0.05	0.08	0.05	0.04	0.01	0.03	0.01	0	-0.01
CaO	0.15	0.29	0.18	0.15	0.22	0.11	0.25	0.26	0.16	0.4	0.34	0.25	0.28	0.34	0.29	0.17
K2O	11.09	10.88	11.21	10.61	9.95	12.35	10.17	11.03	10.54	11.18	10.88	10.31	11.16	9.25	9.87	11.33
Na2O	0.24	0.33	0.14	0.17	0.08	0.06	0.41	0.12	0.06	0.13	0.15	0.39	0.23	0.26	0.16	0.24
Total	95.23	92.03	94.33	95.48	96.67	95.82	94.49	95.69	89.9	95.51	96.23	93.28	91.67	93.35	95.34	94.98
Number of ions based on 20 O																
Si	5.92	5.84	5.97	6.07	6.17	6.10	5.78	5.95	6.11	6.00	5.93	5.89	5.92	6.27	6.13	5.95
Al (iv)	2.08	2.16	2.03	1.93	1.83	1.90	2.22	2.05	1.89	2.00	2.07	2.11	2.08	1.73	1.87	2.05
Al (vi)	2.49	2.38	2.45	2.39	2.51	2.28	2.60	2.38	2.38	2.42	2.53	2.35	2.36	2.34	2.50	2.47
Fe	0.11	0.38	0.09	0.11	0.05	0.07	0.21	0.19	0.11	0.11	0.12	0.21	0.18	0.24	0.11	0.10
Mg	0.22	0.17	0.30	0.37	0.29	0.45	0.10	0.31	0.32	0.28	0.20	0.40	0.29	0.28	0.26	0.27
Mn	0.00	0.01	0.00	0.01	0.00	0.00	0.00	0.01	0.01	0.00	0.00	0.00	0.00	0.00	0.00	0.00
Ti	0.04	0.01	0.02	0.02	0.02	0.02	0.02	0.03	0.02	0.03	0.02	0.02	0.03	0.02	0.01	0.02
Ca	0.02	0.04	0.02	0.02	0.03	0.01	0.03	0.03	0.02	0.05	0.04	0.03	0.04	0.04	0.04	0.02
K	1.71	1.77	1.75	1.62	1.49	1.90	1.58	1.70	1.72	1.72	1.66	1.63	1.80	1.44	1.50	1.75
Na	0.06	0.08	0.03	0.04	0.02	0.01	0.10	0.03	0.01	0.03	0.03	0.09	0.06	0.06	0.04	0.06
Fe/ (Fe+Mg)	0.32	0.69	0.24	0.22	0.16	0.13	0.68	0.38	0.25	0.27	0.37	0.35	0.38	0.46	0.30	0.28

Table D-3 (continued) - Sericite compositions from the Powerhouse Zone

Sample Points	PH-08 n=3	PH-03 n=3	PH-12 n=2	PH-12 n=2	PH-7 n=2	Ph-18 n=2	Ph-02 n=2	Ph-05 n=2	PH-21 n=1
SiO2 (wt. %)	49.43	36.31	49.34	46.44	47.9	47.39	49.73	48.03	42.36
TiO2	0.16	0.13	0.1	0.08	0.15	0.15	0.12	0.17	0.08
Al2O3	31.59	26.17	32.19	30.4	34.02	33.63	31.13	34.8	32.75
FeO	0.3	0.77	0.48	1.79	0.62	0.62	0.35	0.44	0.5
MgO	1.61	0.68	1.64	4.82	0.85	0.8	2.3	0.73	0.51
MnO	0.02	0.01	0.05	-0.04	0.02	-0.03	0.02	0.04	0.04
CaO	0.42	0.13	0.14	0.09	0.1	0.03	0.09	0.02	0.1
K2O	10.81	6.92	10.97	7.85	9.17	9.79	9.68	9.74	7.93
Na2O	0.38	0.69	0.43	0.36	0.48	0.42	0.26	0.48	1.26
Total	94.7	71.8	95.19	91.71	93.29	92.79	93.58	94.33	85.41
Number of ions based on 20 O									
Si	**5.98**	5.72	5.94	5.78	5.83	5.82	6.03	5.79	5.64
Al (iv)	**2.02**	2.28	2.06	2.22	2.17	2.18	1.97	2.21	2.36
Al (vi)	**2.48**	2.77	2.52	2.23	2.71	2.69	2.49	2.74	2.78
Fe	**0.03**	0.20	0.05	0.19	0.06	0.06	0.04	0.04	0.06
Mg	**0.29**	0.12	0.30	0.90	0.15	0.15	0.42	0.13	0.10
Mn	**0.00**	0.01	0.01	0.00	0.00	0.00	0.00	0.00	0.00
Ti	**0.01**	0.01	0.01	0.01	0.01	0.01	0.01	0.02	0.01
Ca	**0.05**	0.02	0.02	0.01	0.01	0.00	0.01	0.00	0.01
K	**1.67**	1.07	1.69	1.24	1.42	1.54	1.50	1.50	1.35
Na	**0.09**	0.17	0.10	0.09	0.11	0.10	0.06	0.11	0.33
Fe/ (Fe+Mg)	**0.09**	0.62	0.14	0.17	0.29	0.30	0.08	0.25	0.36

Table D-3 (continued) - Sericite compositions from the Woodman's Brook Zone

Sample	WB-10	WB-10	WB-15	WB3	WB-01	Wb-6	WB-25	Wb-19	WB-09	Wb-14	WB-31	WB-30
Points	n=3	n=3	n=1	n=2	n=5	n=2	n=1	n=2	n=1	n=3	n=3	n=1
SiO2 (wt. %)	45.47	45.58	45.42	43.86	51.93	48.04	47.21	48.85	48.73	50.65	46.81	40.76
TiO2	0.19	0.11	0.26	0.16	0.11	0.15	0.21	0.18	0.17	0.06	0.27	0
Al2O3	32.87	33.73	32.75	34.15	30.21	31.24	33.6	32.72	32.33	30.2	34.07	15.53
FeO	2.22	1.58	0.95	1.77	1.57	2.94	0.78	0.88	1.69	3.68	1.58	5.19
MgO	0.71	0.67	0.93	0.83	0.93	2.87	1.15	1.18	1.28	0.92	0.98	1.97
MnO	-0.03	0.06	0.01	0.06	0.04	0.11	-0.03	0	0.01	0.03	0.09	0.61
CaO	0.03	0.16	0.05	0.1	0.19	0.05	0.23	0.16	0.05	0.5	0.08	13.08
K2O	9.84	11.54	9.88	9.66	7.93	7.52	9.51	9.41	9.85	8.82	9.28	0.05
Na2O	0.62	0.56	0.51	0.45	1.56	1.7	0.46	0.46	0.45	0.23	0.62	8.07
Total	91.88	93.82	90.7	90.99	94.37	94.59	93.15	93.83	94.5	95.05	93.65	85.22
Number of ions based on 20 O												
Si	5.72	5.66	5.75	5.56	6.22	5.83	5.78	5.92	5.91	6.12	5.72	5.88
Al (iv)	2.28	2.34	2.25	2.44	1.78	2.17	2.22	2.08	2.09	1.88	2.28	2.12
Al (vi)	2.59	2.59	2.63	2.67	2.50	2.29	2.64	2.60	2.53	2.42	2.63	0.52
Fe	0.23	0.16	0.10	0.19	0.16	0.30	0.08	0.09	0.17	0.37	0.16	0.63
Mg	0.13	0.12	0.17	0.16	0.17	0.52	0.21	0.21	0.23	0.16	0.18	0.42
Mn	0.00	0.01	0.00	0.01	0.00	0.01	0.00	0.00	0.00	0.00	0.01	0.07
Ti	0.02	0.01	0.02	0.02	0.01	0.01	0.02	0.02	0.02	0.01	0.03	0.00
Ca	0.00	0.02	0.01	0.01	0.02	0.01	0.03	0.02	0.01	0.06	0.01	2.02
K	1.58	1.83	1.59	1.56	1.22	1.16	1.49	1.46	1.52	1.36	1.45	0.01
Na	0.15	0.13	0.12	0.11	0.36	0.40	0.11	0.11	0.11	0.05	0.15	2.26
Fe/ (Fe+Mg)	0.64	0.57	0.37	0.54	0.49	0.37	0.28	0.30	0.43	0.69	0.47	0.60

Table D-4 - Carbonate microprobe analyses from various zones

Label	LS-26	LS-43	LS-33	LS-28	LS-34	PH-08	PH-03	PH-12	PH-12	PH-02	PH-02
Points	1	2	2	3	3	2	2	1	1	1	1
Na2O	0.02	0	0.01	0.02	0.01	0	0.02	0.01	0.05	0.02	0
MgO	0.07	0.01	0.11	0.13	0.29	0.27	16.48	14.95	15.95	0.12	19.28
Al2O3	0.12	0.03	0.04	0.04	0.05	0.06	0.01	0.03	0.26	0.01	0.04
SiO2	0.24	0.12	0.2	0.21	0.27	0.27	0.09	0.18	0.09	0.12	0.13
K2O	0.07	0.08	0.12	0.07	0.07	0.09	0.03	0.03	0.06	0.08	-0.03
CaO	42.27	57.34	57	55.83	56.24	54.38	27.95	30.5	29.26	55.43	29.14
TiO2	8.11	-0.01	0	0.04	0.03	0	0.03	-0.01	0	0.01	-0.06
MnO	0.62	0.77	0.62	1.88	1.57	1.85	2.22	1.92	0.64	2.05	1.06
FeO	0.04	0.11	0.05	0.1	0.02	0.22	4.32	4.29	5.1	0.03	1.66
Total	51.42	58.38	58.1	58.19	58.44	57.14	51.04	51.84	51.33	57.81	51.26
Number of ions on the basis of 6 O											
Mg	0.00	0.00	0.01	0.01	0.01	0.01	0.82	0.74	0.79	0.01	0.92
Ca	1.54	1.97	1.96	1.92	1.92	1.91	1.00	1.08	1.04	1.93	1.00
Mn	0.02	0.02	0.02	0.05	0.04	0.05	0.06	0.05	0.02	0.06	0.03
Fe	0.00	0.00	0.00	0.00	0.00	0.01	0.12	0.12	0.14	0.00	0.04
Ca/Mg	458.1	2485.6	353.0	302.5	135.4	138.7	1.2	1.5	1.3	343.3	1.1
Ca/(Mg+Fe+Mn)	69.0	80.1	82.4	32.0	33.7	26.9	1.0	1.2	1.1	30.6	1.0
Mg/Fe	3.1	0.3	4.0	2.6	41.4	2.3	6.8	6.2	5.6	5.4	20.7
Species	Calcite	Calcite	Calcite	Calcite	Calcite	Calcite	Dolomite	Dolomite	Dolomite	Calcite	Dolomite

Label	PH-21	WB-10	WB-10	WB-1	WB-7	WB-14	WB-26	WB-21	WB-30	WB-31	MB-1
Points	1	2	1	2	1	2	2	1	1	1	1
Na2O	0	0.03	0.03	0.03	0.08	0.02	0.08	0.05	0.02	0.01	0.03
MgO	0.75	11.23	12.88	10.35	12.41	0.3	0.04	11.42	1.34	0.42	0
Al2O3	0.34	0.14	0.04	0.35	0.61	0.65	0.19	0.01	0.91	0.03	0.37
SiO2	0.2	0.22	0.18	0.5	0.48	0.83	0.63	0.24	0.98	0.3	0.3
K2O	0.08	0.08	0.04	0.06	0.09	0.11	0.06	0.03	0.04	0.05	0.05
CaO	54.3	27.96	28.57	27.28	27.52	54	54.83	28.84	45.99	55.63	57.09
TiO2	0.03	0.01	-0.04	0.05	0.03	-0.01	0.01	-0.03	3.29	0.01	-0.06
MnO	2	3.53	3.7	1.06	1.84	0.58	1	0.75	1.32	1.34	0.16
FeO	0.49	9.49	7.96	14.63	10.93	1.15	0.37	13	2.98	0.41	0.05
Total	58.16	52.65	53.31	54.19	53.96	57.61	57.16	54.3	56.83	58.11	58
Number of ions on the basis of 6 O											
Mg	0.04	0.57	0.64	0.52	0.61	0.01	0.00	0.57	0.06	0.02	0.00
Ca	1.86	1.03	1.02	0.98	0.97	1.85	1.91	1.03	1.55	1.91	1.95
Mn	0.05	0.10	0.10	0.03	0.05	0.02	0.03	0.02	0.04	0.04	0.00
Fe	0.01	0.27	0.22	0.41	0.30	0.03	0.01	0.36	0.08	0.01	0.00
Ca/Mg	52.3	1.8	1.6	1.9	1.6	130.0	792.3	1.8	24.6	96.5	0.0
Ca/(Mg+Fe+Mn)	18.1	1.1	1.1	1.0	1.0	30.4	47.8	1.1	8.8	28.4	351.0
Mg/Fe	2.7	2.1	2.9	1.3	2.0	0.5	0.2	1.6	0.8	1.8	0.0
Species	Calcite	Ankerite	Ankerite	Ankerite	Ankerite	Calcite	Calcite	Ankerite	Ankerite	Calcite	Calcite

Appendix E

APPENDIX E

E.1 Lead Isotope Analysis

Six galena separates were collected from various alteration zones and prospects in the Buchans area. Analyses were carried out at the GEOTOP Laboratory, Université du Québec à Montréal (UQAM). Data are reported as $^{206}Pb/^{204}Pb$, $^{207}Pb/^{204}Pb$, $^{208}Pb/^{204}Pb$ and $^{207}Pb/^{206}Pb$ with an analytical uncertainty of 0.05% amu^{-1} at the 1 σ level (Moritz and Malo, 1996). The data are presented in Table E-1 with accompanying sample descriptions in Table E-2. All other data used in Figure 5-18 and described in text are from Cumming and Krstic (1987).

Table E-1 - Lead isotope ratios for six samples from the Buchans area. Analytical uncertainty for each of the ratios is +/- 0.05%.

Sample	Drill Hole	Depth	206Pb/204Pb	207Pb/204Pb	208Pb/204Pb	206Pb/207Pb
Airport Zone	2837	672'	17.806	15.498	37.55	0.8711
Woodmans Brook Zone	BE-95-03	108.3 m	17.61	15.447	37.494	0.877
Sandfill Prospect	1910	1815.5'	17.845	15.508	37.597	0.8692
Middle Branch Zone	1742	1185'	17.815	15.48	37.569	0.8691
Powerhouse Zone	BE-97-19	178.8 m	17.727	15.471	37.429	1.1457
Middle Branch East	BE-97-18	5 m.	17.958	15.502	37.627	1.1586

Table E-2 - Descriptions of host rock/mineralization style for samples analysed for lead isotope ratios in Table D-2.

Sample	**Description**
Airport Zone	Minor Pb-Zn sulphides in quartz veins cutting chloritic zone.
Woodmans Brook Zone	Stockwork galena - sphalerite in sericite - silica altered felsic volcanic
Sandfill Prospect	Massive Zn-Pb-Ba sulphide clasts in transported ore
Middle Branch Zone	Stringer gal-sph mineralization in altered felsic volcanic
Powerhouse Zone	1 cm wide galena - sphalerite - quartz stringer in altered felsic volcanic
Middle Branch East Zone	~ 1 cm massive Zn-Pb-Ba sulphide clasts in sheared polylithic unit.

Appendix F

Appendix F

F.1 Mass Balance Calculations - Method and Equations

The MacLean method:

Mass balance calculations at the **LSZ/MBZ** were based on Al_2O_3 - Zr fractionation trends (Figure 6-13b). The equation for the curve is:

(1) $y = -0.0067x + 22.5$

Alteration lines intersecting this curve are linear and emanate from the origin:

(2) $y = Al_2O_3/Zr$

Precursor compositions for Zr were derived from the intersection of alteration lines (1) with the fractionation curve (2):

(3) $Zr_{precursor} = 22.5/[(Al_2O_3/Zr) - (-0.0667)]$

Precursor compositions (PC) for each sample of all major oxides and Ba, Rb and Sr were derived from the following equations, where $x = Zr_{precursor}$. These equations represent fractionation curves of the oxide or trace element plotted against Zr. Rather than single quadratic curves, individual linear trends were used for each of the mafic and felsic endmembers as there has been little fractionation within each unit.

	Mafic volcanic rocks	Felsic volcanic rocks
SiO_2	0.049x + 48.61	0.032x + 69.59
TiO_2	-0.00031x + 0.8	-0.0015x + 0.55
Fe_2O_3	-0.0044x + 9.96	-0.006x + 2.75
MnO	0.0008x + 0.15	0.0001x+ 0.084
MgO	-0.033x + 6.96	-0.015x + 2.57
CaO	-0.023x + 10.21	-0.0099x + 2.57
Na_2O	0.035x + 2.11	-0.018x + 6.82
K_2O	0.0074x + 0.23	0.015x - 0.01
P_2O_5	0.003x	0.05
Rb	0.27x + 0.4	0.32x + 4.8

Ba	5.2x + 184	6.7x
Sr	-1.6x + 500	-1.46x + 3.7

The *enrichment factor* (E_f) is derived from:

$$Zr_{precursor}/Zr_{measured}.$$

(E_f) is < 1 for mass loss and > 1 for mass gain.

Reconstructed (RC) values for each oxide per sample are determined from:

(E_f) * oxide (measured)

Mass changes (MC) are calculated as:

$$MC = RC - PC$$

Negative values indicate a mass loss; Positive values are mass gains.

The same method was applied to the WBZ and PHZ.
Equations for the **PHZ** are as follows:

Al_2O_3 - Zr fractionation curve: $y = -0.0068x + 22.5$

All other constituents plotted against Zr are in the table below.

	Mafic volcanic rocks	Felsic volcanic rocks
SiO_2	0.1493x + 57.8	0.049x + 48.61
TiO_2	-0.00487x + 0.71	0.00096x + 0.42
Fe_2O_3	-0.165x + 17.88	-0.0044x + 9.96
MnO	0.00058x + 0.013	0.00008x+ 0.15
MgO	-0.09x + 10.27	-0.033x + 6.96
CaO	0.00659x + 3.32	-0.023x + 10.21

Na_2O	0.02952x + 1.71	0.0035x + 2.91
K_2O	0.00724x + 0.34	0.00738x + 0.229
P_2O_5	0.00001x + 0.042	0.0034x + 0.054
Rb	0.387x - 25	0.276x + 0.37
Ba	2.7x - 142	5.15x + 0
Sr	0.813x + 39	2.21x + 195

Equations for the **WBZ** are as follows:

Al_2O_3 - Zr fractionation curve: -0.0083x + 22.5

All other constituents plotted against Zr are in the table below.

	Mafic volcanic rocks	Felsic volcanic rocks
SiO_2	0.15x + 55.14	0.049x + 48.61
TiO_2	-0.00487x + 0.74	0.00096x + 0.48
Fe_2O_3	-0.10x + 15.88	-0.0044 + 9.96
MnO	0.00058x + 0.04	0.00008x+ 0.15
MgO	-0.09x + 9.7	-0.033x + 6.96
CaO	-0.00659x + 3.0	-0.023x + 10.21
Na_2O	0.030x + 0.9	0.0035x + 2.11
K_2O	0.0072x + 1.34	0.0074x + 0.229
P_2O_5	0.000010x + 0.042	0.0034x + 0
Rb	0.40x + 0	0.30x + 0.37
Ba	2.7x + 40	5.2x + 0
Sr	0.82x + 25	2.2x + 100

Table F-1 - Various alteration indices and important alteration indicator elements.

Sample	Spitz & Darling	Sericite Index	Hashimoto	Cu	Pb	Zn	ZnPbCu %	S	Rb/Sr	Rb	Sr	As	Ba	LOI	MgO	Na2O	K/Ca	K2O	CaO	FeO total	MnO	SiO2	Cl
LS01	87	34	28	45	15	54	0.01	231	0.07	29	398	7	876	2.74	2.71	2.42	0.14	1.26	7.86	8.93	0.17	56.37	141
LS02	78	32	39	4	28	36	0.01	160	0.17	43	208	13	923	2.02	1.30	3.68	0.62	1.71	1.04	2.02	0.08	75.12	112
LS03	95	71	89	3	27	362	0.04	8785	0.69	42	18	39	647	6.53	7.39	0.83	0.85	2.07	0.37	10.05	0.58	56.01	67
LS04	100	98	85	1	20	239	0.03	1706	0.40	36	55	4	6984	4.60	5.28	0.04	0.61	1.88	1.19	4.14	0.23	70.83	60
LS05	99	97	95	513	3095	5573	0.92	12416	0.80	63	16	35	1586	3.14	0.44	0.08	0.97	2.99	0.10	2.32	0.03	77.83	96
LS06	98	81	97	3328	4357	5759	1.34	63681	0.10	10	90	57	5945	8.10	3.96	0.10	0.92	0.44	0.04	13.10	0.13	69.21	92
LS07	89	46	75	10	16	268	0.03	5646	0.38	38	61	42	993	5.36	6.17	2.25	0.83	1.94	0.39	10.30	0.37	54.88	86
LS08	96	86	84	38	1553	3153	0.47	10068	0.73	66	25	33	1585	3.39	0.62	0.57	0.94	3.45	0.21	2.51	0.02	76.45	104
LS09	86	36	45	67	5	53	0.01	159	0.08	32	359	23	684	7.78	11.37	2.32	0.09	1.28	12.95	13.78	0.25	42.08	130
LS10	99	97	94	16	167	27	0.02	33848	0.51	25	24	263	2715	4.91	0.38	0.05	0.95	1.65	0.08	6.82	< .01	79.14	89
LS11	98	94	89	155	37	28	0.02	9873	0.76	82	26	68	1725	4.51	0.91	0.27	0.92	4.54	0.38	3.77	0.05	69.72	51
LS12	85	18	69	76	70	316	0.05	2866	0.10	12	113	34	436	5.53	7.84	2.84	0.42	0.64	0.89	9.77	0.70	55.32	52
LS13	96	81	66	1	27	86	0.01	251	0.44	70	87	5	3115	6.25	3.17	0.63	0.53	2.77	2.44	2.38	0.06	66.69	68
LS14	99	97	94	79	3313	4588	0.80	9988	0.26	76	213	52	15314	4.60	0.65	0.12	0.96	4.36	0.19	2.01	0.02	69.42	43
LS15	99	97	95	n/a	n/a	n/a	n/a	n/a	n/a	n/a	n/a	n/a	n/a	5.70	3.30	0.06	0.89	1.69	0.21	7.95	0.11	71.97	
LS16	93	0	34	23128	2071	4682	2.99	142632	0.00	0	636	238	45418	9.82	0.12	0.02	0.00	< .05	0.21	18.73	0.01	65.06	62
LS17	96	82	86	16	51	451	0.05	10425	0.75	62	21	46	1241	6.15	4.36	0.68	0.85	3.06	0.53	8.79	0.39	58.49	63
LS18	93	75	77	18	26	554	0.06	3626	0.73	63	24	11	1122	3.27	1.50	1.10	0.91	3.35	0.34	2.88	0.20	73.09	93
LS19	98	91	90	52	1116	3956	0.51	5184	0.81	72	17	16	1611	3.28	1.60	0.36	0.94	3.61	0.25	2.45	0.14	74.06	103
LS20	88	17	47	59	21	321	0.04	534	0.08	7	88	1	303	11.17	9.10	1.74	0.04	0.36	8.89	9.55	1.21	43.62	352
LS21	99	97	62	n/a	n/a	n/a	n/a	n/a	n/a	n/a	n/a	n/a	n/a	3.78	0.66	0.12	0.60	3.89	2.63	1.70	0.09	72.80	
LS22	96	81	72	82	43	178	0.03	2067	0.40	59	91	67	901	6.84	7.63	0.75	0.48	3.12	3.43	12.97	0.16	53.18	43
LS23	100	97	97	13	29	219	0.03	6312	0.80	58	14	127	1513	5.58	5.31	0.08	0.93	2.78	0.20	8.48	0.15	60.18	49
LS24	73	27	25	2	18	234	0.03	136	0.15	27	151	9	1440	1.15	0.22	3.60	0.55	1.34	1.09	0.79	0.03	81.61	145
LS25	95	80	74	1	10	91	0.01	77	0.32	89	186	3	2750	4.91	2.73	0.84	0.73	3.46	1.28	1.68	0.04	70.12	89
LS26	89	62	66	360	2288	5414	0.81	35067	0.04	58	1311	88	132142	3.87	2.53	1.27	0.65	2.11	1.16	1.46	0.05	62.42	152
LS27	100	97	90	503	1789	12290	1.46	17905	0.57	28	21	26	2239	5.35	5.77	0.03	0.62	1.16	0.72	7.54	0.37	68.13	79
LS28	98	65	67	10	46	323	0.04	15610	0.15	11	63	18	5605	7.97	9.41	0.26	0.09	0.48	4.62	11.49	0.62	52.94	83
LS29	83	0	72	64	267	2792	0.31	10099	0.04	1	25	7	142	5.72	8.47	2.82	0.00	< .05	0.47	10.32	0.64	58.26	98
LS32	100	95	70	69	85	814	0.10	4199	0.39	27	43	57	698	7.62	6.04	0.07	0.30	1.37	3.14	7.74	0.63	58.27	96
LS33	95	79	80	1	55	322	0.04	105	0.40	76	115	7	2027	5.26	3.20	0.89	0.82	3.44	0.75	1.56	0.05	68.30	90
LS34	99	0	77	1	82	563	0.06	647	0.02	1	68	7	205	16.32	25.58	0.14	0.00	< .05	7.29	2.11	0.40	35.40	194
LS35	100	90	99	26	771	1039	0.18	4816	0.30	8	18	238	493	12.04	25.80	0.04	0.59	0.38	0.26	9.78	0.52	31.24	60
LS36	99	97	94	30	735	1358	0.21	8503	0.46	52	62	140	4317	4.38	4.34	0.08	0.88	2.96	0.40	2.50	0.10	71.59	89
LS37	100	0	80	333	706	1022	0.21	7712	0.04	1	15	6	73	7.84	12.67	0.02	0.00	< .05	3.23	11.01	0.60	54.01	87
LS38	100	95	96	445	2278	11088	1.38	58284	0.26	8	23	55	1422	10.57	9.10	0.02	0.47	0.35	0.40	18.08	0.32	51.52	60
LS39	79	3	64	4	12	172	0.02	8357	0.04	2	66	6	1129	4.85	7.26	3.65	0.17	0.10	0.49	9.01	0.42	58.60	141
LS40	89	13	82	9	15	275	0.03	5542	0.21	7	25	4	109	5.79	9.88	1.88	0.45	0.28	0.34	10.23	0.53	56.17	118
LS41	96	11	93	4	45	430	0.05	23254	0.12	2	14	38	19	10.81	12.65	0.58	0.16	0.07	0.37	19.99	0.69	39.28	42
LS42	85	28	69	4	32	197	0.02	13938	0.37	19	32	8	229	5.09	5.30	2.06	0.54	0.80	0.68	8.62	0.32	64.72	85
LS43	88	0	82	13	13	234	0.03	8074	0.06	1	20	14	21	6.22	10.04	1.80	0.00	< .05	0.35	10.77	0.52	56.53	111
LS44	91	8	81	11	47	320	0.04	23133	0.08	2	24	32	45	8.09	9.40	1.21	0.09	0.10	0.96	13.75	0.51	53.47	92
LS45	87	5	77	23	92	289	0.04	22281	0.06	2	30	28	40	7.43	8.95	1.88	0.09	0.09	0.89	13.89	0.47	53.27	80
LS46	98	92	83	1	3	7	0.00	291	0.61	90	56	18	704	3.59	0.33	0.36	0.89	4.00	0.51	1.61	0.03	73.00	115
Average	**93**	**58**	**76**	**673**	**579**	**1595**	**0.28**	**13602**	**0.31**	**33**	**113**	**45**	**5716**	**6.13**	**6.03**	**1.01**	**0.53**	**1.71**	**1.69**	**7.71**	**0.30**	**61.60**	**96.70**

S-D = Modified Spitz-Darling Alteration Index
Ser = Sericite Alteration Index
Hash = Hashimoto Alteration Index

ZnPbCu refer to combined copper, lead and zinc in wt. %.
All major oxides in wt. %; trace elements in ppm.
n/a = not analyzed

Table F-2 - Correlations for alteration indices and various elements for data from the Lucky Strike area.

	Cl	Spitz - Darling	Sericite Index	Hashimoto	Cu	Pb	Zn	Zn+Pb +Cu	Rb/Sr	K/Ca	As	Rb	Ba	Sr	LOI	MgO	CaO	Na2O	K2O	Total FeO	MnO
	1.000																				
Spitz/Darling	-0.365	1.000																			
Sericite Index	-0.348	0.663	1.000																		
Hashimoto	-0.440	0.696	0.492	1.000																	
Cu	-0.142	0.025	-0.209	-0.307	1.000																
Pb	-0.152	0.324	0.309	0.287	0.313	1.000															
Zn	-0.146	0.294	0.296	0.264	0.228	0.773	1.000														
Zn+Pb+Cu	-0.187	0.193	0.046	-0.010	0.784	0.756	0.772	1.000													
Rb/Sr	-0.283	0.479	0.754	0.494	-0.209	0.011	0.073	-0.091	1.000												
K/Ca	-0.294	0.365	0.800	0.489	-0.206	0.298	0.153	-0.011	0.795	1.000											
As	-0.306	0.329	0.263	0.196	0.471	0.221	0.108	0.383	0.098	0.196	1.000										
Rb	-0.197	0.288	0.703	0.183	-0.206	0.052	-0.043	-0.138	0.711	0.759	-0.077	1.000									
Ba	-0.001	-0.050	0.007	-0.158	0.303	0.366	0.279	0.391	-0.215	0.023	0.255	0.100	1.000								
Sr	0.077	-0.222	-0.108	-0.443	0.368	0.278	0.178	0.365	-0.354	-0.102	0.195	0.089	0.922	1.000							
LOI	0.177	0.288	-0.309	0.154	0.206	0.011	0.056	0.166	-0.405	-0.526	0.195	-0.564	-0.078	-0.108	1.000						
MgO	0.107	0.073	-0.394	0.164	-0.178	-0.220	-0.127	-0.191	-0.412	-0.536	0.030	-0.591	-0.188	-0.208	0.804	1.000					
CaO	0.637	-0.129	-0.258	-0.523	-0.100	-0.257	-0.229	-0.216	-0.370	-0.518	-0.250	-0.178	-0.074	0.177	0.333	0.328	1.000				
Na2O	0.347	-0.971	-0.625	-0.628	-0.175	-0.394	-0.345	-0.321	-0.434	-0.334	-0.401	-0.250	-0.060	0.123	-0.304	-0.026	0.163	1.000			
K2O	-0.218	0.384	0.651	0.182	-0.172	0.086	-0.041	-0.047	0.705	0.707	0.000	0.974	0.069	0.036	-0.559	-0.637	-0.189	-0.372	1.000		
Total FeO	-0.232	-0.041	-0.434	0.007	0.352	0.016	0.114	0.283	-0.429	-0.547	0.196	-0.690	-0.113	-0.078	0.555	0.392	0.105	0.026	-0.718	1.000	
MnO	0.353	-0.137	-0.496	0.006	-0.197	-0.343	-0.178	-0.247	-0.366	-0.594	-0.171	-0.667	-0.249	-0.304	0.536	0.598	0.270	0.191	-0.672	0.510	1.000

Table F-3 - Various alteration indices and important alteration indicator elements.

Sample	S-D	Ser	Hash	Cu	Pb	Zn	ZnPbCu	S	Rb/Sr	Rb	Sr	As	Ba	MgO	Na2O	K/Ca	K2O	CaO	FeO total	MnO	SiO2	Cl
PH-01	82	33	50	768	245	379	0.14	84085	0.22	32	147	99	388	4.09	5.17	1.79	2.57	1.44	12.32	0.07	53.44	88
PH-02	85	39	66	79	316	564	0.10	36987	0.40	45	113	49	368	10.55	4.10	0.97	2.66	2.75	8.38	0.19	49.99	69
PH-03	83	30	63	144	24	107	0.03	33661	0.25	34	136	1	401	8.50	5.13	1.76	2.19	1.24	7.80	0.13	52.44	713
PH-04	98	89	88	24	15	839	0.09	10471	1.84	48	26	31	507	0.55	0.47	30.01	3.85	0.13	1.64	0.00	76.47	86
PH-05	99	94	93	1	12	1	0.00	8364	4.12	49	12	18	631	0.66	0.23	33.32	3.53	0.11	1.37	0.00	79.72	109
PH-06	98	92	93	42	39	205	0.03	19134	2.67	57	21	43	720	2.49	0.36	24.29	3.98	0.16	4.24	0.04	71.18	80
PH-07	99	94	93	6	15	59	0.01	15954	3.58	40	11	69	406	0.98	0.17	23.21	2.73	0.12	2.65	0.01	81.73	68
PH-08	83	27	66	2604	45	178	0.28	31242	0.22	32	146	52	268	10.99	4.45	0.76	1.65	2.18	8.55	0.25	51.04	128
PH-09	95	76	87	1	17	15	0.00	13010	1.17	37	32	1	500	4.45	0.83	10.28	2.62	0.25	3.13	0.03	74.14	46
PH-10	98	88	84	45	474	1653	0.22	16796	1.58	44	28	23	538	1.39	0.45	7.01	3.41	0.49	3.15	0.02	75.37	94
PH-11	96	80	79	11	373	1689	0.21	13028	1.94	51	26	20	476	1.05	0.80	9.53	3.16	0.33	2.79	0.02	76.50	78
PH-12	94	69	61	717	50	100	0.09	16377	1.04	31	30	150	307	3.20	0.96	0.89	2.18	2.46	3.16	0.11	74.44	115
PH-13	76	17	23	1	18	1	0.00	9660	0.12	14	122	1	130	1.26	4.79	0.36	0.97	2.70	1.88	0.07	73.53	128
PH-14	99	93	81	1	28	31	0.01	12256	2.93	41	14	1	562	2.18	0.22	3.01	3.14	1.04	2.53	0.04	76.48	48
PH-15	94	70	76	350	17	31	0.04	17039	0.78	33	43	33	481	4.10	1.04	2.48	2.47	0.99	3.98	0.05	73.25	78
PH-16	93	63	78	12	8	31	0.01	421	0.75	45	60	1	358	5.45	1.46	3.17	2.51	0.79	0.82	0.03	70.97	113
PH-17	89	39	79	41	27	181	0.02	3268	0.35	40	113	1	274	10.83	2.45	1.96	1.57	0.80	9.29	0.09	56.85	152
PH-18	99	93	86	147	11	1787	0.19	13722	4.97	42	8	41	371	2.93	0.25	4.31	3.09	0.72	3.30	0.03	75.98	91
PH-19	94	69	79	31	22	30	0.01	1153	1.01	47	46	1	411	3.33	1.16	6.55	2.57	0.39	1.20	0.03	74.78	101
PH-20	100	100	97	81354	5476	223	8.71	188860	4.11	12	3	182	80	0.00	0.00	33.70	1.06	0.03	20.07	0.02	75.45	52
PH-21	97	86	52	1	10	1	0.00	8410	1.47	50	34	28	447	1.15	0.61	0.98	3.84	3.92	1.84	0.07	69.16	94
PH-22	98	90	90	1	24	1	0.00	6069	2.86	48	17	11	547	0.61	0.37	48.71	3.51	0.07	1.02	0.00	77.10	102
PH-23	98	90	86	81	82	57	0.02	24181	2.12	55	26	48	791	1.17	0.41	10.24	3.59	0.35	3.94	0.01	75.17	105
PH-24	98	90	88	1	2	1	0.00	2505	2.99	59	20	43	372	0.53	0.47	21.37	4.25	0.20	0.53	0.00	71.08	54

S-D = Modified Spitz-Darling Alteration Index
Ser = Sericite Alteration Index
Hash = Hashimoto Alteration Index

ZnPbCu refer to combined copper, lead and zinc in wt. %.
All major oxides in wt. %; trace elements in ppm.

Table F-4 - Correlation Coefficients for Alteration Indices and selected elements from the PHZ.

Variables	Spitz/Darling	Sericite	Hashimoto	Cu	Pb	Zn	Zn+Pb+Cu	S	Rb/Sr	Rb	Sr	As	Ba	MgO	Na2O	K/Ca	K2O	CaO	Total FeO	MnO	SiO2	Cl
Spitz/Darling	1.000																					
Sericite Index	0.982	1.000																				
Hashimoto	0.817	0.767	1.000																			
Cu	0.192	0.221	0.246	1.000																		
Pb	0.192	0.224	0.244	0.993	1.000																	
Zn	0.155	0.171	0.141	-0.046	0.033	1.000																
Zn+Pb+Cu	0.197	0.227	0.251	0.999	0.995	-0.009	1.000															
S	-0.037	0.018	0.073	0.903	0.912	-0.005	0.905	1.000														
Rb/Sr	0.766	0.822	0.680	0.332	0.318	0.219	0.338	0.169	1.000													
Rb	0.497	0.456	0.447	-0.538	-0.516	0.141	-0.533	-0.581	0.226	1.000												
Sr	-0.954	-0.969	-0.700	-0.198	-0.198	-0.154	-0.203	0.056	-0.790	-0.378	1.000											
As	0.120	0.153	0.063	0.663	0.661	-0.007	0.663	0.749	0.227	-0.415	-0.128	1.000										
Ba	0.483	0.491	0.435	-0.467	-0.446	0.043	-0.465	-0.422	0.236	0.755	-0.413	-0.360	1.000									
MgO	-0.620	-0.729	-0.267	-0.197	-0.206	-0.100	-0.201	-0.064	-0.620	-0.155	0.756	-0.166	-0.282	1.000								
Na2O	-0.978	-0.959	-0.749	-0.168	-0.164	-0.132	-0.172	0.106	-0.733	-0.435	0.974	-0.080	-0.431	0.666	1.000							
K/Ca	0.552	0.600	0.639	0.335	0.320	-0.100	0.331	0.192	0.631	0.211	-0.555	0.154	0.249	-0.546	-0.521	1.000						
K2O	0.611	0.635	0.434	-0.425	-0.403	0.190	-0.418	-0.436	0.403	0.890	-0.544	-0.261	0.784	-0.452	-0.542	0.353	1.000					
CaO	-0.557	-0.546	-0.827	-0.181	-0.186	-0.153	-0.186	-0.069	-0.530	-0.278	0.512	0.065	-0.365	0.357	0.527	-0.630	-0.276	1.000				
Total FeO	-0.279	-0.273	-0.031	0.740	0.749	-0.005	0.742	0.895	-0.079	-0.582	0.365	0.623	-0.477	0.334	0.357	-0.034	-0.575	0.049	1.000			
MnO	-0.700	-0.747	-0.529	-0.112	-0.123	-0.104	-0.116	0.062	-0.607	-0.307	0.766	0.080	-0.377	0.832	0.739	-0.569	-0.471	0.676	0.358	1.000		
SIO2	0.741	0.784	0.454	0.098	0.092	0.097	0.101	-0.162	0.647	0.164	-0.879	-0.001	0.301	-0.852	-0.832	0.486	0.340	-0.479	-0.501	-0.830	1.000	
Cl	-0.428	-0.437	-0.249	-0.105	-0.118	-0.100	-0.109	-0.016	-0.312	-0.144	0.461	-0.212	-0.073	0.380	0.499	-0.202	-0.208	0.111	0.130	0.321	-0.438	1.000

Table F-6 - Correlation Coefficients for Alteration Indices and selected elements from the WBZ.

	Spitz/Darling	Sericite	Hashimoto	Cu	Pb	Zn	Zn+Pb+Cu	S	Rb/Sr	Rb	Sr	As	Ba	MgO	Na2O	K/Ca	K2O	CaO	Total FeO	MnO	SiO2	Cl
Spitz/Darling	1.000																					
Sericite Index	0.837	1.000																				
Hashimoto	0.816	0.583	1.000																			
Cu	-0.009	-0.033	-0.032	1.000																		
Pb	0.403	0.410	0.358	-0.129	1.000																	
Zn	0.212	0.126	0.318	-0.127	0.422	1.000																
Zn+Pb+Cu	0.257	0.178	0.348	-0.124	0.540	0.991	1.000															
S	0.364	0.323	0.371	-0.008	0.368	0.435	0.460	1.000														
Rb/Sr	0.722	0.777	0.645	-0.016	0.402	0.074	0.129	0.353	1.000													
Rb	0.496	0.726	0.196	0.058	0.161	-0.224	-0.183	0.175	0.697	1.000												
Sr	-0.713	-0.509	-0.696	-0.121	-0.257	-0.261	-0.283	-0.357	-0.576	-0.312	1.000											
As	0.283	0.284	0.231	-0.054	0.069	0.332	0.319	0.107	0.016	-0.226	-0.191	1.000										
Ba	0.568	0.680	0.375	-0.023	0.627	0.084	0.172	0.180	0.712	0.676	-0.395	-0.163	1.000									
MgO	-0.121	-0.527	0.264	-0.020	-0.223	0.079	0.040	-0.042	-0.370	-0.598	-0.030	-0.096	-0.498	1.000								
Na2O	-0.986	-0.814	-0.840	-0.023	-0.395	-0.221	-0.265	-0.368	-0.711	-0.452	0.756	-0.278	-0.541	0.102	1.000							
K/Ca	0.402	0.492	0.461	-0.023	0.118	-0.062	-0.040	0.142	0.755	0.493	-0.367	-0.038	0.473	-0.293	-0.402	1.000						
K2O	0.431	0.735	0.167	-0.005	0.221	-0.200	-0.153	0.102	0.654	0.916	-0.172	-0.232	0.667	-0.665	-0.408	0.549	1.000					
CaO	-0.187	-0.335	-0.466	-0.046	-0.187	-0.233	-0.245	-0.238	-0.406	-0.198	0.410	-0.148	-0.275	0.131	0.227	-0.551	-0.208	1.000				
Total FeO	-0.092	-0.399	0.300	-0.014	-0.074	0.360	0.323	0.381	-0.209	-0.520	-0.111	-0.033	-0.423	0.800	0.079	-0.231	-0.619	-0.092	1.000			
MnO	-0.280	-0.543	0.083	0.116	-0.231	0.264	0.212	0.017	-0.371	-0.547	0.034	-0.093	-0.487	0.776	0.280	-0.405	-0.648	0.133	0.837	1.000		
SIO2	0.140	0.448	-0.182	0.023	0.179	-0.086	-0.053	-0.170	0.236	0.300	-0.003	0.358	0.366	-0.841	-0.161	0.177	0.403	-0.106	-0.837	-0.782	1.000	
Cl	0.274	0.034	0.320	-0.211	0.265	0.460	0.465	0.051	-0.003	-0.407	-0.192	0.540	-0.095	0.222	-0.255	-0.129	-0.496	-0.097	0.326	0.170	-0.021	1.000

Table F-5 - Various alteration indices and important alteration indicator elements.

Sample	S-D	Ser	Hash	Cu	Pb	Zn	ZnPbCu	S	Rb/Sr	Rb	Sr	As	Ba	MgO	Na2O	K/Ca	K2O	CaO	eO tota	MnO	SiO2	Cl
WB-1	80	15	56	0	6	1	0.00	12575	0.18	13	70	11	168	5.11	4.05	1.45	0.73	0.51	10.78	0.15	62.31	85
WB-2	98	91	83	1	6	1	0.00	6045	2.74	63	23	24	463	1.42	0.44	6.08	4.63	0.76	1.74	0.05	70.59	82
WB-3	86	45	65	1	3	1	0.00	2146	0.97	33	34	14	380	3.11	2.67	11.05	2.22	0.20	5.37	0.07	69.20	79
WB-4	98	92	91	3	17	1	0.00	16678	5.08	55	11	140	570	0.52	0.35	35.73	4.10	0.11	3.07	0.01	71.77	77
WB-5	88	30	81	44	18	206	0.03	15099	0.48	14	29	77	170	9.37	2.07	2.56	0.90	0.35	13.44	0.23	57.51	98
WB-6	92	52	89	6	17	101	0.01	13173	1.27	31	24	52	292	14.61	1.73	8.62	1.87	0.22	14.83	0.22	45.63	76
WB-7	90	61	64	6	5	1	0.00	8553	1.31	47	36	25	590	1.04	2.12	9.94	3.25	0.33	1.93	0.01	72.47	78
WB-8	99	96	78	15	32	1	0.00	31597	1.53	46	30	67	503	1.90	0.14	2.40	3.14	1.31	5.26	0.03	73.42	80
WB-9	93	56	90	3	10	124	0.01	3935	1.04	28	27	7	290	13.94	1.55	12.19	1.97	0.16	13.38	0.20	48.04	109
WB-10	96	75	89	0	21	87	0.01	11049	2.13	34	16	17	289	7.34	0.70	4.00	2.06	0.51	16.29	0.23	54.13	164
WB-11	96	84	76	1	9	1	0.00	15238	2.48	60	24	16	946	2.55	0.76	3.19	4.04	1.27	3.65	0.05	68.13	49
WB-12	83	22	64	0	3	126	0.01	5459	0.42	25	60	11	242	8.63	3.98	0.80	1.12	1.39	13.61	0.44	50.95	77
WB-13	100	100	89	0	134	2772	0.29	15514	1.45	13	9	1061	138	1.92	0.00	2.32	0.75	0.32	4.39	0.05	86.31	195
WB-14	84	42	47	4	2	16	0.00	2208	1.21	47	38	12	445	1.37	3.72	2.96	2.71	0.92	2.55	0.07	68.91	67
WB-15	99	95	94	9	11	9	0.00	12601	5.08	57	11	28	857	1.94	0.23	26.07	4.04	0.15	2.94	0.03	71.91	81
WB-16	99	95	95	15	12	52	0.01	23610	6.02	69	11	36	1008	2.23	0.24	33.79	5.02	0.15	5.12	0.02	64.84	75
WB-17	94	4	79	4	11	132	0.01	709	0.00	0	15	12	60	13.78	0.96	0.02	0.04	2.67	10.91	0.19	57.14	120
WB-18	93	72	73	1	10	1	0.00	13273	2.07	60	29	1	893	1.16	1.64	11.77	4.26	0.36	2.38	0.01	68.13	73
WB-19	86	49	58	17	15	92	0.01	6957	1.20	37	31	21	379	1.62	2.57	6.80	2.42	0.36	2.19	0.03	74.19	87
WB-30	78	12	53	1	1	118	0.01	200	0.06	9	157	9	190	5.88	4.84	0.69	0.64	0.93	8.31	0.13	70.01	131
WB-31	99	93	81	3	7	37	0.00	5265	3.83	53	14	1	904	4.14	0.26	2.35	3.64	1.55	4.14	0.13	71.23	69
WB-20	92	67	72	4	6	88	0.01	3680	2.11	42	20	17	882	1.74	1.50	9.12	3.04	0.33	2.00	0.05	74.07	99
WB-21	87	52	60	1	6	5	0.00	7736	1.09	38	35	1	490	1.51	2.57	8.27	2.78	0.34	2.19	0.03	72.53	73
WB-22	84	42	43	1	8	1	0.00	20525	0.62	36	58	17	240	1.80	3.41	1.09	2.43	2.22	3.36	0.06	67.94	88
WB-23	92	68	65	40	33	468	0.05	16329	1.33	51	38	29	376	0.80	1.60	4.96	3.46	0.70	2.45	0.02	71.80	65
WB-24	86	30	74	1	1	125	0.01	613	0.53	21	39	1	164	10.08	2.47	0.68	1.03	1.52	6.87	0.19	62.62	72
WB-25	88	56	64	25	6	1	0.00	6898	1.66	42	25	17	688	1.32	2.26	16.82	2.91	0.17	1.83	0.02	73.92	89
WB-26	91	60	71	79	52	446	0.06	11308	2.00	42	21	19	559	4.22	1.74	2.65	2.65	1.00	7.16	0.25	65.16	56
WB-27	94	69	71	1	6	16	0.00	7772	0.47	45	96	1	336	5.29	1.61	1.72	3.51	2.04	2.23	0.07	58.13	72
WB-28	85	42	34	4	12	80	0.01	2116	0.33	34	102	1	297	0.82	3.48	0.85	2.55	2.99	2.45	0.05	67.74	87
WB-29	79	56	54	1	1	62	0.01	27	0.33	34	103	1	197	0.21	3.79	8.95	4.91	0.55	0.65	0.04	75.23	1
BE-01-64	98	93	89	0	743	1000	0.17	25363	5.00	60	12	25	1077	1.25	0.32	11.00	4.34	0.39	4.37	0.01	68.92	121
BE-3-106	98	92	84	0	622	1973	0.26	23099	2.58	54	21	54	1437	0.99	0.33	6.55	3.69	0.56	3.56	0.02	72.22	110
BE-8-267	92	65	79	0	36	204	0.02	25880	2.36	36	15	17	239	3.96	1.34	6.13	2.49	0.41	6.20	0.06	69.83	87
BE-10-14	89	40	80	0	10	5311	0.53	13040	1.14	22	19	1	251	8.42	2.07	4.33	1.35	0.31	15.39	0.33	54.15	137
BE-10-18	92	55	85	0	157	2907	0.31	74405	2.26	33	14	68	274	8.10	1.53	6.24	1.86	0.30	22.12	0.25	47.80	79
BE-3-111	100	100	96	0	645	2540	0.32	22999	3.78	30	8	1	1372	0.75	0.00	17.67	3.39	0.19	3.46	0.01	75.02	105

S-D = Modified Spitz-Darling Alteration Index
Ser = Sericite Alteration Index
hash = Hashimoto Alteration Index

Table F-7 - Calculated mass changes for volcanic rocks in the Lucky Strike and Middle Branch Area

Drill Hole	outcrop	196	542	542	2889	2889	2871	2871	2871	2892	202	202	202
From	n/a	146	8	262	385	537	270	444.5	601.5	264	205	214	557
To	n/a	148	10	265	388	540	272.5	447	604	265	207	216	560
Sample	LS-01	LS-03	LS-06	LS-07	LS-20	LS-22	LS-27	LS-28	LS-29	LS-32	LS-35	LS-36	LS-37
Lithology	And-Bas	And-Bas	And-Bas	And-Bas	And-Bas	And-Bas	And-Bas	And-Bas	And-Bas	And-Bas	And-Bas	And-Bas	And-Bas
Raw Data - LOI Free													
Zr	75	47	11	61	27	69	27	42	38	29	68	70	22
Zr precursor	77	52	41	59	36	70	51	62	51	37	57	87	39
Al2O3/Zr	0.23	0.37	0.49	0.31	0.56	0.26	0.38	0.29	0.37	0.55	0.33	0.19	0.51
Enrich Factor	1.02	1.10	3.70	0.98	1.33	1.01	1.88	1.48	1.34	1.26	0.84	1.24	1.78
SiO2	58.01	59.28	75.27	57.58	49.38	53.18	72.76	57.56	61.28	62.99	35.15	74.60	56.31
TiO2	0.83	0.64	0.14	0.81	0.51	0.95	0.37	0.71	0.52	0.51	0.91	0.58	0.40
Al2O3	16.96	17.23	5.35	19.00	15.13	17.68	10.16	12.38	14.23	15.90	22.19	13.51	11.20
Fe2O3	9.19	10.64	14.25	10.81	10.81	12.97	8.05	12.49	10.86	8.37	11.00	2.60	11.48
MnO	0.17	0.85	0.14	0.39	1.37	0.16	0.40	0.67	0.67	0.68	0.59	0.10	0.63
MgO	2.79	7.82	4.31	6.47	10.30	7.63	6.16	10.23	8.91	6.53	29.03	4.52	13.21
CaO	8.09	0.39	0.04	0.41	10.06	3.43	0.77	5.02	0.49	3.39	0.29	0.42	3.37
Na2O	2.49	0.88	0.01	2.36	1.97	0.75	0.03	0.28	2.97	0.08	0.29	0.42	3.37
K2O	1.30	2.19	0.48	2.04	0.41	3.12	1.24	0.52	0.01	1.48	0.43	3.08	0.01
P2O5	0.16	0.08	0.01	0.14	0.06	0.13	0.06	0.13	0.06	0.06	0.12	0.16	0.04
Rb	27	43	10	36	7	59	27	11	1	27	8	54	1
Ba	823	672	5997	937	292	901	2204	5536	136	694	501	4429	71
Sr	374	19	91	58	85	91	21	62	24	42	19	64	15
Precursors													
SiO2	52.37	51.15	50.60	51.53	50.37	52.02	51.10	51.66	51.11	50.40	51.42	52.86	50.52
TiO2	0.78	0.78	0.79	0.78	0.73	0.78	0.75	0.76	0.78	0.74	0.78	0.77	0.74
Al2O3	17.38	19.04	19.79	18.53	20.11	17.85	19.11	18.35	19.10	20.06	18.68	16.72	19.89
Fe2O3	9.62	9.73	9.78	9.70	9.80	9.65	9.74	9.69	9.74	9.80	9.71	9.58	9.79
MnO	0.16	0.15	0.15	0.15	0.15	0.16	0.15	0.15	0.15	0.15	0.15	0.16	0.15
MgO	4.42	5.25	5.62	5.00	5.78	4.66	5.28	4.91	5.28	5.75	5.07	4.10	5.67
CaO	8.44	9.02	9.27	8.84	9.38	8.61	9.04	8.78	9.04	9.37	8.89	8.22	9.31
Na2O	2.38	2.29	2.25	2.32	2.24	2.35	2.29	2.33	2.29	2.24	2.31	2.41	2.25
K2O	0.80	0.61	0.53	0.67	0.49	0.74	0.60	0.69	0.61	0.50	0.65	0.87	0.52
P2O5	0.23	0.16	0.12	0.18	0.11	0.21	0.15	0.19	0.15	0.11	0.17	0.26	0.12
Rb	22	15	12	17	10	20	14	18	14	10	16	24	11
Ba	580	451	394	490	369	543	446	505	447	372	479	630	385
Sr	377	417	435	405	443	389	419	400	418	441	408	361	437
Total	96.58	98.18	98.91	97.69	99.16	97.04	98.22	97.50	98.24	99.12	97.84	95.95	98.96
factor	1.0354	1.0185	1.0111	1.0236	1.0085	1.0305	1.0181	1.0257	1.0179	1.0089	1.0221	1.0423	1.0105
Precursors - normalized to 100%													
SiO2	54.23	52.10	51.17	52.74	50.80	53.61	52.02	52.99	52.02	50.85	52.55	55.09	51.06
TiO2	0.80	0.80	0.80	0.80	0.74	0.80	0.76	0.78	0.80	0.74	0.80	0.81	0.75
Al2O3	17.99	19.39	20.01	18.97	20.28	18.40	19.46	18.82	19.44	20.24	19.09	17.43	20.10
Fe2O3	9.96	9.91	9.89	9.93	9.89	9.95	9.91	9.94	9.91	9.89	9.92	9.98	9.89
MnO	0.16	0.16	0.15	0.16	0.15	0.16	0.16	0.16	0.16	0.15	0.16	0.16	0.15
MgO	4.58	5.34	5.68	5.11	5.83	4.80	5.38	5.03	5.37	5.80	5.18	4.27	5.73
CaO	8.74	9.18	9.38	9.05	9.46	8.87	9.21	9.00	9.20	9.45	9.09	8.56	9.41
Na2O	2.46	2.33	2.28	2.37	2.25	2.43	2.33	2.39	2.33	2.26	2.36	2.52	2.27
K2O	0.82	0.62	0.54	0.68	0.50	0.77	0.61	0.71	0.62	0.50	0.67	0.91	0.52
P2O5	0.24	0.16	0.12	0.18	0.11	0.22	0.16	0.19	0.16	0.11	0.18	0.27	0.12
Rb	22	15	12	17	10	20	15	18	15	11	17	25	11
Ba	600	460	398	502	372	559	454	518	455	376	489	657	389
Sr	390	425	440	414	446	400	426	411	426	445	417	377	442
Total	100.00	100.00	100.00	100.00	100.00	100.00	100.00	100.00	100.00	100.00	100.00	100.00	100.00
Reconstituted													
SiO2	59.4	65.5	278.4	56.2	65.6	53.7	136.9	85.3	82.2	79.5	29.6	92.3	100.0
TiO2	0.9	0.7	0.5	0.8	0.7	1.0	0.7	1.1	0.7	0.6	0.8	0.7	0.7
Al2O3	17.4	19.0	19.8	18.5	20.1	17.9	19.1	18.3	19.1	20.1	18.7	16.7	19.9
Fe2O3	9.4	11.8	52.7	10.5	14.4	13.1	15.1	18.5	14.6	10.6	9.3	3.2	20.4
MnO	0.2	0.9	0.5	0.4	1.8	0.2	0.8	1.0	0.9	0.9	0.5	0.1	1.1
MgO	2.9	8.6	15.9	6.3	13.7	7.7	11.6	15.2	12.0	8.2	24.4	5.6	23.5
CaO	8.3	0.4	0.1	0.4	13.4	3.5	1.4	7.4	0.7	4.3	0.2	0.5	6.0
Na2O	2.6	1.0	0.0	2.3	2.6	0.8	0.1	0.4	4.0	0.1	0.2	0.5	6.0
K2O	1.3	2.4	1.8	2.0	0.5	3.2	2.3	0.8	0.0	1.9	0.4	3.8	0.0
P2O5	0.2	0.1	0.0	0.1	0.1	0.1	0.1	0.2	0.1	0.1	0.1	0.2	0.1
Rb	28	48	37	35	9	60	51	16	1	34	7	67	2
Ba	843	742	22179	914	388	910	4146	8205	183	876	422	5482	126
Sr	383	21	337	57	113	92	40	92	32	53	16	79	27
Total	102.4	110.5	369.8	97.5	132.9	101.0	188.1	148.2	134.2	126.1	84.2	123.8	177.7
Mass Changes													
SiO2	5.2	13.4	227.2	3.4	14.8	0.1	84.8	32.3	30.2	28.6	-23.0	37.2	49.0
TiO2	0.0	-0.1	-0.3	-0.0	-0.1	0.2	-0.1	0.3	-0.1	-0.1	-0.0	-0.1	-0.0
Al2O3	0.0	0.0	0.0	0.0	0.0	0.0	0.0	0.0	0.0	0.0	0.0	0.0	0.0
Fe2O3	-0.5	1.8	42.8	0.6	4.5	3.1	5.2	8.6	4.7	0.7	-0.7	-6.8	10.5
MnO	0.0	0.8	0.4	0.2	1.7	0.0	0.6	0.8	0.7	0.7	0.3	-0.0	1.0
MgO	-1.7	3.3	10.3	1.2	7.9	2.9	6.2	10.1	6.6	2.4	19.3	1.3	17.7
CaO	-0.5	-8.8	-9.2	-8.7	3.9	-5.4	-7.8	-1.6	-8.5	-5.2	-8.8	-8.0	-3.4
Na2O	0.1	-1.4	-2.2	-0.1	0.4	-1.7	-2.3	-2.0	1.7	-2.2	-2.1	-2.0	3.7
K2O	0.5	1.8	1.2	1.3	0.0	2.4	1.7	0.1	-0.6	1.4	-0.3	2.9	-0.5
P2O5	-0.1	-0.1	-0.1	-0.0	-0.0	-0.1	-0.0	0.0	-0.1	-0.0	-0.1	-0.1	-0.0
Rb	5	33	25	18	-1	39	36	-2	-13	24	-10	42	-9
Ba	243	283	21781	412	16	350	3692	7687	-272	500	-68	4825	-263
Sr	-7	-404	-103	-358	-333	-308	-387	-319	-394	-392	-401	-297	-415
Total	2.4	10.5	269.8	-2.5	32.9	1.0	88.1	48.2	34.2	26.1	-15.8	23.8	77.7

Table F-7 continued

Drill Hole	202	202	202	202	202	202	202	202	1916		196	542	2889
From	608	686	835	914	939	1031	1095.5	1214	1819.5		579.5	376	17
To	611	688	837	916	941	1032	1098	1216	1822.5		583.5	378	18
Sample	LS-38	LS-39	LS-40	LS-41	LS-42	LS-43	LS-44	LS-45	MB-10	Average	LS-05	LS-08	LS-16
Lithology	And-Bas	And-Bas	And-Bas	And-Bas	And-Bas	And-Bas	And-Bas	And-Bas	And-Bas	And-Bas	Dacites	Dacites	Dacites
Raw Data - LOI Free													
Zr	19	50	50	56	122	48	79	48	64	49	140	164	1
Zr precursor	36	60	59	61	132	60	96	63	81	59	154	152	60
Al2O3/Zr	0.55	0.31	0.31	0.30	0.10	0.31	0.17	0.29	0.21	0.32	0.08	0.08	0.31
Enrich Factor	1.92	1.20	1.18	1.10	1.08	1.25	1.21	1.32	1.27	1.33	1.10	0.93	59.73
SiO2	57.31	64.31	60.34	44.07	68.88	60.72	57.91	57.97	50.05	56.30	82.26	78.70	75.22
TiO2	0.31	0.66	0.69	0.77	0.81	0.72	0.77	0.66	0.76	0.61	0.34	0.43	0.01
Al2O3	10.45	15.41	15.66	16.76	12.64	14.78	13.34	13.86	13.41	13.79	11.08	13.29	0.31
Fe2O3	20.11	9.89	10.99	22.43	9.17	11.57	14.89	15.11	10.93	11.24	2.45	2.48	21.66
MnO	0.36	0.46	0.57	0.77	0.34	0.56	0.55	0.51	0.17	0.48	0.03	0.02	0.01
MgO	10.12	7.97	10.61	14.19	5.64	10.78	10.18	9.74	4.26	8.76	0.47	0.64	0.14
CaO	0.44	0.54	0.37	0.42	0.72	0.38	1.04	0.97	6.16	2.05	0.11	0.22	0.24
Na2O	0.44	0.54	0.37	0.42	0.72	0.38	1.04	0.97	1.84	0.98	0.08	0.59	2.31
K2O	0.39	0.11	0.30	0.08	0.85	0.01	0.11	0.10	1.12	0.84	3.16	3.55	0.01
P2O5	0.06	0.12	0.11	0.10	0.21	0.11	0.17	0.11	0.08	0.10	0.03	0.08	0.08
Rb	8	3	7	2	20	1	2	2	24	17	63	65	0
Ba	1410	1173	106	19	235	21	44	40	869	1179	1576	1569	41056
Sr	23	69	25	14	33	20	24	30	376	69	16	25	576
Precursors													
SiO2	50.40	51.55	51.51	51.62	55.08	51.55	53.29	51.71	52.60	49.41	74.65	74.58	71.54
TiO2	0.74	0.78	0.78	0.78	0.76	0.78	0.77	0.78	0.78	0.74	0.32	0.32	0.46
Al2O3	20.07	18.50	18.55	18.40	13.69	18.49	16.13	18.28	17.07	17.56	12.21	12.34	18.52
Fe2O3	9.80	9.70	9.70	9.69	9.38	9.70	9.54	9.68	9.60	9.27	1.82	1.84	2.39
MnO	0.15	0.15	0.15	0.15	0.16	0.15	0.16	0.16	0.16	0.15	0.09	0.09	0.08
MgO	5.76	4.98	5.01	4.93	2.60	4.98	3.81	4.87	4.27	4.69	0.29	0.32	1.69
CaO	9.37	8.83	8.85	8.80	7.17	8.83	8.01	8.75	8.34	8.40	1.04	1.06	1.98
Na2O	2.24	2.32	2.32	2.33	2.57	2.32	2.44	2.33	2.40	2.23	4.04	4.08	5.74
K2O	0.50	0.67	0.67	0.68	1.20	0.67	0.93	0.70	0.83	0.66	1.66	1.64	0.58
P2O5	0.11	0.18	0.18	0.18	0.40	0.18	0.29	0.19	0.24	0.18	0.05	0.05	0.05
Rb	10	17	17	17	37	17	27	18	23	17	54	54	24
Ba	372	493	489	501	864	493	676	510	603	482	1035	1022	401
Sr	442	404	405	402	289	404	347	399	370	ERR	139	142	279
Total	99.12	97.66	97.71	97.57	93.01	97.66	95.37	97.45	96.28	93.27	96.16	96.31	103.03
factor	1.0088	1.0240	1.0234	1.0249	1.0751	1.0240	1.0485	1.0262	1.0386	0.9812	1.0399	1.0383	0.9706
Precursors - normalized to 100%													
SiO2	50.84	52.79	52.72	52.91	59.22	52.79	55.87	53.07	54.63	50.70	77.62	77.44	69.43
TiO2	0.74	0.80	0.80	0.80	0.82	0.80	0.81	0.80	0.81	0.75	0.33	0.33	0.45
Al2O3	20.24	18.94	18.98	18.86	14.72	18.94	16.91	18.76	17.73	17.99	12.70	12.81	17.97
Fe2O3	9.89	9.93	9.93	9.93	10.08	9.93	10.00	9.94	9.97	9.50	1.90	1.91	2.32
MnO	0.15	0.16	0.16	0.16	0.17	0.16	0.17	0.16	0.16	0.15	0.09	0.09	0.08
MgO	5.81	5.10	5.12	5.05	2.80	5.10	3.99	5.00	4.44	4.81	0.30	0.33	1.64
CaO	9.45	9.04	9.05	9.02	7.71	9.04	8.40	8.98	8.66	8.61	1.08	1.10	1.92
Na2O	2.26	2.38	2.37	2.38	2.77	2.38	2.56	2.39	2.49	2.28	4.20	4.23	5.58
K2O	0.50	0.69	0.68	0.70	1.29	0.69	0.98	0.71	0.86	0.68	1.72	1.70	0.56
P2O5	0.11	0.18	0.18	0.19	0.43	0.18	0.30	0.19	0.25	0.18	0.05	0.05	0.05
Rb	11	17	17	18	40	17	28	18	24	17	56	56	23
Ba	375	505	500	513	929	505	709	523	627	496	1076	1061	389
Sr	446	414	415	412	310	414	364	409	384	ERR	145	148	271
Total	100.00	100.00	100.00	100.00	100.00	100.00	100.00	100.00	100.00	95.65	100.00	100.00	100.00
econstituted													
SiO2	110.0	77.2	71.5	48.4	74.6	76.0	70.0	76.5	63.7	80.5	90.7	73.1	4492.8
TiO2	0.6	0.8	0.8	0.8	0.9	0.9	0.9	0.9	1.0	0.8	0.4	0.4	0.6
Al2O3	20.1	18.5	18.5	18.4	13.7	18.5	16.1	18.3	17.1	17.6	12.2	12.3	18.5
Fe2O3	38.6	11.9	13.0	24.6	9.9	14.5	18.0	19.9	13.9	16.0	2.7	2.3	1293.7
MnO	0.7	0.6	0.7	0.8	0.4	0.7	0.7	0.7	0.2	0.6	0.0	0.0	0.6
MgO	19.4	9.6	12.6	15.6	6.1	13.5	12.3	12.8	5.4	11.4	0.5	0.6	8.4
CaO	0.8	0.6	0.4	0.5	0.8	0.5	1.3	1.3	7.8	2.6	0.1	0.2	14.3
Na2O	0.8	0.6	0.4	0.5	0.8	0.5	1.3	1.3	2.3	1.3	0.1	0.5	138.0
K2O	0.7	0.1	0.4	0.1	0.9	0.0	0.1	0.1	1.4	1.1	3.5	3.3	0.6
P2O5	0.1	0.1	0.1	0.1	0.2	0.1	0.2	0.1	0.1	0.1	0.0	0.1	4.8
Rb	15	4	8	2	22	1	2	3	31	21	69	60	0
Ba	2707	1408	126	21	254	26	53	53	1106	2225	1737	1457	2452242
Sr	44	83	30	15	36	25	29	40	478	ERR	18	23	34404
Total	192.0	120.0	118.5	109.8	108.3	125.1	120.9	131.9	113.0	132.0	110.2	92.9	5972.3
ass Changes													
SiO2	59.2	24.4	18.8	-4.5	15.4	23.2	14.1	23.4	9.1	29.8	13.0	-4.4	4423.4
TiO2	-0.1	-0.0	0.0	0.0	0.1	0.1	0.1	0.1	0.2	0.0	0.0	0.1	0.2
Al2O3	0.0	0.0	0.0	0.0	0.0	0.0	0.0	0.0	0.0	0.0	0.0	0.0	0.0
Fe2O3	28.7	1.9	3.1	14.7	-0.2	4.5	8.0	10.0	3.9	6.5	0.8	0.4	1291.4
MnO	0.5	0.4	0.5	0.7	0.2	0.5	0.5	0.5	0.1	0.5	-0.1	-0.1	0.5
MgO	13.6	4.5	7.4	10.5	3.3	8.4	8.3	7.8	1.0	6.6	0.2	0.3	6.7
CaO	-8.6	-8.4	-8.6	-8.6	-6.9	-8.6	-7.1	-7.7	-0.8	-6.0	-1.0	-0.9	12.4
Na2O	-1.4	-1.7	-1.9	-1.9	-2.0	-1.9	-1.3	-1.1	-0.1	-1.0	-4.1	-3.7	132.4
K2O	0.2	-0.6	-0.3	-0.6	-0.4	-0.7	-0.8	-0.6	0.6	0.4	1.8	1.6	0.0
P2O5	0.0	-0.0	-0.1	-0.1	-0.2	-0.0	-0.1	-0.0	-0.2	-0.1	-0.0	0.0	4.7
Rb	5	-14	-9	-16	-18	-16	-26	-16	7	4	13	5	-23
Ba	2332	903	-375	-492	-675	-479	-655	-471	479	1728	660	396	2451853
Sr	-401	-331	-385	-396	-275	-389	-335	-370	94	ERR	-127	-125	34133
Total	92.0	20.0	18.5	9.8	8.3	25.1	20.9	31.9	13.0	36.3	10.2	-7.1	5872.3

Table F-7 continued

Drill Hole	2889	2889	2889	2871	202	1662	1662	1683	1798	1662	1778	1910	1910
From	167	214	279	177.5	194.5	1052	1500.5	1267	1463.5	1244	1537	1791	2006
To	170	216	281	180.5	195.5	1054	1502.5	1269	1465	1246	1539	1792.7	2008
Sample	LS-17	LS-18	LS-19	LS-26	LS-34	MB-01	MB-02	MB-03	MB-04	MB-05	MB-07	MB-08	MB-09
Lithology	Dacites	volc sst	Dacites	Dacites	Dacites	Dacites	Dacites	Dacites	Dacites	Dacites	Dacites	Dacites	Dacites
Raw Data - LOI Free													
Zr	131	179	181	147	195	230	228	159	144	184	161	191	252
Zr precursor	109	153	152	148	155	150	138	151	136	152	143	144	140
Al2O3/Zr	0.14	0.08	0.08	0.09	0.08	0.08	0.10	0.08	0.10	0.08	0.09	0.09	0.09
Enrich Factor	0.83	0.85	0.84	1.01	0.80	0.65	0.61	0.96	0.94	0.82	0.89	0.76	0.56
SiO2	62.01	75.45	76.12	76.55	42.08	67.36	66.25	77.11	75.71	72.95	71.86	71.00	62.64
TiO2	0.70	0.38	0.41	0.33	0.39	0.56	0.49	0.34	0.30	0.39	0.35	0.38	0.57
Al2O3	18.29	14.43	14.77	12.58	15.22	19.18	21.84	12.98	14.18	15.02	14.50	17.00	23.74
Fe2O3	9.32	2.97	2.52	1.79	2.51	0.87	0.91	0.92	0.47	1.72	2.96	1.54	3.01
MnO	0.41	0.21	0.14	0.06	0.48	0.00	0.02	0.00	0.01	0.04	0.03	0.02	0.05
MgO	4.62	1.55	1.64	3.10	30.41	1.00	2.44	0.42	0.45	0.36	0.65	0.94	2.92
CaO	0.56	0.35	0.26	1.42	8.67	1.00	0.96	0.80	2.30	2.84	2.79	3.27	0.45
Na2O	0.72	1.14	0.37	1.56	0.17	1.88	1.15	0.57	0.45	4.26	4.31	2.40	0.36
K2O	3.24	3.46	3.71	2.59	0.01	8.07	5.89	6.80	6.07	2.36	2.45	3.39	6.18
P2O5	0.13	0.06	0.05	0.01	0.07	0.06	0.04	0.05	0.05	0.06	0.09	0.05	0.07
Rb	59	64	68	52	1	103	92	92	60	36	47	54	114
Ba	1184	1131	1527	116584	214	153591	2361	17078	7134	986	1512	21875	1632
Sr	20	24	15	1156	71	2588	73	173	101	149	285	370	26
Precursors													
SiO2	73.16	74.59	74.56	74.43	74.68	74.50	74.12	74.55	74.06	74.56	74.29	74.32	74.17
TiO2	0.39	0.32	0.32	0.33	0.32	0.15	0.16	0.14	0.17	0.14	0.15	0.15	0.16
Al2O3	15.23	12.31	12.38	12.64	12.13	12.50	13.27	12.40	13.40	12.39	12.93	12.87	13.18
Fe2O3	2.10	1.83	1.84	1.86	1.82	1.85	1.92	1.84	1.93	1.84	1.89	1.88	1.91
MnO	0.08	0.09	0.09	0.09	0.09	0.09	0.08	0.09	0.08	0.09	0.09	0.09	0.08
MgO	0.96	0.31	0.32	0.38	0.27	0.35	0.52	0.33	0.55	0.33	0.45	0.43	0.50
CaO	1.49	1.06	1.07	1.11	1.03	1.09	1.20	1.07	1.22	1.07	1.15	1.14	1.19
Na2O	4.86	4.07	4.09	4.16	4.02	4.12	4.33	4.09	4.36	4.09	4.24	4.22	4.30
K2O	1.14	1.64	1.63	1.58	1.67	1.61	1.48	1.63	1.46	1.63	1.54	1.55	1.49
P2O5	0.05	0.05	0.05	0.05	0.05	0.05	0.05	0.05	0.05	0.05	0.05	0.05	0.05
Rb	40	54	53	52	55	53	49	53	49	53	51	51	50
Ba	732	1025	1018	991	1043	1006	929	1016	916	1017	963	968	938
Sr	206	142	143	149	138	146	163	144	166	143	155	154	161
Total	99.45	96.28	96.35	96.64	96.08	96.30	97.14	96.19	97.28	96.18	96.77	96.71	97.04
factor	1.0056	1.0387	1.0379	1.0348	1.0408	1.0384	1.0295	1.0396	1.0280	1.0397	1.0334	1.0340	1.0305
Precursors - normalized to 100%													
SiO2	73.57	77.48	77.39	77.02	77.73	77.36	76.31	77.50	76.13	77.52	76.77	76.85	76.43
TiO2	0.39	0.33	0.33	0.34	0.33	0.15	0.17	0.15	0.17	0.15	0.16	0.16	0.17
Al2O3	15.31	12.79	12.85	13.08	12.63	12.98	13.66	12.89	13.77	12.88	13.36	13.31	13.58
Fe2O3	2.11	1.90	1.91	1.93	1.89	1.92	1.98	1.91	1.99	1.91	1.95	1.95	1.97
MnO	0.09	0.09	0.09	0.09	0.09	0.09	0.09	0.09	0.09	0.09	0.09	0.09	0.09
MgO	0.96	0.32	0.34	0.40	0.28	0.36	0.54	0.34	0.57	0.34	0.46	0.45	0.52
CaO	1.50	1.10	1.11	1.15	1.07	1.13	1.24	1.11	1.25	1.11	1.19	1.18	1.22
Na2O	4.88	4.23	4.24	4.31	4.19	4.28	4.46	4.26	4.49	4.25	4.38	4.37	4.44
K2O	1.15	1.70	1.69	1.64	1.74	1.67	1.52	1.69	1.50	1.69	1.59	1.60	1.54
P2O5	0.05	0.05	0.05	0.05	0.05	0.05	0.05	0.05	0.05	0.05	0.05	0.05	0.05
Rb	40	56	55	54	57	55	51	55	50	55	52	53	51
Ba	736	1065	1057	1026	1086	1045	956	1056	941	1057	995	1001	966
Sr	207	147	149	154	143	151	168	149	170	149	161	159	166
Total	100.00	100.00	100.00	100.00	100.00	100.00	100.00	100.00	100.00	100.00	100.00	100.00	100.00
Reconstituted													
SiO2	51.6	64.4	63.8	76.9	33.5	43.9	40.2	73.7	71.5	60.2	64.1	53.8	34.5
TiO2	0.6	0.3	0.3	0.3	0.3	0.4	0.3	0.3	0.3	0.3	0.3	0.3	0.3
Al2O3	15.2	12.3	12.4	12.6	12.1	12.5	13.3	12.4	13.4	12.4	12.9	12.9	13.1
Fe2O3	7.8	2.5	2.1	1.8	2.0	0.6	0.6	0.9	0.4	1.4	2.6	1.2	1.7
MnO	0.3	0.2	0.1	0.1	0.4	0.0	0.0	0.0	0.0	0.0	0.0	0.0	0.0
MgO	3.8	1.3	1.4	3.1	24.2	0.7	1.5	0.4	0.4	0.3	0.6	0.7	1.6
CaO	0.5	0.3	0.2	1.4	6.9	0.7	0.6	0.8	2.2	2.3	2.5	2.5	0.2
Na2O	0.6	1.0	0.3	1.6	0.1	1.2	0.7	0.5	0.4	3.5	3.8	1.8	0.2
K2O	2.7	3.0	3.1	2.6	0.0	5.3	3.6	6.5	5.7	2.0	2.2	2.6	3.4
P2O5	0.1	0.1	0.0	0.0	0.1	0.0	0.0	0.1	0.0	0.1	0.1	0.0	0.0
Rb	49	55	57	52	1	67	56	88	57	29	42	41	63
Ba	986	965	1280	117179	171	100095	1435	16317	6740	813	1348	16568	898
Sr	17	20	13	1162	57	1686	45	166	96	123	254	281	14
Total	83.3	85.3	83.8	100.5	79.7	65.2	60.8	95.5	94.5	82.5	89.1	75.7	55.0
Mass Changes													
SiO2	-21.9	-13.1	-13.6	-0.1	-44.2	-33.5	-36.1	-3.8	-4.6	-17.3	-12.7	-23.1	-42.0
TiO2	0.2	-0.0	0.0	-0.0	-0.0	0.2	0.1	0.2	0.1	0.2	0.2	0.1	0.1
Al2O3	0.0	0.0	0.0	0.0	0.0	0.0	0.0	0.0	0.0	0.0	0.0	0.0	0.0
Fe2O3	5.7	0.6	0.2	-0.1	0.1	-1.4	-1.4	-1.0	-1.5	-0.5	0.7	-0.8	-0.3
MnO	0.3	0.1	0.0	-0.0	0.3	-0.1	-0.1	-0.1	-0.1	-0.1	-0.1	-0.1	-0.1
MgO	2.9	1.0	1.0	2.7	24.0	0.3	0.9	0.1	-0.1	-0.0	0.1	0.3	1.1
CaO	-1.0	-0.8	-0.9	0.3	5.8	-0.5	-0.7	-0.3	0.9	1.2	1.3	1.3	-1.0
Na2O	-4.3	-3.3	-3.9	-2.7	-4.1	-3.1	-3.8	-3.7	-4.1	-0.7	-0.5	-2.5	-4.2
K2O	1.5	1.2	1.4	1.0	-1.7	3.6	2.1	4.8	4.2	0.3	0.6	1.0	1.9
P2O5	0.1	-0.0	-0.0	-0.0	0.0	-0.0	-0.0	-0.0	-0.0	0.0	0.0	-0.0	-0.0
Rb	9	-1	2	-2	-56	12	5	33	7	-26	-11	-12	12
Ba	250	-99	223	116153	-915	99051	478	15260	5799	-244	353	15567	-68
Sr	-191	-127	-136	1008	-87	1535	-123	16	-75	-27	94	121	-152
Total	-16.8	-14.7	-16.2	0.5	-20.3	-34.8	-39.3	-4.5	-5.5	-17.5	-10.9	-24.3	-45.0

Table F-7 continued

Drill Hole	1798	1768	1768	1768		25	196	237	237	243	2871	2871	202
From	1348	873	1572.5	1627		57	525	441	1025	561	88	116.5	108
To	1350	876	1575.5	1630		61	527	443	1027	563	89	117.5	111
Sample	MB-11	MB-12	MB-14	MB-15	Average	LS-02	LS-04	LS-10	LS-13	LS-14	LS-24	LS-25	LS-33
Lithology	Dacites	Dacites	Dacites	Dacites	Dacite	Rhy-Dac	Rhy-Dac	Rhy-Dac	Rhy-Dac	Rhy-Dac	Rhy-Dac	Rhy-Dac	Rhy-Dac
Raw Data - LOI Free													
Zr	199	99	175	213	153	108	116	63	150	156	79	120	145
Zr precursor	148	95	144	141	126	76	76	76	76	76	76	76	76
Al2O3/Zr	0.09	0.17	0.09	0.09	0.09	0.12	0.10	0.11	0.11	0.11	0.12	0.13	0.12
Enrich Factor	0.74	0.96	0.82	0.66	3.43	0.70	0.66	1.21	0.51	0.49	0.96	0.63	0.52
SiO2	70.71	66.73	69.55	67.45	63.99	76.35	74.55	83.46	71.01	74.27	82.95	73.34	71.87
TiO2	0.46	0.24	0.51	0.45	0.37	0.22	0.19	0.11	0.27	0.30	0.14	0.22	0.26
Al2O3	17.02	16.91	15.62	19.74	13.99	13.43	11.82	6.94	16.52	17.56	9.71	15.94	17.45
Fe2O3	1.63	8.20	2.92	1.49	3.29	2.05	4.36	7.19	2.53	2.15	0.80	1.76	1.64
MnO	0.01	0.08	0.05	0.02	0.08	0.08	0.24	0.01	0.06	0.02	0.03	0.04	0.05
MgO	0.78	2.25	0.93	2.62	2.65	1.32	5.56	0.40	3.38	0.70	0.22	2.86	3.37
CaO	2.28	1.60	3.79	1.43	1.61	1.06	1.25	0.08	2.60	0.20	1.11	1.34	0.79
Na2O	2.72	1.13	4.59	0.81	1.44	3.74	0.04	0.05	0.67	0.13	3.66	0.88	0.94
K2O	4.31	2.83	1.97	5.92	3.45	1.74	1.98	1.74	2.95	4.66	1.36	3.62	3.62
P2O5	0.07	0.03	0.08	0.07	0.06	0.01	0.01	0.01	0.01	0.01	0.01	0.01	0.01
Rb	65	56	34	86	55	0	75	36	88	66	24	43	26
Ba	12120	481	3509	29076	18918	748	5885	2506	2440	15381	1332	2009	1936
Sr	259	47	316	385	ERR	206	61	26	86	230	150	186	121
Precursors													
SiO2	74.43	72.68	74.31	74.22	67.38	77.64	77.64	77.64	77.64	77.64	77.64	77.64	77.64
TiO2	0.15	0.23	0.15	0.16	0.21	0.13	0.13	0.13	0.13	0.13	0.13	0.13	0.13
Al2O3	12.65	16.19	12.88	13.08	12.07	10.63	10.63	10.63	10.63	10.63	10.63	10.63	10.63
Fe2O3	1.86	2.18	1.88	1.90	1.75	0.80	0.80	0.80	0.80	0.80	0.80	0.80	0.80
MnO	0.09	0.08	0.09	0.09	0.08	0.03	0.03	0.03	0.03	0.03	0.03	0.03	0.03
MgO	0.38	1.17	0.44	0.48	0.48	0.69	0.69	0.69	0.69	0.69	0.69	0.69	0.69
CaO	1.11	1.63	1.14	1.17	1.09	0.97	0.97	0.97	0.97	0.97	0.97	0.97	0.97
Na2O	4.16	5.12	4.22	4.28	3.94	3.39	3.39	3.39	3.39	3.39	3.39	3.39	3.39
K2O	1.58	0.98	1.54	1.51	1.34	1.77	1.77	1.77	1.77	1.77	1.77	1.77	1.77
P2O5	0.05	0.05	0.05	0.05	0.05	0.01	0.01	0.01	0.01	0.01	0.01	0.01	0.01
Rb	52	35	51	50	45	25	25	25	25	25	25	25	25
Ba	991	635	967	948	844	1421	1421	1421	1421	1421	1421	1421	1421
Sr	149	228	154	159	ERR	96	96	96	96	96	96	96	96
Total	96.46	100.32	96.72	96.93	88.38	96.06	96.06	96.06	96.06	96.06	96.06	96.06	96.06
factor	1.0367	0.9968	1.0339	1.0317	0.9354	1.0410	1.0410	1.0410	1.0410	1.0410	1.0410	1.0410	1.0410
Precursors - normalized to 100%													
SiO2	77.16	72.45	76.83	76.57	69.34	80.82	80.82	80.82	80.82	80.82	80.82	80.82	80.82
TiO2	0.15	0.23	0.16	0.16	0.22	0.14	0.14	0.14	0.14	0.14	0.14	0.14	0.14
Al2O3	13.11	16.14	13.32	13.49	12.39	11.07	11.07	11.07	11.07	11.07	11.07	11.07	11.07
Fe2O3	1.93	2.18	1.95	1.96	1.79	0.83	0.83	0.83	0.83	0.83	0.83	0.83	0.83
MnO	0.09	0.08	0.09	0.09	0.08	0.03	0.03	0.03	0.03	0.03	0.03	0.03	0.03
MgO	0.40	1.17	0.45	0.49	0.48	0.72	0.72	0.72	0.72	0.72	0.72	0.72	0.72
CaO	1.15	1.63	1.18	1.21	1.12	1.01	1.01	1.01	1.01	1.01	1.01	1.01	1.01
Na2O	4.31	5.10	4.37	4.41	4.04	3.53	3.53	3.53	3.53	3.53	3.53	3.53	3.53
K2O	1.64	0.97	1.60	1.56	1.39	1.84	1.84	1.84	1.84	1.84	1.84	1.84	1.84
P2O5	0.05	0.05	0.05	0.05	0.05	0.01	0.01	0.01	0.01	0.01	0.01	0.01	0.01
Rb	54	35	53	52	46	26	26	26	26	26	26	26	26
Ba	1028	633	1000	978	871	1479	1479	1479	1479	1479	1479	1479	1479
Sr	155	227	160	164	ERR	100	100	100	100	100	100	100	100
Total	100.00	100.00	100.00	100.00	90.91	100.00	100.00	100.00	100.00	100.00	100.00	100.00	100.00
Reconstituted													
SiO2	52.5	63.9	57.3	44.7	254.9	53.4	49.2	101.0	36.2	36.4	79.6	46.2	37.4
TiO2	0.3	0.2	0.4	0.3	0.3	0.2	0.1	0.1	0.1	0.1	0.1	0.1	0.1
Al2O3	12.6	16.2	12.9	13.1	12.1	9.4	7.8	8.4	8.4	8.6	9.3	10.0	9.1
Fe2O3	1.2	7.9	2.4	1.0	60.8	1.4	2.9	8.7	1.3	1.1	0.8	1.1	0.9
MnO	0.0	0.1	0.0	0.0	0.1	0.1	0.2	0.0	0.0	0.0	0.0	0.0	0.0
MgO	0.6	2.2	0.8	1.7	2.5	0.9	3.7	0.5	1.7	0.3	0.2	1.8	1.8
CaO	1.7	1.5	3.1	0.9	2.0	0.7	0.8	0.1	1.3	0.1	1.1	0.8	0.4
Na2O	2.0	1.1	3.8	0.5	7.4	2.6	0.0	0.1	0.3	0.1	3.5	0.6	0.5
K2O	3.2	2.7	1.6	3.9	2.8	1.2	1.3	2.1	1.5	2.3	1.3	2.3	1.9
P2O5	0.1	0.0	0.1	0.0	0.3	0.0	0.0	0.0	0.0	0.0	0.0	0.0	0.0
Rb	48	53	28	57	44	0	50	44	45	32	23	27	14
Ba	9008	461	2894	19268	125085	524	3884	3032	1244	7537	1279	1266	1007
Sr	193	45	260	255	ERR	144	40	31	44	113	144	117	63
Total	74.3	95.7	82.5	66.3	343.0	70.0	66.0	121.0	51.0	49.0	96.0	63.0	52.0
Mass Changes													
SiO2	-24.6	-8.6	-19.5	-31.9	185.5	-27.4	-31.6	20.2	-44.6	-44.4	-1.2	-34.6	-43.5
TiO2	0.2	-0.0	0.3	0.1	0.1	0.0	-0.0	-0.0	0.0	0.0	-0.0	0.0	-0.0
Al2O3	0.0	0.0	0.0	0.0	0.0	0.0	0.0	0.0	0.0	0.0	0.0	0.0	0.0
Fe2O3	-0.7	5.7	0.5	-1.0	59.0	0.6	2.0	7.9	0.5	0.2	-0.1	0.3	0.0
MnO	-0.1	-0.0	-0.0	-0.1	0.0	0.0	0.1	-0.0	-0.0	-0.0	-0.0	-0.0	-0.0
MgO	0.2	1.0	0.3	1.2	2.0	0.2	3.0	-0.2	1.0	-0.4	-0.5	1.1	1.0
CaO	0.5	-0.1	1.9	-0.3	0.8	-0.3	-0.2	-0.9	0.3	-0.9	0.1	-0.2	-0.6
Na2O	-2.3	-4.0	-0.6	-3.9	3.3	-0.9	-3.5	-3.5	-3.2	-3.5	-0.0	-3.0	-3.0
K2O	1.6	1.7	0.0	2.4	1.4	-0.6	-0.5	0.3	-0.3	0.4	-0.5	0.4	0.0
P2O5	0.0	-0.0	0.0	-0.0	0.2	-0.0	-0.0	0.0	-0.0	-0.0	-0.0	-0.0	-0.0
Rb	-6	18	-24	5	-2	-26	24	18	19	6	-3	1	-12
Ba	7980	-172	1894	18291	124214	-956	2405	1553	-235	6057	-201	-214	-473
Sr	38	-182	101	91	ERR	44	-60	-69	-56	12	44	17	-37
Total	-25.7	-4.2	-17.5	-33.7	252.1	-30.0	-34.0	21.0	-49.0	-51.0	-4.0	-37.0	-48.0

Table F-7 continued

Drill Hole	2865		202	202	202	202	202	202
From	3209.5		70	75	92	100	110	122
To	3211							
Sample	LS-46	Average	1540715	1540716	1540717	1540697	1540698	1540699
Lithology	Rhy-Dac	Rhy-Dac	Dacites	Dacites	Dacites	Dacites	Dacites	Dacites
Zr	98	104	71	41	79	44	107	51
Zr precursor	76	68	66	67	87	77	99	72
Al2O3/Zr	0.18	0.11	0.27	0.27	0.19	0.23	0.16	0.24
Enrich Factor	0.78	0.65	0.93	1.65	1.10	1.74	0.93	1.42
SiO2	75.19	68.30	69.44	80.00	71.41	80.88	71.65	77.87
TiO2	0.13	0.18	0.25	0.19	0.17	0.13	0.24	0.16
Al2O3	17.19	12.66	19.46	10.94	15.23	9.97	17.15	12.49
Fe2O3	1.66	2.41	1.61	1.73	2.83	1.83	1.77	1.67
MnO	0.03	0.06	0.03	0.06	0.12	0.08	0.05	0.07
MgO	0.55	1.84	2.65	4.08	5.46	4.26	3.66	2.42
CaO	0.53	0.90	1.11	0.71	1.59	1.01	0.71	1.66
Na2O	0.53	1.06	1.39	0.76	1.00	0.66	0.95	0.79
K2O	4.12	2.58	4.06	1.53	2.19	1.18	3.83	2.87
P2O5	0.08	0.02	n/a	n/a	n/a	n/a	n/a	n/a
Rb	78	44	22	34	45	29	80	55
Ba	613	3285	1110	1179	2564	1022	2095	1917
Sr	58	112	314	35	158	45	69	0
Precursors								
SiO2	77.64	69.88	71.74	71.79	72.42	72.09	72.83	71.95
TiO2	0.13	0.12	0.27	0.27	0.24	0.25	0.22	0.26
Al2O3	10.63	9.57	18.10	18.00	16.72	17.38	15.89	17.68
Fe2O3	0.80	0.72	2.35	2.35	2.23	2.29	2.16	2.32
MnO	0.03	0.03	0.08	0.08	0.08	0.08	0.08	0.08
MgO	0.69	0.62	1.59	1.57	1.29	1.43	1.10	1.50
CaO	0.97	0.87	1.92	1.90	1.71	1.81	1.59	1.86
Na2O	3.39	3.05	5.63	5.61	5.26	5.44	5.04	5.52
K2O	1.77	1.59	0.65	0.67	0.89	0.77	1.03	0.72
P2O5	0.01	0.01	n/a	n/a	n/a	n/a	n/a	n/a
Rb	25	22	26	26	33	29	37	28
Ba	1421	1279	443	453	582	515	665	485
Sr	96	87	270	271	272	273	274	275
Total	96.06	86.45	102.39	102.29	100.89	101.61	99.99	101.94
factor	1.0410	0.9369	0.9767	0.9777	0.9912	0.9841	1.0001	0.9810
Precursors - normalized to 100%								
SiO2	80.82	72.74	70.07	70.19	71.79	70.95	72.84	70.58
TiO2	0.14	0.12	0.26	0.26	0.24	0.25	0.22	0.26
Al2O3	11.07	9.96	17.67	17.60	16.57	17.11	15.89	17.35
Fe2O3	0.83	0.75	2.30	2.29	2.21	2.25	2.16	2.27
MnO	0.03	0.03	0.08	0.08	0.08	0.08	0.08	0.08
MgO	0.72	0.65	1.56	1.54	1.28	1.41	1.10	1.47
CaO	1.01	0.91	1.87	1.86	1.70	1.78	1.59	1.82
Na2O	3.53	3.18	5.50	5.48	5.21	5.35	5.04	5.42
K2O	1.84	1.66	0.64	0.65	0.88	0.76	1.03	0.71
P2O5	0.01	0.01	n/a	n/a	n/a	n/a	n/a	n/a
Rb	26	23	25	26	32	29	37	27
Ba	1479	1331	433	443	577	507	665	475
Sr	100	90	263	262	237	250	221	256
Total	100.00	90.00	100.01	100.01	100.00	100.00	100.00	100.01
econstituted								
SiO2	58.6	49.8	64.6	131.7	78.4	141.0	66.4	110.3
TiO2	0.1	0.1	0.2	0.3	0.2	0.2	0.2	0.2
Al2O3	13.4	8.4	18.1	18.0	16.7	17.4	15.9	17.7
Fe2O3	1.3	1.9	1.5	2.8	3.1	3.2	1.6	2.4
MnO	0.0	0.0	0.0	0.1	0.1	0.1	0.0	0.1
MgO	0.4	1.1	2.5	6.7	6.0	7.4	3.4	3.4
CaO	0.4	0.6	1.0	1.2	1.7	1.8	0.7	2.4
Na2O	0.4	0.8	1.3	1.3	1.1	1.2	0.9	1.1
K2O	3.2	1.7	3.8	2.5	2.4	2.1	3.5	4.1
P2O5	0.1	0.0	n/a	n/a	n/a	n/a	n/a	n/a
Rb	61	29	21	57	50	51	74	79
Ba	478	2025	1033	1940	2814	1782	1941	2714
Sr	45	74	292	58	173	78	64	0
Total	78.0	64.6	93.0	164.6	109.8	174.4	92.7	141.6
ass Changes								
SiO2	-22.2	-22.9	-5.5	61.5	6.6	70.1	-6.5	39.7
TiO2	-0.0	-0.0	-0.0	0.0	-0.1	-0.0	0.0	-0.0
Al2O3	0.0	0.0	0.0	0.0	0.0	0.0	0.0	0.0
Fe2O3	0.5	1.2	-0.8	0.6	0.9	0.9	-0.5	0.1
MnO	-0.0	0.0	-0.1	0.0	0.0	0.1	-0.0	0.0
MgO	-0.3	0.5	0.9	5.2	4.7	6.0	2.3	2.0
CaO	-0.6	-0.3	-0.8	-0.7	0.0	-0.0	-0.9	0.5
Na2O	-3.1	-2.4	-4.2	-4.2	-4.1	-4.2	-4.2	-4.3
K2O	1.4	0.1	3.1	1.9	1.5	1.3	2.5	3.4
P2O5	0.1	0.0	n/a	n/a	n/a	n/a	n/a	n/a
Rb	35	6	-5	31	17	22	38	51
Ba	-1001	694	600	1498	2237	1275	1276	2239
Sr	-55	-16	29	-203	-64	-172	-157	-256
Total	-22.0	-25.4	-7.0	64.6	9.8	74.4	-7.3	41.6

Table F-8 - Calculated mass changes for volcanic rocks in the PHZ

Drill Hole	BE-96-11	BE-96-11	BE-96-11	BE-96-11	3326	3326	3326	3326	3326	3326	3326	3319	3319
From	121.7	141.1	151.7	168.5	312.0	193.5	73.8	379.0	133.2	405.0	235.5	237.0	163.5
To	122.4	141.6	152.4	168.9	314.0	195.5	75.3	380.5	134.7	406.8	237.0	239.5	165.5
Sample	PH-04	PH-05	PH-06	PH-07	PH-09	PH-10	PH-11	PH-12	PH-13	PH-14	PH-15	PH-16	PH-17
Lithology	Dacite	Dacite	Dacite	Dacite	Dacite	Dacite	Dacite	Dacite	Dacite	Dacite	Dacite	Dacite	Dacite
Raw data - LOI free													
Zr	113	97	104	84	101	94	107	96	98	87	94	127	91
AL/ZR	0.17	0.18	0.19	0.16	0.16	0.19	0.16	0.16	0.16	0.19	0.17	0.15	0.21
Zr Precursor	93	92	86	97	97	86	97	100	100	87	95	101	82
E factor	0.8211	0.9531	0.8209	1.1551	0.9664	0.9140	0.9032	1.0366	1.0276	0.9937	1.0079	0.7958	0.8986
SiO2	73.50	76.88	68.32	79.47	72.15	72.76	74.05	72.80	72.77	74.05	71.42	69.16	55.94
TiO2	0.26	0.23	0.35	0.19	0.27	0.24	0.29	0.19	0.33	0.23	0.26	0.32	0.54
Al2O3	19.69	17.04	20.31	13.75	16.44	18.23	17.62	15.15	15.26	16.71	15.90	19.63	18.83
Fe2O3	1.57	1.32	4.07	2.58	3.05	3.04	2.70	3.09	1.87	2.45	3.88	0.80	9.14
MnO	0.00	0.00	0.04	0.01	0.03	0.02	0.02	0.10	0.07	0.04	0.05	0.03	0.09
MgO	0.52	0.63	2.39	0.96	4.33	1.35	1.01	3.13	1.25	2.11	4.00	5.32	10.66
CaO	0.12	0.10	0.16	0.11	0.25	0.47	0.32	2.41	2.68	1.01	0.97	0.77	0.79
Na2O	0.45	0.22	0.35	0.17	0.81	0.44	0.78	0.94	4.75	0.22	1.01	1.42	2.41
K2O	3.85	3.53	3.98	2.73	2.62	3.41	3.16	2.18	0.97	3.14	2.47	2.51	1.57
P2O5	0.03	0.03	0.03	0.03	0.05	0.04	0.04	0.02	0.06	0.03	0.04	0.03	0.03
Rb	47	48	55	39	36	43	50	31	14	40	33	44	39
Ba	487	609	691	395	487	520	461	300	129	544	469	349	270
Sr	25	12	21	11	31	27	26	30	121	14	42	59	112
Precursors													
SiO2	71.71	71.54	70.59	72.32	72.32	70.62	72.25	72.73	72.77	70.73	72.01	72.90	70.04
TiO2	0.37	0.37	0.40	0.35	0.35	0.40	0.35	0.33	0.33	0.40	0.36	0.33	0.42
Al2O3	15.74	15.81	16.25	15.46	15.46	16.23	15.49	15.27	15.25	16.18	15.60	15.19	16.49
Fe2O3	2.51	2.70	3.75	1.83	1.83	3.72	1.91	1.38	1.34	3.59	2.18	1.19	4.35
MnO	0.07	0.07	0.06	0.07	0.07	0.06	0.07	0.07	0.07	0.06	0.07	0.07	0.06
MgO	1.89	1.99	2.56	1.52	1.52	2.54	1.56	1.27	1.25	2.47	1.71	1.17	2.89
CaO	2.71	2.71	2.76	2.68	2.68	2.75	2.68	2.66	2.66	2.75	2.69	2.65	2.78
Na2O	4.46	4.43	4.24	4.58	4.58	4.24	4.57	4.66	4.67	4.27	4.52	4.70	4.13
K2O	1.01	1.01	0.96	1.04	1.04	0.96	1.04	1.06	1.07	0.97	1.03	1.07	0.93
P2O5	0.04	0.04	0.04	0.04	0.04	0.04	0.04	0.04	0.02	0.04	0.04	0.04	0.04
Rb	11	11	8	13	13	8	12	14	14	9	12	14	7
Ba	109	106	89	121	121	90	119	128	129	92	115	131	79
Sr	152	157	182	136	136	182	138	125	124	178	144	120	197
Total	100.50	100.66	101.60	99.89	99.89	101.58	99.96	99.49	99.42	101.46	100.20	99.32	102.15
Norm factor	0.9951	0.9934	0.9842	1.0011	1.0011	0.9845	1.0004	1.0052	1.0058	0.9856	0.9980	1.0069	0.9790
Precursors - normalized to 100%													
SiO2	71.36	71.07	69.47	72.40	72.40	69.52	72.28	73.11	73.19	69.72	71.86	73.40	68.57
TiO2	0.36	0.37	0.40	0.35	0.35	0.40	0.35	0.33	0.33	0.39	0.36	0.33	0.41
Al2O3	15.66	15.71	15.99	15.47	15.47	15.98	15.49	15.35	15.34	15.95	15.57	15.30	16.15
Fe2O3	2.50	2.68	3.69	1.83	1.83	3.66	1.91	1.39	1.34	3.53	2.17	1.20	4.26
MnO	0.07	0.07	0.06	0.07	0.07	0.06	0.07	0.07	0.07	0.06	0.07	0.07	0.06
MgO	1.88	1.97	2.52	1.52	1.52	2.50	1.56	1.28	1.25	2.44	1.70	1.18	2.83
CaO	2.69	2.70	2.71	2.68	2.68	2.71	2.68	2.67	2.67	2.71	2.69	2.67	2.72
Na2O	4.44	4.40	4.17	4.59	4.59	4.18	4.57	4.69	4.70	4.21	4.51	4.73	4.04
K2O	1.01	1.00	0.94	1.05	1.05	0.95	1.04	1.07	1.07	0.95	1.03	1.08	0.91
P2O5	0.04	0.04	0.04	0.04	0.04	0.04	0.04	0.04	0.02	0.04	0.04	0.04	0.04
Rb	11	11	8	13	13	8	12	14	14	8	12	14	7
Ba	109	106	88	121	121	88	119	129	129	91	115	132	78
Sr	152	156	179	136	136	179	138	126	125	176	144	121	193
Total	100.00	100.00	100.00	100.00	100.00	100.00	100.00	100.00	100.00	100.00	100.00	100.00	100.00
Reconstituted													
SiO2	60.4	73.3	56.1	91.8	69.7	66.5	66.9	75.5	74.8	73.6	72.0	55.0	50.3
TiO2	0.2	0.2	0.3	0.2	0.3	0.2	0.3	0.2	0.3	0.2	0.3	0.3	0.5
Al2O3	16.2	16.2	16.7	15.9	15.9	16.7	15.9	15.7	15.7	16.6	16.0	15.6	16.9
Fe2O3	1.3	1.3	3.3	3.0	2.9	2.8	2.4	3.2	1.9	2.4	3.9	0.6	8.2
MnO	0.0	0.0	0.0	0.0	0.0	0.0	0.0	0.1	0.1	0.0	0.1	0.0	0.1
MgO	0.4	0.6	2.0	1.1	4.2	1.2	0.9	3.2	1.3	2.1	4.0	4.2	9.6
CaO	0.1	0.1	0.1	0.1	0.2	0.4	0.3	2.5	2.7	1.0	1.0	0.6	0.7
Na2O	0.4	0.2	0.3	0.2	0.8	0.4	0.7	1.0	4.9	0.2	1.0	1.1	2.2
K2O	3.2	3.4	3.3	3.2	2.5	3.1	2.9	2.3	1.0	3.1	2.5	2.0	1.4
P2O5	0.0	0.0	0.0	0.0	0.0	0.0	0.0	0.0	0.1	0.0	0.0	0.0	0.0
Rb	38	45	45	45	35	39	45	32	14	40	33	35	35
Ba	400	580	567	456	470	475	416	311	133	541	473	278	243
Sr	21	11	17	13	30	25	23	31	124	14	42	47	100
Total	82.1	95.3	82.1	115.5	96.6	91.4	90.3	103.7	102.8	99.4	100.8	79.6	89.9
Mass Changes													
SiO2	-11.0	2.2	-13.4	19.4	-2.7	-3.0	-5.4	2.4	1.6	3.9	0.1	-18.4	-18.3
TiO2	-0.2	-0.1	-0.1	-0.1	-0.1	-0.2	-0.1	-0.1	0.0	-0.2	-0.1	-0.1	0.1
Al2O3	0.5	0.5	0.7	0.4	0.4	0.7	0.4	0.4	0.3	0.7	0.5	0.3	0.8
Fe2O3	-1.2	-1.4	-0.3	1.1	1.1	-0.9	0.5	1.8	0.6	-1.1	1.7	-0.6	4.0
MnO	-0.1	-0.1	-0.0	-0.1	-0.0	-0.0	-0.1	0.0	0.0	-0.0	-0.0	-0.0	0.0
MgO	-1.4	-1.4	-0.6	-0.4	2.7	-1.3	-0.6	2.0	0.0	-0.3	2.3	3.1	6.8
CaO	-2.6	-2.6	-2.6	-2.5	-2.4	-2.3	-2.4	-0.2	0.1	-1.7	-1.7	-2.1	-2.0
Na2O	-4.1	-4.2	-3.9	-4.4	-3.8	-3.8	-3.9	-3.7	0.2	-4.0	-3.5	-3.6	-1.9
K2O	2.2	2.4	2.3	2.1	1.5	2.2	1.8	1.2	-0.1	2.2	1.5	0.9	0.5
P2O5	-0.0	-0.0	-0.0	-0.0	0.0	-0.0	-0.0	-0.0	0.0	-0.0	-0.0	-0.0	-0.0
Rb	27	35	37	32	22	31	32	18	1	31	21	21	28
Ba	291	475	479	336	350	387	297	182	3	450	358	146	165
Sr	-131	-145	-163	-123	-106	-154	-115	-95	-1	-162	-102	-75	-93
Total	-17.89	-4.69	-17.91	15.51	-3.36	-8.59	-9.68	3.66	2.76	-0.63	0.79	-20.42	-10.14

Table F-8 continued

Drill Hole	3319	3319	outcrop	BE-97-19	BE-97-19	BE-97-19	BE-96-11	BE-96-11	BE-96-11		BE-96-11	BE-96-11	BE-96-11
From	112.0	282.5		44.0	169.4	184.0	115.8	105.8	62.4		58.5	71.2	84.0
To	113.75	285.0		44.5	169.7	184.3	117.6	106.4	63.1		59.4	72.0	85.1
Sample	PH-18	PH-19	PH-20	PH-21	PH-22	PH-23	E-11-115	E-13-105.	E-13-62.4	Average	PH-01	PH-02	PH-03
Lithology	Dacite	Dacite	Dacite	Dacite	Dacite	Dacite	Dacite	Dacite	Dacite	Dacite	Mafic	Mafic	Mafic
Raw data - LOI free													
Zr	97	108	26	108	103	86	128	95	92	95.88	24	26	28
AL/ZR	0.17	0.17	0.17	0.19	0.18	0.21	0.18	0.12	0.15	0.18	0.95	0.87	0.84
Precursor	96	95	96	87	92	80	90	121	104	92.58	22	24	25
E factor	0.9948	0.8749	3.6843	0.8040	0.9010	0.9293	0.7035	1.2774	1.1399	1.0780	0.9349	0.9094	0.8774
SiO2	73.60	72.84	74.64	67.71	76.27	72.15	65.08	53.97	71.27	72.13	52.05	48.66	51.28
TiO2	0.23	0.27	0.05	0.31	0.18	0.28	0.26	0.21	0.18	0.26	0.40	0.44	0.47
Al2O3	16.04	18.34	4.34	20.66	18.00	18.35	23.27	11.17	13.51	16.86	22.46	22.95	23.73
Fe2O3	3.19	1.17	19.85	1.88	1.04	3.81	4.27	6.65	2.98	3.71	12.00	8.16	7.63
MnO	0.03	0.03	0.02	0.07	0.01	0.01	0.01	0.89	0.18	0.04	0.07	0.19	0.13
MgO	2.84	3.25	0.00	1.10	0.61	1.12	0.83	9.73	0.71	2.45	3.98	10.27	8.31
CaO	0.69	0.38	0.03	3.88	0.08	0.34	0.28	13.78	6.34	0.82	1.40	2.68	1.22
Na2O	0.24	1.13	0.00	0.60	0.37	0.41	0.71	2.84	2.19	0.88	5.03	3.99	5.01
K2O	3.09	2.57	1.06	3.75	3.42	3.49	5.28	0.73	2.60	2.82	2.57	2.66	2.19
P2O5	0.04	0.02	0.02	0.04	0.02	0.04	0.01	0.03	0.03	0.03	0.02	0.02	0.03
Rb	40	46	12	50	48	54	61	15	41	40.35	31	44	33
Ba	360	400	79	436	568	782	682	84	1260	438.72	378	359	392
Sr	8	45	3	35	17	24	24	108	63	35	143	110	133
Precursors													
SiO2	72.16	71.97	72.09	70.73	71.60	69.75	71.26	75.88	73.38	71.62	52.69	52.78	52.82
TiO2	0.35	0.36	0.35	0.40	0.37	0.43	0.38	0.23	0.31	0.37	0.44	0.44	0.44
Al2O3	15.53	15.62	15.56	16.18	15.79	16.63	15.94	13.83	14.97	15.77	21.00	20.87	20.82
Fe2O3	2.01	2.22	2.09	3.59	2.63	4.67	3.00	0.00	0.66	2.60	9.86	9.85	9.85
MnO	0.07	0.07	0.07	0.06	0.07	0.06	0.07	0.08	0.07	0.07	0.15	0.15	0.15
MgO	1.61	1.73	1.66	2.47	1.95	3.07	2.15	-0.63	0.88	1.94	6.23	6.17	6.15
CaO	2.69	2.69	2.69	2.75	2.71	2.79	2.73	2.52	2.63	2.71	9.70	9.66	9.64
Na2O	4.55	4.51	4.54	4.27	4.44	4.07	4.37	5.29	4.79	4.44	2.99	2.99	3.00
K2O	1.04	1.03	1.03	0.97	1.01	0.92	0.99	1.22	1.10	1.01	0.39	0.41	0.41
P2O5	0.04	0.04	0.04	0.04	0.04	0.04	0.04	0.04	0.04	0.04	0.13	0.14	0.14
Rb	12	12	12	9	11	6	10	22	15	10.83	6	7	7
Ba	118	114	116	92	108	74	101	185	140	107.97	113	123	127
Sr	140	145	142	179	155	205	164	41	108	155	437	429	426
Total	100.05	100.24	100.12	101.46	100.60	102.44	100.94	98.47	98.84	100.58	103.59	103.47	103.42
Norm factor	0.9995	0.9976	0.9988	0.9856	0.9940	0.9762	0.9907	1.0156	1.0117	0.99	0.9653	0.9665	0.9669
Precursors - normalized to 100%													
SiO2	72.12	71.79	72.00	69.71	71.17	68.09	70.60	77.07	74.24	71.22	50.86	51.02	51.07
TiO2	0.35	0.36	0.35	0.39	0.37	0.42	0.38	0.23	0.32	0.37	0.43	0.43	0.43
Al2O3	15.52	15.58	15.54	15.95	15.69	16.23	15.79	14.05	15.15	15.68	20.27	20.17	20.13
Fe2O3	2.01	2.22	2.08	3.54	2.61	4.56	2.97	0.00	0.67	2.58	9.52	9.52	9.53
MnO	0.07	0.07	0.07	0.06	0.07	0.06	0.06	0.08	0.07	0.07	0.15	0.15	0.15
MgO	1.61	1.73	1.65	2.44	1.94	2.99	2.13	-0.64	0.89	1.92	6.02	5.96	5.94
CaO	2.68	2.69	2.69	2.71	2.69	2.73	2.70	2.56	2.66	2.69	9.37	9.34	9.32
Na2O	4.55	4.50	4.53	4.21	4.41	3.98	4.33	5.37	4.85	4.42	2.88	2.89	2.90
K2O	1.04	1.02	1.03	0.95	1.00	0.90	0.98	1.24	1.11	1.00	0.38	0.39	0.40
P2O5	0.04	0.04	0.04	0.04	0.04	0.04	0.04	0.04	0.04	0.04	0.12	0.13	0.13
Rb	12	12	12	8	11	6	10	22	16	10.79	6	7	7
Ba	118	114	116	91	107	72	101	188	141	107.50	109	119	123
Sr	140	145	142	176	154	200	163	41	109	154	422	415	412
Total	100.00	100.00	100.00	100.00	100.00	100.00	100.00	100.00	100.00	100.00	100.00	100.00	100.00
Reconstituted													
SiO2	73.2	63.7	275.0	54.4	68.7	67.1	45.8	68.9	81.2	78.3	48.7	44.2	45.0
TiO2	0.2	0.2	0.2	0.2	0.2	0.3	0.2	0.3	0.2	0.2	0.4	0.4	0.4
Al2O3	16.0	16.0	16.0	16.6	16.2	17.1	16.4	14.3	15.4	16.2	21.0	20.9	20.8
Fe2O3	3.2	1.0	73.1	1.5	0.9	3.5	3.0	8.5	3.4	6.4	11.2	7.4	6.7
MnO	0.0	0.0	0.1	0.1	0.0	0.0	0.0	1.1	0.2	0.0	0.1	0.2	0.1
MgO	2.8	2.8	0.0	0.9	0.6	1.0	0.6	12.4	0.8	2.3	3.7	9.3	7.3
CaO	0.7	0.3	0.1	3.1	0.1	0.3	0.2	17.6	7.2	0.8	1.3	2.4	1.1
Na2O	0.2	1.0	0.0	0.5	0.3	0.4	0.5	3.6	2.5	0.8	4.7	3.6	4.4
K2O	3.1	2.3	3.9	3.0	3.1	3.2	3.7	0.9	3.0	2.8	2.4	2.4	1.9
P2O5	0.0	0.0	0.1	0.0	0.0	0.0	0.0	0.0	0.0	0.0	0.0	0.0	0.0
Rb	40	40	45	40	44	50	43	19	46	38.92	29	40	29
Ba	358	350	292	351	512	727	480	107	1436	417.48	353	326	344
Sr	8	39	11	28	15	22	17	138	71	32.62	134	100	117
Total	99.5	87.5	368.4	80.4	90.1	92.9	70.3	127.7	114.0	107.8	93.5	90.9	87.7
Mass Changes													
SiO2	1.1	-8.1	203.0	-15.3	-2.4	-1.0	-24.8	-8.1	7.0	4.9	-2.2	-6.8	-6.1
TiO2	-0.1	-0.1	-0.2	-0.1	-0.2	-0.2	-0.2	0.0	-0.1	-0.1	-0.1	-0.0	-0.0
Al2O3	0.4	0.5	0.4	0.7	0.5	0.8	0.6	0.2	0.3	0.5	0.7	0.7	0.7
Fe2O3	1.2	-1.2	71.1	-2.0	-1.7	-1.0	0.0	8.5	2.7	3.8	1.7	-2.1	-2.8
MnO	-0.0	-0.0	-0.0	-0.0	-0.1	-0.0	-0.1	1.1	0.1	0.0	-0.1	0.0	-0.0
MgO	1.2	1.1	-1.7	-1.6	-1.4	-2.0	-1.5	13.1	-0.1	0.8	-2.3	3.4	1.4
CaO	-2.0	-2.4	-2.6	0.4	-2.6	-2.4	-2.5	15.0	4.6	-0.9	-8.1	-6.9	-8.3
Na2O	-4.3	-3.5	-4.5	-3.7	-4.1	-3.6	-3.8	-1.7	-2.3	-3.5	1.8	0.7	1.5
K2O	2.0	1.2	2.9	2.1	2.1	2.3	2.7	-0.3	1.9	1.7	2.0	2.0	1.5
P2O5	-0.0	-0.0	0.0	-0.0	-0.0	-0.0	-0.0	-0.0	-0.0	-0.0	-0.1	-0.1	-0.1
Rb	28	28	33	32	33	44	33	-4	31	27	23	33	22
Ba	240	236	176	260	405	654	380	-81	1295	340	244	207	221
Sr	-132	-106	-131	-148	-139	-178	-146	96	-37	-121	-288	-315	-296
Total	-0.52	-12.51	268.43	-19.60	-9.90	-7.07	-29.65	27.74	13.99	7.3	-6.51	-9.06	-12.26

Table F-8 continued

Drill Hole	BE-96-11	BE-96-11	
From	97.9	85.9	
To	98.7	86.4	
Sample	PH-08	BE-11A-85.	Average
Lithology	Mafic	Mafic	Mafic
Raw data - LOI free			
Zr	27	19	26.27
AL/ZR	0.80	0.83	0.87
Precursor	26	25	24.12
E factor	0.9552	1.3126	0.9192
SiO2	50.18	31.88	50.54
TiO2	0.45	0.32	0.44
Al2O3	21.71	15.85	22.72
Fe2O3	8.40	9.02	9.05
MnO	0.25	0.65	0.16
MgO	10.81	18.55	8.34
CaO	2.14	19.37	1.86
Na2O	4.38	2.55	4.60
K2O	1.65	1.78	2.27
P2O5	0.02	0.02	0.03
Rb	32	28	35.07
Ba	263	361	347.84
Sr	144	153	132.28
Precursors			
SiO2	52.88	52.83	52.79
TiO2	0.44	0.44	0.44
Al2O3	20.74	20.80	20.86
Fe2O3	9.85	9.85	9.85
MnO	0.15	0.15	0.15
MgO	6.11	6.14	6.16
CaO	9.62	9.64	9.66
Na2O	3.00	3.00	2.99
K2O	0.42	0.41	0.41
P2O5	0.14	0.14	0.14
Rb	8	7	7.03
Ba	133	128	124.23
Sr	422	425	429
Total	103.35	103.40	103.46
Norm factor	0.9676	0.9671	0.97
Precursors - normalized to 100%			
SiO2	51.16	51.09	51.03
TiO2	0.43	0.43	0.43
Al2O3	20.07	20.12	20.16
Fe2O3	9.53	9.53	9.52
MnO	0.15	0.15	0.15
MgO	5.91	5.94	5.96
CaO	9.30	9.32	9.33
Na2O	2.90	2.90	2.89
K2O	0.41	0.40	0.39
P2O5	0.14	0.13	0.13
Rb	7	7	6.79
Ba	129	124	120.09
Sr	408	411	414
Total	100.00	100.00	100.00
Reconstituted			
SiO2	47.9	41.8	46.5
TiO2	0.4	0.4	0.4
Al2O3	20.7	20.8	20.9
Fe2O3	8.0	11.8	8.3
MnO	0.2	0.9	0.1
MgO	10.3	24.4	7.7
CaO	2.0	25.4	1.7
Na2O	4.2	3.3	4.2
K2O	1.6	2.3	2.1
P2O5	0.0	0.0	0.0
Rb	30	36	32.18
Ba	251	474	318.62
Sr	137	201	121.79
Total	95.5	131.3	91.9
Mass Changes			
SiO2	-3.2	-9.3	-4.6
TiO2	0.0	-0.0	-0.0
Al2O3	0.7	0.7	0.7
Fe2O3	-1.5	2.3	-1.2
MnO	0.1	0.7	0.0
MgO	4.4	18.4	1.7
CaO	-7.3	16.1	-7.6
Na2O	1.3	0.4	1.3
K2O	1.2	1.9	1.7
P2O5	-0.1	-0.1	-0.1
Rb	23	29	25
Ba	122	349	199
Sr	-271	-210	-292
Total	-4.48	31.26	-0.21

Table F-9 - Calculated mass changes for volcanic rocks in the WBZ

Drill Hole	BE-95-01	BE-95-01	BE-95-01	BE-96-08	BE-96-08	BE-96-08	BE-96-10	BE-96-10	BE-96-10	BE-96-10	BE-96-09
From	19.4	53.2	129.7	18.6	109.4	281.8	114.5	78.3	193.7	208.5	62
To	20.2	53.6	130.1	19.1	110	282.2	115.1	78.8	194.2	208.8	62.5
Sample	WB-01	WB-02	WB-03	WB-04	WB-05	WB-07	WB-08	WB-11	WB-13	WB-14	WB-15
Lithology	Dacite	Dacite	Dacite	Dacite	Dacite	Dacite	Dacite	Dacite	Dacite	Dacite	Dacite
Raw data - LOI free											
Sample	WB-01	WB-02	WB-03	WB-04	WB-05	WB-07	WB-08	WB-11	WB-13	WB-14	WB-15
Zr	113	105	111	99	117	87	82	100	40	99	91
Al2O3/Zr	0.14	0.19	0.15	0.20	0.13	0.21	0.18	0.19	0.15	0.20	0.20
Zr precursor	100.61	82.32	96.44	80.13	103.31	75.96	86.81	81.74	97.23	80.64	79.03
Enrich Factor	0.8899	0.7844	0.8654	0.8060	0.8868	0.8765	1.0527	0.8207	2.4546	0.8177	0.8675
SiO2	62.31	70.59	69.20	71.77	57.51	72.47	73.42	68.13	86.31	68.91	71.91
TiO2	0.40	0.35	0.36	0.34	0.36	0.32	0.24	0.35	0.19	0.36	0.32
Al2O3	15.90	19.97	16.75	19.66	15.70	18.48	14.53	19.15	5.88	19.33	18.38
Fe2O3	10.78	1.74	5.37	3.07	13.44	1.93	5.26	3.65	4.39	2.55	2.94
MnO	0.15	0.05	0.07	0.01	0.23	0.01	0.03	0.05	0.05	0.07	0.03
MgO	5.11	1.42	3.11	0.52	9.37	1.04	1.90	2.55	1.92	1.37	1.94
CaO	0.51	0.76	0.20	0.11	0.35	0.33	1.31	1.27	0.32	0.92	0.15
Na2O	4.05	0.44	2.67	0.35	2.07	2.12	0.14	0.76	0.00	3.72	0.23
K2O	0.73	4.63	2.22	4.10	0.90	3.25	3.14	4.04	0.75	2.71	4.04
P2O5	0.05	0.05	0.05	0.05	0.05	0.06	0.03	0.05	0.03	0.07	0.05
Rb	13	63	33	55	14	47	46	60	13	47	57
Ba	168	463	380	570	170	590	503	946	138	445	857
Sr	70	23	34	11	29	36	30	24	9	38	11
Precursors											
SiO2	70.16	67.43	69.54	67.10	70.56	66.48	68.10	67.34	69.66	67.18	66.94
TiO2	0.25	0.34	0.27	0.35	0.24	0.37	0.32	0.34	0.27	0.35	0.36
Al2O3	14.15	15.67	14.50	15.85	13.93	16.20	15.29	15.72	14.43	15.81	15.94
Fe2O3	5.82	7.65	6.24	7.87	5.55	8.28	7.20	7.71	6.16	7.82	7.98
MnO	0.10	0.09	0.10	0.09	0.10	0.09	0.09	0.09	0.10	0.09	0.09
MgO	0.65	2.29	1.02	2.49	0.40	2.86	1.89	2.34	0.95	2.44	2.59
CaO	2.34	2.46	2.36	2.47	2.32	2.50	2.43	2.46	2.36	2.47	2.48
Na2O	3.87	3.33	3.75	3.27	3.95	3.14	3.46	3.31	3.77	3.28	3.23
K2O	2.07	1.94	2.04	1.92	2.09	1.89	1.97	1.93	2.04	1.92	1.91
P2O5	0.04	0.04	0.04	0.04	0.04	0.04	0.04	0.04	0.04	0.04	0.04
Rb	39	32	37	31	40	29	34	32	38	31	31
Ba	315	265	303	259	322	247	277	263	305	260	256
Sr	107	92	103	90	109	87	96	91	104	91	89
Total	99.44	101.23	99.85	101.45	99.18	101.86	100.79	101.29	99.78	101.40	101.56
Norm factor	1.0056	0.9878	1.0015	0.9857	1.0083	0.9818	0.9921	0.9873	1.0023	0.9862	0.9847
Precursors - normalized to 100%											
SiO2	70.55	66.61	69.64	66.14	71.15	65.27	67.56	66.49	69.82	66.25	65.92
TiO2	0.25	0.33	0.27	0.34	0.24	0.36	0.31	0.34	0.27	0.34	0.35
Al2O3	14.23	15.48	14.52	15.62	14.04	15.90	15.17	15.52	14.46	15.59	15.70
Fe2O3	5.85	7.56	6.25	7.75	5.60	8.13	7.14	7.61	6.17	7.71	7.85
MnO	0.10	0.09	0.10	0.09	0.10	0.09	0.09	0.09	0.10	0.09	0.09
MgO	0.65	2.26	1.02	2.45	0.41	2.81	1.87	2.31	0.95	2.41	2.55
CaO	2.35	2.43	2.37	2.44	2.34	2.45	2.41	2.43	2.36	2.43	2.44
Na2O	3.89	3.29	3.75	3.22	3.98	3.09	3.44	3.27	3.78	3.24	3.18
K2O	2.08	1.91	2.04	1.89	2.11	1.86	1.95	1.91	2.05	1.90	1.88
P2O5	0.04	0.04	0.04	0.04	0.04	0.04	0.04	0.04	0.04	0.04	0.04
Rb	39	31	37	31	40	29	33	31	38	31	30
Ba	316	262	304	255	325	243	275	260	306	257	252
Sr	107	91	104	89	110	85	95	90	104	89	88
Total	100.00	100.01	100.00	100.00	100.00	100.00	100.00	100.00	100.00	100.00	100.00
Reconstituted											
SiO2	55.5	55.3	59.9	57.8	51.0	63.5	77.3	55.9	211.9	56.4	62.3
TiO2	0.4	0.3	0.3	0.3	0.3	0.3	0.3	0.3	0.5	0.3	0.3
Al2O3	14.2	15.7	14.5	15.8	13.9	16.2	15.3	15.7	14.4	15.8	15.9
Fe2O3	9.6	1.4	4.6	2.5	11.9	1.7	5.5	3.0	10.8	2.1	2.6
MnO	0.1	0.0	0.1	0.0	0.2	0.0	0.0	0.0	0.1	0.1	0.0
MgO	4.5	1.1	2.7	0.4	8.3	0.9	2.0	2.1	4.7	1.1	1.7
CaO	0.5	0.6	0.2	0.1	0.3	0.3	1.4	1.0	0.8	0.7	0.1
Na2O	3.6	0.3	2.3	0.3	1.8	1.9	0.1	0.6	0.0	3.0	0.2
K2O	0.7	3.6	1.9	3.3	0.8	2.8	3.3	3.3	1.9	2.2	3.5
P2O5	0.0	0.0	0.0	0.0	0.0	0.1	0.0	0.0	0.1	0.1	0.0
Rb	11	49	29	44	12	42	49	49	32	38	49
Ba	150	363	328	459	151	517	530	777	340	364	743
Sr	62	18	29	9	26	32	32	20	22	31	10
Total	89.0	78.4	86.5	80.6	88.7	87.6	105.3	82.1	245.1	81.8	86.7
Mass Changes											
SiO2	-15.1	-11.3	-9.8	-8.3	-20.1	-1.8	9.8	-10.6	142.1	-9.9	-3.6
TiO2	0.1	-0.1	0.0	-0.1	0.1	-0.1	-0.1	-0.0	0.2	-0.0	-0.1
Al2O3	-0.1	0.2	-0.0	0.2	-0.1	0.3	0.1	0.2	-0.0	0.2	0.2
Fe2O3	3.7	-6.2	-1.6	-5.3	6.3	-6.4	-1.6	-4.6	4.6	-5.6	-5.3
MnO	0.0	-0.0	-0.0	-0.1	0.1	-0.1	-0.1	-0.0	0.0	-0.0	-0.1
MgO	3.9	-1.1	1.7	-2.0	7.9	-1.9	0.1	-0.2	3.8	-1.3	-0.9
CaO	-1.9	-1.8	-2.2	-2.3	-2.0	-2.2	-1.0	-1.4	-1.6	-1.7	-2.3
Na2O	-0.3	-2.9	-1.4	-2.9	-2.1	-1.2	-3.3	-2.6	-3.8	-0.2	-3.0
K2O	-1.4	1.7	-0.1	1.4	-1.3	1.0	1.4	1.4	-0.2	0.3	1.6
P2O5	0.0	-0.0	0.0	-0.0	0.0	0.0	-0.0	0.0	0.0	0.0	0.0
Rb	-28	18	-9	13	-28	13	15	18	-6	7	19
Ba	-167	102	25	204	-174	274	255	517	33	107	491
Sr	-45	-73	-74	-80	-84	-53	-63	-70	-82	-58	-78
Total	-11.0	-21.6	-13.5	-19.4	-11.3	-12.4	5.3	-17.9	145.1	-18.2	-13.3

Table F-9 continued

Drill Hole	BE-95-02	BE-95-02	BE-95-03	BE-95-03	BJ-46	BE-95-01	BJ-46	BJ-46	BJ-46	BJ-45	BJ-45
From	9.9	119.5	157.8	133.1	226	53.2	501	646	1298.5	109	149
To	10.5	120.1	158.2	133.5	228	53.6	503	647.5	1300.5	111	151
Sample	WB-16	WB-17	WB-18	WB-19	WB-20	WB-21	WB-22	WB-23	WB-24	WB-25	WB-26
Lithology	Dacite	Dacite	Dacite	Dacite	Dacite	Dacite	Dacite	Dacite	Dacite	Dacite	Dacite
Raw data - LOI free											
Sample	WB-16	WB-17	WB-18	WB-19	WB-20	WB-2	WB-22	WB-23	WB-24	WB-25	WB-26
Zr	127	93	106	78	82	86	116	113	107	87	119
Al2O3/Zr	0.17	0.15	0.20	0.21	0.21	0.21	0.16	0.17	0.14	0.20	0.15
Zr precursor	88.25	96.68	78.56	77.01	78.02	77.93	93.31	90.48	101.81	79.80	98.30
E factor	0.6923	1.0386	0.7381	0.9910	0.9482	0.9105	0.8055	0.7984	0.9483	0.9218	0.8233
SiO2	64.84	57.14	68.13	74.19	74.07	72.53	67.94	71.80	62.62	73.92	65.16
TiO2	0.40	0.33	0.34	0.30	0.30	0.37	0.41	0.35	0.35	0.29	0.35
Al2O3	21.92	13.94	21.65	16.25	16.90	17.61	18.32	18.78	14.82	17.22	17.42
Fe2O3	5.12	10.91	2.38	2.19	2.00	2.19	3.36	2.45	6.87	1.83	7.16
MnO	0.02	0.19	0.01	0.03	0.05	0.03	0.06	0.02	0.19	0.02	0.25
MgO	2.23	13.78	1.16	1.62	1.74	1.51	1.80	0.80	10.08	1.32	4.22
CaO	0.15	2.67	0.36	0.36	0.33	0.34	2.22	0.70	1.52	0.17	1.00
Na2O	0.24	0.96	1.64	2.57	1.50	2.57	3.41	1.60	2.47	2.26	1.74
K2O	5.02	0.04	4.26	2.42	3.04	2.78	2.43	3.46	1.03	2.91	2.65
P2O5	0.06	0.04	0.06	0.07	0.06	0.07	0.05	0.04	0.05	0.05	0.05
Rb	69	0	60	37	42	38	36	51	21	42	42
Ba	1008	60	893	379	882	490	240	376	164	688	559
Sr	11	15	29	31	20	35	58	38	39	25	21
Precursors											
SiO2	68.32	69.57	66.87	66.64	66.79	66.77	69.07	68.65	70.34	67.05	69.82
TiO2	0.31	0.27	0.36	0.36	0.36	0.36	0.29	0.30	0.24	0.35	0.26
Al2O3	15.18	14.48	15.98	16.11	16.02	16.03	14.76	14.99	14.05	15.88	14.34
Fe2O3	7.06	6.21	8.02	8.18	8.08	8.09	6.55	6.83	5.70	7.90	6.05
MnO	0.09	0.10	0.09	0.09	0.09	0.09	0.10	0.10	0.10	0.09	0.10
MgO	1.76	1.00	2.63	2.77	2.68	2.69	1.30	1.56	0.54	2.52	0.85
CaO	2.42	2.36	2.48	2.49	2.49	2.49	2.39	2.40	2.33	2.47	2.35
Na2O	3.51	3.75	3.22	3.17	3.20	3.20	3.65	3.57	3.91	3.26	3.80
K2O	1.98	2.04	1.91	1.90	1.90	1.90	2.02	2.00	2.08	1.92	2.05
P2O5	0.04	0.04	0.04	0.04	0.04	0.04	0.04	0.04	0.04	0.04	0.04
Rb	34	37	30	30	30	30	36	35	39	31	38
Ba	281	304	254	250	253	253	295	287	318	258	308
Sr	97	104	89	88	88	88	101	99	108	90	105
Total	100.65	99.83	101.60	101.75	101.65	101.66	100.16	100.44	99.33	101.48	99.67
Norm factor	0.9935	1.0017	0.9842	0.9828	0.9837	0.9836	0.9984	0.9957	1.0068	0.9854	1.0033
Precursors - normalized to 100%											
SiO2	67.87	69.69	65.81	65.49	65.70	65.68	68.96	68.35	70.82	66.08	70.05
TiO2	0.31	0.27	0.35	0.36	0.35	0.35	0.29	0.30	0.25	0.35	0.26
Al2O3	15.08	14.50	15.73	15.83	15.76	15.77	14.73	14.93	14.15	15.64	14.39
Fe2O3	7.01	6.22	7.90	8.04	7.95	7.95	6.54	6.80	5.74	7.78	6.07
MnO	0.09	0.10	0.09	0.09	0.09	0.09	0.10	0.10	0.10	0.09	0.10
MgO	1.75	1.00	2.59	2.72	2.63	2.64	1.30	1.55	0.54	2.48	0.86
CaO	2.40	2.37	2.44	2.45	2.45	2.45	2.38	2.39	2.34	2.44	2.36
Na2O	3.48	3.76	3.17	3.12	3.15	3.15	3.65	3.56	3.93	3.21	3.81
K2O	1.97	2.04	1.88	1.86	1.87	1.87	2.01	1.99	2.09	1.89	2.06
P2O5	0.04	0.04	0.04	0.04	0.04	0.04	0.04	0.04	0.04	0.04	0.04
Rb	34	37	30	29	30	30	36	35	40	30	38
Ba	279	304	250	246	249	249	294	286	320	254	309
Sr	96	104	87	86	87	87	101	98	109	89	105
Total	100.00	100.00	100.00	100.00	100.00	100.00	100.00	100.00	100.00	100.00	100.00
Reconstituted											
SiO2	44.9	59.4	50.3	73.5	70.2	66.1	54.7	57.3	59.4	68.1	53.6
TiO2	0.3	0.3	0.3	0.3	0.3	0.3	0.3	0.3	0.3	0.3	0.3
Al2O3	15.2	14.5	16.0	16.1	16.0	16.0	14.7	15.0	14.0	15.9	14.3
Fe2O3	3.5	11.3	1.8	2.2	1.9	2.0	2.7	2.0	6.5	1.7	5.9
MnO	0.0	0.2	0.0	0.0	0.0	0.0	0.1	0.0	0.2	0.0	0.2
MgO	1.5	14.3	0.9	1.6	1.6	1.4	1.4	0.6	9.6	1.2	3.5
CaO	0.1	2.8	0.3	0.4	0.3	0.3	1.8	0.6	1.4	0.2	0.8
Na2O	0.2	1.0	1.2	2.5	1.4	2.3	2.7	1.3	2.3	2.1	1.4
K2O	3.5	0.0	3.1	2.4	2.9	2.5	2.0	2.8	1.0	2.7	2.2
P2O5	0.0	0.0	0.0	0.1	0.1	0.1	0.0	0.0	0.0	0.0	0.0
Rb	48	0	44	37	39	35	29	40	20	39	35
Ba	698	62	659	375	837	446	193	300	156	634	460
Sr	8	16	21	31	19	32	46	30	37	23	17
Total	69.2	103.9	73.8	99.1	94.8	91.1	80.5	79.8	94.8	92.2	82.3
Mass Changes											
SiO2	-23.0	-10.3	-15.5	8.0	4.5	0.4	-14.3	-11.1	-11.5	2.1	-16.4
TiO2	-0.0	0.1	-0.1	-0.1	-0.1	-0.0	0.0	-0.0	0.1	-0.1	0.0
Al2O3	0.1	-0.0	0.2	0.3	0.3	0.3	0.0	0.1	-0.1	0.2	-0.1
Fe2O3	-3.5	5.1	-6.1	-5.9	-6.0	-6.0	-3.8	-4.8	0.8	-6.1	-0.2
MnO	-0.1	0.1	-0.1	-0.1	-0.0	-0.1	-0.0	-0.1	0.1	-0.1	0.1
MgO	-0.2	13.3	-1.7	-1.1	-1.0	-1.3	0.1	-0.9	9.0	-1.3	2.6
CaO	-2.3	0.4	-2.2	-2.1	-2.1	-2.1	-0.6	-1.8	-0.9	-2.3	-1.5
Na2O	-3.3	-2.8	-2.0	-0.6	-1.7	-0.8	-0.9	-2.3	-1.6	-1.1	-2.4
K2O	1.5	-2.0	1.3	0.5	1.0	0.7	-0.1	0.8	-1.1	0.8	0.1
P2O5	0.0	-0.0	0.0	0.0	0.0	0.0	-0.0	-0.0	0.0	0.0	-0.0
Rb	14	-37	14	8	10	5	-7	5	-20	9	-3
Ba	419	-242	408	130	588	197	-101	15	-164	380	151
Sr	-88	-88	-66	-55	-68	-55	-54	-68	-72	-65	-88
Total	-30.8	3.9	-26.2	-0.9	-5.2	-8.9	-19.5	-20.2	-5.2	-7.8	-17.7

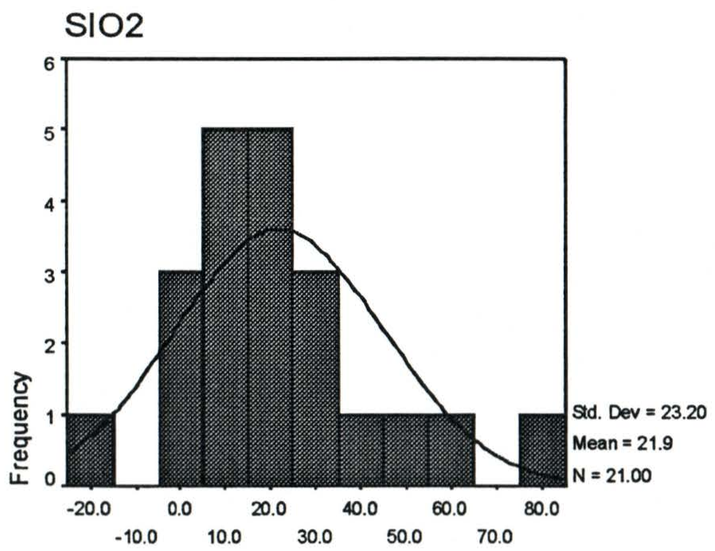
Table F-9 continued

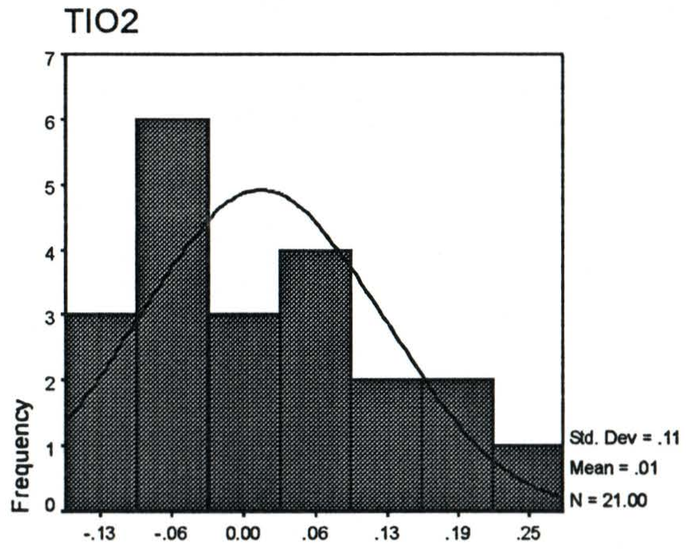
Drill Hole	BJ-41	BJ-41	BJ-41	BE-97-15	BE-97-16	BE-95-02	BE-95-03	BE-95-03	BE-95-08		BE-96-08
From	266.5	526.5	471	5	74.2	64.1	106.5	111.7	267.8		249
To	268.5	528.5	473	5.3	74.4	65.4	108.2	112.7	269.6		249.5
Sample	WB-27	WB-28	WB-29	WB-30	WB-31	BE-01-64	BE-3-106	BE-3-111	BE-8-267	Avg Felsic	WB-06
Lithology	Dacite	Dacite	Dacite	Dacite	Dacite	Dacite	Dacite	Dacite	Dacite	Dacite	Bas-And
Raw data - LOI free											
Sample	WB-27	WB-28	WB-29	WB-30	WB-31	BE-01-64	BE-3-106	BE-3-111	BE-8-267	Avg Felsic	WB-06
Zr	134	101	105	93	108	109	75	47	80	109	19
Al2O3/Zr	0.20	0.19	0.14	0.17	0.17	0.18	0.24	0.36	0.19	0.17	1.08
Zr precursor	80.11	81.81	101.74	90.34	90.67	84.53	68.67	50.96	82.01	87.60	20.00
E factor	0.5965	0.8097	0.9695	0.9671	0.8363	0.7741	0.9184	1.0843	1.0209	0.8052	1.0526
SiO2	58.13	67.74	75.23	64.19	68.28	68.92	72.22	75.02	69.83	68.60	45.63
TiO2	0.49	0.44	0.11	0.52	0.32	0.34	0.29	0.28	0.30	0.33	0.44
Al2O3	26.57	19.40	14.50	15.51	17.91	20.00	18.29	16.85	15.37	18.95	20.42
Fe2O3	2.23	2.45	0.65	8.31	4.14	4.37	3.56	3.46	6.20	4.25	14.83
MnO	0.07	0.05	0.04	0.12	0.13	0.01	0.02	0.01	0.06	0.07	0.22
MgO	5.29	0.82	0.21	5.40	3.97	1.25	0.99	0.75	3.96	2.61	14.61
CaO	2.04	2.99	0.55	0.85	1.48	0.39	0.56	0.19	0.41	0.94	0.22
Na2O	1.61	3.48	3.79	4.43	0.25	0.32	0.33	0.00	1.34	0.29	1.73
K2O	3.51	2.55	4.91	0.59	3.49	4.34	3.69	3.39	2.49	3.91	1.87
P2O5	0.05	0.09	0.02	0.08	0.04	0.05	0.04	0.04	0.04	0.05	0.03
Rb	45	34	34	8	51	60	54	30	36	56	31
Ba	336	297	197	174	866	1077	1437	1372	239	972	292
Sr	96	102	103	144	13	12	21	8	15	13	24
Precursors											
SiO2	67.10	67.35	70.33	68.63	68.68	67.76	65.39	62.75	67.38	68.22	49.59
TiO2	0.35	0.34	0.24	0.30	0.30	0.33	0.41	0.49	0.34	0.31	0.50
Al2O3	15.85	15.71	14.06	15.00	14.97	15.48	16.80	18.27	15.69	15.23	17.87
Fe2O3	7.87	7.70	5.71	6.85	6.81	7.43	9.01	10.78	7.68	7.12	9.87
MnO	0.09	0.09	0.10	0.10	0.10	0.09	0.08	0.07	0.09	0.09	0.15
MgO	2.49	2.34	0.54	1.57	1.54	2.09	3.52	5.11	2.32	1.82	6.30
CaO	2.47	2.46	2.33	2.40	2.40	2.44	2.55	2.66	2.46	2.42	9.75
Na2O	3.26	3.31	3.90	3.57	3.58	3.40	2.93	2.40	3.32	3.49	2.18
K2O	1.92	1.93	2.08	1.99	2.00	1.95	1.84	1.71	1.93	1.97	0.38
P2O5	0.04	0.04	0.04	0.04	0.04	0.04	0.04	0.04	0.04	0.04	0.07
Rb	31	32	39	35	35	33	27	20	32	34	6
Ba	259	263	318	287	288	271	227	179	264	279	103
Sr	90	92	108	98	99	94	81	66	92	96	144
Total	101.45	101.28	99.33	100.45	100.42	101.02	102.57	104.30	101.26	100.72	96.66
Norm factor	0.9857	0.9873	1.0067	0.9955	0.9958	0.9899	0.9750	0.9588	0.9875	0.9929	1.0346
Precursors - normalized to 100%											
SiO2	66.81	66.50	70.80	68.32	68.39	67.08	63.76	60.16	66.54	67.73	51.31
TiO2	0.35	0.34	0.25	0.30	0.30	0.33	0.40	0.47	0.34	0.31	0.52
Al2O3	15.78	15.51	14.15	14.93	14.91	15.33	16.38	17.52	15.50	15.12	18.49
Fe2O3	7.84	7.60	5.74	6.82	6.78	7.35	8.79	10.34	7.58	7.07	10.21
MnO	0.09	0.09	0.10	0.09	0.10	0.09	0.08	0.07	0.09	0.09	0.16
MgO	2.48	2.31	0.55	1.56	1.53	2.07	3.43	4.90	2.29	1.80	6.52
CaO	2.46	2.43	2.35	2.39	2.39	2.42	2.48	2.55	2.43	2.41	10.09
Na2O	3.25	3.27	3.93	3.55	3.56	3.36	2.85	2.31	3.28	3.46	2.26
K2O	1.91	1.91	2.09	1.99	1.99	1.93	1.79	1.64	1.91	1.96	0.39
P2O5	0.04	0.04	0.04	0.04	0.04	0.04	0.04	0.04	0.04	0.04	0.07
Rb	31	31	40	35	35	32	26	19	31	34	6
Ba	258	260	320	285	286	268	222	172	261	277	107
Sr	90	90	108	98	98	93	79	64	91	96	149
Total	101.01	100.00	100.00	100.00	100.00	100.00	100.00	100.00	100.00	100.00	100.00
										ERR	
Reconstituted											
SiO2	34.6	54.9	73.0	62.1	57.1	53.3	66.3	81.3	71.3	55.2	48.0
TiO2	0.3	0.4	0.1	0.5	0.3	0.3	0.3	0.3	0.3	0.3	0.5
Al2O3	15.8	15.7	14.1	15.0	15.0	15.5	16.8	18.3	15.7	15.2	21.5
Fe2O3	1.3	2.0	0.6	8.0	3.5	3.4	3.3	3.8	6.3	3.4	15.6
MnO	0.0	0.0	0.0	0.1	0.1	0.0	0.0	0.0	0.1	0.1	0.2
MgO	3.2	0.7	0.2	5.2	3.3	1.0	0.9	0.8	4.0	2.1	15.4
CaO	1.2	2.4	0.5	0.8	1.2	0.3	0.5	0.2	0.4	0.8	0.2
Na2O	1.0	2.8	3.7	4.3	0.2	0.2	0.3	0.0	1.4	0.2	1.8
K2O	2.1	2.1	4.8	0.6	2.9	3.4	3.4	3.7	2.5	3.1	2.0
P2O5	0.0	0.1	0.0	0.1	0.0	0.0	0.0	0.0	0.0	0.0	0.0
Rb	27	27	33	8	43	47	50	33	37	45	33
Ba	200	240	192	168	724	834	1319	1487	244	779	307
Sr	57	83	100	139	11	9	19	9	16	10	25
Total	59.6	81.0	97.0	96.7	83.6	77.4	91.8	108.4	102.1	80.5	105.3
										ERR	
Mass Changes											
SiO2	-32.2	-11.6	2.2	-6.2	-11.3	-13.7	2.5	21.2	4.8	-12.5	-3.3
TiO2	-0.1	0.0	-0.1	0.2	-0.0	-0.1	-0.1	-0.2	-0.0	-0.0	-0.1
Al2O3	0.1	0.2	-0.1	0.1	0.1	0.2	0.4	0.7	0.2	0.1	3.0
Fe2O3	-6.5	-5.6	-5.1	1.2	-3.3	-4.0	-5.5	-6.6	-1.3	-3.6	5.4
MnO	-0.0	-0.0	-0.1	0.0	0.0	-0.1	-0.1	-0.1	-0.0	-0.0	0.1
MgO	0.7	-1.6	-0.3	3.7	1.8	-1.1	-2.5	-4.1	1.8	0.3	8.9
CaO	-1.2	-0.0	-1.8	-1.6	-1.2	-2.1	-2.0	-2.3	-2.0	-1.6	-9.9
Na2O	-2.3	-0.5	-0.3	0.7	-3.4	-3.1	-2.6	-2.3	-1.9	-3.2	-0.4
K2O	0.2	0.2	2.7	-1.4	0.9	1.4	1.6	2.0	0.6	1.2	1.6
P2O5	-0.0	0.0	-0.0	0.0	-0.0	-0.0	-0.0	0.0	0.0	-0.0	-0.0
Rb	-4	-4	-6	-27	8	14	24	14	6	11	27
Ba	-57	-20	-128	-117	438	566	1097	1316	-16	502	201
Sr	-32	-8	-8	41	-87	-83	-59	-55	-75	-85	-124
Total	-41.4	-19.0	-3.0	-3.3	-16.4	-22.6	-8.2	8.4	2.1	-19.5	5.3

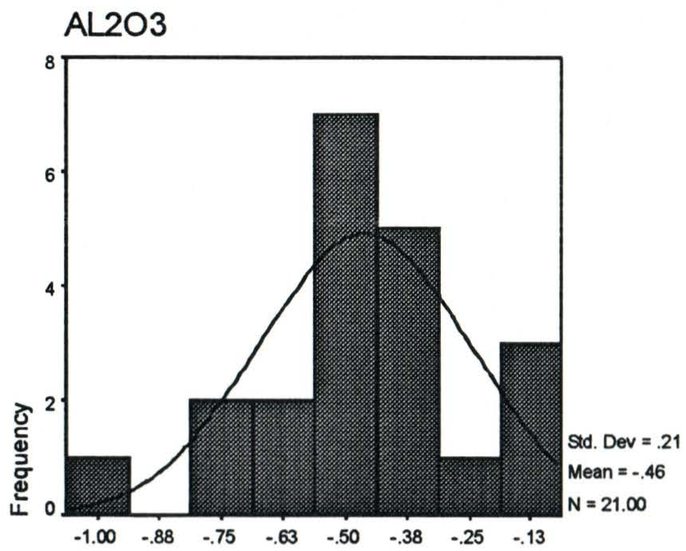
Table F-9 continued

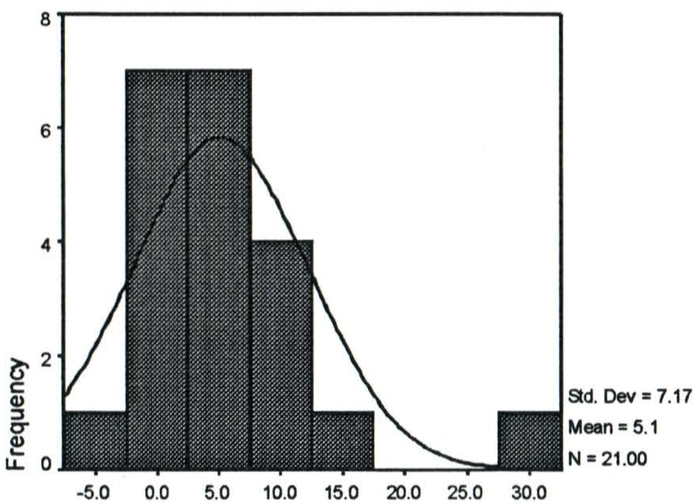
Drill Hole	BE-96-10	BE-96-10	BE-96-10		BE-95-10	BE-95-10	BE-93-11	BJ-42	BJ-42	BJ-47	BJ-49
From	124.3	154.7	190.7		186.1	140.0	111.7	447.0	980.0	344.0	263.0
To	124.8	155.5	191.1		186.6	143.0	112.7				
Sample	WB-09	WB-10	WB-12	Avg Mafic	BE-10-186	BE-10-140	BE-3-111	*BJ42447	*BJ42980	*BJ47344	*BJ49263
Lithology	Bas-And	Bas-And	Bas-And	Bas-And	Bas-And	Bas-And	Bas-And	Dacite	Dacite	Dacite	Dacite
Raw data - LOI free											
Sample	WB-09	WB-10	WB-12	Avg Mafic	BE-10-186	BE-10-140	BE-3-111	"BJ42447	"BJ42980	"BJ47344	"BJ49263
Zr	18	20	25	21	22	22		103	113	113	102
Al2O3/Zr	1.12	0.89	0.78	0.97	0.80	0.78	0.36	0.13	0.11	0.14	0.14
Zr precursor	20.00	24.00	28.00	23.00	27.00	28.00	61.00	104.60	118.74	101.70	101.97
E factor	1.1111	1.2000	1.1200	1.1209	1.2273	1.2727	1.2979	1.0160	1.0543	0.9028	1.0011
SiO2	48.04	54.13	50.95	49.69	47.80	54.15	75.02	74.64	77.22	70.20	72.96
TiO2	0.40	0.42	0.53	0.45	0.41	0.43	0.28	0.25	0.04	0.47	0.33
Al2O3	20.33	18.29	19.30	19.59	17.60	17.50	16.85	13.60	11.99	15.57	14.02
Fe2O3	13.38	16.29	13.61	14.53	22.12	15.39	3.46	2.91	1.23	3.91	3.88
MnO	0.20	0.23	0.44	0.27	0.25	0.33	0.01	0.13	0.04	0.07	0.08
MgO	13.94	7.34	8.63	11.13	8.10	8.42	0.75	1.00	0.94	2.09	1.26
CaO	0.16	0.51	1.39	0.57	0.30	0.31	0.19	1.71	0.48	1.92	1.76
Na2O	1.55	0.70	3.98	1.99	1.53	2.07	0.00	3.04	3.68	2.19	2.11
K2O	1.97	2.06	1.12	1.76	1.86	1.35	3.39	2.84	3.34	2.92	2.37
P2O5	0.02	0.02	0.04	0.03	0.04	0.04	0.04	n/a	n/a	n/a	n/a
Rb	28	34	25	30	33	22	30	85	68	60	54
Ba	290	289	242	278	274	251	1372	628	984	173	152
Sr	27	16	60	32	14	19	8	95	142	47	30
Precursors											
SiO2	49.59	49.79	49.98	49.74	49.93	49.98	51.60	70.76	72.87	70.32	70.36
TiO2	0.50	0.50	0.51	0.50	0.51	0.51	0.54	0.23	0.16	0.24	0.24
Al2O3	17.87	18.13	18.39	18.07	18.33	18.39	20.54	13.82	12.64	14.06	14.04
Fe2O3	9.87	9.85	9.84	9.86	9.84	9.84	9.69	5.42	4.01	5.71	5.68
MnO	0.15	0.15	0.15	0.15	0.15	0.15	0.15	0.10	0.11	0.10	0.10
MgO	6.30	6.17	6.04	6.20	6.07	6.04	4.95	0.29	-0.99	0.55	0.52
CaO	9.75	9.66	9.57	9.68	9.59	9.57	8.81	2.31	2.22	2.33	2.33
Na2O	2.18	2.19	2.21	2.19	2.20	2.21	2.32	3.99	4.41	3.90	3.91
K2O	0.38	0.41	0.44	0.40	0.43	0.44	0.68	2.10	2.20	2.08	2.08
P2O5	0.07	0.08	0.10	0.08	0.09	0.10	0.21	0.04	0.04	0.04	0.04
Rb	6	7	8	7	8	8	17	40	46	39	39
Ba	103	124	144	118	139	144	314	326	364	318	318
Sr	144	153	162	151	160	162	235	110	122	108	108
Total	96.66	96.93	97.21	96.86	97.14	97.21	99.48	99.05	97.67	99.34	99.31
Norm factor	1.0346	1.0316	1.0287	1.0324	1.0294	1.0287	1.0052	1.0096	1.0238	1.0067	1.0069
Precursors - normalized to 100%											
SiO2	51.31	51.36	51.42	51.35	51.40	51.42	51.87	71.44	74.60	75.04	70.85
TiO2	0.52	0.52	0.52	0.52	0.52	0.52	0.54	0.23	0.17	0.26	0.25
Al2O3	18.49	18.70	18.92	18.65	18.86	18.92	20.64	13.95	12.95	15.00	14.13
Fe2O3	10.21	10.17	10.12	10.18	10.13	10.12	9.74	5.47	4.10	6.09	5.72
MnO	0.16	0.16	0.16	0.16	0.16	0.16	0.16	0.10	0.11	0.11	0.10
MgO	6.52	6.36	6.21	6.40	6.25	6.21	4.97	0.29	-1.01	0.58	0.53
CaO	10.09	9.96	9.84	9.99	9.87	9.84	8.85	2.33	2.27	2.49	2.34
Na2O	2.26	2.26	2.27	2.26	2.27	2.27	2.34	4.03	4.51	4.16	3.94
K2O	0.39	0.42	0.45	0.41	0.44	0.45	0.68	2.12	2.25	2.22	2.09
P2O5	0.07	0.08	0.10	0.08	0.09	0.10	0.21	0.04	0.04	0.05	0.04
Rb	6	7	8	7	8	8	17	41	47	42	40
Ba	107	128	148	122	143	148	316	329	373	339	321
Sr	149	158	167	156	164	167	236	111	124	115	109
Total	100.00	100.00	100.00	100.00	100.00	100.00	100.00	100.00	100.00	105.99	100.00
				ERR							
Reconstituted											
SiO2	53.3	65.0	57.1	55.8	58.8	68.8	97.5	75.8	81.4	63.4	73.0
TiO2	0.4	0.5	0.6	0.5	0.5	0.5	0.4	0.3	0.0	0.4	0.3
Al2O3	22.6	21.9	21.6	21.9	21.6	22.2	21.9	13.8	12.6	14.1	14.0
Fe2O3	14.9	19.5	15.2	16.3	27.2	19.5	4.5	3.0	1.3	3.5	3.9
MnO	0.2	0.3	0.5	0.3	0.3	0.4	0.0	0.1	0.0	0.1	0.1
MgO	15.5	8.8	9.7	12.3	10.0	10.7	1.0	1.0	1.0	1.9	1.3
CaO	0.2	0.6	1.6	0.6	0.4	0.4	0.2	1.7	0.5	1.7	1.8
Na2O	1.7	0.8	4.5	2.2	1.9	2.6	0.0	3.1	3.9	2.0	2.1
K2O	2.2	2.5	1.3	2.0	2.3	1.7	4.4	2.9	3.5	2.6	2.4
P2O5	0.0	0.0	0.0	0.0	0.0	0.1	0.1	n/a	n/a	n/a	n/a
Rb	31	41	28	33	41	28	39	87	72	55	54
Ba	322	347	271	312	337	319	1784	638	1037	156	152
Sr	30	19	67	35	17	24	10	96	150	42	30
Total	111.0	120.0	112.0	112.1	123.0	127.0	130.0	101.7	104.3	89.7	98.9
				ERR							
Mass Changes											
SiO2	2.0	13.6	5.6	4.5	7.4	17.4	17.4	4.4	6.8	-11.6	2.2
TiO2	-0.1	-0.0	0.1	-0.0	-0.0	0.0	17.4	0.0	-0.1	0.2	0.1
Al2O3	4.1	3.2	2.7	3.3	2.8	3.3	17.4	-0.1	-0.3	-0.9	-0.1
Fe2O3	4.6	9.4	5.1	6.1	17.1	9.4	17.4	-2.5	-2.8	-2.6	-1.8
MnO	0.1	0.1	0.3	0.1	0.2	0.3	17.4	0.0	-0.1	-0.0	-0.0
MgO	9.0	2.4	3.5	5.9	3.7	4.5	17.4	0.7	2.0	1.3	0.7
CaO	-9.9	-9.4	-8.3	-9.4	-9.5	-9.4	17.4	-0.6	-1.8	-0.8	-0.6
Na2O	-0.5	-1.4	2.2	-0.1	-0.4	0.4	17.4	-0.9	-0.6	-2.2	-1.8
K2O	1.8	2.1	0.8	1.6	1.8	1.3	17.4	0.8	1.3	0.4	0.3
P2O5	-0.0	-0.1	-0.1	-0.1	-0.0	-0.0	17.4	-0.0	-0.0	-0.0	-0.0
Rb	25	34	20	26	33	20	17	46	25	13	14
Ba	215	219	123	190	194	170	17	309	665	-183	-169
Sr	-119	-139	-99	-120	-147	-142	17	-15	25	-73	-78
Total	11.0	20.0	12.0	12.1	23.0	27.0	173.5	1.7	4.3	-16.3	-1.1

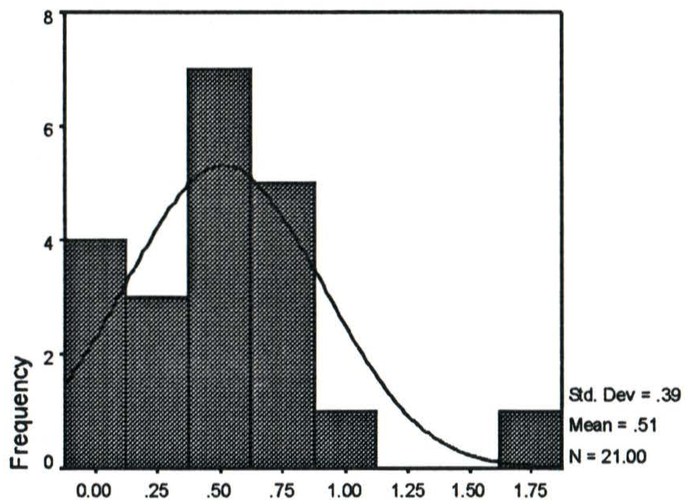
* indicates data from Thurlow (1981).

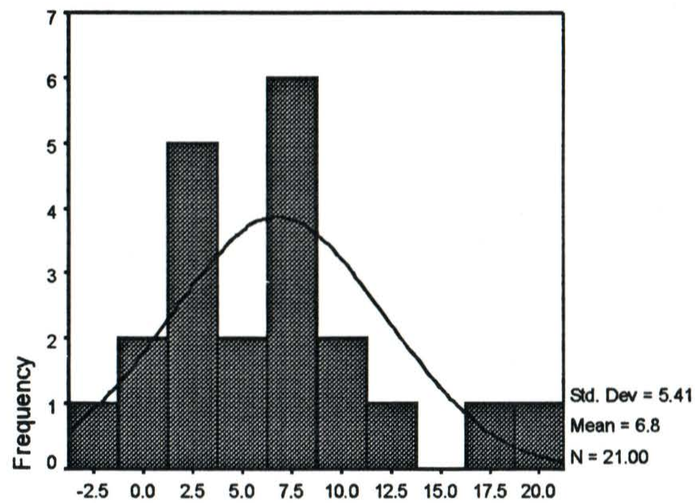


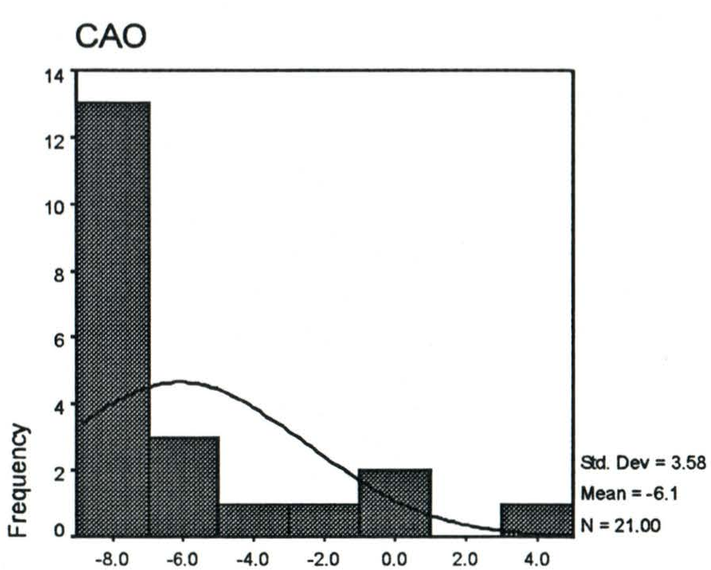


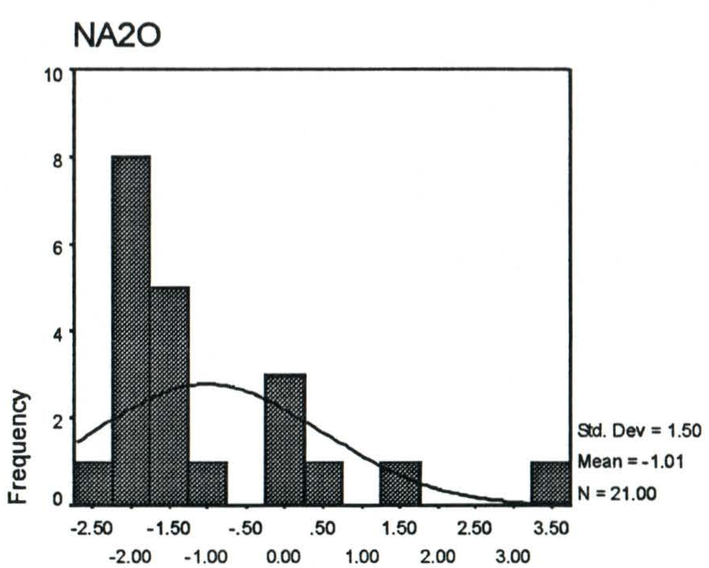












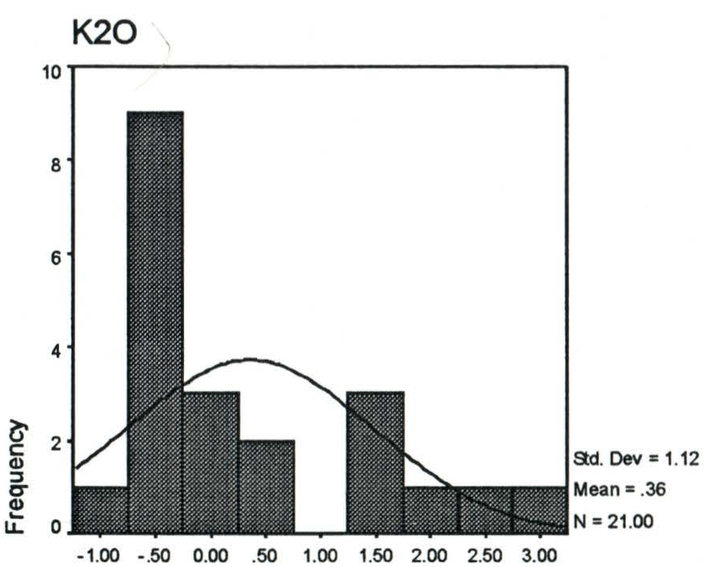
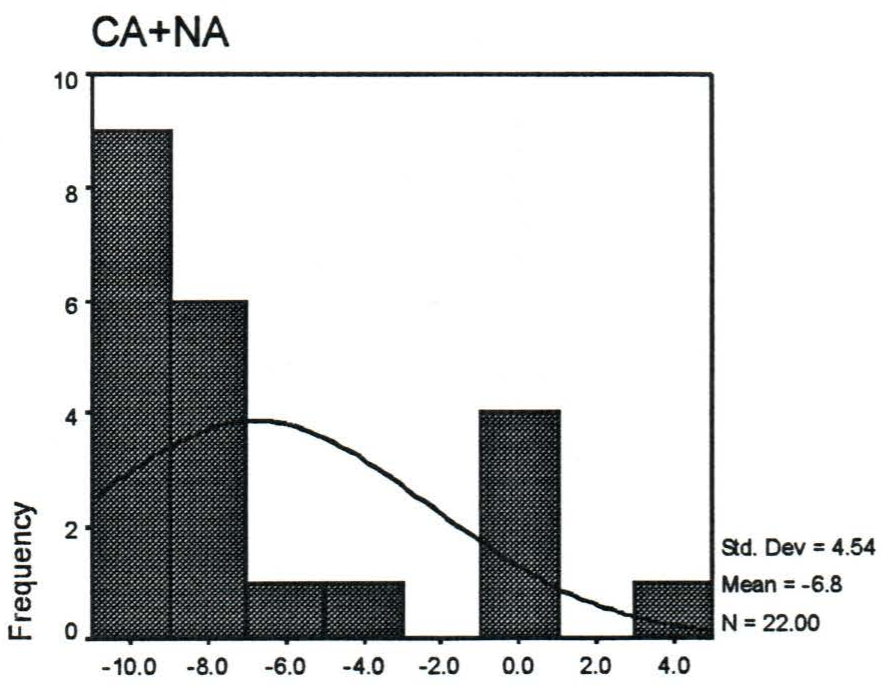
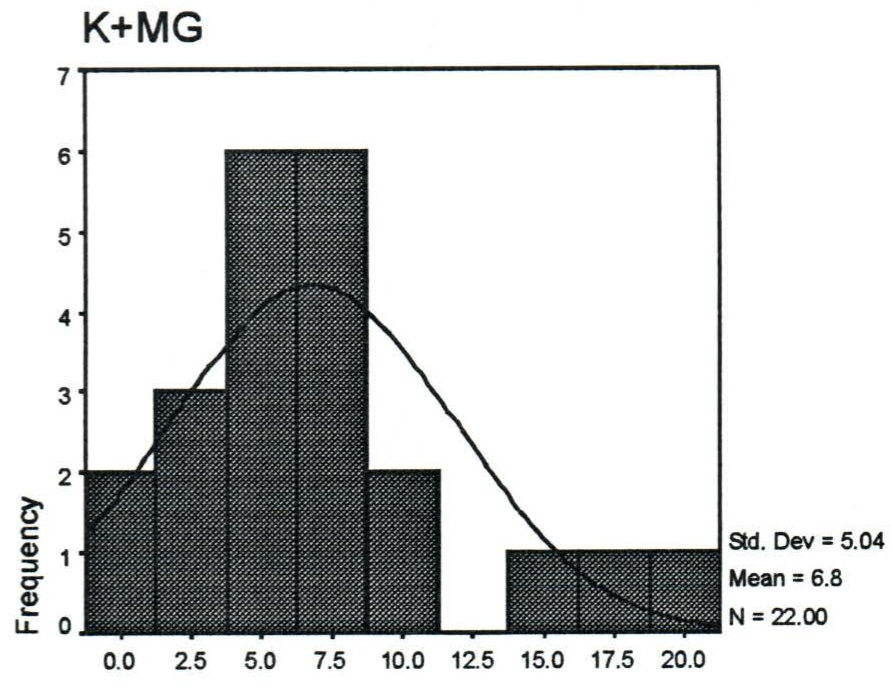
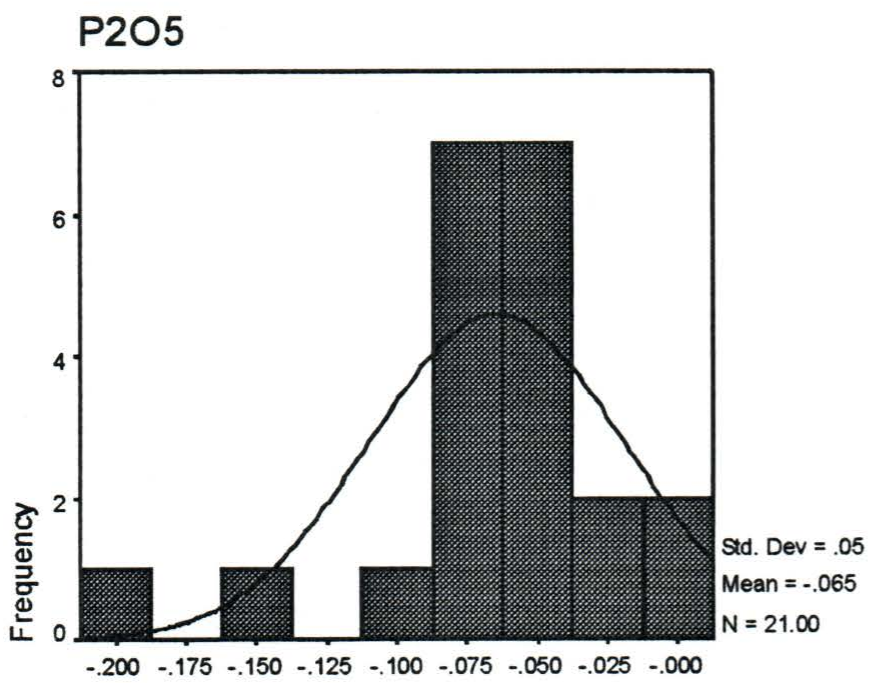
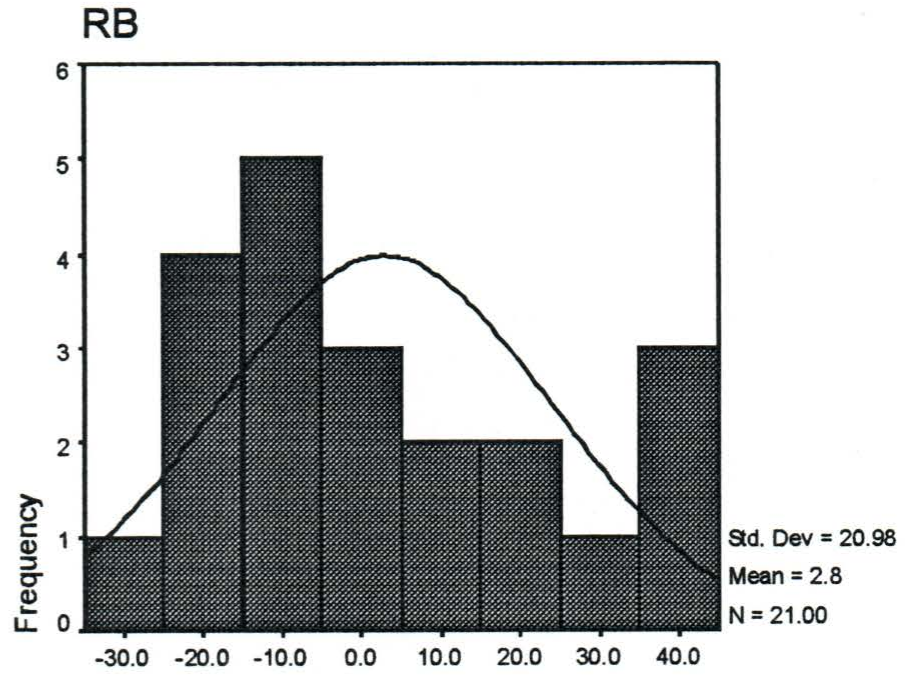


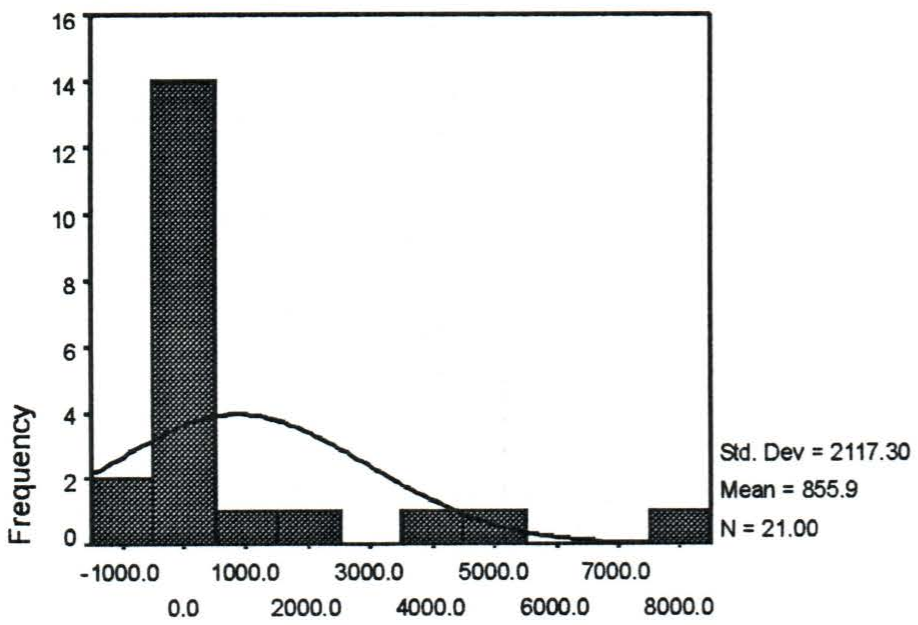
Figure F-1 - Oxide and trace element mass change histograms for SHF andesitic basalts.

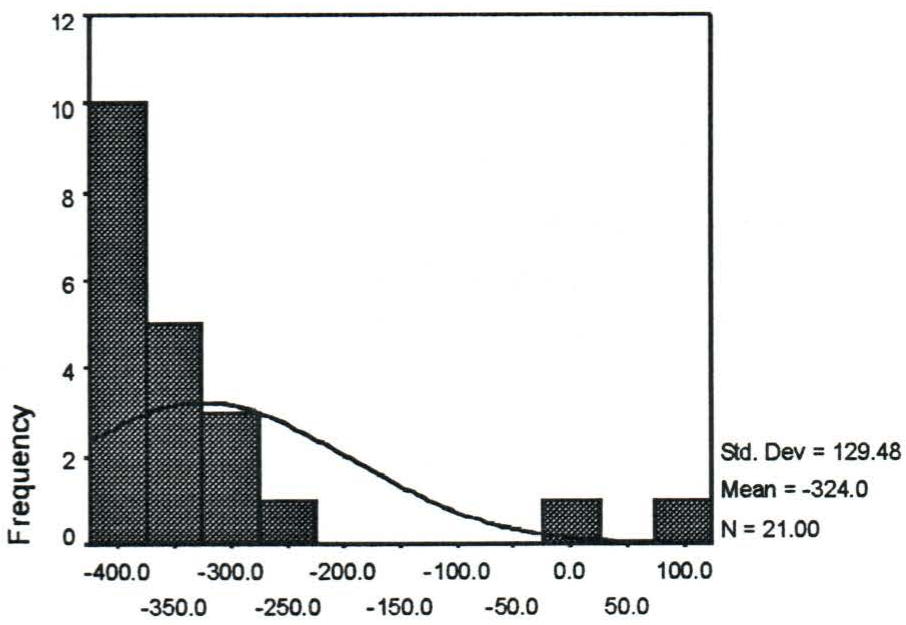












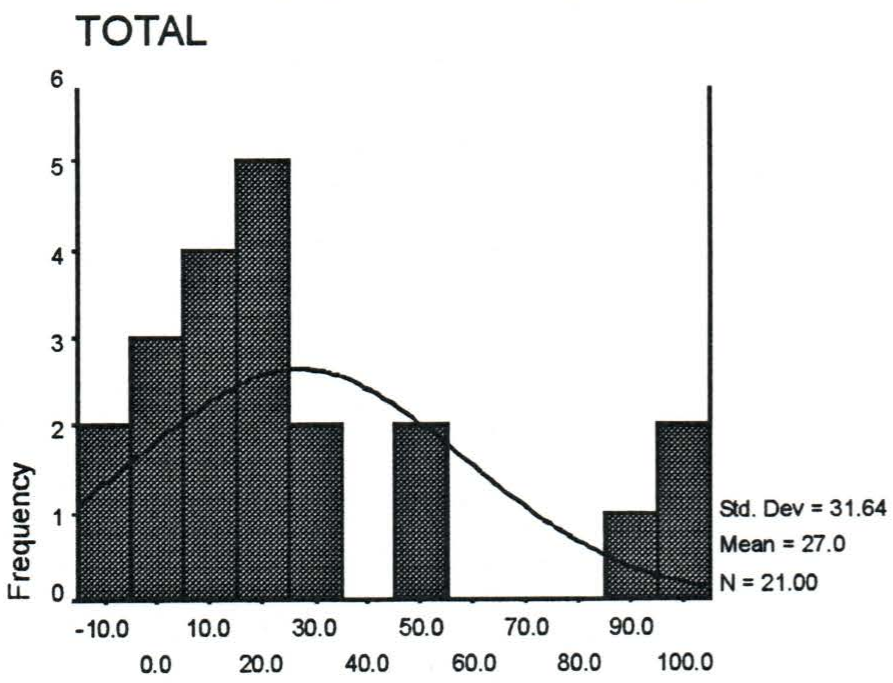
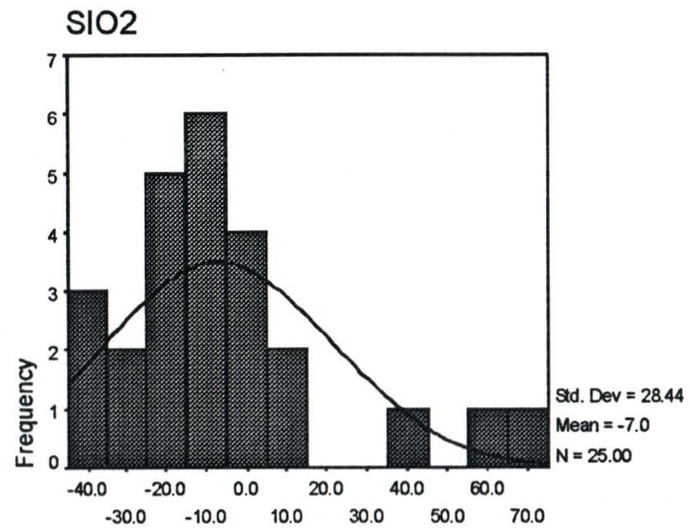
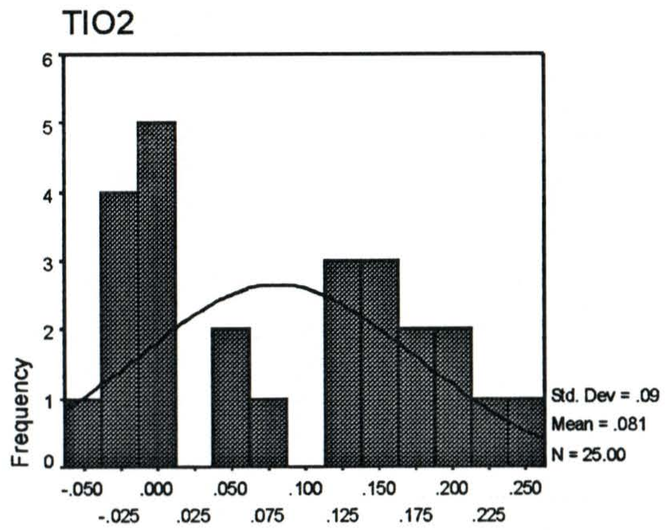
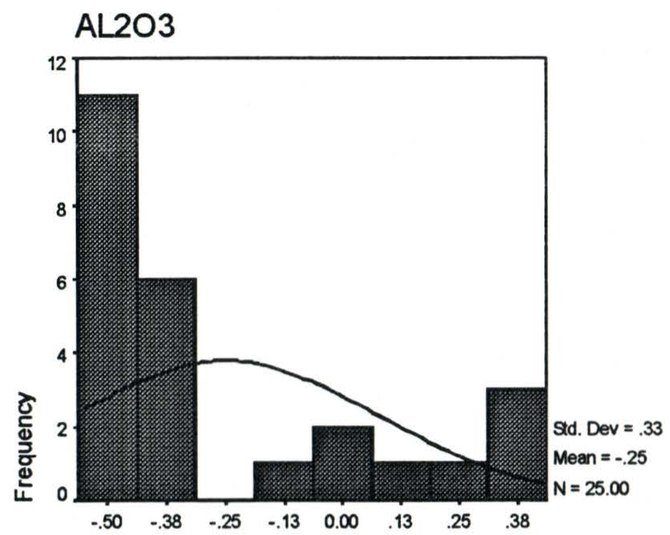
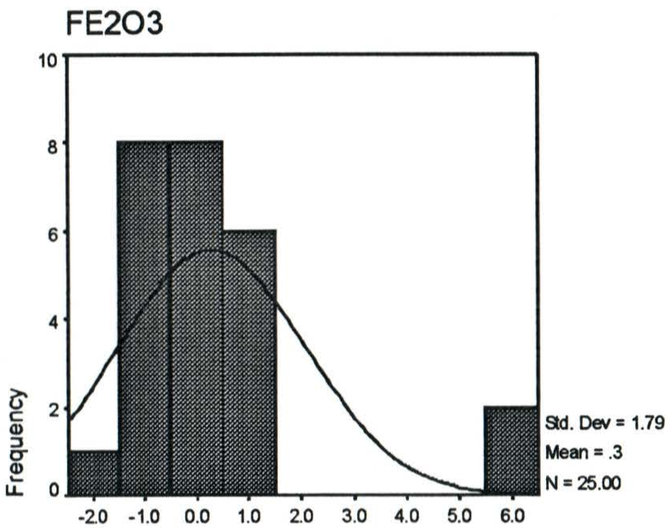


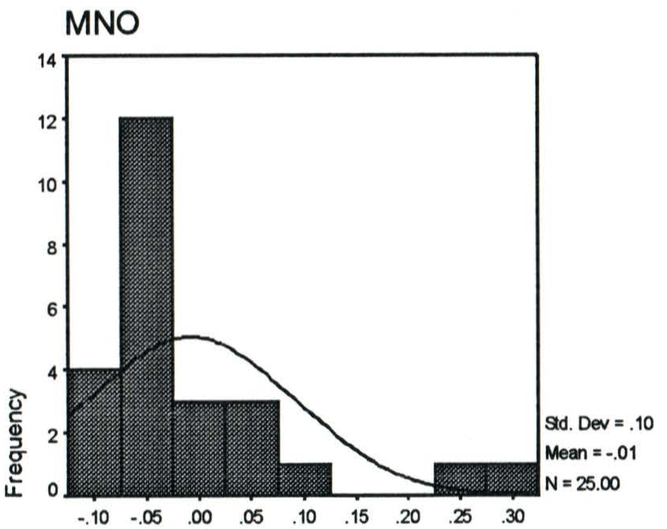
Figure F-1 - (continued) Oxide and trace element mass change histograms for SHF andesitic basalts.

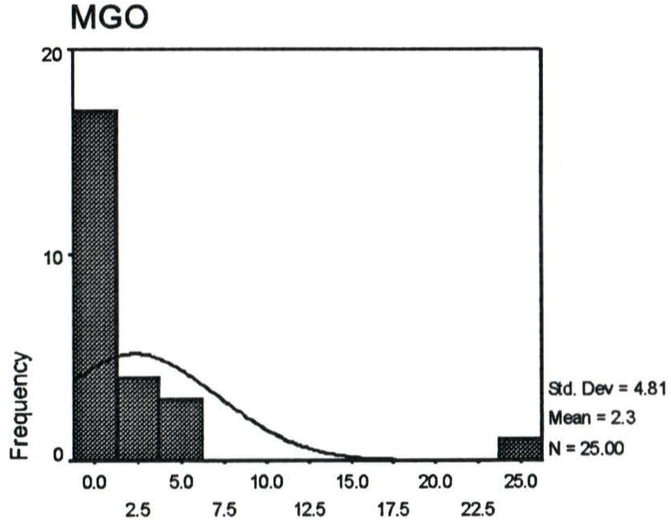


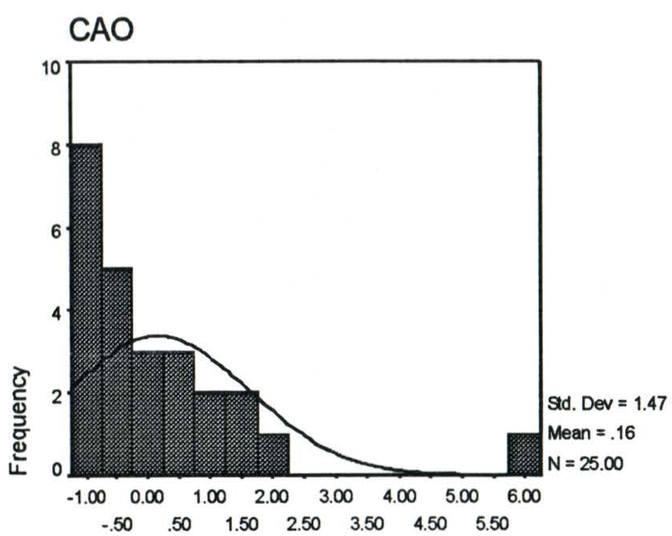


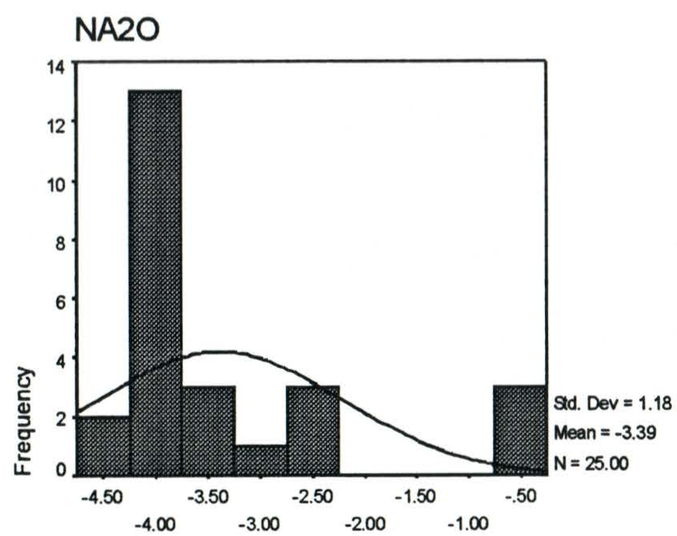












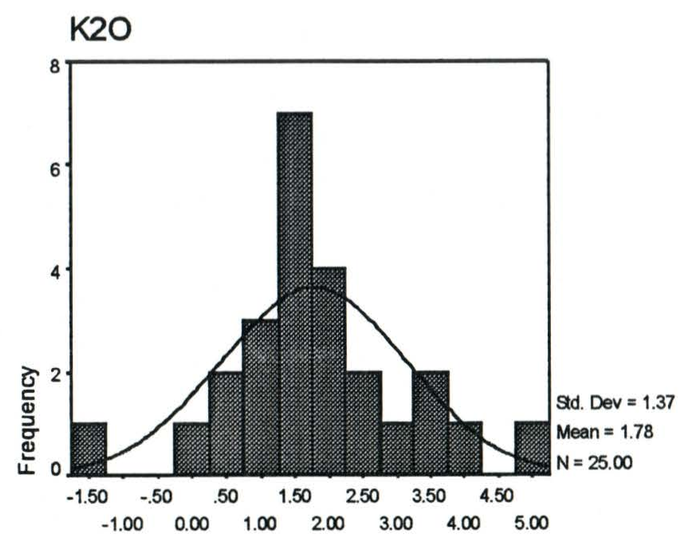
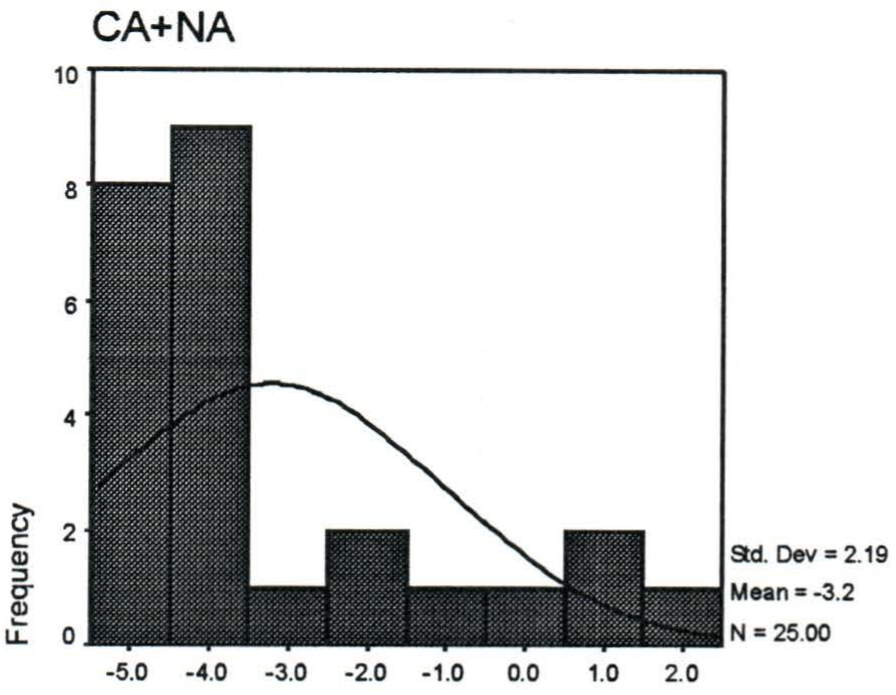
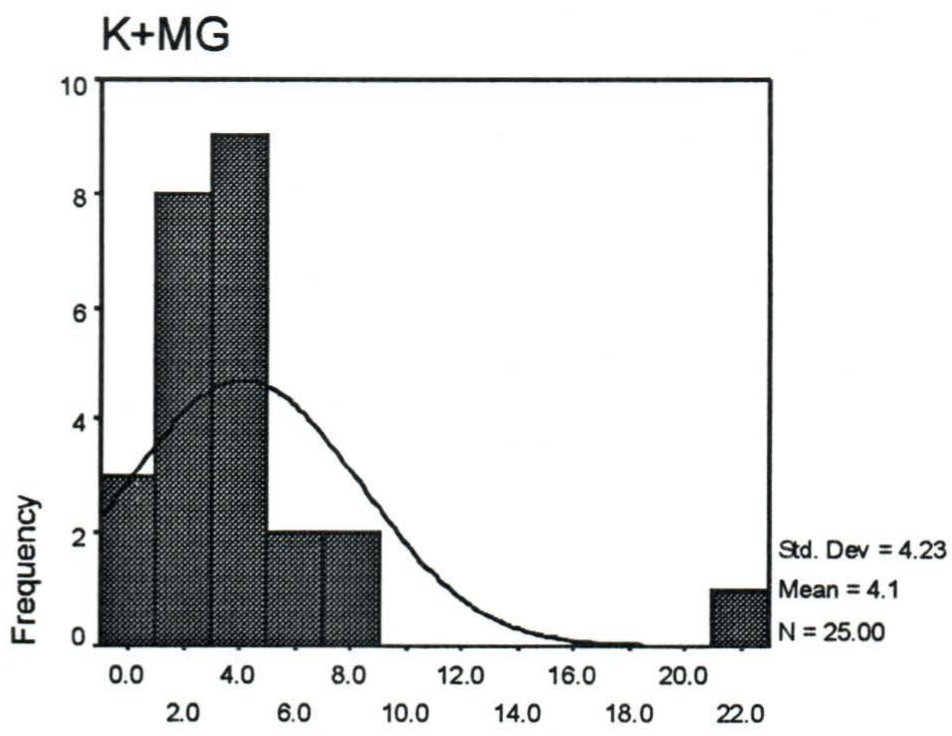
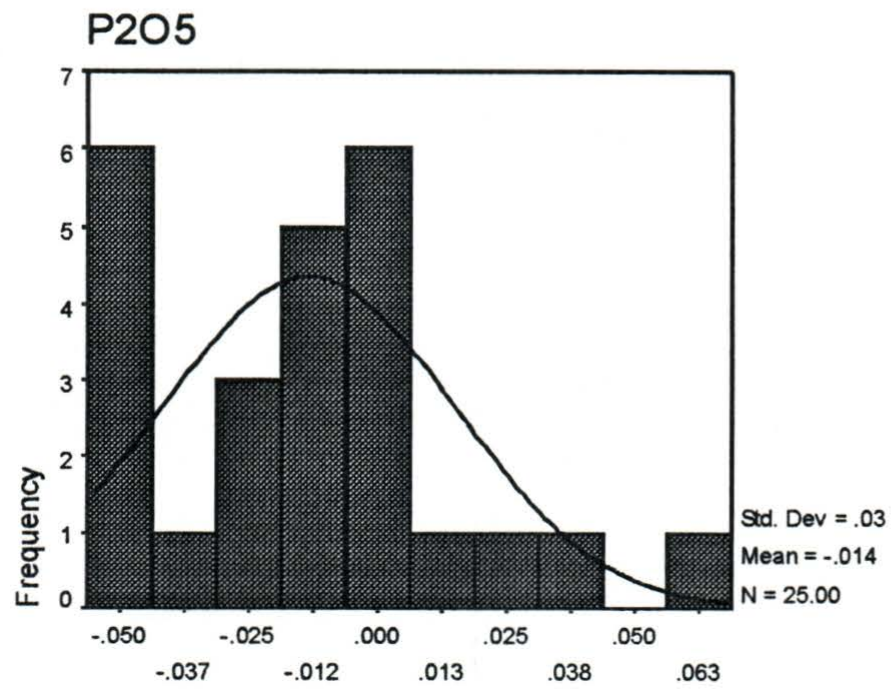
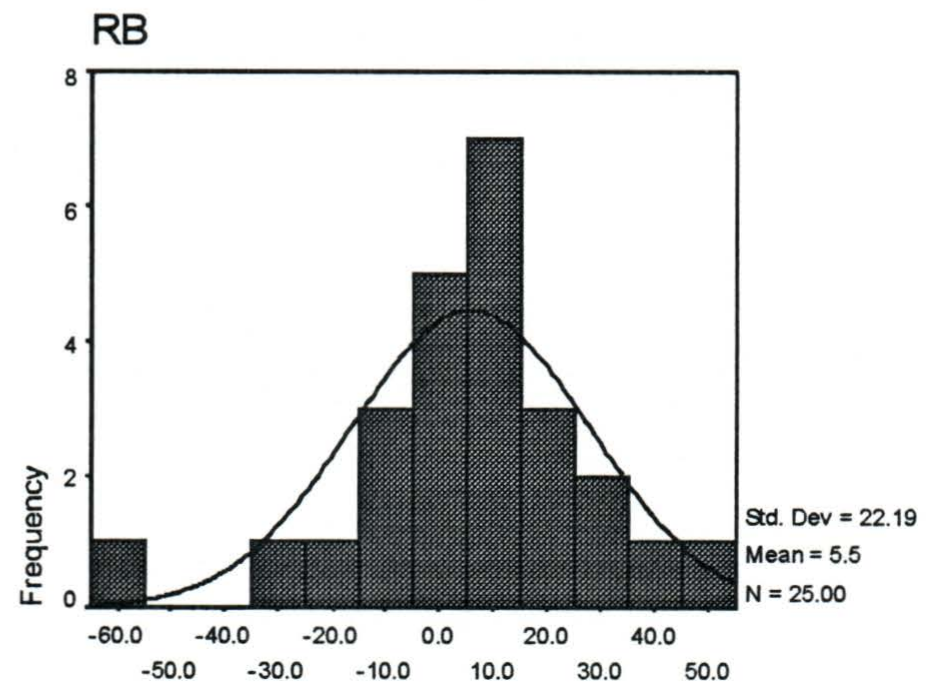


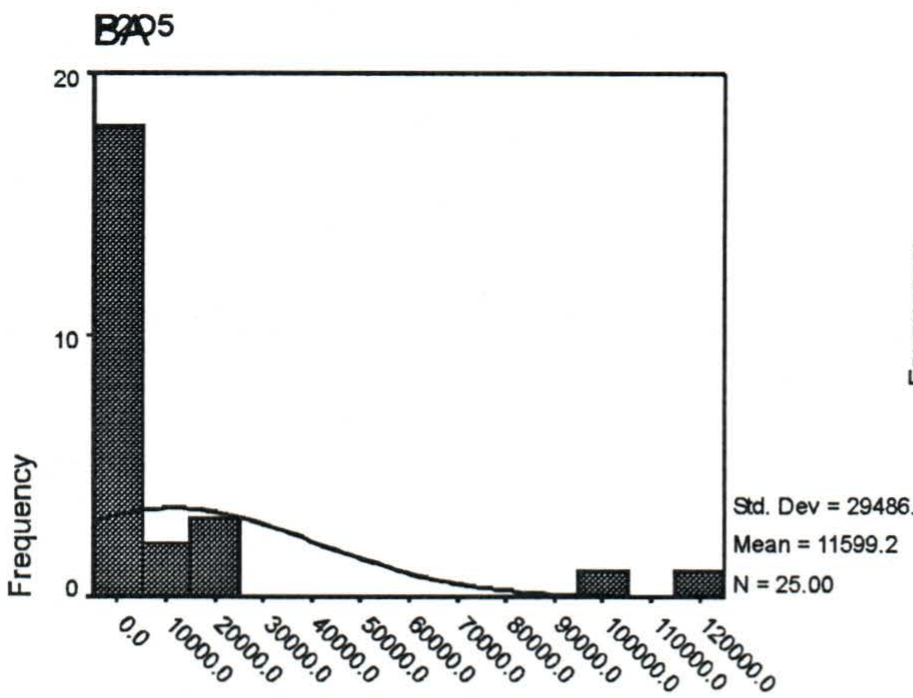
Figure F-2 - Oxide and trace element mass change histograms for BRF dacites.

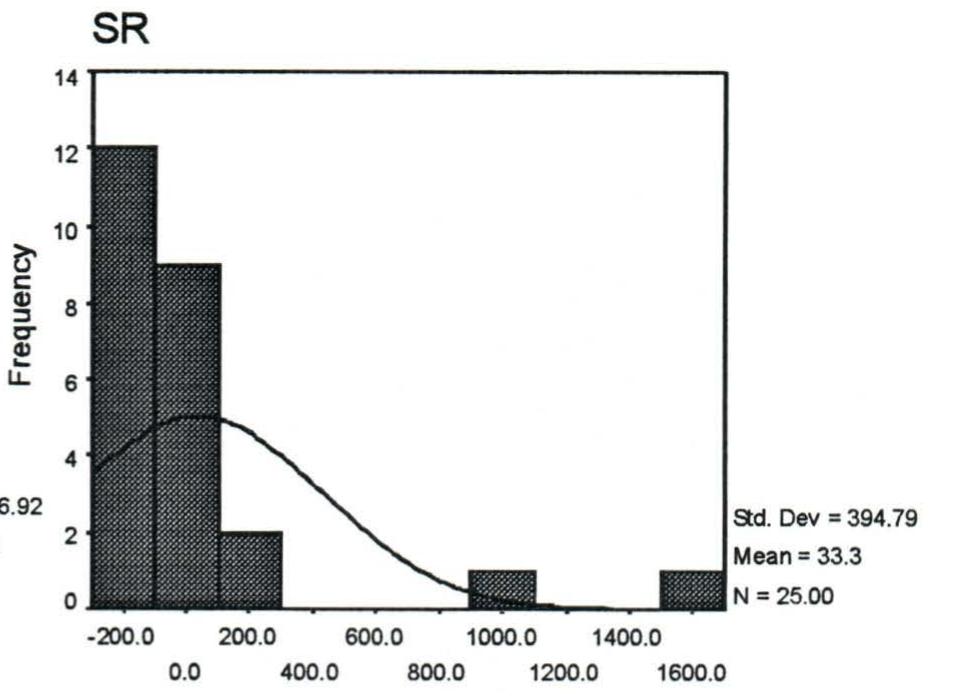












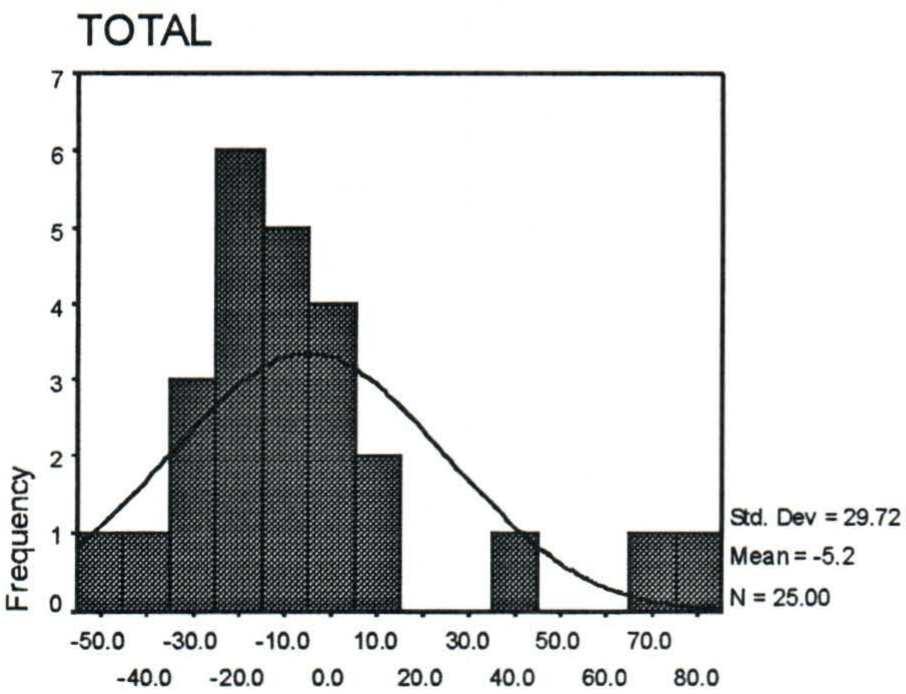
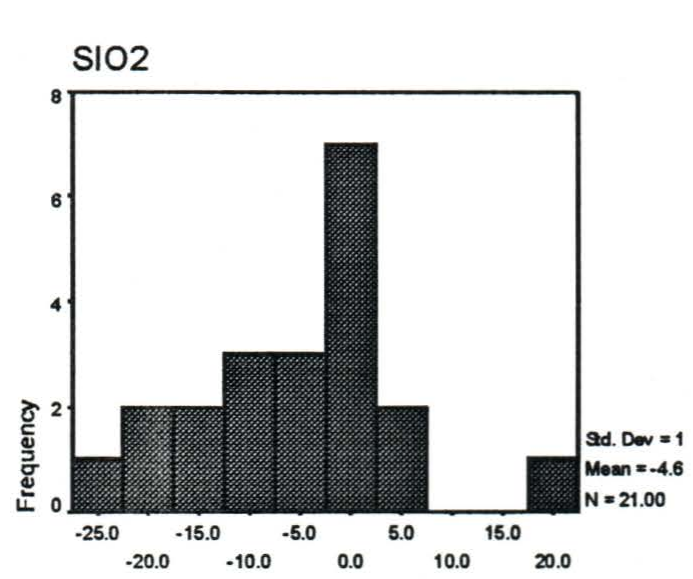
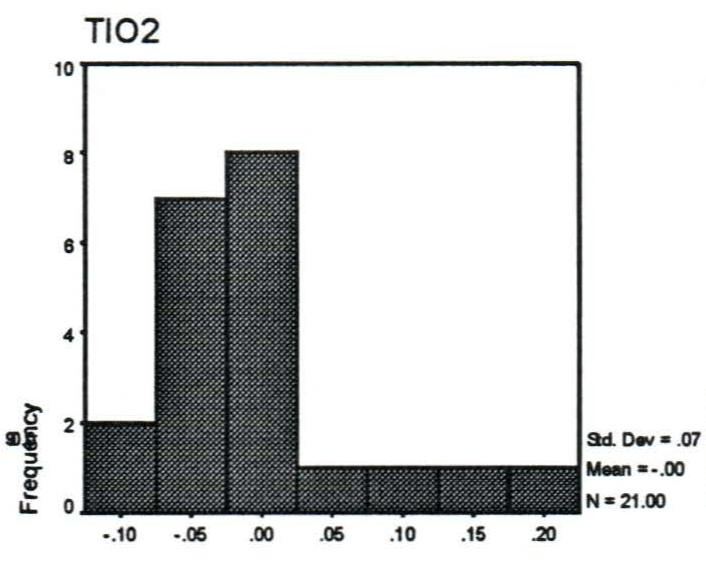
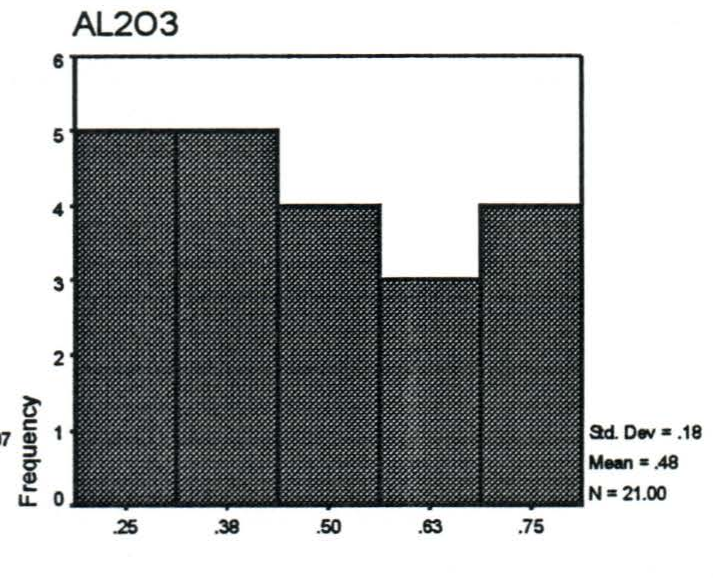
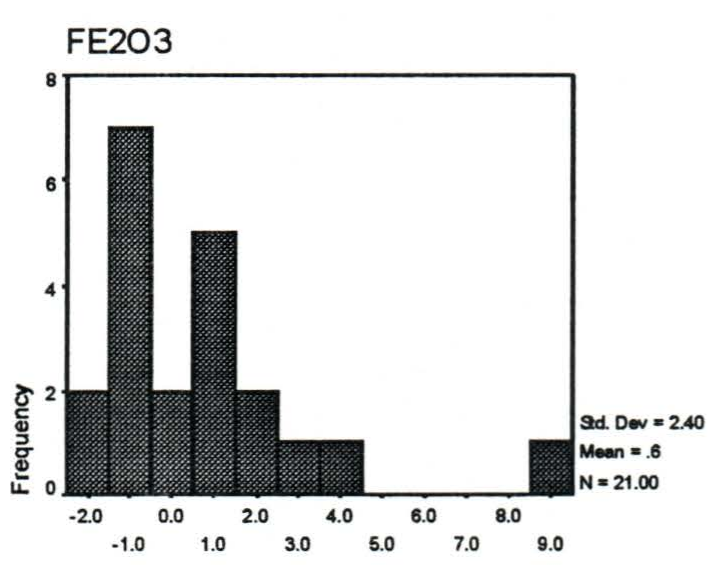


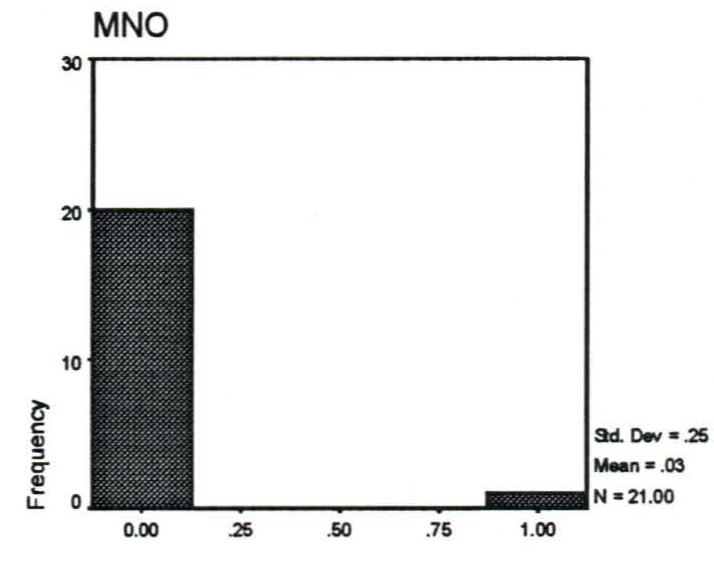
Figure F-2 - (continued) Oxide and trace element mass change histograms for BRF dacites.

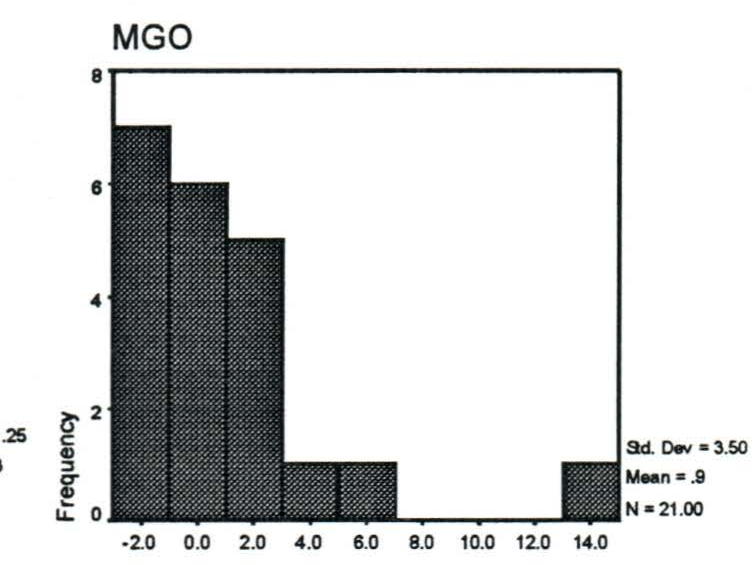


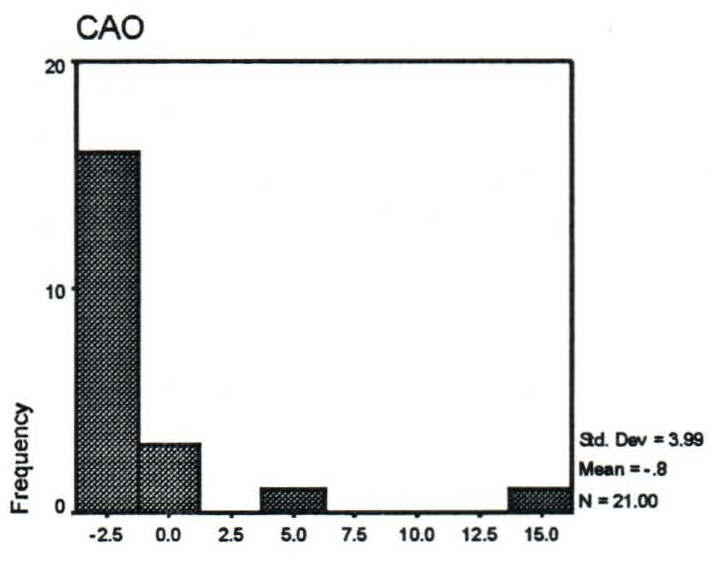


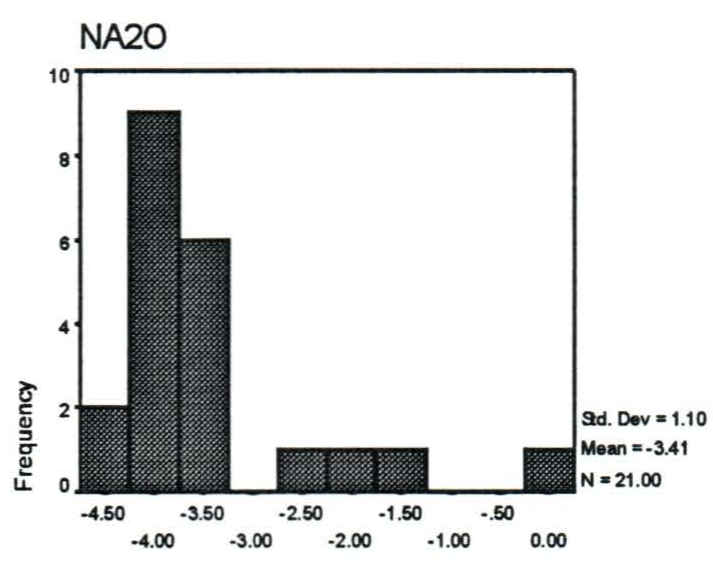


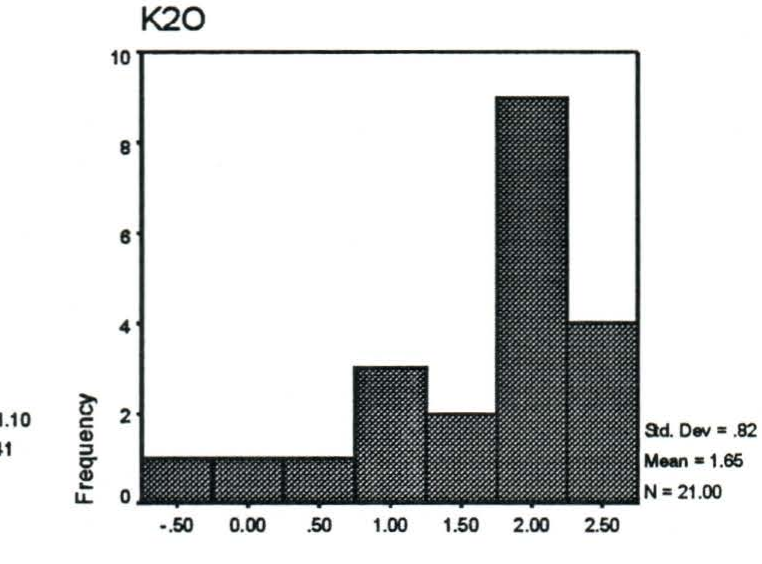


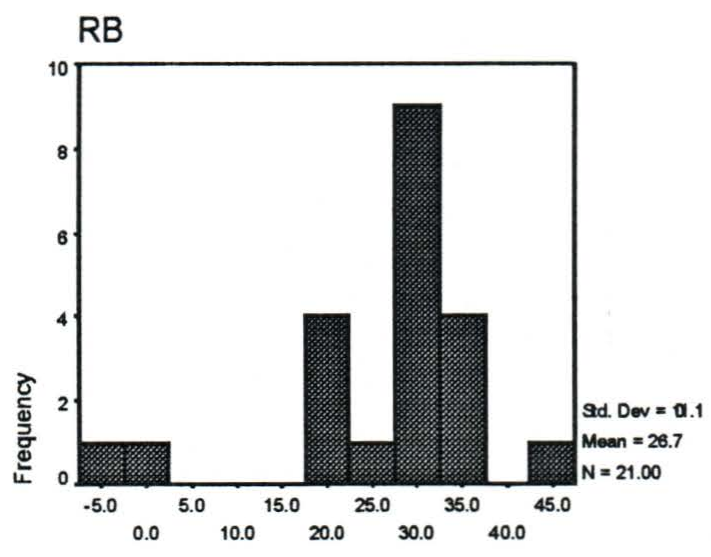


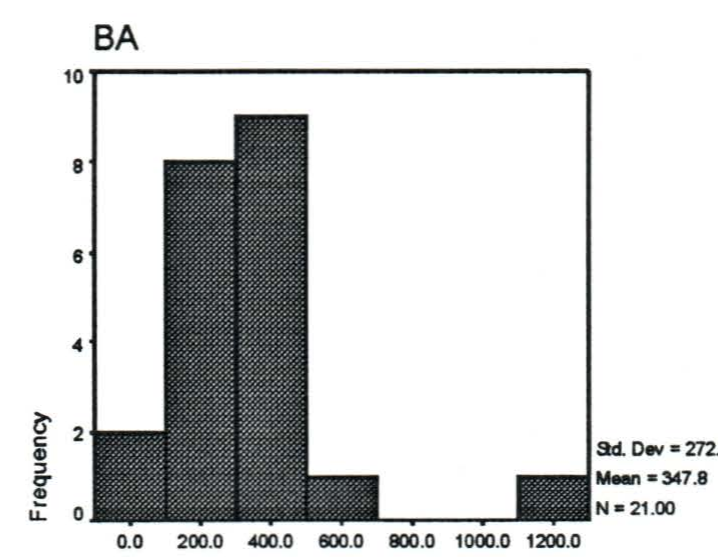












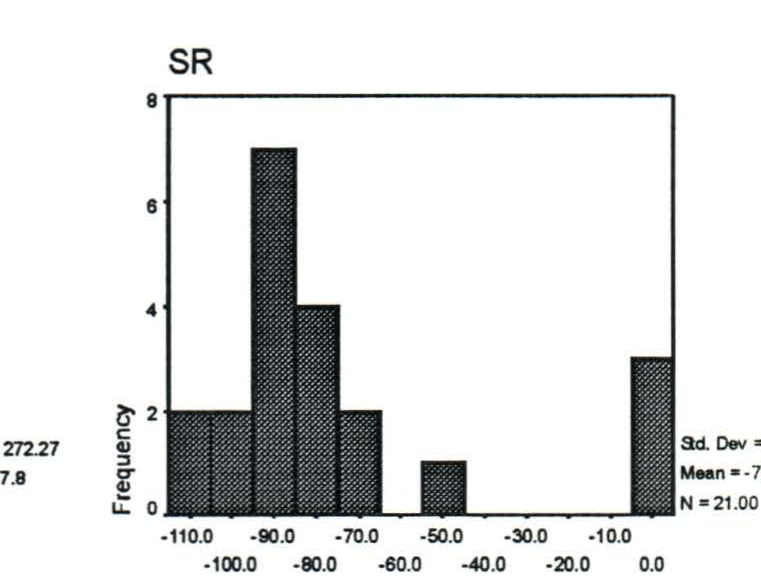
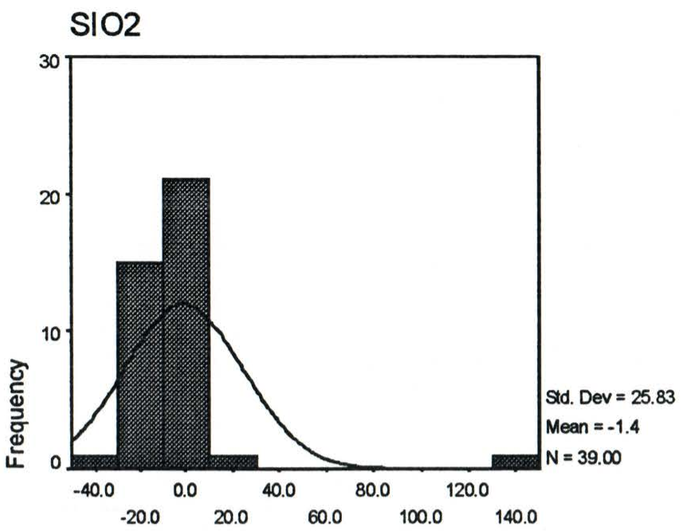
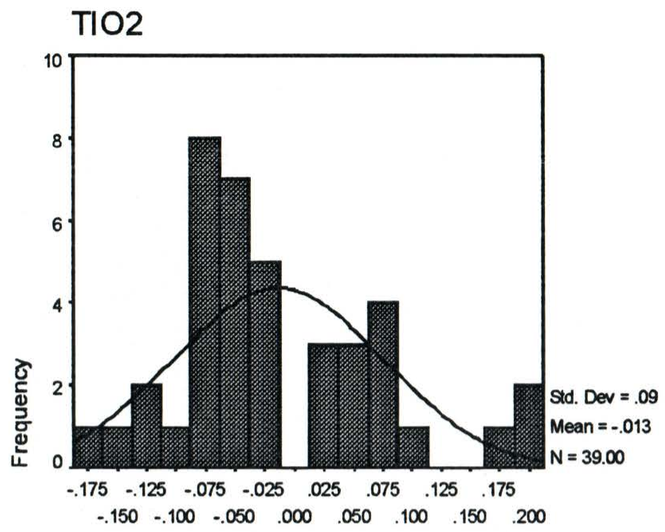
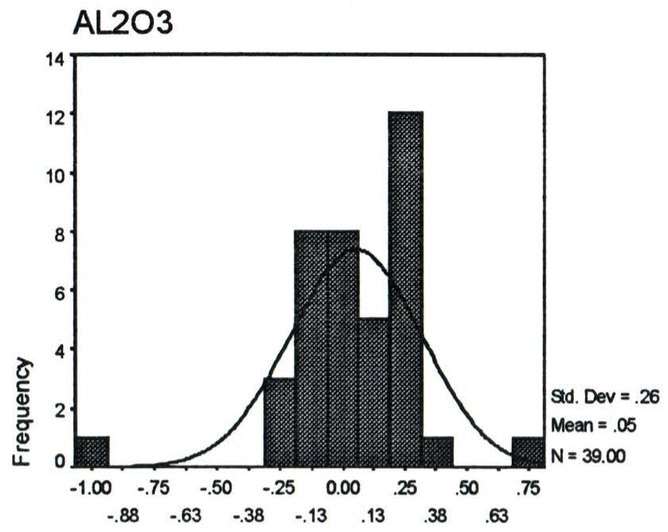
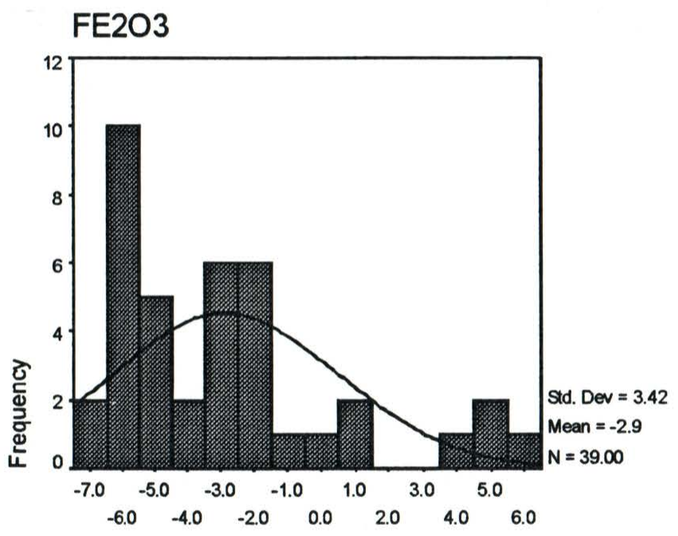


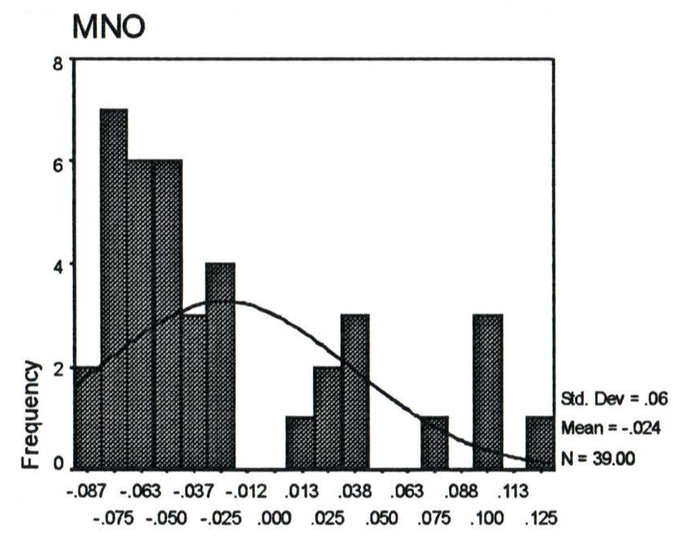
Figure F-3 - Oxide and trace element mass change histograms for PHZ dacites.

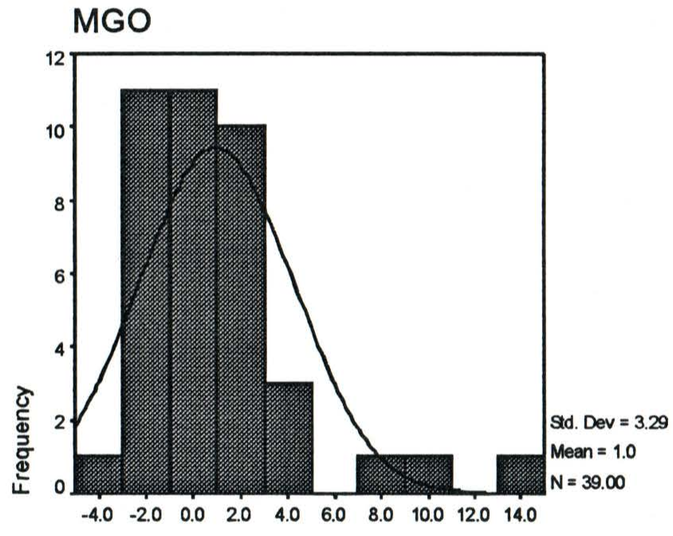


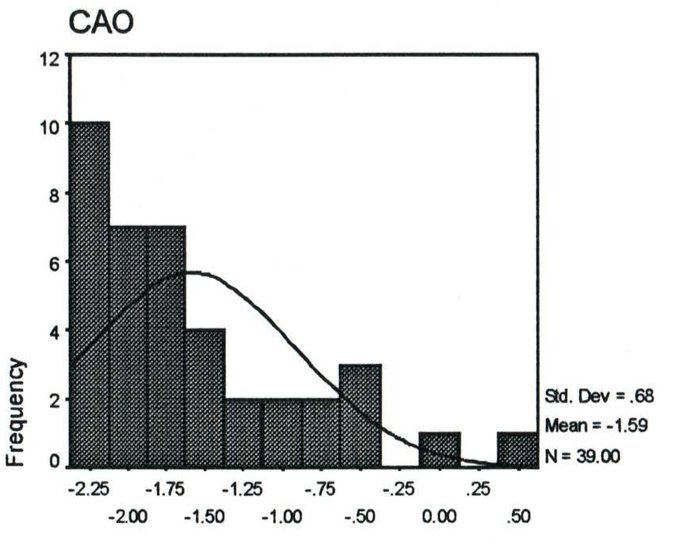


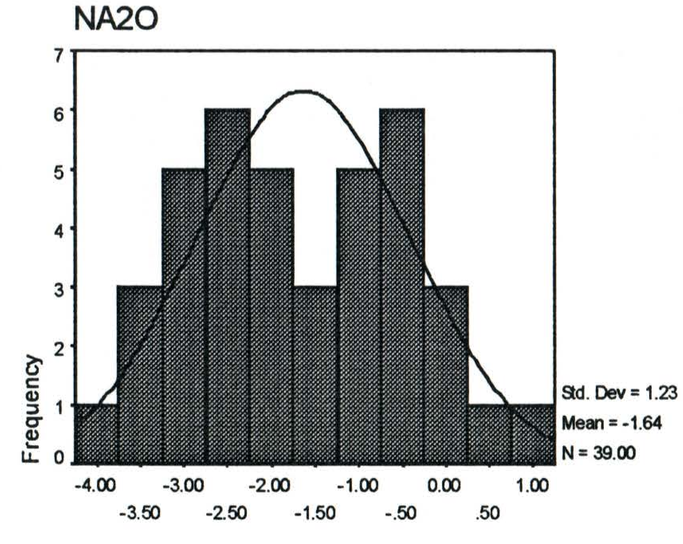












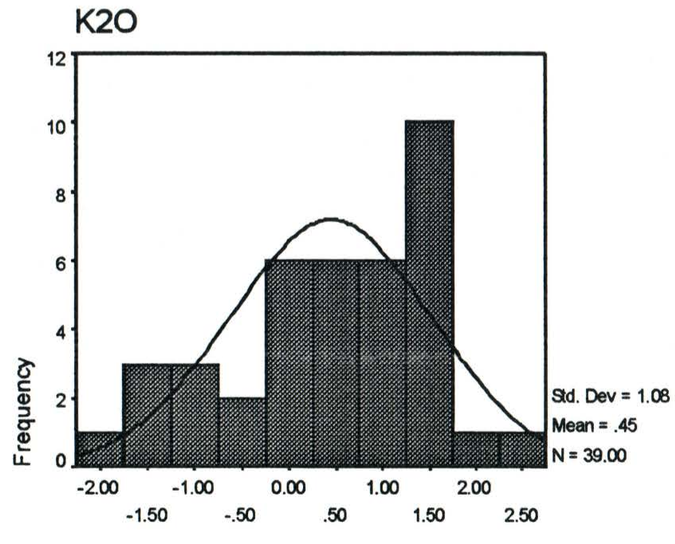
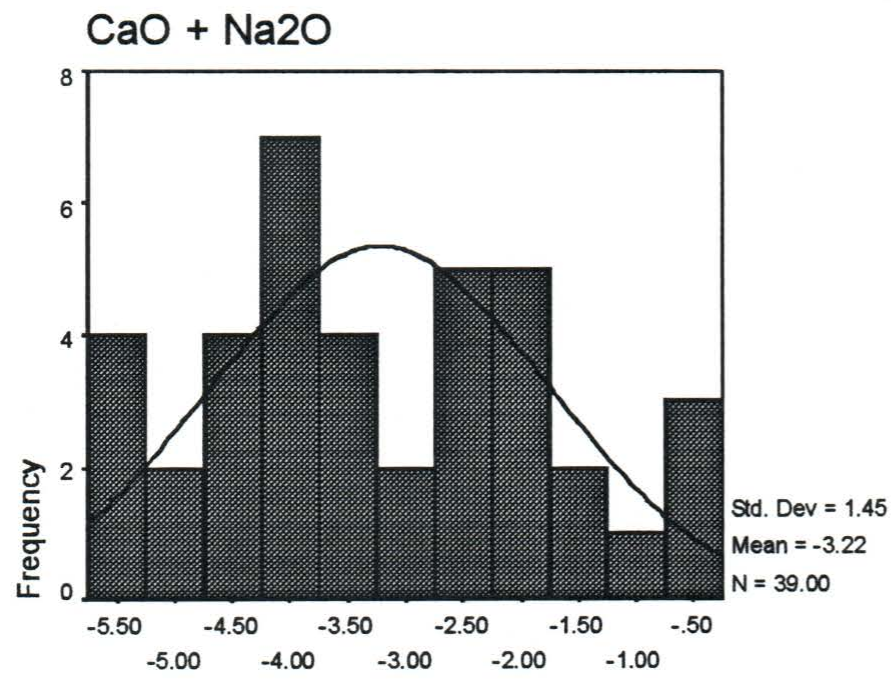
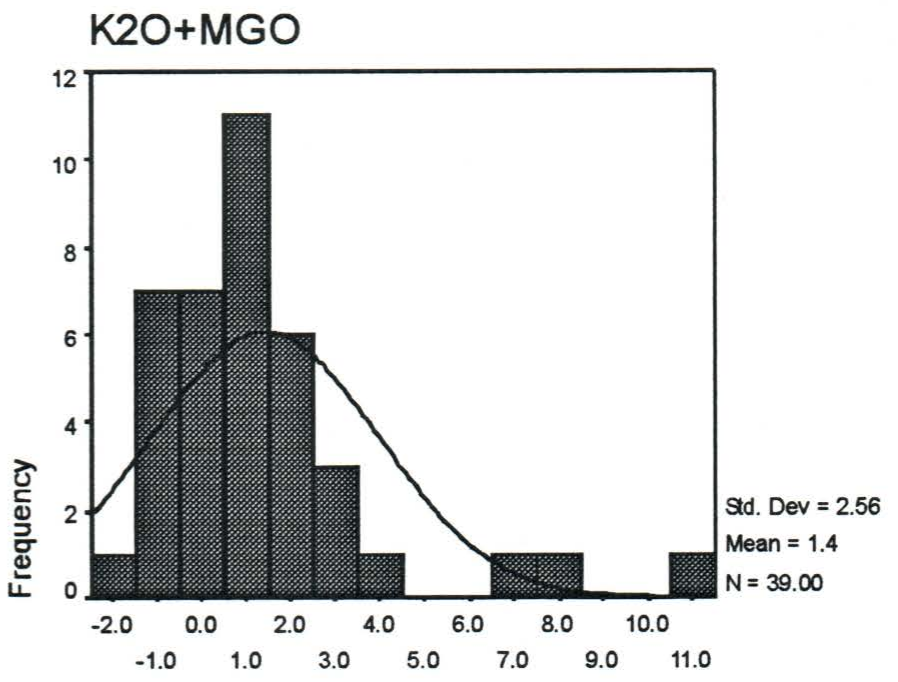
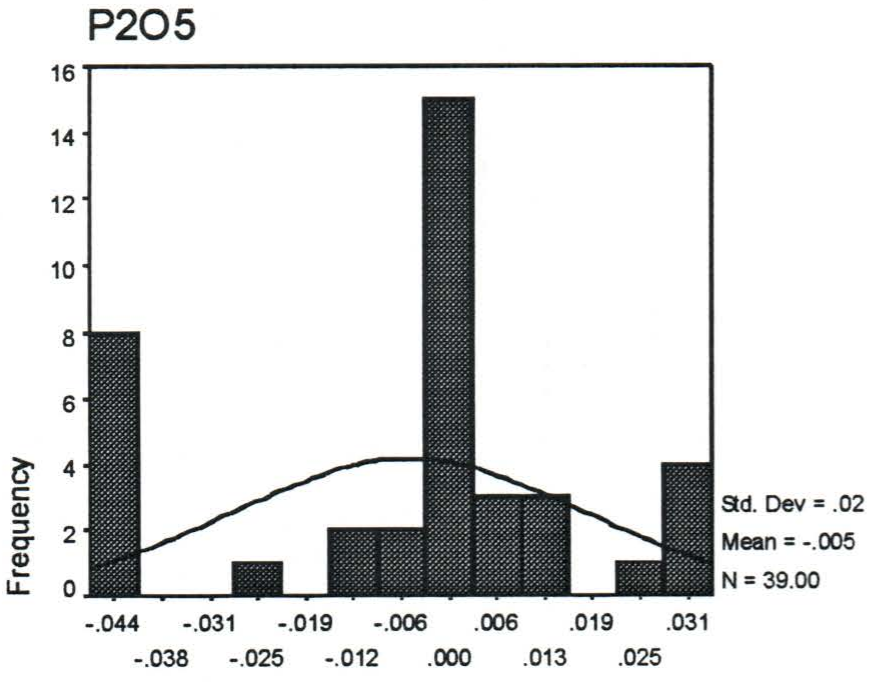
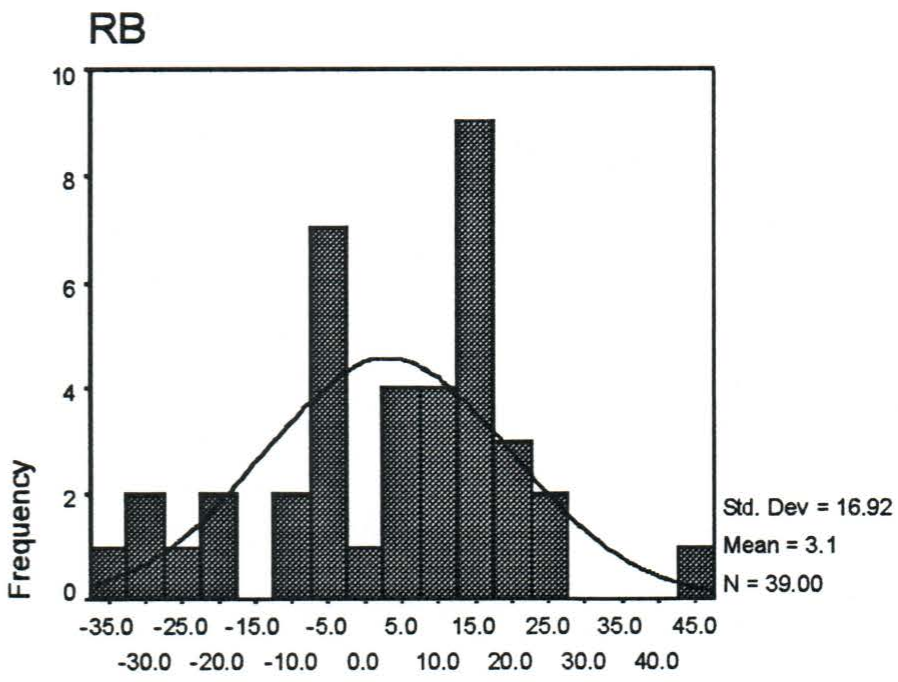


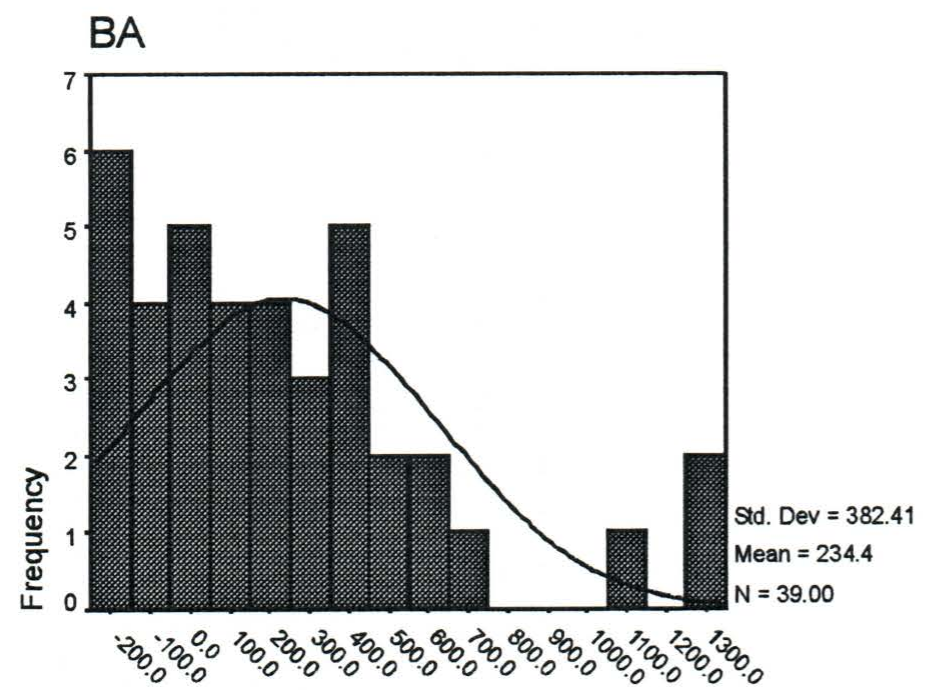
Figure F-4 - Oxide and trace element mass change histograms for WBZ dacites.

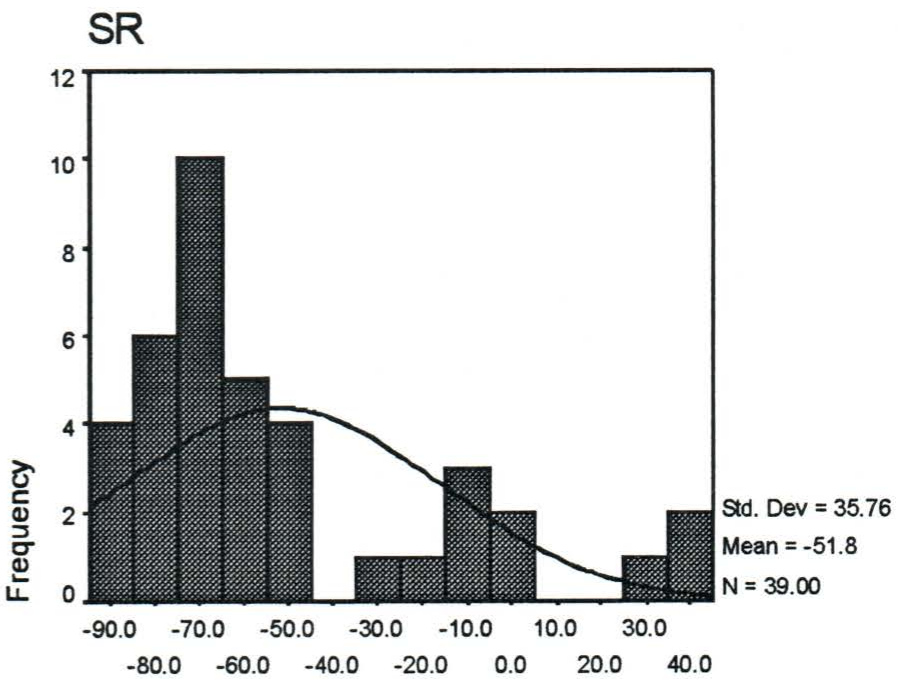












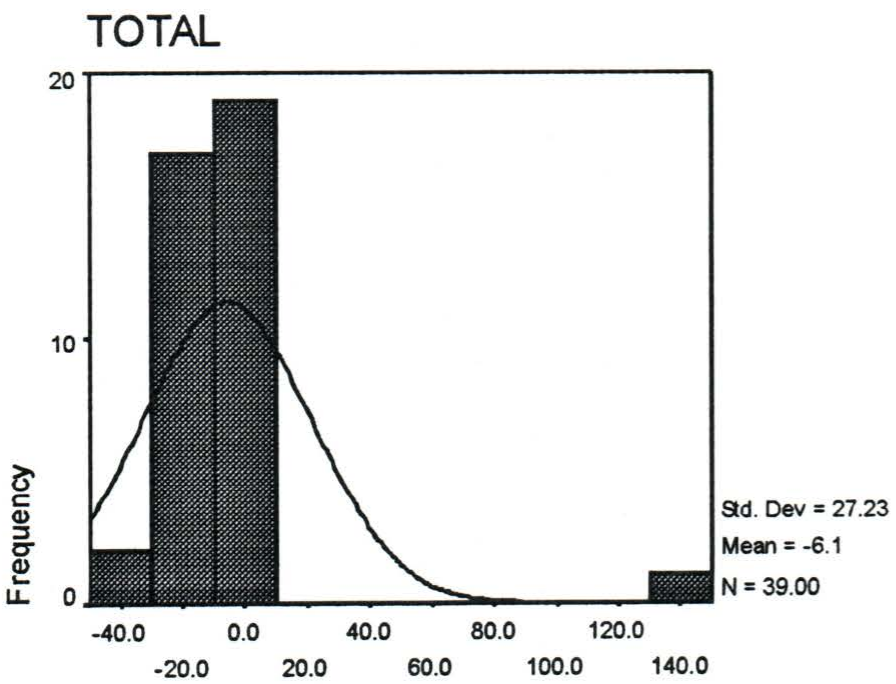


Figure F-4 - (continued) Oxide and trace element mass change histograms for WBZ dacites.